UNIVERSIDADE DE LISBOA
INSTITUTO SUPERIOR TÉCNICO

RESTORATION OF ANCIENT PORTUGUESE INTERIOR PLASTER COATINGS: CHARACTERIZATION AND DEVELOPMENT OF COMPATIBLE GYPSUM-BASED PRODUCTS

Maria Teresa de Almeida Gouveia Geraldes Freire

Supervisor: Doctor Maria do Rosário da Silva Veiga
Co-Supervisors: Doctor António Manuel dos Santos Silva
Doctor Jorge Manuel Caliço Lopes de Brito

Thesis approved in public session to obtain the PhD Degree in Civil Engineering
Jury final classification: Pass with Distinction

Jury:

Chairperson: Chairman of the IST Scientific Board
Members of the Committee:
Doctor Ana Luísa Pinheiro Lomelino Velosa
Doctor José Manuel Aguiar Portela da Costa
Doctor Inês dos Santos Flores Barbosa Colen
Doctor Maria do Rosário da Silva Veiga
Doctor António José Estevão Grande Candeias
Doctor Ana Paula Patrício Teixeira Ferreira Pinto França de Santana

2016

UNIVERSIDADE DE LISBOA
INSTITUTO SUPERIOR TÉCNICO

RESTORATION OF ANCIENT PORTUGUESE INTERIOR PLASTER COATINGS: CHARACTERIZATION AND DEVELOPMENT OF COMPATIBLE GYPSUM-BASED PRODUCTS

Maria Teresa de Almeida Gouveia Geraldes Freire

Supervisor: Doctor Maria do Rosário da Silva Veiga

Co-Supervisors: Doctor António Manuel dos Santos Silva

Doctor Jorge Manuel Caliço Lopes de Brito

Thesis approved in public session to obtain the PhD Degree in Civil Engineering

Jury final classification: Pass with Distinction

Jury:

Chairperson: Chairman of the IST Scientific Board

Members of the Committee:

Doctor Ana Luísa Pinheiro Lomelino Velosa, Associate Professor, Universidade de Aveiro

Doctor José Manuel Aguiar Portela da Costa, Associate Professor, Faculdade de Arquitectura, Universidade de Lisboa

Doctor Inês dos Santos Flores Barbosa Colen, Associate Professor, Instituto Superior Técnico, Universidade de Lisboa

Doctor Maria do Rosário da Silva Veiga, Senior Researcher (with habilitation), Laboratório Nacional de Engenharia Civil

Doctor António José Estevão Grande Candeias, Assistant Professor, Escola de Ciências e Tecnologia, Universidade de Évora

Doctor Ana Paula Patrício Teixeira Ferreira Pinto França de Santana, Assistant Professor, Instituto Superior Técnico, Universidade de Lisboa

Funding Institutions:

FCT - Fundação para a Ciência e Tecnologia, PhD scholarship SFRH/40128/2007

Thesis carried out in collaboration with the National Laboratory of Civil Engineering within the framework of the cooperation protocol between IST and LNEC

2016

Aos meus pais

Ao João e à Mariana

À minha Ninô

Acknowledgments

"De sonhar ninguém se cansa, porque sonhar é esquecer, e esquecer não pesa e é um sono sem sonhos em que estamos despertos."

"Nobody gets tired of dreaming, because dreaming is to forget, and forget does not weigh and is a dreamless sleep in which we are awake."

Fernando Pessoa (Portuguese poet, philosopher and writer, 1888-1935)

The idea to undertake this thesis first came up in 2002, when I was still working at SIVAL. The subject was obviously related to gypsum and the person elected to supervise the work was Eng. Maria do Rosário Veiga, from LNEC. This initial project soon had to be abandoned due to professional compromises that were not compatible with the time needed to perform it. However, it was not forgotten and some years later the decision to proceed was definitely made.

In spite of having been a long, hard road I never regretted my decision. One of the main reasons for that was the pleasure I had to work with Eng. Maria do Rosário. Although we had had only few professional contacts before starting to work in this project time showed that my first impression was right: I found in Eng. Maria do Rosário not only an extremely competent and dedicated supervisor, that was always available to support me and to contribute with her invaluable scientific knowledge and advice, but also my best friend during the whole process. Words are not enough to express my gratitude.

Another very important thing I owe to Eng. Maria do Rosário is the choice of my co-supervisors, Professor Jorge de Brito, from Instituto Superior Técnico and Doctor António Santos Silva from LNEC. The three form an outstanding team whom I feel honoured to have worked with.

To Professor Jorge de Brito and his extraordinary working capacity I have to thank the permanent willingness to cooperate and to keep me motivated, the attention given to the minimum details despite being overworked and the patience that he had with me.

To Doctor António Santos Silva for the excellent work conditions provided, for understanding and sharing with me the enthusiasm for these subjects and for all the knowledge transmitted during our numerous discussions. His unlimited availability, patience, sympathy and friendship made me reinforce the feeling that it was worth running the risk of my decision.

To LNEC for creating the conditions that allowed the realization of all the experimental work. It is, no doubt, a great institution. In LNEC I also had the opportunity to meet many colleagues that are now my friends. They have always encouraged me, in the best and worst moments, showing a spirit of cooperation and friendship uncommon to find. For that I am very grateful to Sofia Malanho, Ana Rita Santos, Sílvia Costa, Ana Fragata, Sandro Botas, Giovanni Borsoi, Claúdio Cruz, António Vilhena, Luís Matias, Nádia Lampreia, Ana Marques, Dora Santos and Eng. Pina dos Santos.

To the technicians of LNEC that gave their invaluable support to the experimental work: Ana Paula Menezes and Susana Couto from the Materials Department; Bento Sabala, Acácio Monteiro, Luís Carmo and especially Ana Maria Duarte from the Buildings Department. Great part of the work would have been impossible without their cooperation.

To other people from LNEC that contributed with their friendship, so important in a work of this kind: Sónia Raposo, who had the generosity of lending me many books without delivery time limit; Fátima Meneses, Luzia Barracha, Fátima Forreta and Vanda Cardoso for making me feel as being part of the "family".

To FCT (Fundação para a Ciência e Tecnologia) for financial support through the PhD scholarship SFRH/BD/40128/2007 and to ICIST (Instituto de Engenharia de Estruturas, Território e Construção) also for financial support.

To Isabel Pombo Cardoso, my "gypsum friend", for the encouragement, the fruitful discussions and for sharing with me the passion for gypsum; only she can really understand it.

To Dulce Henriques, Ana Silva, José Silvestre and Manuela Amado, my "PhD friends", for their contribution to keep me motivated; without their incentive it would have been even harder.

To my dear friends Ana Paula Figueiredo and Helena Freitas for their constant encouragement; they know how it was important to me.

To my colleagues from SIVAL, Eng. Carlos Pereira and Eng. Ângela Sousa, for their prompt cooperation whenever I asked for it, for their friendship, their interest in my work and for the enthusiasm about "gypsum matters" we always share when we are together.

To Eng. Pedro Faria for the facilities provided at SIVAL and for the supply of materials and to Dr. Mário Marques from LUSICAL also for the supply of materials.

To all the entities and people who gave an invaluable contribution in the process of collection of the samples I express here my gratitude. They were so many that I will not take the risk of enumerating all. I have, however, to name Architects Irene Frazão and Luísa Cortesão, from Direcção Geral do

Património Cultural (DGPC), Paulo Ludgero, Miguel Figueiredo and João Oliveira from the firm CRERE, Doctor Virgílio Correia and Dr. Pedro Sales from the Monographic Museum of Conímbriga.

And last, but not least, my family: to my cousins Joana and Catarina for supporting me always, even when they were in need of support; to my brother Joaquim and his family, Rita, Afonso and Inês for receiving me so well in their home during my numerous stays in Lisbon; to my brother Pedro who encouraged me a lot in the final part of the work as he wanted desperately to see me ending it; to my mother-in-law for helping me and for giving support to my husband and children in my absence; to all the other members of my family, just for being part of it.

To my parents, from whom I inherited the will to learn; their example and unconditional love are my guiding lines.

To my children, João and Mariana, that early had to learn what a PhD was and never complained about it. They have always been generous offering me support, comprehension and love.

To Carlos Pedro, for many of the excellent photos and for bearing during all these years something that has always been unbearable to him: my unavailability.

Abstract

This thesis aims at contributing to promote the preservation of the Portuguese ancient gypsum-based plaster coatings.

A literature review showed that there is little information about this heritage and no products in the market especially designed for its preservation.

A systematic study of the composition of the interior plaster coatings belonging to several periods of the Portuguese history was conducted. More than 100 samples were collected from north to south of the country, representing different types of constructions (dwellings, palaces, churches, etc.) and epochs: Roman and Late Roman, Islamic, Low Middle-Age and Renaissance, Baroque and Post Baroque. A mineralogical survey was made, showing that the use of gypsum-based plasters in Portugal was significant only from the mid 1800's to the first decades of the 20th century, mainly as wall and ceilings' decorative programmes.

A detailed mineralogical, physical and mechanical characterization was performed on the later period samples. Three main compositional patterns, directly related with the type of plastered elements and their application, were revealed: smooth surface, moulded on site and pre-moulded.

Compatibility requirements for the restoration products were established, which, together with experimental application tests, allowed defining seven mixes. They were then submitted to physical and mechanical characterization tests and three mixes that best fulfilled the requirements established were selected.

Keywords: Gypsum-based plasters; Characterization; Microstructure; XRD; Physical and mechanical properties; Interior plaster coatings; Compatible materials; Restoration products; Portuguese heritage; Traditional construction

Resumo

Esta tese pretende contribuir para a preservação dos revestimentos interiores antigos Portugueses com base em gesso.

A revisão da literatura permitiu concluir que há pouca informação sobre este património e não há produtos disponíveis no mercado especialmente concebidos para a sua preservação.

Realizou-se um estudo sistemático da composição dos revestimentos interiores de paredes em vários períodos da história de Portugal. Recolheu-se mais de 100 amostras de norte a sul, representando vários tipos de construções (edifícios de habitação, palácios, igrejas, etc.) e épocas: Romana e tardo-Romana, Islâmica, Baixa Idade Média e Renascimento, Barroca e Pós-Barroca. A avaliação da composição mineralógica mostrou que o uso de gesso em revestimentos de paredes e tectos só foi significativo entre a segunda metade do século XVIII e as primeiras décadas do século XX.

As amostras deste último período foram objecto de caracterização mineralógica, física e mecânica. Foi revelada a existência de três padrões principais de composição, directamente relacionados com o tipo de elementos estucados e respectivas técnicas de aplicação: superfícies lisas, elementos moldados no local e elementos pré-moldados.

Foram ainda estabelecidos requisitos de compatibilidade para os produtos de restauro que, juntamente com a realização de testes de aplicação, conduziram à definição de sete formulações. Seguiu-se a sua caracterização física e mecânica e as três misturas que melhor preencheram os requisitos de compatibilidade estabelecidos foram seleccionadas.

Palavras-chave: Revestimentos de gesso; Caracterização; Microestrutura; DRX; Propriedades físicas e mecânicas; Revestimentos interiores estucados; Materiais compatíveis; Produtos de restauro; Património Português; Construção tradicional

List of contents

List of figures

List of tables

1

Introduction

"El progreso no consiste en aniquilar hoy el ayer, sino, al revés, en conservar aquella esencia del ayer que tuvo la virtud de crear ese hoy mejor"

José Ortega y Gasset (Spanish philosopher and essayist, 1883-1955)

1.1 Motivation and scope

The preservation of the built heritage is considered of major importance to understand human History. In fact, the knowledge of the materials and techniques used and of their evolution throughout the different historical periods and geographical regions worldwide is considered a precious source of information, not only from the architectural and constructive points of view, but also from the human and social sciences' (Gourdin & Kingery 1975; Kingery et al. 1988; Philokyprou 2012).

In the twentieth century the importance of all forms of cultural heritage started to be highlighted, particularly in Europe, with the elaboration of several international documents and charters for its preservation, notably the Venice Charter of 1964. Since architectural assets are an important part of the cultural heritage, it is strongly recommended that interventions should comply with a global perspective of buildings and the built environment they belong to, preserving their structure and external image, as well as their interior spaces and original materials. When this cannot be achieved, the design and use of new products for restoration should be based on similar materials and their compatibility with the original ones be ensured before application, according to the Krakow Charter of 2000. In this document the architectural decoration is specifically mentioned as being part of the built heritage (DGPC n.d.).

This research work was developed within this context and consists on the study of ancient Portuguese interior wall and ceilings' coatings based on gypsum and gypsum-lime plasters in order to develop compatible, efficient and durable solutions for their preservation.

The first step was to acquire complete knowledge of the materials and compositions of the referred coatings. An extensive bibliographic review allowed concluding there is very little information on this important heritage, especially from the materials' point of view (even in international literature studies on gypsum plasters' composition are surprisingly scarce).

On the other hand, the Portuguese word for "plaster" - *estuque* - means "a kind of mortar *with gypsum* used for the plastering of walls, relief ornaments and sculpture works" (Machado 1991), but is assigned in general bibliography to all kinds of plastered elements independently of their composition.

In spite of lacking raw material sources of gypsum in Portugal, in opposition to the greater availability of limestone, this question of terminology has induced some scientific communities to think that gypsum plasters could have been used since the Roman period, especially for the manufacture of elaborated decorations or as a base of wall paintings (Vieira 2002; Silva 2005).

Therefore, it was absolutely paramount to clarify this issue through a study that allowed writing the real history of the materials used in the manufacture of plasters of the Portuguese architectural heritage. With this purpose, an extensive set of original samples from several historical periods, from smooth surfaces to decorative elements, all in rather good conditions, belonging to various types of buildings (either of patrimonial value or of common use, both with architectural interest), were collected from the north to the south of the country.

A first mineralogical survey was made using XRD and the results showed that the use of gypsum plasters in Portugal was only particularly significant between the mid-eighteenth century and the first half of the twentieth century, mainly as wall and ceilings' decorative programmes. In fact, according to a classification used by the Council of Europe it is the second most representative decorative art in the Portuguese architecture, only superseded by *azulejos* (ceramic tiles) (Vieira 2008). Even though, information about this important heritage is very scarce leading to the systematic adoption of substitutive practices by modern solutions, contributing to its rapid loss.

In the last decade an effort has been made to turn this situation around, with art history studies (Vieira 2002; Vieira 2008; Silva 2005) as well as architectural and civil engineering studies (Cotrim et al. 2007; Cotrim et al. 2008; Malta da Silveira et al. 2007) in order to stand up for the preservation of gypsum-based plasters and contribute to their promotion. However, the distinction between lime and gypsum plasters, records about their correct preparation and application and the development of adequate conservation and/or restoration solutions from the materials' point of view have not been made so far.

By giving an insight into the materials used in the past, clarifying some techniques of application and developing gypsum and gypsum-lime based restoration products compatible with the original

materials, this study intends to draw attention to this important heritage, contribute to the implementation of better conservation and restoration practices and reduce its indiscriminate destruction, assuming a preliminary character in this research field in Portugal.

1.2 Research aims and objectives

This thesis aims at contributing to applying the principles expressed in the Krakow Charter of 2000 to the specific case of the Portuguese ancient gypsum and gypsum-lime plaster coatings.

In order to accomplish these principles, the following objectives have been established:

1) To make a systematic study on the composition of the Portuguese interior plaster coatings along the most important civilizational periods that characterized the country's history and to understand which were the main factors that determined the choice of materials. In fact, most of the references to these constructive elements are very generic, based almost exclusively on visual observation, without any analytical support;
2) To develop interdisciplinary studies on those plasters where gypsum is the main constituent (gypsum and gypsum-lime plasters), establishing relationships between the chemical, mineralogical and microstructural characterization results and the physical and mechanical properties determined;
3) To define compatibility requirements based on the results of the referred characterization studies;
4) To define mixes with composition similarities to the ancient materials and determine their physical and mechanical properties;
5) To select the mixes that best fulfil the compatibility requirements previously established;
6) To contribute to clarify the differences between gypsum and lime plasters.

1.3 Organization of the thesis

The thesis is organized in six chapters. The first chapter is the present introductory section. The remaining five chapters address the following subjects:

- Chapter 2 consists on a literature review about most topics covered in the thesis, namely questions of terminology and the state-of-the-art concerning the materials under study. This compilation is based on scientific publications and on ancient construction manuals.

  A survey of the state-of-the-practice is also presented and the information obtained is compared to that of literature. This survey is mostly based on interviews of plasterers still

using traditional materials and working according to traditional practices. It also comprises the attendance of a workshop about the application of gypsum and gypsum-lime traditional plastering systems, including some techniques used in decorative finishes.

All subjects addressed are more detailed in the case of gypsum because it is a material much less studied in the Portuguese traditional construction than air lime.

The state-of-the-art concerning very specific issues, namely some properties of the materials (qualitative and quantitative composition, porosity and water vapour permeability) is presented in chapters 4 and 5 along with the respective discussion of results.

- Chapter 3 is about the chronological study of the materials used in the Portuguese interior plaster coatings from the Roman period until the first quarter of the 20th century. It consists on a mineralogical survey using XRD performed on 139 samples of original plaster coatings still in good condition. The methodology used and the results obtained are presented and the periods when gypsum was one of the main constituents of those plaster coatings are identified. The relationships between the materials used and the main factors that conditioned that choice (availability of raw materials, external influences from other people, socioeconomic aspects, etc.) are discussed.
- Chapter 4 presents the analytical characterization of the gypsum and gypsum-lime plaster samples from eleven case studies belonging to the period where they are more representative in the Portuguese architecture: from the second half of the 18th century till the first quarter of the 20th. This characterization work comprises the determination of mineralogical, microstructural, physical and mechanical properties and the materials and methods used to achieve the desired information are described. The compilation of the results obtained as well as the interrelations established between the several properties are presented and discussed.
- Chapter 5 is dedicated to the development of compatible gypsum and gypsum-lime based products for restoration of the ancient plasters. The compatibility requirements are defined based on the overall results presented in Chapter 4.

  The materials and methods used to perform the experimental work are described and seven mixes are designed according to the established requirements. These mixes are characterized with respect to the same physical and mechanical properties determined in the ancient samples. The respective results are discussed and the fulfilment of the pre-established criteria is verified, allowing the choice of three products considered to be the most adequate.
- Chapter 6 presents the overall conclusions of the thesis focusing on the research aims and objectives previously defined. In this final chapter some topics for future developments are also proposed.

2

Literature review

2.1 Cultural framework of the study

The concepts of *"heritage", "conservation"* and *"restoration"* evolved together, moving from the mere association to historical, archaeological and architectural tangible assets, to a much broader definition, where concepts such as traditions, culture, landscape, sites of memory, of symbolic or social value, etc. (intangible assets) acquired sufficient importance to constitute together what is now called *"cultural heritage"*.

This evolution came from the discussion of a set of ideas whose origins can be situated in the late eighteenth century, following the French Revolution. The massive destruction of works of art and monuments that took place then led to the publication of an official edict towards their protection. In this document, for the first time in the history of the western civilization, new and important concepts are referred such as the award of a public nature to these goods and the recognition that they deserve to be preserved (Rivera-Blanco 2008).

In the twentieth century a good example of such evolution is reflected in the subtitles of the international charters for the protection of cultural heritage (DGPC n.d.).

In fact, the Athens Charter of 1931 refers to the restoration of *"historic monuments"* while in 1964 the subtitle of the Venice Charter already refers the *"conservation and restoration of monuments and sites"*; the preamble of the Nara Document on Authenticity of 1994 says that it is a document *"conceived in the spirit of the Venice Charter and builds on it and extends it in response to the expanding scope of cultural heritage concerns and interests in our contemporary world"* (ICOMOS 2004).

The Athens Charter was signed by 20 European countries. It was the first international document published in order to raise awareness among governments about the importance of protecting and safeguarding the *"art of the people*" as a universal good. It also played a key role in the development of heritage protection legislation in several European countries, namely the so-called Italian Restoration Charter of 1932 and the Spanish Historical Heritage Act of 1933 (Rivera-Blanco 2008).

Regarding their content, this evolution was accompanied by the inclusion of new concepts, namely the use of the words *"authenticity"* and *"antiquity*" in the Venice Charter and the notion that the conservation and restoration of monuments intend to double their value as *"works of art"* and as *"historical evidence",* a clear influence of Cesare Brandi and his *Teoria del Restauro* (Brandi 2006) whose first edition had been published in Rome a year earlier.

The Venice Charter was also the foundation stone of the International Council on Monuments and Sites - ICOMOS - a non-governmental organization created one year later in Krakow and defined by its first President as *"the institution which constitutes the court of highest appeal in the area of the restoration of monuments, and of the conservation of ancient historical centres, of the landscape and in general of places of artistic and historical importance"* (ICOMOS 2004).

These were the first steps for the creation of a universal conscience towards the existence of something that does not belong exclusively to a people or place, but to all mankind. From that moment on a new dynamic was created and in 1972 the General Conference of UNESCO, held in Paris, adopted a convention concerning *"the protection of the world cultural and natural heritage"*. Since then, many other documents have been written by experts and adopted by ICOMOS, though always having in mind the Venice Charter as the world's official code in the field of the conservation of cultural properties (ICOMOS 2004).

The framework of historical monuments as an urban space to safeguard puts into practice an idea that Gustavo Giovannoni had focused already on the methodology for conservation that he developed and defined as "Scientific Restoration". It valued the poor architecture, which could not have great individual value, but as a whole symbolized the "how to build" of a certain time/epoch and formed an urban environment without which the monuments would not have the same value or the same understanding (Rivera-Blanco 2008).

In the year 2000 a group of experts that prepared and participated in the International Conference on Conservation "Krakow 2000", aware of the profound values of the Venice Charter and working towards the same aims, elaborated a document entitled "The Charter of Krakow 2000". There they proposed the principles for conservation and restoration of the built heritage in *"our time",* where concepts like *"cultural heritage"*, *"mobile heritage and intellectual property"*, *"collective memory"*, *"urban and landscape architectural heritage"* and *"restoration project"* were included. In spite of having not been adopted officially by ICOMOS it is considered a very important document by those whose work is related with the conservation and restoration fields.

In fact, the idea behind *"cultural heritage"* is the identity of a people, which in turn consists of the memory of the past and the experience of the present, being a legacy for the future. However, the cultural heritage of a people is not exclusive of that people; it is part of a more diverse world: *"The*

cultural heritage of each is the cultural heritage of all" is a fundamental principle of UNESCO, a concept that the Conference of 1972 helped to develop and implement in particular through guidelines for heritage conservation (the "safeguard plans") and the establishment of an intergovernmental committee for the protection of cultural and natural heritage of outstanding universal value called the "World Heritage Committee".

The idea of continuity along the timeline means that the loss of cultural heritage is synonymous with loss of references. Therefore, the presence of gaps in that line should be avoided, at the risk of losing an important part of memory. That is why it is so difficult to establish selection criteria and intervention methodologies in a work of conservation and restoration, so as not to misrepresent the historical and heritage value inherent in it: removing traces of different epochs, for example, in a clear influence of the "Stylistic restoration" of Viollet-le-Duc, was practiced in most European countries until the mid-twentieth century, Portugal included.

In the Krakow Charter it is highlighted that *"the maintenance and repairs are a fundamental part of the heritage conservation process"*, being strongly recommended *"the adoption of preventive measures"* based on comprehensive studies and *"appropriate reports"*, reinforcing the idea that, in historical sites, even in cases where the buildings do not stand out for their individual architectural value, they *"must be protected as urban elements of continuity, owing to their dimensional, technical, spatial, decorative and chromatic characteristics, irreplaceable connecting elements to the organic unity of the city"*.

Last but not least, two very important remarks, essential to the framework of this study: the idea that the interior spatiality of the old buildings is one of its core values, which is paramount to safeguard, in a broad sense, historical town centers and the architectural heritage in general; the inclusion in the Krakow Charter of the architectural decoration as part of the built heritage that must be preserved through a specific project linked to the overall restoration project.

2.2 Materials

Before the description of the materials themselves, some terminology issues that arise specifically in the Portuguese language will be addressed.

2.2.1 Terminology

Estuque **-** word for gypsum plaster, defined in the Portuguese written sources as:

a) "A kind of mortar *with gypsum* used for the plastering of walls, relief ornaments, sculpture works, etc." (Machado 1991);

b) "Coating used for finishing interior walls and ceilings with a paste of lime *and gypsum"* (Themudo-Barata n.d.);
c) "Mortar composed of lime, fine sand *and gypsum"* (D'Assumpção n.d.)**.**

Although there is no consensus on the exact definition of the word *estuque*, there is no doubt that gypsum is part of its composition. However, the widespread use of the word to designate both gypsum-containing coatings and coatings made of lime only, especially when it comes to decoration, creates the need to use the expression *"estuque de gesso"* (gypsum plaster), a redundancy in Portuguese.

This language imprecision should be due, on the one hand, to the fact that the words e*stuco,* in Spanish, and *stucco*, in Italian, designate "mortars made of gypsum, gypsum and lime, or lime, with or otherwise without the addition of other materials..." (Gárate-Rojas 1999) and, on the other hand, to the random use of the words "plaster" *(estuque)*, "gypsum" and "lime" to designate the same elements in the Portuguese literature without the materials having been analysed. These facts mean that many people, some of which working in the archaeological, construction, rehabilitation, conservation and/or restoration areas, think that the differences between gypsum and lime are irrelevant.

Gypsum - it is used to designate both natural raw material (calcium sulphate dihydrate, $CaSO_4.2H_2O$) and one of the products derived from its calcination (hemihydrate or bassanite, $CaSO_4.1/2H_2O$).

In French (and in English also) a distinction is made between the two products whereas *gypse* (gypsum) is the word for raw material and *plâtre* (plaster of Paris) designates the hemihydrate.

Air lime - it is also used to designate two different phases, the calcium oxide (CaO) and the calcium hydroxide ($Ca(OH)_2$) resulting from its hydration. In everyday language, and as a way to tell them apart, the first is also called by quicklime and the second by slaked or hydrated lime.

Anhydrite - word used to designate the anhydrous calcium sulphate ($CaSO_4$), both referring to the natural mineral or to the product resulting from the calcination of calcium sulphate dihydrate at temperatures higher than those used to obtain the hemihydrate.

2.2.2 Binders used in construction: historical evolution

Several archaeological studies demonstrate the use of lime and gypsum mortars in architecture since the Natufian period (10,300-8,500 BC), in the area of the Near East (now Israel, Syria and Turkey) (Gourdin & Kingery 1975; Kingery et al. 1988) and in Cyprus (Philokyprou 2012).

The quantities involved presupposed already some knowledge of the technologies of production, preparation and application, processes that may have taken some millennia to materialize, since the

authors state that the "discovery" of air lime masses occurred occasionally, some 14,000 years ago (12,000 BC) (Kingery et al. 1988).

All this knowledge has been gradually extended to neighbouring regions. In ancient Egypt, gypsum mortars strongly predominated over lime, although there are plenty of both raw materials (Álvarez Galindo et al. 1995). According to these authors, the high temperature needed for the calcination of lime (800-900 °C) compared with the temperatures required to obtain the different types of gypsum plasters (hemihydrate: 120-180ºC; anhydrite: 300-500 °C) in a region where wood, the main source of energy, was scarce, was at the origin of this phenomenon. The same authors also claim that the presence of gypsum plaster is always much more significant in Egyptian mortars, than in Europe, whatever the historical period.

The knowledge of how to manufacture and use this material is thought to have passed to the Greeks by the Egyptians and the Minoans and then to the Romans, remaining in Europe until the end of the Classical Antiquity (Stark & Wicht 1999).

Via the Romans, this knowledge also reached Central and Northern Europe. Throughout the centuries it became part of the traditional European way of building, alone or mixed with other materials, like lime, sand or other aggregates and/or organic admixtures. Contrary to what is thought it had not only applications in interior relieved decorations of walls, architectural elements or as base for decorative frescoes but also in masonry mortars (Ghorab et al. 1986; Ragai et al. 1987; Ragai 1988a; Ragai 1988b; Ragai 1989; Kawiak 1991; Turriano 1996; Vogel et al. 1999; Middendorf 2002; Fischer & Vtorov 2002; Lucas 2003a; Lucas 2003b; Igea et al. 2010; Igea et al. 2012; Philokyprou 2012), floor screeds (Gourdin & Kingery 1975; Kawiak 1991; Fischer & Vtorov 2002; Philokyprou 2012) and exterior wall coverings (S.N.I.P. 1982; Fischer & Vtorov 2002; Lucas 2003a; Lucas 2003b; Sanz 2009).

However, in the classical civilizations the use of lime predominated over that of gypsum. By incorporating small additions of other materials to increase the durability and stability of the lime mortars against the action of water, the Greeks contributed decisively to their popularity. In the island of Thera (present-day Santorini) a mortar made of lime, sand and volcanic ashes (also called "earth of Santorini") was used for the first time, with a water resistance comparable to that of mortars of hydraulic binders (Álvarez Galindo et al. 1995).

The Romans were the heirs of the Greek building technology, in particular as regards the use of air lime mortars. Known as outstanding in their use, they owe that fame to the excellent condition with which many of these materials survived till today. They were used not only in the settlement of masonry, but also in floor screeds, wall coatings, among others.

The quality and durability of the Roman lime mortars are attributed to various factors among which the following stand out (Álvarez Galindo et al. 1995):

a) The careful selection of materials used in the composition of the mortars, from the choice of the raw materials to produce lime, to the selection of the aggregates, incorporation, in specific cases, of other substances, both of organic origin - albumin, casein, oil - and inorganic - terracotta, baked clay and, above all, pozzolan, the volcanic rock from Puzzuoli, Naples;
b) The improvement of lime manufacturing procedures;
c) The careful preparation of the mortars, to obtain homogeneity and a correct ratio of mixing with water;
d) The importance given to the application techniques, namely compaction and polishing.

All these factors confer to the material a greater resistance to the action of external agents and therefore greater durability and possibility of use in aggressive environments (tanks, aqueducts, bridges).

With the fall of the Roman Empire, these practices started being lost and one may even say that, in the field of mortars, there was no remarkable technical progress in the Middle Ages (Álvarez Galindo et al. 1995). This idea was put forward very clearly by Philokyprou (2012), stating that "it is rather impressive that during the prehistoric period man developed such a high level of technology in the manufacture of mortars, and no major innovations have taken place in this area until recently".

On what concerns gypsum its use almost disappeared in Europe in the medieval times, emerging again with the presence of the Arabs, between the 8th and 15th centuries (Gárate-Rojas 1999). Nevertheless, it was only in the 17th century that gypsum plasters definitely assumed great relevance within the European decorative arts, a role held throughout the whole Baroque and Rococo periods. The possibility of imitating noble materials, like marble, porphyry, wood, often richer in colour and veining than the originals, contributed to maintain and even expand its use until the end of the 19th century (Stark & Wicht 1999; Gárate-Rojas 1999).

It was precisely in the 19th century that the appearance of Portland cement revolutionized the history of mortars, in particular air lime mortars. The high mechanical strength that cement can reach rapidly and its insolubility in water have decisively contributed to its rapid emergence as a construction material, replacing in a short period of time the traditional materials previously used in several applications: masonry mortar, walls and floors coatings outside and inside the buildings, concrete structures, etc.

Despite representing an unprecedented technical progress, such a rapid change in the way of building led to the irreparable loss of ancient knowledge and proved to be, in some cases, harmful, especially for constructions previous to its appearance. The high strength and impermeability of cement composites associated with an increased risk of transfer of soluble salts to the substrates produced a

combination that is generally detrimental to ancient constructions. Basically it contributed to unbalance the proper functioning of the pre-existing (thick and porous) walls, mostly with moisture problems, increasing their degradation rate.

The numerous negative testimonies about the use of cement-based products on ancient constructions given by the interventions made during most part of the 20th century led to a change, in the last decades, in the way of acting towards the preservation of architectural heritage. Concepts like compatibility have been given more importance, namely on what concerns the materials used in restoration/conservation. Nowadays there are many research groups working on the characterization of traditional materials and their manufacture technologies, where gypsum and lime mortars and plasters have a very important role.

2.2.3 Gypsum

2.2.3.1 General considerations

Gypsum is a natural mineral rock quite abundant in the Earth's crust, of chemical formula $CaSO_4.2H_2O$ (calcium sulphate dihydrate) and hardness 1.5-2 in the Mohs scale. It also occurs in the form of natural anhydrite, the non-hydrated phase, of chemical formula $CaSO_4$ and hardness 3-4 in the Mohs scale (Karni & Karni 1995; Gárate-Rojas 1999; Wirsching 2005).

Both minerals are found throughout the world. There are considerable deposits in North America, Brazil, Near and Middle East, North Africa and Europe; here the main gypsum quarries are located in Spain, France, Italy, Germany, UK, Poland, Russia and the Ukraine (Eurogypsum 2007).

These deposits are mainly of sedimentary origin resulting from the evaporation of large bodies of saline water with precipitation of layers of different minerals according to their solubility (in increasing order, i.e. the less soluble accumulate in the bottom). In this process, known as “evaporite sequence” carbonates are the first to be deposited, followed by sulphates and finally chlorides. Depending on the deposition conditions, very thick beds of pure gypsum may occur (Figure 2.1 (a)), or otherwise they can be interbedded in very thin layers whose exploitation is not economically viable (Figure 2.1 (b)). It is relatively easy to mine the gypsum stone due to its low hardness. Mining can be subterranean or in open quarries (Figure 2.1 and Figure 2.2)

Under conditions of increased pressure and temperature, natural gypsum deposits can be converted into anhydrite; the opposite also occurs, with anhydrite being converted into gypsum due to the infiltration of water. This gypsum is called of secondary origin while that formed upon initial crystallization is the primary gypsum. The best known deposits of the latter are in the Paris Basin (Figure 2.2) and in the areas around the Mediterranean (Wirsching 2005).

Figure 2.1 - Gypsum natural deposits: (a) open quarry in Almeria, Spain, with very thick gypsum beds (http://www.panoramio.com/); (b) thin layer of satin spar gypsum embedded in a clayed ground (http://academic.emporia.edu/aberjame/student/corley3/rdhil.htm); [accessed 15 September 2015]

According to some authors cited by Karni & Karni (1995) and Wirsching (2005), the relative amounts of natural gypsum and anhydrite formed depend on the geological history/conditions of the formation. In some deposits, the two minerals appear side by side, both horizontally and vertically, and occasionally as a mixture. The differentiation of the two rocks is absolutely crucial for the gypsum industry, as the manufacture of some products demand the use of a very pure dihydrate (ex: plaster of Paris).

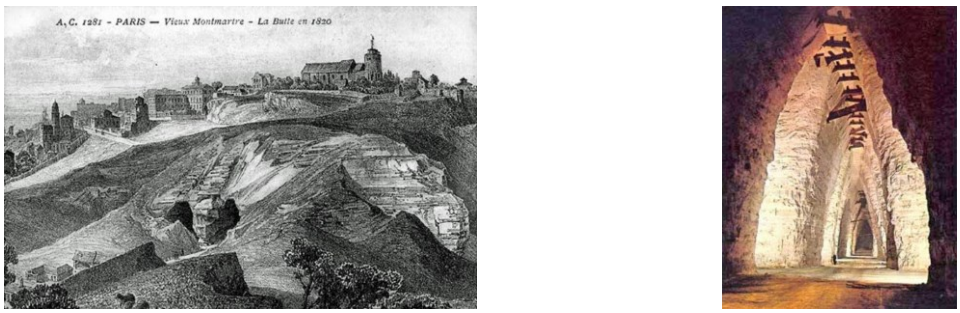

Figure 2.2 - Montmartre, Paris: (a) view of the hill in 1820, where urbanization had already begun, yet the gypsum quarries, both open and underground, active since Roman times were still present; (b) actual view of an underground cathedral-like vault gypsum quarry with wooden timbers to prevent collapse (http://written-in-stone-seen-through-my-lens.blogspot.pt/2014/04/geological-legacies-of-paris-basin-part.html, accessed 15 September 2015)

The most important rock textures of natural gypsum are selenite (made of large, lamellar, transparent crystals, whose name is due to Selena, the Greek goddess of the Moon, because of its moon-like glow), satin spar (with translucent fibrous crystals) and alabaster (with a compact, very fine crystalline structure used for statuary since antiquity and for interior decorations since the Middle Ages (Figure 2.3)). Anhydrite has also several varieties but these are of little importance compared with dihydrate (S.N.I.P. 1982; Karni & Karni 1995; Livingston et al. 1998; Wirsching 2005).

(a) (b)

(c) (d)

Figure 2.3 - Some gypsum natural varieties: (a) massive beams of selenite in Mexico's Cave of Crystals, deep below the Chihuahuan desert; (b) fragment of a giant crystal of selenite showing the transparent lamellar structure; (c) Satin spar (fibrous structure); (d) alabaster (marble-like gypsum, with massive, very fine crystalline structure) (http://www.johnbetts-fineminerals.com/jhbnyc/mineralmuseum/ accessed 15 September 2015)

The gypsum and anhydrite deposits differ also in purity and in colour depending on the impurities present. The most common ones are limestone, dolomite, celestine, marl, clay and, less frequently, silica, bitumen, polyhalite, among others. If they are present since the deposits formation they are called "primary impurities"; otherwise if they result from contamination during exposure to materials flushed into cracks and cavities they are called "secondary impurities".

Both minerals have several applications, such as (S.N.I.P. 1982; Wirsching 2005):

a) In building construction, for the production of gypsum based products (in powder form, as precast elements, plasterboards, for floor screeds or self-levelling floor plasters, etc.);
b) In the cements industry, directly added to the clinker before grinding in order to regularize (retard) the setting of cements;
c) In the ceramic industry as moulding material for roof tiles, decorative and tableware;
d) In medicine, for dental moulds, surgical casts and orthopaedic bandages;
e) In agriculture and livestock, as soil corrector, to control the clarity of wines or in the preparation of cattle feed;
f) As filler for adhesives, paints and plastics;
g) In the glass industry as substitute for sodium sulphate (more expensive).

2.2.3.2 Sources of raw material in Portugal

There is lack of raw material sources of gypsum in Portugal, in opposition to the greater availability of limestone (calcium carbonate content > 98%) (Figure 2.4).

(a) (b)

Figure 2.4 - Geological maps representing the limestone and gypsum deposits in Portugal: (a) Limestone(http://geoportal.lneg.pt/geoportal/mapas/index.html) ; (b) Gypsum (Zbyszewski & Almeida 1964)

Besides existing in lower amounts, the known gypsum deposits have usually problems of purity (gypsum dihydrate content < 90%) and/or whiteness. Some frequent contaminations are dark coloured marls, clays and dolomitic limestone (Graça Costa 1986), giving rise to the so-called "grey gypsum". White gypsum" occurs in smaller quantities (sometimes only 10% of the total) and usually together with "grey gypsum", being very expensive to separate them. Moreover many of the deposits would have to have a subsurface exploitation (Zbyszewski & Almeida 1964).

In the region of *Óbidos*, located in the centre of Portugal, there are some of the few active gypsum quarries in the country. The "grey gypsum" extracted is mainly consumed by the cement industry and only a small part is used in the production of plasters for the building construction.

Some years ago, flue gas desulphurization (FGD) gypsum, a by-product resulting from the desulphurization of flue gases of fossil fuels by reaction with very pure, finely divided calcium carbonate started to be produced in a Portuguese power plant. The calcium sulphate dihydrate obtained by this process is moist, very fine and has high purity (> 95%). It is classified as a product and not as a waste, and is also used in the cement and gypsum industries, together with natural raw materials (Wirsching 2005).

(a) (b)

Figure 2.5 - Active gypsum quarries in Óbidos, Portugal: (a) Avarela 1, underground exploitation; (b) Avarela 2, open quarry (Copyright © Rui Nunes 2004, http://www.mindat.org/, accessed 17 September 2015)

2.2.3.3 The $CaSO_4$ - H_2O system

The $CaSO_4$-H_2O system is composed by five solid phases. Four of them exist at room temperature and are of interest to industry; the fifth (anhydrite I) only exists above 1180 ºC (S.N.I.P. 1982; Wirsching 2005):

a) *Calcium sulphate dihydrate* - it is the starting material before dehydration and the final product after rehydration. The density and crystal structure are the main differences between them, with the former having a dense, compact microstructure and the latter a considerable porosity due to the evaporation of the surplus kneading water (only about 18% of the water added is consumed in the reaction of hydration; 82% evaporate, creating a porous structure);

b) *Calcium sulphate hemihydrate* - it occurs in two forms, α and β with different crystal sizes and shapes, directly related to the conditions of calcination, but with the same crystallographic structure (Lewry & Williamson 1994a). They constitute two limiting states of a series of intermediate crystallization varieties.

   α hemihydrate is obtained by dehydration of gypsum in autoclaves at water vapour pressures above 1 bar through a "dissolution-recrystallization" process (wet process), giving rise to compact, well-formed, transparent crystals with sharp edges; β form dehydrates at pressures slightly under 1 bar (dry process) and the resulting particles have high micro-porosity and are made up of extremely small crystals (also called crystallites).

   α plaster needs much smaller amount of kneading water than the β form, leading to denser, stronger and harder products. However, it has very limited use in building construction due to its brittleness.

   α and β forms can only be distinguished by microscopy or by differential thermal analyses (DTA): the exothermic peak due to the transformation of anhydrite III to anhydrite II is around 220 ºC for α and 350ºC for β.

c) *Anhydrite III* - also known as soluble anhydrite, it owes its instability to its water greediness, even at low humidity environments. Industrially it is impossible to obtain isolated, only in a mixture of phases. Its presence in a plaster product can either be desirable, or not, as it accelerates the hydration of the paste.

d) *Anhydrite II* - it can be either a naturally occurring form or an industrial product obtained from the calcination of dihydrate at higher temperatures (300-700 ºC). Its hydration kinetic is inversely proportional to the calcination temperature and time. When burnt between 500 ºC and 700 ºC it is called "insoluble anhydrite" and usually needs an activator to start hydration.

e) *Anhydrite I* - it is a defined phase above 1180 ºC but does not exist below that temperature, transforming into anhydrite II. It is impossible to obtain as a pure phase, since it is always contaminated by products resulting from the dissociation of anhydrite (CaO and SO_2/SO_3).

Table 2.1 summarizes the main characteristics of the different phases of the $CaSO_4$ - H_2O system.

Table 2.1 - Phases of the $CaSO_4$ - H_2O system (adapted from Wirsching 2005)

Phase	Calcium sulphate dihydrate	Calcium sulphate hemihydrate		Anhydrite III	Anhydrite II	Anhydrite I
		α form	β form			
Chemical formula	$CaSO_4.2H_2O$	$CaSO_4.1/2H_2O$		$CaSO_4$	$CaSO_4$	$CaSO_4$
Molecular mass (g/mol)	172.17	145.15	145.15	136.14	136.14	136.14
Water of crystallization (%)	20.92	6.21	6.21	0.00	0.00	0.00
Density (kg/m^3)	2.31	2.76	2.62-2.64	2.58	2.93-2.97	undetermined
Hardness (Mohs)	1.5	-	-	-	3-4	-
Water solubility at 20 ºC (g $CaSO_4$/100 g solution)	0.21	0.67	0.88	hydrates to hemihydrate	(0.27)*	-
Production temperature (ºC)	< 40	80-180	120-180	variable if α or β	200-1180	not produced commercially
Stability at room temperature	stable	metastable in dry air		metastable	stable	not observable

* Value referred to slowly soluble anhydrite II (Eq. 2.3)

2.2.3.4 Thermal decomposition of gypsum

When heated, gypsum easily loses its water of hydration. The progressive rise of temperature originates several calcium sulphate compounds, partially or totally dehydrated (Murat & Foucault 1977; S.N.I.P. 1982; Wirsching 2005):

Dihydrate-→ hemihydrate → anhydrite III → anhydrite II → Anhydrite I

These compounds together with calcium sulphate dihydrate constitute the phases of the $CaSO_4$ - H_2O system. The chemical transformations corresponding to the dehydration of gypsum are represented in Eq. 2.1 to Eq. 2.6:

$$CaSO_4.2H_2O_{(s)} \xrightarrow{120\text{-}180\ ºC} CaSO_4.1/2H_2O_{(s)} + 3/2H_2O_{(g)} \quad \text{(Eq. 2.1)}$$

$$CaSO_4.1/2H_2O_{(s)} \xrightarrow{\approx 220\ ºC} CaSO_{4\ (s)\ (soluble)} + 1/2H_2O_{(g)} \quad \text{(Eq. 2.2)}$$

$$CaSO_4.2H_2O_{(s)} \xrightarrow{300\text{-}500\ ºC} CaSO_{4\ (s)\ (slowly\ soluble)} + 2H_2O_{(g)} \quad \text{(Eq. 2.3)}$$

$$CaSO_4.2H_2O_{(s)} \xrightarrow{500\text{-}700\ ºC} CaSO_{4\ (s)\ (insoluble)} + 2H_2O_{(g)} \quad \text{(Eq. 2.4)}$$

$$CaSO_4.2H_2O_{(s)} \xrightarrow{700\text{-}1180\ ºC} CaSO_{4\ (s)\ (partially.\ dissociated)} + 2H_2O_{(g)} \quad \text{(Eq. 2.5)}$$

$$\downarrow\ > 1180\ ºC$$

$$CaO_{(s)} + SO_{3\ (g)} \quad \text{(Eq. 2.6)}$$

In spite of being known as a building construction material for several millennia, the gypsum plaster manufacture remained undeveloped for a long time, being carried out on an empirical basis using rudimentary processes of transformation. It was only in 1768 that Lavoisier, considered the "father" of modern chemistry, undertook the first scientific study of the fundamental phenomena in gypsum preparation. He pointed out that the dehydration of gypsum rock occurs in two steps: the first corresponds to the elimination of three quarters of the water of crystallization and the second to the transformation of the previously formed hemihydrate into anhydrous calcium sulphate. The reference to the intermediate phase as "hemihydrate" that he regarded as the true constituent of plaster was made for the first time.

Only one century after another French chemist, Le Châtelier, determined as precisely as possible the temperatures to which the two dehydration levels experimentally recognized by Lavoisier are taking place. He also demonstrated that the quantity of water released in the first level corresponds exactly to one and half water molecules. The Dutch physical and organic chemist Van't Hoff, first winner of the Nobel Prize in Chemistry, also authored remarkable works on the decomposition of gypsum, determining the temperature at which gypsum and hemihydrate are in equilibrium.

These works, together with the investigations carried out by contemporary research scientists and the development of industrial techniques, supported and inspired the transformation efforts in the field of plaster manufacturing that occurred in the 20th century. This technological revolution in the gypsum

production process homogenized and improved the quality of the plasters obtained, allowing the manufacture of new products and the development of new applications, a dynamic process that is in constant evolution.

2.2.3.5 Hydration, setting and hardening

The products resulting from the dehydration of gypsum (hemihydrate, anhydrite III and anhydrite II) when in contact with water undergo hydration under ambient conditions, converting again into calcium sulphate dihydrate (Murat 1982; S.N.I.P. 1982; Karni & Karni 1995; Wirsching 2005; Singh & Middendorf 2007). The corresponding chemical reactions are represented in Eq. 2.7 to Eq. 2.9:

$$CaSO_{4\ (s)\ (soluble)} + 1/2H_2O_{(g)} \longrightarrow CaSO_4.1/2H_2O_{(s)} + heat \qquad \text{(Eq. 2.7)}$$

$$CaSO_4.1/2H_2O_{(s)} + 3/2H_2O_{(l)} \longrightarrow CaSO_4.2H_2O_{(s)} + heat \qquad \text{(Eq. 2.8)}$$

$$CaSO_{4\ (s)\ (slowly\ soluble\ or\ insoluble)} + 2H_2O_{(l)} \longrightarrow CaSO_4.2H_2O_{(s)} + heat \qquad \text{(Eq. 2.9)}$$

In spite of having the same chemical composition as the raw material, the products obtained have very different density, porosity and microstructure, which also results in very different characteristics.

In this process, called “rehydration”, hemihydrate and anhydrite II are converted directly into dihydrate, while anhydrite III is converted via hemihydrate. These reactions have very different kinetics, with anhydrite III being the fastest (Eq. 2.7), followed by hemihydrate (Eq. 2.8), slowly soluble anhydrite and insoluble anhydrite (Eq. 2.9).

The mechanism of hydration of the different phases has been the subject of many studies but it is not consensual yet. Once again, it was Lavoisier who first described and tried to explain the observations made during the hydration of plaster (cited in S.N.I.P. 1982)

> *“L'endurcissement du plâtre avec l'eau n'est autre chose qu'une véritable cristallisation, la pierre spéculaire, privée de son eau par le feu, la reprend avec avidité et recristallise de nouveau en formant une masse dont la dureté surpasse celle de la plupart de nos pierres”.*
>
> (“The hardening of the plaster with water is nothing other than a true crystallization, the specular stone, deprived of its water by fire recovers it greedily and recrystallizes again forming a mass of hardness exceeding that of most of our stones”).

Two main theories have been formulated: the crystallization theory and the colloidal theory. The first is the eldest and has been presented in 1887 as conclusions of the works of Le Châtelier; the second appeared in 1909 and intended to question the first one.

Nowadays the theory of crystallization is the most commonly accepted (Wirsching 2005; Singh & Middendorf 2007) for the hydration of hemihydrate. According to this theory, the following stages occur:

a) Calcium hemihydrate is mixed with water and a part of it immediately dissolves (about 8 g/l at 20 ºC), forming a saturated solution with respect to Ca^{2+} and SO_4^{2-} ions;
b) This saturated solution is actually supersaturated with respect to calcium sulphate dihydrate which, at 20 ºC, has a solubility of 2 g/l, leading to nuclei formation. When nuclei acquire a certain critical size, crystallization takes place and $CaSO_4.2H_2O$ precipitates;
c) The plaster sets and develops strength due to the intergrowth and interlock of the newly formed crystals.

All these stages have been identified by Le Châtelier that considered the reaction of rehydration of plaster a combination of chemical (hydration), physical (crystallization) and mechanical (hardening) phenomena.

In the hydration of anhydrite II, or in other phases with crystals of higher dimensions and difficult total solubilisation, some authors advocate a colloidal mechanism, though it is still under study (Sievert et al. 2005).

The crystallization process influences the microstructure of hardened gypsum which in turn affects its physical and mechanical properties. In fact, the morphology of calcium sulphate dihydrate crystals depends on the formation conditions such as solution saturation/supersaturation (directly related with the solubility of the reactant and to the temperature of the water/plaster mixture), type of subhydrate (hemihydrate α, β or anhydrite) and the respective crystal habit and surface area, water/plaster ratio, the presence and type of chemical admixtures, etc.

The rate of hydration is also related to the previous factors, as well as to the fineness and purity of the material and to the mixing conditions (time and speed). The reaction kinetics is represented by a sigmoidal function (Figure 2.6).

The hydration of the sub-hydrated gypsum phases are exotermic reactions accompanied by a volume increase (swelling) of the paste. The evolution of the hydration of a plaster using calorimetry is one of the most common procedures to evaluate the setting times of gypsum-based products, namely in quality control industrial laboratories.

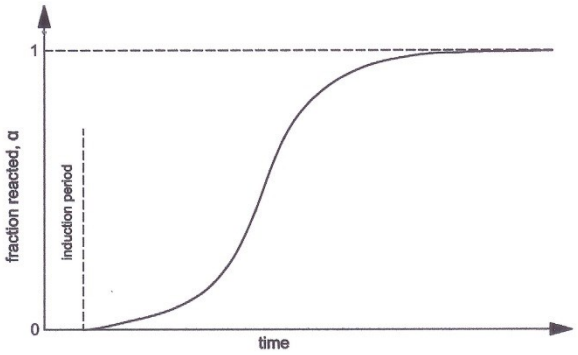

Figure 2.6 - Schematic representation of the fraction of hemihydrate hydrated as a function of time showing a sigmoidal distribution (Singh & Middendorf 2007)The hydration of the sub-hydrated gypsum phases are highly exothermic reactions accompanied by a volume increase (swelling) of the paste. The evolution of the hydration of a plaster using calorimetry is one of the most common procedures to control the setting times of gypsum-based products, namely in quality control industrial laboratories.

The graphical representation of the temperature rise as a function of time has also the form of a sigmoid (Figure 2.7), though with a slight difference from that of Figure 2.6:

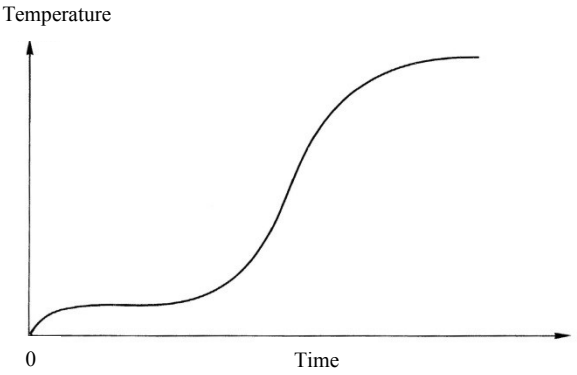

Figure 2.7 - Schematic representation of the temperature rise during hydration of the hemihydrate as a function of time showing a sigmoidal distribution (S.N.I.P. 1982)

In this curve an immediate rise in temperature is observed during the addition of the plaster to the gauging water. It results from the overlap of two phenomena: the wetting heat of the plaster particles and the hydration reaction of any soluble anhydrite eventually present. After that, an induction period occurs corresponding to the dissolution of the plaster into Ca^{2+} and SO_4^{2-} ions and formation of calcium sulphate dihydrate crystallization nuclei from the supersaturated solution formed in the meantime.

The seed crystals begin to grow then and the temperature starts to rise due to the ongoing exothermic reaction. When the maximum temperature is reached about 95% of the plaster phases are hydrated and the reaction continues at a much slower rate. Then the temperature of the hardened mass starts to decrease but the expansion of the paste proceeds until the reaction is complete. This volume increase is due to the forces arising from the growth of the gypsum crystals and the readjustments of the matrix.

These factors and the way they influence and relate to the main properties of gypsum products will now be more thoroughly discussed.

2.2.3.6 Properties of gypsum paste and hardened product

The three main phenomena that characterize the hydration of the products resulting from the dehydration of gypsum are the setting, expansion and temperature rise of the paste.

Setting

The setting or development of strength of gypsum plasters is a three-stage process (Lewry & Williamson 1994b):

a) Development of an interlocking matrix of dihydrate needles as result of the hydration reaction of hemihydrate. In the case of anhydrite, both natural and processed, the morphology of the resulting crystals is stocky and less needle-like (Gourdin & Kingery 1975; Sanz 2009; Schlütter et al. 2010; Philokyprou 2012);
b) The second stage is the release of internal stress caused by the build-up of pressure as crystal needles grow against each other. This stage is accompanied by a period of reduced strength;
c) The final stage involves the removal of water in excess, not required for the chemical reaction. During this stage there is an increase in strength due to the loss of lubrication effect that excess water induces in the dihydrate structure and simultaneously the reinforcement of that structure by the precipitation of dihydrate from the remaining solution with formation of small crystallites. The final structure is characterized by a large open porosity.

In practice, after addition of a plaster hemihydrate to the water, the resulting mixture starts to be fluid (a paste in the case of a multiphase plaster, i.e. made of a mix a sub-hydrated phases: β-hemihydrate, anhydrite III, Anhydrite II, etc., evolving to a paste and finally to a rigid state. The initial setting time corresponds to the moment where the mixture becomes a paste (or a thicker paste) and the final setting time occurs when the mass is hardened.

It is very important to understand these different stages of gypsum plaster products reaction with water from the point of view of the application of the materials (Figure 2.8).

β-hemihydrate is not adequate for plastering because of its fluid consistency and very low time interval between initial and final time. Only with admixtures, namely retarders, it is possible to produce formulations of plastering products based on this phase (Wirsching 2005). However, its characteristics are adequate to be used for the production of casting moulds in the ceramic industry.

As stated before, α-plasters are not commonly used in construction because of its brittleness. Besides, they also have lack of smoothness and insufficient coating capacity, two important properties during application of the products.

Multiphase plasters are the most suitable for the manufacture of gypsum plastering products as their phase composition results in quick initial setting time and a smooth evolution of setting until the end. They also need less water to achieve an adequate consistency, leading to denser and higher strength finished plasterwork. In fact, the calcination of raw gypsum results always in a multiphase mixture, although nowadays the control of the production processes allows a much higher homogeneity when the intention is to produce a single phase (Wirsching 2005).

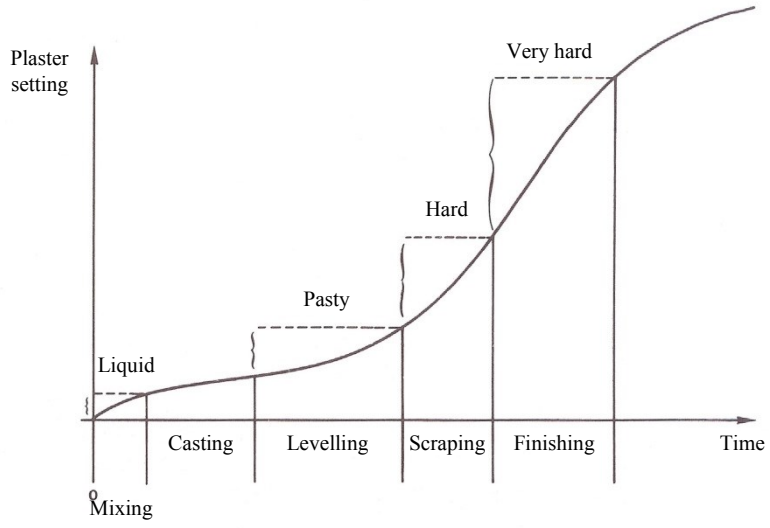

Figure 2.8 - Schematic evolution of gypsum plasters setting: successive phases of a plasterer's work (adapted from S.N.I.P. 1982)

Expansion

When plaster is added to the water there is an initial volume reduction (S.N.I.P. 1982; Karni & Karni 1995) due to the difference between the volume of the reaction products and the sum of the volumes of the reagents.

For example, in the case of the hydration of β-hemihydrate (Eq. 2.8), the most used phase, the calculation of the volume decrease using the stoichiometry of the reaction and the data from Table 2.1 is presented below.

It shows that β-hemihydrate has an initial volume contraction of about 10%. This stage is difficult to detect, especially in non-retarded plasters. As soon as the setting process starts, even though only a small portion of the material is hydrated, expansion begins.

	Reagents			Reaction product
	$CaSO_4.1/2H_2O$ +	$3/2H_2O$	⟶	$CaSO_4.2H_2O$
Mass (g)	145.15	27.02		172.17
Density (g/cm^3)	2.63	1.00		2.31
Volume (cm^3)	55.2	27.0		74.5
Total volume (cm^3)	82.2			74.5
Volume variation	**7.7 cm^3 or 9.4 %**			

The gypsum crystals grow freely until the mass hardens. After that, the formation of a rigid structure restrains the motions of the crystals' ends, giving rise to forces that induce a phenomenon known by "crystal growth pressure", (Chatterji & Jeffery 1964) or "swelling pressure" (Murat 1982) and to some reordering of the structure, causing an expansion of the skeleton of the porous material under formation.

It proceeds even after the final setting time has been reached and the resulting gypsum mass has hardened. In the case of the non-retarded hemihydrates, more than 90% of the swelling takes place in the first hour, slowing down after that until stopping one or two days later (Karni & Karni 1995).

During drying, the gypsum masses usually shrink but it corresponds only to about 10% of the initial expansion. The reverse situation occurs, i.e. the wetting of the dried hardened gypsum mass leads to a small increase of volume (about 0.01-0.02%) (S.N.I.P. 1982; Karni & Karni 1995). That is the reason why gypsum building materials are considered to have volume stability (Wirsching 2005)

This volume variation behaviour is a great advantage when gypsum is cast, both for use in the ceramic industry and to precast decorative elements. Even if they have complicated forms it ensures accurate dimensions and shapes of the reproduced elements (Karni & Karni 1995; Gárate-Rojas 1999).

This behaviour is also advantageous when gypsum is used in coarse mortars as interface cracks are avoided, in contrast to lime, lime-cement or cement mortars with much higher shrinkage.

Like with other properties, certain limits are recommended for expansion of the gypsum pastes, especially critical when used in restrained conditions (e.g. to make moulds for casting); the development of internal tensions can originate micro cracks in the hardened product, reducing its strength and durability.

The values found in the literature for linear expansion due to hydration of a hemihydrate plaster are not consensual, ranging from ≥ 1% (Karni & Karni 1995), to 0.07-0.5 % (S.N.I.P. 1982) and finally to about

0.17% (Chatterji & Jeffery 1964). However, none of these authors indicates the plaster/water ratios corresponding to the referring values, an important lacuna as it is one of the factors that affects the magnitude of expansion: the higher the weight of plaster per volume of water the more the paste expands.

In practice, a freshly calcined hemihydrate plaster with a particle size < 300 micron and a plaster/water ratio of 1.25 kg/L can have an average expansion of 0.15% one hour after adding the plaster to the water. The same type of plaster with a coarser particle size distribution is mixed with a plaster/water ratio of 1.45 kg/l and the average expansion then can be near 0.2% (personal experience of the author).

The fineness of the plaster, the use of setting modifiers (accelerators or retarders), fillers and aggregates, lime, are some of the factors that also influence the expansion of the paste.

Strength

The strength of set and dried gypsum is directly related with the crystallization of the calcium sulphate dihydrate and the evaporation of the excess water used to prepare the mixture. It is proportional to the density of the mass and therefore depends on its porosity which, in turn, is related to the plaster/water ratio and the pore size distribution.

Strength is also affected by the moisture content of the hardened product and by the use of admixtures, without changes in density (Wirsching 2005).

a) Plaster/water ratio

The temperature and conditions of calcination (vapour pressure, duration, type of kiln) give rise to different phases of the system $CaSO_4$ - H_2O. For the same phase, distinct crystal morphologies can be obtained which is directly related to the respective specific surface areas.

These characteristics, together with the purity and type of raw material, the reactivity of the phases, the particle size distribution and the type of application of the products are the major factors that determine the plaster/water (P/W) ratio of a gypsum plaster.

The P/W ratio is the most determinant parameter that affects strength of hydrated gypsum. In fact, the water amount influences the strength of gypsum by influencing the void fraction which, in turn, influences the formation of the gypsum crystals and the bonds between them during the hydration reaction (Yu & Brouwers 2011).

These authors measured the void fraction (porosity) of several gypsum mixtures prepared with different P/W ratios and observed that the higher it was, the lower the P/W ratio. They also determined the flexural and compressive strengths of the mixtures and the values obtained were plotted *versus* the

voids fraction. The results show a clear relation between both factors: the strength decreases with the increase of the voids fraction. It is important to notice, however, that brittleness increases with decreasing porosity (Coquard et al. 1994).

Yu & Brouwers (2011) observed the microstructures of two samples with different P/W ratios in the scanning electron microscope (SEM) and it was clear that the matrix corresponding to the higher P/W ratio exhibited smaller void fraction and had much tighter and homogeneous crystals than in the other sample matrix. This shows that the gypsum produced with lower water content had a better bonding between the gypsum crystals leading to better mechanical properties.

However, different plasters prepared with the same P/W ratio can have distinct mechanic performances. A comparison of the hydrated products resulting from the hydration and setting of both types of hemihydrate at the same P/W ratio indicates that α-plaster gives rise to higher strength (Lewry & Williamson 1994b). In the reaction of the α-plaster with water the precipitation of the dihydrate crystals is slower than with the β-form. SEM observations revealed that the microstructure of the set α-plaster consists of relatively short stubby dihydrate needles with a greater degree of inter-crystalline bonding and hence greater strength. On the contrary, the set β-plaster microstructure has longer, fibrous dihydrate needles with less inter-crystalline bonding and therefore has lower strength.

Murat et al. (1975) stated that the growth rate can be very variable: a very rapid growth results in more numerous and less well formed crystals per unit volume; a slow-growing promotes the formation of larger crystals whose structure is better organized (it has fewer defects). In other words, the growth rate of the gypsum crystals influences their morphology and, consequently, the microstructure of the matrix, having a direct relation with strength of the hardened product.

So, for the same type of plaster the P/W ratio is directed related with the mechanical strengths but for different plasters with the same P/W this is not necessarily true, demonstrating that many factors have to be taken into account when comparing their characteristics.

Other mechanical properties of the gypsum plasters, like dynamic modulus of elasticity and hardness shore C are also affected by the porosity (related with the P/W ratio) of the hardened masses, in the same way as the flexural and compressive strengths (Coquard et al. 1994).

b) Impurities

The main impurities present in hardened gypsum come from the raw materials (Wirsching 2005). Their influence in the properties of the final product depends on the way they interfere with the hydration process, namely by changing the growing orientation of the crystals which affects their packing and interlock in the microstructure (Murat et al. 1975).

The presence of contaminants in the mixing water can also affect the strength of gypsum. Two examples are clay and sodium chloride: the first one retards the hydration and setting and leads to less resistant masses; the second one accelerates the reaction but also contributes to lower the strength (Murat et al. 1975).

The admixtures often used by manufacturers to change the behaviour and/or properties of the gypsum products can also be considered as impurities. Due to its importance the main admixtures will be addressed in a section ahead.

c) Use of admixtures

Nowadays, most of the gypsum based materials are already supplied as "factory-made" products, i.e., the plaster (usually β-hemihydrate or multiphase) has been previously mixed with aggregates and admixtures. In the worksite they only have to be mixed with water before application.

Admixtures are added to the plasters in the powder form. They can be either of organic or inorganic origin and their use intends to improve the mixing of the dry product with water and the properties of the wet and hardened pastes/mortars, such as rheological behaviour, workability, setting time adhesion, etc. (Bayer & Lutz 2000).

Some of the most common admixtures are those that modify the kinetic of the hydration process, either accelerating or retarding it. Both organic and inorganic substances can be used. These admixtures generally alter the surface properties of the crystals which leads to changes in nucleation, growth, and hydration kinetics, resulting in variations in size and morphology as well as crystal habit (Murat et al. 1975; Lewry & Williamson 1994c; Singh & Middendorf 2007; Song et al. 2010).

The accelerators are substances that increase the solubility or the rate of dissolution of the plaster phases in water. Many strong inorganic acids like sulphuric, hydrochloric or nitric and their salts (of sodium, potassium, calcium, etc.) and also strong bases are some examples (S.N.I.P. 1982; Lewry & Williamson 1994c). They can also act providing additional sites for nucleation. Calcium sulphate dihydrate finely ground is extensively used with this purpose, the very fine grains being considered as crystallization seeds, whereas salts modify the transport properties of ions and increase the dissolution rate of the hemihydrate (Song et al. 2010).

Set retarders are usually weak organic acids (malic, succinic, tartaric, and citric) and their salts, organic colloids that are the decomposition and hydrolysis products of biopolymers such as proteins (ex: keratin), and salts of phosphoric and boric acids. The mechanism of retardation of the crystallization of gypsum varies according to the type of substance. High molecular mass colloids act as nuclei poisons: they involve the crystals and difficult their diffusion (Wirsching 2005).

The carboxylic acids are adsorbed on the surface of growing gypsum nuclei during the induction period delaying the crystallization and hardening processes. Citric acid, for example, has been explained as providing a significant retarding effect because the acid molecules preferentially adsorb on the gypsum surface. This preferential adsorption reduces the number of active sites available for water-gypsum interaction (Singh & Middendorf 2007; Song et al. 2010).

In the case of tartaric acid, it has been reported as having almost no retardation effect on the hydration of hemihydrate in a pH neutral solution. However, in alkaline medium (through addition of hydrated lime to the plaster mix) it is one of the most widely used retarders in the manufacture of gypsum products for building construction producing the greatest retarding effects with the smallest quantity (Forg 1989). The reason is that at high pH tartaric acid inhibits both the growth of gypsum crystals and the dissolution of hemihydrate, while in neutral pH it only inhibits the growth of gypsum (Singh & Middendorf 2007).

The mechanical properties of the hardened products where set modifiers (accelerators or retarders) had been used were found to be, in the majority of the cases, inferior to those obtained when hydration occurred in a pure medium (Murat et al. 1975; Forg 1989).

Lewry & Williamson (1994c) studied the effect of accelerators (calcium sulphate dihydrate crystals and potassium sulphate) in the setting time, microscopic structure and strength of α-hemihydrate. They concluded that the increased nucleation rates induced by the admixtures gave rise to finer and smaller dihydrate needles with reduced inter-crystalline bonding and lower mechanical strengths.

With respect to retarders, a very dramatic example is given by Murat et al. (1975) that studied the hydration of an industrial hemihydrate plaster with increasing quantities of citric acid. The evolution of the crystals facies formed was observed in fractured surfaces using SEM. It showed that the acicular facies (hydration in a pure medium) starts to diminish in favour of the formation of thick crystals embedded in gypsum needles for 0.05% to 0.1% concentrations of citric acid. The needle-like shape progressively disappears as thicker crystals around 10 microns big form, variable in shape depending on the amount of citric acid used. With 0.5% the crystals assume the shape of thick hexagons whereas in the case of an addition of 0.2% citric acid they are trapezoidal or prismatic and cubic.

It is further noticed that these massive crystals are poorly formed and have many growth defects (presence of cavities). The mechanical properties of these materials change in a very unfavourable way with the increase of the amount of citric acid. In fact, with an addition of 0.5% the mechanical strength is so low that the mass behaves like a sandy material, showing no coherence.

So, the citric acid retarding action induces radical changes in crystals facies. On the contrary, the retardation effect of degraded proteins (like keratin) does not change the crystal facies although the

setting time can reach several hours. In this case the fall of the mechanical strength is much less important. There are even some organic products, like animal glues, that besides increasing the setting time, also improve workability and strength.

The changes produced in the microstructure due to the use of accelerators or retarders reduces expansion of the plasters during setting (Karni & Karni 1995).

Other examples of admixtures used in factory-made gypsum plaster mixes are those that regulate the water demand, either to reduce or to increase it (Wirsching 2005). Plasticizers are included in the first group (melamine resins, sulfonates). They are often used to improve strength of the hardened products as they act as "wetting agents" reducing the water needed to obtain a workable mass. The second group comprises the thickeners and water retaining agents (starch and cellulose ethers). They influence the stability of the plaster slurry, the workability and the yield.

Cellulose ethers are of major importance as admixtures although they are added in small contents. They are commonly known as "water retaining agents" and the mostly used formulas are methyl hydroxyethyl and methyl hydroxypropyl cellulose (MHEC and MHPC, respectively) (Bayer & Lutz 2000). They are absolutely essential in plaster mixes with long setting time, as they have the capacity of retaining water and slowly release it to the plaster slurry, maintaining it with a soft and plastic consistency until the work is complete (Wirsching 2005). Otherwise the suction of the support and the evaporation through the external surface of the plaster would drastically reduce its water content before the end of the hydration reaction. In practice, less coherent microstructures would form and the products would show lower strength. These admixtures also benefit the stability of the plaster slurry preventing its segregation and sedimentation and improve the shrinkage behaviour and the bonding to the base.

In this work, admixtures have been used in the developed gypsum-lime plaster mixes only when their use was proved to be imperative. The contents were always the minimum needed to obtain the desired characteristics, so that any negative effects were as small as possible.

d) Moisture content

The moisture content of hardened gypsum products influences several properties such as hardness, mechanical strength or thermal conductivity (Murat 1982).

According to Wirsching (2005) a moisture content of 1% results already in evident strength decrease while 5% makes it drop to half that of air-dried gypsum products.. On the contrary, Andrews (1946) studied the effect of moisture in the strength of hardened plaster of Paris and found that with 0.06% humidity the strength was 93.5% that of dried product, with 1% the strength was almost half (56%), decreasing to 51.5%

at 3% water content. From these results it seems that the major difference occurs between the dried state till 1% moisture content as between 1% and 3% the difference is already very small.

Anyway, there is no doubt that even at low contents, moisture seriously affects the gypsum products' mechanical properties. The reason is that water layers inside the microstructure of gypsum have a lubricating effect between the crystals lowering its strength and transforming it into a more deformable material (Wirsching 2005). The experimental results of Reynaud et al. (2006) evidenced that a relative sliding of gypsum crystals was enhanced in the presence of water and proposed a simple viscoelastoplastic rheological model to describe this effect.

It is consensual, however, that this loss of strength is reversible, unless the gypsum remains wet during long periods. In that case, the dissolution of some material occurs and the structural changes induced affect negatively its performance.

Concerning the effects of exposure to wetting/drying cycles without a long permanence in the wet condition, Henning & Eggert (1999) concluded that it can even be beneficial to the hardness of the gypsum surface due to crystallization/recrystallization phenomena. However, in their study the test specimens were only submitted to 10 cycles, and it is important to increase that number to confirm whether this is really the trend.

Similar conclusions had already been stated by several authors (Kingery et al. 1988; Middendorf & Knöfel 1998b; Middendorf & Knöfel 1998a; Middendorf 2002; Philokyprou 2012) but their objects of study were weathered ancient gypsum mortars submitted to countless wetting/drying cycles for centuries.

e) Microstructure

The relationship between the microstructure and the properties of the hardened masses resulting from the reaction with water of the several dehydrated phases of gypsum has been discussed, with reference to some of the main factors that induce morphological changes. The mechanisms of actuation of each factor have been addressed in order to better understand their influence on the properties of the gypsum plasters.

In spite of being far from exhaustive, this discussion allowed concluding that the factors affecting the development of the microstructure can be divided in two types: factors internal to the process of hydration, where they induce modifications in each of the steps (dissolution, nucleation and crystal growth) with special emphasis on the relative speeds at each stage and the mechanisms of interaction between the crystals; external factors, such as the presence of mechanical stress, environmental changes during setting and the effects of adsorption, humidification and drying.

Among the external factors, it is important to highlight the influence of the conditions of application of the products on their future behaviour and durability (S.N.I.P. 1982).

In fact, the internal layers, usually applied to regularize the background, must be adequately compressed in order to reduce shrinkage and obtain better mechanical performances. The same procedure is recommended to the finishing layer, although in this case special attention must be paid to the consistency of the plaster: when it begins thickening, it means that crystal growth is already occurring and excessive working will markedly reduce strength. For the same reason, remixing or adding more water at this stage is also totally unadvised. This is especially critical in the lime-gypsum plasters, as lime is gummier and confers more plasticity to the paste, even after formation of the dihydrate, looking as if it still can be worked or remixed (Karni & Karni 1995).

The adequate smoothing of the final plaster layer is desirable as it originates an effect known as "oriented crystallization". The hardness measured on such surfaces is greater than that of non-polished ones (Murat et al. 1975). A similar effect occurs when a plaster is poured into a mould and the crystals close to the internal surface of the mould will grow oriented in a given direction (Kingery et al. 1988).

2.2.3.7 Other properties of gypsum building products

Besides being a sustainable material, with much lower energy incorporation than other inorganic binders and an endless potential of recycling, there are other important properties that make gypsum plaster products very suitable to be used in construction.

Thermal insulation

Gypsum plaster is one of the traditional building materials with better thermal insulation characteristics (S.N.I.P. 1982). This is mainly due to low density and high porosity (around 50-60%).

It has an average thermal conductivity of 0.35 W m^{-1} K^{-1} for a bulk density of 1000 $kg.m^{-3}$, at temperature of 23 ºC and 50% relative humidity (EN 13279-1:2008). However, this value is dependent on the conditions of application on site and in use, namely the P/W ratio in the former and moisture in the latter (Murat & Foucault 1977).

Fire protection

The remarkable fire resistance of gypsum plaster is due the high content of water in its structure (about 18% of its weight). When temperature increases the crystallization water is gradually released in the form of vapour and the heat consumed in the reaction retards the temperature rise.

So, if fire is near gypsum products, calcination of their exposed surfaces begins. However, it progresses slowly into the bulk as the layer of calcined gypsum adheres to the underlying uncalcined gypsum making it more difficult for the calcination process to continue.

The temperature of the materials behind/under the surfaces of gypsum usually does not exceed 150 ºC by the time calcination is completed, which is a value much below the ignition temperatures of the majority of the building materials. So, gypsum is naturally a fire retardant and this capacity is responsible for its fire protection characteristics (S.N.I.P. 1982; Karni & Karni 1995; Wirsching 2005).

It was due to this behaviour during the great fire of London in 1666, that in 1667 king Louis XIV of France decreed as compulsory the use of gypsum plasters and renders to cover the half-timbered structures of buildings. The aim was to promote their resistance to fire (S.N.I.P. 1982).

Also in Germany the material of choice for exterior rendering was high temperature gypsum, where it was available. Numerous half-timbered buildings in southern Germany were retrospectively rendered with this material on their exteriors (Lucas 2003a).

Thermo-hygrometric regulation

Gypsum plasters have the capacity to adsorb water vapour when ambient relative humidity increases and to release it when humidity decreases. This is known as "breathing capacity"(Wirsching 2005).

Although the velocity of these exchanges depends on the compactness, P/W ratio, exposed surface area and ambient conditions of temperature and humidity, there is no doubt that gypsum building materials play an important role in the thermo-hygrometric regulation of the spaces where they have been applied. This capacity together with its good thermal insulation properties prevent the occurrence of condensation phenomena under normal conditions, i.e. the plaster surfaces do not "sweat", feeling warm to the touch (S.N.I.P. 1982; Wirsching 2005).

Gypsum building materials have also volume stability undergoing very small changes in size with variations in moisture content (Wirsching 2005).

2.2.3.8 Production process

The technological developments of the twentieth century were naturally felt in the gypsum and lime industries. The processes presently used to produce any of these products have little or nothing to do with those of a few centuries ago, or even, of the first half of the twentieth century.

In fact, if one looks at the description on the plaster manufacture made by Luiz Augusto Leitão (1896) in his book *"Curso elementar de construcções"* (Elementary course of constructions), there is a time consuming process based on extensive hand craft and empirical knowledge:

> *"A calcinação da pedra gypsosa produz o gesso. A operação póde effectuar-se quer em telheiros ou fornos do campo (...) quer em fornos ordinários (...). Os telheiros são abertos em uma só face; as três restantes são fechadas por muros"* (Figure 2.9).
>
> "The calcination of gypsum stone produces plaster. The operation can take place in sheds or field kilns (...) or in ordinary kilns (...). The sheds are open on one side only; the remaining three are closed by walls" (Figure 2.9).

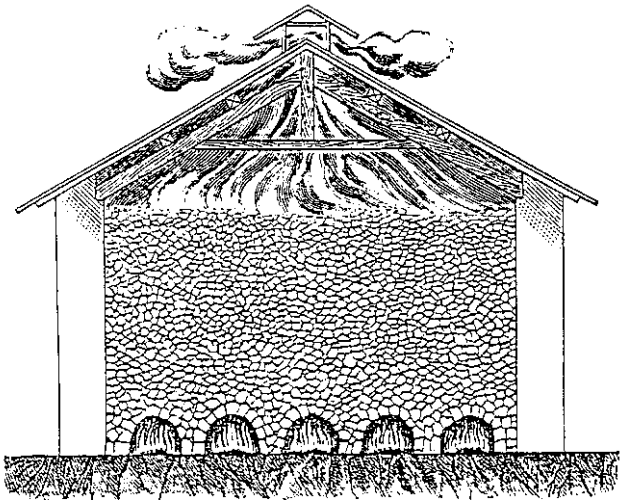

Figure 2.9 - Shed-type intermittent kiln (Leitão 1896)

> *"(...) Procede-se ao carregamento d'estes fornos, começando por formar abobadas ou fornalhas com as pedras mais grossas, e dispondo sobre estas as pedras cada vez menores, de modo que na parte superior da carga há apenas pó e fragmentos miúdos* (Figure 2.10 (a)). *Accendem-se as fornalhas com lenha ou matto, eleva-se a temperatura a 120º ou 160º, e alimenta-se o fogo durante dez a quinze horas, conforme o estado atmospherico, a qualidade da pedra e o combustivel empregado* (Figure 2.10 (b)). *Considera-se completa a operação quando principiam a estar vermelhas as pedras das abobadas; (...) tapam-se todos os respiradouros e deixa-se arrefecer* (Figure 2.10 (c))*."*
>
> "The loading of these kilns is performed, starting by making domes or furnaces with coarser stones, and laying on these increasingly smaller stones, so that in the top of the load there is only dust and small fragments (Figure 2.10 (a)). The furnaces are lit with wood or bush, the temperature is raised to 120 ºC or 160 ºC, and the fire is fed for ten to fifteen hours, depending on the atmospheric state, the quality of the stone and the employed fuel

(Figure 2.9 (b)). The operation is considered complete when the stones of the vaults begin to be red; (...) all vents are covered up and the kiln is allowed to cool (Figure 2.10 (c)).”

“A calcinação intermittente em telheiros ou em fornos ordinários e a calcinação contínua nestes últimos não fornecem o gesso branco e fino de que se faz uso nos estuques esmerados, porque o fumo, atravessando a massa de pedras gypsosas, ennegrece-a; o grau de cozedura está também longe de ser uniforme. Obvia-se a estes inconvenientes cozendo a pedra com o vapor de agua, em um apparelho que consta de um gerador de vapor e de três tinas de alvenaria communicando entre si e com o gerador por meio de tubos munidos de chaves. (...) A cozedura pode ainda effectuar-se em torradores cylindricos, quando se pretenda um gesso fino ou de boa qualidade.”

“Intermittent calcination in sheds or in ordinary kilns and continuous calcination in the latter does not provide the fine white plaster that is used in the neat stuccos because the smoke across the mass of gypsum stones blackens it. The degree of firing is also far from being uniform. These drawbacks are obviated by firing the stone with the water vapour in one apparatus consisting in a steam generator and three masonry tanks communicating with each other and with the generator by means of tubes fitted with keys. (...) The cooking can still be carried out in cylindrical roasters, when planning a fine plaster or of good quality.”

(a)

(b)

(c)

Figure 2.10 - Traditional intermittent gypsum kiln with four openings: (a) freshly prepared, ready to start calcination; (b) during the calcination process; (c) after calcination, ready to be dismounted (Sanz 2007).

So, to get coarser plasters (used in masonry settlement work, preparatory layer for plaster, etc.), the process of calcination was different from that of a plaster for "neat" works, very fine and white. The same principle was applied to the choice of raw material, in which the plasters of lower purity and more greyish colour were intended for rough works and the higher purity and whiteness for the delicate ones (Graça Costa 1986).

A very similar description (probably based on the book of Leitão) is still made by Segurado (Segurado_b n.d.), around the 1930's. Little or no progress is noticed between the writing of the two manuals. The second only adds the use of bread ovens as a possibility for the calcination of gypsum for white stucco works.

Regarding current processes, developed and implemented mostly from the second half of the twentieth century, gypsum plasters are calcined in directly fired rotary kilns (Figure 2.11) or else in indirectly heated vertical or horizontal kettles. The last ones, also known as *Beau* kettles, work in batches and are more commonly used in France.

The automation as well as the control systems associated with the various stages of production, homogenized quality and lead to products necessarily different from any gypsum produced using the old, traditional processes. In spite of being impossible to produce a one-phase plaster, it is possible to be close to it. Multiphase plasters can be then a tailored mix of different phases (hemihydrate, anhydrite III, anhydrite II, etc.) or they can be obtained industrially combining the type of kiln, the granulometry of the raw material and the calcination temperatures (Wirsching 2005).

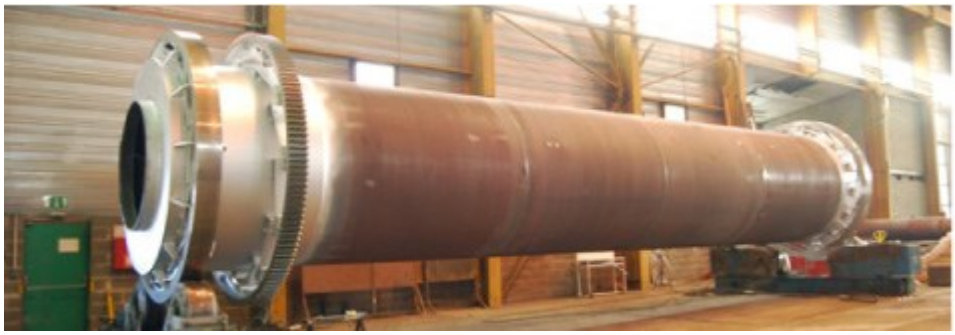

Figure 2.11 - Directly fired rotary kiln used to produce β–hemihydrate and multiphase plasters

Furthermore, the possibility of obtaining plasters with different particle size distributions and mix them with a wide range of materials (aggregates, water retainers, plasticizers, thickeners, lightweight aggregates) allows designing products to almost all purposes and provide them to the customers ready to use, or ready to knead on site.

Summarizing, the dehydration and rehydration processes are the basis of all production technology and application of gypsum products. This loop process, together with the low temperatures of calcination required when compared to other calcium based binders (about 900 ºC for air lime, 1200 ºC for hydraulic lime and 1450 ºC for Portland cement), allows gypsum to be defined as "the magic mineral indefinitely recyclable" (Figure 2.12) and to be considered as "the sustainable material for the 21st century" (Eurogypsum 2007).

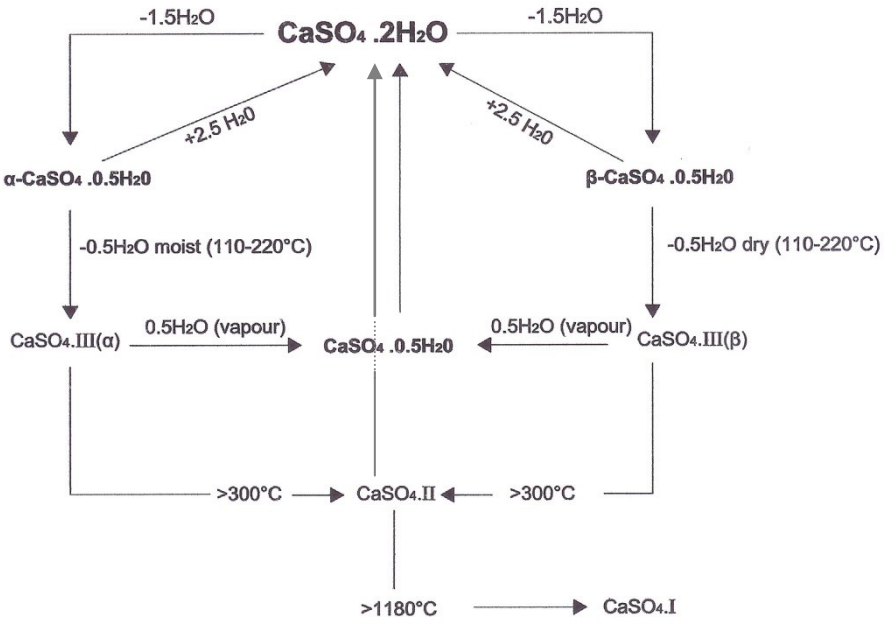

Figure 2.12 - The cycle of gypsum (adapted from Singh & Middendorf 2007)

2.2.4 Air lime

2.2.4.1 General considerations

Calcium carbonate or calcite rocks are widespread over almost the whole world. They were the first rocks to be quarried due to their abundancy (they were easy to find), to their softness and to their layered structure, qualities that make them easy to work. It has hardness of 3 in the Mohs scale and chemical formula $CaCO_3$. The limestones quarried today are classified according to their compactness as chalk, limestone and marble (increasing order) depending on the degree of cementation of the calcite grains. It is relatively easy to mine limestone due to its low hardness. Mining can be subterranean or in open quarries (Tegethoff 2001).

Calcium carbonate occurs in three different crystal modifications: calcite, aragonite and vaterite. The dominant in nature is clearly calcite, not only in the massive limestone rocks, but also in combination with quartz, barite and fluorite forming the parent rock of many mineral veins.

In spite of the biggest amounts of limestone being consumed by the construction industry (as masonry or decorative stone, in the production of cement, concrete, quick and slaked lime, as crushed stone for road construction, etc.) calcium carbonates have still the most diverse applications, among which some examples are given (Tegethoff 2001):

a) In sculpture;
b) As filler for paper, plastics, paints and coatings, putties and adhesives;
c) In agriculture and livestock, as fertilizer, soil corrector, or in the preparation of cattle feed;
d) In environmental protection, used as flue gas desulphurisation in power plants, for the preparation of drinking water, neutralisation of over acidified lakes and rivers;
e) In everyday products, as blackboard chalk, cosmetics, dental care products.

2.2.4.2 The air lime cycle

The processing of the air lime used in construction has many points in common with the gypsum cycle. It starts with the calcination of the raw material, passing then through a process of hydration and finally reacts with carbon dioxide, originating a product chemically identical to the starting raw material but with a markedly different microstructure.

However, the type of chemical reactions, the kinetic and the thermodynamic of the processes involved are different from those of gypsum plaster and will now be described:

$$CaCO_{3\,(s)} \xrightarrow{800\text{-}900\ ^{o}C} CaO_{\,(s)} + CO_{2\,(g)} \qquad \text{(Eq. 2.10)}$$

$$CaO_{\,(s)} + H_2O_{\,(l)} \longrightarrow Ca(OH)_{2\,(powder\ or\ slurry)} + heat \qquad \text{(Eq. 2.11)}$$

$$Ca(OH)_{2\,(slurry)} + CO_{2\,(g)} \longrightarrow CaCO_{3\,(s)} + H_2O_{\,(l)} + heat \qquad \text{(Eq. 2.12)}$$

During calcination of the calcium carbonate the carbon dioxide is released to the atmosphere and the only product remaining is calcium oxide (CaO) or quicklime (Eq. 2.10).

Quicklime is very unstable, having a high reactivity with water. The hydration reaction (Eq. 2.11), also called extinction of lime, is accompanied by a significant increase in the apparent volume, which can reach 3 to 3.5 times the original volume, and the release of a considerable amount of energy, in the form of heat, reaching temperatures above 300 °C (Margalha 2010).

In this process, if the water added is only the one necessary for the reaction then the product obtained is hydrated lime (also called slaked lime) in the powder form. On the contrary, if excess water is

added, lime putty or limewash can be obtained, depending on whether the respective quantities are lower or higher (Margalha 2010).

The last stage of the air lime cycle is the reaction of calcium hydroxide ($Ca(OH)_2$) with the carbon dioxide (CO_2) present in the atmospheric air, resulting in the formation of calcium carbonate, a less soluble and harder product (Eq. 2.12). This process, known as carbonation, is accompanied by significant shrinkage that occurs mainly in the first days (Margalha 2010).

Carbonation is not a single step process, occurring in several stages (Lawrence et al. 2006a; Arizzi & Cultrone 2013), such as:

a) Diffusion of gaseous CO_2 through the pores of the paste;
b) Dissolution of CO_2 and of $Ca(OH)_2$ in the pore water;

$$CO_{2\,(g)} + H_2O_{\,(l)} \longleftrightarrow H_2CO_{3\,(aq)} \qquad \text{(Eq. 2.13)}$$

$$Ca(OH)_{2\,(s)} + H_2O_{\,(l)} \longrightarrow Ca^{2+}_{(aq)} + 2OH^-_{(aq)} \qquad \text{(Eq. 2.14)}$$

c) Precipitation of $CaCO_3$.

$$Ca^{2+}_{(aq)} + 2OH^-_{(aq)} + H_2CO_{3\,(aq)} \longrightarrow CaCO_{3\,(s)} + 2H_2O_{\,(l)} \qquad \text{(Eq. 2.15)}$$

The factors that influence these stages are mainly CO_2 permeability, relative humidity and temperature (Moorehead 1986; Houst & Wittmann 1994).

Carbonation of lime causes an increase of 35% in weight and 11.8% in volume in the initial pastes, with significant changes in the microstructure, leading to more compact and less porous systems (Moorehead 1986; Arandigoyen et al. 2006; Lawrence et al. 2007). This volume increase in the transformation of calcium hydroxide into calcite is found inside the mortar pores, filling the voids occupied by the water that evaporates which, in turn, reduces the porosity of the matrix and can reduce the access of carbon dioxide to its most inland areas.

It is in the hydrated form that lime is used in construction, simple or mixed with other materials such as gypsum, to form pastes, or aggregates, to form lime mortars; the addition of any of these materials counteracts shrinkage (Livingston et al. 1998). Once applied, the hydrated lime reacts slowly with atmospheric carbon dioxide in the presence of water - favourable relative humidity of the air 60-93% (Cizer, Rodriguez-Navarro, et al. 2012) - where it partially dissolves. The chemical composition of the initial rock is then reconstituted.

The carbonation process can take months, or even years until being complete and in some cases portlandite is still detected in mortars with centuries (Adams et al. 1998).

2.2.4.3 Production process

All data available about lime technology result from ongoing research that was developed in a more systematic and scientific form since the 18th century. Before that, the knowledge was essentially empirical and most practices adopted were based on the observation of the performance and durability of the different solutions. Regard ing air lime, some of the aspects referred to in the literature are now enumerated (Leitão 1896; Segurado_b n.d.; Paz Branco 1993; Mateus 2002):

a) *Selection of the raw material* - hardness, colour, impurities;

b) *Calcination* - type of kiln, arrangement of the stones in the kiln, duration of cooking, cooling and unloading, type of fuel, etc.

   The distinction between lime cooked with bush and lime cooked with coal was made. The first was recommended for "works of responsibility, like plasters and garnishes as well as in masonry that must endure great efforts" (Segurado_b n.d.). This is because lime cooked with coal had many impurities resulting from the combustion, consisting of a large volume of ash and even slag intimately mixed with it being difficult to separate them. Besides the colour is not so white, with this lime the paste formed was less homogeneous, less oily and less bright than the lime fired with bush. According to Mateus (2002), in the 18th century one of the criteria proposed by Higgins to assess the quality of an air lime immediately after firing was precisely the colour: it should be bright white, to ensure that the lime was free from any impurities. Another criterion was to dissolve it in hydrochloric or acetic acid and check whether its dissolution was made without effervescence and without noise, factors that guarantee a perfect homogeneity;

c) *Extinction of quicklime* - explanation of the different methods (by immersion, spraying, mixed with wet sand or spontaneously) and recommendations depending on the purpose intended for the lime, always with the goal of guaranteeing a special quality for the finishing layer/garnish of wall coatings and for masonry that must endure greater efforts.

   The speed of dissolution of lime in water immediately after cooking, was another of the criteria proposed by Higgins to assess its quality (Mateus 2002);

d) *Sieving of slaked lime* - essentially to eliminate undercooked or overcooked fragments;

e) *Storage of slaked lime in the worksite* - usually as putty, in barrels or pits made especially for that in the ground. Use of lime with longer maturity in works of more responsibility as stone/ashlar masonry settlement, repointing of joints, finishing layer of wall coatings, fresco paintings, etc.

In the late 19th century lime production in large industrial scale was a reality. Notable developments in scientific knowledge had been already made and quality control tests started to be applied (some of them still in use) like the determination of bulk density, setting time (in hydraulic limes) and strength, tested on mortars prepared with a volumetric proportion of 1:3. However, small craft productions continued to be responsible for a significant amount of the lime used in construction until the mid-20th century (Mateus 2002).

2.2.4.4 Sources of raw material in Portugal

There is great availability of limestone and marble in Portugal, as shown in Figure 2.4, section 2.2.3.2.

2.2.5 Aggregates

The aggregates used in the preparation of the traditional multi-coat plastering systems shall be of siliceous or calcareous nature, free of clay and any impurities like organic material, soluble salts, dirt, etc. In the plasters for the finishing layer the colour of the aggregates is also important and shall be as white as possible (Segurado_a n.d.; Sawyer 1951; Hannouille 1959; Paz Branco 1993).

In fact, organic material can strongly affect the setting time of gypsum and the resulting materials have lower mechanical strength.

Soluble salts, in turn, can cause efflorescence, always undesirable and harmful in construction.

The clay content must be controlled because it can be beneficial to the workability of the mortars in given contents, but its excessive presence may increase shrinkage on drying. When it exceeds 6%, the aggregate should be rejected (Malta da Silveira 2000).

Regarding the grain size of the aggregates used in the ancient traditional plasters, it is extremely difficult to know its parameters, because the literature, with few exceptions, invariably states that "the sands should be fine." One of these exceptions is the book by Hannouille (1959) that distinguishes between "fine sand (with particles of 0.5 to 1 mm)" and "coarse sand (1.5 to 3mm)".

Such an absence of more precise information is not surprising if one considers that it still happens today. In fact, the European standard EN 13279-1:2008 that specifies the characteristics and performance of powder products based on gypsum, including pre-dosed plasters, makes no reference to this matter.

2.2.6 Kneading water

The quality of water used in the preparation of any mortar was also given the utmost importance in the technical literature, in the form of the most varied recommendations, as stated by Leitão (1896):

"(...) água que convem seja tirada das fontes ou dos rios e ribeiras, porque não contém, como a dos poços, tanques ou lagoas, princípios que ás vezes prejudicam as boas qualidades da argamassa. As aguas do mar só se utilisam nas argamassas que tiverem de ficar immersas em agua salgada".

"(…) water that is appropriate is taken from sources or from rivers and streams, because it does not contain, such as that of wells, ponds or lagoons, principles which sometimes hinder the good qualities of the mortar. Sea waters are used only on mortars that will be immersed in salt water."

In fact, it was intended that the water was clean and free of impurities, organic material and harmful salts for the same reasons as described above for the aggregates (*cf.* 2.2.5).

These recommendations were later explained on the basis of scientific studies, again started by Higgins in the 18th century and developed throughout the 19th century by other researchers, closely assisted by the equally intense development of Chemistry (Mateus 2002).

The importance of the quality of the water used to prepare building materials is still of great concern as is attested by the references made to this subject in the respective standards. In the case of gypsum plastering systems the technical report CEN/TR 15124 recommends that "the water should be of a quality such that it does not adversely affect the plaster. Water fit for drinking is suitable for mixes for plastering".

2.2.7 Gypsum *versus* air lime: characteristics and behaviour

As stated before, gypsum and lime are both calcium minerals and have both a very similar processing cycle: the raw material exploitation, the production (based on calcination and milling processes), the type of binder (air hardening) and the similar appearance after application from an aesthetic point of view. This aesthetic similarities are enhanced by Livingston et al. (1998) when they argue that gypsum mortars may have been more widely used than is reported in the literature because of that.

However, the differences in their chemistry lead to distinct physical and mechanical properties, which, in turn, determine their form and type of application in construction:

a) *Setting and hardening* - in lime mortars it is the calcium hydroxide that reacts with atmospheric carbon dioxide to form a porous hard structure. This reaction (carbonation) involves the exchange of water vapour for carbon dioxide and does not occur in a wet environment (air binder reaction). The rate of gas transfer is progressively slowed down by the reduction of porosity caused by carbonation and the complete hardening of lime can take many years (Adams et al. 1998; Livingston et al. 1998). On the contrary, the setting and

hardening of gypsum is due to the hydration and drying of the mass and results in very quick processes: the first takes about 30 minutes and the second a few weeks (about one month in winter) (Karni & Karni 1995);

b) *Dimensional variations* - gypsum products expand during hydration while lime products shrink;
c) *Use of aggregates* - gypsum plasters and mortars do not need the addition of aggregates (Livingston et al. 1998). In the European standard on design considerations and essential principles for internal plastering systems (EN 13914-2:2005) it is specified that "the aggregate can be omitted from mortars made from gypsum plaster or anhydrite binders", while for lime mixes they play a very important role in the reduction/control of shrinkage;
d) *Deformability* – lime-based plasters and mortars have a much more elastic behaviour than those of gypsum, a more brittle material. This is easily translated in the respective values of dynamic modulus of elasticity, much lower in the case of lime;
e) *Strength* - gypsum materials have higher strength that lime's, especially tensile strength;
f) *Solubility* - calcite (0.0015%) is about 130 times less soluble than gypsum (0.2%), at room temperature and almost-neutral pH (Kingery et al. 1988). Therefore, lime mortars can be used in exterior without restrictions and gypsum masses are mainly used indoors, with the exception of those made from high temperature gypsum plasters.

The distinction between gypsum and lime plasters remained obscure up to the 18th century. Only by that time, research into the principles of gypsum technology was begun by Lavoisier and has continued till today. However, such traditional craft was slow to accept the scientific conclusions and only in the second half of the last century has developed into a modern industry. A similar path has been taken by lime massive production (Wirsching 2005).

For all these reasons, it is considered relevant to differentiate between gypsum and lime, which takes on added importance in the context of conservation and restoration interventions. Yet, it is also important to have in mind and to know how to exploit their extremely high affinity, complementing each other in a positive way. As stated by Gárate-Rojas (1999) the use of these two materials together gives rise to products of an almost endless versatility, both in composition and in application.

2.3 The Portuguese traditional plaster coatings: current knowledge

In Portugal, the lack of good quality gypsum raw material contributed to the predominant use of lime in construction. Only in the Islamic and Renaissance periods are there some occasional remains of the application of gypsum plasters, both in smooth surfaces and in decorative elements, always associated to buildings of some architectural value (Freire, Santos Silva, et al. 2015). Prior to this study, many authors suggest that gypsum has been used since the Roman occupation (Malta da Silveira 2000; Vieira 2002;

Vieira 2008; Silva 2005), an hypothesis with no analytical evidence so far; in this study all results indicate that gypsum plasters mainly came into the Portuguese architecture in the second half of the 18th century.

Still, most ancient buildings (from 19th century to the 40's of the 20th) have interior walls and ceilings' gypsum plaster coatings. Some of them have high historical, architectural and aesthetic value and are part of the cultural heritage. In fact, the knowledge, the mastery and the art inherent to the design and application of such coatings cannot be regarded as belonging only to the buildings they are physically connected to; they are also part of art history, collective memory and Portuguese traditions.

In the 1930's, the emergence of modernism in Portugal made gypsum plasters definitely lose a decorative role in architecture. Since then they are almost exclusively used in interior smooth surface walls and ceilings coatings.

According to a classification used by the Council of Europe, decorative plasterwork is the second most represented decorative art in Portugal, only superseded by *azulejos* (ceramic tiles) (Vieira 2008). Its importance contrasts, however, with the lack of value it has been voted to, mainly due to the antipathy of the dictatorial regime (*Estado Novo*) towards the historical period corresponding to the 18th century, to which it was closely linked (the 18th century was connoted with the absolutist regime, represented by king *D. João V* and later the anti-clericalism of the Marquis of *Pombal*) (Cotrim 2004). The fact that it was considered for a long time a "worthless" and "minor" art is clear in the text that the Director of the National Buildings and Monuments signed in 1935: "Our artistic and architectural heritage is being recovered from the attacks that were made against it in the 17th and 18th centuries." Among the buildings intervened at the time are the cathedrals of Lisbon and Oporto in respect of which he says that the walls and columns were "covered in stucco and woodcarving of no value", calling them "useless and outrageous additions to the original project" (cited by Silva 2005).

This attitude of the authorities responsible for the conservation of historic buildings led to the total disregard for its study and for the definition of strategies for its preservation, either through maintenance actions, or through conservation and/or restoration interventions.

For all these reasons, it is therefore not surprising the state of degradation and loss of most of this heritage, either by collapse or by rehabilitation actions that, in most cases, are actions of "cleansing" of the interior of the buildings. Its impressive lack of inventory is also not oblivious to this fact.

In the 1960's the first works on the Portuguese decorative plasters were published by the art historian Flórido de Vasconcelos (Vasconcelos 1961; Vasconcelos 1966). Until the late 1990's he could be considered a single voice in what concerns studies dedicated to this art in the country.

Recently, thanks to a group of researchers coming from the National Laboratory for Civil Engineering and IST, studies were performed on ancient stuccos: constructive characterization and pathological analysis (Malta da Silveira 2000); a survey of the issues considered most important for the establishment of a methodology applied to their rehabilitation (Cotrim 2004); studies of historical-artistic character and survey of the techniques in the field of decorative plasters (Vieira 2002; Vieira 2008; Silva 2005; Leite 2008).

Besides constituting a set of high interest, these works were pioneer in the compilation of information and called the attention of the institutions with responsibilities in the field of cultural heritage, as well as the public in general, to the existence of this important heritage. Yet, studies addressing the point of view of the materials used in its execution were still lacking.

The scarcity of bibliography about this subject is also a reality, mainly due to an intended secrecy about this art, which remained concentrated in a few people (usually handed down from generation to generation within the same family). On the other hand, the quick abandonment of the traditional materials and techniques in the mid-20th century led to an irreversible loss of important information that is now impossible to recover.

It was therefore necessary to work on the mitigation of these lacunae, an objective that this research would like to contribute to.

In a first stage, to know which materials were involved in the execution of ancient plasterworks it was necessary to collect original samples, preferably *in situ*, and characterize them. It was also important to complement the previous study with interviews to some of the plasterers that still work with traditional materials and techniques, in order to gather as much information as possible about the knowledge on "how to do it" and compare it with the analytical results obtained.

Only after that was it possible to establish compatibility requirements and move towards developing well-founded solutions for the conservation and restoration of the old materials. The design and selection of the most adequate mixes were then based on the results of their characterization with respect to the same properties evaluated in the ancient samples and on the fulfilment of the referred compatibility requirements.

2.3.1 Composition

The most common plaster elements in ancient buildings - decorative (precast, moulded on bench or moulded on site) and smooth surface finishing layers - were the object of study in this work.

The Portuguese literature is not consensual about their constitution, especially the smooth surface plasters (Leitão 1896; Segurado_a n.d.; Füller n.d.; Paz Branco 1993; Veiga et al. 1995; Malta da Silveira 2000). The variability is found in several aspects like the number of layers and their composition, which, in turn, also varied according to the type of constructive elements to be covered (walls or ceilings), if the plasters were for decorative purposes or if, on the contrary, were for smooth unpainted surfaces, the addition of retarders (type and quantity), etc.

Two traditional plasterers, still active and working mainly in rehabilitation works, have been interviewed (in 2010 and 2011) in order to know the composition and application procedure they use, particularly in the smooth surface coatings. Information about the materials used is as following:

Gypsum plaster (hemihydrate) - both use the product *Estuque* produced by the Portuguese firm SIVAL;

Lime - Plasterer 1 buys quicklime (in stones) and slakes it with excess water (Figure 2.13):

a) In a container of 200 1itres he introduces 45 kg of quicklime and adds water until reaching about 160-170 litres of its capacity (Figure 2.13 (a));
b) He lets it stay for, at least, one week, stirring once in a while;
c) After that, he passes the slaked lime through a sieve (Figure 2.13 (b)) and transfers the lime putty obtained into buckets, covering it with water (Figure 2.13 (c), left);
d) Before using it, he rejects the excess water and works with the putty (Figure 2.13 (c), right).

Plasterer 2 - buys lime putty, available in the market in closed buckets;

Sand - both use white sand from *Coina*. Only plasterer 2 gave information about the grain size, saying that "it should be between 1 and 2 mm".

The information collected was then compared with that of the literature (Table 2.2).

Both plasterers said they usually apply three layers to make the coating:

1. Spatterdash (*chapisco*) - It is used with a very fluid consistency to regularize the absorption and promote adhesion between the substrate and the subsequent layers. They said it is often applied by the masons and is usually a mix of cement (sometimes lime, if the place is damp) and coarser sand in the proportions 1:6.
2. Regularization layer (*reboco*) - Both use a mix of lime putty and sand from *Coina* to which they add a bit of cement or gypsum plaster when they want to accelerate hardening.
   Plasterer 1 said this layer had an approximate thickness of 3-5 mm but did not specify its composition (it seemed to be a bit random).

Plasterer 2 prepared a mix and the proportions were approximately 1:9. Then he applied a small quantity approximately 5-10 mm thick;

3. Finishing layer (smooth surface) (*estuque*) - Plasterer 1: 20 litres of lime putty, 4 litres of water and then gypsum plaster until there is no water available to soak any more plaster (it is said that the water is saturated of gypsum). He applies this paste in a very thin-layer (1-2 mm). Plasterer 2 did a similar application (1-2 mm thick) but used a mix with more lime: 20 litres of lime, 3 litres of water and gypsum plaster until saturation of the water;
4. Moulded on site elements - Plasterer 1 adds 8 litres of water to the lime putty and then gypsum plaster.
   Plasterer 2 adds 5 litres of water (a paste richer in lime than that of plasterer 1).

(a)

(b)

(c)

Figure 2.13 - Extinction of quicklime: (a) general view of the material; (b) sieving of slaked lime; (c) conservation of lime with excess water (left); putty (right)

Table 2.2 - Composition of the traditional interior plaster coatings: comparison between practice and literature

Plaster element	Interviews		Literature [1]		
	Plasterer 1	Plasterer 2	(Leitão 1896)	(Füller n.d.)	(Paz Branco 1993)
	HH : Lime putty (volumetric proportions) [2]		HH : Lime putty (volumetric proportions)		
Thin-layer (smooth surface)	1:2.8	1:4	1:1	1:1.7	1:1.5
Moulded on site	1:1.4	1:2.2	?	1:1	1:1
Precast and moulded on bench	1:0	1:0	?	1:0	1:0

HH - gypsum hemi-hydrate; HL - calcitic hydrated lime; [1] References of Segurado_a and _b not included as the receipts were based on Leitão (1996); [2] Bulk density of HH = 0.69 kg/dm^3

The main differences between these procedures and those mentioned in the literature are the number of layers and the composition of the first two layers: in former times the binder was always lime and nowadays the spatterdash is usually cement; it was common to have more than three layers (Malta da Silveira et al. 2007). A reduction on the number of layers can be due to the costs of labour and/or to the need of building faster.

The total thickness of the plaster coating is consequently lower, estimated as 18-23 mm against 19-33 mm for ancient coatings (Veiga et al. 1995). These are only approximate values, depending on several factors like state and type of the substrate, the level of professionalism of the plasterer, application techniques (in particular if the regularization/preparation layer is applied using the "points" and "lines" (*pontos e mestras*) procedure, used when the coating has demanding flatness tolerances, thereby increasing its thickness, etc. (Figure 2.14) (Malta da Silveira et al. 2007).

However, there are also many similarities, like the fact of being applied as a multilayer coating and the gradual reduction of the particle size of the layers from the inside to the outside, so important for the adhesion between them and, consequently, the quality and durability of the coating (Veiga et al. 1995; Malta da Silveira et al. 2007).

Figure 2.14 - Wall partition made of lathing with coatings of different thicknesses

Finally, one last note to highlight the importance of the procedure of measurement of each constituent.

The contents defined to prepare the mixes of materials have always been given special attention, being an issue that is transversal in the literature of all times and to all types of construction. The old treatises and construction manuals always had a section dedicated to these matters, although during many centuries the receipts were almost exclusively a reproduction of the contents indicated by Vitruvius, Plinius the Elder and Faventinus (Mateus 2002). Only rarely did they result from precise and systematic experiments. In any case, the preciseness was relative as these contents were, with few exceptions, volumetric.

Even during all the 20th century volumetric measurements were predominant in the mortars prepared on site, with all the errors associated. It is difficult to make an accurate measurement of volumes at work, due to the size and shape of containers used as reference measure, the moisture content of the materials, their degree of compactness, etc.

Although this question is highly relevant in the case of the aggregates - the volume of voids of coarse sand is lower than that of fine sand so, for equal volumetric contents, one coarse sand mortar is poorer in binder - it was perhaps easier to understand the problem in the case of products with very fine particle sizes. In his book of 1896, Leitão states already that "the cement is weighed by kilograms. (...) Some people think that the lime and pozzolan should also be weighed because it is difficult to measure twice the same amount of powder in the same way" and Segurado (Segurado_b n.d.) claims that "in general for cement, hydraulic lime and pozzolan the content is indicated by the number of kilograms of active substance for one cubic meter of sand". In practice, no one knows the actual application of this procedure but probably it was just used in works of larger dimension.

The question of volume or weight measurement of the different constituents of a mortar is a controversial issue, whose importance was only truly enhanced with the advent of concrete. For this material there are rules and procedures that define as more correct, because more accurate, the weighing of sand and cement. However, volumetric measurements may still be used since the determination of bulk density and moisture content of the sand is made several times a day (Sousa Coutinho 2006).

In spite of being consensual with respect to concrete, these requirements failed to be applied to other mixes made on site (mortars and plasters), probably because they are regarded of less "responsibility". Only with the use of pre-dosed products, ready to be mixed with water on site, can this lacuna be fulfilled.

2.3.2 Preparation

The preparation of a mortar or plaster on site consists of dosing and mixing very well all the constituents with each other and with water, so that it results in a homogeneous paste. If not well kneaded any of the constituents can be told apart by the naked eye.

Another key point in the preparation of a mortar/plaster is the amount of water used in mixing which, in turn, is directly related to its consistency. In fact, if the material has excess water, it will be too fluid, although easier to apply. However, it will not have the adequate characteristics for a good performance, particularly in terms of porosity (too high) and mechanical strength (too low). It is desirable that "its cohesion should be such that it can withstand the destructive external agents it is subjected to" (Leitão 1896).

On the contrary, if the mortar/plaster is too consistent this means that it does not have enough water and is more difficult to apply. Besides, its early drying will not allow the formation of a cohesive internal structure and will result in high shrinkage.

All the requirements the preparation of a mortar/plaster should comply with demonstrate why it is another important step, determining both a correct application and a good performance in service.

Regarding the preparation of pastes resulting from the mixture of gypsum plaster with lime putty, the common procedure is as following:

a) The lime putty is placed in a clean, smooth surface and a clearing is open in its center (Figure 2.15 (a));
b) The water is added at the intended content, and is deposited in the clearing (Figure 2.15 (b));
c) The gypsum powder is sprinkled into the water (Figure 2.15 (c));
d) The components are kneaded with a trowel until forming a homogeneous mass (Figure 2.15 (d)).

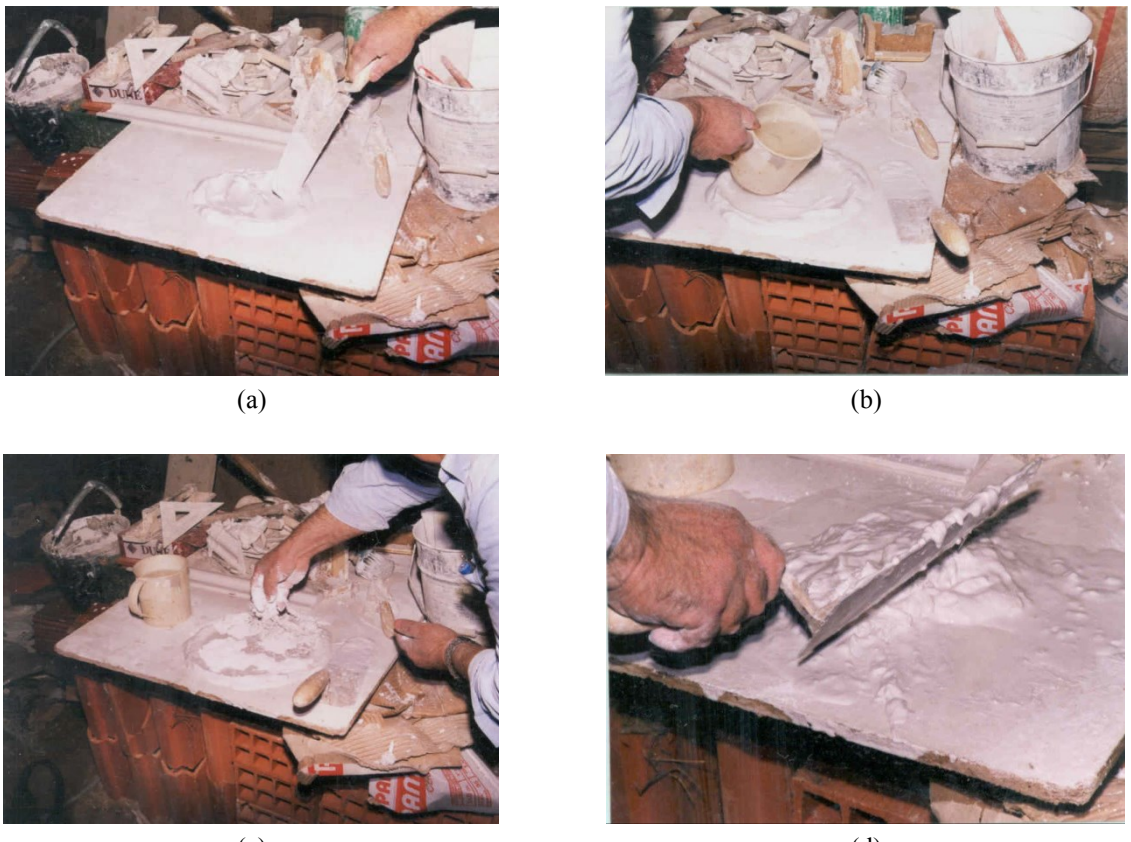

(a) (b) (c) (d)

Figure 2.15 - Preparation of a lime-gypsum plaster paste: (a) opening of a clearing in the lime putty; (b) addition of water; (c) gypsum plaster sprinkled into the water; (d) mixture of materials (Margalha, s/d)

2.3.3 Application

The first layer is applied on the substrate, usually ordinary masonry, wood lathing or, sometimes, rammed earth (Figure 2.16). The mortar consistency shall be more fluid when the substrate is masonry to simultaneously adhere to the mortar in the joints and to the masonry units. If these are already very dry (e.g. in case of an interrupted work) the wall should be first moistened, to promote adhesion between the facing and the coating.

When the mortar is applied to a wood lathing it has to have a regular consistency (neither too fluid nor too thick) in order to penetrate through the spaces between the laths when pressed hard and made to slide perpendicularly to them. Then, the surface is further straightened with the panel trowel, creating points of anchorage (Malta da Silveira et al. 2007).

(a) (b)

(c) (d)

Figure 2.16 - First layer of a multi-coat plastering system: (a) mixing lime and sand; (b) and (c) lime mortar, ready to be applied; (d) rammed earth substrate after application of the first layer

The regularization layer is applied over the first undercoat usually using a square trowel. The trowel contains the paste that is taken to the wall and pressed against it with the border of the tool in upwards movements (Figure 2.17 (a)). Afterwards, the coating needs planing with a ruler and again smoothing with the trowel which also functions as a float (Figure 2.17 (b)).

(a)

(b)

Figure 2.17 - Regularization layer (second coat): (a) application of the mortar with the border of the tool in upwards movements; (b) straightening of the surface

At the end, the finishing layer is usually applied as a very thin coat (2-3 mm). To promote adhesion it should also be pressed against the wall with the border of the trowel, in upwards movements (Figure 2.18). It can have several types of finishes that will be explained in the next section (*cf.* 2.3.4).

Figure 2.18 - Finishing layer: application of the lime-gypsum paste over the regularization layer

2.3.4 Types of plaster finish

Some types of finishes used in the traditional plastered surfaces in Portugal are now briefly explained.

Smooth finish by polishing

After applying the finishing layer, the whole surface it stroked with a soft damp cloth, in order to remove any irregularities (Segurado_a n.d.; Veiga et al. 1995).

If t no colouring of the surface is intended and the plaster is sufficiently white, the application of paint is not required, and it is enough to polish the surface after drying. This operation fills the pores and provides greater surface hardness increasing its resistance to abrasion, dirt, washing and other actions resulting from the use. However, if the surface is located in a persistently moist area, it is advisable to use a paint containing fungicide.

The plaster can still be burnished with pumice or jasper's very fine powder. Before burnishing, the surface must be moistened with a sponge. The procedure ends up by rubbing vigorously the surface with a felt cloth soaked in soapy water (Segurado_a n.d.; Veiga et al. 1995).

Rough finish

It is made with a sponge, lightly impregnated with plaster slurry (optionally coloured) pressed actively against the surface (Paz Branco 1993).

Coloured plaster

Traditionally coloured plaster surfaces can be obtained by: (i) *fresco* painting (a work that in general results very imperfect); (ii) diluting the pigment in the water to be used in the preparation of the mixture; (iii) incorporating it, also diluted, in the paste before application (Figure 2.19 (a) and (b)) (Veiga et al. 1995; Gárate-Rojas 1999).

(a) (b)

Figure 2.19 - Coloured plaster: (a) incorporation of the pigment in the paste; (b) homogeneous pigmented paste, ready to apply; (c) application of the coloured layer; (d) smoothing the surface; (e) final appearance; (f) pigmented paste being applied as paint

The pigmented paste can be applied in thin-layer to obtain a smooth surface (Figure 2.20 (a) to (c)) or with a brush, resulting in a lighter shade (Figure 2.20 (d)).

Nowadays plaster surfaces can be painted with several types of paints available in the market, although this operation significantly reduces its moisture regulation capacity, one of the great advantages of gypsum and lime coatings (Ramos et al. 2010).

The indefinite versatility of the lime-gypsum plasters also allows imitating nobler materials, such as stone or wood, using pigmented masses or specific techniques of painting and polishing (Gárate-Rojas 1999; Malta da Silveira 2000).

(a)

(b)

(c)

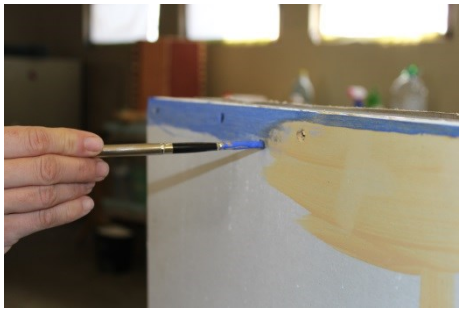

(d)

Figure 2.20 - Coloured plaster: (a) application of the coloured layer; (b) smoothing the surface; (c) final appearance; (d) pigmented paste being applied as paint

Plaster decorative elements

The frames, cornices or half-columns used to decorate the walls and ceilings of buildings often have straight or curved constant sections. They can therefore be moulded on site. The profile of the element is usually made of zinc plate (Figure 2.21 (a)) that is fixed to a wood base and runs on a wooden ruler, previously fixed to the wall (Figure 2.21 (b)). The plaster is placed between the surface of application and the mould. The mixes prepared for this purpose have commonly a higher proportion of gypsum than those used in thin-layer plaster finishings (Freire et al. 2010).

The same moulds can be used to produce this type of elements on a bench. The procedure is similar to that of moulding on site but the material used is most of the times pure gypsum plaster, as it is possible to work much faster.

The decorative elements can also be precast. This technique is used essentially to manufacture pieces without constant section. It consists on filling the moulds with gypsum plaster slurry, prepared with fluid consistency to reproduce all the details (Figure 2.22).

(a)

(b)

(c)

(d)

Figure 2.21 – Decorative elements with constant section: (a) zinc profile; (b) moulding on site; (c) moulds made of wooden base and zinc profile; (d) element moulded on bench

(a)

(b)

(c)

(d)

Figure 2.22 - Process of manufacture of precast decorative elements: (a) opening of the mould through which the gypsum plaster slurry is poured; (b) demoulding the piece; (c) complete view of the parts that constitute the mould with the corresponding piece inside; (d) view of some precast decorative elements

On site the pre-manufactured elements are pasted to the surfaces with a mass consisting of a plaster mixture with more gypsum than lime (to harden faster). That mass is pressed hard against the base. To help improving adhesion, the back of the pieces have often grooves deliberately made (Figure 2.23). When the ornaments have higher weight and/or size, they cannot be applied using only the plaster "glue"; they also have to be fixed mechanically, by means of screws and nails (Malta da Silveira 2000).

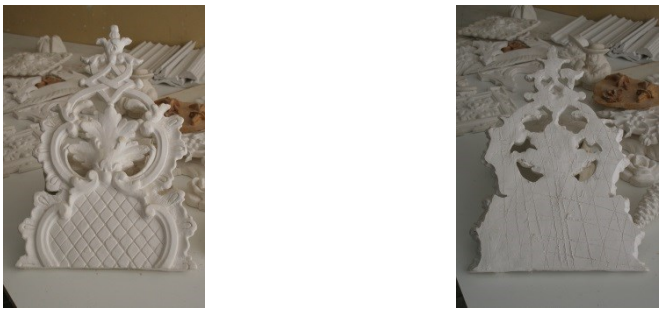

(a) (b)

Figure 2.23 - Half ceiling precast ornament: (a) Front view; (b) back view, with grooves

Nowadays these elements are all previously manufactured and applied by bonding and/or mechanical fastening to the base. The exception is the elements of regular profile that, in some cases, are still moulded directly on site. Since all these ornaments are finished with a thin layer of a finishing mass, it is often not possible to tell whether they are made of plaster, or synthetic materials, e.g. expanded polystyrene or PVC.

2.3.5 Quality requirements

Although there are some exceptions, like the ashlar stone walls, in ancient buildings the majority of the walls are coated. Thus, the coatings have a significant influence on the living conditions in buildings and have a decisive importance in the performance of walls as a whole.

In fact, in ordinary masonry, where the joints can reach a few centimeters and are very difficult to regularize, it is important to protect the walls from the action of aggressive agents, which outdoors are primarily the weather conditions (rain, wind, extreme temperature ranges) and inside are due to common use. In the latter case, the regularity of the surfaces also contributes to comfort, in particular visual and tactile.

So that the traditional plaster coatings meet the functional requirements inherent to their use, it is paramount to check a set of quality rules (Veiga et al. 1995, EN 13914-2:2005; CEN/TR 15124:2005). Some of these rules, concerning aesthetic appearance are now listed:

a) Flatness of the surfaces;
b) Verticality of the plastered finish;
c) Horizontality of the ceilings coatings;
d) Regularity and smoothness of the surface;
e) Resistance to cracking.

In the case of ancient buildings, the materials used in conservation and restoration works must also comply with some specific and fundamental requirements of historical authenticity and compatibility with the buildings and the backgrounds where they are applied, being the following issues particularly important (Veiga et al. 2001):

a) Not to degrade the pre-existing walls;
b) Protect them;
c) Chemical, physical and mechanical compatibility with the original materials in contact;
d) Reversibility or, at least, reparability of the interventions;
e) Respect the historical authenticity, namely in the case of higher value architectural heritage.

3

The history of Portuguese interior plaster coatings: A mineralogical survey using XRD

3.1 Introduction

In order to achieve the proposed objectives of this thesis it was concluded that a systematic study of the composition of the Portuguese interior plaster coatings along the most important civilizational periods that characterised the country's history was needed. A total of 139 samples were then collected from north to south of the territory, representing several types of constructions (either civil and religious buildings of value as heritage or current, both interesting from an architectural point of view) and different epochs: Roman and Late Roman (1st century B.C. to 6th century A.D.), Islamic (9th - 13th centuries), Low Middle-Ages and Renaissance (14th - 16th), Baroque (17th - 18th) and Post Baroque (19th - 20th). A mineralogical survey using XRD was made and the results showed that lime was the main binder until the end of the 18th century with gypsum overcoming its use in the 19th century mainly in wall and ceilings' decorative coatings.

Relationships are established between the evolution of the materials used and several influencing aspects, namely other cultures, the neighbouring countries and their traditional construction techniques, raw materials availability, the purposes/techniques of application, and geographical location.

3.2 Experimental work

3.2.1 Materials

Samples from thin layer (thickness between 1 and 5 mm) smooth surfaces or decorative plasters, of five historical periods (Roman, Islamic, Low Middle Age-Renaissance, Baroque and Post-Baroque) were collected in several regions (Figure 3.1).

The majority of the Roman and Islamic samples came from the most important Portuguese archaeological sites, as it is the case of *Conímbriga* (Roman, in the centre near *Coimbra*) (Figure 3.2) and *Silves* or *Mértola* (both Islamic and both in the south). Other samples result from the

archaeological monitoring of some civil engineering interventions (construction of buildings, motorways, bridges), either in urban historical centres (like *Coimbra* and *Loulé*) or in the countryside, the *Alcariais dos Guerreiros de Cima*, a rural Islamic village in *Alentejo's* southern region. Indeed, the Islamic influence is more noticeable in the south of Portugal (Figure 3.1).

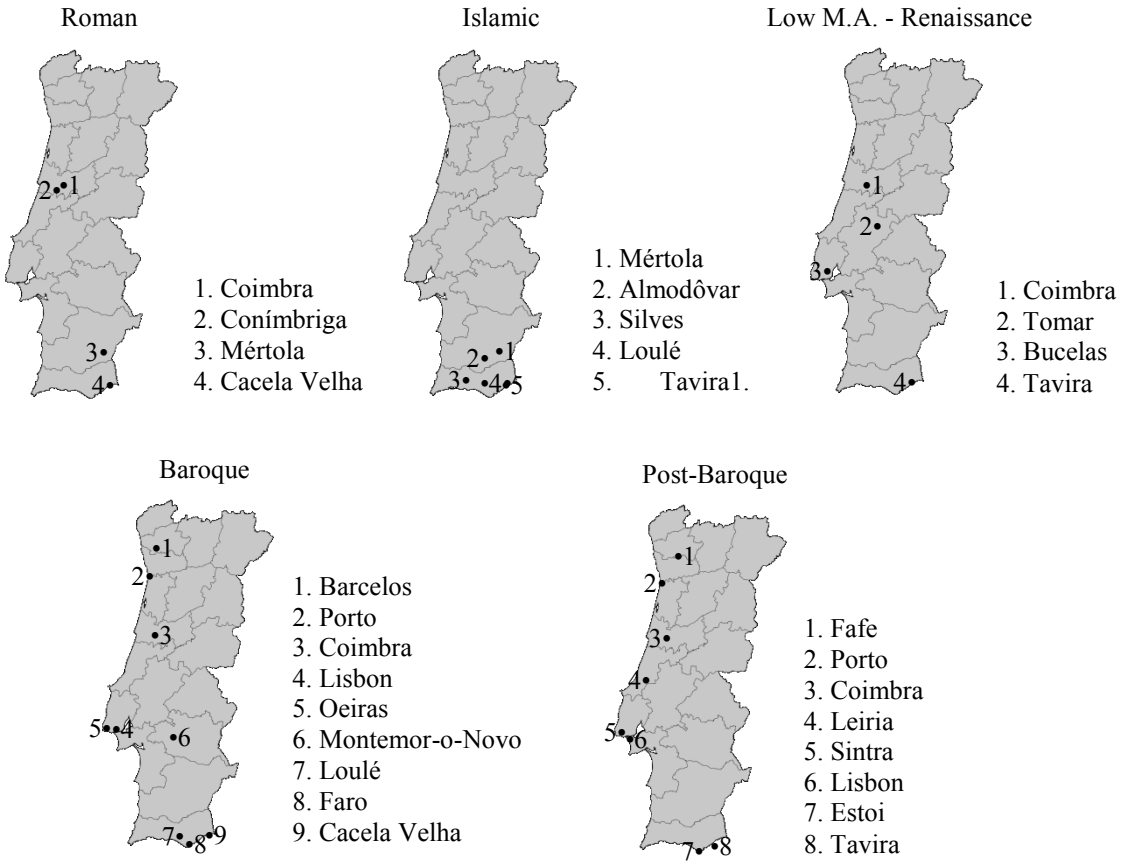

Figure 3.1 - Geographical location of the case studies by historical period

Only few samples of the Low Middle Age-Renaissance period were available, from archaeological sites (CG11 and LC1) or collected directly on site (CC1 to CC7 and IB1). However they comprise one of the most important case studies of the referred period: the unique and very rare stucco work from the *Charola* of the Convent of Christ, in *Tomar*, a monument classified as World Heritage by UNESCO (Figure 3.3).

Finally, the most recent periods, Baroque and Post-Baroque, have the highest number and variety of case studies, the majority of which corresponding to buildings still in service. This made it possible for all samples to be collected on site (with the exception of CV2, from an archaeological excavation). In all cases the buildings were about to be restored and/or rehabilitated, or were being intervened. Among them are some of the most emblematic buildings of Portuguese architectural heritage, like St. Michael's Chapel (University of *Coimbra*), *Santíssimo Sacramento's* Chapel (*Porto* Cathedral) and *Saudação* Convent

(*Montemor-o-Novo*) from the Baroque period or the palaces of *Bolsa* (*Porto*) (Freire et al. 2012), *Monserrate* (*Sintra*) (Gil & Calvet 1992) and *Estoi* (*Faro*) (Freire et al. 2009; Freire et al. 2010; Gil & Calvet 1992), which have the richest decorative programs from the 19th and beginning of the 20th century.

(a)

(b)

(c)

Figure 3.2 - *Conímbriga*, House of the Fountains: (a) general view; (b) and (c) details of mosaic floors and interior wall coatings

Figure 3.3 - *Charola* of the Convent of Christ, in *Tomar*: general view

The main information about the materials studied is reported in Table 3.1

This research work is focused on the plaster finishing elements. Whenever these elements were made of more than one layer, they were separated, numbered according to their order of application on site (number one being the inner layer of a multilayer plaster) and analysed individually (Figure 3.4). If a pictorial layer existed above, it was first carefully removed.

Table 3.1 - Plaster samples - Identification, provenance and dating

Identification	Site	Provenance	Sampling location	Approximate date (century)
Roman (I BC - V AD) and Late Roman (VI - VIII AD) period				
C1	*Conímbriga*	Amphitheater	Wall plaster (polychromic)	1st B.C. - 3rd A.D.
C2, C3, C4		House of *Cantaber*	Frieze	
C5			Wall plaster (polychromic)	
C6, C7, C8		House of the Fountains	Pilaster	
C9, C10, C11		*Thermae*	Frieze (polychromic)	
C12		*Tabernae*	Cornice (polychromic)	
C13, C14		Museum's reserve	Cornice	
C15			Frieze (polychromic)	
C16			Decorative stucco (with leaf)	
C17, C18		Museum's	Capital	
CT1	Coimbra	*Trindade* College	Wall plaster (polychromic)	1st
CV1	Cacela Velha	Fortress's Square	Wall plaster (polychromic)	4th - 6th
M1 to M3	Mértola	*Afonso Costa* St.	Wall plaster	6th - 7th
Islamic period (IX - XIII centuries)				
M4	Mértola	*Beira-Rio* excavations	Wall plaster	9th - 13th
M5		Old Mosque	Wall plaster	12th
M6		Citadel	Wall plaster	
M7				13th
M8				10th - 13th
BS1	Silves	Library excavations	Wall plaster	10th - 12th
BS2, BS3			Wall plaster (polychromic)	
AG1, AG2	Almodôvar	*Alcariais dos Guerreiros* arch.	Wall plaster	12th
CS1/1, CS2/1	Silves	Citadel	Wall plaster - inner layer	12th - 13th
CS3/1, CS11/1				
CS15/1, CS16/1				
CS17/1, CS18/1				
CS20/1, CS23/1				
CS1/2, CS2/2			Wall plaster - upper layer	
CS3/2, CS11/2				
CS15/2, CS16/2				
CS18/2, CS23/2				
CS4 to CS10			Wall plaster	
CS12 to CS14				
CS19, CS21				
CS22.F			Wall plaster - front	
CS22.T			Wall plaster - back	
CB1	Loulé	*Bicas*' House	Wall plaster	
TMF1		*Martim Farto's* Lane	Wall plaster (polychromic)	
CG1 to CG10	Tavira	*Graça's* Convent	Wall plaster	

Table 3.1 - Plaster samples - Identification, provenance and dating (cont.)

Identification	Site	Provenance	Sampling location	Approximate date (century)
Low Middle Age and Renaissance period (14th - 16th centuries)				
CG11	Tavira	*Graça's* Convent	Wall plaster (polychromic)	14th - 16th
CC1 to CC7	Tomar	Conv. Christ - *Charola*	Decorative panels	Early 16th
LC1	Coimbra	*Chimico* Laboratory arch. excavations	Wall plaster	16th
IB1	Bucelas	Church of *Bucelas*	Ceiling plaster	16th - 17th
Baroque period (17th - 18th centuries)				
CvS1	Montemor-o-Novo	*Saudação* Convent	Wall plaster	1st half 17th
IM1	Coimbra	*Misericórdia* Church	Ceiling plaster	17th
CSM1		St. Michael's Chapel	Wall plaster	
SP1	OPorto Cathedral	*Santíssimo's* Chapel	Ornament (gilded)	2nd half 18th
SP3			Frieze (thin finishing coat)	
SP4			Ceiling plaster (polychromic)	
LC2	Coimbra	*Chimico* Laboratory	Ceiling plaster	
LC3			Wall plaster	
LC4			Frieze (thick finishing coat)	
CP1	Oeiras	*Casa de Pesca* of the Marquis of *Pombal*	Ceiling plaster (polychromic)	
CP2			Frieze	
CP3			Ornaments	
CSA1	Loulé	St. Antonio Convent	Ornaments	
PRM1	Lisbon	*Rodrigues de Matos* Palace	Wall plaster (polychromic)	End 18th
PRM2			Ornament	
PRM3			Plaster bonding layer of PRM2	
IVF1	Barcelos	*Vilar de Frades* Church	Ceiling plaster	18th
IVF2			Ornament	
SC1	Faro	Captain's Mansion	Wall plaster	
CV2	Cacela Velha	Fortress's Square	Wall plaster	
Post-Baroque period (19th - 20th centuries)				
SA1/1	Coimbra	Room of the Arms, University	Ceiling plaster (polychromic) - inner layer	Early 19th
SA1/2			Ceiling plaster (polychrome) - upper layer	
CT2/1	Coimbra	*Trindade* College	Wall plaster (polychromic) - inner layer	Middle 19th
CT2/2			Wall plaster (polychromic) - upper layer	
PBS1	Leiria	*Barão Salgueiro* Manor house	Ceiling plaster	
PBS2			Frieze	
PBS3			Ornaments	

Table 3.1 - Plaster samples - Identification, provenance and dating (cont.)

Identification	Site	Provenance	Sampling location	Approximate date (century)
Post Baroque period (19th - 20th centuries)				
ERR1, ERR2	Porto	Building - *Restauração* St.	Wall plaster (polychromic)	2nd half 19th
ERR3			Frieze	
ERR4			Ornament	
PB1	Porto	*Bolsa* Palace	Frame from ceiling (gilded)	
PB2			Ornament (gilded)	
PB3			Frame (base of PB2, gilded)	
PB4			Ornaments	
PB6/1			Regularization layer for PB6/3	
PB6/2			Preparation layer of PB6/3	
PB6/3			Ornament (polychromic)	
PM1	Sintra	*Monserrate* Palace	Stone like skirting board	
PM2			Ornaments	
PM3			Frieze (gilded)	
PM4			Regularization layer of ceiling	
PM5/1			Wall plaster - inner layer	
PM5/2			Wall plaster - upper layer	
IS1/1	Lisbon	*Sacramento* Church	Wall plaster - inner layer	
IS1/2			Wall plaster - upper layer	
EDB1	Lisbon	Building - 5, *Duques de Bragança* St.	Wall plaster (polychromic)	
EDB2		Building - 5J, *D. B.* St.	Wall plaster	
EDB3			Wall plaster (polychromic)	
ISF1	Tavira	*S. Francisco* Church	Ornament (polychromic)	End 19th
ISF2			Ornament	
PE1/1	Estoi, Faro	*Estoi* Palace	Regularization layer for PE1/2	Transition 19th - 20th
PE1/2			Ornament (polychromic)	
PE2/1			Regularization layer for PE2/2	
PE2/2			Ornament (polychromic)	
PE4/1			Ornament - inner layer	
PE4/2			Ornament - upper polychromic layer	
PE5/1			Wall plaster (polychromic) - inner layer	
PE5/2			Wall plaster (polychromic) - middle layer	
PE5/3			Wall plaster (polychromic) - upper layer	
EG1 to EG4	Leiria	*Garage* building	Wall plaster (polychromic)	Early 20th
EG5/1			Regularization layer of EG5/2	
EG5/2			Frieze	
EBR1	Leiria	*Beira Rio* building	Ceiling plaster (polychromic)	
EBR2/1			Wall plaster (polychromic) - inner layer	
EBR2/2			Wall plaster (polychromic) - upper layer	
EBR3			Frieze	
CTF1	Fafe	Cine-Theater building	Ornaments (polychromic)	1st quarter 20th
CTF2			Wall plaster (polychromic)	
CTF3			Plaster bonding layer of CTF1	
EAL	Lisbon	Liberty's Av. building	Ceiling plaster (polychromic)	

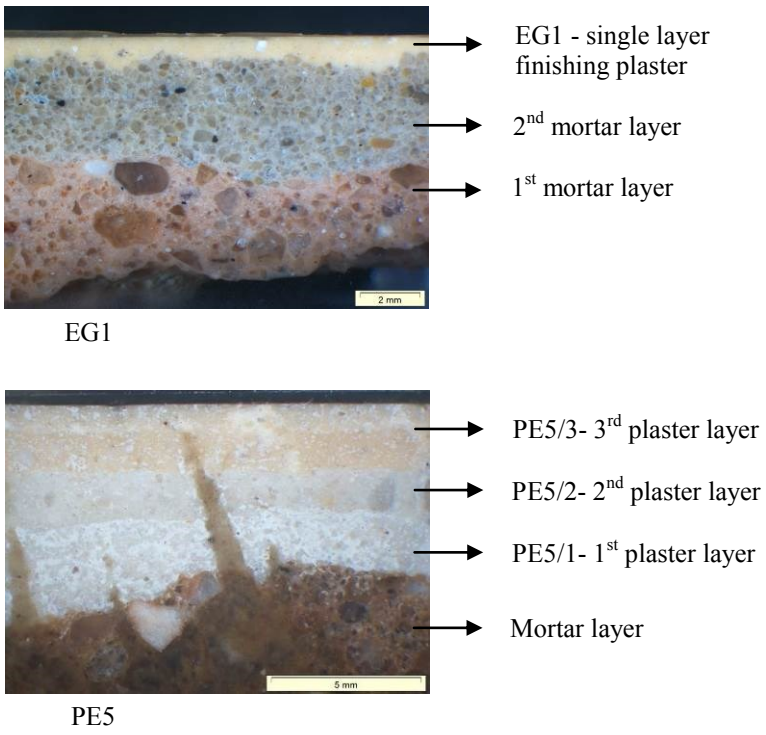

Figure 3.4 - Nomenclature adopted in the process of identification of the samples: examples of a single layer (EG1) and multilayer finishing plaster (PE5)

Most of the decorative elements were precast or moulded on site with a single plaster mix; the corresponding samples are representative of the whole. However, in few of them the core was made of mortar and only the final coating was plastered, being mentioned in Table 3.1 as "finishing coat". In these cases only that coat was analysed.

3.2.2 Experimental data

X-ray powder diffraction analyses (XRD) were performed using a Philips X'Pert diffractometer with Fe filtered cobalt Kα radiation (λ=1.7903 Å), operating at 35kV and 45 mA. Powder diffraction data were collected in the range 10º-50º (2θ) in steps of 0.05ºwith a 1 second measuring time per step. The samples were previously grinded and sieved until all the powder particles passed through a sieve of 106 microns. Afterwards, the grinded samples were deposited on a sample-holder with a flat support made of single crystal silicon transparent to Co Kα radiation. The data was collected using a X'Pert Quantify © software and the diffractograms were analysed with a X'Pert HighScore © software, which determines the background, locates peaks and identifies the minerals and phases present using the XRD cards from the International Centre for Diffraction Data Powder Diffraction Files (ICDD PDF).

As a complement to XRD analysis, thermogravimetric analysis (TG) was performed in some samples in order to obtain quantitative information about the gypsum and calcite contents. A Setaram TGA92

TG-DTA simultaneous analyser was operated in an argon atmosphere with a uniform heating rate of 10 ºC/min from room temperature to 1000 ºC. The samples, prepared as mentioned for XRD, were weighted in platinum-rhodium crucibles of 50 µl capacity in quantities that varied between 30 and 50 mg.

3.3 Results and discussion

The mineralogical characterization of the samples is summarized in Table 3.2 to Table 3.5. In spite of XRD being a method traditionally used for qualitative analyses, it is possible to distinguish with a reasonable approximation the major constituents from those that are only slightly detectable (the trace compounds).

Table 3.2 - Plaster samples - Mineralogical composition by XRD of Roman and Late Roman period

Identification	Major constituents	Minor constituents
Roman and Late Roman period		
C2, C6	Calcite	
C5, C7, C9, C11, C13	Calcite	Quartz, Feldspars
C1	Calcite, Quartz	Feldspars
C8, C12, C15, C16, C18	Calcite	Quartz, Feldspars, Dolomite (C8, C16, C18), Magnesite (C8, C16), Aragonite (C12, C15), Hematite (C8), Halite (C12)
C3, C4, C10, C14, C17	Calcite	Quartz (C4, C10, C14, C17), Diopside (C3, C4, C10), Dolomite (C3, C4), Magnesite (C4, C10), Aragonite (C14, C17), Halite (C3, C14), Barite (C4), Hematite (C14), Cristobalite (C17), Micas (C10)
CT1, CV1	Quartz, Calcite	Feldspars, Micas (CT1), Kaolinite (CT1), Hematite (CV1)
M2	Calcite	Quartz, Aragonite, Micas
M1, M3	Calcite, Quartz	Feldspars, Micas (M3), Dolomite (M3), Aragonite (M3), Hematite (M3)

Table 3.3 - Plaster samples - Mineralogical composition by XRD of Islamic period

Identification	Major constituents	Minor constituents
Islamic period		
M5, M8	Calcite	Quartz, Magnesite (M5)
M4, M6	Calcite, Quartz	Feldspars, Micas (M4), Diopside (M4), Hematite (M6)
M7	Gypsum, Quartz	Calcite, Feldspars
BS3	Calcite	Quartz, Feldspars, Aragonite
BS1, BS2	Calcite, Quartz	Feldspars, Cristobalite, Halite (BS1), Thermonatrite (BS1), Aragonite (BS2)
AG1, AG2	Calcite	Quartz, Dolomite (AG1), Magnesite (AG1), Goethite (AG2)
CS3/2, CS4	Calcite	Quartz, Gypsum, Magnesite (CS3/2),
CS21, CS22.F	Calcite	Quartz, Dolomite, Hematite (CS22.F)
CS8	Calcite	Quartz, Feldspars, Dolomite, Gypsum?
CS14, CS20/1, CS22.T	Calcite	Quartz, Feldspars, Dolomite (CS14, CS22.T), Goethite (CS22.T)
CS2/1, CS2/2, CS5, CS18/2, CS23/1	Calcite	Quartz, Gypsum, Feldspars, Maghemite (CS2/1), Aragonite (CS23/1)
CS9, CS10, CS16/1, CS18/1	Calcite	Quartz, Feldspars, Gypsum (CS10, CS16/1), Dolomite (CS16/1, CS18/1), Aragonite (CS9), Cristobalite (CS10)
CS16/2, CS19	Calcite, Quartz	Feldspars, Gypsum, Dolomite
CS6, CS7, CS15/1, CS15/2	Calcite, Quartz	Gypsum (CS6), Dolomite (CS15/1, CS15/2), Goethite (CS6), Hematite (CS15/1)
CS3/1, CS17/1	Calcite, Quartz	Feldspars, Gypsum, Magnesite (CS3/1), Dolomite (CS17/1), Chlorite (CS17/1)
CS1/1, CS1/2, CS23/2	Calcite, Quartz	Feldspars, Gypsum (CS1/2, CS23/2), Aragonite (CS1/2, CS23/2), Cristobalite (CS1/2), Diopside (CS1/1)
CS11/2, CS12	Gypsum	Calcite, Quartz, Feldspars
CS13	Gypsum, Quartz	Calcite, Hematite
CS11/1	Gypsum, Quartz, Calcite	Feldspars
TMF1	Calcite	Quartz, Gypsum, Feldspars
CB1	Calcite, Quartz	Feldspars, Hematite, Vaterite
CG5, CG7, CG9	Calcite	Quartz, Gypsum
CG3, CG4, CG6, CG8, CG10	Calcite	Quartz, Gypsum, Feldspars
CG2	Calcite	Quartz, Feldspars, Magnesite, Hematite, Hydrocalumite
CG1	Quartz, Calcite	Feldspars, Dolomite, Magnesite, Hematite

Table 3.4 - Plaster samples - Mineralogical composition by XRD of Low Middle Age-Renaissance period and Baroque period

Identification	Major constituents	Minor constituents
Low Middle Age - Renaissance period		
CG11	Calcite, Quartz	Gypsum, Feldspars
CC1 to CC7	Gypsum	Quartz, Anhydrite (CC5?, CC7), Calcite (CC5?, CC6?)
LC1	Calcite	Quartz, Feldspars
IB1	Calcite	Quartz, Gypsum
Baroque period		
CvS1	Calcite	Quartz, Feldspars, Dolomite
IM1	Quartz, Calcite	Barite, Feldspars
CSM1	Calcite	Quartz, Feldspars, Magnesite
SP1	Gypsum	Calcite, Quartz, Celestine, Feldspars
SP3	Calcite, Gypsum	Quartz, Feldspars, Anhydrite, Barite
SP4	Gypsum, Calcite	Celestine, Feldspars, Anhydrite, Quartz
LC2	Calcite	Quartz, Feldspars
LC3	Calcite	Gypsum, Quartz, Feldspars
LC4	Calcite	Quartz, Gypsum
CP1	Calcite, Gypsum	Dolomite, Quartz
CP2	Gypsum	Dolomite
CP3	Calcite, Gypsum	Dolomite, Quartz
CSA1	Calcite, Gypsum, Hydrocalumite	
PRM1	Calcite	Quartz, Gypsum, Feldspars
PRM2	Calcite	Gypsum, Quartz, Diopside, Feldspars
PRM3	Calcite	Gypsum, Quartz, Aragonite
IVF1	Calcite, Quartz, Gypsum	Feldspars, Micas, Dolomite, Hydromagnesite
IVF2	Calcite, Gypsum	Aragonite, Quartz
SC1	Calcite	Magnesite, Feldspars, Dolomite, Hydrocalumite, Gypsum, Quartz
CV2	Calcite, Quartz	Aragonite

Table 3.5 - Plaster samples - Mineralogical composition by XRD of Post-Baroque period

Identification	Major constituents	Minor constituents
Post-Baroque period		
SA1/1, SA1/2	Calcite	Gypsum, Quartz, Feldspars, Dolomite (SA1/2), Magnesite (SA1/2)
CT2/1, CT2/2	Gypsum, Calcite	Quartz, Dolomite (CT2/1)
PBS1	Calcite, Gypsum	Quartz
PBS2	Gypsum, Calcite	Quartz, Anhydrite
PBS3	Gypsum	Anhydrite
ERR1	Calcite, Quartz	Feldspars, Hematite, Aragonite
ERR2	Quartz, Calcite, Feldspars	Gypsum
ERR3	Gypsum, Calcite	Celestine, Quartz
ERR4	Calcite, Gypsum, Feldspars	Celestine, Quartz
IS1/1, IS1/2	Calcite, Gypsum	Quartz, Halite
PB1, PB6/2	Gypsum, Calcite	Feldspars, Quartz, Anhydrite (PB1), Celestine (PB6/2)
PB3, PB4, PB6/1	Gypsum, Calcite	Celestine (PB3, PB6/1), Quartz (PB4, PB6/1), Anhydrite (PB3)
PB2, PB6/3	Gypsum	Feldspars (PB2), Anhydrite (PB2), Quartz (PB2), Celestine (PB6/3)
PM1	Gypsum, Anhydrite	Quartz
PM2	Gypsum	
PM3	Gypsum, Calcite	Quartz, Anhydrite
PM4	Gypsum, Calcite, Quartz	
PM5/1, PM5/2	Calcite, Gypsum, Quartz	Feldspars
EDB1	Calcite, Gypsum	Quartz
EDB2	Calcite	Gypsum, Quartz
EDB3	Quartz, Calcite	Rutile, Gypsum
ISF1, ISF2	Gypsum, Calcite	Feldspars, Quartz, Dolomite (ISF1)
PE2/1	Gypsum, Calcite	Feldspars
PE1/1, PE1/2, PE2/2, PE4/1	Gypsum, Calcite	Quartz, Anhydrite (PE1/2, PE2/2), Feldspars (PE1/1, PE1/2)
PE5/1, PE5/2, PE5/3	Calcite, Gypsum	Quartz, Halite (PE5/1, PE5/3), Feldspars (PE5/3), Aragonite (PE5/3)
PE4/2	Gypsum, Anhydrite	Hematite
EG1, EG2, EG3, EG4, EG5/1	Calcite, Gypsum	Quartz, Feldspars, Anhydrite (EG2, EG4, EG5/1)
EG5/2	Gypsum, Calcite	Quartz, Feldspars, Anhydrite
EBR1	Calcite, Gypsum	Anhydrite, Quartz, Feldspars
EBR2/1, EBR2/2	Calcite, Gypsum	Kaolinite, Quartz, Feldspars, Anhydrite (EBR2/2), Talc (EBR2/2)
EBR3	Gypsum, Calcite	Quartz, Feldspars
CTF1	Gypsum, Dolomite	Calcite, Quartz, Talc
CTF2, CTF3	Gypsum, Calcite	Dolomite, Quartz, Feldspars, Talc, Portlandite (CTF2), Magnesite (CTF2), Kaolinite (CTF2), Weddelite (CTF3)
EAL	Gypsum, Calcite	Quartz, Anhydrite

The results allowed the mineralogical compositions of the Portuguese interior plaster coatings in the historical periods studied to be determined, with the exception of the Low Middle Age-Renaissance period, due to the insufficient number of samples collected. Figure 3.5 shows the evolution of the mentioned composition throughout those periods in relation to the predominant binder (i.e. the binder with the greatest content).

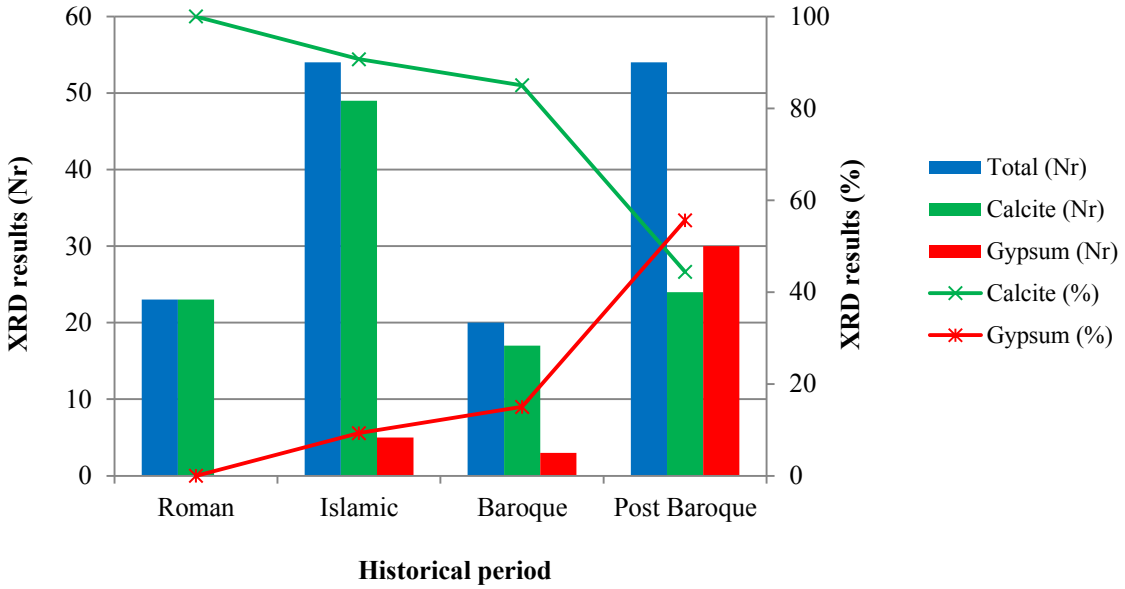

Figure 3.5 - Predominant binder used in the historical periods studied

3.3.1 Roman and Late Roman period

Twenty-three samples dated between the centuries 1st B.C. and 7th A.D. belonging to four archaeological sites were collected and analysed.

Their manipulation and visual observation revealed, in general, a high matrix cohesion, which explains the good state of conservation of most of them (Figure 3.6). XRD results show that they have been manufactured with calcitic air lime, as calcite is the unique constituent resulting from a binder reaction (Figure 3.7).

Five samples had also quartz, which can be explained by the use of fine aggregates; in all the others the presence of aggregates was not detected, meaning they have not been used at all or they consisted of very fine limestone particles, not distinguishable from carbonated lime using XRD.

Previous studies on the composition of Roman mortars in several archaeological sites of Portugal showed similar results (Santos Silva, Paiva, et al. 2006; Santos Silva, Ricardo, et al. 2006; Velosa et al. 2007; Borsoi et al. 2010), with the exception of one sample from the beginning of the edification of

the city of *Ammaia* that revealed to be a mud mortar (Cardoso et al. 2014). The presence of aggregates, or minerals associated to them, was always detected in those cases.

Even though the referred studies focused mainly other types of mortars - masonry/joint mortars, foundation/pavement mortars and rendering solutions for hydraulic structures - it is significant that the binder used was always the same, irrespectively of the mortar's function. So far, the assumptions of some scientific communities on the use of gypsum plasters since that period are not confirmed (Vieira 2002; Silva 2005).

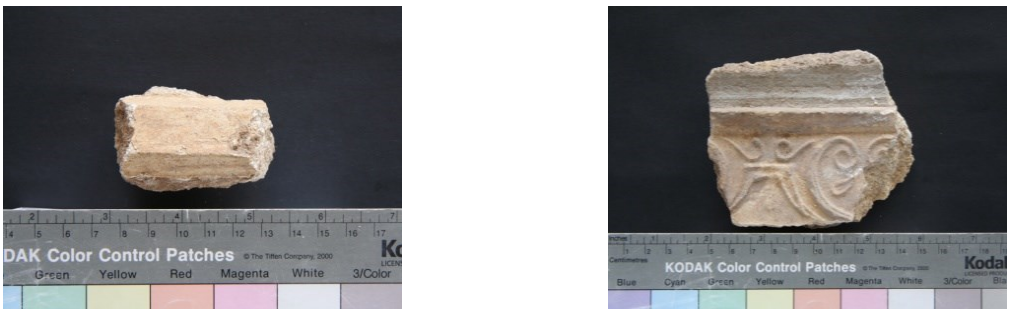

(a) (b)

(c) (d)

Figure 3.6 - Samples from the Roman period: (a) C6, House of the Fountains, *Conímbriga*; (b) C9, *Thermae, Conímbriga*; (c) CT1, *Trindade* College, *Coimbra*; (d) CV1, Fortress's square, *Cacela Velha*

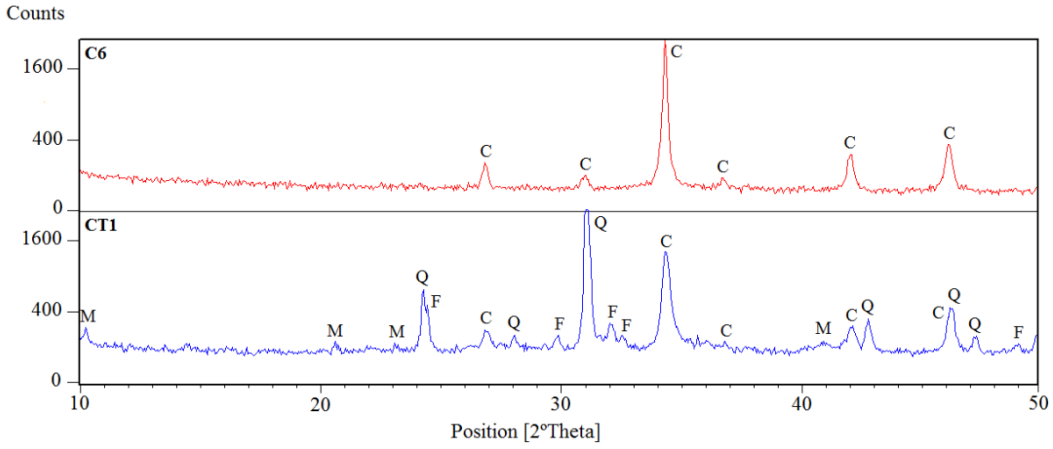

Figure 3.7 - Diffractograms of the samples C6 and CT1. Notation used: C - Calcite, Q - Quartz; F - Feldspars, M - Micas

Another important feature underlined by all authors is the quality and durability of the mortars analysed. This is not surprising considering that Romans were known for their outstanding skills in working lime and the careful procedures they used in the production of lime mortars (from the choice of raw materials to their mix and application) (Álvarez Galindo et al. 1995). In *Ammaia*, for example, the calcitic binder used was not correlated to the local geology. The authors think this is possibly due to the dolomitic content of the local calcareous formations, a fact that, if confirmed, is an evidence of the importance given to the quality of the materials used in the composition of Roman mortars.

Up to now, the results from the Portuguese characterization studies follow the trend of most other Roman archaeological sites located in countries like Spain (Robador et al. 2010), Italy (Miriello et al. 2010), Greece (Papayianni et al. 2013) or Turkey (Miriello et al. 2011), to mention only some. The few exceptions to the use of aerial lime binder seem to be related with geographic restrictions, as it is the case of *Pollentia*, situated in the Spanish island of Mallorca (Genestar et al. 2006), where the binder used was hydraulic lime.

3.3.2 Islamic period

The historical period of the Islamic occupation left a stronger imprint in the south of Portugal (Figure 3.1), which conditioned the geographical location of the case studies presented.

Forty-five samples of wall plasters (Figure 3.8) dated between the 9th and the 13th centuries were collected. As some had more than one layer, a total of fifty-four XRD analyses were performed (Table 3.2). The results obtained showed that lime was used in fifty cases, sometimes mixed with quartz aggregates.

Gypsum was detected as major constituent in samples from the citadels of *Mértola* (M7), and *Silves* (CS11, CS12 and CS13) (Figure 3.9) alone or together with quartz aggregates (M7 and CS13). In the case of CS11/1 a small addition of calcite was also detected. Considering its thickness (> 20 mm) it probably corresponds to a mortar used to even the support before the application of the gypsum thin finishing coat CS11/2.

Similar results were obtained in a study of ancient plasters from important constructions (convents, churches and palaces) in Mallorca, Spain, where two of the smooth surface' samples from the Islamic period (10th - 12th centuries) were also mainly composed of gypsum (with very small additions of lime) (Genestar & Pons 2003).

(a) (b) (c)

Figure 3.8 - Samples from the Islamic period: (a) TMF1, *Martim Fartos's* Lane, *Loulé*; (b) M7, Citadel, *Mértola*; (c) CS11, Citadel, *Silves*

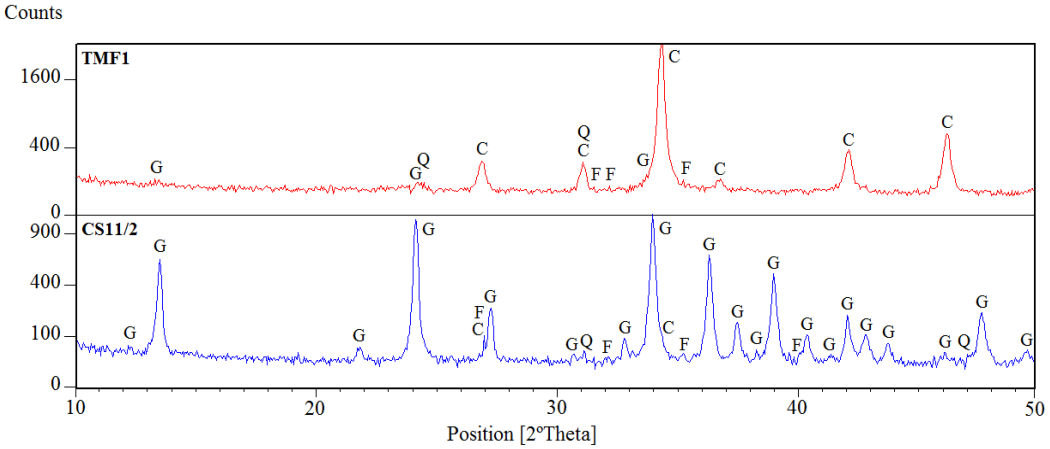

Figure 3.9 - Diffractograms of samples TMF1 and CS11/2. Notation used: C - Calcite; G - Gypsum; Q - Quartz; F – Feldspars

The presence of gypsum in samples from the Islamic period agrees with a previous characterization study of Roman and Islamic mortars from *Mértola* performed in the National Laboratory of Civil Engineering in 2006 (Report LNEC 200/2006 - DM/NMM), in which gypsum was identified in a sample from the decorative wall plaster of the *Mirhab* of the old Mosque (presently the town Mother Church). The presence of aggregates, or minerals associated to them, was also detected in very small quantities.

It also agrees with the statements of the archaeologists responsible for the works at *Silves* that the multiple fragments of richly decorated and relief elements found were made of gypsum (Gomes 2003). However, these statements did not have until now an analytical support and seem to have been exclusively based on historical comparative analyses. In fact, the referred fragments were part of the decorative arches and ceilings of the courtyard of a house denoting the high social status of their owners and built during the *Almoada Period* in *Silves*. Its architecture presented many similarities with

several contemporary structures of the south of the Iberian Peninsula (*Al-Andalus*, during the Islamic occupation, (Figure 3.10)), namely *Murcia*, *Granada* and *Malaga* (Gomes 2003; Rúbio Domene 2011). Similarities between the decorative patterns of the referred arches and those from the *Mirhab* of the old Mosque of *Mértola* (Gomes 2003) are also emphasized.

As stated before, the use of gypsum in the Portuguese architecture is always somehow unexpected due to the scarcity of sources of raw material. In the specific cases mentioned, a strong argument can be the influence generated by the intense relation and trade that existed between the several kingdoms of the *Al-Andalus,* equally observed in many other architectural aspects (defensive constructions, for example) or daily life objects (like ceramics) (Simões de Abreu et al. 2008).

Figure 3.10 - The Iberian peninsula in the beginning of the 10th century (Mattoso 1985)

An important question is therefore the origin of the gypsum used both in *Mértola* as in *Silves*. In the south of the territory there are some geological formations (Zbyszewski & Almeida 1964), but the information available presently indicates that their purity and particularly their whiteness is not in agreement with the colour of some of the samples analysed, such as CS11/2 (Graça Costa 1986). The north of Africa or the south of Spain - both very rich in high quality gypsum beds - are the most probable sources. However, the absolute need to preserve calcined gypsum away from moisture, a very difficult task to undertake by that time during its transport over long distances, leads to the assumption that probably it would be imported as raw material and processed in a place near the construction site.

In fact, documents from the 19th century recommend such procedure, namely the book from Juan de Villanueva (Madrid, 1827), where the author refers that "the calcination of gypsum should be done, when possible, on the job, or nearby: because it is better to use it soon after calcination" (cited in

Gárate-Rojas 1999), or a French treatise: "If it is not possible to use the gypsum soon after it is burnt and grinded, in countries where it is rare, and therefore gypsum needs to be brought over long distances, it is necessary to bring it in lumps and not burnt" (Rondelet, 1802: cited in Cardoso 2010). Even though these documents were written many centuries after the Islamic occupation of Portugal, it is very plausible that the procedures were the same by that time, as it happened with many other traditional construction techniques.

Such procedures involved considerable costs and were probably restricted to constructions of higher patrimonial value. In fact, up until now the presence of gypsum in constructions of the Islamic period has been detected in elements belonging exclusively to buildings that fit these requirements (Mosque of *Mértola* and houses from the citadels of the castles of *Silves* and *Mértola*).

According to the historical sources, the nobler materials used in the classical world (like stone based structures and decorations) were then exclusively reserved to monuments (Simões de Abreu et al. 2008). However, if an important man or emir from a *taifa* kingdom ordered so, an attempt was made to mimic the brightness of the capital by using very rich decorative programs, though made with more accessible building materials, as it was the case of gypsum plasters. It is then, mainly in the 11th and 12th centuries, that the use and development of alternative techniques and materials undergo stylistic creative processes of adaptation that will origin and embody the uniqueness of Andalusian art. It is also by that time that the use of gypsum plasters is more generalized in the *Al-Andalus* (Simões de Abreu et al. 2008; Rúbio Domene 2011). The traditional use of decorative surfaces to cover a poor structure (often made from rubble masonry and/or earthen binding materials) is characteristic of the Islamic architecture and a heritage from the time of the Parthians, in Iran (Gárate-Rojas 1999).

Another interesting feature related to the samples of the citadel of *Silves* is the presence of traces of gypsum in most of the lime plasters. There are two possible explanations: either gypsum was used as setting time accelerator or it is a contamination from the numerous gypsum plasters' elements found. The last one seems to be the most logical, since for centuries all these materials have been buried together and gypsum is slightly soluble in water (much more than calcite: 2.3 g/l of $CaSO_4$, at 20º C (Innorta et al. 1980) against 0.015 g/l of $CaCO_3$ (Kingery et al. 1988)).

The same can be observed in most of the samples from the archaeological excavations of *Graça's* Convent, in *Tavira* and the explanation seems to be the same, as the settlement mortar of a 15th-16th century's ceramic tile work of Moorish influence (*alicatado*) thought to have been used as pavement was found together with the Islamic material and proved to be a gypsum mortar. In spite of the previous considerations about the solubility of gypsum the samples analysed showed, in general, a good state of conservation.

3.3.3 Low Middle Age and Renaissance period

A set of ten samples available from this period represent four case studies, from the centre to the south of the country (Figure 3.1). In three of them they correspond to wall and ceiling finishing plasters (smooth surfaces) and were mainly made of calcite. The fourth case study consists of the valuable stucco decorative panels of the *Charola* of the Convent of Christ, where a group of seven samples were collected directly on site.

The XRD analyses showed that the panels' surface had already been covered by very thin (≤ 1 mm) layers of lime-gypsum plasters, probably applied with very fluid consistency in order to work as "painting" layers. The purpose of these interventions was to restore the whiteness of the original materials. However, its application was not only made over the relief elements but also over the bottom of the panels (deliberately pigmented in a bluish-dark grey to highlight the decorative language), which made its interpretation much more difficult (Figure 3.11).

(a) (b)

Figure 3.11 - *Charola* of the Convent of Christ, Tomar: (a) panels from window 1; (b) detail of a panel with and without the "painting" layers of lime-gypsum plaster

Under these "painting" layers a powdered dark grey layer of dirt covering the original materials could be seen. After cleaning it, samples were prepared for analyses and the results showed that the original panels were entirely made of high quality gypsum (Figure 3.12). Few other constituents were also detected but in such low quantities that the results were inconclusive (Report LNEC 3/2012 - DED/NRI - DM/NMM).

The origin of the panels is still not clear but the plasterers that worked there show artistic influences from the Spanish *Plateresque* and *Mudéjar*, leading Art History researchers to presume that they have been taught by the "school of Seville plasterers" (Pereira 2003). However, it is also very plausible that, if not the panels themselves, at least the gypsum and the moulds to produce them could have been originated there.

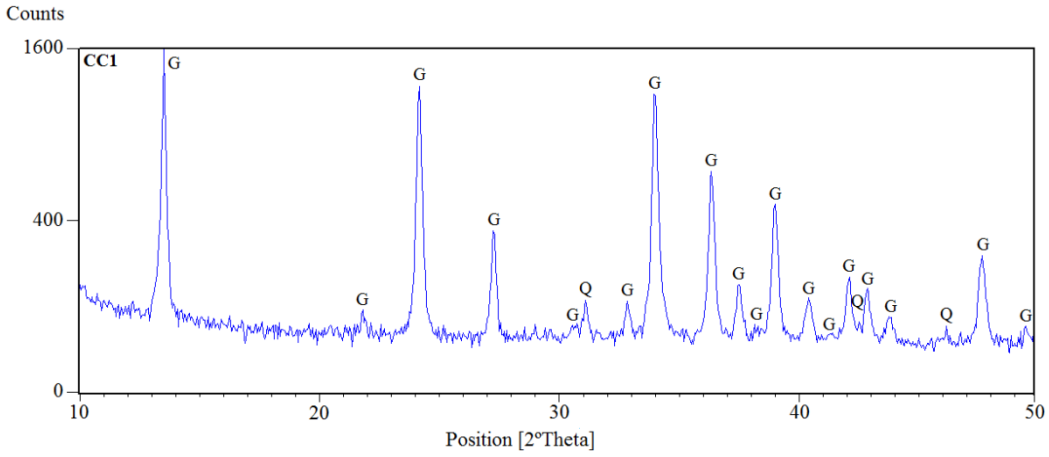

Figure 3.12 - Diffractogram of sample CC1. Notation used: G - gypsum; Q - quartz

It would be very interesting to confirm these assumptions and see if there is any relation between this case and others where the Spanish plasterers could have also had its influence. One example is the decoration of a gothic tomb from the 15th century belonging to the Knight *Rui Valente,* discovered a few years ago in the cathedral of *Faro* (Figure 3.13 (a)), which is "a funereal monument of the utmost importance (…), denoting *Mudéjar* influence" (Llera 2006) and "the first known tomb monument in Portugal to use plaster instead of stone" (Vieira da Silva 2006). The other example is the already referred *alicatado* pavement of *Tavira* (Figure 3.13 (b)). In this last case, archaeologists think that the tiles and the settlement gypsum plaster are both from the region of Seville, Spain (Cavaco & Covaneiro 2009), a fact reinforced by the intense commercial trade, military relations and artistic influences that existed then between the two regions - *Algarve* and *Andalucía* (AA.VV. 2008).

(a) (b)

Figure 3.13 - Examples of *Mudéjar* influence in Portugal: (a) 15th century tomb, cathedral of *Faro*; (b) 15th - 16th century *alicatado* pavement and corresponding settlement mortar, *Tavira*.

3.3.4 Baroque period

The mineralogical characterization by XRD was performed in twenty samples from the 17th and 18th centuries representing eleven case studies, the number of samples and of case studies being equally distributed between two types of constructions: religious and civil occupation buildings.

Calcite is the major constituent in seventeen samples, i.e. calcitic air lime was the predominant binder (Figure 3.14). However, for the first time gypsum is also present in considerable amounts in almost half of the samples, all belonging to the 18th century, and is the only binder in samples SP1 and CP2. These samples belong to elements moulded before application: SP1 are ornaments that seem to have been roughly precast and afterwards worked with tools; CP2 is a voluminous frieze moulded on a bench with sisal fibres inside (Figure 3.15).

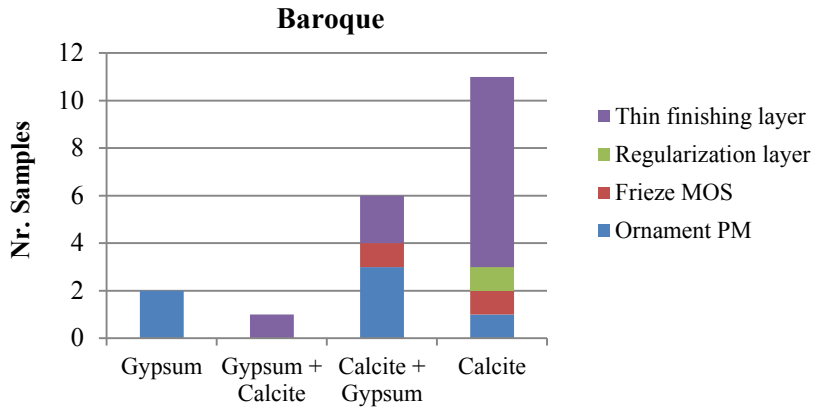

Figure 3.14 - Baroque period: type of plastered elements related to binder composition (MOS - moulded on site; PM - pre-moulded)

Out of the six samples of decorative elements analysed, only PRM2 did not have gypsum as one of the major constituents. This sample, together with CP3, IVF2 (Figure 3.15) and CSA1 belong to ornaments that have first been sculpted by hand and then attached to the support.

For this technique to perform well the plaster has to be sufficiently hard to endure the tools when sculpted but soft enough to allow the execution of delicate shapes. Such behaviour can be better achieved by using mixes of gypsum and lime since the former gives the plasters some hardness in a short time and the latter allows them to remain softer and less brittle for a longer period (Turco 2008). With the exception of PRM2, the other three samples are lime-gypsum plasters with a very similar composition (Figure 3.16).

In the group of seventeen samples where lime is the predominant compound, twelve correspond to thin layer coatings. Besides being the most logical binder to use in Portuguese mortars' composition due to the geological abundance of limestone, lime is also easier to work in this type of application allowing a much longer working time. The exception is sample SP4, a smooth surface thin layer ceiling plaster (Figure 3.15 and Figure 3.16).

The presence of quartz was detected in three samples, all belonging to very thin finishing layers (≤ 1 mm): IM1, IVF1 and CV2. However, as stated before, it is also possible that some samples have

additions of calcitic aggregates, especially those composed only by calcite.

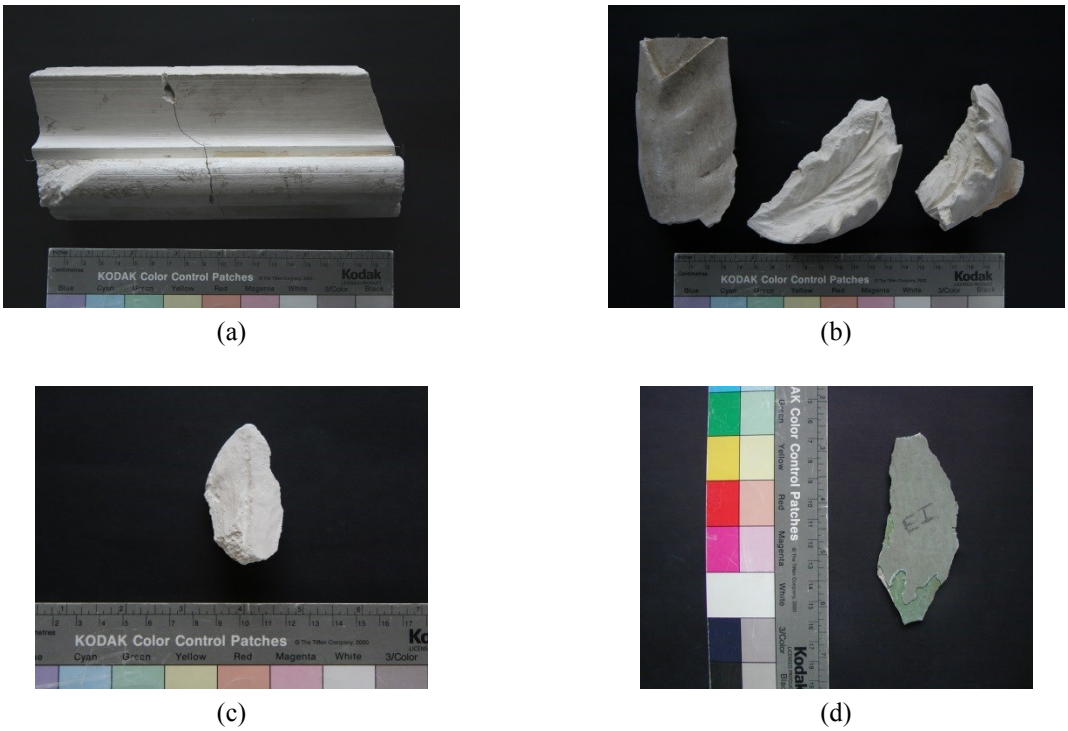

Figure 3.15 - Samples from the Baroque period: (a) CP2 and (b) CP3, *Casa de Pesca* of the Marquis of *Pombal*, *Oeiras*; (c) IVF2, *Vilar dos Frades* Church, *Barcelos*; (d) SP4, *Santíssimo Sacramento's* Chapel, *Porto*

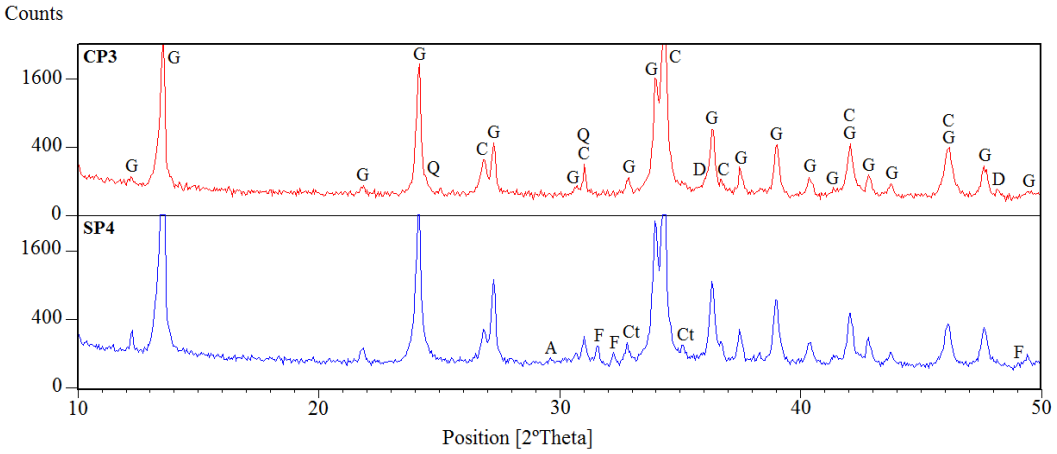

Figure 3.16 - Diffractograms of samples CP3 and SP4. Notation used: G - Gypsum; C - Calcite; Q - Quartz; D - Dolomite; A - Anhydrite; F - Feldspars; Ct – Celestine

Similar results have been obtained by Genestar & Pons (2003)on the already referred study of ancient finishing smooth surface thin layer plasters from Mallorca, belonging to several periods (10th -12th centuries, 14th century and 17th century), where only two of the nineteen samples analysed had gypsum as the main binder. Those two samples were from the Islamic period.

3.3.5 Post Baroque period

Forty-one samples belonging to fourteen buildings from the 19th to mid-20th centuries were collected. As some had more than one layer, a total of fifty-four XRD analyses were performed (Table 3.2). Gypsum was the predominant compound detected in 30 diffractograms, either used alone or together with calcite. The binder composition of the samples related to the type of plastered elements they correspond to is presented in Figure 3.17 and some of the samples analysed are shown in Figure 3.18.

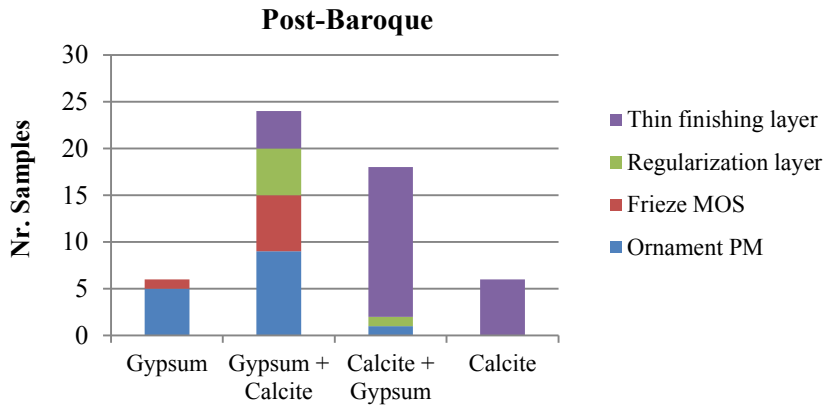

Figure 3.17 - Post Baroque period: type of plastered elements related to binder composition (MOS - moulded on site; PM - pre-moulded)

The careful analysis of Figure 3.17 allows concluding that most of the samples where gypsum is the predominant compound correspond to pre-moulded (PM) or moulded on site (MOS) decorative elements. As seen in Figure 3.14 , in the Baroque period calcitic air lime was still the most used binder, even in this type of elements, meaning that the use of gypsum plasters in the Portuguese architecture was only fully implemented in the 19th century.

Though less expressive, the so-called regularization layers used to prepare the surfaces before application of these elements were also mainly gypsum-calcite plasters, sometimes with aggregates mixed (PM4).

Contrarily, in the group of twenty-four samples of lime-based plasters, twenty-two correspond to thin layers, either smooth surfaces or friezes' finishing coatings, confirming that lime was the chosen binder for this kind of applications. However, it was only used alone in five samples: SA1, EDB2, EDB3, ERR1 and ERR2, the last three with some quartz or feldspar, probably incorporated as aggregates. All the other samples have gypsum in their composition.

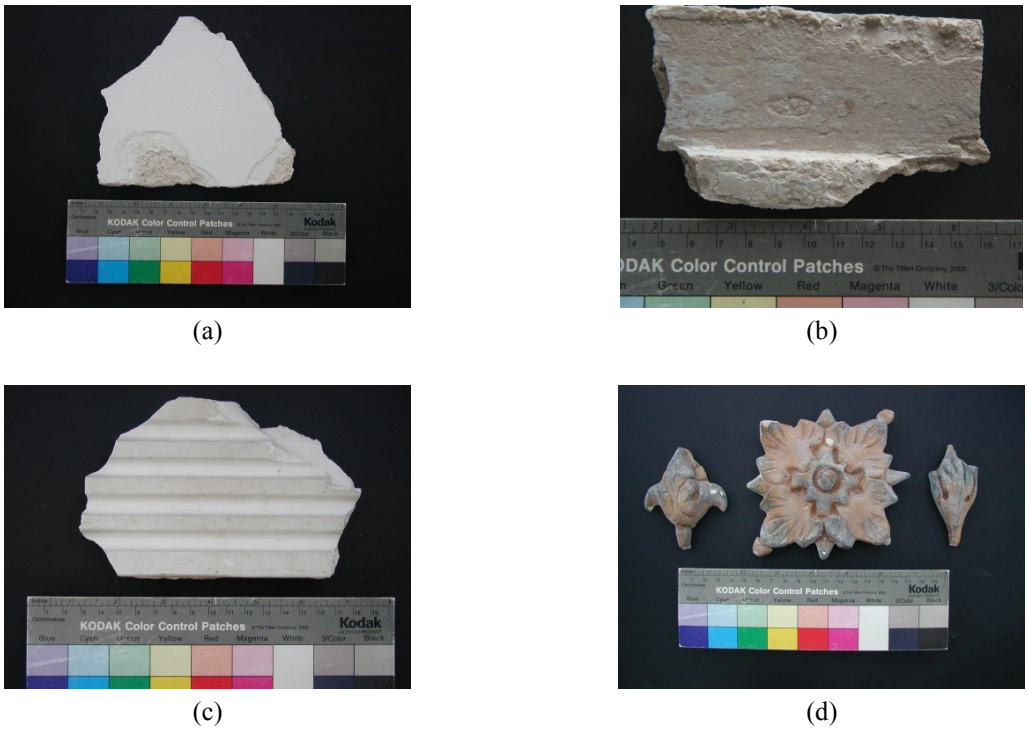

(a) (b)

(c) (d)

Figure 3.18 - Samples from the post-Baroque period: (a) PBS1, *Barão Salgueiro* Manor house, *Leiria*; (b) PM1, *Monserrate* Palace, *Sintra*; (c) EBR3, *Beira Rio* building, *Leiria*; (d) CTF1, Cine-Theatre, *Fafe*

Considering that gypsum expands when setting and lime shrinks, the combination of the two materials has a "compensation" effect, avoiding high volume variations and making it possible not to use aggregates when they are mixed together. Likewise mentioned for the Baroque period, a relation can be established between the proportions of gypsum and calcite used to prepare the plasters and their purpose/technique of application. In this case, the compensating effect is the balance between workability and hardness (Turco 2008). The main reason to avoid the use of aggregates is achieving smoother surfaces, a requirement in accordance with the most demanding aesthetic standards of the Post-Baroque period.

Another interesting observation is the presence of anhydrite as major constituent in two samples used with the purpose of simulating decorative stones: PM1 (marble) (Figure 3.18 (b) and Figure 3.19) and PE4/2 (imperial red porphyry) (Freire et al. 2009). They both seem to be denser and harder than the other samples. In fact, the presence of anhydrite in significant quantities is evidence that the gypsum was calcined at higher temperatures, probably already with the aim of producing stronger materials, as the mixes with anhydrite require much less water to be prepared than those with calcium sulfate hemihydrate. They also have better workability and longer setting (Wirsching 2005; Turco 2008).

In the case of sample PE4, a voluminous frieze, it was clearly moulded on a bench and its internal structure is made of a thick layer of gypsum plaster (PE4/1), sisal fibers and an iron wire. Only the

finishing layer (PE4/2), with 5-15 mm thickness, simulates the decorative stone imperial red porphyry. PM1 is a stone like skirting board moulded directly on site.

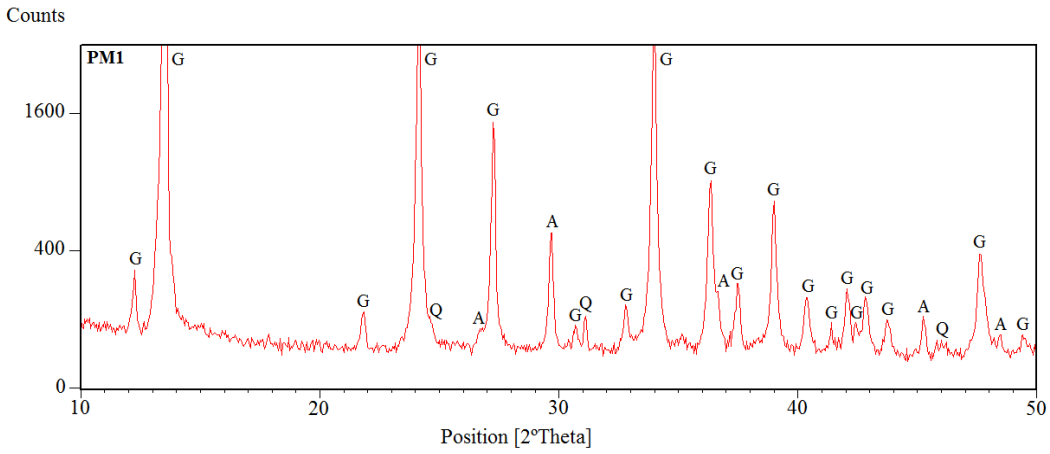

Figure 3.19 - Diffractogram of sample PM1. Notation used: G - gypsum; A - anhydrite; Q - quartz

3.3.6 Minor constituents

The residual constituents detected in almost all samples (Table 3.2) can give additional information, like the origin of the raw materials, the exposure to weathering conditions or the use of pigments and painted layers. Traces of other compounds, like quartz and feldspars, are usual in the earth's crust so they are considered to be impurities and their detection has no special meaning.

The presence of aragonite and vaterite, both polymorphs of calcium carbonate, are due to the occurrence of calcite dissolution-recrystallization phenomena (Santos Silva et al. 2011), while halite is mainly attributed to the action of saline water or saline soils and to salt spray maritime environment. In this work only the first two could have been influential.

On the opposite, celestine is a mineral often associated with gypsum deposits and can give important clues on studies of the raw materials' origin. The samples where celestine was detected in this preliminary study are all from case studies located in the city of *Porto*, independently of their date of construction (18th, 19th or 20th centuries). The same observation has been made during a study about gypsum preparatory layers of Portuguese gilded altarpieces from the 17th and 18th centuries (Cardoso, I. P., Personal Communication, 2006) in samples from the northern region of the country. However, such compound has also been found in a sample from *Estoi* Palace after using a multi-analytical approach (*cf.* Chapter 4, "SEM-EDS and PLM observations" section) and in samples from the calcium sulphate-based preparatory layers of a group of 16th century paintings from the *Alentejo* region (Melo et al. 2014), leading to suppose that it is not only in gypsum used in the north that this constituent is present.

Hematite and goethite were detected in samples with a reddish colour and its origin could be either an impurity of the raw materials or a deliberate addition, as it is clearly the case of sample PE4/2. Talc is present in samples from two case studies of the 20th century and is probably due to a contamination coming from the painting layers covering their surfaces.

3.4 Conclusions

The mineralogical study by XRD of Portuguese plasters since the Roman occupation of the territory showed that aerial calcitic lime was the main binder used until the 19th century, when gypsum definitely became important. This agrees with the abundance of high quality limestone and lack of gypsum beds in Portugal.

However, it is noticed that the traditions deep rooted in the different cultures associated with the various periods also had an influence, as in the case of constructions of higher heritage status in the Islamic period where the presence of gypsum has been detected.

The introduction of the Islamic decorative language in the Iberian Peninsula evolved to different forms of art in architecture, of which the *Mudéjar* and *Plateresque* styles are two important examples, an influence that persisted until the Renaissance period.

With the Baroque style the importance given to decorative arts in architecture widely increased and gypsum started to be more used, even though associated with lime and mainly for the manufacture of decorative elements.

It was only in the 19th century that gypsum topped lime. However, the later continued to be the main binder in the composition of plasters for thin layer applications, a practice that proved to be common to all the historical periods studied.

The use of aggregates, namely quartz, seems to be less frequent in the finishing plaster layers than in mortars used with other purposes. This trend has been accentuated throughout the centuries, and is almost inexistent in the Baroque and Post Baroque periods. The possibility of the existence of aggregates of calcitic origin, not distinguishable from carbonated lime using XRD, has always to be considered in the cases where calcite was present.

These facts allowed starting to build the first reliable database on Portuguese historical plasters composition and to establish a clear relationship with their purposes/techniques of application, in which the geographical location within Portugal seemed to have no influence.

4

The Portuguese gypsum and gypsum-lime based plasters from the 18th to the 20th century: Analytical characterization

4.1 Introduction

The introduction of decorative gypsum based plasters in the Portuguese architecture was partly due to the arrival in the 18th century of two Italian artists to *Porto* and Lisbon: the architect *Nicolau Nasoni* (Vasconcelos 1991, 1997) and the plasterer *Giovanni Grossi* (Silva 2005).

They had a strong and indelible influence on the expression of the Baroque and Rococo styles, attested by the huge number of high-quality works authored by them and/or their disciples. Whereas in the 18th century the era of industrialization had not yet arrived, this assumes a paramount importance.

Grossi, in particular, had a privileged position: he arrived in Portugal in 1748, few years before the earthquake of 1755 that almost destroyed Lisbon (Silva 2005). After the catastrophe the need to quickly rebuild the city created an extraordinary opportunity to disseminate his art.

Alongside *Grossi*, several other Italian masters worked in Lisbon, namely *Gomassa*, *Chantoforo* and *Toscanelli*, constituting the first generation of plasterers to work there. However *Grossi* has always been the most influential (Silva 2005).

Between 1764 and 1777 he was responsible for the "Class of Plaster" (*Aula do Estuque*), established by the Marquis of *Pombal*, where he taught young apprentices on his craft. Since 1773 that some of them were considered qualified to perform works in stucco. Those that had their education in the "Class of Plaster" or contacted directly with *Grossi* can be clearly identified by Art History specialists, not only through the decorative language they used but also due to their "great mastery of technique, which implied a thorough knowledge of the rules of perspective and of the composition of plasters" (Silva 2005). They left magnificent works in Lisbon and throughout the country.

The prominent place given to the decorative arts in the Baroque period proceeded into the 19th century, with inspirations based on old artistic styles, originating the "Neo" currents and movements (Leite et al. 2008; Arruda et al. 2008).

In what concerns the architectural heritage, some important testimonies of Moorish influence arose in the mid-century, with two of the most emblematic case studies being presented in this work: the Arabian Room of the *Bolsa* Palace, in *Porto*, and the *Monserrate* Palace, located in *Sintra*.

In both cases the decoration of walls and ceilings was mainly based on gypsum plasters and was executed by the Portuguese plasterers *Luís Pinto Meira* and *Domingos Meira*, respectively, both coming from a small village in the north of Portugal called *Afife* (Mendonça 2012).

Besides *Monserrate*, *Domingos Meira* was responsible for the decoration of several other important constructions throughout the country, namely the *Estoi* Palace, located in the Algarve, another case study presented in this work. *Meira* was considered the most important Portuguese plasterer of the second half of the 19th century (Mendonça 2012).

The fashion based on historicist revivalisms, where Paris remained the guiding beacon of the arts of decoration, proceeded into the first decades of the 20th century though slowly changing to a smaller scale. Other styles with softer lines and much simpler decorative programs, like *Art Nouveau*, were also introduced in Portugal by that time under the influence of some architects. *Ernesto Korrodi*, whose work is represented here in two case studies, was one of them: he authored the project of the *Beira Rio* building and influenced the design of the *Garage* building, both located in the city of *Leiria*. He was also the author of other important works from the north to the south of Portugal (Verdelho da Costa 1997).

In order to study the materials and techniques of application used in that period of almost two centuries (from the second half of the 18th century to the first decades of the 20th), a mineralogical, physical and mechanical characterization was performed in 33 original samples corresponding to 44 distinct materials/components, from smooth surfaces to decorative elements, all in rather good conditions. The samples belong to 11 case studies representing several types of buildings (either of patrimonial value or of common use, both with architectural interest) and comprising different geographical locations throughout Portugal (Figure 4.1).

Some compositional patterns have been detected. They are related with the way the materials were applied: the smooth surface coatings are the richest in air lime, the precast elements are mainly composed of gypsum and the elements moulded on site usually result from a balanced mixture of these two binders.

The characterization work performed and the results obtained are detailed in this chapter.

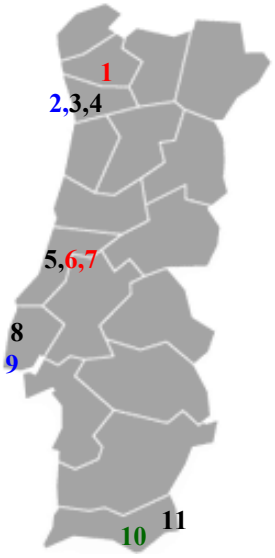

North
1. *Fafe* - Cine-Theater, 20th century
2. *Porto* - Cathedral, *Santíssimo Sacramento's* Chapel, 18th century
3. *Porto* - *Restauração* Street building, 19th century
4. *Porto* - *Bolsa* Palace, 19th century

Centre
5. *Leiria* - *Barão Salgueiro* Manor house, 19th century
6. *Leiria* - *Garage* building, 20th century
7. *Leiria* - *Beira Rio* building, 20th century

Center-South (Lisbon area)
8. *Sintra* - *Monserrate* Palace, 19th century
9. *Oeiras* - *Casa de Pesca*, Marquis of *Pombal*, 18th century

South
10. *Estoi, Faro* - *Estoi* Palace, 19th-20th centuries
11. *Tavira* - Church of the former Convent of *S. Francisco*, 19th century

Figure 4.1 - Geographical location of the case studies

4.2 Experimental work

4.2.1 Analytical procedure

The mineralogical and chemical properties of the samples were determined using the analytical methodology developed by Santos Silva et al. (2006).

The analytical characterization started with a photographic recording followed by a detailed visual observation, sometimes assisted by a stereo-zoom microscope, in order to register information about the presence, type and shape of aggregates, additions (like fibres) and pigments, and the number of layers of the finishing coat.

Afterwards, the samples were dried at 40 ºC for approximately 12 h, to enable the detection of potential hygroscopic compounds or soluble salts, whose crystalline structure could be damaged if samples were dried to constant mass.

Each specimen was then split into several fractions to be used in the various techniques (Figure 4.2).

In order to study the textural properties of the layers in the samples (stratigraphy) and to identify the mineralogy and morphology of the aggregates and possible pigments, fragments of the samples were prepared by impregnation under vacuum with an epoxy resin, followed by a precision cut and polishing procedures. The polished surfaces obtained were observed with the stereo-zoom microscope and images were recorded digitally (Figure 4.3 and Figure 4.4).

(a) (b)

Figure 4.2 - Sample ISF1: (a) as it arrived on the lab; (b) divided in several fragments

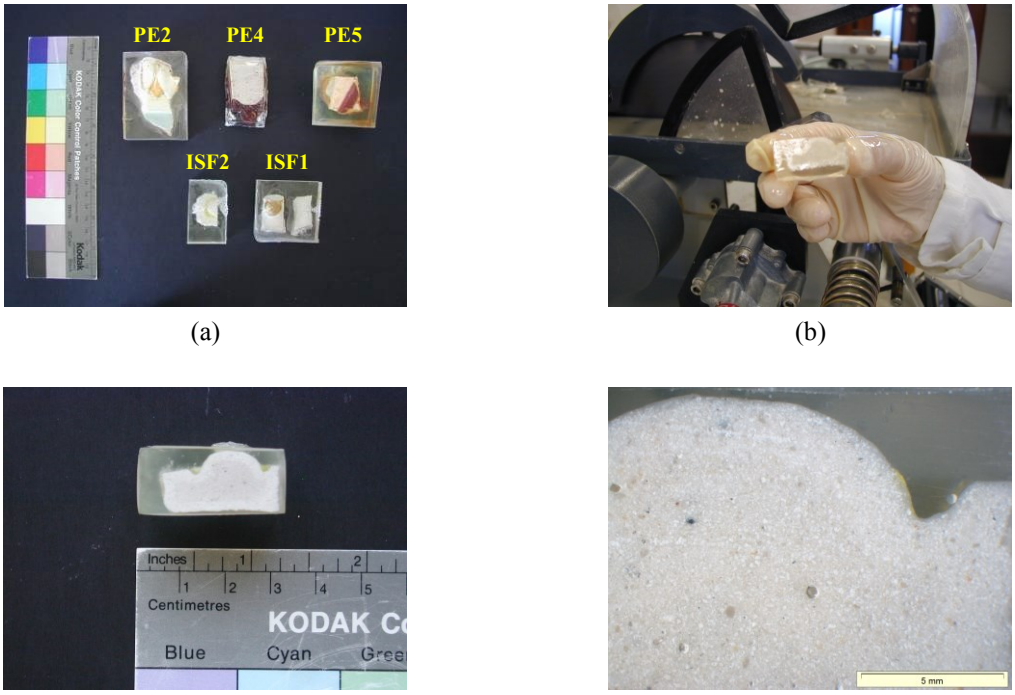

(a) (b)

(c) (d)

Figure 4.3 - Preparation of polished surfaces: (a) fragments of some samples impregnated with an epoxy resin; sample ISF2 after precision cut (b) and after being polished (c); (d) stereo-zoom image of the polished surface shown in (c)

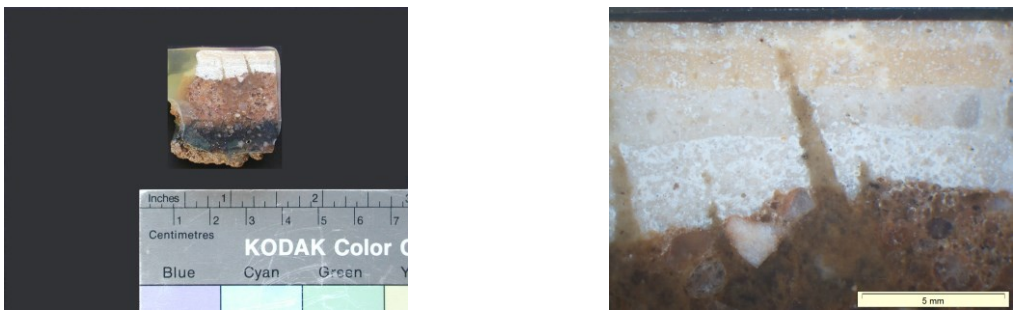

(a) (b)

Figure 4.4 - Detail of a thin-layer plaster fragment (PE5) (a) after impregnation, cut and polishing operations; (b) stereo-zoom image of the polished surface shown in (a)

X-ray diffraction analysis was performed to determine the mineralogical composition of the binder and other possible constituents such as aggregates.

The thermogravimetric and differential thermal analysis (TG-DTA) provided additional data on the quantitative composition of the samples, namely the relationship between the gypsum and carbonates contents.

Polarized light microscopy (PLM) was used occasionally to observe thin sections and help clarifying some issues related to the presence and/or morphology of aggregates as well as to determine the presence of different thermally originated phases in the matrix.

Scanning electron microscopy coupled with energy dispersive X-ray spectrometer (SEM-EDS) was used in observations of polished and fractured surfaces allowing further insight into the microstructure and crystal morphology of the matrix and provided semi-quantitative chemical analyses of individual particles and phases.

FT-IR and micro FT-IR spectroscopy analyses were performed in the samples where the presence of organic compounds was suspected.

Micro Raman was used in the different parts of the sample PE4 to search for the presence of other constituents than those obtained by XRD and TG-DTA, as well as to confirm the eventual presence of goethite, a question raised by micro FT-IR spectra.

Some physical and mechanical properties were also determined, namely water absorption by capillarity, hygroscopic behaviour, water vapour permeability, dynamic modulus of elasticity and compressive strength using test procedures often adapted taking into account the irregular shape and friability of some of the samples.

4.2.2 Experimental data

The **photographic recording** of the samples was made using either CANON 350D or OLYMPUS Camedia C-2020 Z photo-cameras.

The **optical microscopy observations** were made with an Olympus SZH stereo-zoom microscope equipped with a video camera Olympus DP20 for the corresponding image recording and an Olympus BX60 petrography microscope in transmission using crossed polarizers for the PLM observations.

X-ray powder diffraction analyses (XRD) were performed using a Philips X'Pert diffractometer with Fe filtered cobalt Kα radiation (λ=1.7903 Å), operating at 35kV and 45 mA. Powder diffraction data were collected in the range 3º-74º (2θ) in steps of 0.05ºwith a 1 second measuring time per step.

The samples were previously grinded and sieved until all the powder particles passed through a sieve of 106 microns. Afterwards, the grinded samples were deposited on a XRD sample-holder, using the back-loaded process. The data was collected using a X'Pert Quantify © software and the diffractograms were analysed with a X'Pert HighScore © software, which determines the background, locates peaks and identifies the minerals and phases present using the XRD cards from the International Centre for Diffraction Data Powder Diffraction Files (ICDD PDF).

A Setaram TGA92 **TG-DTA** simultaneous analyser was operated in an argon atmosphere with a uniform heating rate of 10 ºC/min from room temperature to 1000 ºC. The samples, prepared as mentioned for XRD, were weighted in platinum-rhodium crucibles of 50 μl capacity in quantities that varied between 30 and 50 mg.

SEM-EDS analysis at L.N.E.C. were made using a microscope JEOL JSM-6400 coupled with an OXFORD energy dispersive X-ray detector (EDS), both on polished (with backscattered electrons - BSE images) and freshly fractured surfaces (using secondary electrons - SEI images) that were previously sputtered with carbon in a JEOL JEE-4X vacuum evaporator or with gold-palladium film in a BALTEC sputter coater.

In the observations of sample PE4 at MPA Bremen a field emission scanning electron microscope (FESEM) Hitachi S 4000 coupled with EDAX detector was used.

In the case of the samples from *Bolsa* Palace, scanning electron microscopy observations of polished surfaces in BSE mode were made on a FESEM JEOL JSM-7001F coupled with an OXFORD EDS detector. These polished surfaces were also sputtered with a gold palladium film in a BALTEC sputter coater.

FT-IR spectroscopic analyses were performed at the University of Évora on a Perkin Elmer apparatus, with scan from 4000 cm^{-1} to 400 cm^{-1}, spectral resolution of 4 cm^{-1}, in transmission mode. Powdered samples were prepared, mixed with potassium bromide and placed in a pellet (KBr pellet method).

The **micro Raman** spectra were obtained in the University College of London using a Renishaw InVia Raman microscope with a diode Laser operating at 785 nm, x50 objective and the spatial resolution down to c. 1μm. The instrument is calibrated every day using a silicon pattern. The laser power was 1% and the acquisitions were made with 1 scan during 10 seconds.

The **water absorption** tests were performed using a capillary absorption by contact technique developed for irregular and/or friable samples (Veiga et al. 2004) (Figure 4.5 (a)).

After 24 h, the baskets with the samples are taken out of the vat and placed on two narrow stands in order to prevent contact with water or any other surface; the capillary absorption stops then and the drying process begins (Figure 4.5 (b)), proceeding until the test specimens achieve constant weight.

(a) (b)

Figure 4.5 - Determination of the capillary water absorption in ancient samples using a contact technique: (a) samples in a vat where water reaches the bottom of the baskets (absorption procedure); (b) baskets placed in stands outside the vat (drying procedure)

The **water vapour permeability** was determined using the method described in EN 1015-19:1998, adapted to the size of each sample (Figure 4.6). This method is based on the measurement of the water vapour flux through the sample due to the pressure differential between the internal (relative humidity approximately 100%) and the external surface conditions (relative humidity = 50 ± 5 %) at 23 ± 2 ºC The vapour flux is quantified by the weight variations of the test devices (Figure 4.7).

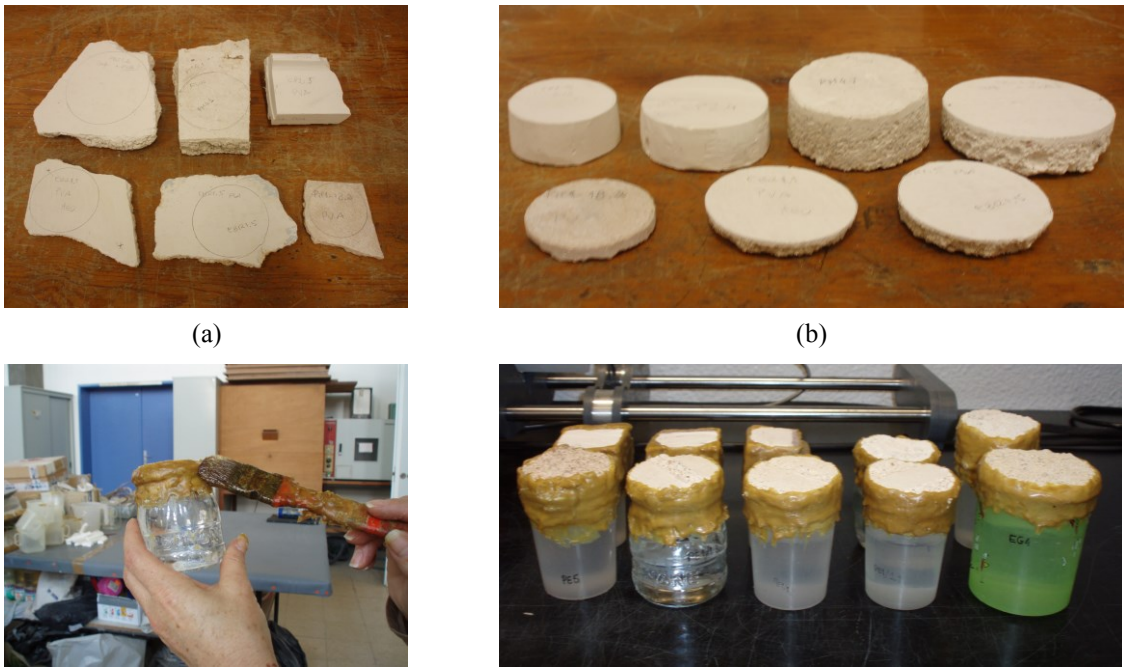

(a) (b)

(c) (d)

Figure 4.6 - Determination of the water vapour permeability in ancient samples: (a) original samples; (b) adapted test specimens; (c) application of the insulating material; (d) devices after completing the preparation

(a)

(b)

Figure 4.7 - Determination of the water vapour permeability: (a) ongoing test, in the climatic chamber; (b) weighing procedure

The procedure used to evaluate **hygroscopicity** (Magalhães & Veiga 2007) consisted on measuring the weight variations of samples previously dried at 40 ºC until constant mass and then placed in a climatic chamber at a temperature of 23 ± 2 ºC and increasing moisture conditions: 30%, 50%, 70% and 90% (adsorption conditions). The samples were kept at each moisture level until constant mass was achieved (Figure 4.8). They were then subjected to the same relative humidity levels in reverse order (desorption conditions) using the same weighing procedure.

(a)

(b)

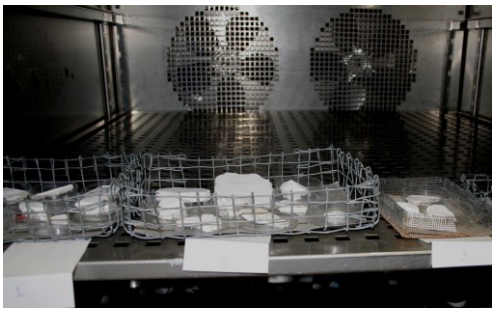

(c)

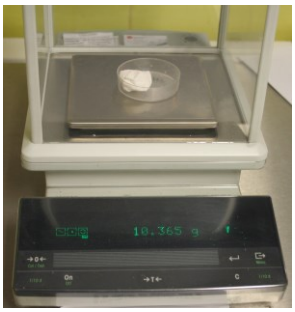

(d)

Figure 4.8 - Determination of the hygroscopic behaviour: (a) test specimens ready to start the procedure; (b) climatic chamber; (c) ongoing test inside the chamber; (d) weighing of a test specimen

It is important to notice that the study of the hygroscopic behaviour was the most difficult to perform due to the long period of time required and to the very particular and sensitive conditions of the procedure (relative humidity). It has been done in three different moments (2010, 2012 and 2014) though only two are considered in this work: 2010 and 2014 (in 2012 the climatic chamber had a breakdown and it was not possible to obtain 90% relative humidity).

The repetition of the test in some samples revealed that the adopted procedure did not have a good reproducibility in terms of quantitative values; only the curve profiles and the relative results between samples of the same case study are comparable. Nevertheless, as the most important information intended to be the determination of the curve profile and not so much the precise quantification of the hygroscopic capacity of the samples, it is considered that the main objective of the study has been accomplished: contributing to understand better the hygroscopic behaviour of these materials.

Tests to determine the **pore size distribution curves** using mercury intrusion porosimetry were based on ASTM D4404-84:2004 and carried out using the equipment FILLING APPARATUS and AUTOSCAN 60 of QUANTACHROME. The estimated uncertainty for the standard intrusion value assuming a normal distribution with k = 2 was ± 0.0168 cm^3g^{-1}.

Each sample consisted of two specimens previously grinded to granular form and dried to constant mass at 40 ºC. After that they were placed in individual bags identified with the name followed by the numeral "1" or "2" (bag 1 and bag 2, Figure 4.9) and maintained in a desiccator until testing.

At the beginning of the test procedure they were subjected to degasification for at least 30 minutes, at room temperature and using a vacuum of 50 or 60 mmHg. For the contact angle a standardized value of 140º was used in all determinations.

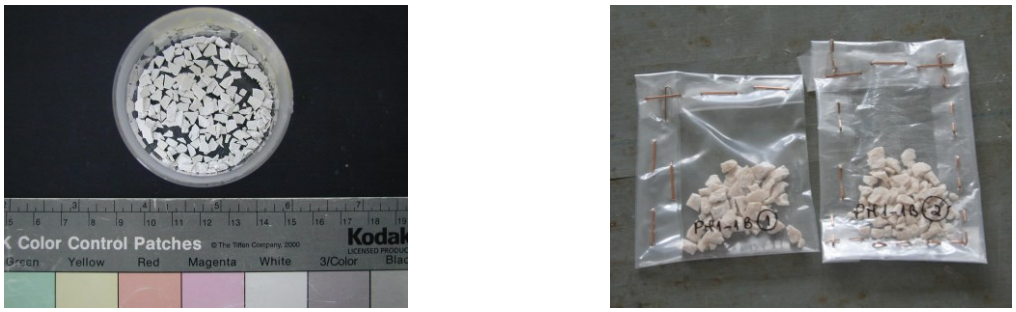

(a) (b)

Figure 4.9 - Preparation of the test specimens for mercury intrusion porosimetry: (a) sample EG4 (thin-layer plaster) before drying; (b) sample PM1 ready to be tested

The determination of the **bulk density,** needed for the calculation of the dynamic modulus of elasticity, was made using two methods adapted to the irregular shape and size of the test specimens: the *water displacement method* and the *sand method*.

The *water displacement method* is based on the measurement of the water volume variation inside a graduated cylinder immediately after the insertion of previously weighed fragments of the sample. However, this method soon revealed to be inappropriate for most of the samples because it required the use of very small fragments and a very quick measurement of the water volume variation due to the high absorption of the materials under study. Finally, this can be considered a destructive method, as the referred fragments can no longer be used in other procedures.

(a)

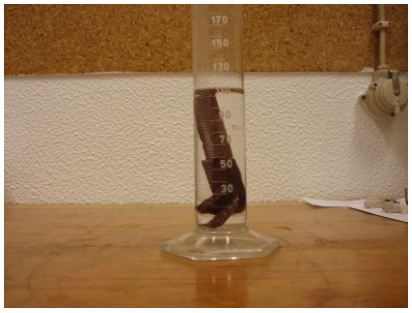

(b)

Figure 4.10 - Determination of the bulk density by the water displacement method

The *sand method* (Figure 4.11) is based on the determination of the volume of a test specimen previously dried at 40 ºC and weighted, using the bulk density of calibrated sand (reference APAS 30 from the supplier AREIPOR, previously dried at 105 ºC) according to the NP EN 1097-3:2002. The difference of weight between the metal measuring vessel with 1 litre capacity filled with "test specimen + sand" and only filled with sand is registered and the volume of the test specimen is calculated.

The sand method allows the repetition of the procedure and the use of larger test specimens without affecting their integrity.

In most of the samples where the bulk density had already been determined by the water displacement method it was not possible to perform the sand method anymore. In spite of having different quantitative results, a logical and direct relationship between both methods could be established. It is important to notice however that the error associated to the dynamic modulus of elasticity is significant in any case and the ultrasonic pulse velocity is the most reliable result.

Finally, in a few samples it was possible to use a third and more precise method based on the *weighing and measurement of the size of the test specimens* (length, width and height).

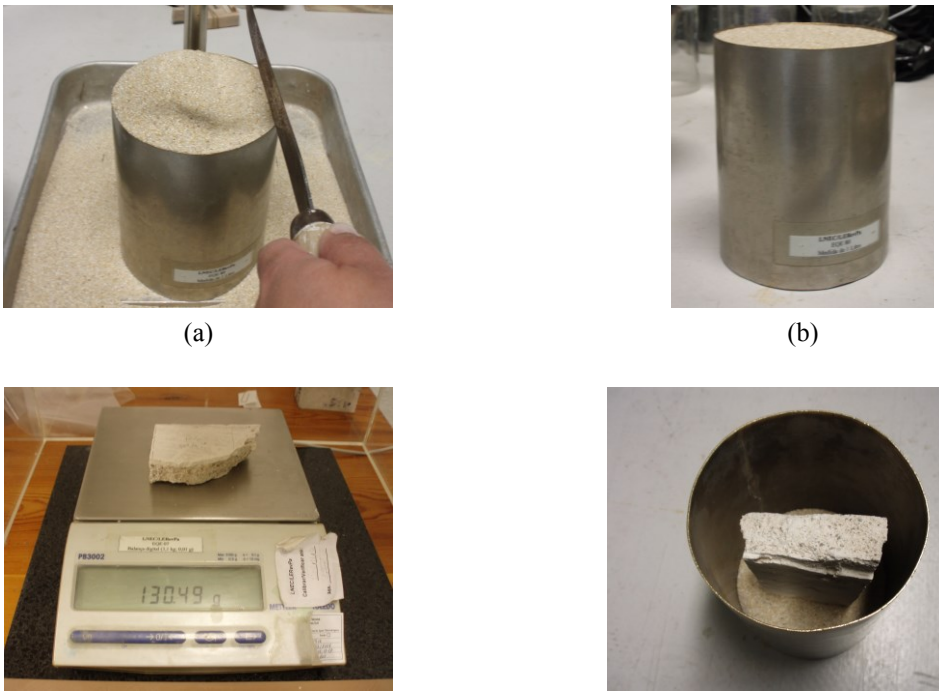

(a) (b)

(c) (d)

Figure 4.11 - Determination of the bulk density of the samples by the sand method: (a) and (b) bulk density of sand; (c) weighing of test specimen; (d) test specimen inside the vessel before the addition of sand

The **dynamic modulus of elasticity** was determined using the method of ultrasounds that is based on the measurement of the velocity of high frequency sound waves through the material under study, allowing the calculation of elastic parameters (NP EN 12504-4:2007). Special exponential probes with pointed ends were used to provide good and precisely located contact with the samples' surfaces.

(a) (b)

Figure 4.12 - Determination of the dynamic modulus of elasticity in ancient samples using ultrasound waves: (a) indirect method, probes in the same surface (superficial transmission); (b) direct method, probes in opposite surfaces (transmission through the material)

In the **compressive strength** test, an electromechanical testing device complying to the requirements of EN 1015-11, from the Spanish company Hoytom S.L., model HM-S, with a load cell of 200 kN, was used. The load rate was adjusted according to EN 1015-11 so that failure occurred within a period of 30 to 90 s; in most cases it was equal to 100 N/s and in a few cases 50 N/s, 200 N/s and 500 N/s.

The regular shape of the samples necessary for adaptation to the test device and for the calculations was often achieved through the use of a shaping mortar designed to be stronger than the samples and composed of CEM II 32.5 cement and siliceous sand with volumetric proportions of 1:3 (Magalhães & Veiga 2009; Válek & Veiga 2005) (Figure 4.13).

(a) (b)

Figure 4.13 - Adaptation of ancient plaster samples to the compressive strength test device: (a) application of the shaping mortar; (b) samples ready to be tested

This research work is focused on the plaster finishing elements. Whenever there was a pictorial layer, it was first carefully removed.

4.3 Case studies

4.3.1 18th century: the dawn of a new era for the decorative arts in the Portuguese architecture

The XRD survey presented in Chapter 0 showed that only two case studies from the 18th century, from a total of eleven, had gypsum or gypsum-lime based interior plaster coatings: the *Santíssimo Sacramento's* Chapel of *Porto* Cathedral, in the north of Portugal, and the *Casa da Pesca* (House of Fishing) of the Marquis of *Pombal* farm located in *Oeiras*, centre-south of the country (Figure 4.1).

4.3.1.1 The *Santíssimo Sacramento's* Chapel

The *Santíssimo Sacramento's* Chapel is located on the left side of the *Porto* Cathedral's presbytery. In 1707 it was expanded to the shape it has nowadays: a simple centred plant with three lateral lobes (semi-circular) and a domed roof with skylight (Ferreira-Alves 1991).

In the 18th century several interventions, mainly decorative-oriented, were performed in the Cathedral in order to adapt its Medieval structure to the new Baroque style. During one of these work campaigns, more precisely in the second half of the century, the *Santíssimo Sacramento's* Chapel was

decorated with very fine stucco motifs, Rococo style, most of them gilded, framed by walls in shades of green (Botelho & Costa 2004) (Figure 4.14).

Figure 4.14 - The *Santíssimo Sacramento's* Chapel: general view

Due to the poor condition of the plasters, in 2008 an intervention for their conservation and restoration took place, which results can be seen in Figure 4.15.

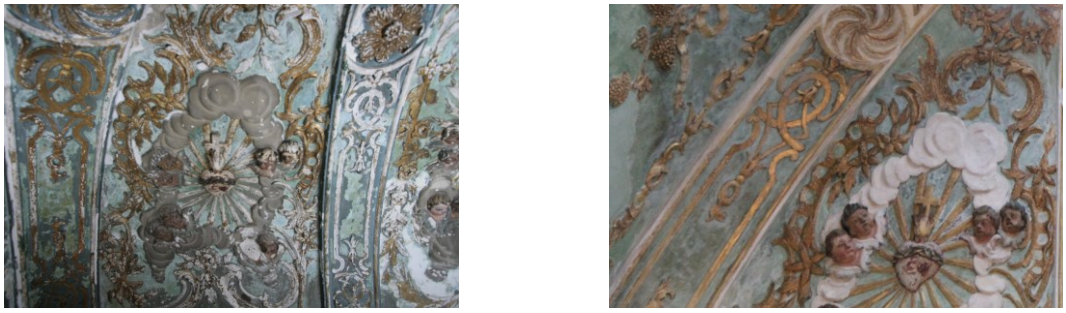

(a) (b)

Figure 4.15 - Decorative plasters of the *Santíssimo Sacramento's* Chapel: (a) before restoration; (b) after restoration

Samples

A total of five samples were collected in two ways: indirectly, meaning they had been previously detached due to some anomaly in the building (samples SP1, SP2 and SP3) and directly on site (samples SP4 and SP5).

After the first visual observation, two samples (SP2 and SP5) were rejected due to strong suspicions of not being original (Figure 4.16): in the case of SP2, a sample from the cornice of the domed roof, different finishing coatings were detected in the several fragments collected, making it difficult to establish which was (or were) the original one(s); concerning SP5, another sample from the ceiling (domed roof) but collected in a different area than SP4, it had a completely distinct colour (dark grey)

and was more friable. As in other cases along this work, whenever doubts arose about the originality of a sample, it was decided to exclude it.

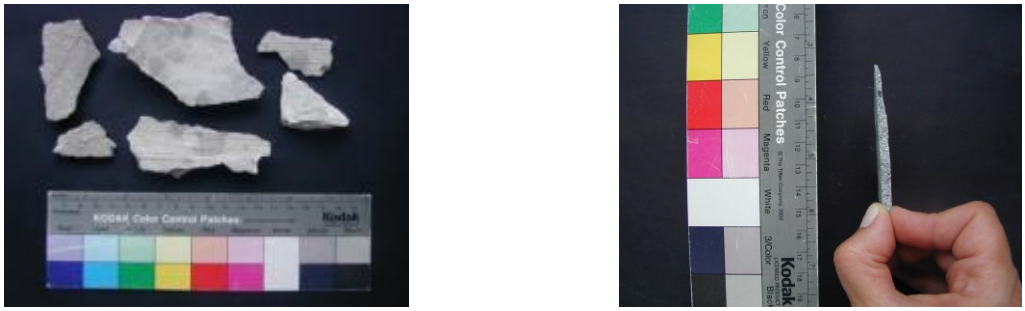

(a) (b)

Figure 4.16 - Photographs of the rejected samples: (a) SP2; (b) SP5 (side view)

The images of the samples studied are shown in Figure 4.17 and the respective identification and description are summarized in Table 4.1.

(a)

(b) (c)

Figure 4.17 - Photographs of the analysed samples from *Santíssimo Sacramento's* Chapel: (a) SP1; (b) SP3; (c) one of the fragments from SP4

Table 4.1 - Identification and description of the samples from *Santíssimo Sacramento's* Chapel

Sample identification	Description
SP1	Ornaments from the dome (gilded)
SP3	Frieze (frame) from the arch (finishing layer)
SP4	Ceiling plaster (polychrome)

Results and discussion

- Visual observation of the samples

The information obtained by visual observation of the samples is summarized in Table 4.2.

Table 4.2 - Visual observation of the samples from *Santíssimo Sacramento's* Chapel

Sample	Description
SP1	Three fragments of **ornaments** from the dome that were already detached (Figure 4.17 (a));
	Surfaces seem to have been originally gilded but show now the presence of several pictorial layers on the gild, the last one blue;
	Very hard exterior surfaces contrast with a very friable inside;
	The method used in their preparation is not clear: at first, they seemed precast but a careful observation of the surfaces indicates they have been worked/retouched with tools. A plausible hypothesis is that they have been prepared in two steps;
	The two fragments from the right (Figure 4.17 (a)) had traces of a light beige paste on their back, applied on a thin layer.
SP3	One fragment of irregular shape, approximately 10 cm long and 3 cm wide (Figure 4.17 (b));
	Composed by one thick layer (10-20 mm) of a coarse aggregate mortar (showing a high percentage of aggregates, very small wood pieces and contamination of coal) and a **thin (1-2 mm) plaster layer**, of beige colour, with much finer particles size (object of this study);
	Surface showing the presence of several beige painting layers (probably limewash).
SP4	Several fragments of the **smooth** painted **surface** from the dome;
	Consists of a plaster layer approximately 5 mm thick with several pictorial layers applied over it (Figure 4.17 (c));
	Plaster very friable on the back, becoming progressively stiffer as it approaches the opposite surface, with the paint.

It is interesting to notice that none of the decorative elements can be considered simply precast. The sample closer to that is SP1: it seems to have been roughly precast and then finished by hand, as its surface shows signs of having been worked with tools. The observation of the decorations still remaining in the chapel also shows that all the elements are different (Figure 4.15), not typical of a pure "series manufacture", as observed in most of the decorative elements of the 19th century.

- XRD results

The qualitative mineralogical composition determined by XRD showed that gypsum and calcite are the main constituents (Figure 4.18, Table 4.3).

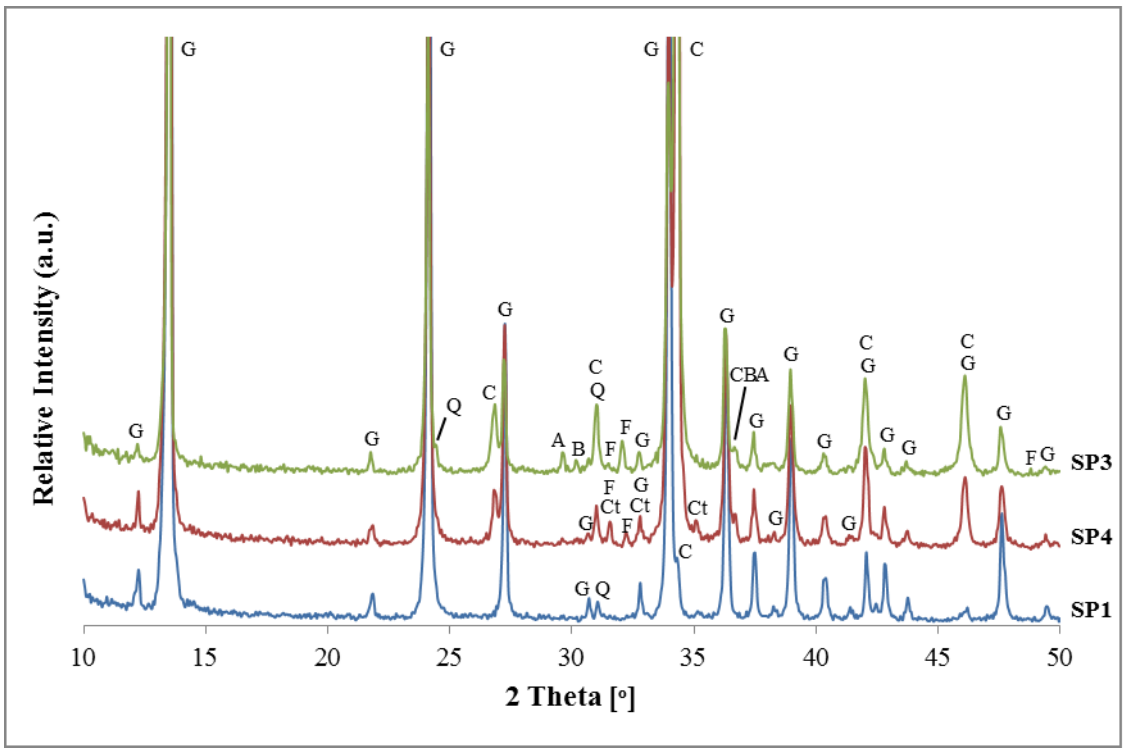

Figure 4.18 - XRD patterns of the samples from *Santíssimo Sacramento's* Chapel
Notation: G - Gypsum; C - Calcite; Q - Quartz; Ct - Celestine; A - Anhydrite; F - Feldspars; B - Barite

Table 4.3 - XRD qualitative mineralogical composition of the samples from *Santíssimo Sacramento's* Chapel

Sample	Identified crystalline compounds						
	Gypsum	Calcite	Quartz	Feldspars	Celestine	Anhydrite	Others
SP1	++++	trc	trc	trc	trc	-	-
SP3	++/+++	+++	trc	trc	-	trc	Barite (trc)
SP4	+++	++/+++	trc	trc	trc	trc	-

Notation used in XRD peak analysis:

++++	Very high proportion (predominant compound)	+	Weak proportion
+++	High proportion	trc	Traces
++	Medium proportion	-	Not detected

Traces of other compounds (impurities) were also found, namely quartz and feldspars, minerals usual in the Earth's crust whose detection has no special meaning. On the opposite, the presence of celestine (in SP1 and SP4), a mineral often associated with gypsum deposits, can give important clues on studies of the raw materials' origin, a fact discussed in the previous chapter. The detection of barite in sample SP3 could have the same meaning as it is usually associated in nature with celestine, forming a solid solution of $(Ba,Sr)SO_4$. (barite and celestine sometimes occur as a replacement of the mineral anhydrite (Hanor 2000)). However, SP3 was the only sample where celestine was not detected, so the origin of barite can be different (may be associated with the use of a consolidating agent in the past).

Finally, traces of anhydrite were found in some samples (SP3 and SP4), which can be due to the calcination process, where there was always a given amount of over burnt gypsum (Sanz 2009; Cardoso 2010), or/and to the raw material, as it is also a common impurity of the gypsum deposits.

- TG-DTA results

Mass and thermal variations associated with the chemical and physical transformations that occur during heating of the test specimens, such as dehydration of gypsum (calcium sulphate dihydrate, $CaSO_4.2H_2O$) in the range 85 - 250 ºC, decomposition of carbonates (mainly calcite, $CaCO_3$) in the range 600 - 850 ºC or crystalline transitions (like soluble to insoluble anhydrite, i.e., from anhydrite III to anhydrite II, around 350 ºC) (Adams et al. 1992; Borrachero et al. 2008; Paama et al. 1998) were obtained by TG-DTA analysis. From these data, the amount of gypsum and calcite were calculated and the results of XRD could be confirmed (Table 4.4, Figure 4.19).

Table 4.4 - Weight loss and calculated gypsum/calcite contents of the samples from *Santíssimo Sacramento's* Chapel

Sample	Temperature range (ºC)						Calculated contents (%)	
	25→85	85→250	250→600	600→850	850→1000	Loss of ignition	Gypsum	Calcite
SP1	0.2	19.4	0.4	1.4	0,0	21.4	93	3
SP3	0.2	8.3	1.4	23.6	1.0	34.5	39	54
SP4	0.0	11.6	0.8	17.5	1.5	31.4	55	40

The doublet of peaks corresponding to the two steps of dehydration of gypsum are well defined in the DTG and DTA curves (Figure 4.19): the first peak refers to the transformation of dihydrate into hemihydrate, comprising the removal of 3/4 of the water of crystallization (Eq. 4.1) and the second represents the loss of the remaining water from hemihydrate, to form soluble anhydrite (also known as anhydrite III) (Eq. 4.2) (S.N.I.P. 1982; Adams et al. 1992; Borrachero et al. 2008):

$$CaSO_4.2H_2O_{(s)} \longrightarrow CaSO_4.1/2H_2O_{(s)} + 3/2\ H_2O_{(g)} \quad \text{(Eq. 4.1)}$$

$$CaSO_4.1/2H_2O_{(s)} \longrightarrow CaSO_4\ (\text{soluble}) + 1/2\ H_2O \quad \text{(Eq. 4.2)}$$

The changes in the slope of the respective TG curves, corresponding to the mass loss of these two dehydration steps, are also perceptible.

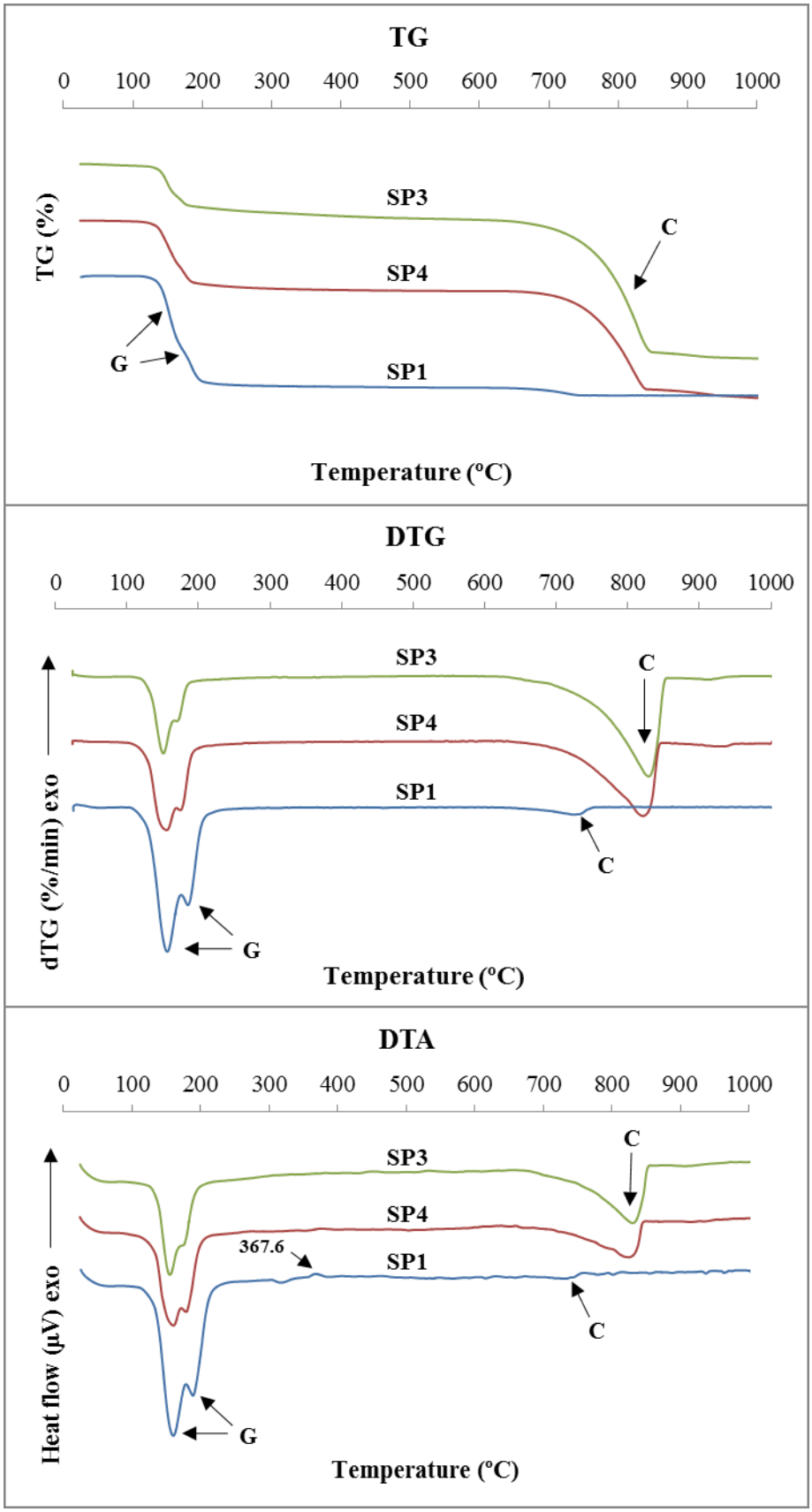

Figure 4.19 - TG, DTG and DTA curves of the samples from *Santíssimo Sacramento's* Chapel. Notation: G - Gypsum dehydration; C - Calcite decarbonation

In the sample SP1 the phase change of soluble to insoluble anhydrite (or anhydrite II) (Eq. 4.3), a pure crystallographic transformation, can be detected through the exothermic peak at 367.6 ºC (Figure 4.19, DTA curve) (S.N.I.P. 1982):

$$CaSO_{4\,(s)}\ (\text{soluble}) \longrightarrow CaSO_{4\,(s)}\ (\text{insoluble}) \qquad \text{(Eq. 4.3)}$$

On what concerns the decarbonation of calcite (Eq. 4.4) the range of temperatures is broader (600-850 ºC) for the samples with greater content of this compound (SP3 and SP4) than for the other that has only traces (SP1). It is also perceptible that the peak corresponding to the maximum decomposition rate occurs at lower temperatures in the samples with less calcite (and higher gypsum) content. In other words, it seems that the temperature of conversion of calcite to quicklime is influenced by the gypsum to calcite proportions, an observation also made by Ragai (1988).

$$CaCO_{3\,(s)} \longrightarrow CaO_{(s)} + CO_{2\,(g)} \qquad \text{(Eq. 4.4)}$$

In the case of SP1, the amount of calcite is so low that it is most probably an impurity of the raw material, i.e. gypsum was the only binder used to produce the corresponding decorative elements.

- Physical properties

Hygroscopic behaviour

In this group of samples was not possible to evaluate any physical property beyond the hygroscopic behaviour, due to their small size.

Figure 4.20 shows the image of the test specimens and the graphical representation of the results obtained for sample SP4; Table 4.5 provides more accurate quantitative information. The values of hygroscopicity were also determined in the sample SP1 but were too high, indicating the probable presence of hygroscopic contaminants. In this case as well as in all the others with a similar behaviour it was decided to present only the quantitative information (Table 4.5).

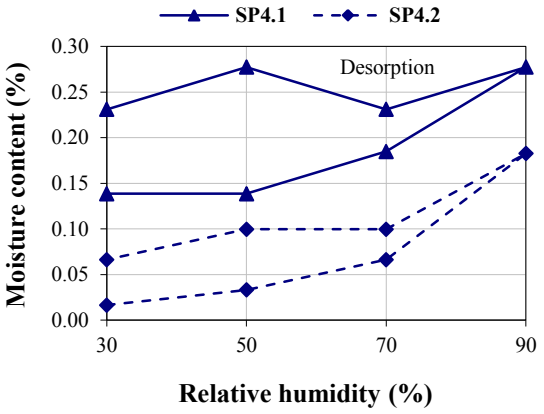

(a) (b)

Figure 4.20 - Hygroscopic behaviour of sample SP4: (a) test specimens; (b) graphical representation

Table 4.5 - Hygroscopicity results of the samples from *Santíssimo Sacramento's* Chapel (SP1, 2014; SP4, 2010)

	RH (%)	MC (%) SP1 (1TS)	MC (%) SP4.1*	MC (%) SP4.2*
Adsorption	30	0.07	0.14	0.02
	50	0.23	0.14	0.03
	70	0.47	0.18	0.07
	90	**1.61**	**0.28**	**0.18**
Desorption	70	0.51	0.23	0.10
	50	0.25	0.28	0.10
	30	0.09	0.23	0.07

* Too high variation between the test specimens, thus there is no sense in presenting the average result; RH - relative humidity; MC - moisture content; TS - test specimen

In spite of showing different values of adsorption/desorption (Table 4.5), the two test specimens of the sample SP4 can be considered to have a similar hygroscopic behaviour. In fact, the difference observed is constant along the whole procedure leading to very similar curve profiles (Figure 4.20). The exception is the result of desorption at 50% relative humidity of the test specimen SP4.1, which is not logical and can be due to a weighing error: SP4.1 was much smaller than SP4.2 (the initial weights were, respectively, 2.163 g and 6.024 g), and is more susceptible to interferences.

The quantitative gap between the two curves, observed since the first weighing step at 30% relative humidity with test specimen SP4.1 already showing a higher adsorption, can be due to the differences observed in the external surface of the two test specimens: in SP4.2 it was impossible to remove completely the preparatory layer used between the plaster and the layer of polychromes. This can lead

to an obstruction of some pores and cause a lower adsorption at each relative humidity step without changing the general hygroscopic behaviour of the material.

Another important feature of the curves of Figure 4.20 is the non-recovery of the weight of both test specimens during the desorption process. In other words, the adsorption and desorption curves deviate from each other. This phenomenon is called "hysteresis", or "adsorption hysteresis" and is usually associated with capillary condensation in mesopore structures (IUPAC 1972); however, if it occurs even at the lowest attainable vapour pressures, it is called "low pressure hysteresis" and the system has to have micropores (IUPAC 1985). In these specific documents, the mesopores are considered to have a diameter in the range 0.002 - 0.05 micron and micropores are those with a diameter below 0.002 micron.

- Mechanical properties

Dynamic modulus of elasticity

Among the mechanical characteristics only the dynamic modulus of elasticity of sample SP1 could be obtained (Table 4.6).

Table 4.6 - Dynamic modulus of elasticity results of the samples from *Santíssimo Sacramento's* Chapel

Sample	Bulk density[(1)] ($kg.m^{-3}$)	SD	CV (%)	Distance (m)	Time (μs)	SD	CV (%)	Speed ($m.s^{-1}$)	DME (MPa)
SP1	1376	116	8.4	0.061	33.3	0.1	0.3	1816	4064

[(1)] Sand method; SD - standard deviation; CV - coefficient of variation

The scarce information found in the literature indicates that results around 4000 MPa are normal for the dynamic modulus of elasticity of a gypsum plaster mixed with a plaster/water ratio of approximately 1.3 kg/l (Coquard et al. 1994), a value close to what has probably been used in the preparation of SP1, considering the fluidity required for the gypsum paste.

It is important to notice that the procedures adopted for the determination of the bulk density of the samples under study (with irregular shapes) often have a considerable error associated. So, the ultrasonic pulse velocity through the material is thought to be a more reliable result as does not involve calculations using that parameter.

4.3.1.2 The *Casa da Pesca* of the Marquis of *Pombal* farm

The Marquis of *Pombal* farm presents one of the most important works of art of the garden in Portugal with its design and layout falling into some of the most representative of the Baroque period in the Lisbon region (Pereira de Lima 2006). The *Casa da Pesca* is part of it and owes its name to the theme of fishing, an activity then currently practiced in the huge tank located on its right side. The simple aspect and architecture of the building contrast with its interior, where a room with the walls extensively covered with tile panels and stuccos can be found (Figure 4.21).

(a) (b)

Figure 4.21 - *Casa da Pesca*: (a) outside view of the building; (b) view of the room on the first floor

The ceiling is decorated with very delicate and high quality stuccos representing scenes of fisheries, executed by Giovanni Grossi (Silva 2005). Even though it is the shelter of such a valuable work of art, the building is in a poor state of conservation and imminent ruin, endangering this important heritage (Figure 4.22).

(a) (b)

Figure 4.22 - Ceiling of *Casa da Pesca's* interior room: (a) north side; (b) west side, in poor condition

Samples

A total of three samples, previously detached due to anomalies in the building, were collected. Their identification and description are summarized in Table 4.7 and the corresponding images are shown in Figure 4.23.

Table 4.7 - Identification and description of the samples from *Casa da Pesca*

Sample identification	Description
CP1	Ceiling plaster (polychrome)
CP2	Frieze
CP3	Ornaments

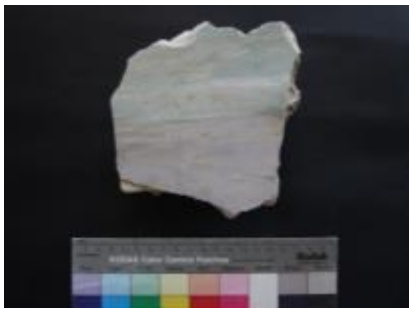

(a)

(b)

(c)

Figure 4.23 - Photographs of the analysed samples from *Casa da Pesca*: (a) one fragment from CP1; (b) two fragments from CP2; (c) CP3

Results and discussion

- Visual observation of the samples

The information obtained by visual observation of the samples is summarized in Table 4.8.

Similarly to what was observed in the *Santíssimo's* Chapel, the decorative elements are all different from each other, with no signs of having been made by an "industrial manufacture" process. The sample closer to that is CP2, a frieze moulded on a bench which implied the use of a profile, made of wood or metal, reproducing the required shape.

Table 4.8 - Visual observation of the samples from *Casa da Pesca*

Sample	Description
CP1	Six fragments from the **smooth surface** of the painted ceiling: three consisted of the final layer where the paint was applied and the other three had also a layer of mortar attached (Figure 4.23 (a));
	The final plaster layer had fine particles size but relatively high thickness (7-12 mm), and was very stiff and compact.
CP2	Three fragments of a bulky **frieze moulded on a bench** (Figure 4.23(b)) with sisal fibres inside and a film of brown paper attached to the back;
	Moulded in two steps: first the core was made and then the finishing layer, with a very low thickness, seemingly having been applied consecutively;
	The fragments showed a pellicle of a painting (limewash type) that could be easily detached due to the dust it had behind (between the surface of the plaster and the paint), i.e. it was not applied originally.
CP3	Three fragments of **ornaments** of considerable volume representing vegetal related motifs (Figure 4.23(c));
	They seem to have been **sculpted before application**: there are many similar ornaments on site even though all different, i.e. they have not been precast.

- XRD results

The qualitative mineralogical composition of the samples determined by XRD showed that gypsum and calcite are the main constituents (Figure 4.24, Table 4.9).

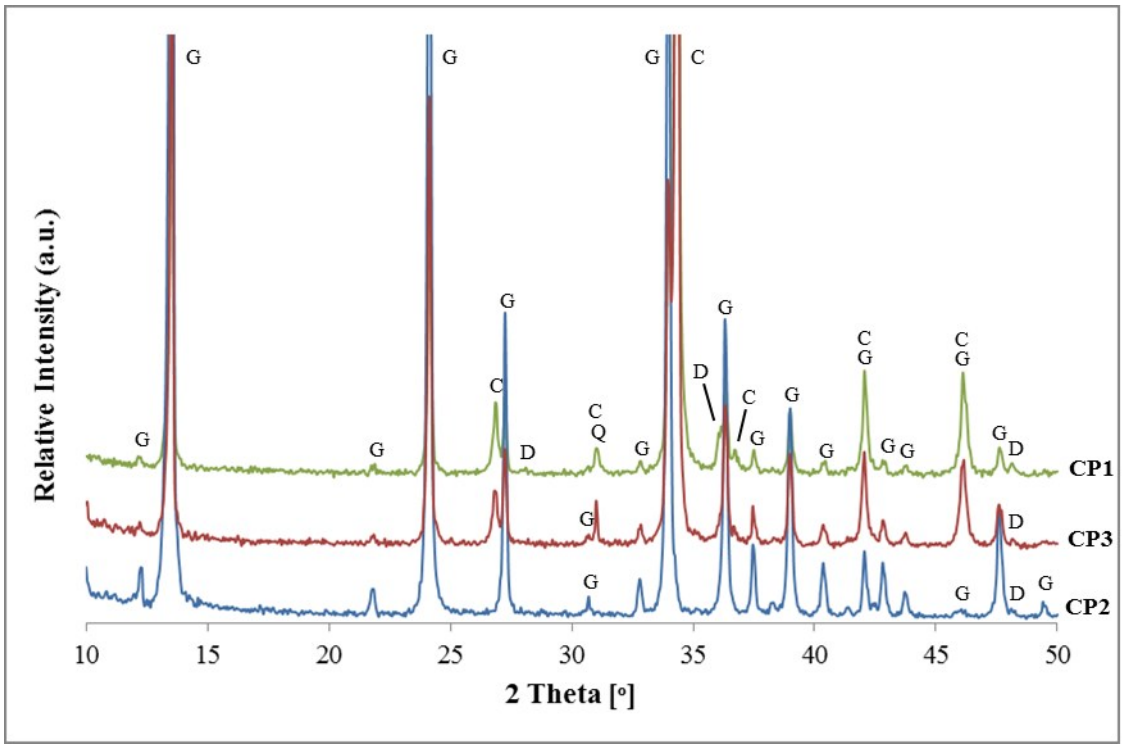

Figure 4.24 - XRD patterns of the samples from *Casa da Pesca*. Notation: G - Gypsum; C - Calcite; Q - Quartz; D - Dolomite

Table 4.9 - XRD qualitative mineralogical composition of the samples from *Casa da Pesca*

Sample	Identified crystalline compounds				
	Gypsum	Calcite	Quartz	Dolomite	Others
CP1	++	+++/++++	trc	trc	-
CP2	++++	-	-	trc	-
CP3	++/+++	+++	trc	trc	-

Notation used in XRD peak analysis:

++++	Very high proportion (predominant compound)	+	Weak proportion
+++	High proportion	trc	Traces
++	Medium proportion	-	Not detected

Traces of other compounds were also found (impurities), namely quartz and dolomite: the first is a mineral usual in the Earth's crust whose detection has no special meaning; the second is commonly associated with gypsum and calcite deposits and can give important clues on studies of the raw materials' origin, as referred for other compounds (celestine, for example).

- TG-DTA results

The amounts of gypsum and calcite were calculated through TG-DTA analysis and the results of XRD could be confirmed (Table 4.10, Figure 4.25).

Table 4.10 - Weight loss and calculated gypsum / calcite contents of the samples from *Casa da Pesca*

Sample	Temperature range (ºC)						Calculated contents (%)	
	25→85	85→250	250→600	600→850	850→1000	Loss of ignition	Gypsum	Calcite
CP1	0.2	5.6	1.1	30.9	0.7	38.5	27	70
CP2	0.1	19.8	0.8	1.5	0.6	22.8	94	3
CP3	0.2	8.2	1.2	25.1	0.2	34.9	39	57

Again, in the samples with more gypsum (CP2 and CP3) the doublet of peaks corresponding to the two steps of dehydration of this material are well defined in the DTG and DTA curves and the changes in the slope of their TG curves, corresponding to the mass loss of these two dehydration steps, are clearly perceptible for CP2 (Figure 4.25).

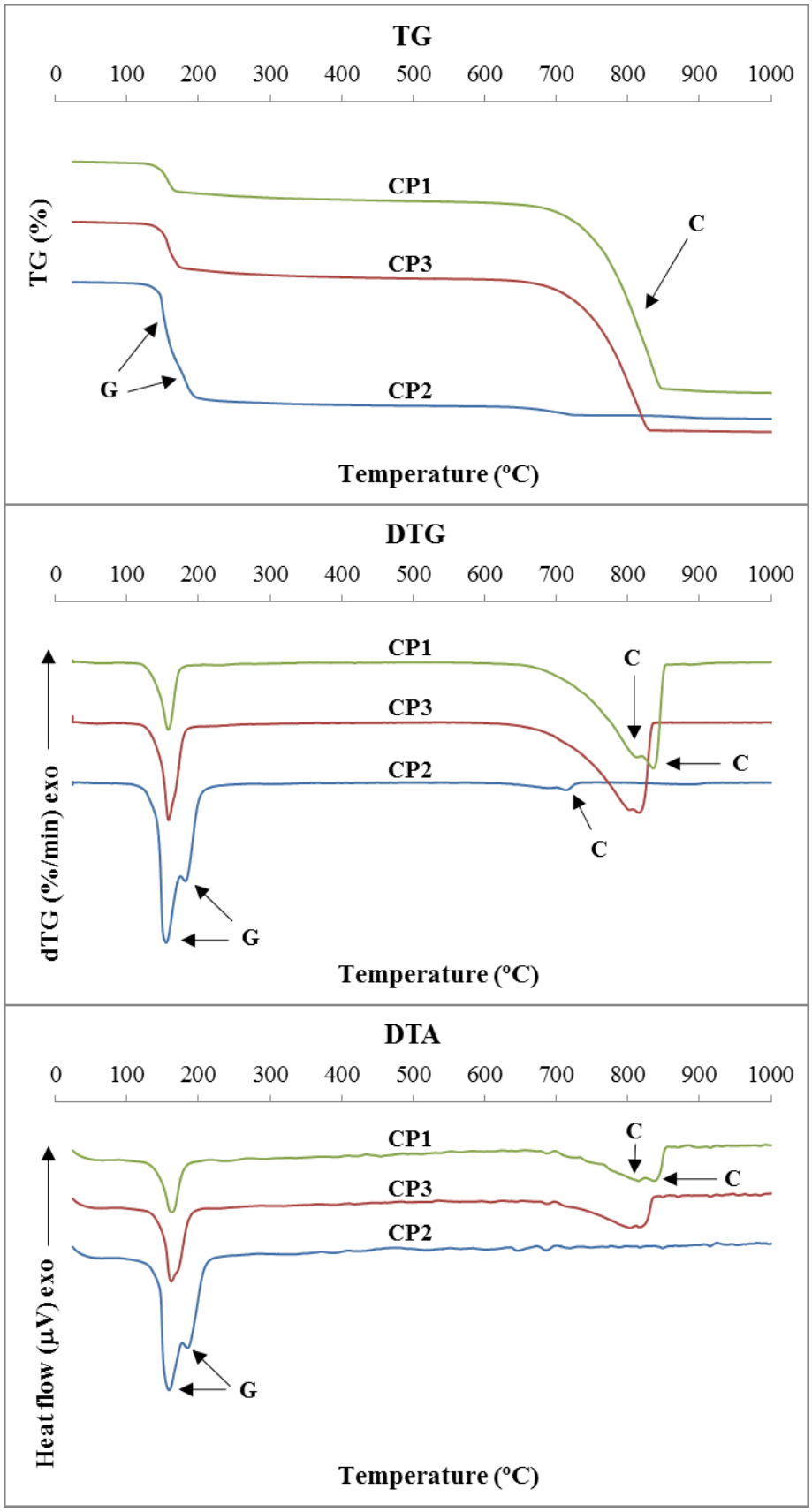

Figure 4.25 - TG, DTG and DTA curves of the samples from *Casa da Pesca*. Notation: G - Gypsum dehydration; C - Calcite decarbonation

In what concerns the decarbonation of calcite (Eq. 4.4), similar observations to those of the samples from *Santíssimo's* Chapel can be made: (a) the range of temperatures of the correspondent chemical transformation is broader (600-850 ºC) for the samples with greater content of this compound (CP1 and CP3) and narrower (better defined) for CP2, with trace quantities (probably an impurity of the raw material); (b) the samples with more gypsum show lower decarbonation temperatures for calcite.

Another important observation is the presence of two differentiated peaks in the DTG curves of the samples CP1 and CP3 (Figure 4.25), more precisely at 811.9 ºC and 835.2 C for CP1 and at 802.2 ºC and 815.0 C for CP3. These peaks can also be detected in the respective DTA curves at temperatures slightly superior (about 1 ºC), though in a less perceptible way.

When the decarbonation of calcite occurs in two steps it can be due to one (or more) of the following reasons (Alvarez et al. 2000; Anastasiou et al. 2006; Gourdin & Kingery 1975; Igea et al. 2012; Montoya et al. 2003; Moropoulou et al. 1995; Vecchio et al. 1993):

a) The presence of material with different degrees of crystallinity, as is the case of natural calcite (carbonate of primary origin) and calcite resulting from the carbonation of lime or from dissolution-recrystallization cycles (both of secondary origin);
b) The presence of an amorphous phase together with a crystalline one;
c) A mixture of different sized crystallite particles, resulting from an incomplete calcination of some raw material grains;
d) The presence of carbonated compounds of different origins and/or compositions.

Any of the previous hypotheses is plausible in this case:

a) Although the presence of aggregates was not detected through either visual observation or the manipulation of the samples during preparation for XRD and thermal analyses, there is always a possibility of a small content of natural calcite as an impurity of the gypsum raw material. As the thermal decomposition is a process limited by heat transfer, the rate of which is a function of particle size, larger size crystals (natural calcite) need higher energy to decompose than smaller and less well crystallized ones (secondary origin carbonates);
b) It is also plausible but could only be confirmed with microscopy techniques, not used in this case;
c) It could only be confirmed using microscopy techniques;
d) The presence of traces of dolomite was detected in the three samples analysed, thus making this explanation plausible. In fact, dolomite is a carbonated compound of chemical formula $CaMg(CO_3)_2$, whose thermal decomposition occurs in two phases: the first corresponds to the decarbonation of magnesium carbonate ($MgCO_3$) and takes place at temperatures that can vary from 450 ºC (Adriano 2008) to 700 ºC (Montoya et al. 2003); the second, at about 700 ºC to

900 ºC ((Montoya et al. 2003; Vecchio et al. 1993), is due to the decarbonation of calcite remaining from the dolomite lattice. The last temperature range is coincident with that of the previously referred calcium carbonates of primary and secondary formation meaning that the respective peaks in the DTG and DTA curves can appear very close (or even overlapped), producing an effect like the one observed in CP1 and CP3 (Figure 4.25).

Another feature that can be attributed to the presence of dolomite is the existence of disturbances around 700 ºC in all DTA curves, which is possibly related to the decomposition of its magnesium carbonate content.

The temperature gaps between the two decarbonation peaks found in the present study - 23.3 ºC for CP1 and 12.8 ºC for CP3 - agree with a study cited by Gourdin and Kingery (1975), which indicates a temperature gap of 13 to 38 ºC, and with Igea et al.'s study (2012) that found a 22 ºC gap. However, in both cases the peaks are linked to the presence of calcite with different crystallization origins and not to the presence of dolomite; other authors that specify gaps in the decomposition temperatures refer to much bigger differences (about 100 ºC) but the same explanation is given (Anastasiou et al. 2006; Vecchio et al. 1993). This illustrates the variability of results and interpretations that this kind of observations can have.

Finally, in the TG curves of Figure 4.25 and according to expectations, this phenomenon is so discrete that it is not perceptible. Only by using high resolution thermogravimetric analysis (HRTG) would it probably be clarified (Borrachero et al. 2008).

- Physical properties

The water absorption by capillarity and the water vapour permeability were determined in sample CP2; the hygroscopic behaviour was studied in the three samples collected.

Capillary absorption

The results obtained are shown graphically in Figure 4.26 and the quantitative values are summarized in Table 4.11.

Although they are unrepresentative at this point, some remarks will be made. Later, when all the characterization results have been presented, a global and deeper discussion will be possible.

The capillary coefficient by contact shows that the rate of suction is very high in the first 5 minutes, with the water absorbed during this period representing 73.05% of the total amount absorbed during the time of the procedure (24 h). In fact, the major part of the absorption (92.56%) occurs in the first 10 minutes (3.16 $min^{1/2}$, Figure 4.26 (b)), which usually indicates a great content of capillary pores

with a high percentage of the larger ones (considered to have r > 0.5 micron according to Magalhães et al. 2004; Rato 2006; the upper limits for the radii of capillary pores are much more divergent with values like 50 micron (Stefanidou 2010), 500 micron (Rato 2006) or 1000 micron (Meng 1996, cited by (Thomson et al. 2004)).

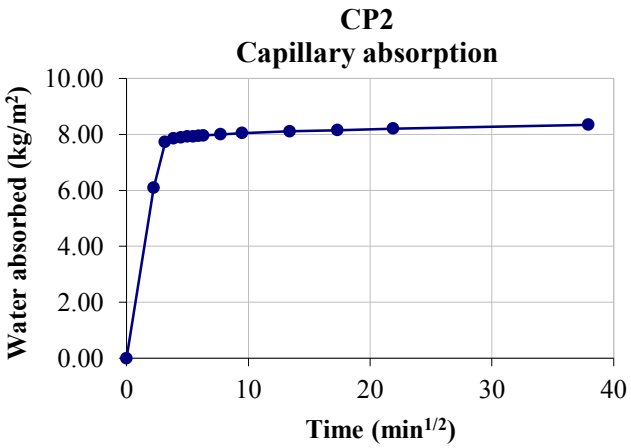

(a) (b)

Figure 4.26 - Capillary water absorption by contact of sample CP2: (a) test specimen during the determination; (b) graphical representation of the results

Table 4.11 - Capillarity coefficient by contact results of sample CP2

Test specimen	
Surface (cm^2)	28.68
Weight (g)	70.57
Capillary absorption at 5 min:	
(g)	17.48
($kg.m^{-2}$)	**6.09**
(%, relative to weight of sample)	24.77
(%, relative to total absorption)	73.05
Capillary absorption at 24 h:	
(g)	23.93
($kg.m^{-2}$)	**8.34**
(%, relative to weight of sample)	33.91
Ccc at 5 min ($kg.m^{-2}min^{-1/2}$)	**2.73**

Ccc - capillarity coefficient by contact

The total amount of water absorbed is equally high (Figure 4.26 (b)), which is usually related to a significant and well-connected open porosity (Magalhães et al. 2004; Rato 2006).

The drying behaviour of sample CP2 was also evaluated and is presented in Figure 4.27.

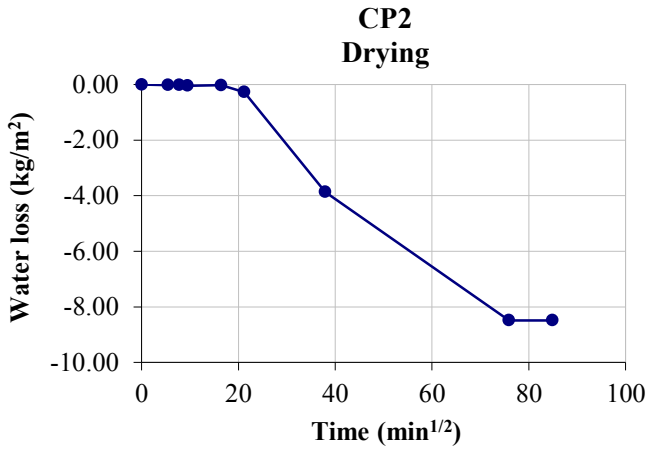

Figure 4.27 - Graphical representation of the drying behaviour of the sample CP2

In the first hours the loss of weight was negligible. Only in the period between 21.21 and 37.95 $min^{1/2}$ (corresponding to 450 and 1440 minutes, respectively) did it start to be significant, becoming quick after that. The initial drying inertia was probably longer than it would be if only the test specimen was involved but the friability of the old samples required the development of a procedure where a set "basket + geotextile + sample" had to be used (Veiga et al. 2004) (*cf.* 4.2.2, "Experimental data" section).

Hygroscopic behaviour

The hygroscopic behaviour was studied in all the samples from *Casa da Pesca*.

Figure 4.28 shows the graphical representation of the results obtained for sample CP2; the values of hygroscopicity of the other two samples (CP1 and CP3) were too high (Table 4.12), indicating the probable presence of hygroscopic contaminating substances (e.g. soluble salts).

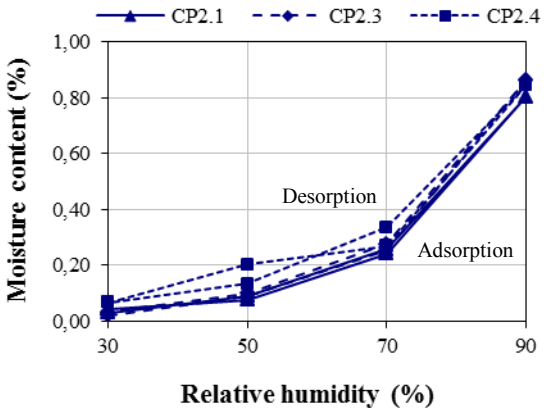

(a) (b)

Figure 4.28 - Hygroscopic behaviour of sample CP2: (a) test specimens; (b) graphical representation

Table 4.12 - Average hygroscopicity results of the samples from *Casa da Pesca* (2014)

RH (%)	MC (%) CP1 (2TS)	SD	CV (%)	MC (%) CP2 (3TS)	SD	CV (%)	MC (%) CP3 (3TS)	SD	CV (%)
30	0.03	0.010	30.88	0.04	0.023	50.35	0.10	0.011	10.49
50	0.15	0.035	23.01	0.12	0.070	57.01	0.25	0.006	2.30
70	0.58	0.279	48.05	0.26	0.014	5.33	0.72	0.027	3.69
90	**2.03**	0.829	40.89	**0.84**	0.030	3.59	**2.50**	0.136	5.43
70	0.63	0.269	42.77	0.29	0.042	14.30	0.80	0.038	4.75
50	0.24	0.050	21.22	0.11	0.023	21.46	0.39	0.027	6.79
30	0.08	0.010	11.73	0.04	0.021	47.32	0.14	0.018	12.72

RH - relative humidity; MC - moisture content; TS - test specimens; SD - standard deviation; CV - coefficient of variation

Contrarily to what was observed in sample SP4 from the *Santíssimo Sacramento's* Chapel, the CP2 test specimens show negligible hysteresis and have very similar quantitative values, represented by almost overlapped curve profiles. The absence of hysteresis is usually related to a pore size distribution curve shifted to high pore radii (without capillary condensation phenomena). This supposition is also in agreement with the other physical properties determined.

The maximum value of adsorption of the sample CP2 (at 90% relative humidity) is high when compared to most of the samples analyzed, namely SP4. So, it can be either due to the presence of some hygroscopic contaminants or it is the real value, as there were other cases with similar results.

Water vapour permeability

The test procedure to determine this property can only be performed in specimens with a flat surface. In *Casa da Pesca* it corresponded to sample CP2; the device used and the results obtained are shown in Figure 4.29 and in Table 4.13, respectively.

The values found indicate that sample CP2 has a very high permeability, even higher than (about twice) the values obtained from literature for gypsum-lime test specimens (Ramos et al. 2010: Sd = 0.059 m) and for lime-based mortars formulations for restoration purposes prepared in laboratory (Veiga et al. 2010: Sd < 0.10 m; Margalha 2010: Sd = 0.05-0.12 m).

However, they are in agreement with the capillary absorption and drying behaviours presented above, denoting high and very well connected open porosity.

(a)

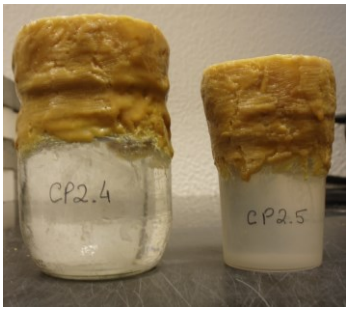

(b)

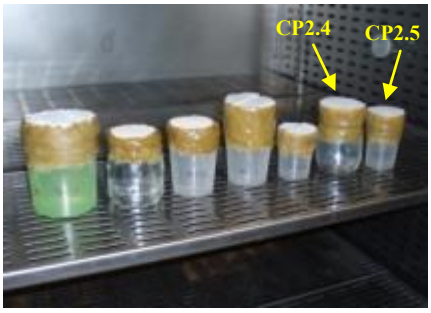

(c)

Figure 4.29 - CP2's water vapour permeability determination: (a) preparation of the test specimens; (b) devices used (adapted to ancient samples); (c) ongoing test

Table 4.13 - Water vapour permeability results of sample CP2

Sample (test specimens)	Thickness (d) (mm)	ΔM/24h (g)	Permeability ($ng.m^{-1}.s^{-1}.Pa^{-1}$)	Sd (d=10 mm) (m)
CP2 (2)	19.70	0.42	51.47	**0.033**
SD	0.07	0.06	1.21	0.001
CV (%)	0.35	13.47	2.35	2.77

SD - standard deviation; CV - coefficient of variation; Sd - thickness of air layer with equivalent diffusion of water vapour

- Mechanical properties

Dynamic modulus of elasticity and compressive strength

The results of the mechanical properties determined, dynamic modulus of elasticity and compressive strength are presented in Table 4.14 and Table 4.15, respectively. Figure 4.30 shows samples CP2 and CP3 being tested at compression.

In what concerns the dynamic modulus of elasticity, sample CP2 shows a value of the same order of magnitude as SP1, with a similar composition, and slightly above what is considered to be the moderate range for lime mortars (2500-4000 MPa) (Veiga et al. 2010). Also in this case the result

obtained can be considered current for a gypsum plaster that had to be moulded before application, i.e., with a plaster/water ratio adequate to achieve a relatively fluid consistency. As for sample CP3, the value is much lower (less than half) but in accordance with its different composition, where calcite resulting from carbonated lime is the major constituent (Table 4.10).

Table 4.14 - Dynamic modulus of elasticity results of the samples from *Casa da Pesca*

Sample	Bulk density[(1)] ($kg.m^{-3}$)	SD	CV (%)	Distance (m)	Time (µs)	SD	CV (%)	Speed ($m.s^{-1}$)	DME (MPa)
CP2	1135	61	5.4	0.117	54.7	0.1	0.3	2139	4672
CP3	1387	89	6.4	0.048	36.4	0.3	0.7	1304	2121

[(1)] Sand method; SD - standard deviation; CV - coefficient of variation; DME - dynamic modulus of elasticity

Table 4.15 - Compressive strength results of the samples from *Casa da Pesca*

Sample	Confinement mortar age (days)	Bulk density[(1)] ($kg.m^{-3}$)	SD	CV (%)	Load rate ($N.s^{-1}$)	Maximum load (N)	Compressive strength* (MPa)
CP2	31	1115	26	2.4	50	5317	3.32
CP3	-	1387	89	6.4	50	2152	1.35

[(1)] Sand method; SD - standard deviation; CV - coefficient of variation; * When SD and CV are not presented it means that the result refers to one test specimen only

(a) (b)

Figure 4.30 - Adapted compressive strength tests: (a) CP2 with confinement mortar; (b) CP3 with two fibre cement boards to obtain the target height

The same considerations can be made for the mechanical strengths, only possible to determine in samples CP2 and CP3. The first presents again a higher value than the moderate range for lime mortars (1.5-2.5 MPa) and the second has a value slightly below, both in accordance with the respective dynamic modulus of elasticity.

However, in the case of sample CP2 the result obtained is completely in agreement with that of the gypsum plaster sample from the *Mirhab* of the old Mosque of *Mértola* (3.5 MPa, Veiga 2012) already referred in Chapter 3. In fact, this was the only result of mechanical properties found in the literature for ancient gypsum plasters of the same type (made with the same kind of binder and having a similar application). Furthermore, it was only possible to make a comparison with studies of test specimens prepared in laboratory.

The lowest experimental values for a gypsum plaster are referred by Dalui *et al.* (1996) and were obtained with a plaster/water ratio of 1.0 kg/l: 2 MPa for compressive strength and 2000 MPa for dynamic modulus of elasticity. Coquard et al. (1994) report a lower plaster/water ratio (0.92 kg/l) achieving the same result for the dynamic modulus of elasticity and 2.5-2.9 MPa for flexural strength, values that do not seem logical when compared to the example of Dalui; compressive strength were not evaluated. However, these plaster/water ratios are usually very difficult to work with due to the excessive fluidity of the paste, and not very probable to be used in practice.

For the manufacture of ordinary gypsum elements the hemihydrate form most commonly used is (and was) β-hemihydrate, whose suitable workability can be usually achieved with plaster/water ratios between 1.2 kg/l and 1.5 kg/l. These pastes lead to much harder plasters: 5 to 8 MPa were the results obtained for the compressive strength of the gypsum plaster mixes tested during the elaboration of this work (*cf.* Chapter 5) and 9 to 12 MPa were the values found in the literature (S.N.I.P. 1982; Dalui et al. 1996; Wirsching 2005; Yu & Brouwers 2011).

The reasons for such difference can be many – the smaller and more irregular size of the ancient test specimens, the aging effects, the original procedures of preparation and application of the plaster elements, etc. - making it difficult to compare results without more approximate references.

Similarly, it is only possible to compare the results obtained for sample CP3, a gypsum-lime plaster, with ancient lime mortars or with formulations prepared in laboratory even though not always of the same type: (i) the gypsum-lime plaster mixes with similar compositions to that of CP3 tested during this work (M1 and M2) had about 3 MPa of compressive strength (*cf.* Chapter 5); (ii) Igea Romera et al. (2013) developed several gypsum-lime repair mortars with incorporation of quartzitic and gypsum alabaster aggregates and prepared them with plaster/water ratios that varied between 1.2 kg/l and 1.8 kg/l in the former case and between 1.0 kg/l and 1.6 kg/l in the latter. The compressive strength results obtained were respectively in the ranges 4-12 MPa and 1-6.5 MPa, i.e. the majority are also well above CP3's; (iii) six samples of lime mortars from Portuguese ancient buildings, have been tested using the confinement mortar method and the results obtained varied between 1.9 MPa and 2.5 MPa (Magalhães & Veiga 2009), with the exception of one render from a 16th century Convent in Lisbon

that presented 4.7 MPa (Válek & Veiga 2005). Such values (1.9-2.5 MPa) are found to be the most approximate to CP3's.

As the presence of aggregates was not detected, the differences found between CP2 and CP3 are mainly related to the type of binders used in their composition: gypsum plaster in the former and a mix of hydrated lime (now carbonated and appearing as calcite) and gypsum plaster in the later one (Table 4.10).

In fact, as it is well known, gypsum and lime plasters have distinct physical and mechanical behaviour. To explain this, several reasons can be given, namely the different nature of the chemical reactions (with water, in the case of gypsum, and with carbon dioxide from the air, in the case of lime) and the plaster/water ratio used to prepare the mixtures (lower in the case of lime because of its finer particles size). These factors influence both the microstructure and the porous structure of the resulting hardened products which, in turn, are determinant to their main physical and mechanical characteristics (Igea Romera et al. 2013; Rato 2006; Thomson et al. 2004; Yu & Brouwers 2011): gypsum plasters are more brittle, exhibit a microstructure composed of prismatic needle-like crystals which intergrow and interlock during hydration and setting, have a coarser particles size and show higher porosity values (Coquard et al. 1994); lime plasters, though also considered very porous materials, have a lower global porosity(Thomson et al. 2004).

In spite of having a higher porosity, usually inversely related to the mechanical properties values, gypsum plasters have higher DME and mechanical strength than lime plasters (Igea Romera et al. 2013).

It is though very important to conclude that the statement about porosity being the most determinant parameter influencing the mechanical characteristics of this type of materials (Wirsching 2005; Thomson et al. 2004) is only valid when they have the same chemical composition and that the results obtained for the samples analysed in this work are totally in agreement with all the previous remarks.

4.3.2 The 19th century

From the 19th century five case studies have been considered: two located in the city of *Porto*, representing the north of Portugal - a dwelling in *Restauração* Street and the Arabian Room of the *Bolsa* Palace; one in the centre - the *Barão Salgueiro* Manor house, in *Leiria*; one in the centre-south - *Monserrate* Palace, in *Sintra*; one in the south - the *S. Francisco's* church, in *Tavira* (Figure 4.31).

The case studies are presented according to their geographical location, from the north to the south of the country.

1. Porto
2. Leiria
3. Sintra
4. Tavira

Figure 4.31 - Geographical location of the 19th century case studies

4.3.2.1 The *Restauração* Street building

The *Restauração* Str. building is located in *Porto's* city centre. It was built in the second half of the 19th century to be the dwelling house of a wealthy family (Figure 4.32). The stucco decoration is simple but denoting a good quality of execution. Some of the ceilings have already collapsed due to the poor condition of the building (Figure 4.33).

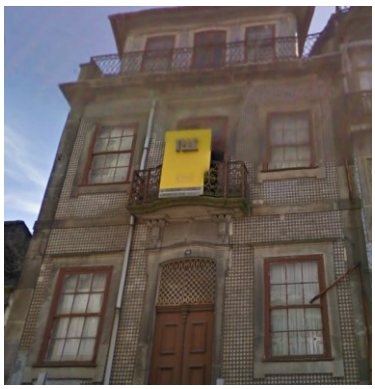

Figure 4.32 - *Restauração* Street building: general view of the façade

(a)

(b)

Figure 4.33 - *Restauração* Street building: (a) entrance hall; (b) detail of a collapsed ceiling (the yellow line indicates the place where sample ERR4 was collected)

Samples

A total of four samples were collected on site (Figure 4.34).

(a) (b)

Figure 4.34 - Collection of samples at *Restauração* Street building: (a) sample ERR2; (b) sample ERR3

After the mineralogical survey using XRD (Chapter 3), two samples (ERR1 and ERR2) did not proceed for further study as they did not have gypsum in the major constituents.

The identification and description of the samples studied are summarized in Table 4.16 and their images are shown in Figure 4.35.

Table 4.16 - Identification and description of the samples from *Restauração* Street building

Sample identification	Description
ERR3	Finishing layer of a cornice
ERR4	Ornament

(a) (b)

Figure 4.35 - Photographs of the analysed samples from *Restauração* Street building: (a) ERR3; (b) ERR4

Results and discussion

- Visual observation of the samples

The information obtained by visual observation of the samples is summarized in Table 4.17.

Table 4.17- Visual observation of the samples from *Restauração* Street building

Sample	Description
ERR3	Six fragments from the **final layer** of a cornice (Figure 4.35 (a)); The fragments had high thickness (10-15 mm), low density and were very friable; The frieze seems to have been moulded on site as its internal structure, consisting of a thick layer of mortar, was attached to the wall with iron rods (Figure 4.36).
ERR4	One **ornament** of considerable volume representing an acanthus leaf (Figure 4.35 (b)); It seems to have been **sculpted before application** as it belongs to a set of similar ornaments even though all different (Figure 4.32 (c)), meaning they have not been precast.

Figure 4.36 - Cross-section of the cornice from where sample ERR3 (red arrow) was taken, with iron rods (yellow arrows)

Similarly to what was observed in the case studies from the 18th century, the decorative elements corresponding to sample ERR4 are all different from each other (Figure 4.32 (c)) with no signs of having been made by an "industrial manufacture" process. However, there is a big skylight in the centre of the house, to illuminate the staircase, framed by plaster decorations that have been clearly precast (Figure 4.37).

(a) (b)

Figure 4.37 - Skylight framed by plaster decorations that have been precast: (a) top frame; (b) bottom frame

- XRD results

The qualitative mineralogical composition of the samples determined by XRD showed that gypsum and calcite are the main constituents (Figure 4.38, Table 4.18).

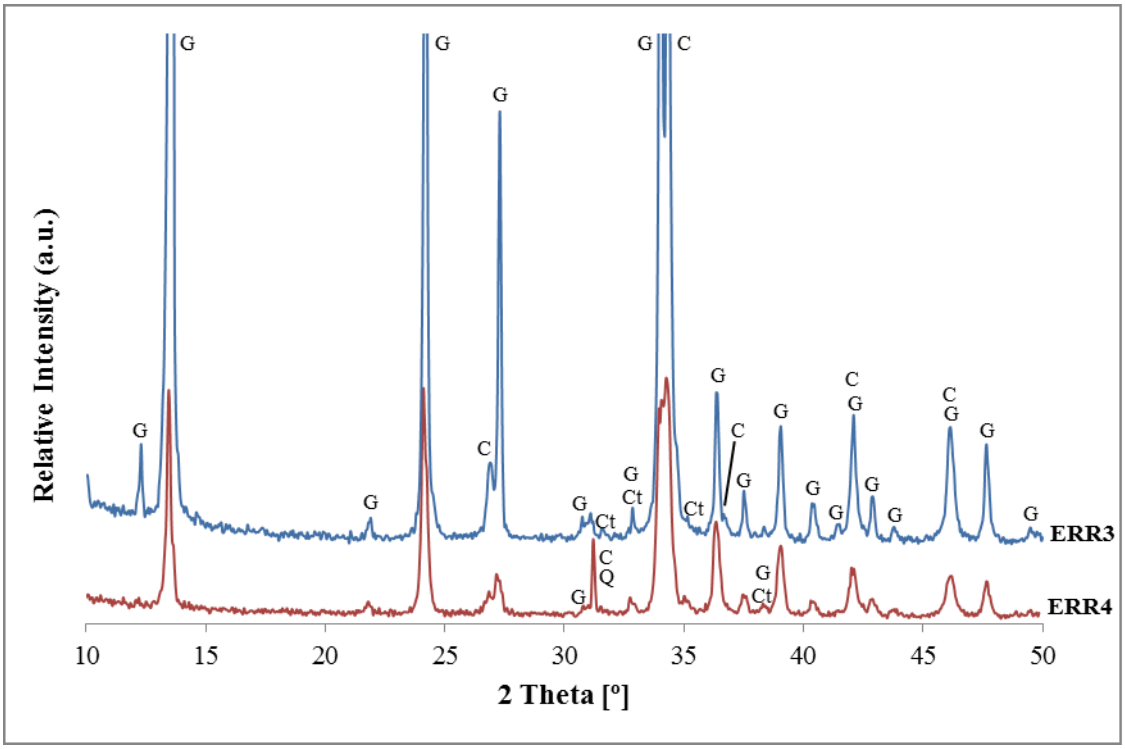

Figure 4.38 - XRD patterns of the samples from *Restauração* Street building.
Notation: G - Gypsum; C - Calcite; Q - Quartz; Ct – Celestine

Table 4.18 - XRD qualitative mineralogical composition of the samples from *Restauração* Street building

Sample	Identified crystalline compounds				
	Gypsum	Calcite	Quartz	Celestine	Others
ERR3	+++	++	trc	trc	-
ERR4	++/+++	++/+++	trc	trc	-

Notation used in XRD peak analysis:

++++	Very high proportion (predominant compound)	+	Weak proportion
+++	High proportion	trc	Traces
++	Medium proportion	-	Not detected

Again, the traces of quartz and celestine found are considered impurities, as discussed in Chapter 3.

- TG-DTA results

Sample ERR3 was analysed using TG-DTA (Figure 4.39). The amounts of gypsum and calcite were calculated and the results of XRD could be confirmed (Table 4.19).

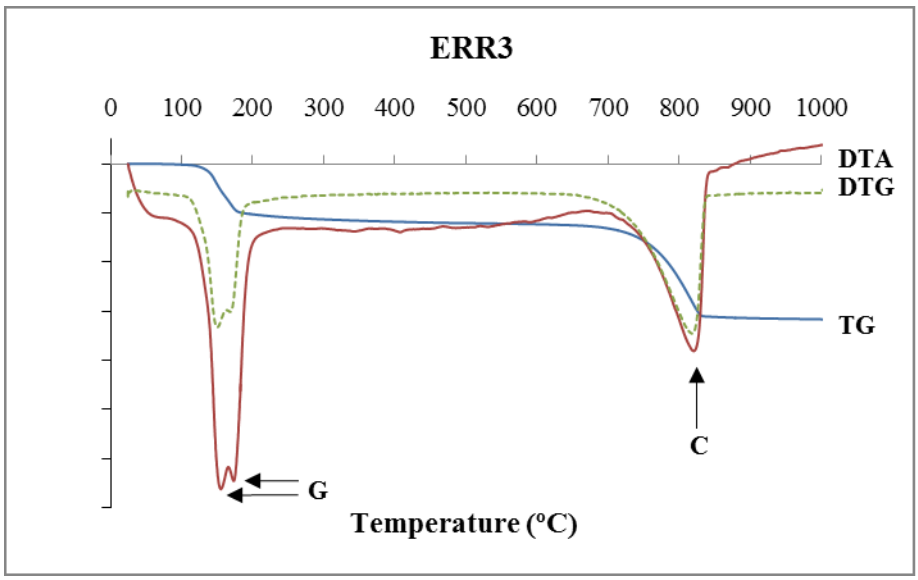

Figure 4.39 - TG, DTG and DTA curves of the sample ERR3.
Notation: G - Gypsum dehydration; C - Calcite decarbonation

Table 4.19 - Weight loss and calculated gypsum/calcite contents of the sample ERR3

Sample	Temperature range (ºC)						Calculated contents (%)	
	25→85	85→250	250→600	600→850	850→1000	Loss of ignition	Gypsum	Calcite
ERR3	0.1	10.8	1.4	19.1	0.2	31.6	52	43

The TG-DTA chart for sample ERR3 (Figure 4.39) is characteristic of a gypsum-lime plaster. The doublet of peaks corresponding to the two steps of dehydration of gypsum is well defined in the DTG and DTA curves in the range 100-200 ºC, while the peak related with the decarbonation of calcite occurs between 700 ºC and 850 ºC.

- Physical properties

Hygroscopic behaviour

In this case study, of the physical properties it was only possible to evaluate the hygroscopic behaviour of the sample ERR3.

Figure 4.40 shows the graphical representation of the results obtained and Table 4.5 gives more accurate quantitative information.

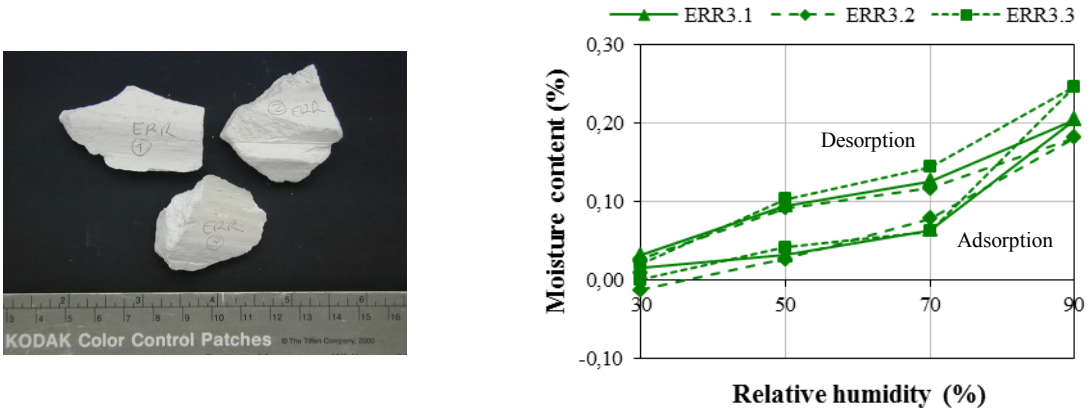

(a) (b)

Figure 4.40 - Hygroscopic behaviour of sample ERR3: (a) test specimens; (b) graphical representation

Table 4.20 - Average hygroscopicity results of the sample ERR3 (2010)

	Relative humidity (%)	Moisture content (%)	SD	CV (%)
Adsorption	30	*	*	*
	50	0.03	0.008	23.37
	70	0.07	0.009	13.38
	90	**0.21**	0.033	15.64
Desorption	70	0.13	0.014	10.72
	50	0.10	0.006	6.40
	30	0.03	0.005	20.94

SD - standard deiation; CV - coefficient of variation; * Too high CV value that preclude presenting the results

The curve profiles of Figure 4.40 indicate the presence of hysteresis in the three test specimens of the sample ERR3, and are more significant at 50% and 70% relative humidity. As stated before (sample SP4), this type of hysteresis is due to the occurrence of condensation in mesopore structures while at 30% relative humidity ("low pressures hysteresis") it is already related to the presence of some microporosity.

The hygroscopic behaviour of the sample ERR3 is similar to that of the sample SP4 except at 30% relative humidity where the difference between adsorption and desorption curves is smaller, and is probably negligible or even absent at lower vapour pressures.

These observations seem to indicate that the chemical composition of the materials under study is directly related to their main characteristics. In fact, SP4 and ERR3 have very similar gypsum and calcite contents which probably led to a similar pore size distribution which, in turn, led to a similar hygroscopic behaviour.

4.3.2.2 The Arabian Room of the *Bolsa* Palace

The *Bolsa* Palace is located in *Porto's* historical centre classified as World Heritage by UNESCO. It was built from the ruins of the former *S. Francisco* Convent and its construction took over sixty years. It is the *Porto* Trade Association headquarters, but it was once the Court of Commerce and later the Stock Exchange, a function that originated the palace's present name (ARTEDITORES 2009).

Considered an architectural icon of the 19th century where several decorative styles blend together it is classified as national monument. Its façade is one of the greatest examples of neoclassical style in Portugal (Figure 4.41).

Figure 4.41 - *Bolsa* Palace: view of the façade

The Arabian Room is the most emblematic of the palace's rooms as it embodies the clearest expression of the neo-Moorish art in Portugal. Its construction began in 1862 and was finished only in 1880. The coloured stucco decorations were inspired by the Palace of the *Alhambra*, in *Granada*, Spain (Rúbio Domene 2011), and cover the walls and ceiling, constituting one of the richest and most original decorative Portuguese gypsum plasters of that period (ARTEDITORES 2009) (Figure 4.42 and Figure 4.43).

As there are no historical records about the materials and techniques of application used in the decoration works performed in this room, the present characterization study became an essential basis for the restoration works that took place there in 2010 (Freire et al. 2012).

(a)

(b)

Figure 4.42 - Arabian Room of the *Bolsa* Palace: (a) general view; (b) closer view, showing the richness of the stucco decoration

Samples

A total of six samples were collected in two different ways: indirectly, i.e. they had been previously detached due to some anomaly in the building (five samples, Figure 4.43 (a) and (b)) and directly on site (sample PB6, Figure 4.43 (c)). They all belong to decorative elements.

After the first visual observation, sample PB5 was rejected due to strong evidence of not being original: the golden layer is painted and the interior metal frame is not rusted like the others, showing a superficial blue colour (possibly copper reacting to copper sulphate) (Figure 4.44).

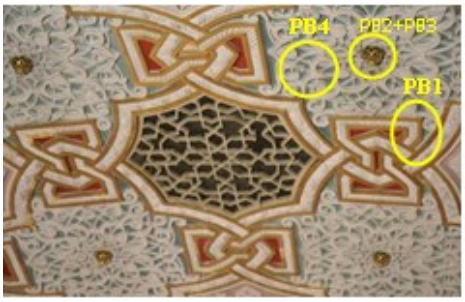

(a)

(b)

(c)

Figure 4.43 - Detail of some stucco decorations with indication of the ornaments corresponding to the samples collected: (a) ceiling; (b) crowning of the cornice that delimits the ceiling; (c) wall of the gallery on the first floor

Figure 4.44 - Sample PB5, excluded from the study

The identification and description of the samples studied is summarized in Table 4.21 and the corresponding images are shown in Figure 4.45.

(a) (b) (c) (d) (e) (f)

Figure 4.45 - Photographs of the analysed samples from *Bolsa* Palace: (a) PB1; (b) PB2; (c) PB3; (d) PB2+PB3; (e) PB4; (f) PB6

Table 4.21 - Identification and description of the samples from *Bolsa* Palace

Sample identification	Description
PB1	Frame from the ceiling (gilded)
PB2	Ornaments from the breathing holes of the ceiling (gilded)
PB3	Octagonal base of PB2 (gilded)
PB4	White ornaments from the ceiling
PB6	Preparation layers (PB6/1 and PB6/2) and ornament (PB6/3) of a wall of the gallery on the first floor (with polychromes)

Results and discussion

The experimental results of the samples analysed are reported in this section.

- Visual observation of the samples

It was difficult to determine how many layers composed samples PB1 and PB6 and only after observation under the stereo-zoom microscope was it decided which of them would be able to be separated and analysed by XRD and TG-DTA (Figure 4.46.

The data obtained by visual observation of the samples is summarized in Table 4.22.

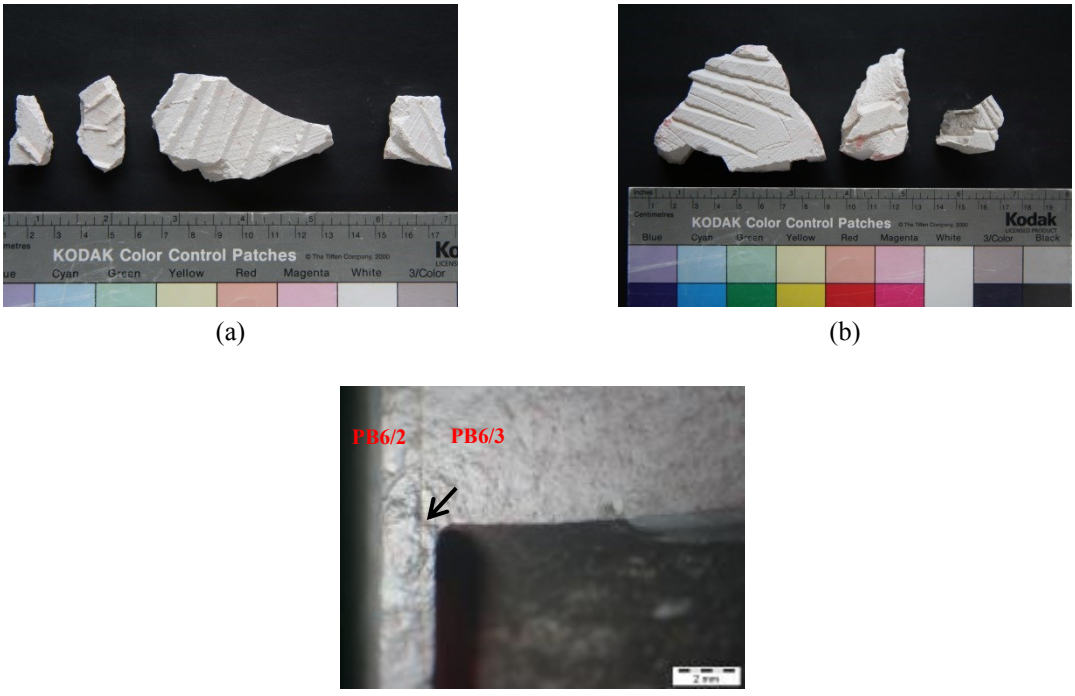

(a) (b)

(c)

Figure 4.46 - Process of execution of ornaments corresponding to sample PB6: (a) outer surface of PB6/1 (b) inner surface of PB6/2 (c) stereo-zoom microscope image showing the interface between PB6/2 and PB6/3

Table 4.22 - Visual observation of the samples from *Bolsa* Palace

Sample	Number of layers	Identification	Description
PB1	Min.10	PB1/1+PB1/2	White plaster layers from within the **moulded frame***.
		PB1/3	Very thin yellowish plaster layer, immediately above PB1/1+PB1/2 that seemed to display some flexibility.
		PB1/4...	Very thin layers (at least 7), consisting on the preparation for the 1st gold leaf application and subsequent restoration operations, till the 2nd gold leaf (the last layer, already decayed).
PB2	1	PB2	Several fragments (> 7) from a breathing hole/**ornament** of the ceiling with traces of gold leaf, an orange pigment (preparation layer of bole?) and restoration plaster(s);
PB3	1	PB3	Octagonal **base of PB2** seeming to have been originally attached to the ceiling with metallic elements that rusted and damaged the piece; It had restoration plaster(s), traces of gold leaf and an orange pigment (rests of bole?); The restoration plasters seem to have been used to paste the several pieces of the damaged octagon to each other and to the ceiling.
PB4	1	PB4	Three fragments of white **ornaments** from the ceiling, less dense than any of the other samples; They presented traces of a blue paint in the base of the side faces that had a different hue in one of them (Figure 4.45, PB4, fragment on the left); That fragment had a much harder surface than the other two, indicating a different preparation; it was rejected with the assumption that it probably resulted from a restoration (with no certainties about that).
PB6	3	PB6/1	**Regularization layer** applied over the mortar with an average thickness of 6 mm; It presented a textured pattern in the outer face that was printed by the grooves of PB6/2 (Figure 4.46 (a) and (b)).
		PB6/2	Thin layer that is the **finishing layer** in the surfaces where there are no ornaments (with polychromes) and is the back layer of the ornaments (PB6/3); It was poured sometime after the first slurry (maybe some minutes, as there is a clear interface between PB6/2 and PB6/3), probably to fill the last millimetres of the mould. It had grooves at the back to promote adhesion to the substrate which are the negative of the pattern observed in sample PB6/1 (Figure 4.46 (b)).
		PB6/3	Precast **ornaments** (with polychromes) moulded in panels; Traces of gilding in some fragments (visible under the stereo-zoom microscope) (Figure 4.47 (a)); Traces of an orange pigmented layer covered with a white painting layer (Figure 4.47 (b) and (c)).

* Analysed together by XRD and TG-DTA as is was very difficult to have a physical separation with 100% certainty.

The grooves in the back surface of the ornaments and the corresponding textured pattern they print in the fresh plaster (or mortar) layer over which they are applied have the function of promoting the adhesion between them. It is a common procedure that was found in sample PB6 and in other case studies, like the *Monserrate* Palace (PM4, Figure 4.79 (c)) or the *Alhambra* complex (Rúbio Domene 2011).

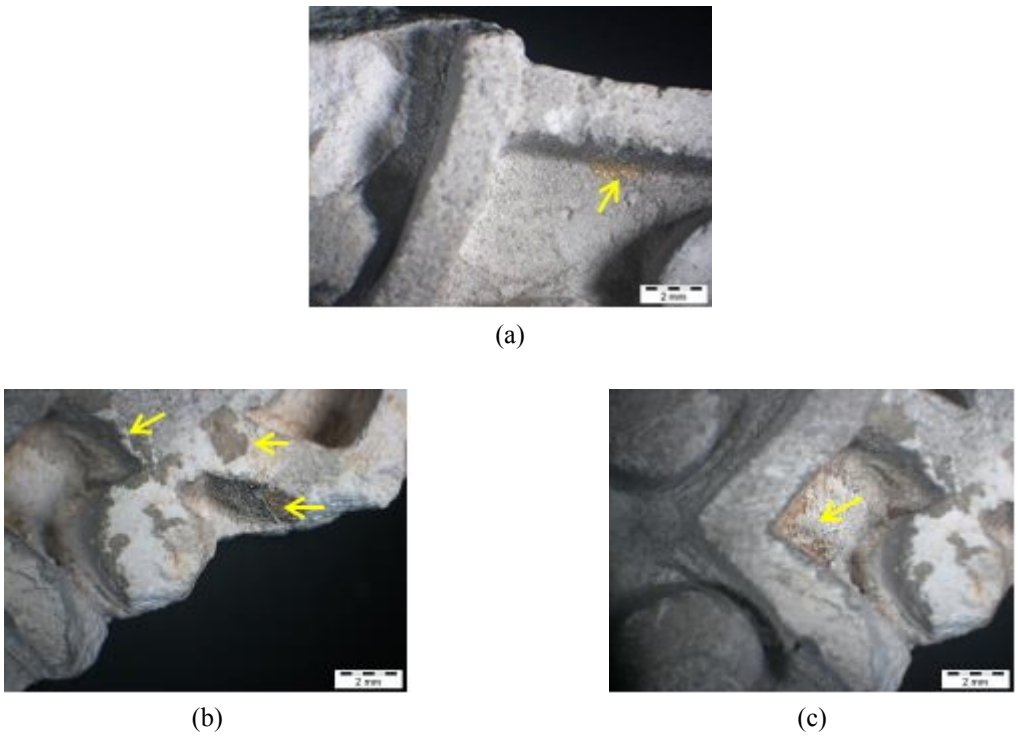

(a) (b) (c)

Figure 4.47 - Stereo-zoom microscope images of previous decorative layers in PB6/3: (a) traces of gilding; (b) and (c) white painting, limewash type, over orange pigmented layer

The visual observation of the samples also allowed seeing that the polychromes of the decorations have suffered already significant changes, meaning that the visual effect originally produced should have been different from what it is presently.

In fact, traces of gilding can be found in the two larger fragments from sample PB6/3 (Figure 4.47 (a)). It is also visible that a white painting layer (lime wash?) now blackened by dust, is covering their surfaces, sometimes over traces of an orange pigmented layer (Figure 4.47 (b) and (c)).

This orange layer was also observed in samples PB2 and PB3. It is most probably due to the material used as preparation layer before the application of the gold leaf, commonly known as “bole”, a supposition that would have to be confirmed by chemical analysis. Other hypotheses are that clay moulds have been used to cast the original ornaments or that clay was pressed against the decoration motifs in order to reproduce parts of them *in loco*, to obtain moulds for the production of new restoration elements.

Once again there is a parallelism with the *Alhambra*, where most of the plaster decorations have an orange layer. Rúbio Domene concluded that, depending on the period the plasters belong to, that layer can have distinct origins, including the hypotheses previously mentioned for the *Bolsa* Palace samples. The loss of many of the original materials was also observed there, namely in the pictorial layers. An example is the detection of traces of gilding in a few decorative elements. All these features are thought to be related to inadequate restoration and/or cleaning procedures.

- Optical microscopy and FESEM-EDS - observation of polished surfaces

  Sample PB1

A cross-sectional polished surface of sample PB1 (Figure 4.48) has been prepared for stratigraphic analysis with the purpose of determining the different layers that compose it.

Figure 4.48 - Polished surface of PB1: global view

Figure 4.49 shows the ten layers observed. A change in the design of the frame due to restoration procedures was also noticed, with the lines of the original piece being slightly straightened.

Due to the large number of layers and low thickness of most of them, a separation without contaminations was impossible and it was decided to determine their composition using FESEM-EDS (Figure 4.50, Table 4.23).

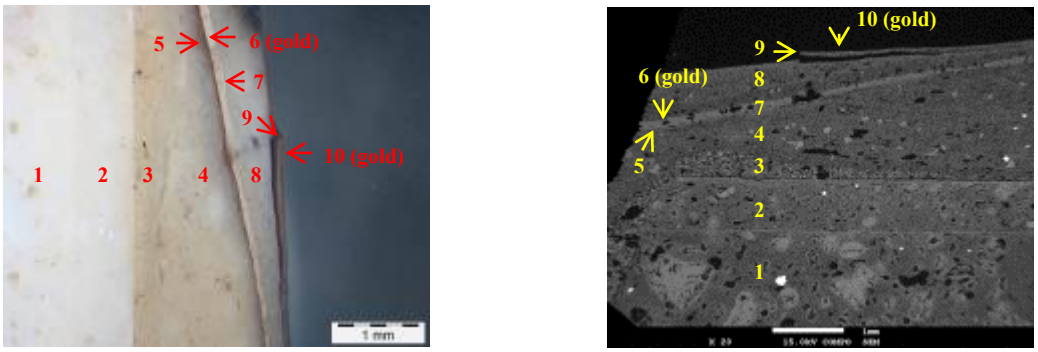

(a) (b)

Figure 4.49 - Polished surface images of PB1 (yellow frame of Figure 4.48) with identification of layers: (a) stereo-zoom microscope; (b) FESEM-BSE

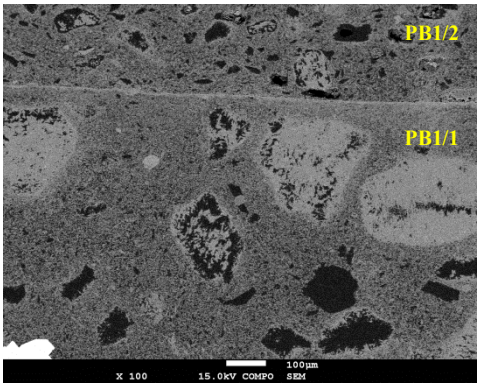

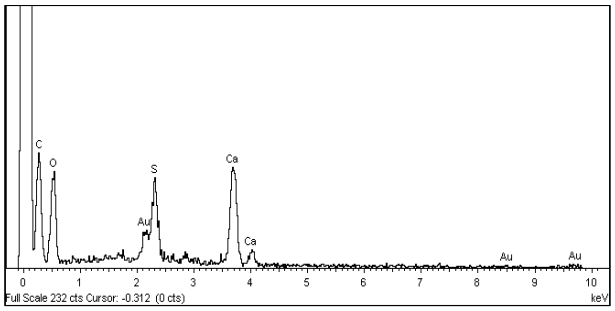

PB1/1

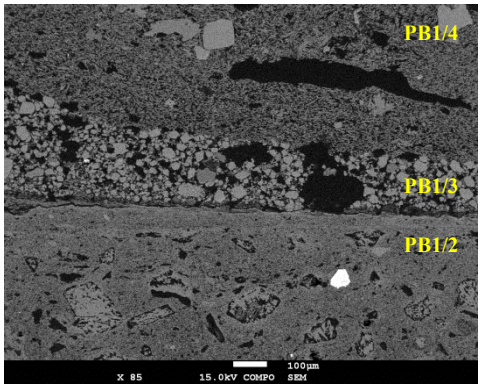

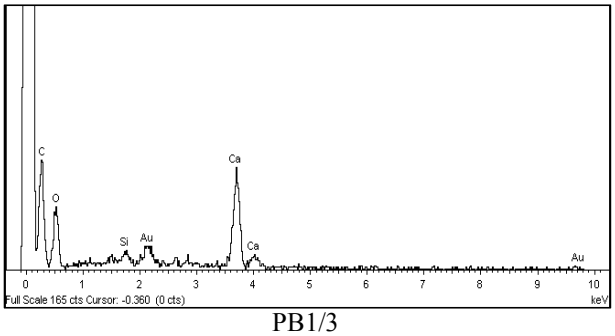

PB1/3

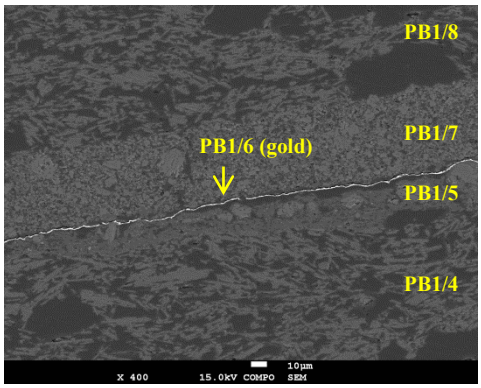

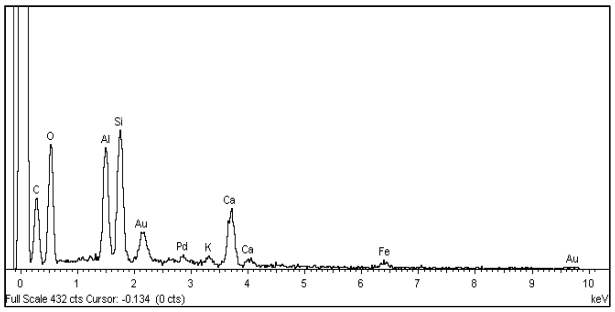

PB1/5

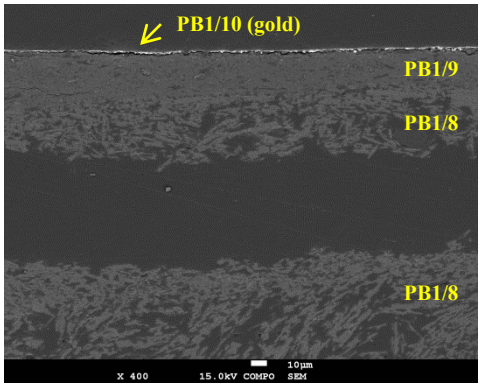

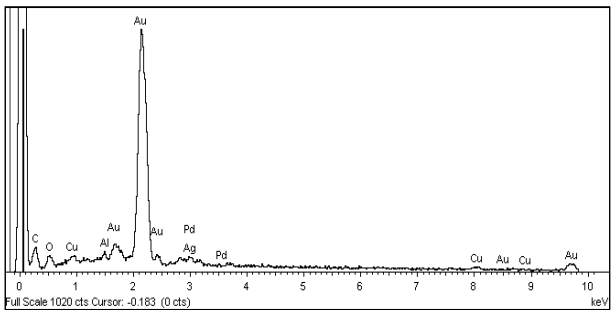

PB1/10

Figure 4.50 - PB1 polished surface: FESEM images and EDS of some layers

Table 4.23 - FESEM-EDS results for sample PB1 stratigraphic analysis

Sample	Layers				
PB1	1+2	3, 7	4, 8	5, 9	6, 10
EDS	Ca, S, C, O (gypsum, calcite)	Ca, C, O (calcite)	Ca, S, O (gypsum)	Si, Al, Mg, Ca, Fe (bole)	Au, traces of Ag

It was concluded that only the first six layers belong to the original piece.

The 7th is the first restoration layer and it was applied over the original gold leaf (6th layer). Its composition - calcite - is similar to that of the 3rd layer though with much smaller grain size (Figure 4.50 (b) and (c)). The function of both is also similar and consists of the promotion of a good adhesion with the precedent layers. The repetitious pattern of composition/function was observed between the other original *versus* restoration layers (4, 5 and 6 similar to 8, 9 and 10, respectively) (Table 4.23).

Finally the first two layers are composed of gypsum and calcite. The morphology of the respective binder matrixes is very similar and the shape of the pores too, differing only in size, bigger in layer 1 than in layer 2 (Figure 4.50 (a)).

The shape of the pores gives interesting indications about the process of execution of a plaster element: angular shaped pores indicate that the plaster mix suffered some kind of compression while round pores mean it was poured with a fluid consistency and let set without further intervention (Rúbio Domene 2011). In sample PB1 all the layers have pores with an angular shape and PB1/1 and PB1/2 are not an exception, i.e. the gypsum-lime plaster that composes them was not poured. The smaller sized pores of layer 2 indicate that it probably was more compressed that layer 1 during execution.

It is also worth pointing out that these two layers (gypsum + calcite) are much whiter than layers 4 and 8 (gypsum) (Figure 4.49 (a)), a fact related to the use of hydrated lime in the composition of the former.

Sample PB6/1

The polished surface of sample PB6/1 was also observed under the stereo-zoom microscope to clarify some uncertainties about the number of layers that composed it, as it showed a preferential fracture pattern typical of the presence of different layers.

In fact, a very discrete interface can be detected (Figure 4.51), meaning that the plaster was applied in two parts. However, as the intergrowth of the crystals between them seems to be very high, each part must have been applied immediately after the other (fresh on fresh) and cannot be considered as a distinct layer.

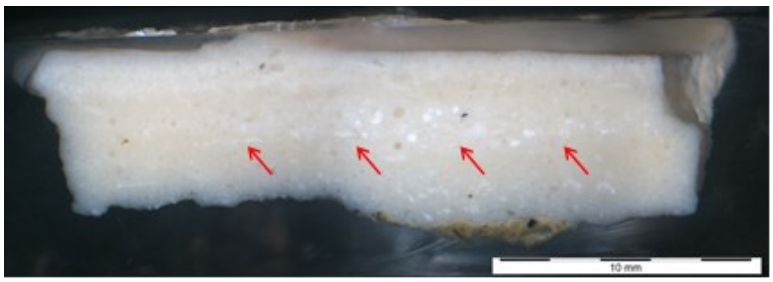

Figure 4.51 - Polished surface of sample PB6/1 and discrete interface between two "layers"

Through an accurate observation of the decorative surfaces of the walls of the Arabian Room it is possible to see that there are joints forming quadrangular patterns. However, they are so well executed that a regular observation would not detect them. In the photos they are not visible either.

This fact indicates that the decorative elements are composed of panels that were first precast and then applied to the base wall. A similar process has been used in the Alhambra in the *Nazarí* period (especially 14th and 15th centuries), though using a different procedure of application of the panels to the walls: they were first fixed in their final position with the aid of some anchorage points made of clay and only afterwards a relatively fluid mix of "grey gypsum" was poured through their back, filling the gap between the wall and the panels and fixing both (Rúbio Domene 2011).

In the Arabian Room the observation of sample PB6/1 indicates that the procedure of application of the panels was different: the base plaster (corresponding to PB6/1) has been first applied to the wall and the panels fixed while it was still fresh. The adhesion is enhanced by the grooves sculpted in the back of the panels and it is probable that some metallic bolts have been used too, as it was observed in *Monserrate* Palace (Figure 4.79). However, there were no panels detached and it was not possible to confirm this hypothesis.

- XRD results

The qualitative mineralogical composition of the samples was determined by XRD and the results obtained showed that gypsum and calcite are the main constituents (Figure 4.52, Figure 4.53, Figure 4.54 and Table 4.24).

In sample PB1, XRD analyses were only performed in the first three layers. All the others were impossible to separate with 100% certainty. Even though, layers 1 and 2 had to be analysed together.

For the mix of these two layers, XRD results are in agreement with those obtained by FESEM-EDS, indicating that they are mainly composed of gypsum, with calcite being the second constituent. However, in the third layer (PB1/3) EDS analyses detected only calcite while XRD clearly indicates

the presence of gypsum. This difference is probably due to a contamination of PB1/3 with the surrounding layers occurred during its preparation for XRD and TG-DTA analyses.

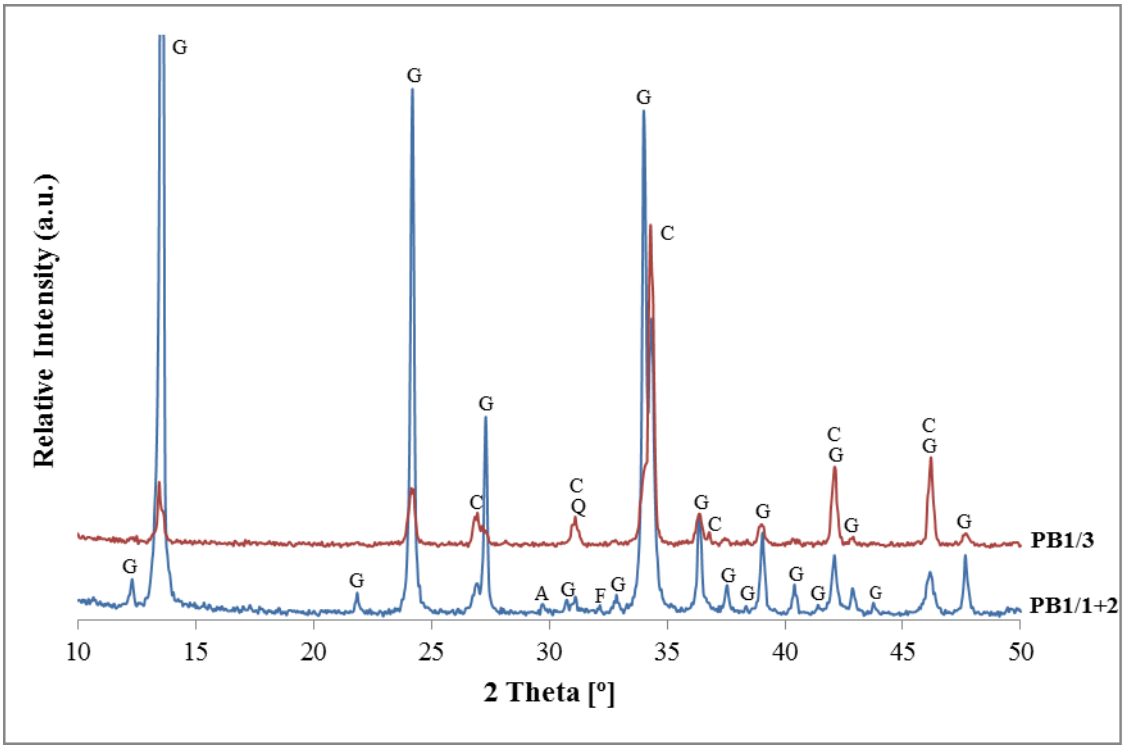

Figure 4.52 - XRD patterns of layers 1 to 3 of sample PB1 from *Bolsa* Palace.
Notation: G - Gypsum; C - Calcite; Q - Quartz; A - Anhydrite; F – Feldspars

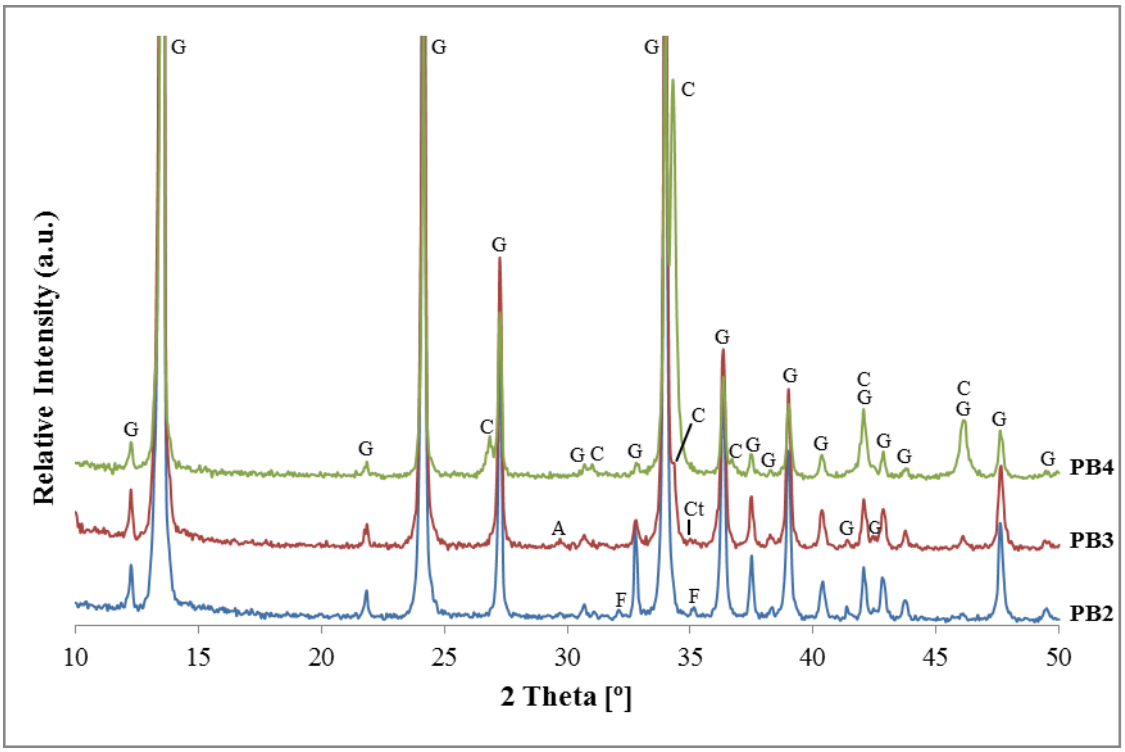

Figure 4.53 - XRD patterns of samples PB2 to PB4 from *Bolsa* Palace.
Notation: G - Gypsum; C - Calcite; A - Anhydrite; F - Feldspars; Ct – Celestine

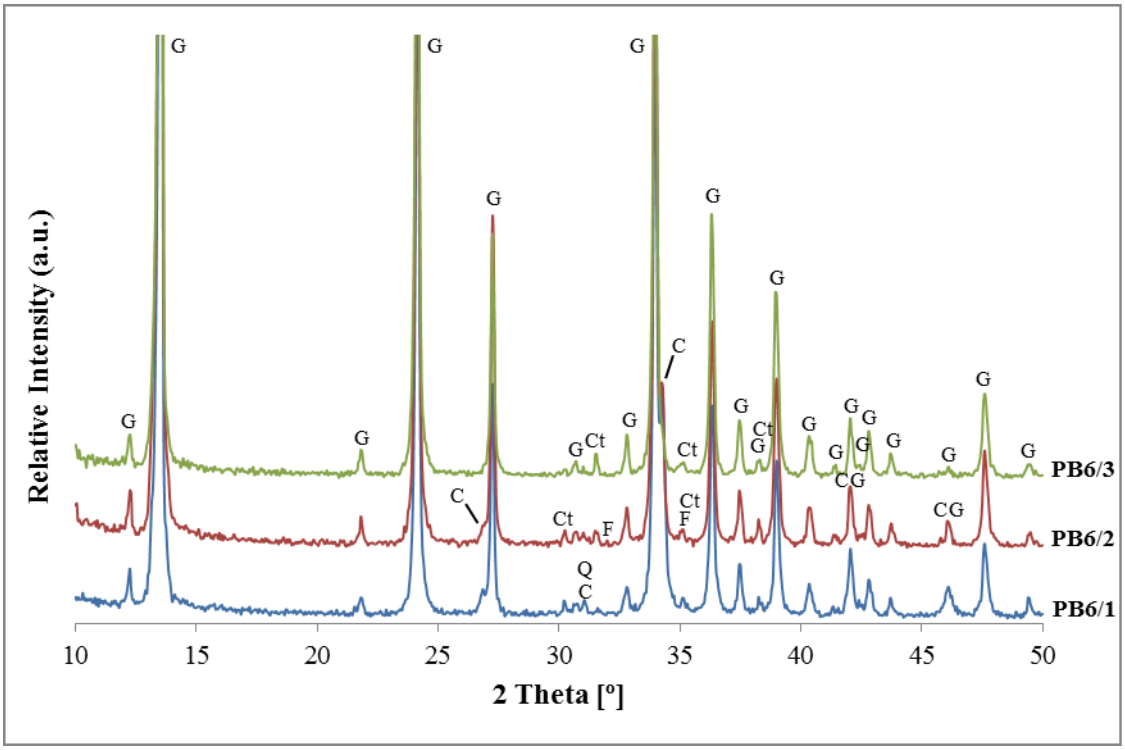

Figure 4.54 - XRD patterns of the 3 parts of sample PB6 from *Bolsa* Palace.
Notation: G - Gypsum; C - Calcite; Q - Quartz; F - Feldspars; Ct - Celestine

Traces of quartz and celestine were also detected and their presences have already been discussed in previous case studies. However, once again it is worth stressing that celestine has been so far only detected in samples from case studies located in the north of Portugal, like the *Bolsa* Palace.

Table 4.24 - XRD qualitative mineralogical composition of the samples from *Bolsa* Palace

Sample	Identified crystalline compounds					
	Gypsum	Calcite	Quartz	Anhydrite	Celestine	Others
PB1/1+2	+++/++++	++/+++	trc	trc	-	Feldspars (trc)
PB1/3	++	+++/++++	trc	-	-	-
PB2	++++	-	-	trc	-	Feldspars (trc)
PB3	++++	+	-	trc	trc	-
PB4	+++	++/+++	-	-	-	-
PB6/1	+++/++++	++	trc	-	trc	-
PB6/2	+++/++++	+	trc	-	trc	Feldspars (trc)
PB6/3	++++	-	-	-	trc	-

Notation used in XRD peak intensity:

++++	Very high proportion (predominant compound)	+	Weak proportion
+++	High proportion	trc	Traces
++	Medium proportion	-	Not detected

- TG-DTA results

The gypsum and calcite contents were determined using TG-DTA analysis and the results of XRD could be confirmed (Table 4.25).Due to the significant amount of thermal analyses performed, it was decided to present the corresponding diagrams in several figures (Figure 4.55, Figure 4.56 and Figure 4.57).

Once again, the samples with more gypsum show the doublet of peaks corresponding to the two steps of dehydration of this material in their DTG and DTA curves. The changes in the slope of the correspondent TG curves referred to the mass loss of these two dehydration steps are more difficult to detect, but they are clearly perceptible in PB2, PB3 and in all the parts of PB6 (Figure 4.56 and Figure 4.57).

The curves also showed lower temperatures of decarbonation of calcite but, unlike what happened in other case studies, the range of the correspondent chemical transformation was not always proportionally broader in the samples with greater content of this compound: in sample PB1/3 it is narrower than in PB1/1+2 and PB4. However, PB1/3 can be considered a special case as it has a certain flexibility indicating that it must have other constituents than calcite and gypsum.

The phase change of soluble to insoluble anhydrite, a pure crystallographic transformation, was detected by DTA in the samples with greater amounts of gypsum, where small exothermic peaks appear between 350 ºC and 400 ºC (Figure 4.56 and Figure 4.57, DTA curves) (S.N.I.P. 1982).

Table 4.25 - Weight loss and calculated gypsum/calcite contents of the samples from *Bolsa* Palace

Sample	Temperature range (ºC)						Calculated contents (%)	
	25→85	85→250	250→600	600→850	850→1000	Loss of ignition	Gypsum	Calcite
PB1/1+ PB1/2	0.1	13.3	1.2	13.9	0.1	28.6	63	32
PB1/3	0.6	5.4	4.2	30.4	5.9	46.5	26	69*
				600→930	930→1000			
PB3	0.1	18.8	0.9	2.5	0.7	23.0	90	6
PB4	0.1	10.7	1.5	20.0	0.2	32.5	51	45
PB6/1		16.1	0.8	8.0	0.9	25.8	77	18
PB6/2		17.4	0.6	4.0	0.3	22.3	83	9
PB6/3	0.0	19.4	0.4	0.6	0.0	20.4	95	1
				600→930	930→1000			
PB2	0.0	20.7	0.8	1.6	0.1	23.2	99	4

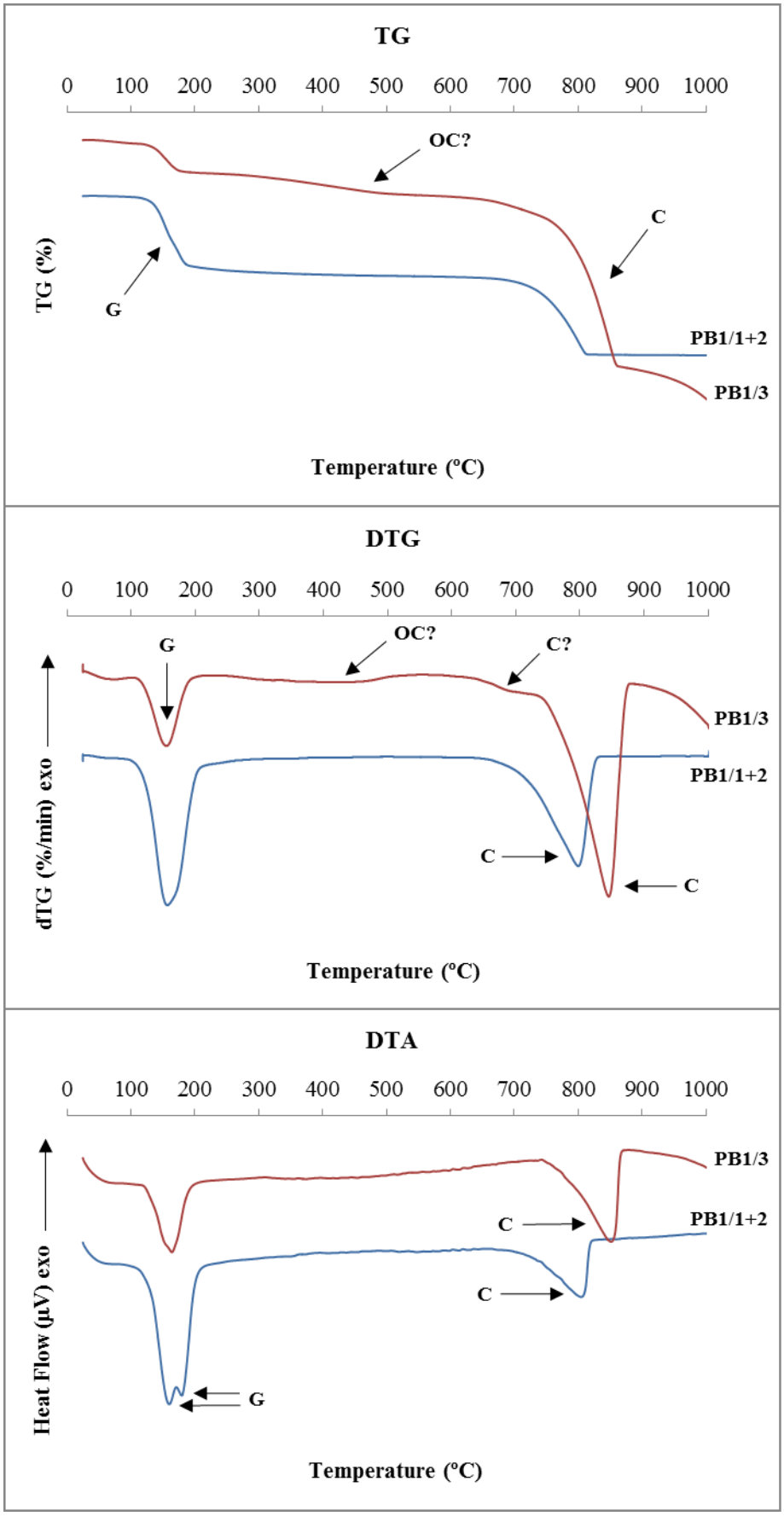

Figure 4.55 - TG, DTG and DTA curves of the samples PB1/1+2 and PB1/3.
Notation: G - Gypsum dehydration; C - Calcite decarbonation

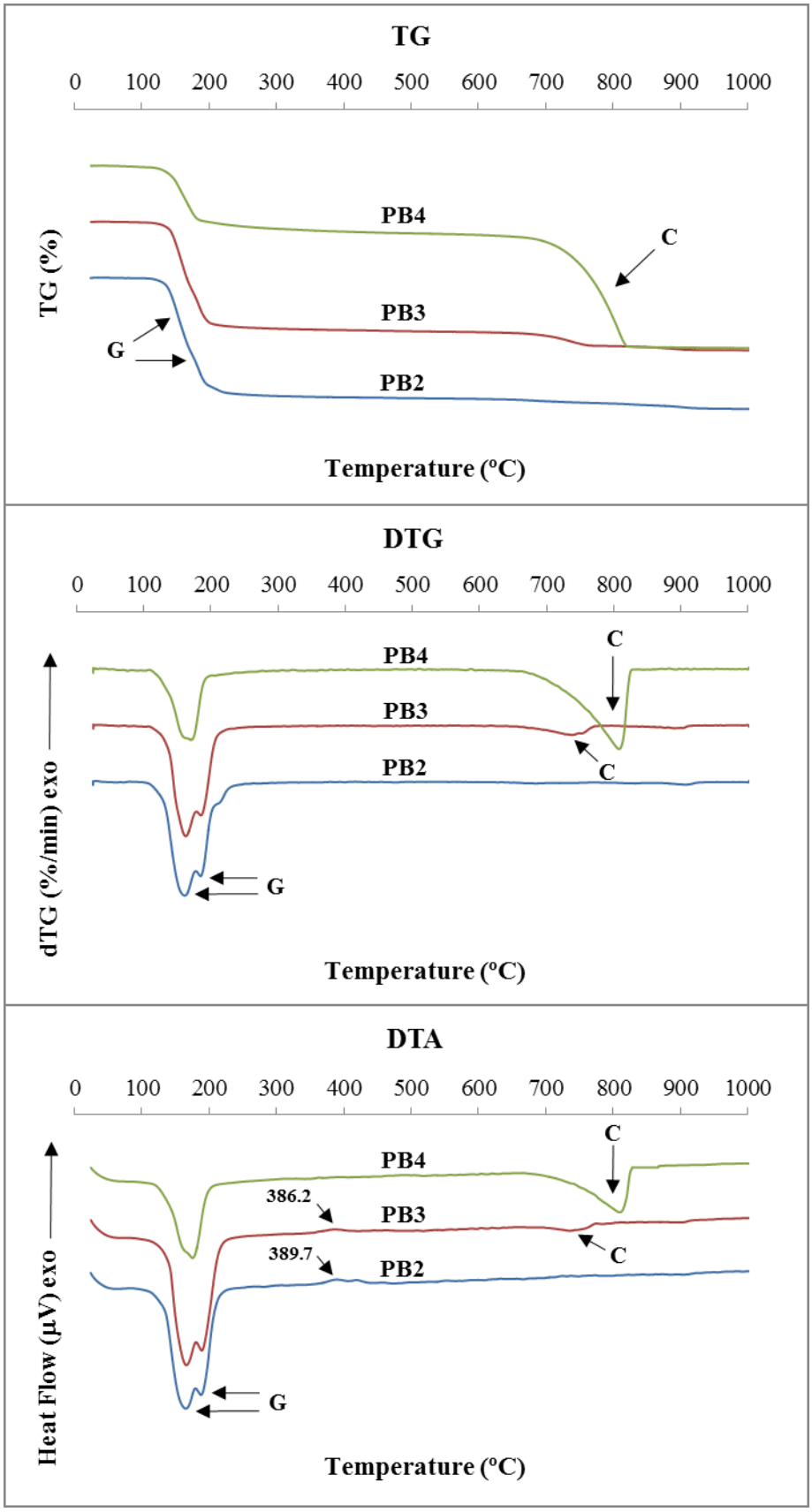

Figure 4.56 - TG, DTG and DTA curves of the samples PB2, PB3 and PB4.
Notation: G - Gypsum dehydration; C - Calcite decarbonation

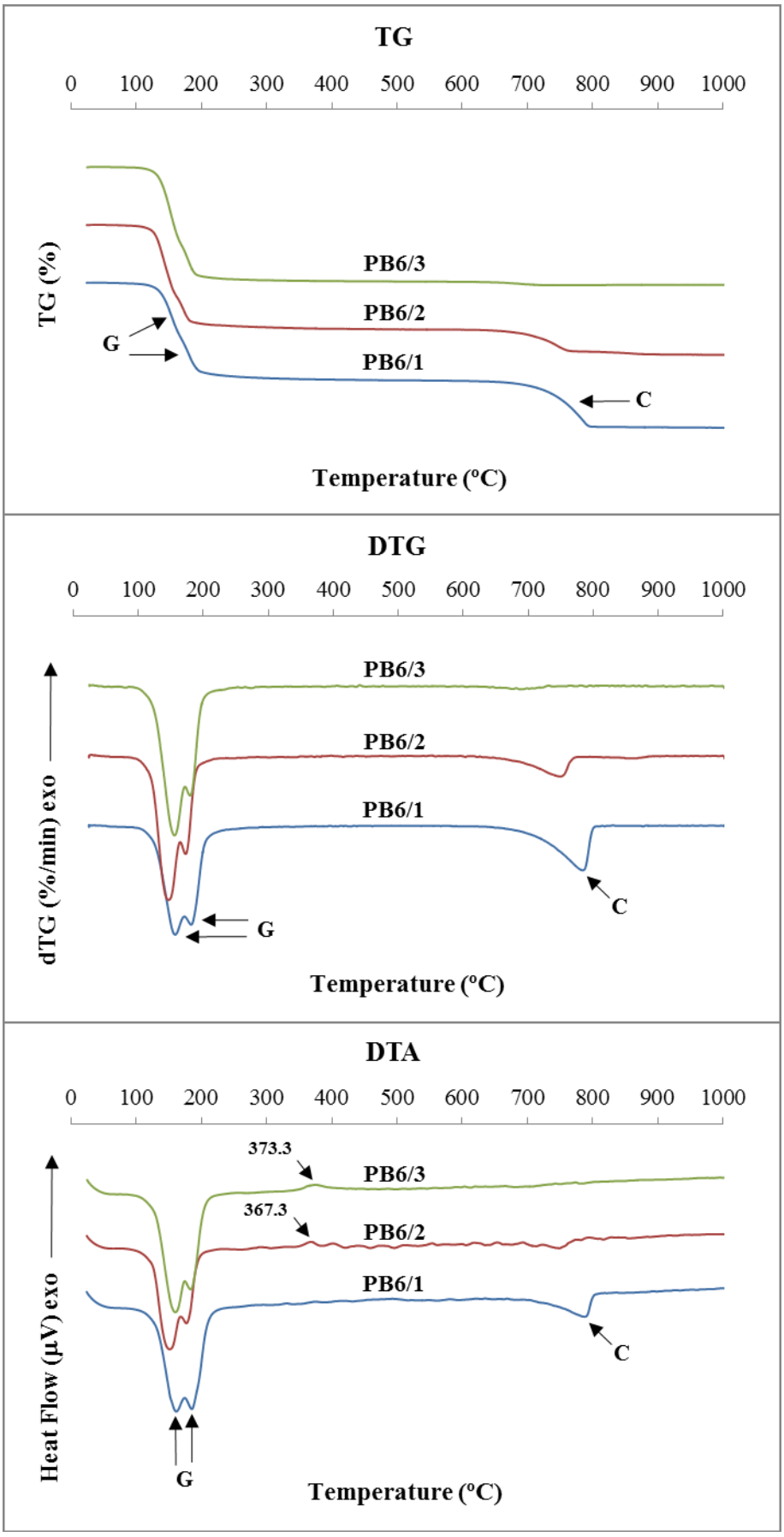

Figure 4.57 - TG, DTG and DTA curves of the samples PB6/1, PB6/2 and PB6/3
Notation: G - Gypsum dehydration; C - Calcite decarbonation

For the mix of the first two layers of sample PB1 (PB1/1+PB1/2), TG-DTA results are in agreement with those obtained by FESEM-EDS. However, as for XRD, the results of the third layer clearly indicate the presence of gypsum while EDS detected only calcite; the hypothesis of a contamination has been pointed out.

The FESEM observations also showed that the calcite is in the form of very round particles without a connection resulting from a chemical reaction between them (Figure 4.50). So, it is very plausible that an organic binder has been used. The atomic ratio between carbon and calcium quantified by EDS (C/Ca = 54/9) also supports this hypothesis, as it is too high to be only due to a contribution of the resin used in the impregnation of the samples. Finally, the loss of weight between 250 ºC and 600 ºC detected by thermal analysis (Figure 4.55 and Table 4.25), possible to attribute to the decomposition of organic compounds, is also in line with these suppositions.

Still in sample PB1/3, other uncommon features were observed in the respective TG-DTA results:

(a) The unfolding of the decomposition temperatures in two levels (a very discrete loss of weight between 650 ºC and 750 ºC, before the big loss at 750-850 ºC) that can be either due to the presence of two types of carbonates, or to the same type but with two distinct particle size;
(b) The continuous loss of weight above 850 ºC, until the end of the procedure (1000 ºC).

Regarding item a) some remarks have already been made in 4.3.1.2 (*cf.* "TG-DTA results"). In this case, the most plausible explanation seems to be the presence of grains of very different size, as can be seen in Figure 4.58.

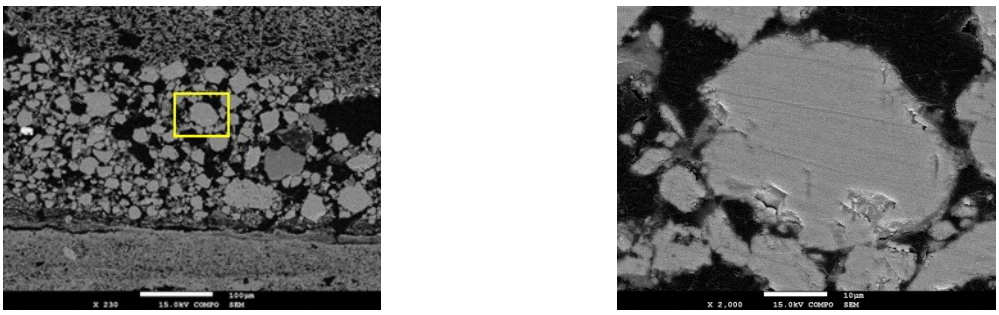

(a) (b)

Figure 4.58 - FESEM images of PB1 polished surface: (a) highlight of PB1/3 where calcite grains of very different sizes are visible; (b) area corresponding to yellow frame of (a)

To explain the phenomenon described in b), further analytical techniques were needed to help clarifying if other substances than those detected by XRD and TG-DTA analyses were present.

The same can be said about sample PB2, where the sum of the gypsum and calcite contents is above 100%. In this case, the gypsum content seems to be inflated by the presence of any substance that undergoes weight loss in the same range of temperatures.

- Physical properties

Physical properties were determined in the samples where the quantity and shape were appropriate to perform the corresponding experimental techniques.

Capillary absorption

The coefficient of capillary absorption by contact (Ccc) was determined in sample PB4 (Figure 4.59) and the results obtained are summarized in Table 4.26.

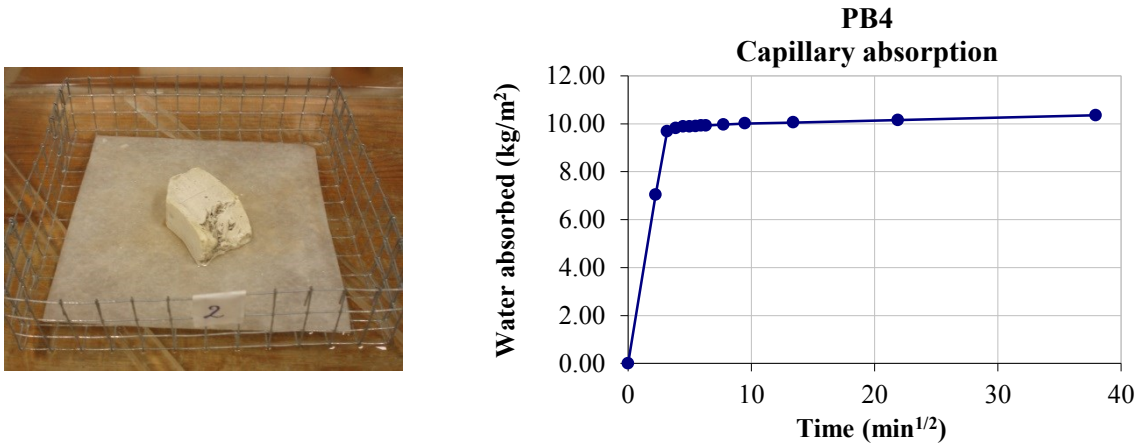

(a) (b)

Figure 4.59 - Water absorption by capillarity of sample PB4: (a) test specimen during the determination; (b) graphical representation of the results

These results are very similar to those of sample CP2: the rate of suction is very high in the first 5 minutes, with the water absorbed during this period representing 67.97% of the total amount absorbed during the time of the procedure (24 h); the major part of the absorption (93.52%) occurs in the first 10 minutes (Figure 4.59 (b)), which usually indicates a great content of capillary pores with a high percentage of the larger ones (considered to have r > 0.5 micron) (Magalhães et al. 2004; Rato 2006); the total amount of water absorbed is also high (Table 4.26) which is usually related to a well-connected open porosity (Magalhães et al. 2004; Rato 2006).

Table 4.26 - Capillary absorption by contact results of sample PB4

Test specimen	
Surface (cm^2)	12.36
Weight (g)	20.83
Capillary absorption at 5 min:	
(g)	8.70
($kg.m^{-2}$)	**7.04**
(%, relative to weight of sample)	41.77
(%, relative to total absorption)	67.97
Capillary absorption at 24 h:	
(g)	12.80
($kg.m^{-2}$)	**10.36**
(%, relative to weight of sample)	61.45
Ccc at 5 min ($kg.m^{-2}min^{-1/2}$)	**3.15**

Ccc - capillarity coefficient by contact

The loss of the water absorbed in the capillarity test was evaluated and is represented in Figure 4.60.

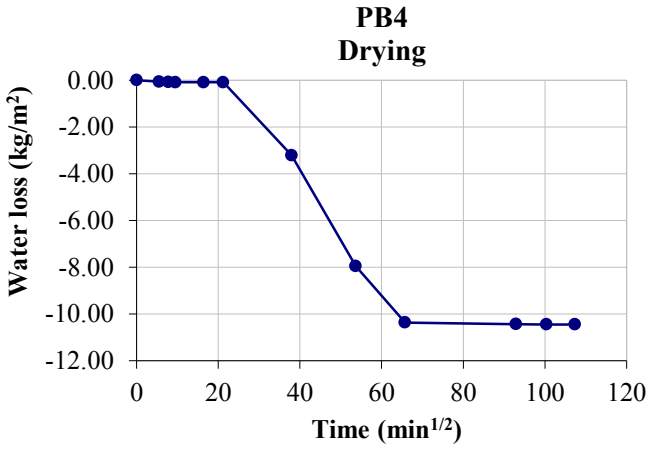

Figure 4.60 - Graphical representation of the drying behaviour of the sample PB4

The drying behaviour of the sample PB4 is also similar to that of the sample CP2: in the first hours the loss of weight was negligible and in the period between 21.21 and 37.95 $min^{1/2}$ (corresponding to 450 and 1440 minutes, respectively) it started to be significant.

Pore size distribution

The pore size distribution was determined by mercury intrusion porosimetry (MIP) in the samples PB4 and PB6/3 (Figure 4.61). The previous supposition about PB4 having a significant amount of pores with radius larger than 0.5 micron was confirmed.

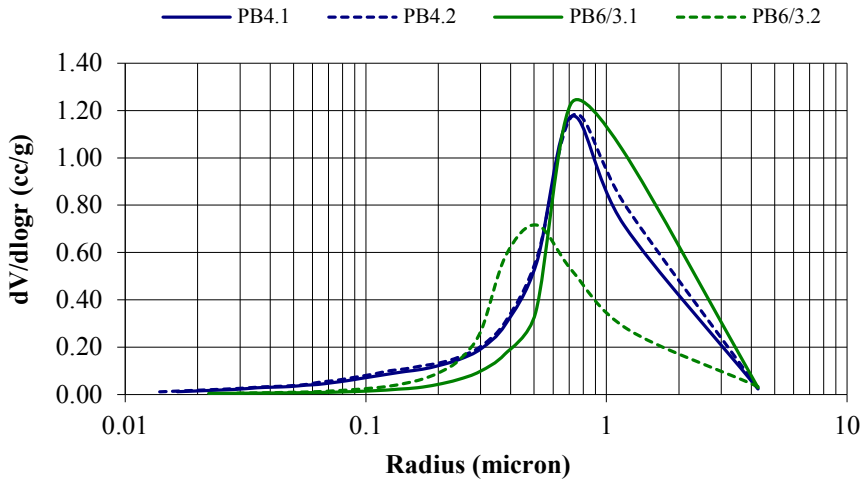

Figure 4.61 - Pore size distribution curves of samples PB4 and PB6/3

In what concerns PB6/3, the results of the two test specimens have a very bad reproducibility. Taking into account that PB6/3 corresponds to a precast element, it is not plausible to assign it to some heterogeneity of the sample's pore structure, being probably originated by any irregularity in the procedure.

In spite of all the previous remarks, a careful analysis of the diagrams displayed in Figure 4.61 shows that the amount of pores with radius under 0.3 micron is different between samples PB4, a gypsum-lime plaster and PB6/3, a gypsum plaster: the first has a higher volume of pores with $r < 0.3$ micron, a difference that is still observed at 0.1 micron. Under that value ($r < 0.1$ micron) the amount of pores of the sample PB6/3 is almost negligible. In spite of the bad reproducibility of the results of sample PB6/3 (Table 4.27), these observations agree with the respective average pore radius, which is clearly smaller in sample PB4.

Table 4.27 - Results obtained by MIP analysis in samples PB4 and PB6/3

Sample. .test specimen	Weight	Bulk density	Density	Porosity (MIP)	Pore radius with max. vol.	Average pore radius
	(g)	($kg.m^{-3}$)	($kg.m^{-3}$)	(%)	(μm)	(μm)
PB4.1	0.78	967	2236	56.8	0.716	0.342
PB4.2	0.79	912	2183	58.2	0.731	0.338
PB6/3.1	0.79	1028	2380	56.8	0.711	0.626
PB6/3.2	0.81	1211	2348	48.4	0.515	0.399

Hygroscopic behaviour

The hygroscopic behaviour was studied in samples PB6/1 and PB6/3 and the results are shown in Figure 4.62 and in Table 4.28.

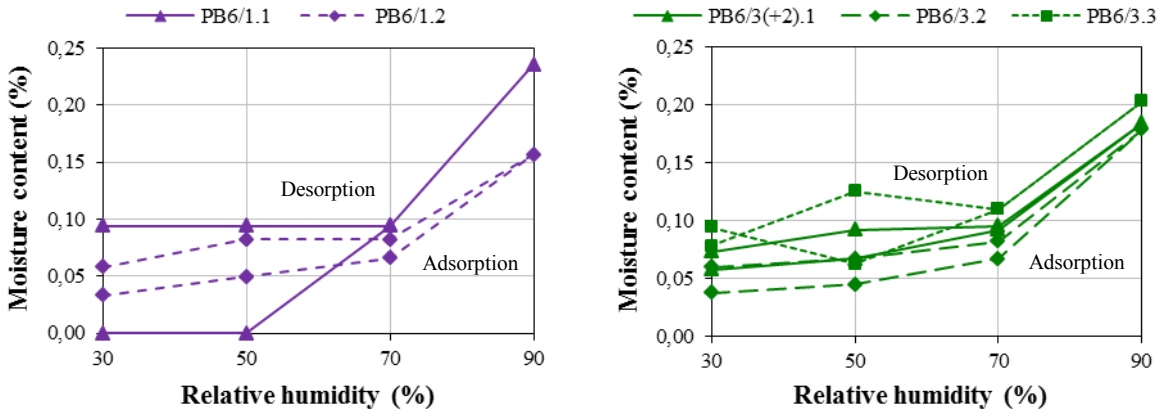

Figure 4.62 - Hygroscopic behaviour of samples PB6/1 and PB6/3

Table 4.28 - Average hygroscopicity results of the samples PB6/1 and PB6/3 (2010)

	RH (%)	MC (%) PB6/1	SD	CV (%)	MC (%) PB6/3	SD	CV (%)
Adsorption	30	*	*	*	0.06	0.029	45.76
	50	*	*	*	0.06	0.012	20.14
	70	0.08	0.020	25.01	0.09	0.021	23.83
	90	**0.20**	0.056	28.51	**0.19**	0.013	6.84
Desorption	70	0.09	0.008	9.48	0.10	0.014	14.41
	50	0.09	0.008	9.48	0.09	0.029	30.75
	30	0.08	0.026	34.04	0.07	0.010	13.66

* Too high CV value making no sense to present the results; RH - relative humidity; MC - moisture content; SD - standard deviation; CV - coefficient of variation

It is important to notice that in this case study both the results of pore size distribution and hygroscopic behaviour are not significant enough to draw trustful conclusions: the graphs of Figure 4.62 have one curve with a very different profile from the other(s) of the same set that correspond to the test specimens of lower weight, PB6/1.1 (2.123 g) and PB6/3.3 (6.393 g), whose higher susceptibility to errors and/or interferences is probably in the origin of this occurrence.

Anyway, these results show that the phenomenon of hysteresis exists in both samples and seem to be slightly clearer in PB6/1. In spite of the pore size distribution of this sample not having been determined, some remarks made in previous case studies about the relationship between the

gypsum-calcite composition and the hygroscopic behaviour, namely that the plasters with a higher content of calcite have a higher volume of pores with radii under 0.1 micron and are more prone to show hysteresis, seem to be also applicable here.

- Mechanical properties

Dynamic modulus of elasticity

The dynamic modulus of elasticity was the only mechanical property determined in the samples from *Bolsa* Palace (Table 4.29). Due to their shape, it was not possible to perform the compressive strength test method in any of them.

Table 4.29 - Dynamic modulus of elasticity results of the samples from *Bolsa* Palace

Sample	Bulk density[(1)] ($kg.m^{-3}$)	Distance (m)	Time (μs)	SD	CV (%)	Speed ($m.s^{-1}$)	DME (MPa)
PB4	995	0.031	29.9	0.2	0.6	1041	970
PB6/3	1045	0.045	27.1	0.1	0.3	1659	2590

[(1)] Calculated: weight/(area of the base x height); SD - standard deviation; CV - coefficient of variation; DME - dynamic modulus of elasticity

The ultrasonic pulse velocity and the DME of sample PB4 are significantly lower than usually found in samples with similar gypsum-calcite composition and bulk density (Freire et al. 2010). The use of air-entraining admixtures to reduce the density of the decorative elements corresponding to this sample is a possible explanation as they are profusely present in the ceiling of the Arabian Room (Figure 4.43). Nevertheless it is a supposition very difficult to prove.

In the case of sample PB6/3 the same parameters (ultrasonic pulse velocity and DME) are in the lower limit of the most common results obtained in samples with the same gypsum-calcite composition (Freire et al. 2011). Yet, this can be also due to its density being slightly lower than that of the referred samples.

4.3.2.3 The *Barão Salgueiro* Manor house

The *Barão Salgueiro* Manor house is located in *Leiria's* city centre, more precisely in the current *Largo Cândido dos Reis*, a noble area of the city since the 17th century. There stood the manor houses of the prominent families where the Baron of *Salgueiro's* was included (C. M. Leiria n.d.).

It is a robust construction dated from the mid-19th century and the first building of such dimensions in the city having more than one floor (Figure 4.63 (a)). The records of the name of the architect that

authored the project have not been found so far but it was clearly designed with the intent of provoking a strong visual impact and to be well integrated in the Romantic spirit.

The main façade was originally painted to simulate a marbled surface that time destroyed remaining now a few traces of a bad restoration work (Figure 4.63 (b)). The entire building is in a poor condition but the intervention already planned has been abandoned due to the economic crisis starting in 2008.

The walls and ceilings' interior coatings are quite simple; only the assembly room (Figure 4.63) and a contiguous small dining room have more elaborated decorative surfaces.

(a)

(b)

(c)

(d)

(e)

Figure 4.63 - *Barão Salgueiro* Manor house: (a) general view; (b) detail of the façade; (c) assembly room with partially collapsed ceiling; (d) and (e) decorative elements

Samples

A total of three samples, all previously detached, were analysed. Their identification and description are summarized in Table 4.30 and the respective images are shown in Figure 4.64.

Table 4.30 - Identification and description of the samples from *Barão Salgueiro* Manor house

Sample identification	Description
PBS1	Ceiling plaster
PBS2	Friezes
PBS3	Ornaments

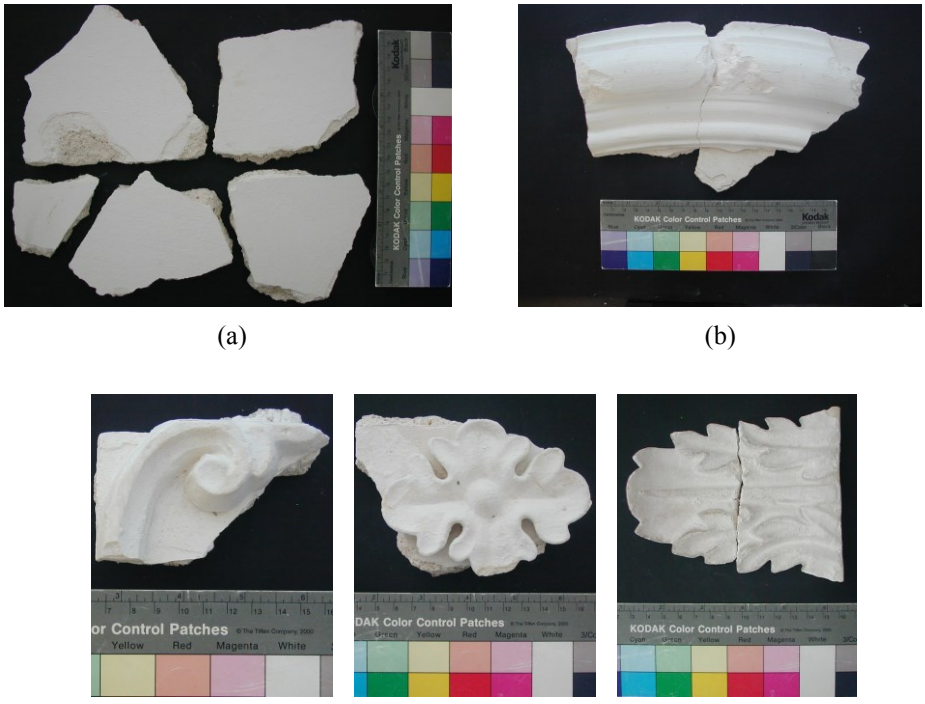

(a) (b)

(c)

Figure 4.64 - Photographs of some fragments of the analysed samples from *Barão Salgueiro* Manor house: (a) PBS1; (b) PBS2; (c) PBS3

Results and discussion

The experimental results of the samples analysed are reported in this section.

- Visual observation of the samples

The information obtained by visual observation of the samples is summarized in Table 4.31 and some details are shown in Figure 4.65.

Table 4.31 - Visual observation of the samples from *Barão Salgueiro* Manor house

Sample	Description
PBS1	Several fragments from the **smooth surface** thin-layer plaster of the ceiling of the main room (Figure 4.64 (a)), all with mortar still attached; The mortar layer was light coloured (almost white), had a thickness of 12-15 mm and was very stiff and compact (Figure 4.65 (a)); The finishing plaster was white, had a much finer particles size and 2-4 mm thickness. It was composed by two layers, seemingly having been applied consecutively as they were so strongly attached that it was impossible to separate them. The compositional analyses made to PBS1 are therefore referred to these two layers together; The fragments showed a pellicle of a white painting that could be removed with some effort (probably a lime wash).
PBS2	Five fragments from moulded on site **voluminous friezes** of the main room, some from the ceiling (Figure 4.64 (b)) and others from the cornice (Figure 4.63 (c), yellow arrow); Four of these fragments still had mortar attached and consisted of a thick layer of plaster strongly bonded to the base (Figure 4.65 (b)); They all had a painting layer, very easy to remove, that seemed to be more brittle than that of PBS1 fragments.
PBS3	Seven precast **ornaments** from the decoration of the main room, four of which still attached to the ceiling's finishing surface (Figure 4.65 (c); A pellicle of white painting with a similar aspect to that of PBS1 was observed. Below that pellicle the surface of the plaster was yellow, seeming that a preparation product had been applied before the paint; In spite of being a bit difficult to remove (like in PBS1) it seemed to be a lime wash type painting due to the brittleness observed. After its removal, the relief and small details present in the surface of the ornaments became much more visible.

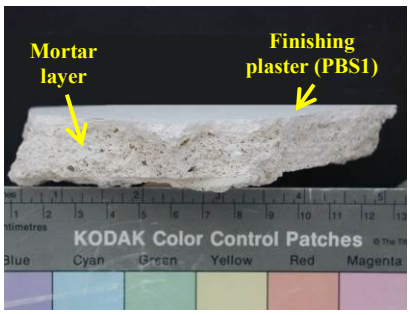

(a)

(b)

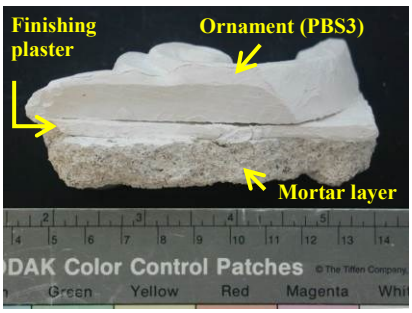

(c)

Figure 4.65 - Cross section images of the samples from *Barão Salgueiro* Manor house: (a) PBS1; (b) PBS2; (c) PBS3

Contrarily to what was observed in the case studies from the 18th century, the decorative elements corresponding to sample PBS3 are all similar to each other (Figure 4.63 (d)), having been precast by an "industrial manufacture" process.

It is interesting to notice that in *Restauração* Street building, approximately of the same time as *Barão Salgueiro* Manor house, only part of the ornaments (the skylight plaster decorations) were produced using the same method; the others showed signs of having been handmade (Figure 4.32 (c)).

- XRD results

The qualitative mineralogical composition of the samples was determined by XRD and the results obtained showed that gypsum and calcite are the main constituents (Figure 4.66, Table 4.32).

Traces of quartz are considered to be impurities whose detection has no special meaning due to its common occurrence in the Earth's crust.

In what concerns anhydrite, traces of this compound were found in the samples with higher contents of gypsum (PBS2 and PBS3) and can be due to the calcination process, where some over burnt material was always present (Sanz 2009; Cardoso 2010), or/and to the raw material, as it is a common impurity of the gypsum deposits.

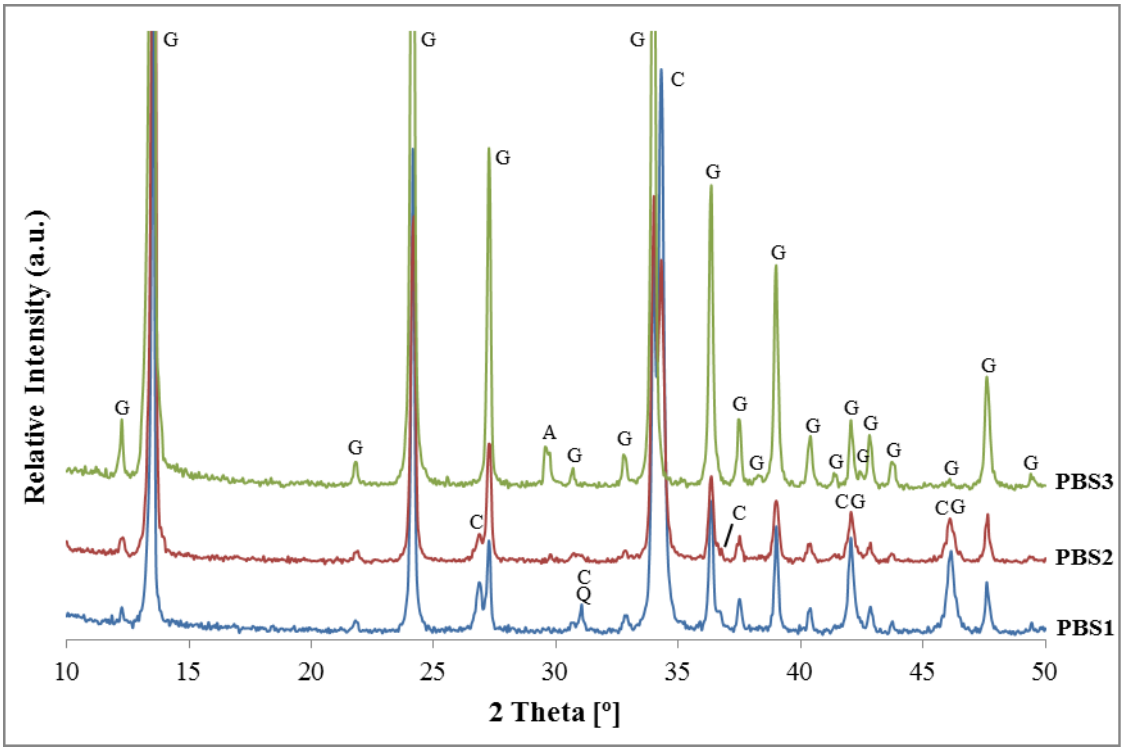

Figure 4.66 - XRD patterns of the samples from *Barão Salgueiro* Manor house
Notation: G - Gypsum; C - Calcite; Q - Quartz; A - Anhydrite

Table 4.32 - XRD qualitative mineralogical composition of the samples from *Barão Salgueiro* Manor house

Sample	Identified crystalline compounds				
	Gypsum	Calcite	Quartz	Anhydrite	Others
PBS1	++/+++	+++	trc	-	-
PBS2	+++	++/+++	trc	trc	-
PBS3	++++	-	-	trc	-

Notation used in XRD peak intensity:

++++	Very high proportion (predominant compound)	+	Weak proportion
+++	High proportion	trc	Traces
++	Medium proportion	-	Not detected

- TG-DTA results

The amounts of gypsum and calcite were determined using TG-DTA analysis and the results of XRD could be confirmed (Table 4.33 and Figure 4.67).

Table 4.33 - Weight loss and calculated gypsum/calcite contents of the samples from *Barão Salgueiro* Manor house

Sample	Temperature range (ºC)						Calculated contents (%)	
	25→85	85→250	250→600	600→850	850→1000	Loss of ignition	Gypsum	Calcite
PBS1	0.1	9.2	1.5	22.3	0.4	33.5	44	51
PBS2	0.1	11.9	1.3	17.6	0.4	31.3	57	40
PBS3	0.0	19.9	0.5	0.6	0.6	21.6	95	1

The doublet of peaks corresponding to the two steps of dehydration of gypsum is well defined in all the DTG and DTA curves (Figure 4.67). However, the phase change of soluble to insoluble anhydrite is only perceptible in the DTA curves of the samples with greater amounts of gypsum (PBS2 and PBS3) through the visualization of small exothermic peaks between 360 ºC and 370 ºC.

In what concerns the decarbonation of calcite, it occurs between 700 ºC and 850 ºC an interval typical of the presence of considerable amounts of this compound, as is the case of samples PBS1 and PBS2.

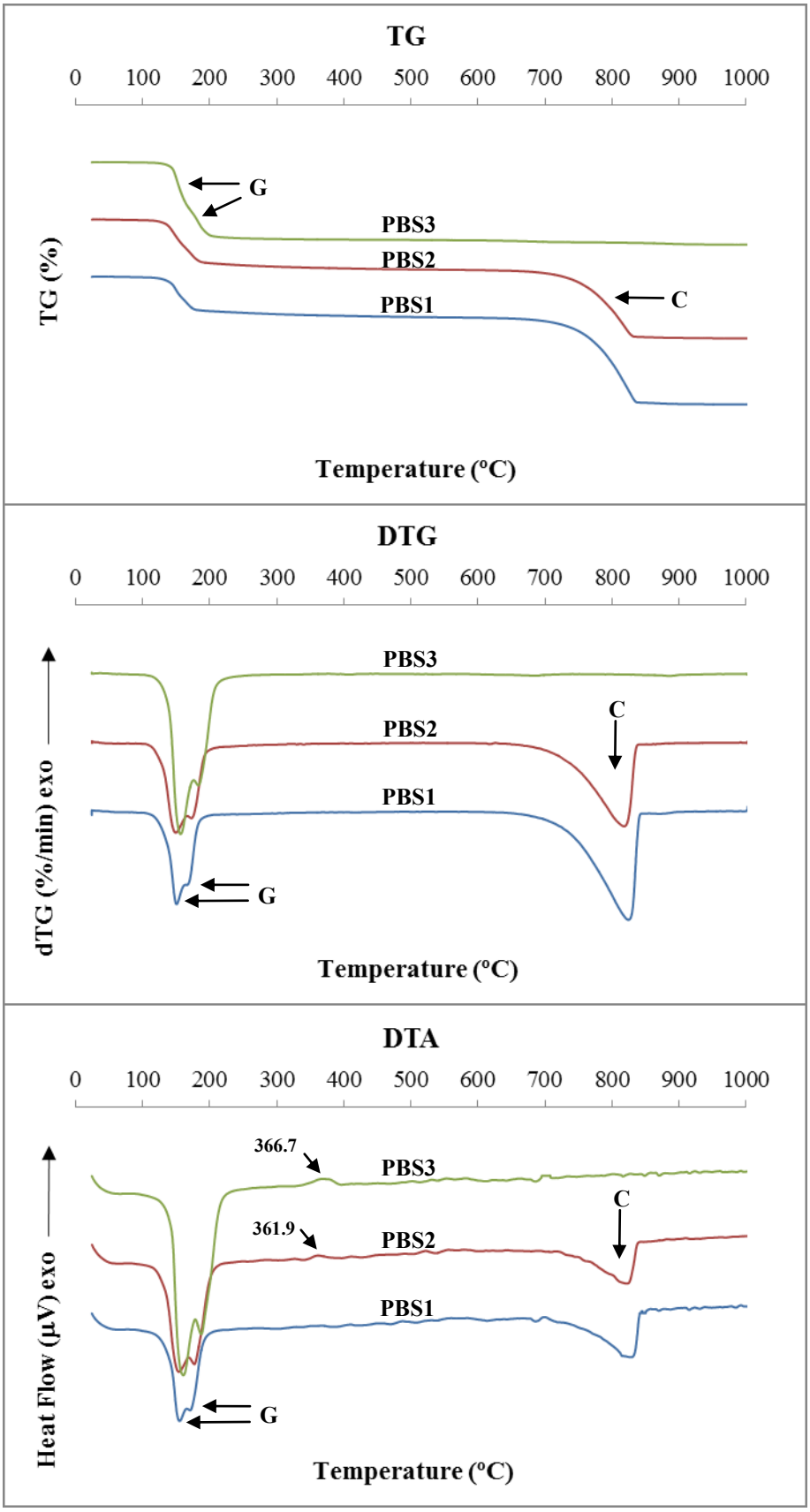

Figure 4.67 - TG, DTG and DTA curves of the samples from *Barão Salgueiro* Manor house. Notation: G - Gypsum dehydration; C - Calcite decarbonation

- Physical properties

Capillary absorption

The coefficient of capillary absorption by contact (Ccc) was determined in samples PBS1 and PBS2 (Figure 4.68) and the results obtained are summarized in Table 4.34.

(a)

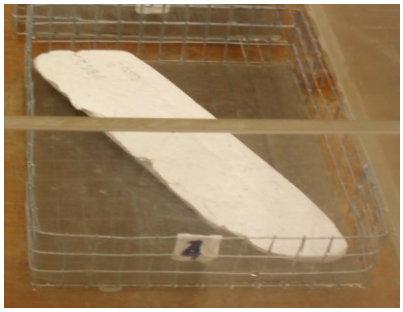

(b)

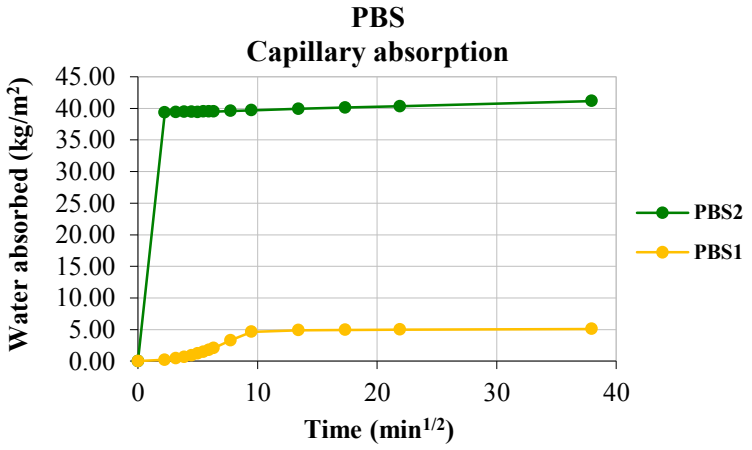

(c)

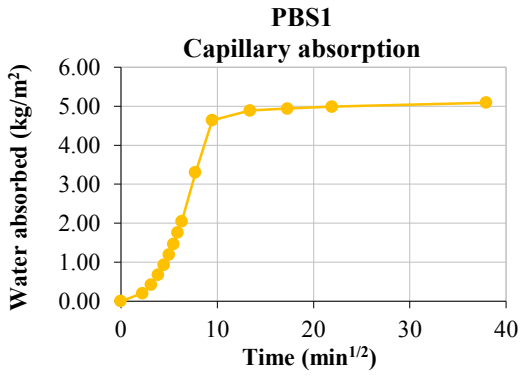

(d)

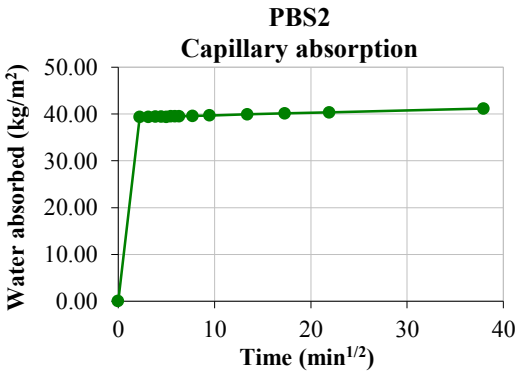

(e)

Figure 4.68 - Water absorption by capillarity of samples PBS1 and PBS2: (a) PBS1 and (b) PBS2 during the determination; (c) to (e) graphical representation of the results

Table 4.34 - Capillary absorption by contact results of samples PBS1 and PBS2

Test specimen	**PBS1**	**PBS2**
Surface (cm^2)	24.92	17.09
Weight (g)	47.00	101.48
Capillary absorption at 5 min:		
(g)	0.51	67.21
($kg.m^{-2}$)	**0.20**	**39.33**
(%, relative to weight of sample)	1.09	66.23
(%, relative to total absorption)	4.02	95.55
Capillary absorption at 24 h:		
(g)	12.68	70.34
($kg.m^{-2}$)	**5.09**	**41.16**
(%, relative to weight of sample)	26.98	69.31
Ccc at 5 min ($kg.m^{-2}min^{-1/2}$)	**0.09**	**17.59**

Ccc - capillarity coefficient by contact

The two samples had a completely different behaviour regarding capillary absorption, with PBS2 showing an unusually high absorption rate in the first minutes (Ccc at 5 minutes = 17.59 $kg.m^{-2}min^{-1/2}$, absorbing more than 95% of the total in this period) and very high global absorption capacity (41.16 $kg.m^{-2}$ corresponding to 69.31% of the weight of the sample).

On the contrary, sample PBS1 had a low initial absorption rate, clearly shown in Figure 4.68 (d), with the first 5 minutes representing only 4.02% of the global absorption, which was much lower as well (5.09 $kg.m^{-2}$ corresponding to 26.98% of the weight of sample).

According to Thomson *et al.* (2004), the capillary water rise occurs in pores with radius between 0.05 micron and 50 micron; yet, they cite other authors that consider the upper limit to be 1 mm (Meng 1996).

Rato (2006) states that the bigger pores are the major contributors to the driving force (higher perimeters lead to higher surface tensions) and the smaller pores offer resistance to the capillary rise (they have a higher capillary pressure), concluding that the first ones are responsible for the initial rates of suction and the later for the rhythm of absorption observed after that, until the stabilization of the system is achieved.

Taking these remarks into account, the results obtained seem to indicate that sample PBS1 has low total porosity and a pore size distribution where the capillary pores of smaller size ($r < 0.5$ micron) must be predominant, while in sample PBS2 the opposite is likely to occur, i.e. extremely high porosity with predominance of pores with radius above 0.5 micron. It is important to notice, however, that in this last case the capillary absorption behaviour is too unusual to be explained based only on the

pore size distribution; the friability of the test specimen used, probably due to a bad preparation of the corresponding plaster (with excess water) or to a long exposure to high moisture contents, has certainly a direct relation with it.

The loss of the water absorbed in the capillarity test was also evaluated and is represented in Figure 4.69.

In spite of having absorbed a much higher quantity of water, PBS2 started to lose weight before PBS1, in agreement with the respective capillary absorption rates. However, PBS1 can also be considered to have a good drying capacity, as it stabilizes even before PBS2. So, the drying behaviour is good for both samples, i.e. different pore size distributions and global porosities are not incompatible with having a well-connected open porosity.

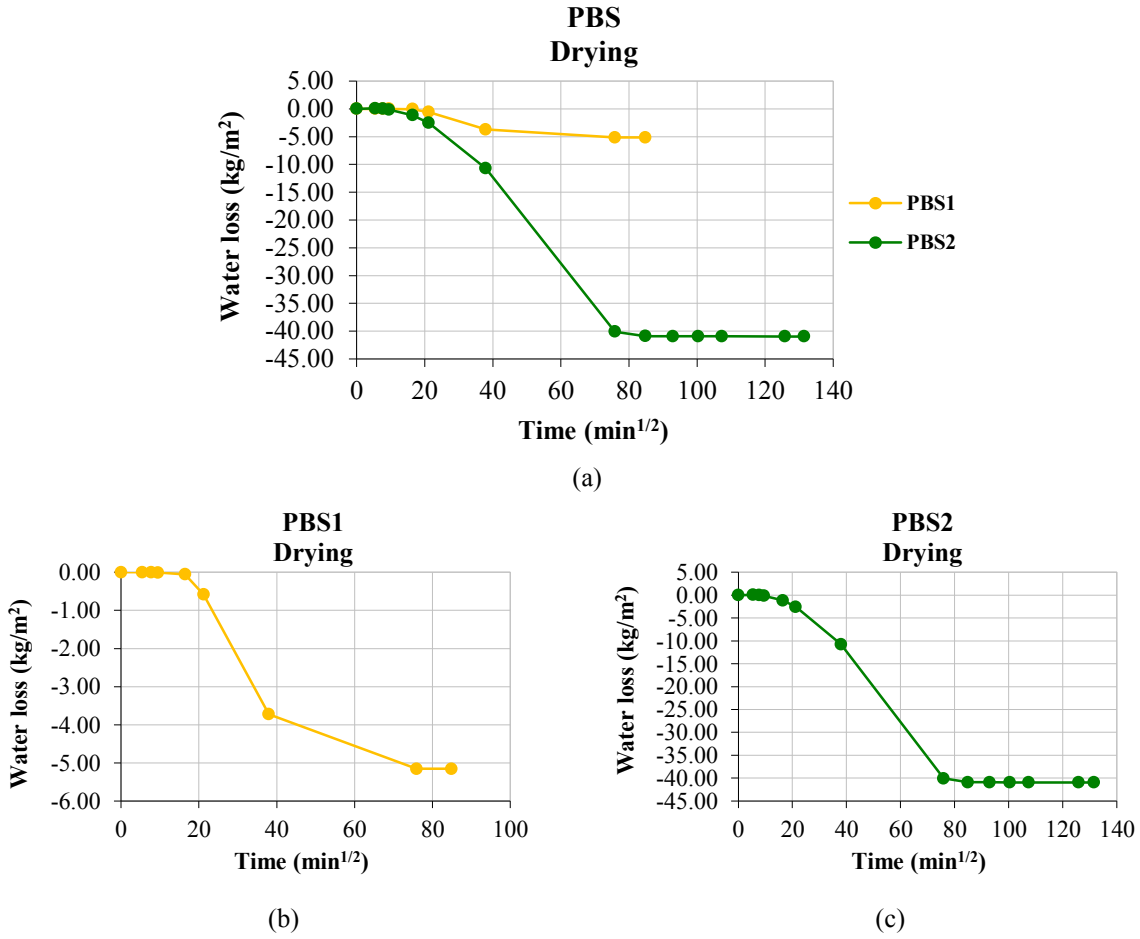

Figure 4.69 - Graphical representation of the drying behaviour of the samples from *Barão Salgueiro* Manor house: (a) joint analysis, for relative comparison; (b) and (c) individual analysis

Hygroscopic behaviour

The hygroscopic behaviour was studied in all the samples from this case study and the results are shown in Figure 4.70 and Table 4.35.

(a)

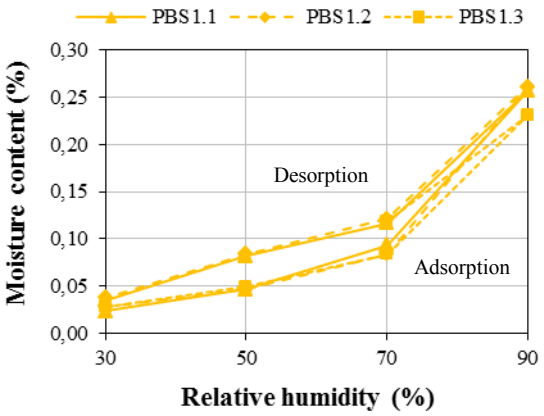

(b)

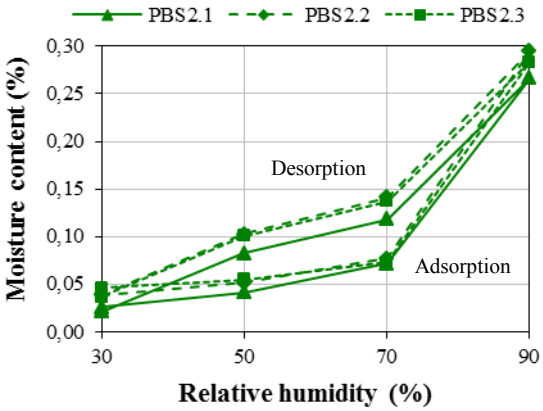

(c)

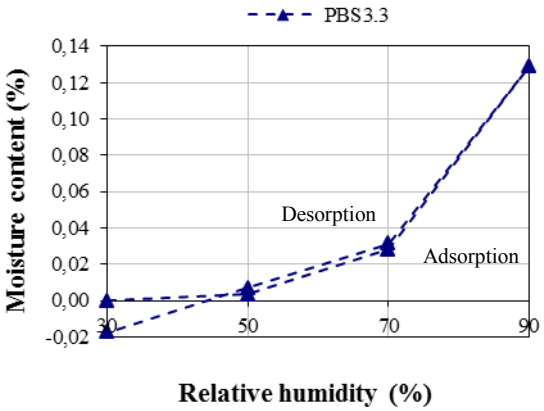

(d)

Figure 4.70 - Hygroscopic behaviour of the samples from *Barão Salgueiro* Manor house: (a) Test specimens; (b) graphical representation of the results

Table 4.35 - Average hygroscopicity results of the samples from *Barão Salgueiro* Manor house (2014)

RH (%)	MC (%) PBS1	SD	CV (%)	MC (%) PBS2	SD	CV (%)	MC (%) PBS3**
30	0.03	0.003	10.14	0.04	0.010	27.76	0.00
50	0.05	0.001	2.72	0.05	0.007	14.62	0.00
70	0.09	0.005	6.24	0.07	0.003	3.59	0.03
90	**0.25**	0.017	6.65	**0.28**	0.014	5.03	**0.13**
70	0.12	0.002	1.97	0.13	0.012	9.35	0.03
50	*	*	*	0.10	0.011	11.89	0.01
30	*	*	*	0.03	0.010	30.96	-0.02

* Too high CV value precluding presenting the results; ** Determined in one test specimen only; RH - relative humidity; MC - moisture content; SD - standard deviation; CV - coefficient of variation

Looking at the curve profiles of Figure 4.70, it seems that sample PBS2 is the one with more pores of smaller size, as it has the highest hygroscopic adsorption and the most pronounced hysteresis effect. In

the case of sample PBS3, such effect is not even present and the hygroscopicity at 90% relative humidity is about half of the values observed in PBS1 and PBS2.

The relationship established in other case studies between hygroscopic behaviour and gypsum-lime content of the plasters, can be considered also applicable here: sample PBS3 is only composed of gypsum, meaning it must have a pore radius distribution more shifted to values above 0.5 micron; the other two samples - both gypsum-lime plasters - must have a higher volume of pores with radii under that value.

However, two facts could have masked the capillary absorption and the hygroscopic behaviour results of these two samples: PBS1 is a thin-layer smooth surface plaster and was tested together with some mortar behind; PBS2 was very friable.

Water vapour permeability

Similarly to other case studies, in *Barão Salgueiro* Manor house it was only possible to determine the water vapour permeability in one test specimen of a sample with a flat surface: PBS1. The device used is shown in Figure 4.71 and the results obtained are presented in Table 4.36.

(a) (b) (c)

Figure 4.71 - PBS1's water vapour permeability determination: (a) preparation of the test specimen; (b) device used (adapted to ancient samples), (c) view of the back surface of the sample (mortar layer)

Table 4.36 - Water vapour permeability results of sample PBS1

Test specimen thickness (d) (mm)	ΔM/24h (g)	Permeability ($ng.m^{-1}.s^{-1}.Pa^{-1}$)	Sd (d=10 mm) (m)
16.57 (2.66 plaster + 13.91 mortar)	0.83	34.71	**0.050**

The values found indicate that sample PBS1 has a high permeability to water vapour, close to the results obtained for gypsum-lime test specimens (Ramos et al. 2010: Sd = 0.059 m) and for lime-based mortars formulations for restoration purposes prepared in laboratory (Veiga et al. 2010: Sd < 0.10 m; Margalha 2010: Sd = 0.05-0.12 m).

In spite of having a low capillary absorption when compared to other samples, its good drying behaviour denotes a well-connected open porosity which, in turn, is usually related to a good water vapour diffusion capacity. So, the results obtained in the various physical properties are in agreement.

- Mechanical properties

As stated before, the object of study in the smooth surface samples is the finishing plaster layers. However, some properties had to be determined in the set "plaster + mortar" due to the impossibility of keeping their physical integrity after a separation process. The mechanical properties are included in this group.

When interpreting the results it is though important to have in mind that the plaster layer is the thinnest one and that in some cases it may not have the most significant contribution to the overall characteristics.

Dynamic modulus of elasticity and compressive strength

The dynamic modulus of elasticity and compressive strength results obtained for the three samples analysed are presented in Table 4.37 and Table 4.38, respectively. Figure 4.72 shows the samples being tested in compression.

Table 4.37 - Dynamic modulus of elasticity results of the samples from *Barão Salgueiro* Manor house

Sample (test specimen)	Bulk density[(1)] ($kg.m^{-3}$)	SD	CV (%)	Distance (m)	Time (µs)	SD	CV (%)	Speed ($m.s^{-1}$)	DME (MPa)
PBS1 (PBS1.1)	1591	16	1.0	0.100	67.2[(2)]	0.3	0.5	1488	3168
PBS1 (PBS1.2)	1648	28	1.7	0.070	51.7[(2)]	0.3	0.5	1353	2716
PBS2 (PBS2.1)	1148	70	6.1	0.116	80.3	0.3	0.3	1444	2154
PBS3 (PBS3.1)	1259	82	6.5	0.077	44.5	0.1	0.2	1725	3370
PBS3 (PBS3.2)	1325	68	5.1	0.059	33.1	0.1	0.3	1785	3799

[(1)] Sand method; [(2)] Measured at the surface (indirect method); SD - standard deviation; CV - coefficient of variation; DME - dynamic modulus of elasticity

Table 4.38 - Compressive strength results of the samples from the *Barão Salgueiro* Manor house

Sample (test specimen)	Confinement mortar age (days)	Bulk density[(1)] ($kg.m^{-3}$)	SD	CV (%)	Load rate ($N.s^{-1}$)	Maximum load (N)	Compressive strength (MPa)
PBS1 (PBS1.1)	31	1591	16	1.0	50	4983	3.11
PBS2 (PBS2.1)	-	1148	70	6.1	50	1628	1.02
PBS3 (PBS3.1)	27	1259	82	6.5	100	6829	4.27

[(1)] Sand method; SD - standard deviation; CV - coefficient of variation

(a) (b) (c)

Figure 4.72 - Adapted compressive strength tests: (a) PBS1 with confinement mortar; (b) PBS2 with three fibre cement boards to achieve the target height; (c) PBS3 with confinement mortar and one fibre cement board

In the smooth surface samples the measurement of the ultrasonic pulse velocity on the surface of the plaster layer proved to be the procedure with less interference/contribution of the mortar. The reason is that the longitudinal propagation of the waves does not reach a great depth and the values obtained are more approximate to those expected for plasters with similar gypsum-calcite composition than a direct measurement, where the probes are positioned in the opposite ends of the thin-layer material under study, very close to the mortar.

However, it is important to consider other issues as well, namely the chemical composition and its direct relationship with the speed of propagation of the waves through the matrix. It is the case of samples PBS1 and PBS2: they have different bulk density/porosity, some difference in the gypsum-lime composition, with PBS1 having less gypsum and more calcite than PBS2, but similar values of speed of propagation of the ultrasound waves. The reason can be either the higher content of gypsum in PBS2 that compensates its higher porosity, or the existence of some influence of the mortar in the sample PBS1 measurement.

In the contrary, the calculation of the dynamic modulus of elasticity is directly influenced by the bulk density, leading to more divergent values. In the smooth surface plasters the mortar contributes to increase the overall bulk density and, consequently, the respective dynamic modulus of elasticity. For example, the values obtained for both parameters in the sample PBS1 would be lower if only the plaster layer was evaluated and the same could be said about the compressive strength, where the cohesiveness of the mortar has surely contributed to increase the result (Table 4.38).

In sample PBS3 the type of material was clearly the most influential issue, as it presented the highest values of ultrasonic pulse velocity and dynamic modulus of elasticity but not of bulk density. As previously discussed (*cf.* item 4.3.1.2, “Mechanical properties”), gypsum is a harder material than calcite resulting from the carbonation of lime even in cases where its porosity is higher. The results obtained for PBS3 are in agreement with these remarks as well as with the most common results

obtained in samples with the same gypsum-calcite composition (Freire et al. 2011) and the very few values available in the literature for gypsum plasters with a plaster/water ratio adequate for the manufacture of precast elements (Coquard et al. 1994; Dalui et al. 1996).

This discussion strengthens the idea that the analysis of the mechanical properties has to be made in a global way, taking into consideration several issues at the same time and not only one perspective. The scarcity of information available in the literature about the characteristics of these materials (gypsum and gypsum-lime based plasters without the addition of aggregates) prevented a reliable comparison with the experimental results obtained in this work, an issue extensively discussed in the *Casa da Pesca's* specimens mechanical properties.

The lowest values of bulk density, DME and compressive strength were those of sample PBS2 and are in agreement with its friability and extremely high porosity

Concerning the compressive strength results, in the case of sample PBS1 (3.11 MPa) it cannot be exclusively assigned to the composition of the finishing layer as the mortar behind plays also an important role. However, if that was the only issue to consider, the value obtained would be in total agreement with those of the gypsum-lime plaster mixes with approximate compositions studied in this work, M1 and M2 (about 3 MPa) (*cf.* Chapter 5). It is also approximate to those of the six samples of lime mortars tested using the confinement mortar method that varied between 1.9 MPa and 2.5 MPa (Magalhães & Veiga 2009), with the exception of one render from a 16th century Convent in Lisbon that presented 4.7 MPa (Válek & Veiga 2005).

Considering now the case of sample PBS3, a gypsum plaster precast element, its compressive strength - 4.27 MPa - is very close to the results obtained for the gypsum plaster mixes tested in this work -5 to 8 MPa (*cf.* Chapter 5) - as well as to that of the sample from the *Mirhab* of the old Mosque of *Mértola* (3.5 MPa, Veiga 2012), already referred. Yet, they are far from the range 9 to 12 MPa found in the literature (S.N.I.P. 1982; Dalui et al. 1996; Wirsching 2005; Yu & Brouwers 2011). The reasons for such difference have already been discussed in the *Casa da Pesca's* case study (*cf.* item 4.3.1.2, "Mechanical properties").

4.3.2.4 The *Monserrate* Palace

The Park and Palace of *Monserrate*, located four kilometres away from *Sintra's* historic centre, are included in the Cultural Landscape of *Sintra,* classified by UNESCO as World Heritage since 1995 (http://www.parquesdesintra.pt [accessed 22 September 2014]).

In 1856 Sir Francis Cook, a wealthy English merchant awarded the title of Viscount of *Monserrate* in 1870, subrogated the estate that could only be acquired in 1863. The construction of the palace began

in 1862, under a project authored by the English architect James Knowles Junior, taking advantage of the structure of an existing neo-Gothic house built in the 18th century by *Gérard Devisme*, another rich merchant that had rented the property in 1789. The works were completed in 1864 (Figure 4.73) (Mendonça 2012).

(a)

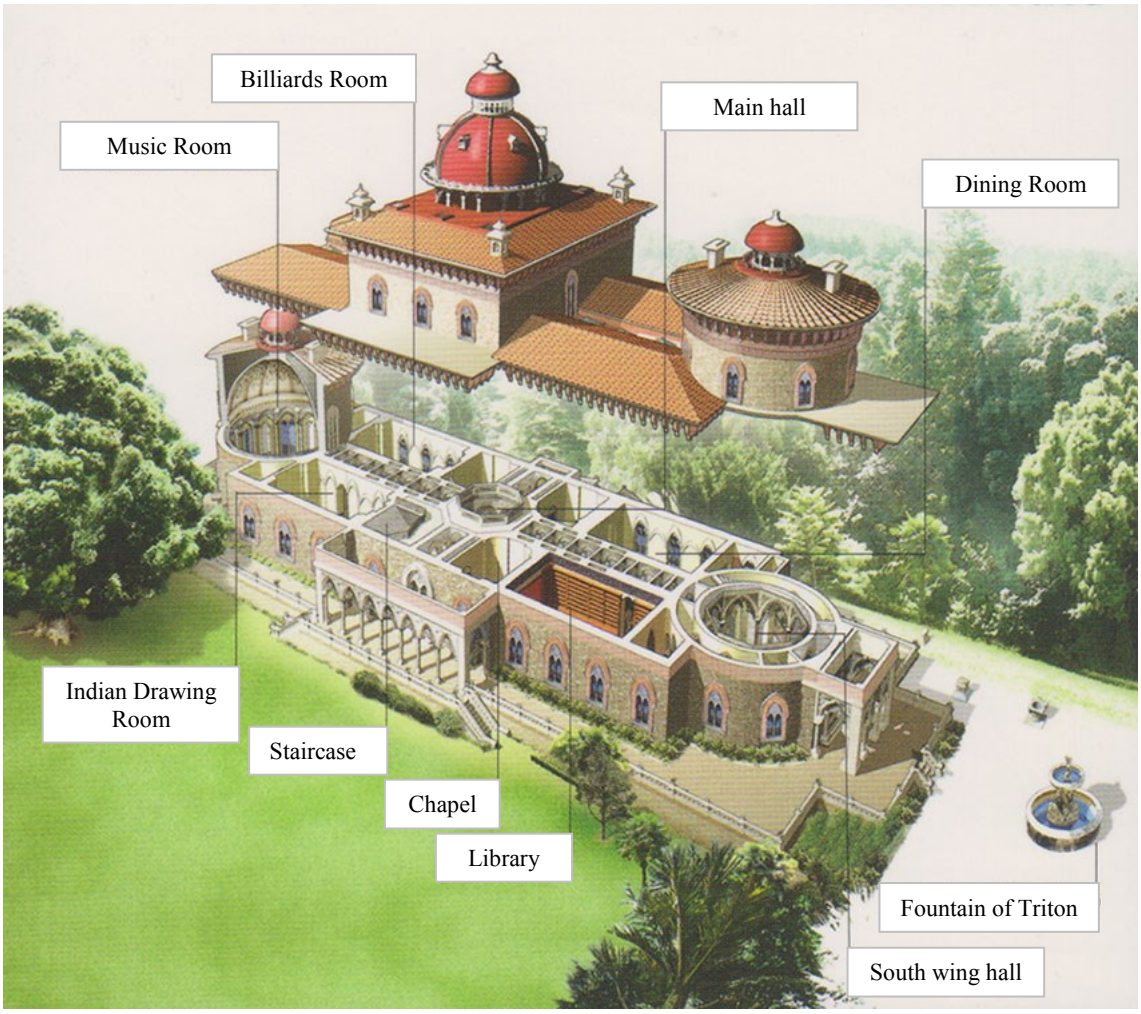

(b)

Figure 4.73 - *Monserrate* Palace: (a) general view; (b) plant of the main spaces of the palace (images adapted from http://www.parquesdesintra.pt [accessed 22 September 2014])

The *Monserrate* Palace is a valuable witness of the eclectic tastes of the 19th century displaying distinctly medieval (Moorish and Gothic) and oriental-style influences, which makes it one of the most important examples of Romantic architecture in Portugal (Figure 4.74), along with the Palace of *Pena* also located in the Cultural Landscape of *Sintra* (http://www.parquesdesintra.pt [accessed 22 Sptember 2014]).

(a)

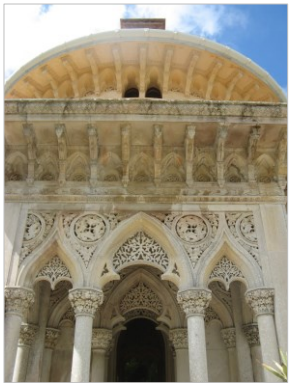

(b)

(c)

(d)

(e)

Figure 4.74 - *Monserrate* Palace: (a) view of the south wing and fountain of Triton; (b) detail of the exterior decoration of the south wing (stone); (c) interior of the south wing hall with different decorative motifs (plasterwork); (d) patterns of wall coverings; (e) dome of the Music room after restoration

In parallel with the above referred influences, a significant part of the building's interior stucco decorations entirely covering walls and ceilings represent exotic vegetal motifs, extending harmoniously to the gardens outside.

Among the plasterers that participated in the stucco works of *Monserrate* was *Domingos Meira*, by the time with the age of 20 but already considered to be *"an excellent sculptor-ornamenter"* (João de Mendonça, 1894 (cited by Mendonça 2012)).

If *Meira* had a merely performing role or exerted already an influence in the options taken by architect Knowles in the interior decoration of the palace is an issue that is still not clarified. However, regardless of the authorship there seems to be no doubt that some of these ornamental plasterworks were based on the reference work of Owen Jones (1809-1874), one of the most influential design theorists of his time, entitled "The Grammar of Ornament". In fact, the main patterns used in corridor walls and ceilings are a faithful copy of a Moorish decor drawn from one of the stucco decorations of the *Alhambra* Palace, in Granada (Mendonça 2012).

Finally, it is interesting to notice that *Domingos Meira* used some of the motifs found in *Monserrate* in other works where he participated elsewhere in the country, namely the mansion of the Viscount of *Estoi* in the Algarve (the *Estoi* Palace, Figure 4.105 (f) and (g)) and its own house in *Afife* where the same carpeted ceilings of leaves appear (Mendonça 2012).

The property has not been given the adequate attention for several decades, suffering extensive damage (Figure 4.75).

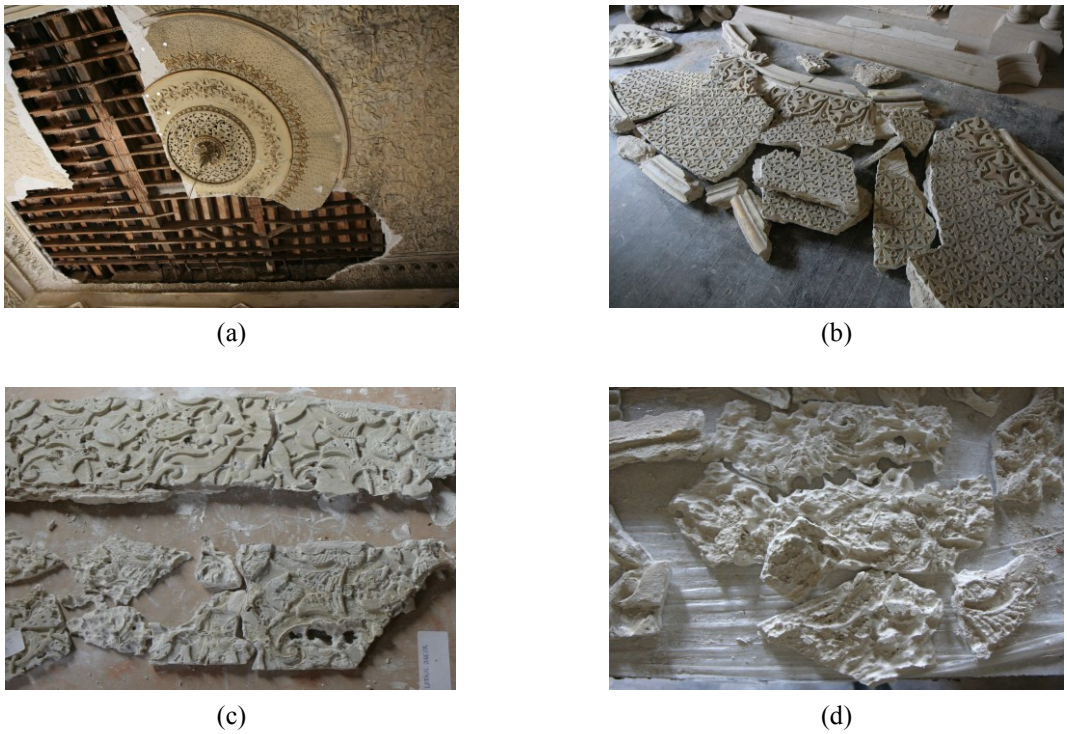

(a) (b)

(c) (d)

Figure 4.75 - Damage at *Monserrate* Palace before the restoration works: (a) collapsed ceiling of the Indian drawing room; (b) fragments corresponding to (a); (c) and (d) examples of deterioration of some plaster decorations due to long water exposure

Only in 2007 was the palace reopened to the public. In 2008 the project of conservation and restoration of the plasters finally began and is still proceeding. The restoration works take place in several stages but always in public view, with the aim of functioning as a workshop (Noé et al. n.d.).

Many decorative motifs and elements had to be totally replaced. Their reproduction was made with flexible materials, like silicon, from parts that were still in good condition to be used as models (Figure 4.76).

(a) (b) (c)

Figure 4.76 - Reproduction of damaged elements in *Monserrate* Palace: (a) mould of a panel; (b) several pieces made from the mould shown in (a); (c) capital being demoulded

Samples

A total of five samples were collected in two different ways: indirectly, as they were already detached due to some anomaly in the building (three samples, two of them shown in Figure 4.77 (b)) and directly on site (Figure 4.77 (a) and (c)).

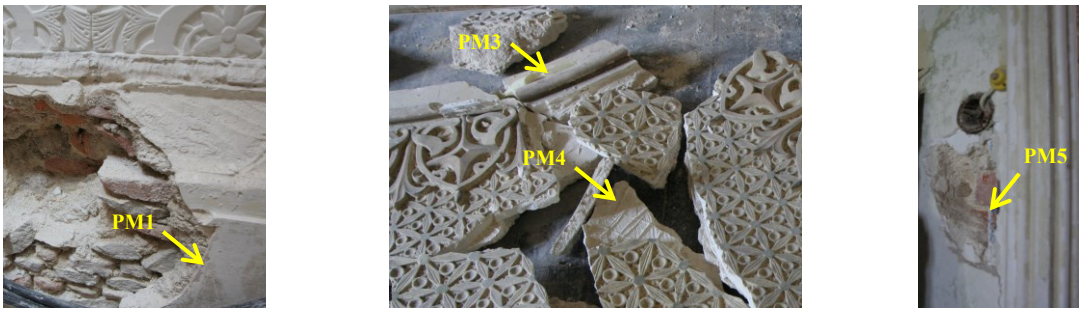

(a) (b) (c)

Figure 4.77 - Detail of the places in the *Monserrate* Palace corresponding to some of the samples collected: (a) stone-like skirting board of the corridor of the south wing; (b) fragments of the decorative ceiling centre of the Indian drawing room; (c) wall of the dining room

After initial visual observation, sample PM2 (belonging to precast panels of the totally collapsed ceiling of the south wing hall) was rejected because it raised doubts about being original: the back surface of the fragments had a film of a substance that seemed to be synthetic (not contemporary of the

original decoration) and was probably used to fix the panels to the ceiling during previous restoration works (Figure 4.78).

(a) (b)

Figure 4.78 - Sample PM2: (a) front view; (b) back view, with synthetic film (yellow arrows)

The images of the samples are shown in Figure 4.79 and their identification and description are summarized in Table 4.39.

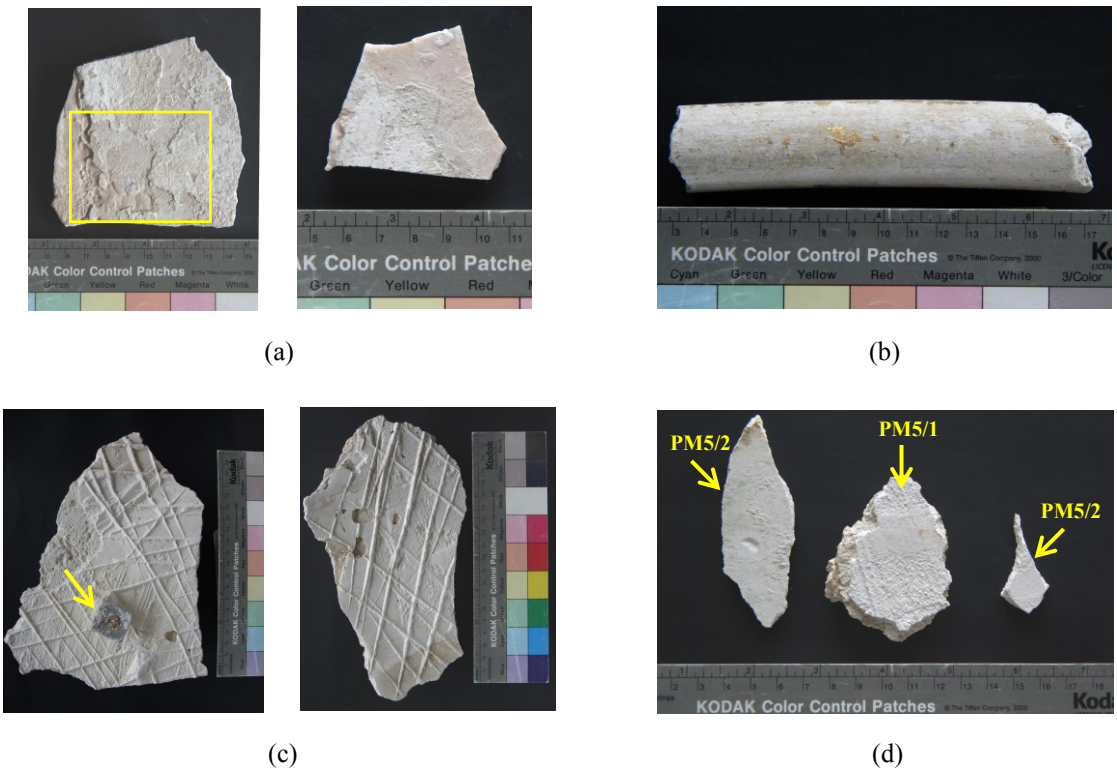

(a) (b)

(c) (d)

Figure 4.79 - Photographs of the analysed samples from *Monserrate* Palace: (a) PM1 (2 fragments); (b) PM3; (c) PM4 (2 fragments), one with a metal bolt (yellow arrow); (d) PM5

Table 4.39 - Identification and description of the samples from *Monserrate* Palace

Sample identification	Description
PM1	Skirting board simulating a noble stone (probably marble)
PM3	Frieze belonging to the decorative ceiling centre of the Indian drawing room (gilded)
PM4	Plaster regularization layer of a ceiling for application of ornaments
PM5	Finishing plaster (made in two layers: PM5/1 and PM5/2) from a wall of the dining room

Results and discussion

- Visual observation of the samples

The information obtained by visual observation of the samples is illustrated in Figure 4.80 and is summarized in Table 4.40.

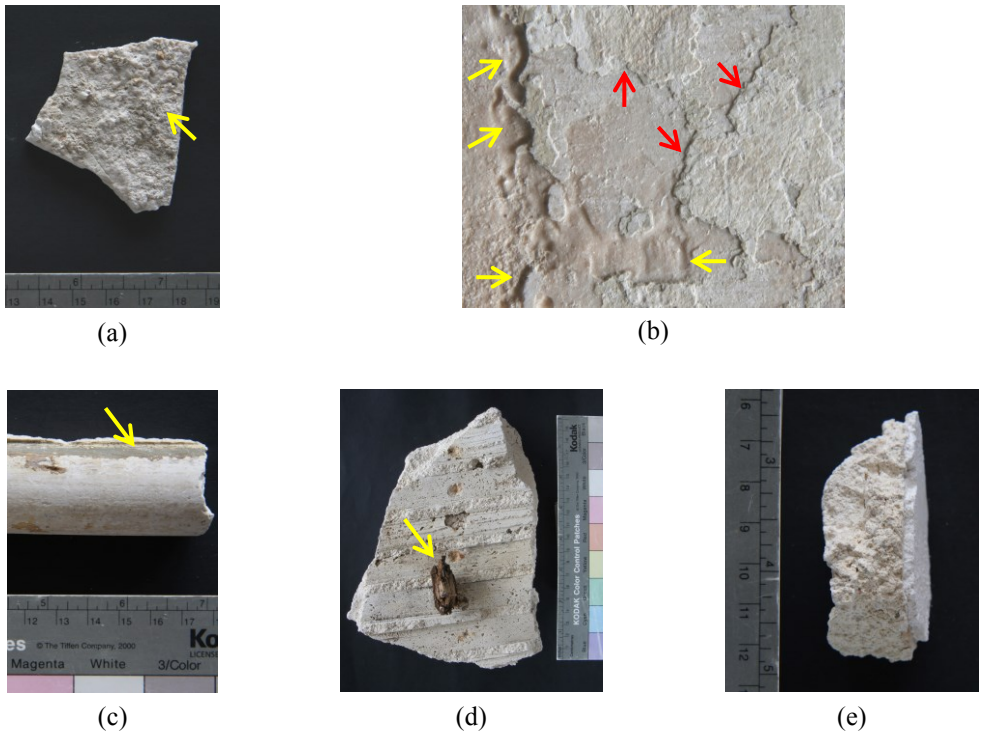

Figure 4.80 - Photographs of the samples from *Monserrate* Palace showing some specific details: (a) back view of a fragment of PM1 with mortar; (b) front view of PM1 (yellow frame of Figure 4.79 (a)) showing grooves (yellow arrows) and painting layers (red arrows); (c) green preparation layer for gilding in PM3; (d) back view of a fragment of PM4, with rotting wood still attached to the metal bolt; (e) side view of a fragment of PM5 showing the mortar and the PM5/1 layer

The cohesiveness of the mortars used in the ceilings of this case study is similar to that observed in the *Estoi* Palace, denoting a special care in the choice of the raw materials, preparation of the mixtures and application on site. In fact, the use of a solid support structure is an absolutely paramount issue to prevent the collapse and/or degradation of the ceilings in current conditions, over which very heavy and precious decorations have been applied in both cases.

Unfortunately in *Monserrate* these procedures were not enough to preserve their integrity due to the water exposure of the building for years, leading to the irreversible degradation of many plaster decorations (Figure 4.75 (c) and (d)) and to the rotting of the wooden structure, with consequent collapse of some ceilings (Figure 4.75 (a) and (b) and Figure 4.80 (d)).

Table 4.40 - Visual observation of the samples from *Monserrate* Palace

Sample	Description
PM1	Stone-like **skirting board**, approximately 6 mm thick, **applied directly over the mortar** behind (Figure 4.80 (a)), to which it was extremely well connected making it very difficult to separate them; Very stiff material, with a light pink colour, looking like a precipitated calcium carbonate. Some areas of the surface were "corroded", with grooves that seem to have been carved by the passage of water during a long period of time (Figure 4.80 (b), yellow arrows); It had several very thin "finishing" layers, some white and others beige coloured (Figure 4.80 (b), red arrows) probably with a paint function. At first they were thought to be lime based but the analytical results obtained did not confirm this hypothesis.
PM3	Fragment of a **frieze** with an approximate tubular form (3 cm wide x 2.7 cm height) belonging to a round, very large decorative element (ceiling centre). It was moulded directly on that element, i.e., **moulded on site**; It had few remains of gilding (Figure 4.79 (b)) in the centre and of a green layer in the sides, in the area where it makes an angle of 90º with the base surface (Figure 4.80 (c), yellow arrow). The green layer was probably the preparation layer for the application of the gilding. Both could be easily detached with a scalpel; It had also a beige layer behind all the previous ones that seemed to result from the polishing operation of the final surface of the plaster: the scalpel slipped on it and it was not separable from the base without damaging it.
PM4	**Regularization / fixing layer** of beige colour with an average thickness of 4-5 mm applied over a very cohesive mortar with 22-23 mm thickness; It presented a textured pattern printed by the grooves of the decorative panels that have been attached to it (Figure 4.79 (c)); The panels were also fixed with the aid of metal bolts (Figure 4.79 (c)) fastened to the wooden structure of the ceiling (Figure 4.80 (d)).
PM5	This sample is made of a fragment of the first layer (PM5/1, approximately 3 mm thick) of a **smooth surface plaster** and the corresponding mortar behind (20-25 mm thick) (Figure 4.80 (e)) and two fragments of the second (and last) layer (PM5/2) (Figure 4.79 (d)); In one of the fragments of PM5/2 some traces of a pale green paint can still be seen (Figure 4.79 (d), left); In both PM5/1 and PM5/2 yellowish-orange sand in the plaster is visible to the naked eye, similar to that observed in sample PM4.

- XRD results

The qualitative mineralogical composition of the samples was determined by XRD and the results obtained showed that gypsum, calcite, quartz and anhydrite are the main constituents found (Figure 4.81 and Table 4.41).

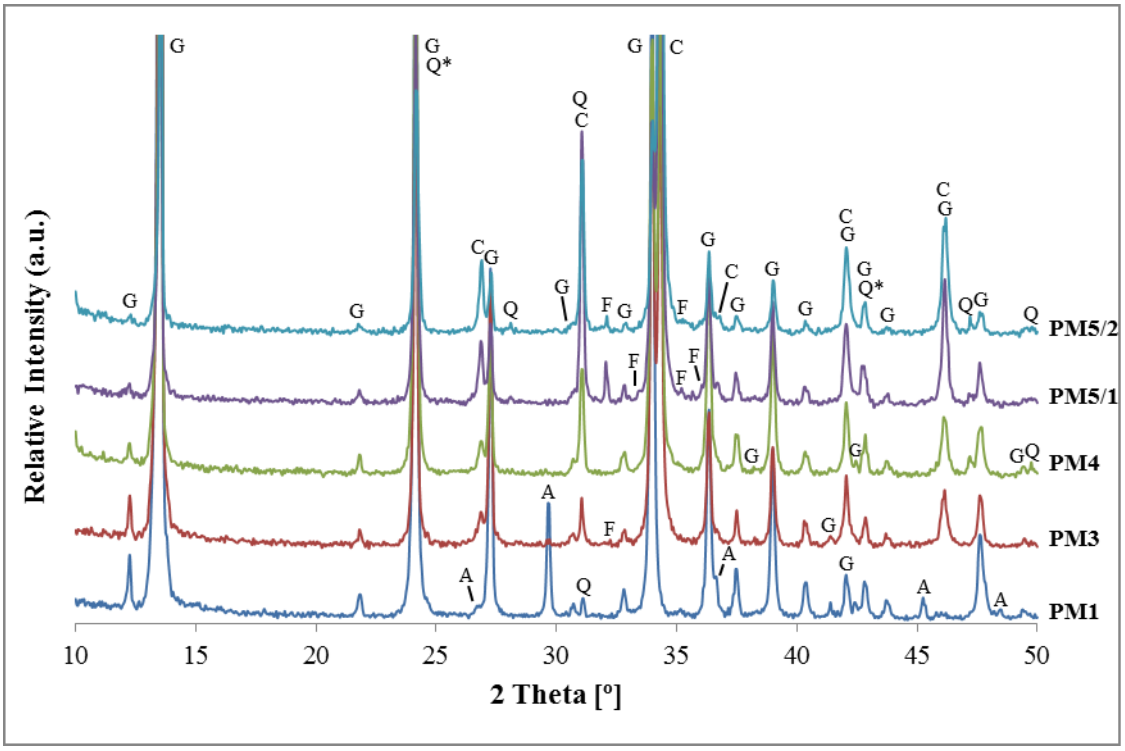

Figure 4.81 - XRD patterns of the samples from *Monserrate* Palace
Notation: G - Gypsum; C - Calcite; Q - Quartz (*PM4, PM5/1, PM5/2); A - Anhydrite; F - Feldspars

Table 4.41 - XRD qualitative mineralogical composition of the samples from *Monserrate* Palace

Sample	Identified crystalline compounds				
	Gypsum	Calcite	Quartz	Anhydrite	Others
PM1	+++/++++	-	trc	+	-
PM3	+++	++/+++	trc	trc	Feldspars (trc)
PM4	+++	++/+++	+	-	-
PM5/1	++/+++	++/+++	+	-	Feldspars (microcline, trc+)
PM5/2	++	+++	++	-	Feldspars (microcline, trc)

Notation used in XRD peak intensity:

++++	Very high proportion (predominant compound)	+	Weak proportion
+++	High proportion	trc	Traces
++	Medium proportion	-	Not detected

During grinding of sample PM1 the presence of a very small quantity of what seemed to be an aggregate was noticed, made of round brown grains, very stiff (they were very difficult to grind), although only gypsum, anhydrite and traces of quartz were detected by XRD (Table 4.41). The sample had a light pink colour before grinding but looked white in powder form.

In sample PM4 the presence of aggregates (fine sand) was also detected during grinding and in both layers of sample PM5 it was visible to the naked eye. The grains had a yellowish-orange colour, were stiffer than the plaster and were probably only quartz in PM4; in the case of sample PM5 feldspars were also detected (Table 4.41).

- TG-DTA results

The thermal behaviour of the samples associated with temperature variations was evaluated using TG-DTA analysis and allowed the quantification of the gypsum and calcite contents (Table 4.42 and Figure 4.82), confirming the results of XRD. Quartz and anhydrite, also present in some of the samples, are not detected by this technique as they do not meet the referred conditions in the temperature range used.

Table 4.42 - Weight loss and calculated gypsum / calcite contents of the samples from *Monserrate* Palace

Sample	Temperature range (ºC)						Calculated contents (%)	
	25→85	85→250	250→600	600→850	850→1000	Loss of ignition	Gypsum	Calcite
PM1	0.0	18.9	0.4	0.1	0.0	19.4	90	0
PM4	0.1	12.5	1.1	14.7	0.7	29.1	60	33
PM5/1	0.1	8.3	1.2	20.5	0.1	30.2	40	47
PM5/2	0.1	5.1	1.5	26.2	0.4	33.3	25	60
				600→900	900→1000			
PM3	0.1	11.8	1.3	18.1	0.9	32.2	57	41

The doublet of peaks corresponding to the two steps of dehydration of gypsum is well defined in all the DTG and DTA curves of Figure 4.82 with the exception of sample PM5/2, which is related to its lower content of this material.

The phase change of soluble to insoluble anhydrite is only visible in the DTA curve of sample PM1, the one with the greatest gypsum content, through a small exothermic peak at 369.3 ºC (Figure 4.82).

In what concerns calcite, the higher content in a sample, the higher the temperatures of decarbonation is. Similar observations have been made throughout all the case studies, with very few exceptions.

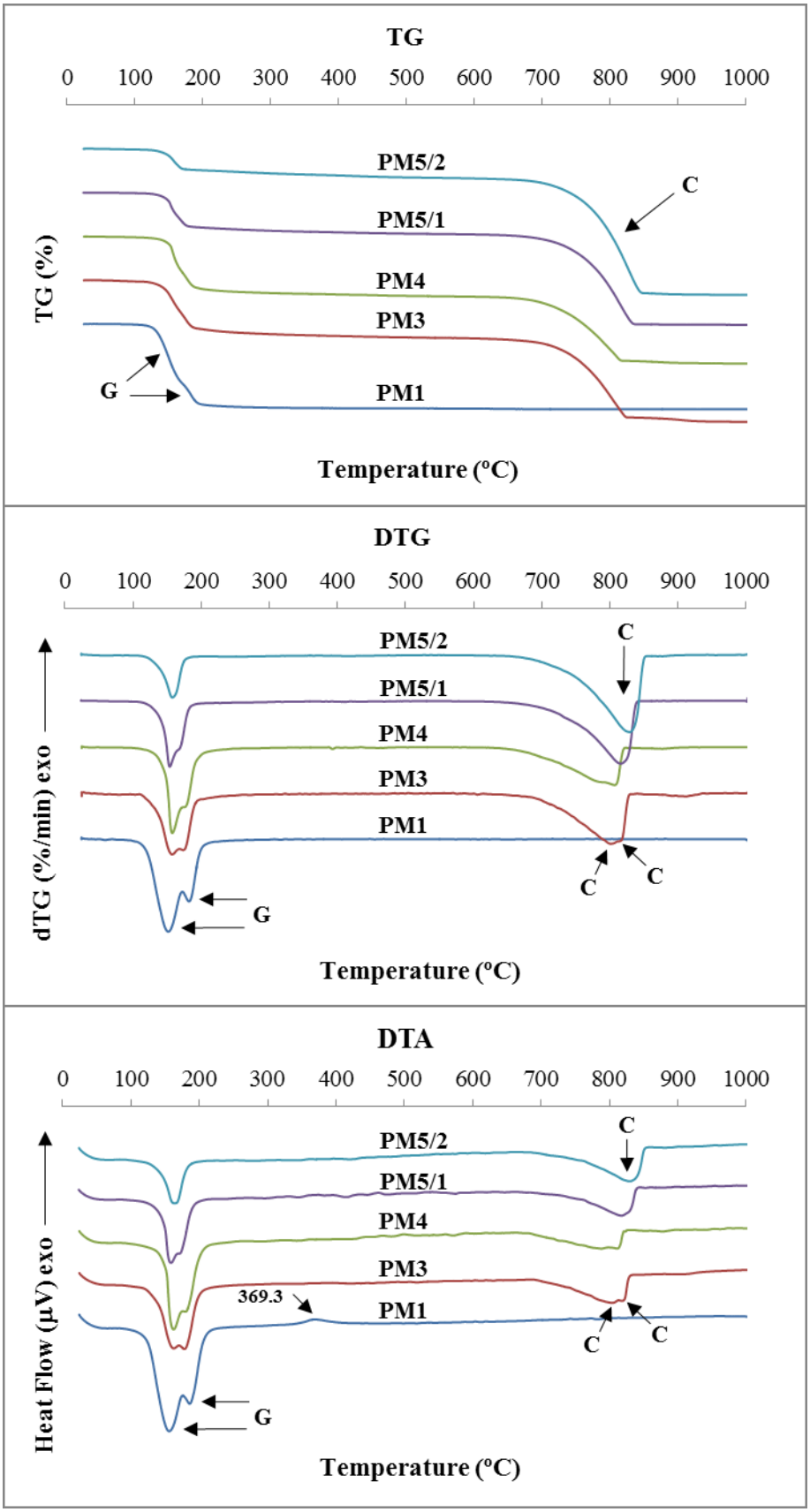

Figure 4.82 - TG, DTG and DTA curves of the samples from *Monserrate* Palace. Notation: G - Gypsum dehydration; C - Calcite decarbonation

Another important observation is the clear unfolding of the decomposition temperatures of calcite in samples PM3 and PM4, occurring in two levels, an issue extensively discussed in 4.3.1.2, "TG-DTA results" section, namely the reasons that are usually in its origin.

In this case, the most plausible reason is the presence of material with different degrees of crystallinity, like natural calcite (carbonate of primary origin) and calcite resulting from the carbonation of hydrated lime or from dissolution-recrystallization cycles (both of secondary origin).

The source of natural calcite is probably the gypsum raw material. In fact, the unfolding becomes fainter with the decrease of gypsum and the increase of hydrated lime contents, i.e., by the following order: PM3, PM4, PM5/1 and PM5/2. This fact is more perceptible in the DTA curves (Figure 4.82).

Another important feature of this set of samples is the weight losses between 250 ºC and 600 ºC; with the exception of sample PM1, the others lose 1.1% to 1.5% of their weight, which is usually associated to the presence of clay minerals and/or organic compounds.

In the case of sample PM3, a small contamination with any material eventually used to polish the external surface of the plaster or with the preparatory layer for the gilding may have occurred, despite the intention of analysing only the composition of the core of the samples and all the care taken on their handling (the preparation layers for gilding have usually clay materials, as referred in the discussion of the results of the samples from the Arabian Room of the *Bolsa* Palace). The same argument can be used to explain the increase of the temperature range considered to be due to the calcite decomposition, where some overlapping with the transformation of any additional compound may occur, as well as the small endothermic weight loss observed between 900 ºC and 1000 ºC.

In what concerns samples PM4 and PM5 the contamination with clay materials is also possible, even though with a different origin (and possibly a different composition): the aggregates; the use of organic compounds is unlikely in both samples.

- SEM observations

In order to understand the special properties of sample PM1, observations and analysis of the micro structure using scanning electron microscopy (SEM) coupled with energy dispersive X-ray spectroscopy (EDS) were performed on the fractured surface. The information obtained is discussed in this section.

Sample PM1

A general view of the matrix at a low magnification is shown in Figure 4.83. In order to facilitate the discussion, the area observed was divided in three fictitious zones that do not represent independent

layers. It is possible to see that the matrix is slightly more compact in the border of zone 1, corresponding to the external surface of the sample. The most logical explanation for that is the application procedure: in the final surface the plasters are usually pressed harder.

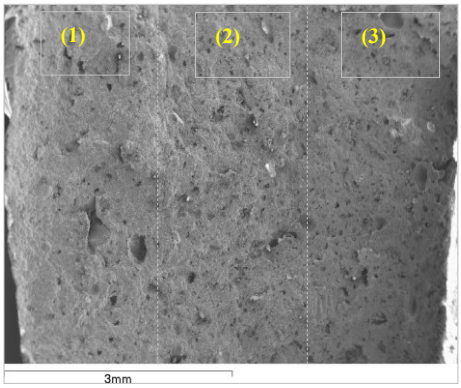

Figure 4.83 - SEM-SE image of the fractured surface of sample PM1, divided longitudinally in three parts: (1) external zone; (2) core of the sample; (3) internal zone (in contact with the mortar)

At higher magnifications it seems that each zone has different morphology, with zone 1 showing the flattest crystals and zone 3 the ones with the more rounded shape (Figure 4.84).

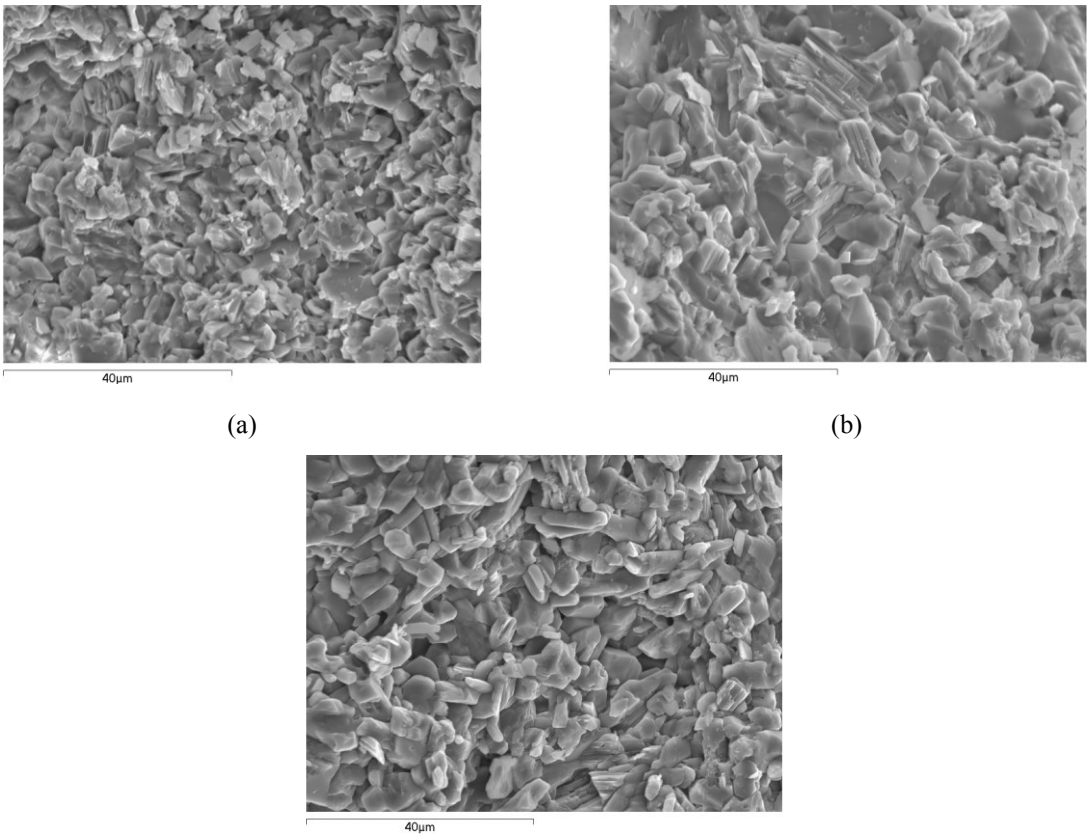

(a) (b)

(c)

Figure 4.84 - SEM-SE images of the crystal morphologies in the three zones of sample PM1: (a) zone 1; (b) zone 2; (c) zone 3

In zone 2 very compact larger masses with no specific morphology were detected. Bustamante & de Rojas (2007) and Igea et al. (2012) reported similar observations in gypsum mortar and plaster samples obtained from high temperature calcined gypsums and described these masses as grains of dihydrate or over burnt anhydrite considered to be sub products of the calcination. They also said that these "inert" phases were separated by sieving, and then they were grinded and added as aggregates to the mixtures. The resulting materials had enhanced compactness and showed very high mechanical characteristics; this situation was observed in sample PM1 (*cf*. "Mechanical properties" section).

The rounded shape of the crystals in zone 3 (Figure 4.84 (c)) is more consistent with a multiphase gypsum plaster that was exposed to weathering, i.e. the water attack induces dissolution-recrystallization processes that wear out the edges of the crystals and improve their growth and compactness (Middendorf & Knöfel 1998b; Middendorf 2002). It can also promote the hydration of the remaining anhydrite along time.

Additional images illustrating the presence of compact masses embedded in the matrix, thought to be grains of anhydrite and/or gypsum showing water and/or thermal attack, are shown in Figure 4.85. Several EDS analyses were performed but the very approximate chemical composition of gypsum (calcium sulfate dihydrate) and anhydrite (anhydrous calcium sulfate) made it difficult to distinguish them, especially when the crystal morphology was uncommon.

For example, based on similar observations reported in the literature (Sanz 2009), the fasciculate crystals shown in Figure 4.85 (a) (black dashed frame) have a morphology usually associated to anhydrite. However, if based on the chemical formulae where the relationship between oxygen and calcium is higher in gypsum than in anhydrite, the respective EDS spectra (numbers 1 and 2, corresponding respectively to the areas of the black and aquamarine coloured frames) seem to indicate that the referred crystals are most probably gypsum. On the contrary, the spectrum of the grains pointed out by pink arrows (spectrum number 4, indigo coloured frame) is more according to the anhydrite chemical formula but their morphology is similar to others observed by Bustamante & de Rojas (2007) and identified as gypsum.

The same can be said about the image shown in Figure 4.85 (b) where similar morphologies of lamellar structure, usually associated to anhydrite, originated spectra with different oxygen-calcium proportions (ex: 1 and 4) or, on the opposite, similar spectra were obtained for different morphologies (ex: 4 and 8).

Concerning Figure 4.85 (c) and (d), three crystal morphologies out of four have spectra supposed to correspond to gypsum and only one (the crystal with a green frame) seems to be not completely hydrated (at higher magnification of the image some remaining fasciculate forms, typical of anhydrite, can still be observed).

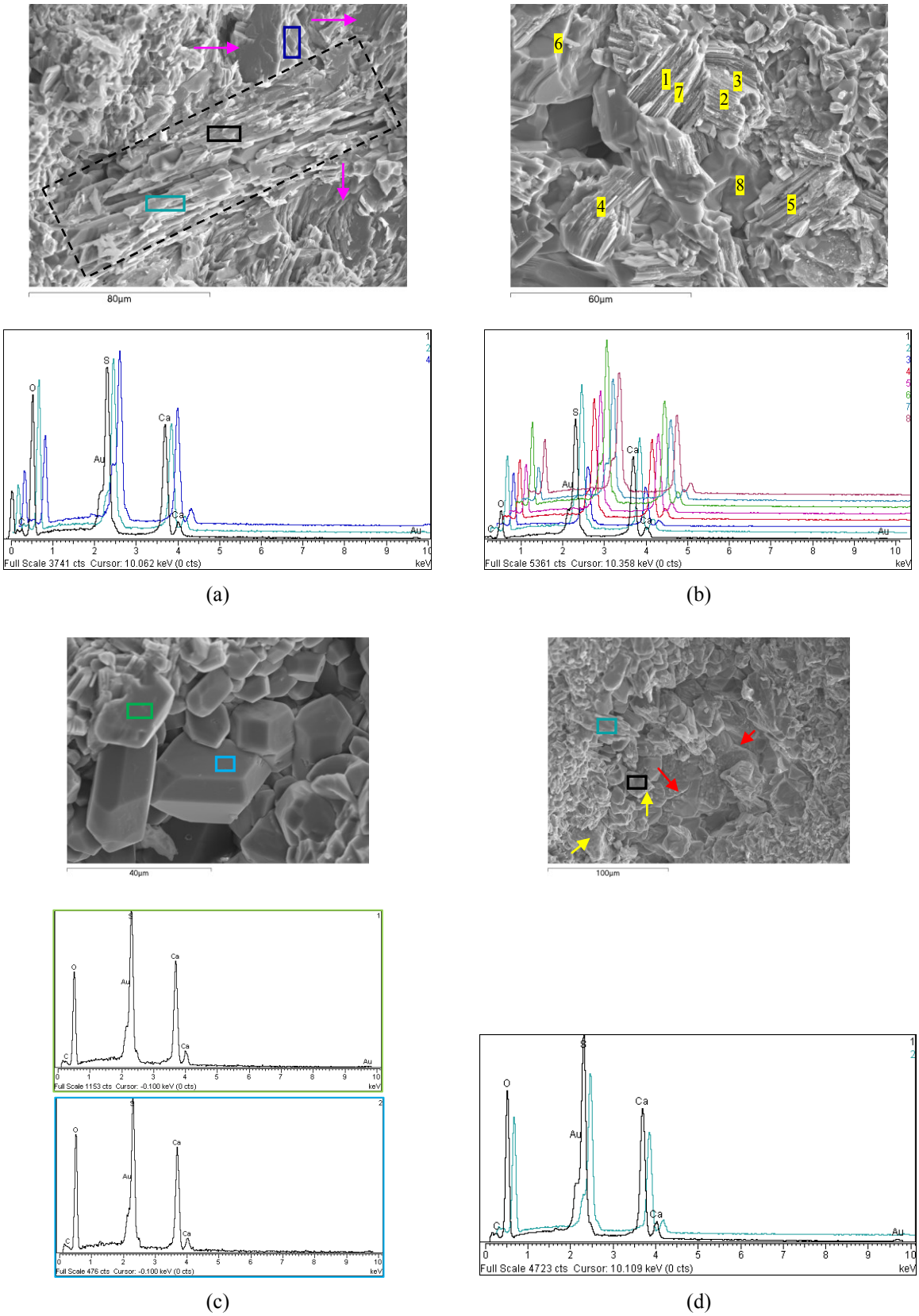

Figure 4.85 - SEM-SE images of crystal masses in sample PM1: (a) fasciculate crystals (black dashed frame), a morphology usually associated with anhydrite and flat, laminated, compact crystals (gypsum? anhydrite?) embedded in the matrix, probably working as aggregates (pink arrows); (b) high dimensions crystals with lamellar internal structure, probably anhydrite still turning into gypsum; (c) crystals in a pore with a polyhedral form, typical of gypsum obtained from anhydrite; (d) pore with eroded crystals (yellow arrows) and a mass at the bottom supposed to be anhydrite (thermal cracks pointed out by red arrows)

Crystals with a polyhedral morphology similar to that of Figure 4.85 (c) have also been observed in sample PE4 from the *Estoi* Palace (*cf.* item 4.3.3.1, "SEM-EDS" section, Figure 4.140 (a)) and the binder used was a multiphase gypsum plaster.

Concerning the properties determined, PE4 was also the closest to PM1, both showing much lower values of porosity, average pore radius and capillary absorption than the other samples analysed. In the case of the mechanical properties (dynamic modulus of elasticity and compressive strength), the results obtained for PM1 were even outstanding (*cf.* "Mechanical properties" section).

Taking into account that no further studies of sample PM1 were made, namely using complementary analytical techniques like in sample PE4, it is not possible at this point to proceed with additional remarks. However, the few issues raised are already interesting and intriguing enough to justify a deeper analysis of sample PM1. Finding the explanations for such peculiar characteristics can help understanding the technology behind the manufacture of these materials which, in turn, can contribute to their conservation and restoration and to open new perspectives concerning the use of different gypsum based products in the future.

- Physical properties

  Capillary absorption

The coefficient of capillary absorption by contact (Ccc) was determined in samples PM1 and PM4 (Figure 4.86 and Figure 4.87) and the quantitative results are summarized in Table 4.43.

(a) (b) (c)

Figure 4.86 - Water absorption by capillarity of samples from *Monserrate* Palace: (a) PM1; (b) and (c) test specimen of PM4 at different moments of the determination

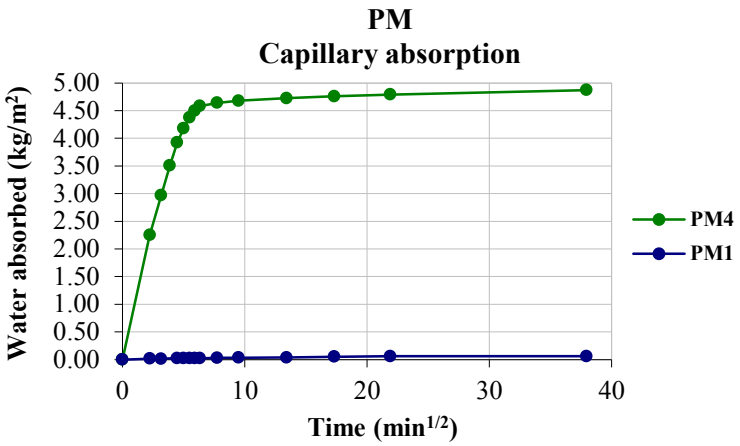

Figure 4.87 - Water absorption by capillarity of samples from *Monserrate* Palace: graphical representation of the results

Table 4.43 - Capillary absorption by contact results of samples PM1 and PM4

Test specimen	**PM1**	**PM4**
Surface (cm^2)	59.63	46.45
Weight (g)	68.18	150.87
Capillary absorption at 5 min:		
(g)	0.10	10.45
($kg.m^{-2}$)	**0.02**	**2.25**
(%, relative to weight of sample)	0.15	6.93
(%, relative to total absorption)	28.57	46.18
Capillary absorption at 24 h:		
(g)	0.35	22.63
($kg.m^{-2}$)	**0.06**	**4.87**
(%, relative to weight of sample)	0.51	15.00
Ccc at 5 min ($kg.m^{-2}min^{-1/2}$)	**0.01**	**1.01**

Ccc - capillarity coefficient by contact

The Ccc at 5 minutes of sample PM1 as well as the total absorption capacity are extremely low but in agreement with other characteristics determined.

In fact, the SEM observations showed a very compact material, with completely different micro structure and crystal morphology from the most common gypsum plasters (Wirsching 2005).

The results of the mercury intrusion porosimetry analysis (pore size distribution, porosity, etc.) are also unusually low, close to the values obtained for sample PE4/2 whose micro structure and crystal morphology have similarities.

The main feature these two samples have in common is the presence of anhydrite in the matrix, first detected by XRD and later confirmed by SEM observations. A thorough study of the sample PE4/2 was made and all the information obtained is detailed in the corresponding case study. It allowed concluding that the use of anhydrite II as binder is in the origin of the particular compositional, structural, physical and mechanical characteristics observed in both samples.

Regarding sample PM4 it showed a value of Ccc at 5 minutes in the low-moderate range with the first 5 minutes representing 46.18% of the global absorption. Comparing it with the sample PBS1 whose total absorption capacity is very similar (5.09 $kg.m^{-2}$), it can be observed that the initial rate of absorption is considerably higher in PM4, which seems to have a greater amount of larger capillary pores. On the contrary, the stabilization at the maximum value of absorption, an issue usually related to the pores of lower dimensions ($r < 0.50$ micron), was slower. These two features, apparently contradictory, are possible when a material has balanced amounts of both types of pores.

In spite of all the previous remarks, in the case of the sample PM4 the explanation is probably different. In fact, the plaster/mortar ratio is lower in PM4 than in PBS1, meaning that the influence of the mortar must be more significant in the first than in the second.

Looking thoroughly at the system of sample PM4, it has a thinner layer of plaster (4-5 mm), which is the absorbent surface and a thicker layer (22-24 mm) of a very cohesive mortar behind. So, the initial rate of absorption is mainly due to the plaster but the final rate until stabilization and the total absorption capacity, directly related to the total porosity, are more influenced by the mortar. Taking into account that the plaster of PM4 had a higher content of gypsum and did not have any type of finishing material applied (PBS1 had a painting layer; the surface of PM4 was irregular and rough, favouring the absorption), it is logical to have an initial rate of suction considerably higher. On the contrary, its thick, very stiff and compact mortar layer had probably much lower porosity and higher content of smaller capillary pores leading to slower final absorption rates and (slightly) lower global absorption values than sample PBS1.

The loss of water absorbed after the capillarity tests was also evaluated and represented in Figure 4.88.

The profile of the curves agrees with the respective capillary absorption behaviour of the samples. In fact, it is interesting to observe that PM4 showed a lower drying rate and took longer to stabilize than PBS1, reinforcing the conviction that is must have a higher content of smaller pores.

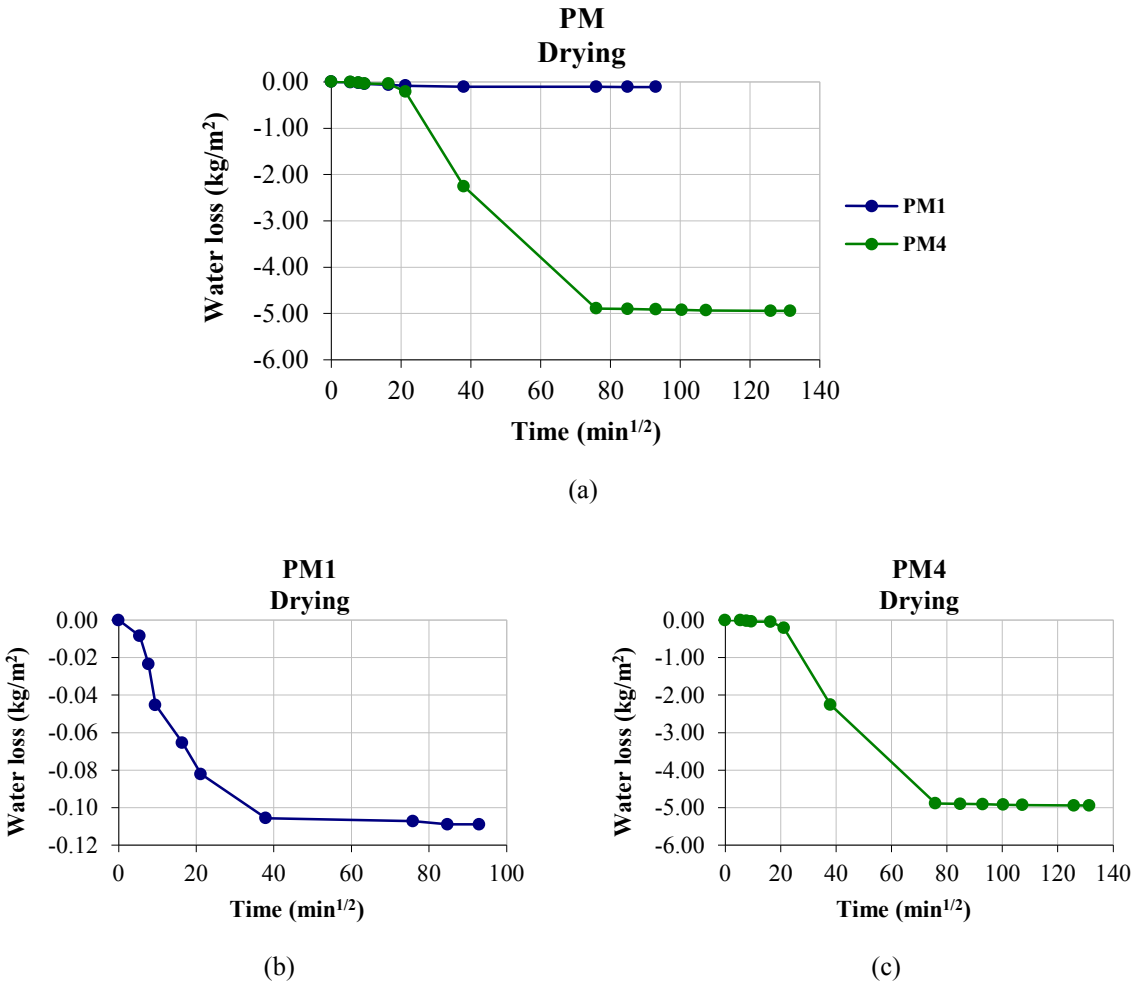

Figure 4.88 - Graphical representation of the drying behaviour of the samples from *Monserrate* Palace: (a) joint analysis, for relative comparison; (b) and (c) individual analysis

Pore size distribution

The pore size distribution by mercury intrusion porosimetry (MIP) was determined in the sample PM1 (Figure 4.89) and the previous suppositions about having a completely different distribution curve from the most common gypsum and gypsum-lime plasters were confirmed (*cf.* items 4.3.2.2, 4.3.3.1 and 4.3.4.2," Pore size distribution" sections).

In spite of having a bad reproducibility, the average pore radius (Table 4.44) is also significantly smaller than (about ten times) the values observed in the other samples of this study (usually in the range 0.1 to 0.6 micron), with the exception of PE4/2. A comparison between the curves of these two samples is presented in the equivalent section of the *Estoi* Palace case study and more thorough considerations are made there.

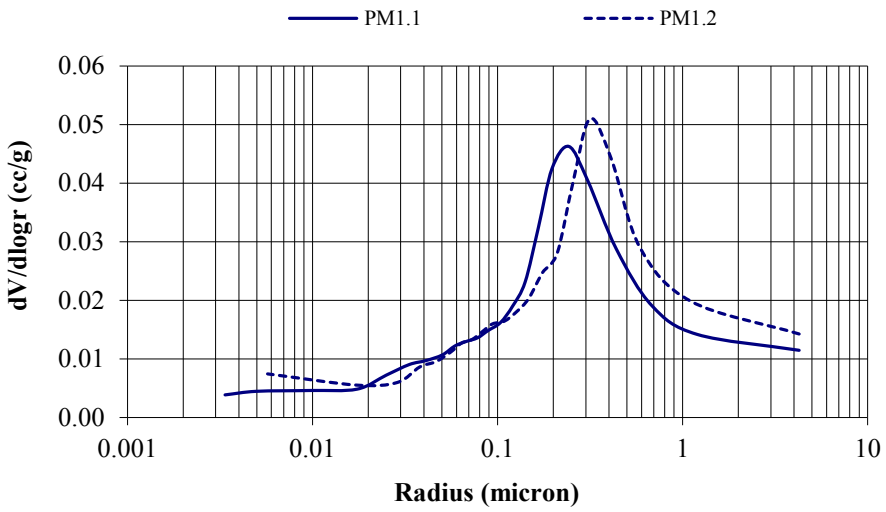

Figure 4.89 - Pore size distribution curves of sample PM1

Table 4.44 - Results obtained by MIP analysis in sample PM1

Sample. .test specimen	Weight (g)	Bulk density ($kg.m^{-3}$)	Density ($kg.m^{-3}$)	Porosity (%)	Pore radius with max. vol. (μm)	Average pore radius (μm)
PM1.1	2.09	2080	2295	9.4	0.243	0.0615
PM1.2	2.18	2063	2290	9.9	0.317	0.0968

Hygroscopic behaviour

The quantitative results of the hygroscopic behaviour of the samples PM1, PM3 and PM5 are summarized in Table 4.45 and the respective graphical representation is shown in Figure 4.90.

Table 4.45 - Average hygroscopicity results of the samples from *Monserrate* Palace: PM1 and PM4 (2010); PM3 and PM5 (2014)

RH (%)	MC (%) PM1	SD	CV (%)	MC (%) PM3	SD	CV (%)	MC (%) PM4	SD	CV (%)	MC (%) PM5	SD	CV (%)
30	0.04	0.002	5.89	0.05	0.002	4.01	0.07	0.033	46.07	*	*	*
50	0.05	0.012	25.93	0.09	0.001	1.23	0.11	0.045	40.25	0.05	0.005	10.36
70	0.09	0.001	1.01	0.18	0.001	0.34	0.53	0.102	19.41	0.17	0.017	9.95
90	**0.24**	0.001	0.23	**0.78**	0.000	0.06	**2.03**	0.476	23.39	**0.98**	0.037	3.81
70	0.19	0.002	1.01	0.26	0.000	0.12	0.75	0.191	25.49	0.30	0.023	7.48
50	0.17	0.004	2.44	0.15	0.002	1.00	0.23	0.029	12.35	0.18	0.045	24.80
30	0.15	0.007	4.55	0.07	0.001	0.87	0.14	0.062	43.67	*	*	*

* Too high CV value precluding presenting the results; RH - relative humidity; MC - moisture content; SD - standard deviation; CV - coefficient of variation

Sample PM4 was also studied but the values of hygroscopicity were too high indicating the probable presence of hygroscopic contaminants (Table 4.45).

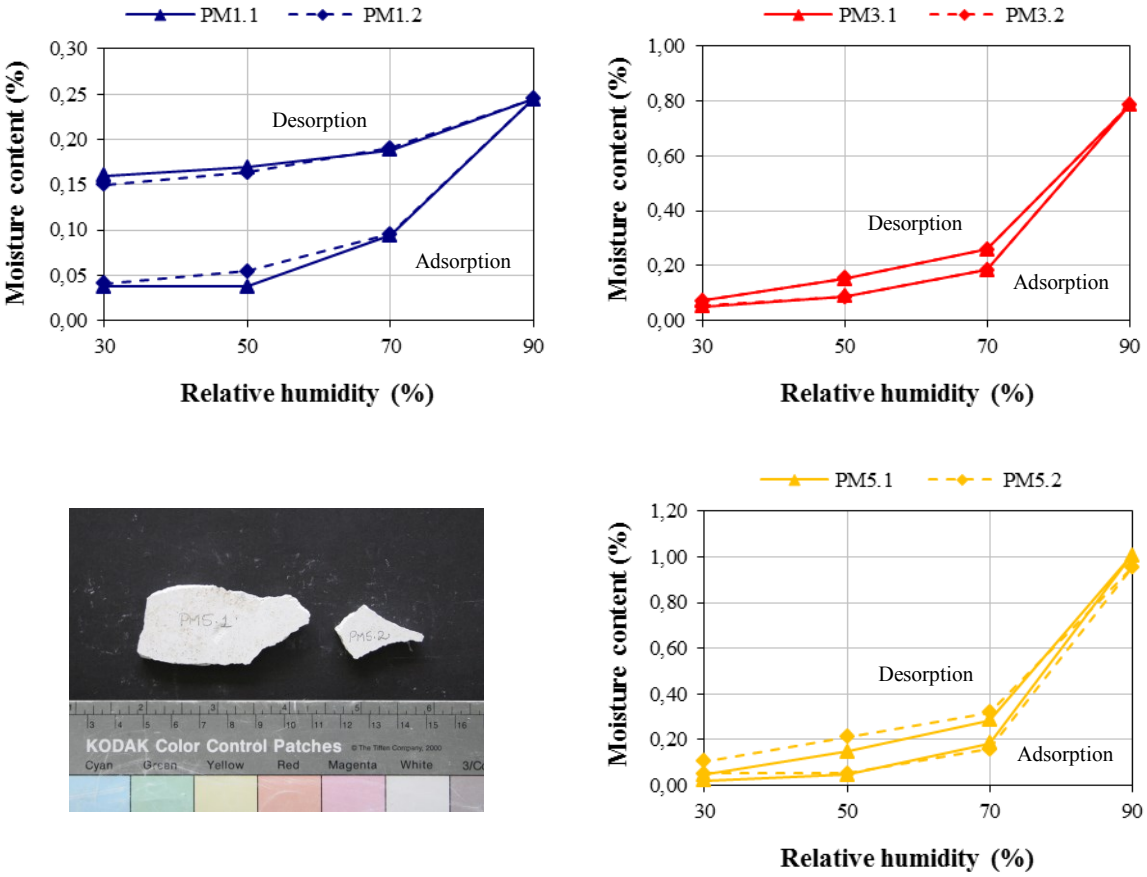

Figure 4.90 - Hygroscopic behaviour of samples from *Monserrate* Palace

A very important characteristic of sample's PM1 hygroscopic behaviour is the existence of significant hysteresis, with the respective adsorption and desorption curves deviating considerably from one another. As referred above (*cf.* 4.3.1.1, "Hygroscopic behaviour" section), this phenomenon is usually associated with capillary condensation in mesopore structures (0.001 micron < r < 0.025 micron, (IUPAC 1972). However, if it still occurs at the lowest attainable vapour pressures, it is called "low pressure hysteresis" and the system has to have micropores (r < 0.001 micron, IUPAC 1985; the pore size classification can be very diverse depending on the authors).

In fact, the process that really occurs is "micropore filling" and it is incorrect to call it "capillary condensation" as it does not involve the formation of liquid menisci. The volume of the micropores is filled with liquid water, more tightly bound to the surface of the absorbent than in meso and macropores, thus not contributing to moisture transfer (Thomson et al. 2004).

The pore size distribution curves of Figure 4.89 show that sample PM1 still has a considerable number of pores in the lower limit achieved by the MIP apparatus, i.e. at radius around 0.004 micron for test specimen

PM1.1 and 0.006 micron for PM1.2. This means that there must be pores with radius below that limit where the "micropore filling" phenomenon occurs, contributing to such significant hysteresis effect.

Regarding the hygroscopic behaviour of samples PM3 and PM5 two main observations were made: the presence of some hysteresis effect (though incomparably lower than that of sample PM1) and higher values of water adsorption at 90% relative humidity than most of the samples analysed.

The first observation suggests the presence of a given number of micro and mesopores in both samples (slightly higher in PM5), in agreement with the respective gypsum-calcite compositions; the second one can be due to the presence of hygroscopic contaminants (e.g. soluble salts).

Water vapour permeability

The water vapour permeability was determined in two samples of the *Monserrate* Palace: PM1 and PM4. Both had flat surfaces of test and were available in sufficient quantity. The devices used are shown in Figure 4.91 and the results obtained are presented in Table 4.46.

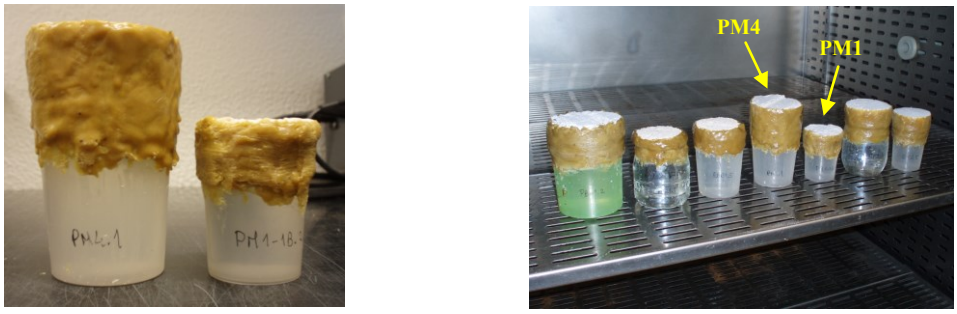

(a) (b)

Figure 4.91 - Water vapour permeability determination in samples PM1 and PM4: (a) devices used (adapted to ancient samples); (b) ongoing test

Table 4.46 - Water vapour permeability results of samples PM1 and PM4

Test specimen	Thickness (d) (mm)	ΔM/24h (g)	Permeability ($ng.m^{-1}.s^{-1}.Pa^{-1}$)	Sd (d=10 mm) (m)
PM1	6.25	0.00542[(1)]	0.23	**8.539**
PM1	6.25	0.00583[(2)]	0.25	**7.933**
PM4	27.47 (3.84 plaster + 23.63 mortar)	0.28	30.23	**0.061**

[(1)] Average value of 11 days in the climatic chamber; [(2)] Average value of 1008 days outside the chamber at non-controlled conditions

The values found indicate that the vapour permeability of sample PM1 is extremely low, completely outside the values obtained in samples of common gypsum plaster materials. It strengthens the

plausibility of a low and almost not connected porous structure, in agreement with all the other properties determined: capillary water absorption (very compact micro structure), very low porosity and average pore radius and extremely high mechanical properties (DME and compressive strength).

Regarding sample PM4, it has a high water vapour permeability, in accordance with the values found for similar materials in the literature: gypsum-lime test specimens (Ramos et al. 2010: Sd = 0.059 m) and lime-based mortars formulations for restoration purposes prepared in laboratory (Veiga et al. 2010: Sd < 0.10 m; Margalha 2010: Sd = 0.05-0.12 m).

Comparing again this sample with sample PBS1, although the difference is not very significant, the permeability of the first is lower (Sd = 0.061 m) than that of the second (Sd = 0.050 m). As the vapour permeability of a material is usually related with its drying behaviour (Rato 2006) and average pore radius (Magalhães et al. 2004) and PBS1 had higher drying rate than PM4, the results obtained are in agreement. In fact, they point out to a slightly higher and better connected open porosity of the sample PBS1 and probable higher average pore radius as well. It would be interesting to have the pore size distribution curves of more samples; a better understanding of the relations between the different properties studied would then be possible.

- Mechanical properties

Dynamic modulus of elasticity and compressive strength

The dynamic modulus of elasticity and compressive strength results obtained for the samples of *Monserrate* Palace are presented in Table 4.47 and Table 4.48, respectively. Figure 4.92 shows the test specimens being tested in compression.

The results of sample PM1 were completely outside what is usually expected for gypsum plaster samples but in agreement with all the other characteristics already discussed.

The highest values found in the literature for gypsum plaster materials are those of Dalui et al. (1996) with 22000 MPa for the DME determined by ultrasonic pulse velocity and 38 MPa for the compressive strength, Wirsching (2005), which indicated a compressive strength value of 40.4 MPa and Middendorf & Knöfel (1998) with 21350 MPa in the DME and 43 MPa compressive strength. Nevertheless, in all cases the authors referred to products obtained from hemihydrate alpha plasters, not used in building materials due to their high brittleness.

Middendorf & Knöfel also determined the compressive strength of old gypsum and gypsum-anhydrite based masonry mortars but the values obtained seldom reached 40 MPa.

Table 4.47 - Dynamic modulus of elasticity results of the samples from *Monserrate* Palace

Sample	Bulk density[1] ($kg.m^{-3}$)	SD	CV (%)	Distance (m)	Time (μs)	SD	CV (%)	Speed ($m.s^{-1}$)	DME (MPa)
PM1	2495	251	10.1	0.114	38.1	0.1	0.3	2999	20194
PM3	1158	41	3.6	0.072	43.3	0.2	0.5	1660	2872
PM4	1702	57	3.4	0.190	93.6[2]	1.0	1.1	2029	6308
PM4	1702	57	3.4	0.212	89.8[3]	0.3	0.4	2361	8543

[1] Sand method; [2] Measured at the surface (indirect method); [3] Direct method; SD - standard deviation; CV - coefficient of variation; DME - dynamic modulus of elasticity

Table 4.48 - Compressive strength results of the samples from *Monserrate* Palace

Sample (test specimen)	Confinement mortar age (days)	Bulk density[1] ($kg.m^{-3}$)	SD	CV (%)	Load rate ($N.s^{-1}$)	Maximum load (N)	Compressive strength (MPa)
PM1 (PM1.1)	-	2380	137	5.8	500	128123	80.08
PM1 (PM1.2)	-	2305	90	3.9	200	110129	68.83
PM4	27	1747	36	2.1	100	3370	2.11

[1] Sand method; SD - standard deviation; CV - coefficient of variation

(a) (b) (c)

Figure 4.92 - Adapted compressive strength tests: (a) PM1 with three fibre cement boards to achieve the target height; (b) PM1 after failure; (c) PM4 with confinement mortar and one fibre cement board

Concerning sample PM4, the DME has been determined by measuring the ultrasonic pulse velocity in two different ways: (1) on the surface of the plaster (indirect method); (2) with the probes positioned at the ends of the plaster layer (direct method). The results were different and show that the mortar was more influential in the direct method increasing the values obtained, which is logical attending to the high thickness and cohesiveness of the mortar.

In fact, if only the plaster layer were considered, both the bulk density and the DME would be much lower. This statement is well supported by the results obtained in samples with similar compositions (PBS2, PM3 and EBR3) whose dimensions allowed the determination of the bulk density and DME without other materials associated.

Taking into account the previous considerations, the compressive strength value of sample PM4 was below expectations.

4.3.2.5 The *S. Francisco* Church

It is a medieval construction located in Tavira, Algarve, thought to date back to the late 13th century (Figure 4.93). It is supposed to have been originally built for the Templars and donated later by king *D. Dinis* to the Franciscans and it was, at times, part of the Convent of *S. Francisco*.

The church was destroyed several times, namely in 1722 and 1755 by earthquakes and in 1881 by a devastating fire, undergoing reconstruction processes after that. From the original gothic structure only the sacristy, with ample window and vault, and two chapels in the old fence are left (Documentar n.d.).

Two domes stand out at the top. During the reconstruction works that took place at the end of the 19th century, the presbytery and the dome close to it were profusely decorated with plaster elements of Neo-Arab influence a job once again authored by *Domingos Meira* (Figure 4.94).

Like in *Monserrate* Palace, water infiltration problems severely affected the plasters destroying some of them. In 2008, even though the annomalies were not totally solved, the plasters were restored. Many of the decorative motifs have been reproduced from the originals using silicone based materials that were later embedded in a gypsum plaster base in order to be fixed, allowing the production of several copies (Figure 4.95).

(a)

Figure 4.93 - *S. Francisco* Church: view of the front façade and the dome (image taken from Documentar n.d.)

(a)

(b)

(c)

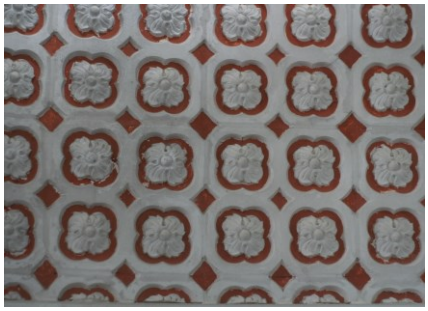

(d)

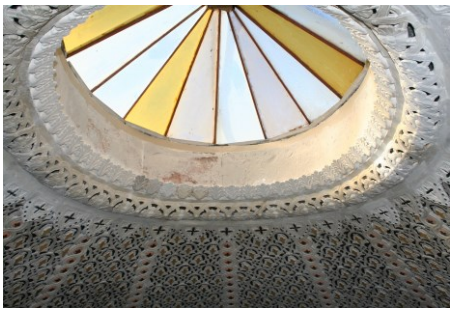

(e)

(f)

(g)

(h)

Figure 4.94 - *S. Francisco* Church: (a) ceiling of the presbytery, in poor condition; (b) decorative plasters of the presbytery; (c) and (d) details of some decorative motifs; (e) dome with skylight after restoration; (f), (g), (h) details of the restored decoration of the dome

(a)

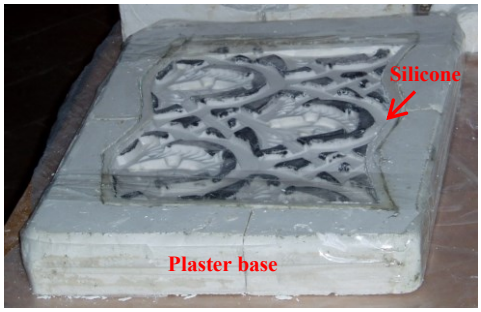

(b)

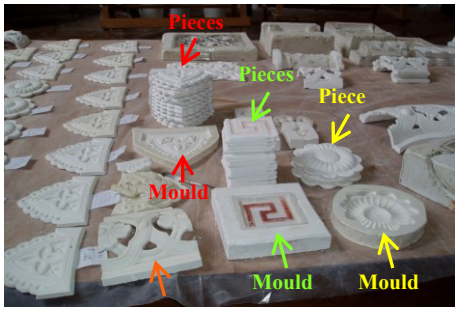

(c)

(d)

Figure 4.95 - Reproduction of damaged elements in *S. Francisco* church: (a) moulds; (b) mould corresponding to sample ISF1; (c) moulds and respective pieces (orange arrow corresponds to sample ISF2); (d) reproduced elements

Samples

Three samples of ornaments previously detached due to anomalies in the building were collected. They all belonged to the decorative program of the dome. Their identifications and corresponding images are shown in Figure 4.96 and Figure 4.97.

(a)

(b)

Figure 4.96 - Samples from *S. Francisco* church: (a) ISF1; (b) ISF3 showing signs of pink coloured biological colonization (yellow arrow)

(a)

(b)

Figure 4.97 - Samples from *S. Francisco* church: (a) ISF2, front view; (b) ISF2, back view with the fixing plaster visible in one of the fragments (red arrow)

Results and discussion

- Visual observation of the samples

The information obtained by visual observation of the samples is summarized in Table 4.49.

Table 4.49 - Visual observation of the samples from *S. Francisco* church

Sample	Description
ISF1	**Precast ornament** representing one "fleur de lis" light-beige coloured, over which there is another "fleur de lis", gilded, smaller and narrower (Figure 4.94 (g) and Figure 4.96 (a));
	It seems to have been attached to a smooth surface base plaster, approximately 5 mm thick, painted in black to enhance the decorative effect of the whole (Figure 4.98 (a));
	The stratigraphic analysis showed that everything has been precast together, i.e. it is only one piece (Figure 4.98 (b)). In fact, looking at Figure 4.95 (b) it can be seen that these ornaments were precast in panels, and then assembled like a puzzle, similarly to what was observed in *Monserrate* Palace or in *Bolsa* Palace;
	It also shows that there is a very thin white layer at the surface of the plaster that seems to have been applied with regularization and/or whitening functions. If this supposition is right, it is probably lime based and its application was immediately after the unmoulding, as there is no visible interface with the core of the sample (Figure 4.98 (c)).
ISF2	Three fragments of a **precast hollow frieze** from the dome with a convex shape representing a floral motive (Figure 4.94 (h) and Figure 4.97 (a));
	It had few remains of what seems to be a yellow pigmented layer in the flower eye rim (Figure 4.98 (d) to (f));
	One of the fragments still had the plaster used to fix it behind (Figure 4.97 (b)).
ISF3	Fragment of a **precast ornament** with a light beige colour and an average thickness of 9 mm (Figure 4.96 (b));
	It had a small area of the surface with pink coloured biological colonization (Figure 4.96 (b)).

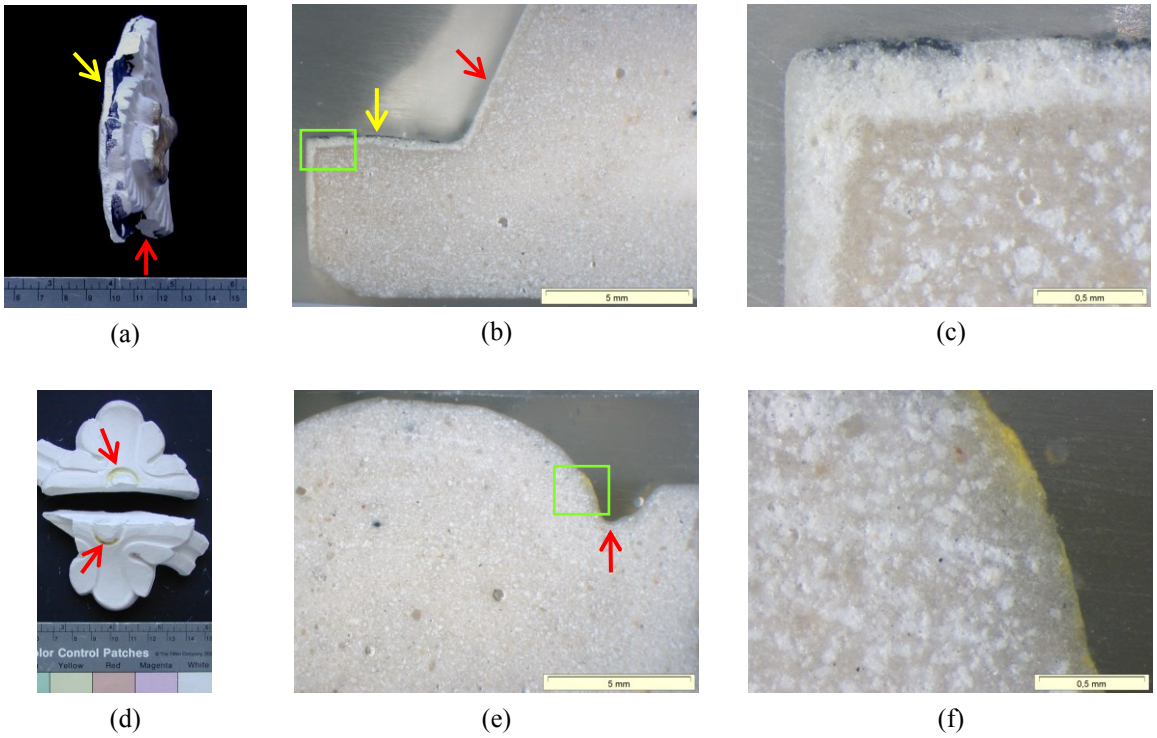

(a) (b) (c)

(d) (e) (f)

Figure 4.98 - Images of the samples from *S. Francisco* church showing some specific details: (a) side view from the top of ISF1 showing the ornament (red arrow) and its "base" (yellow arrow); (b) stereo-zoom microscope cross section view of a polished surface of ISF1 showing that the ornament (red arrow) was precast together with the "base" (yellow arrow); (c) detail of (b) (green frame) showing the very thin white layer all around the surface of the sample and the black pigment in the upper part of the "base"; (d) yellow pigmented layer in the flower eye rim of ISF2 (red arrows); (e) stereo-zoom microscope cross section view of a polished surface of ISF2 showing the flower eye rim area (red arrow); (f) detail of (e) (green frame) where the yellow pigment can be clearly observed

- XRD results

As the samples of *S. Francisco* Church were all from ornaments of the dome it was decided to start by determining the qualitative mineralogical composition of only two of them: ISF1 and ISF2. If significant differences were found, then ISF3 would also be tested, which was not the case. The results obtained showed that gypsum is the main constituent and calcite is also present but in much smaller amounts (Figure 4.99 and Table 4.50).

Traces of quartz and feldspars were also found but are considered to be common impurities due to their abundance in the Earth's crust.

In the case of dolomite, it was only detected in sample ISF1 but in such small quantities that it is surely an impurity of the gypsum raw material, and is probably present in ISF2, too.

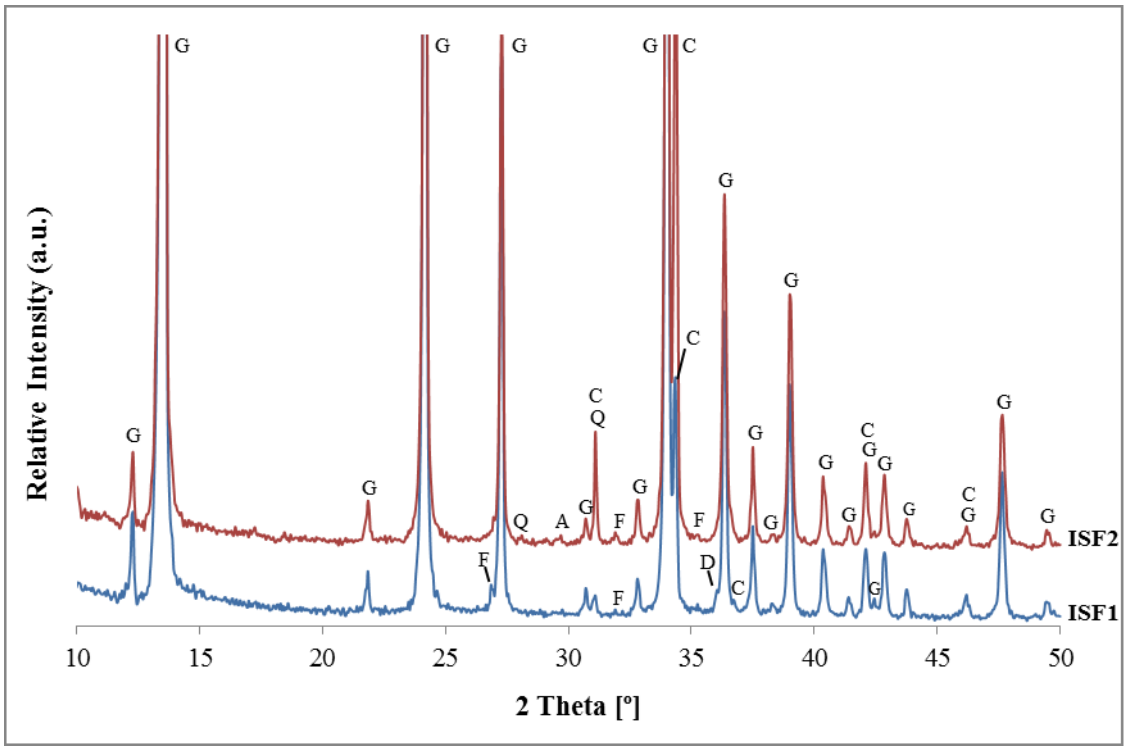

Figure 4.99 - XRD patterns of the samples from *S. Francisco* Church
Notation: G - Gypsum; C - Calcite; Q - Quartz; A - Anhydrite; D - Dolomite; F - Feldspars

Table 4.50 - XRD qualitative mineralogical composition of the samples from *S. Francisco* Church

Sample	Identified crystalline compounds					
	Gypsum	Calcite	Quartz	Dolomite	Anhydrite	Others
ISF1	+++/++++	+/++	trc	trc	-	Feldspars (trc)
ISF2	+++/++++	+	trc	-	trc	Feldspars (trc)

Notation used in XRD peak intensity:

++++	Very high proportion (predominant compound)	+	Weak proportion
+++	High proportion	trc	Traces
++	Medium proportion	-	Not detected

- TG-DTA results

The TG-DTA analyses were also performed only in samples ISF1 and ISF2. The gypsum and calcite contents were determined (Figure 4.100) and the results of XRD could be confirmed (Table 4.51).

The doublet of peaks corresponding to the two steps of dehydration of gypsum is well defined in the DTG and DTA curves of Figure 4.100, which is not surprising as it is the main constituent of both samples.

However, the small exothermic peak that corresponds to the phase change of soluble to insoluble anhydrite is not visible in the DTA curves contrarily to what it is usual in other samples with identical composition.

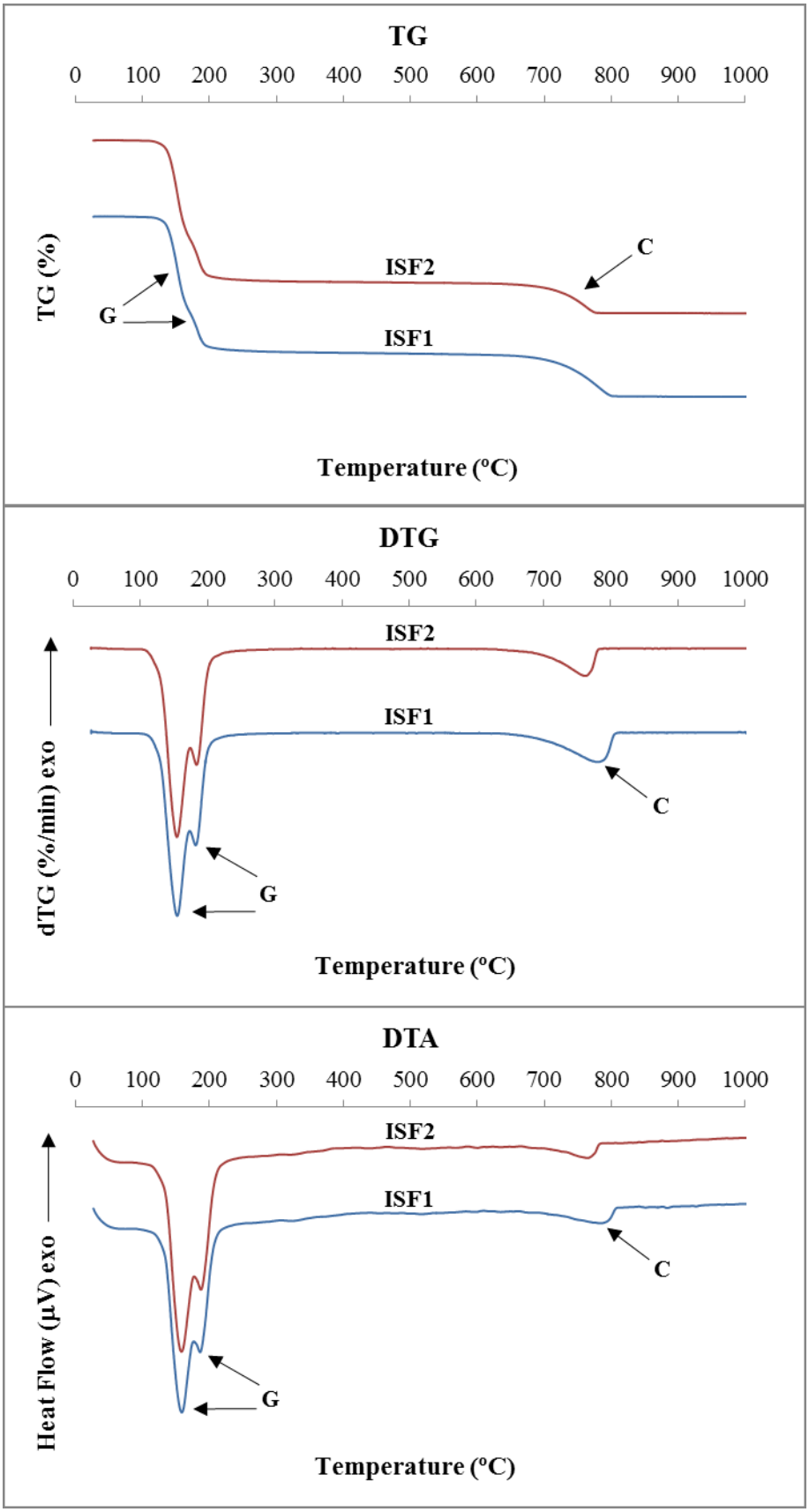

Figure 4.100 - TG, DTG and DTA curves of the samples from *S. Francisco* Church.
Notation: G - Gypsum dehydration; C - Calcite decarbonation

Table 4.51 - Weight loss and calculated gypsum/calcite contents of the samples from *S. Francisco* church

Sample	Temperature range (ºC)						Calculated contents (%)	
	25→85	85→250	250→600	600→850	850→1000	Loss of ignition	Gypsum	Calcite
ISF1	0.0	17.6	0.6	5.4	0.0	23.6	84	12
ISF2	0.0	18.3	0.5	3.9	0.0	22.7	88	9

In what concerns calcite, even though the difference between both samples is small, the temperature of decarbonation is higher in sample ISF, the one with a higher content. Similar observations have been made throughout all the case studies, with very few exceptions.

- Physical properties

Capillary absorption

The water absorption by capillarity behaviour was determined in sample ISF1 (Figure 4.101) and the quantitative results are summarized in Table 4.52.

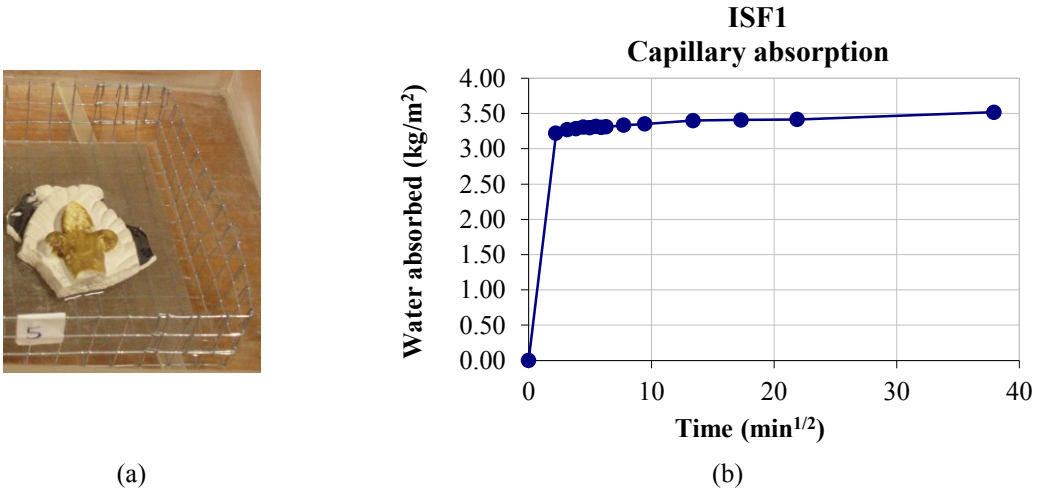

(a) (b)

Figure 4.101 - Water absorption by capillarity of sample ISF1: (a) test specimen during the determination; (b) graphical representation of the results

The curve profile shows a high rate of suction in the first 5 minutes; the water absorbed in this period represents 91.61% of the total amount absorbed during the time of the procedure (24 h). In spite of being a gypsum plaster sample from a precast element, ISF1's curve profile is very similar to those of samples PBS2, PE2/1 and EG5/2, all gypsum-lime plasters from moulded on site elements with approximate compositions. This capillary absorption behaviour usually indicates a great content of capillary pores with a high percentage of the larger ones (considered to have $r > 0.5$ micron) (Magalhães et al. 2004; Rato 2006).

Table 4.52 - Capillary absorption by contact results of sample ISF1

Test specimen	
Surface (cm^2)	33.54
Weight (g)	42.64
Capillary absorption at 5 min:	
(g)	10.81
($kg.m^{-2}$)	**3.22**
(%, relative to weight of sample)	25.35
(%, relative to total absorption)	91.61
Capillary absorption at 24 h:	
(g)	11.80
($kg.m^{-2}$)	**3.52**
(%, relative to weight of sample)	27.67
Ccc at 5 min ($kg.m^{-2}min^{-1/2}$)	**1.44**

Ccc - capillarity coefficient by contact

The loss of the water absorbed in the capillarity test was also evaluated and represented in Figure 4.102.

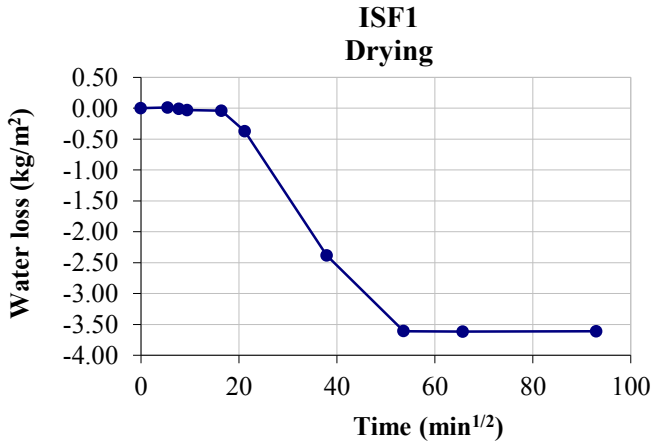

Figure 4.102 - Graphical representation of the drying behaviour of sample ISF1

The profile of the curve shows that sample ISF1 has a good drying capacity, in agreement with its capillary absorption behaviour. This reinforces the conviction that is must have a significant content of large capillary pores (r > 0.5 micron) and indicates a well-connected open porosity (Magalhães et al. 2004; Rato 2006).

Hygroscopic behaviour

The graphical representation of the hygroscopic behaviour of the samples ISF2 and ISF3 is shown in Figure 4.103.

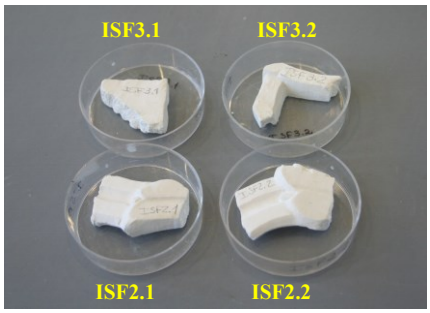

(a)

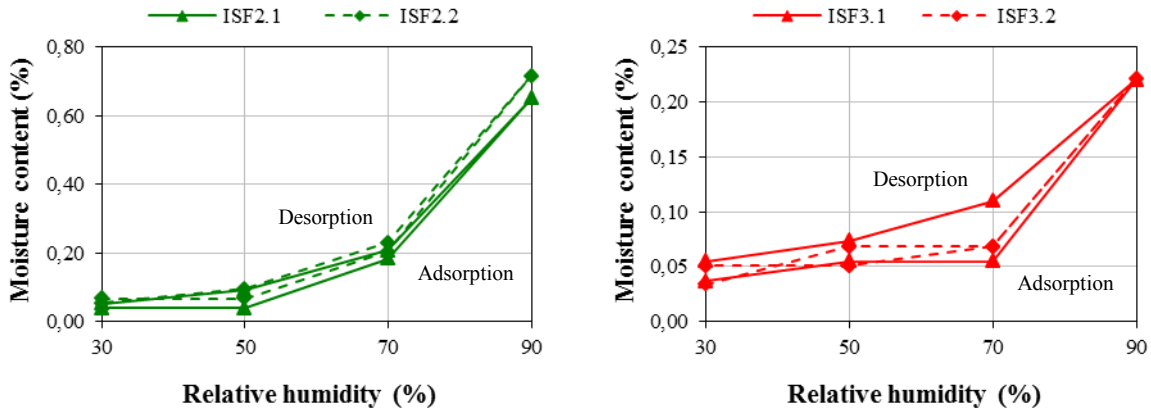

(b)

Figure 4.103 - Hygroscopic behaviour of samples ISF2 and ISF3: (a) test specimens; (b) graphical representation of the results

Table 4.53 - Average hygroscopicity results of samples ISF2 and ISF3 (2014)

	RH (%)	MC (%) ISF2	SD	CV (%)	MC (%) ISF3	SD	CV (%)
Adsorption	30	0.05	0.020	37.86	0.04	0.002	5.29
	50	0.05	0.020	37.86	0.06	0.009	15.00
	70	0.19	0.015	7.56	0.06	0.009	15.00
	90	**0.68**	0.046	6.80	**0.22**	0.001	0.37
Desorption	70	0.22	0.015	6.97	0.09	0.030	33.32
	50	0.09	0.002	2.69	0.06	0.016	25.35
	30	0.05	0.001	2.69	0.07	0.010	13.66

RH - relative humidity; MC - moisture content; SD - standard deviation; CV - coefficient of variation

With the exception of test specimen ISF3.1, the curve profiles do not show the presence of hysteresis effect. This observation is in agreement with the relationship between composition and pore size distribution: the gypsum plaster samples are expected to have negligible amounts of pores in the range where hysteresis usually occurs (< 0.05 micron (IUPAC 1985)).

The results of adsorption at 90% relative humidity are very different, i.e. three times higher in sample ISF2. The probable explanation for that is a contamination with hygroscopic substances, e.g. soluble salts, as the value obtained for sample ISF3 is more consistent with those of other gypsum plaster samples.

- Mechanical properties

Dynamic modulus of elasticity and compressive strength

The dynamic modulus of elasticity results of the samples from *S. Francisco* Church are presented in Table 4.54.

Table 4.54 - Dynamic modulus of elasticity results of the samples from *S. Francisco* Church

Sample (test specimen)	Bulk density ($kg.m^{-3}$)	SD	CV (%)	Distance (m)	Time (μs)	SD	CV (%)	Speed ($m.s^{-1}$)	DME (MPa)
ISF1	1385[(1)]	55	3.9	0.070	35.6	0.2	0.4	1964	4809
ISF2	N.D.	-	-	0.051	30.5	0.1	0.3	1671	-
ISF3	1242[(2)]	-	-	0.070	37.8	0.1	0.1	1854	3841

[(1)] Sand method; [(2)] Water displacement method; N.D. - Not determined; SD - standard deviation; CV - coefficient of variation; DME - dynamic modulus of elasticity

The values obtained for the ultrasonic pulse velocity through the matrixes (1600 - 2000 $m.s^{-1}$) and for the bulk densities (1200 - 1400 $kg.m^{-3}$) are of the same order of magnitude as those of other gypsum plaster samples (SP1, PB6/3, PBS3, PE1/2, PE2/2, etc.).

The corresponding dynamic moduli of elasticity are more divergent (3800-4800 MPa), as their calculation is directly influenced by both parameters. However, they are still in agreement with the most common results obtained in samples with the same composition (Freire et al. 2011) and the very few values available in the literature for gypsum plasters with a plaster/water ratio adequate for the manufacture of precast elements (Coquard et al. 1994; Dalui et al. 1996).

The compressive strength has been determined in sample ISF3 (Figure 4.104) and the results are presented in Table 4.55.

Figure 4.104 - Adapted compressive strength test: ISF3 "sandwiched" between two layers of confinement mortar

Table 4.55 - Compressive strength results of sample ISF3

Sample	Confinement mortar age (days)	Bulk density[(1)] ($kg.m^{-3}$)	SD	CV (%)	Load rate ($N.s^{-1}$)	Maximum load (N)	Compressive strength (MPa)
ISF3	20[(2)]	1242	-	-	100	2350	1.47

[(1)] Water displacement method; [(2)] on both sides; SD - standard deviation; CV - coefficient of variation

The value obtained is lower than expected taking into account the dynamic modulus of elasticity and the values of the majority of the ancient samples with a similar composition (Freire et al. 2011; Veiga 2012). It is also far from the results obtained for the gypsum plaster mixes tested in this work: 5 to 8 MPa (*cf.* Chapter 5). The reason for that is probably the low thickness of the sample (9 mm average).

4.3.3 The transition between the 19th and 20th centuries

4.3.3.1 The *Estoi* Palace

The *Estoi* Palace is situated in the village of *Estoi*, district of Faro, in the south of Portugal (Figure 4.105). Its construction started in the middle of the 19th century but it was only finished between 1893 and 1909, with the decoration of the house and gardens. The decorative program of the Palace was conceived by *Domingos Meira* and results from a mix of architectonic styles, where Neoclassic, Neorocaille and *Art Nouveau* are predominant (Gil & Calvet 1992; Magalhães 2002); it is said to have "the finest plaster ceilings in the Algarve" (Figure 4.106). In 2008, an extensive works campaign promoted the restoration and adaptation of the building to a luxury hotel.

Figure 4.105 - *Estoi* Palace: view of the south façade, to the gardens

(a)

(b)

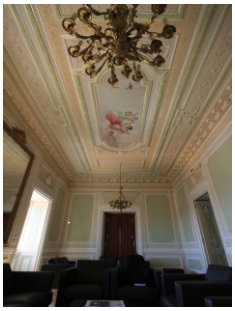

(c)

(d)

(e)

(f)

Figure 4.106 - *Estoi* Palace: Noble room - general view (a) and ceiling (b); Blue room: general view (c) and ceiling (d); (e) and (f) ceiling of the entrance lobby carpeted with leaves

Samples

A total of five samples were collected in two different ways (Figure 4.107): indirectly (samples PE1 to PE4), i.e. they had been previously detached due to some anomaly in the building and directly on site (sample PE5).

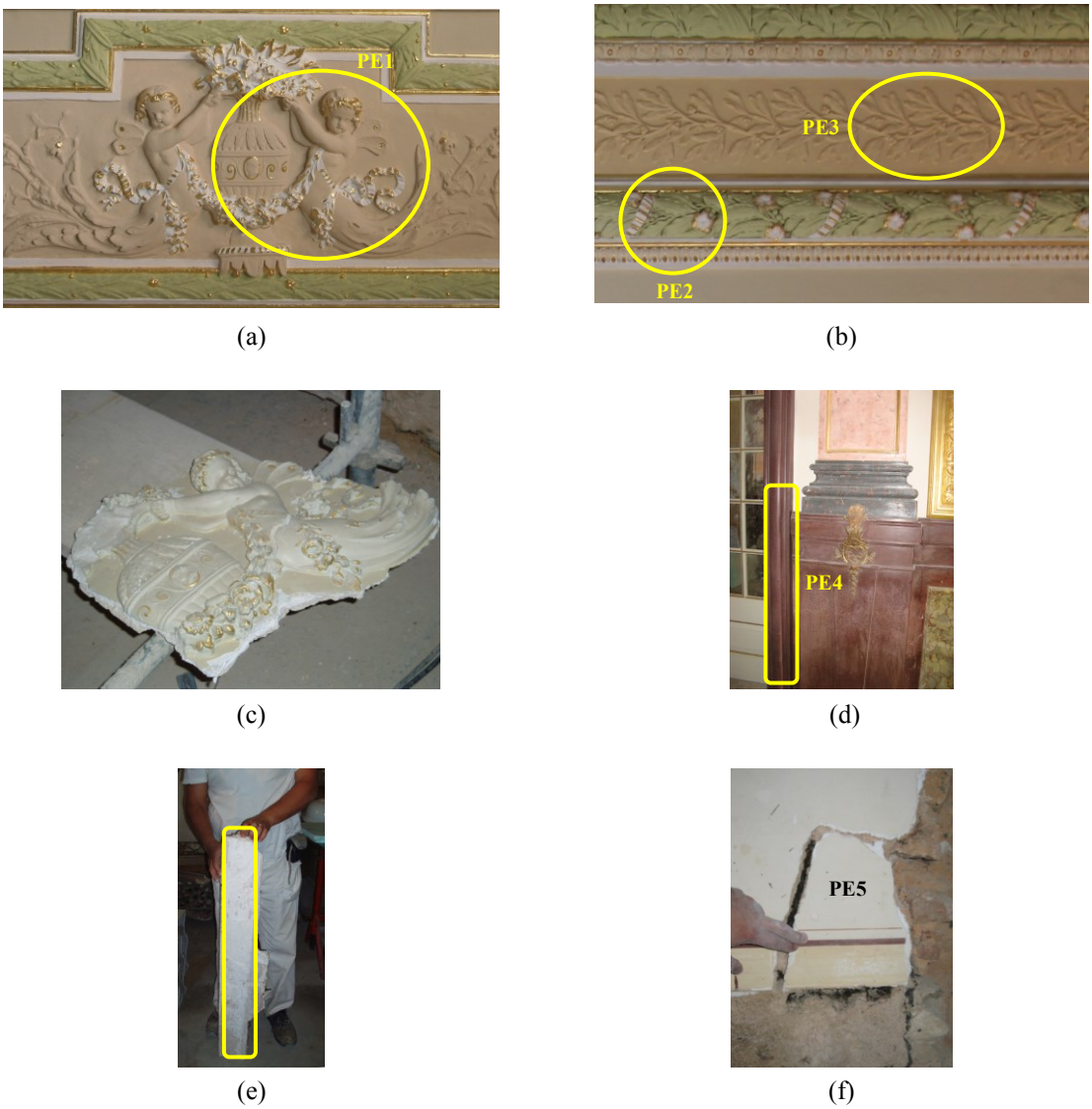

(a) (b) (c) (d) (e) (f)

Figure 4.107 - Details of some plastered surfaces with indication of the corresponding samples collected: (a) and (b) ceiling of the Blue room; (c) sample PE1 lying on the floor, after detachment; (d) door frame of the Noble room; (e) sample PE4 after detachment (back view); (f) wall of a small room, currently the disabled toilet

After initial visual observation, it was decided not to study sample PE3 as it belonged to a precast decorative element like PE1 and PE2 (Figure 4.108).

The identification and description of the samples analysed is presented in Table 4.56 and the corresponding images are shown in Figure 4.109 and Figure 4.110.

Figure 4.108 - Sample PE3, excluded from the study

Table 4.56 - Identification and description of the samples from *Estoi* Palace

Sample identification	Description
PE1	Preparation layer (PE1/1) and decorative putty (PE1/2) from the ceiling of the Blue room (polychromic)
PE2	Preparation layer (PE2/1) and decorative frame (PE2/2) from the ceiling of the Blue room (polychromic)
PE4	Door-frame from the Noble room simulating an imperial red porphyry (PE4/2, polychromic) and respective interior plaster structure (PE4/1)
PE5	Finishing plaster (made in three layers: PE5/1, PE5/2, PE5/3) from a wall of a small room, currently the disabled toilet (polychromic)

(a)

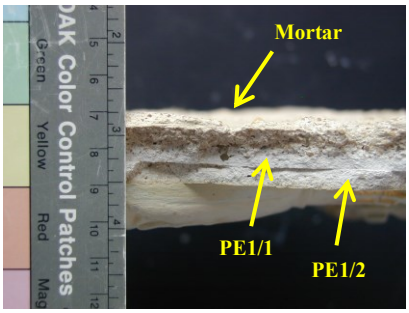

(b)

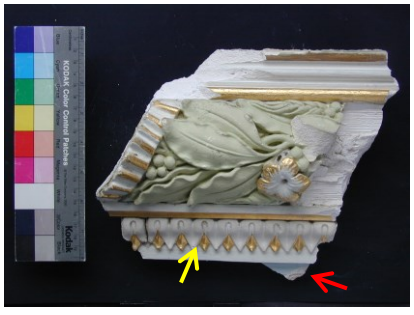

(c)

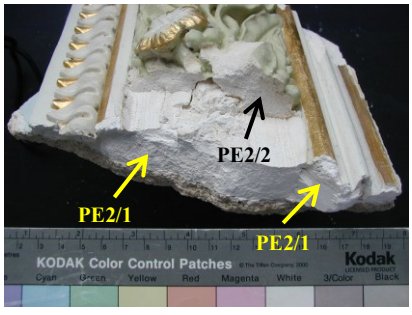

(d)

Figure 4.109 - Photographs of the samples PE1 and PE2 from *Estoi* Palace: (a) PE1 (front view); (b) PE1 (side view); (c) PE2 (front view); (d) PE2 (side view)

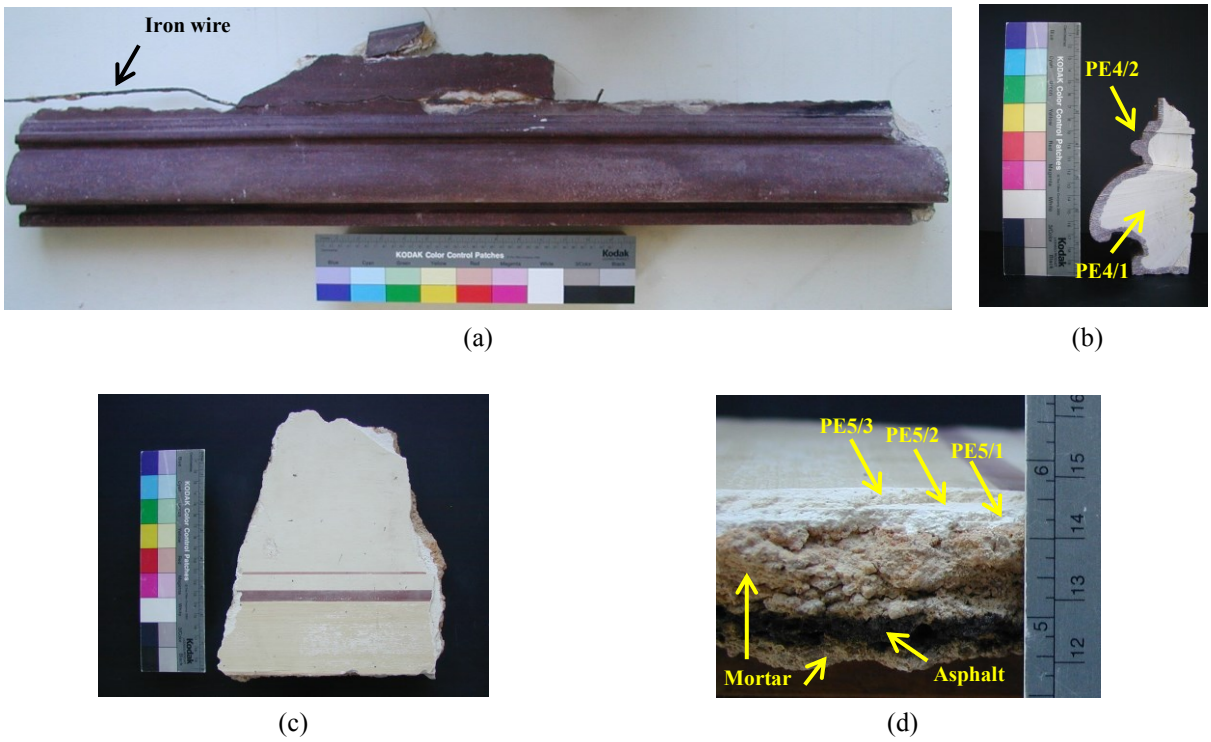

Figure 4.110 - Photographs of the samples PE4 and PE5 from *Estoi* Palace: (a) PE4 (front view); (b) PE4 (side view); (c) PE5 (front view); (d) PE5 (side view)

Results and discussion

Among the samples from *Estoi* Palace, PE4 soon revealed to be a very special case study. The numerous questions raised after the first characterization results triggered using a larger number of techniques than in any other sample analysed during this research work and involved the cooperation of researchers from other institutions: Dr Isabel Pombo Cardoso, by the time PhD student at the University College of London, England (micro-Raman analyses), Dr Frank Schlütter from MPA Bremen Institute for Materials Testing, Germany (Polarized Light Microscopy and SEM-EDS observations of thin sections), Dr José Mirão (Polarized Light Microscopy observations of thin sections) and Dr António Candeias (FT-IR analyses), both from the University of *Évora*, Portugal, and Giovanni Borsoi (micro FT-IR analyses), colleague at LNEC, Portugal.

- Visual observation of the samples

The information obtained by visual observation of the samples is summarized in Table 4.57.

Table 4.57 - Visual observation of the samples from *Estoi* Palace

Sample	No. layers	Identification	Description
PE1	3	PE1/1	White **preparation plaster layer**, approximately 5 mm thick, applied between the mortar and the moulded putty (Figure 4.109 (b)); Extremely well connected to the mortar beneath; Presence of some sisal fibres.
		PE1/2A	White part from the interior of **precast putty** (PE1/2); Structured with a considerable amount of sisal fibres.
		PE1/2B	Yellowish part from the interior of the **putty**, with very irregular thickness (1-3 mm), situated closer to the surface than PE1/2A and immediately below the painted layer.
PE2	3	PE2/1	White thick plaster layer, applied over the mortar, where a part works as **preparation layer** for pasting of precast elements and the other part was **moulded on site** (Figure 4.109 (d) and Figure 4.111 (b)).
		PE2/2A	White part from the interior of the **precast frame** pasted to PE2/1 (Figure 4.111 (d) and (e)).
		PE2/2B	Yellowish part from the interior of the **precast frame** pasted to PE2/1, with very irregular thickness, situated closer to the surface than PE2/2A and immediately below the painted layer (Figure 4.111 (d) and (e)); There were also some **ornaments** consisting of low thickness **precast frames** (Figure 4.109 (c), yellow arrow), structured with iron wires (Figure 4.111 (b), red circle), whose interior had a yellowish colour (total absorption of the key-coat), and so designated by PE2/2B, too (Figure 4.111 (b)).
PE4	3	PE4/1A	Beige **thick plaster layer**, reinforced with sisal fibres and iron wire (Figure 4.110 (a)); The wire was rusted and its expansion caused a fracture in the piece which, together with some moisture, led to its detachment from the wall; It had also a thin layer of a white plaster used to stick the piece to the wall (not visible in the images shown).
		PE4/1B	Very similar to PE4/1A though seeming to be a bit whiter, finer and less porous. It was applied immediately after it due to the perfect union existing between them (Figure 4.112 (b)).
		PE4/2	**Finishing purple decorated plaster layer** (Figure 4.110 (b)), simulating imperial red porphyry with what seemed to be aggregates of different colours (orange and light purple-brown) with grain sizes up to 3 mm (Figure 4.112 (c)). Very stiff and compact.
PE5	3 (Figure 4.110 (c) and Figure 4.112 (e))	PE5/1	Beige **plaster layer**, applied over the mortar, approximately **2-3 mm thick**.
		PE5/2	Intermediate very pale yellow **plaster layer**, approximately **1-1.5 mm thick**; Extremely well connected to the layers beneath and above, making it very difficult to separate them; This observation means that the layers were probably applied with short time intervals (“fresh on fresh” technique) and were very compressed with the tools.
		PE5/3	Light yellow **final plaster layer**, approximately **2-2.5 mm** thick, painted in yellow and brown (Figure 4.110 (c)).

In the case of samples PE1/2 and PE2/2, corresponding to painted precast ornaments, their interior seemed to be made of two layers of different materials. However, it is the difference in colour in the first millimetres of plaster, caused by the absorption of a product applied as key-coat (thought to be shellac), which created what is probably an illusion. In fact, the thickness of the external layer is so low and irregular (especially in PE1/2) that it would be difficult to obtain by the precast technique. It is more logical that the plaster is all the same and that the differences observed are due to a phenomenon of absorption. Nevertheless, the two areas of the interior of the ornaments were given a different designation (A and B) (Figure 4.111 (e)) and were analysed separately by XRD and TG-DTA.

Another observation concerning samples PE1/2 and PE2/2 is the change of the final colour exhibited: PE1/2 is now beige coloured but was previously painted in a very similar colour to PE2/2's actual green; contrarily, the first painted layer of sample PE2/2 was beige. This probably means that the pictorial effect of the ceiling of the Blue room has changed somewhere in time (restoration works?).

An additional detail corroborates this hypothesis: in Figure 4.109 (c) the transition between the relieved decorative part of this ceiling and the central pictorial smooth surface, indicated by a red arrow and corresponding to Figure 4.111 (b), shows a blue coloured surface. However, the stereo-zoom microscope observation (Figure 4.111 (c)) indicates that this surface was originally beige, the colour presently exhibited after the restoration works of 2008 (Figure 4.107 (c)).

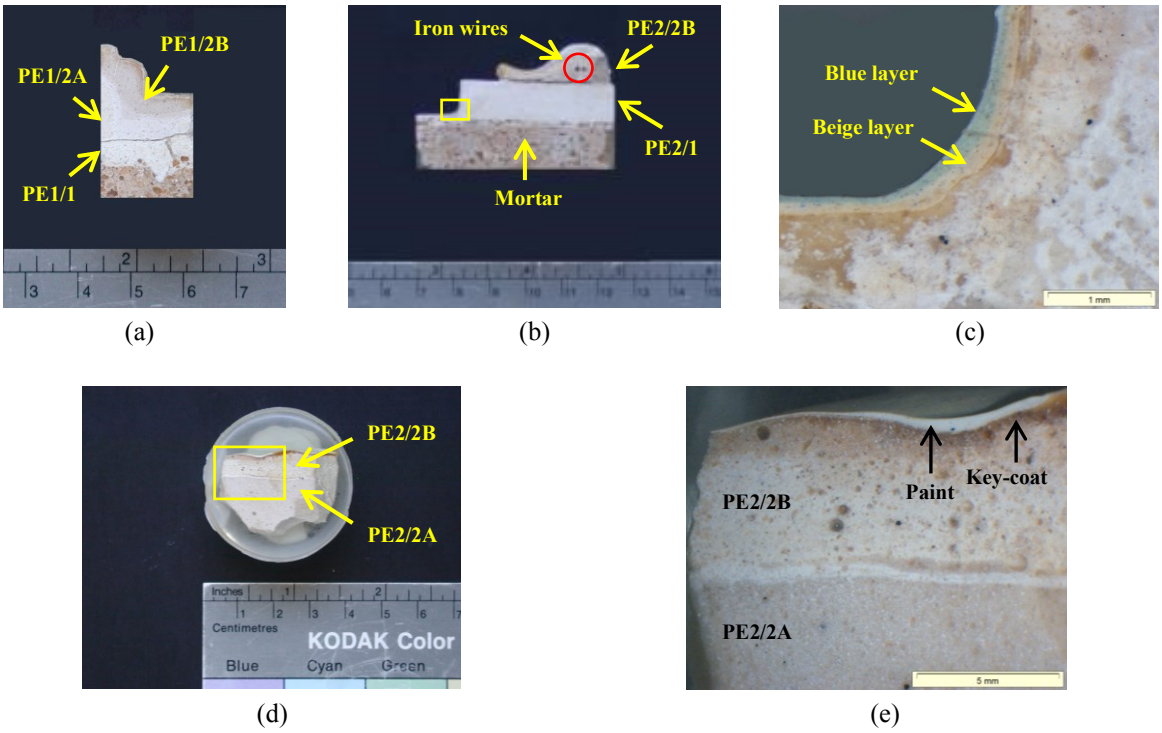

(a) (b) (c)

(d) (e)

Figure 4.111 - Stratigraphic analysis of the samples PE1 and PE2 from *Estoi* Palace: photographs of PE1 (a) and PE2 ((b) and (d)) after preparation of polished surfaces; stereo-zoom microscope images of PE2/1 ((c), yellow frame of (b)) and PE2/2 ((e), yellow frame of (d))

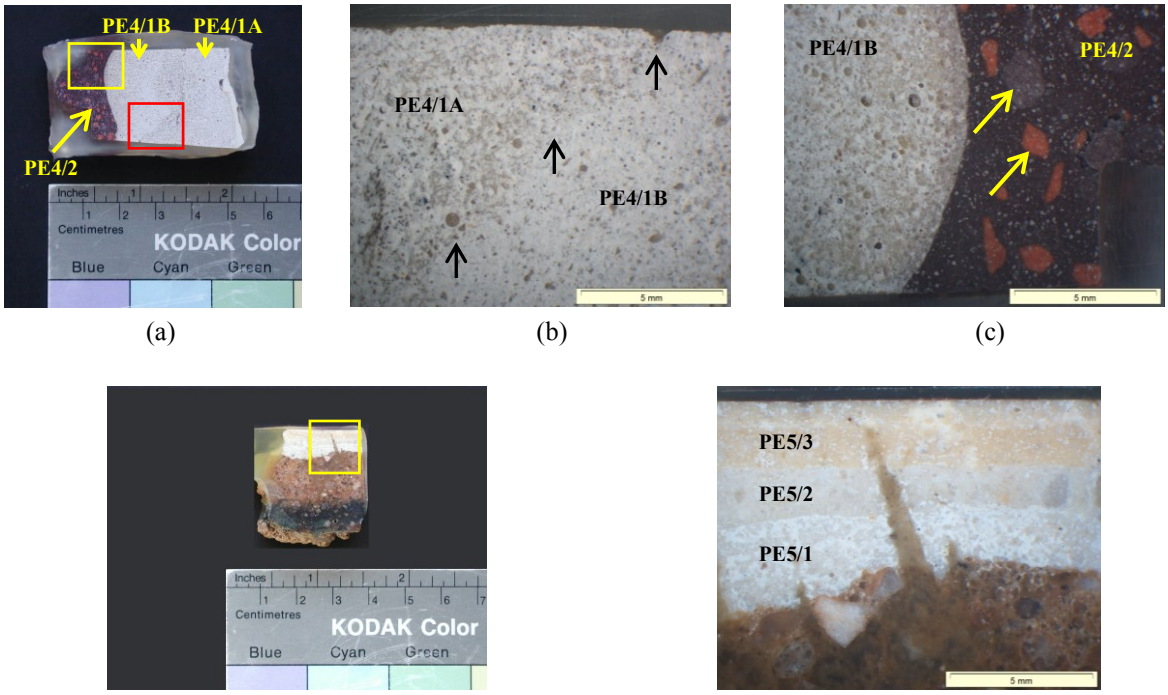

(a) (b) (c)

(d) (e)

Figure 4.112 - Stratigraphic analysis of the samples PE4 and PE5 from *Estoi* Palace: photographs of PE4 (a) and PE5 (d) after preparation of the polished surfaces; stereo-zoom microscope images of PE4/1 ((b), red frame of (a), inverted), PE4/2 and PE4/1B ((c), yellow frame of (a), inverted); and PE5 ((e), yellow frame of (d))

Concerning sample PE4, when looking at it from a front view, it really seems made of stone. The brightness and stiffness of the decorative layer, together with the perfect *porphyry* effect given by the aggregates, are remarkable and highlight the high quality of execution. These aspects were confirmed by the observation of the sample at the stereo-zoom microscope (Figure 4.112 (c)). More detailed images of the visual effect of these elements in the Noble room are presented in Figure 4.113.

Figure 4.113 - *Estoi* Palace: plaster decorative elements simulating imperial red porphyry in the Noble room

The decorative layer of sample PE4 represents, however, only a few millimetres of its structure (Figure 4.110 (b)). The core is constituted by a very thick, less dense white plaster reinforced with sisal fibres and an iron wire.

Looking at Figure 4.112 (b), the small fracture at the top (first arrow) and the slight difference in colour and texture that starts diagonally from there seem to indicate that this very thick element was produced in two phases, one immediately after the other, as the interface between them is almost imperceptible. This area was carefully observed with magnifications up to 60 times but it was even less perceptible, though inconclusive. The solution was to look directly into the sample and do some fracture tests with the aid of a chisel and a hammer: PE4/1 was broken in two parts, clearly showing a preferential fracture pattern through a smoother surface - the joint surface (Figure 4.114):

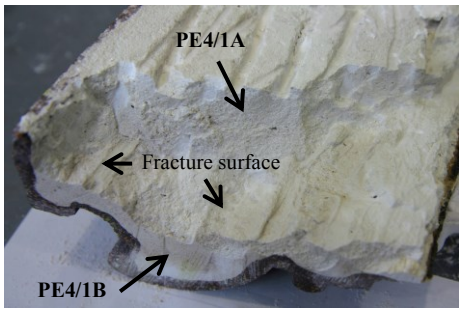

Figure 4.114 - Fracture pattern attesting the existence of a joint surface between PE4/1A and B

The perfection of the union between layers PE4/1B and PE4/2 is also remarkable (Figure 4.112 (c)) and will be further illustrated in the "SEM-EDS and PLM observations" section.

In PE4/2 the required decorative effect was achieved through the use of two types of aggregates (Figure 4.112 (c), yellow arrows): those with a light brown effect, thought to be quartz on the first observations at the stereo-zoom microscope due to its apparent transparency, and the orange ones, thought to be pieces of burned clay. These hypotheses were not confirmed afterwards as XRD and TG-DTA analyses detected only the presence of gypsum, anhydrite and hematite.

Concerning sample PE5, it was also difficult to determine how many layers composed it. The observation under the stereo-zoom microscope clarified that they were three (Figure 4.112 (e)). After it they were separated and analysed individually by XRD and TG-DTA.

This sample belongs to a wall that had a layer of asphalt between two layers of mortar (Figure 4.109 (h) and Figure 4.112 (d)). This is usually a strong indication of moisture problems with the asphalt being used as a barrier between the external and the internal surfaces of the wall. The detection of traces of halite in the XRD analysis of PE5/1 and PE5/3 (Table 4.58) and in the SEM-EDS observations (Figure 4.152) confirmed these suppositions.

Finally, the external surface, corresponding to layer PE5/3, was painted in yellow and brown with a lime wash based paint.

- XRD results

The qualitative mineralogical composition of the samples was determined by XRD and the results obtained showed that gypsum and calcite are the main constituents. In the case of sample PE4/2, calcite was not detected but anhydrite and hematite are also present (Table 4.58, Figure 4.115, Figure 4.116 and Figure 4.117).

Table 4.58 - XRD qualitative mineralogical composition of the samples from *Estoi* Palace

Sample	Identified crystalline compounds					
	Gypsum	Calcite	Quartz	Anhydrite	Feldspars	Others
PE1/1	+++	++	trc	-	trc	-
PE1/2A	+++/++++	+/++	trc	trc	trc	-
PE1/2B	+++/++++	+/++	trc	trc	trc	-
PE2/1	++/+++	++/+++	-	-	trc	-
PE2/2A	+++/++++	+/++	trc	trc	trc	-
PE2/2B	+++/++++	+/++	trc	-	trc	-
PE4/1	+++/++++	+	-	-	trc	Celestine (trc) Dolomite (trc)
PE4/1A	+++/++++	+	trc	-	-	Celestine (trc)
PE4/1B	+++/++++	+/++	trc	trc	-	Dolomite (trc)
PE4/2	+++/++++	-	-	trc+	-	Hematite (trc+) Celestine (trc)
PE5/1	++	+++	trc	-	trc	Halite (trc)
PE5/2	+	+++/++++	trc	-	-	-
PE5/3	++/+++	++/+++	trc	-	-	Halite (trc)

Notation used in XRD peak intensity:

++++	Very high proportion (predominant compound)	+	Weak proportion
+++	High proportion	trc	Traces
++	Medium proportion	-	Not detected

Once again, traces of quartz and feldspars are present due to their common occurrence in the Earth's crust. Dolomite and celestine are also impurities, but associated to the gypsum deposits. It is worth noting that celestine is here detected in a sample that does not belong to a case study located in the north of Portugal.

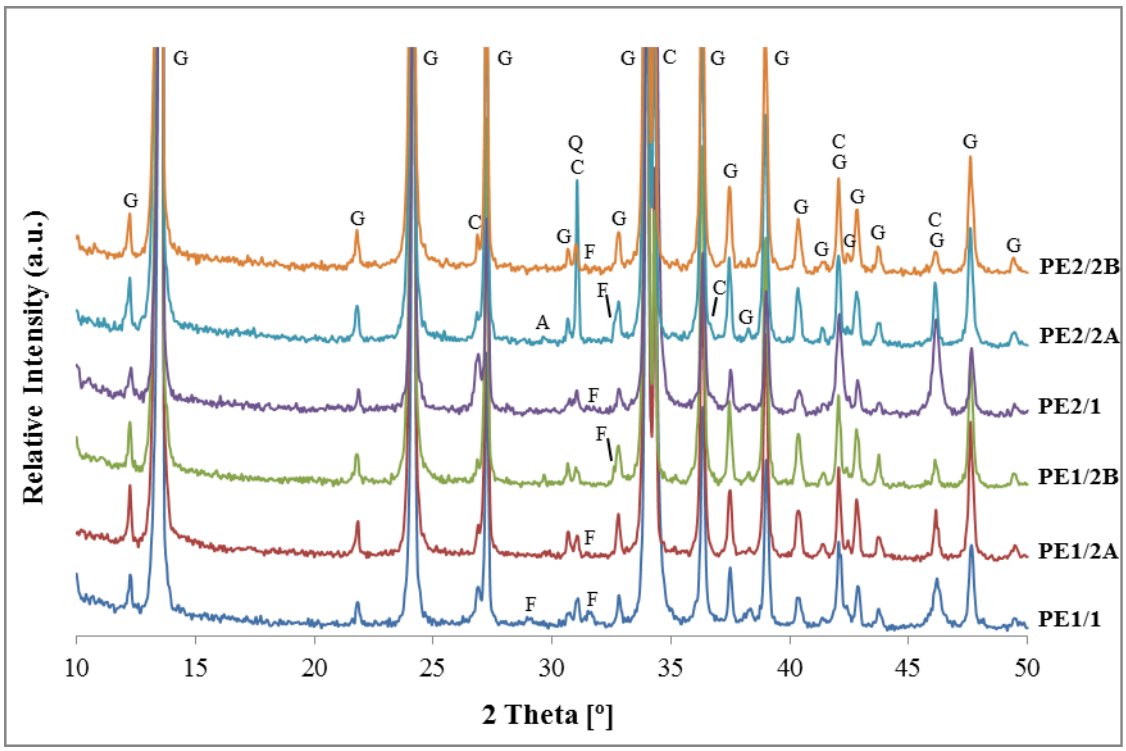

Figure 4.115 - XRD patterns of samples PE1 and PE2.
Notation: G - Gypsum; C - Calcite; Q - Quartz; A - Anhydrite; F - Feldspar

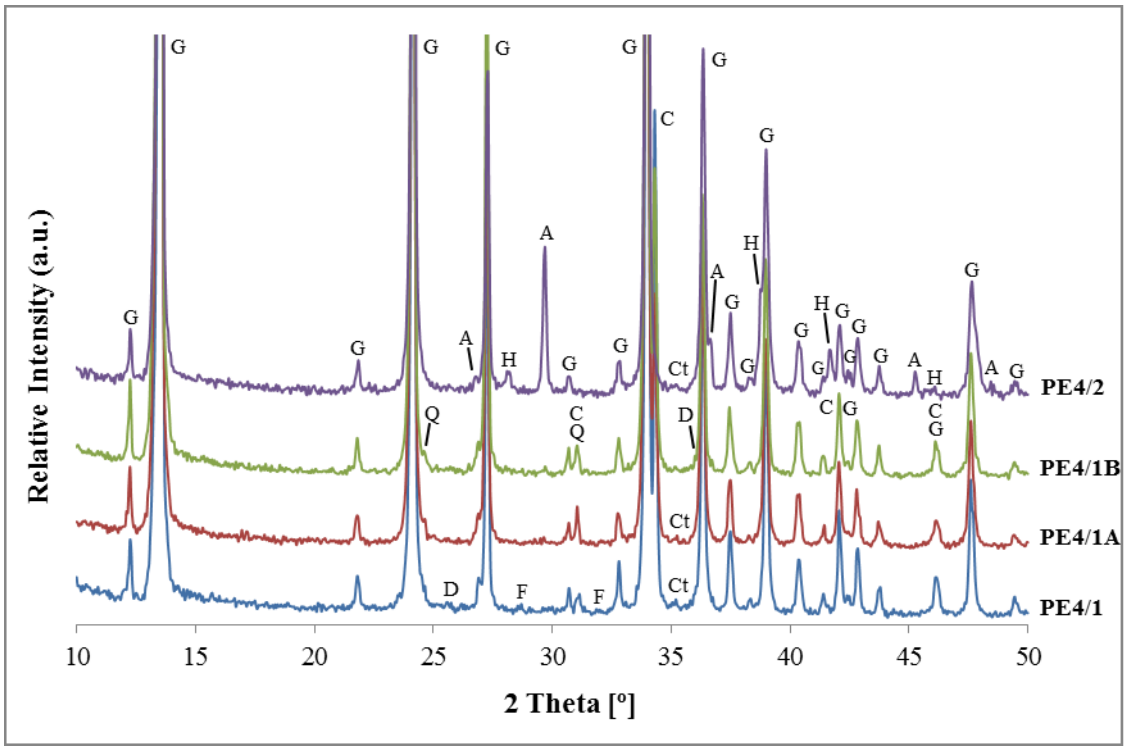

Figure 4.116 - XRD patterns of sample PE4.
Notation: G - Gypsum; C - Calcite; Q - Quartz; A - Anhydrite; H - Hematite; D - Dolomite; Ct - Celestine; F - Feldspar

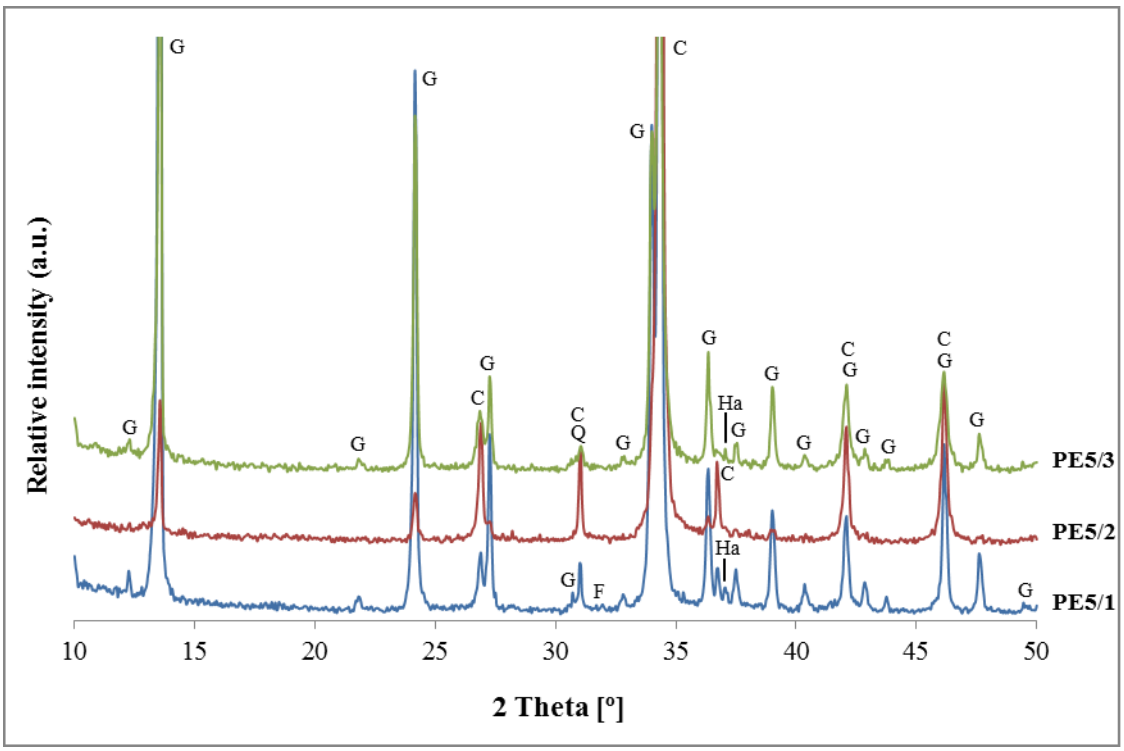

Figure 4.117 - XRD patterns of sample PE5.
Notation: G - Gypsum; C - Calcite; Q - Quartz; F - Feldspar; Ha - Halite

In what concerns anhydrite, traces of this compound were found in the samples with higher contents of gypsum and can be due to the calcination process, where a given amount of over burnt material was always present (Sanz 2009; Cardoso 2010), or/and to the raw material, as it is also a common impurity of the gypsum deposits. The exception is sample PE4/2, a subject that will be further discussed in the next sections.

Besides a higher amount of anhydrite than usual, the presence of hematite is also clearly detected in sample PE4/2.

As stated before, the use of a layer of asphalt between the mortar layers of sample PE5 was already a strong evidence of the existence of a phenomenon of water transport. The detection of halite confirms the presence of soluble salts owing to high moisture contents, probably transmitted to the walls by capillary absorption from the soil.

- TG-DTA results

The thermal behaviour of the samples associated with temperature variations was evaluated using TG-DTA analysis and allowed the quantification of the gypsum and calcite contents (Table 4.59, Figure 4.118, Figure 4.119 and Figure 4.120), confirming the results of XRD. Hematite and anhydrite,

both present in PE4/2, do not undergo transformations with weight losses associated in the temperature range used.

Table 4.59 - Weight loss and calculated gypsum/calcite contents of the samples from *Estoi* Palace

Sample	Temperature range (ºC)						Calculated contents (%)	
	25→85	85→250	250→600	600→850	850→1000	Loss of ignition	Gypsum	Calcite
PE1/1	0.1	13.3	1.6	14.4	0.4	29.8	63	33
PE1/2A	0.0	18.2	0.5	4.3	0.0	23.0	87	10
PE2/1	0.1	10.1	1.5	20.4	0.1	32.2	48	46
PE2/2A	0.0	17.5	0.4	6.3	0.1	24.3	83	14
PE4/1A	0.1	18.1	0.5	4.3	0.7	23.7	87	10
PE4/1B	0.0	18.1	0.6	4.7	0.7	24.1	87	11
PE4/1	0.3	18.2	0.8	4.2	0.2	23.7	87	10
PE4/2	0.1	17.9	0.6	0.8	0.3	19.7	85	2
PE5/1	0.5	8.9	2.0	23.0	0.5	34.9	42	52
				600→900	900→1000			
PE5/2	0.6	1.9	2.3	37.9	0.4	43.1	9	86
PE5/3	0.8	8.0	3.3	24.5	0.6	37.2	38	56
				600 - 725	725 - 850	850→1000		
PE1/2B	0.1	17.9	3.4	2.1	4.6	5.0	33.1	85	15
PE2/2B	0.1	17.0	3.7	2.1	5.9	4.8	33.6	81	18

PE4/1 = PE4/1A + PE4/1B

The doublet of peaks corresponding to the two steps of dehydration of gypsum is well defined in all the DTG and DTA curves of Figure 4.118 and Figure 4.119 but not in those of Figure 4.120. This difference is due to the higher amount of gypsum in samples PE1, PE2 and PE4 than in sample PE5.

In what concerns the decarbonation of calcite, it occurs at lower temperatures in samples PE1, PE2 and PE4 (between 760 - 825 ºC) than in PE5 (820 - 840 ºC) with higher contents of this compound. However, inside the set of samples represented in Figure 4.118, this behaviour is not linearly followed by PE2/2B, a layer of gypsum plaster "contaminated" by the key-coat used to regularize the surface.

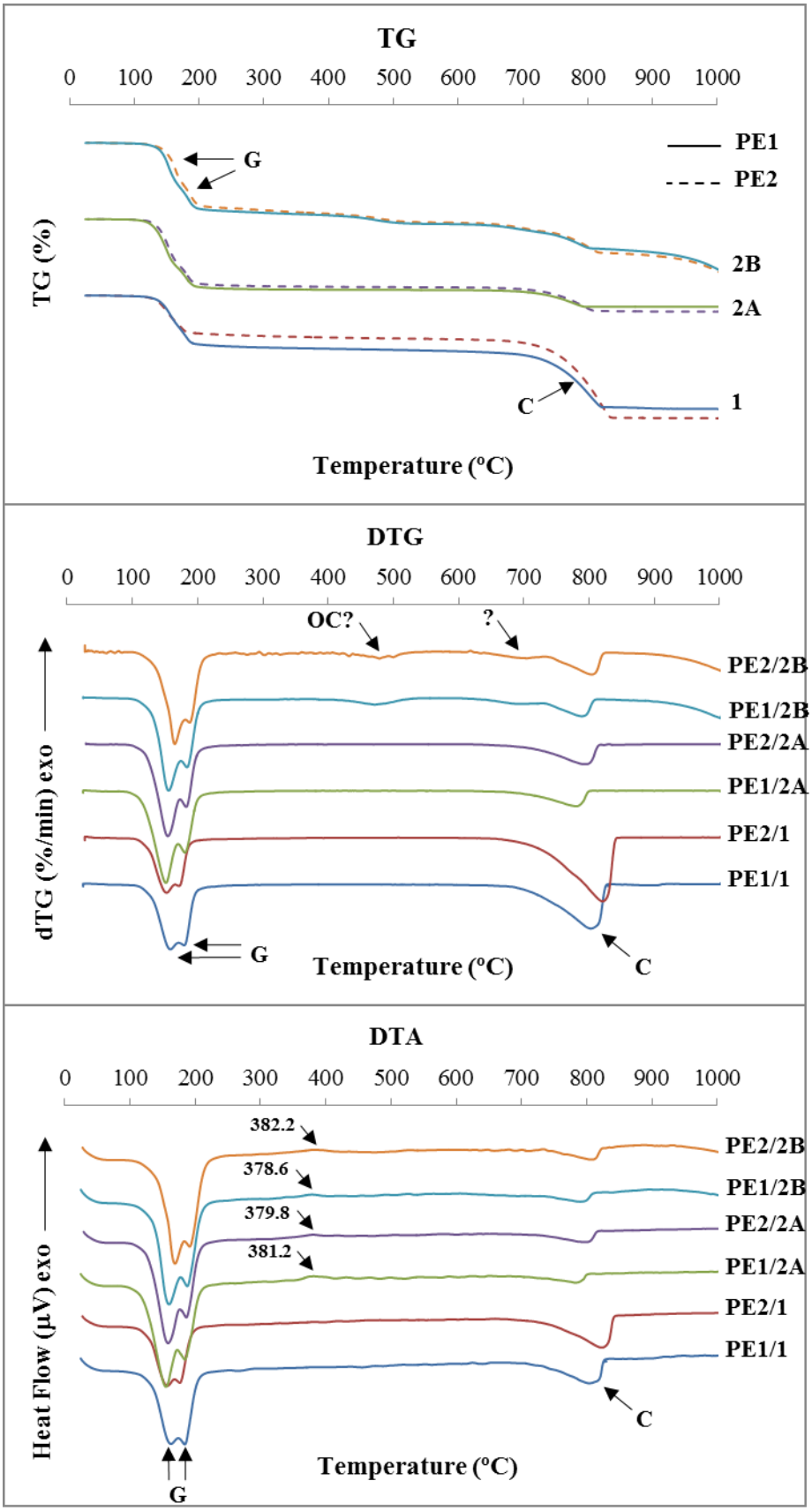

Figure 4.118 - TG, DTG and DTA curves of the samples PE1 and PE2.
Notation: G - Gypsum dehydration; C - Calcite decarbonation; OC - organic compounds

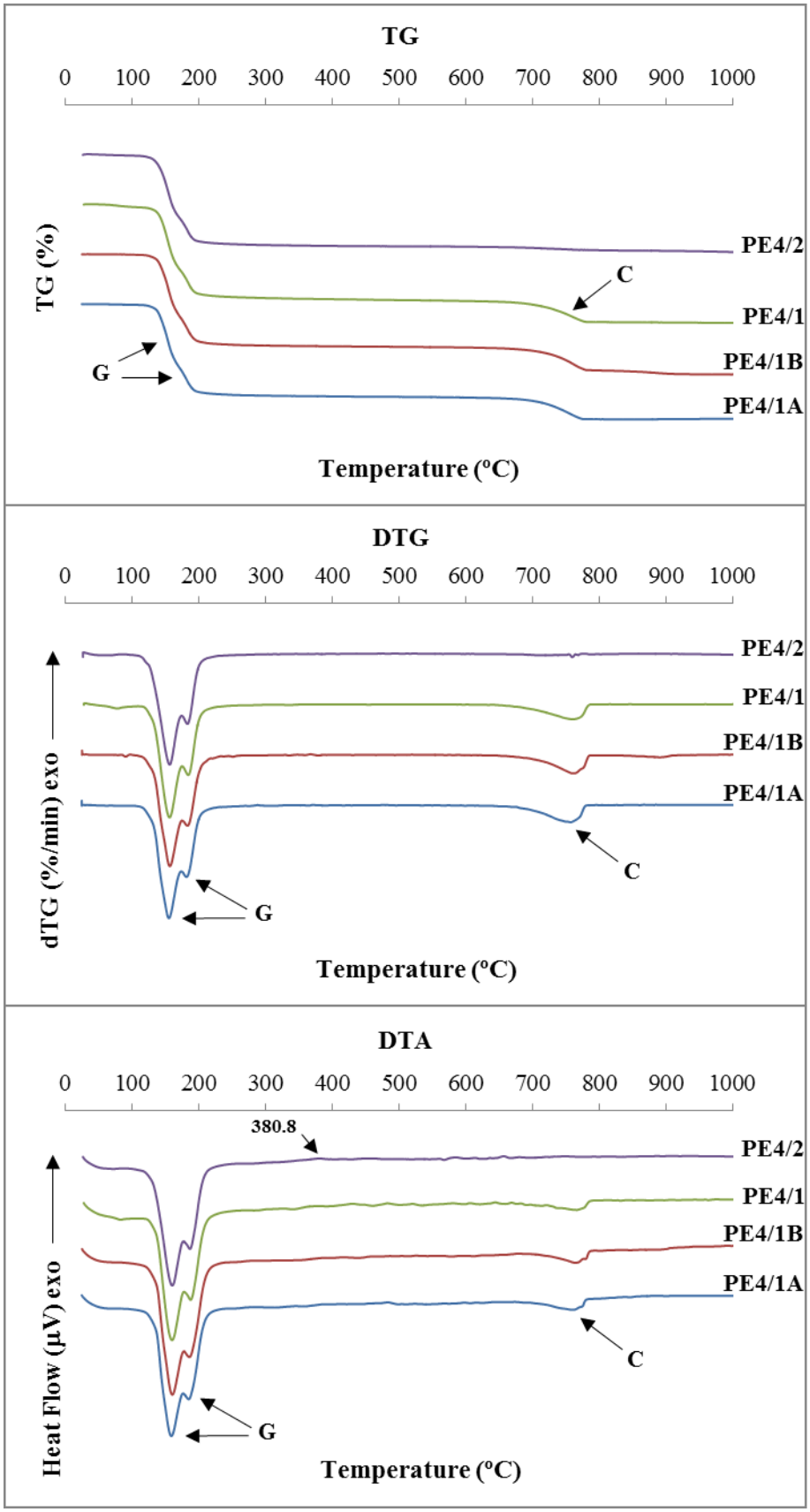

Figure 4.119 - TG, DTG and DTA curves of the sample PE4.
Notation: G - Gypsum dehydration; C - Calcite decarbonation

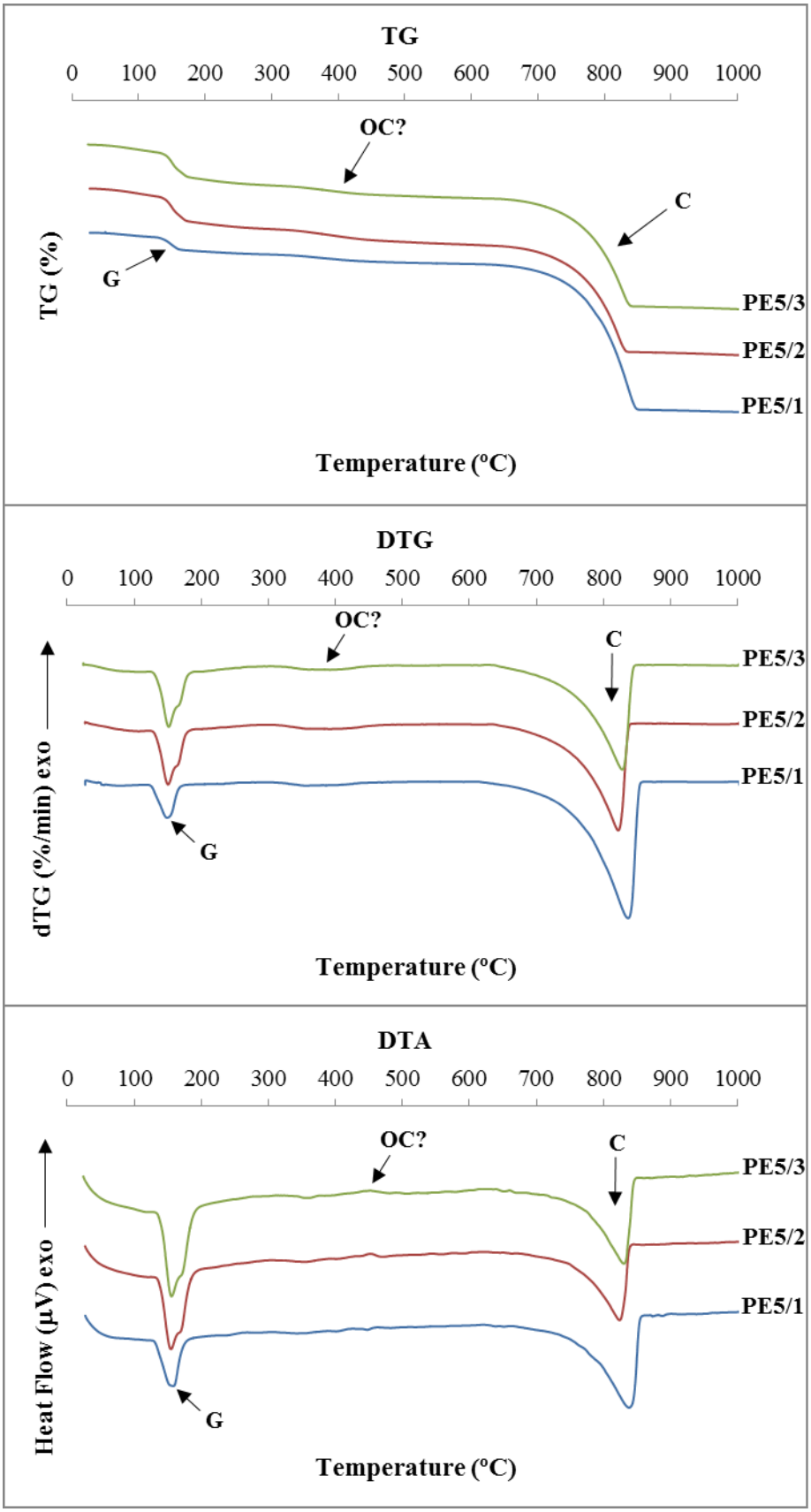

Figure 4.120 - TG, DTG and DTA curves of the sample PE5.
Notation: G - Gypsum dehydration; C - Calcite decarbonation; OC - organic compounds

In spite of being low, the calcite content of samples PE1/2 (A and B), PE2/2 (A and B) and PE4/1 (A and B) (Table 4.59) is probably not exclusively due to impurities present in the gypsum raw material as they all correspond to pre-moulded elements of a high quality of execution decorative program. In these cases the selection of a very pure raw material was a common procedure. So, the addition of small quantities of an aggregate of calcitic origin or of hydrated lime can be two possible explanations for that. Taking into account that the first two elements have been precast, the first hypothesis is more plausible than the second from the workability point of view; the opposite can be said about PE4/1 where the fact of having been moulded on a bench increases the possibility of the use of hydrated lime. These issues were further investigated using SEM but none of them has been confirmed, meaning that the raw material used in *Estoi* Palace was less pure than expected. The reason for that might be the intention of painting most of the decorative elements.

Another important observation is the very identical TG and DTG curve profiles from samples PE1/2B and PE2/2B (almost overlapping in the case of TG) with some uncommon features associated (Figure 4.118 and Table 4.59):

(a) A small loss of weight around 500 ºC;
(b) The unfolding of the decomposition temperatures of calcite in two levels;
(c) The continuous loss of weight after 800 ºC, until the end of the analysis (1000 ºC).

The observation described in a) is probably due to the presence and decomposition of organic compounds.

Regarding item b) some considerations were made in 4.3.1.2 ("TG-DTA results" section), namely the reason(s) that are usually in the origin of a double-step decarbonation of calcite (Alvarez et al. 2000; Anastasiou et al. 2006; Gourdin & Kingery 1975; Igea et al. 2012; Montoya et al. 2003; Moropoulou et al. 1995; Vecchio et al. 1993).

However, in this specific case, an additional fact can be contributing to the unfolding of temperatures: the presence of organic compounds. Considering that PE1/2A belongs to the same plaster piece as PE1/2B and correspondingly PE2/2A to PE2/2B, the difference in the respective calcite contents, lower in the "A" layers, cannot be due to the use of distinct mixtures to produce each of them. So, the most plausible explanation is the presence of some kind of compound, probably organic, whose temperature of decomposition partially overlaps with that of calcite, masking its quantification.

Finally, for item c) an explanation has not been found so far. The same kind of observations ((a), b) and c)) has been previously made in sample PB1/3 from *Bolsa* Palace (see 4.4.2.2, Figure 4.55) and the presence of organic compounds there was also almost sure, the only common feature between them. So, it is possible that the organic compounds are also in the origin of the weight loss in the range 800 ºC - 1000 ºC.

The phase change of soluble to insoluble anhydrite is clearly represented in the DTA curves of the samples PE1/2 (A and B) and PE2/2 (A and B) through the visualization of small exothermic peaks between 378.6 ºC and 382.2 ºC (Figure 4.118).

Similar TG curve profiles of samples PE4/1A and PE4/1B, corresponding to similar weight losses, indicate that they were made of the same gypsum plaster mixture, which is also in accordance with the perfect interface between them (Figure 4.112 (b)). The difference in colour is probably caused by the incorporation of sisal fibres in PE4/1A and the lower porosity of PE4/1B can possibly be due to the fact that PE4/2, applied over it, has been surely pressed hard during its execution.

Another important feature of these samples is the low and very similar weight losses ranging between 250 º and 600 ºC. These results are not surprising for the two internal layers as the sisal fibres of PE4/1A were retained in the sieve, but are somehow unexpected for the external one (PE4/2). In fact, the smoothness and brightness of its surface seem to indicate that some kind of organic addition was used, like wax or oil. However, in the preparation of the samples the criterion of collecting only their core was always respected, in order to avoid the contamination between consecutive layers. That is probably the reason why the hypothetical additions were not detected in PE4/2. Later, further analytical techniques were used to investigate the presence of organic compounds, namely FT-IR spectroscopy; this matter is clarified ahead.

Finally, all the layers of sample PE5 show a small weight loss between 350 ºC and 450 ºC (Figure 4.120) that is probably associated with the presence of pigments in their composition. In fact, the yellower the layer (Figure 4.112 (e)) the higher its weight loss is (Table 4.59).

- FT-IR and micro FT-IR spectroscopic analyses

In order to search for the presence of organic compounds, the samples PE1/2B, PE2/2B and PE5/3 were analysed using FT-IR spectroscopy.

The infrared spectra of the first two samples showed two peaks around 2925 cm^{-1} and 2850 cm^{-1} that correspond to the C−H elongation in methylene groups (CH_2) and two peaks around 1574 cm^{-1} and 1548 cm^{-1} that possibly correspond to C=C elongations (Figure 4.121). The referred observations confirm the existence of organic compounds but in such low quantities that it was difficult to be sure about their nature. It was only possible to conclude that *"the spectral bands attributed to C−H elongation in methylene groups indicate the presence of hydrocarbons whose chain is long enough so that the bands of CH3 groups do not appear. Thus, one can consider the possibility of the presence of materials such as polyethylene or other polymers of the same type; or oils. Excluded are natural resins, acrylic resins, protein glues, gums"* (Valadas & Candeias 2010).

In the case of PE5/3 nothing was detected.

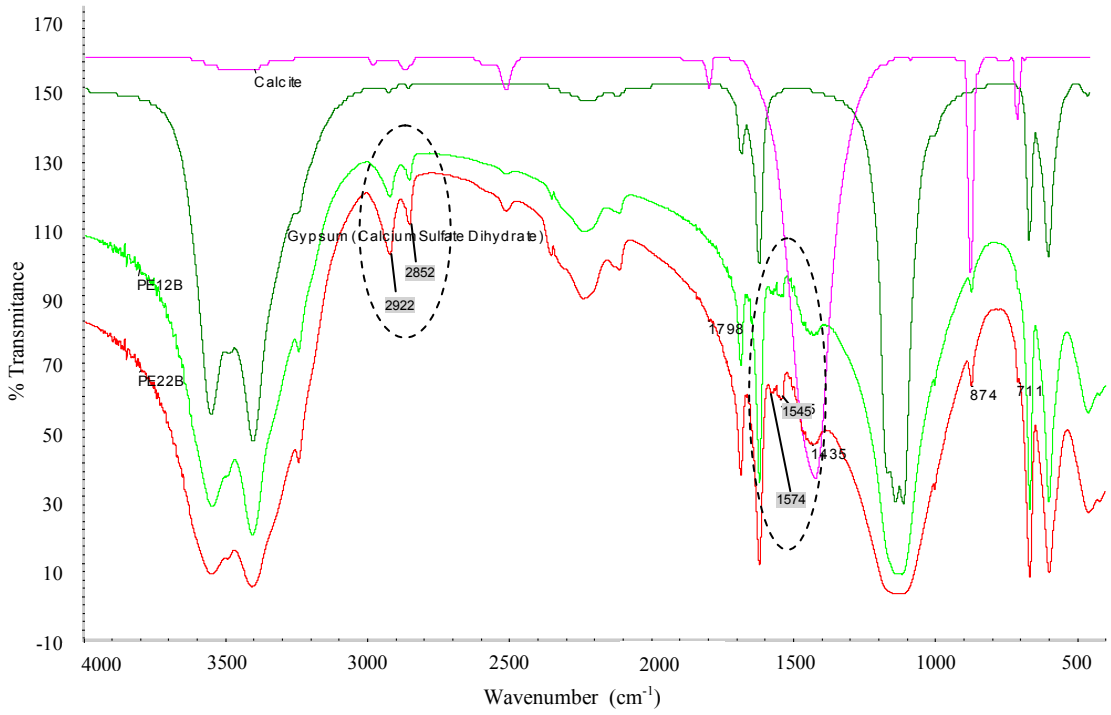

Figure 4.121 - FT-IR spectra of calcite and gypsum (standard substances) and of samples PE1/2B and PE2/2B (KBr pellets method)

The previous hypothesis that the key-coat used to regularize the absorption of the surfaces of PE1/2 and PE2/2 was shellac has not been confirmed. An oil-based product is the most probable one as polyethylene was only discovered in 1933, so it is completely out of question.

Nevertheless, this technique is considered to be indicative only; it was used because it was the only available at the time. To obtain results with improved accuracy, further studies would have to be performed using more sensitive techniques (e.g. Raman, micro FT-IR, etc.).

This is what was made in PE4/2: 1 g of sample was prepared taking care to include a part of the surface (i.e. not only the core, like in the specimen analysed in TG-DTA) and an extraction with ether during 24 h was performed. After that, the resulting solution was filtered and the filtrate was dried and analysed by micro FT-IR. The spectra obtained are shown in Figure 4.122.

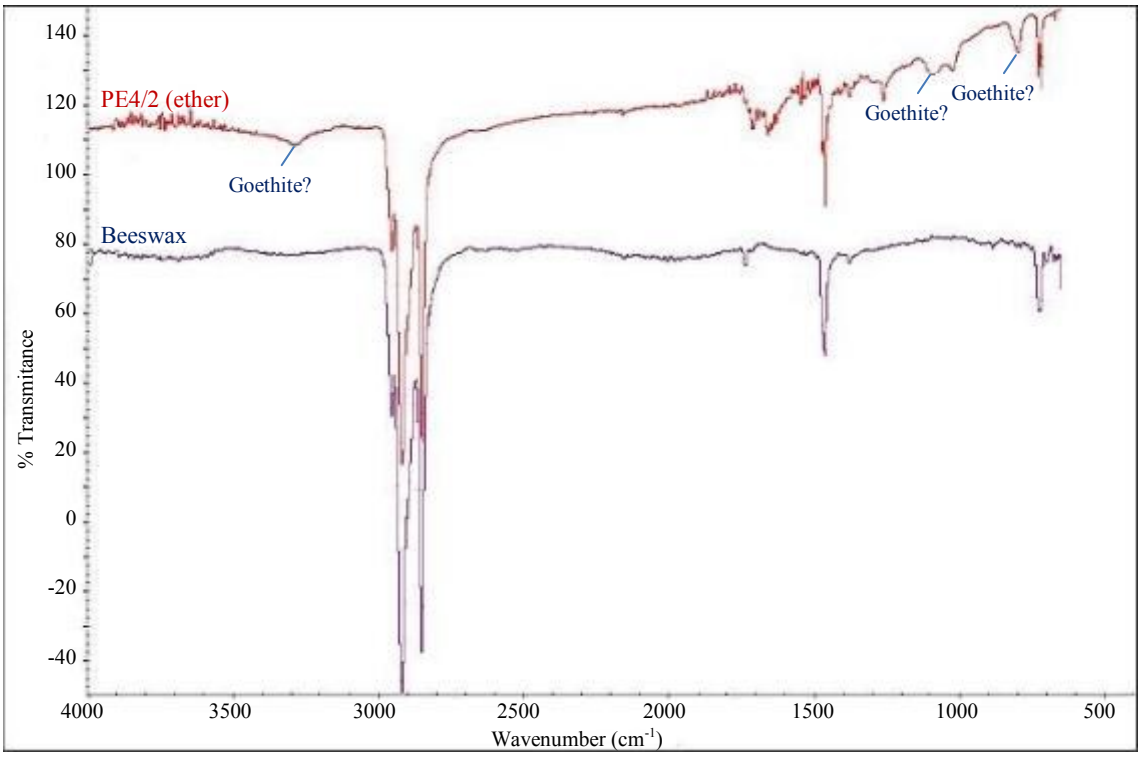

Figure 4.122 - Micro FT-IR spectra of pure beeswax (standard substance) and of sample PE4/2 after extraction with ether (procedure made by Giovanni Borsoi)

The presence of beeswax was detected, a compound that was surely used to polish the external surface and give it the brightness of a real stone.

The presence of goethite was also questioned but further analyses, namely using micro Raman, did not confirm this hypothesis.

- Micro Raman analysis

The micro Raman spectra of the different parts of the sample PE4 (Figure 4.123) were determined in order to investigate the presence of goethite, a suspicion raised by micro FT-IR analysis (Figure 4.122) and of other constituents than those obtained by XRD and TG-DTA.

The data used for the interpretation of the spectra of Figure 4.123 has been essentially based on two Raman spectroscopic libraries (Bell et al. 1997; Burgio & Clark 2001); the respective compilation is presented in Table 4.60.

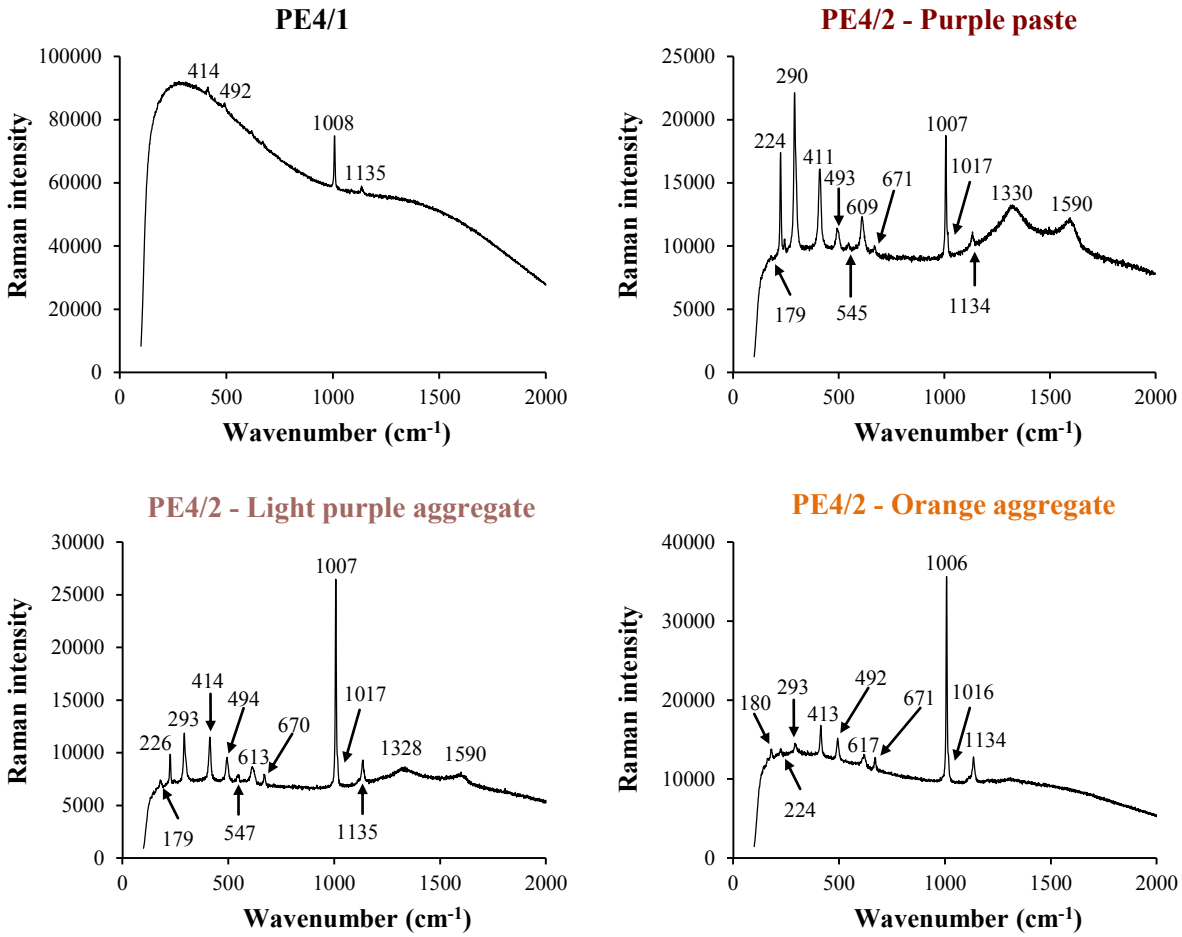

Figure 4.123 - Micro Raman spectra of the different constituents of sample PE4 (authored by Isabel Pombo Cardoso)

The PE4/1 spectrum, with bands at 414, 492, 1008 and 1135 cm^{-1}, confirmed that gypsum is its main constituent.

In PE4/2 the presence of anhydrite (bands at around 609, 671 and 1134 cm^{-1} and a shoulder at 1017 cm^{-1}) and hematite (224 and 290 cm^{-1}) can also be detected in all the different coloured pastes, with the purple paste having a significant concentration of this pigment, followed by the light purple and the orange aggregates by decreasing order. The purple paste and the light purple aggregate spectra showed also the presence of carbon black (broad bands at 1330 and 1590 cm^{-1}) and ultramarine blue (545-547 cm^{-1}).

The bands at 492-494 cm^{-1} in the three spectra of PE4/2 result from the presence of gypsum (493 cm^{-1}, weak intensity), anhydrite (498 cm^{-1}, medium intensity) and hematite (495 cm^{-1}, medium intensity).

Besides hematite, the use of micro Raman allowed detecting the presence of two additional pigments in the purple matrix of PE4/2 and in the light purple aggregates: carbon black and ultramarine blue.

The main function of the first was to darken the pastes; the second, when used in very small quantities, usually had the purpose of giving a purple hue.

Finally, the presence of goethite was not confirmed.

Table 4.60 - Raman spectroscopy data used for the interpretation of the spectra of sample PE4

Compound	Bands wavenumbers (cm^{-1})	Relative intensity
Gypsum	179-181, 493	weak
	414-415, 1132-1136	medium
	619, 670	weak to very weak
	1007-1009	very strong
Anhydrite	416, 498, 608, 626, 675, 1130	medium
	1018	strong
	1161	weak
Hematite	224, 291	strong to very strong
	407-408, 608-610	medium
	494-495	weak
Carbon black	1325, 1579-1580	very strong and broad
Ultramarine blue [(1)]	258, 822	weak
	548	very strong
	1096	medium

Note: The bands wavenumbers are presented in intervals according to the values given by the experimental conditions of the bibliographic references used; [(1)] synthetic pigment that substituted lapis lazuli since 1828

- SEM-EDS and PLM observations

In order to have a further insight into the microstructure and elemental chemical analysis of some samples, polished surfaces, fractured surfaces and thin section preparations have been observed using scanning electron microscopy (SEM) coupled with energy dispersive X-ray spectroscopy (EDS). The thin sections were also observed using polarized light microscopy (PLM). The images and information obtained are shown and discussed in this section.

Sample PE2/2

The cross-sectional polished surface of sample PE2/2 corresponding to Figure 4.111 (e) has been observed using SEM-BSE and the respective images are shown in Figure 4.124.

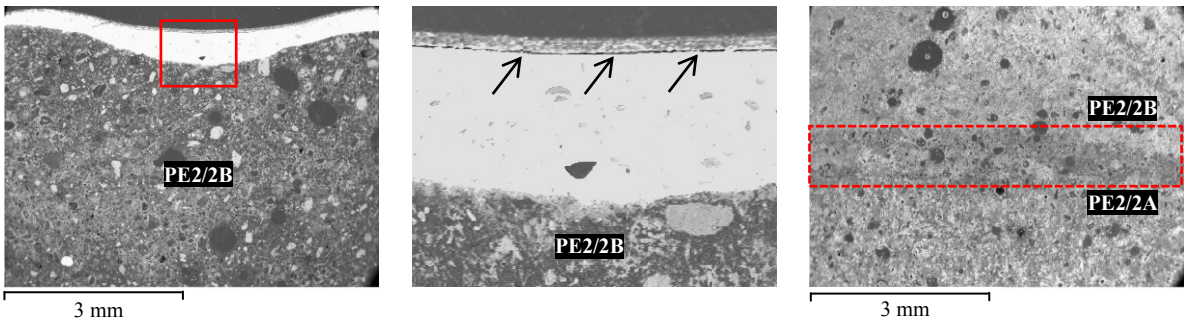

(a) (b) (c)

Figure 4.124 - SEM-BSE images of PE2/2 polished surface: (a) PE2/2B and two layers of paint; (b) detail of (a) (red frame) showing a crack between the layers of paint; (c) interface between PE2/2A and B

The area corresponding to Figure 4.124 (b) has been also observed in fractured surface (SEM-SE mode) and the composition of the different layers was determined by EDS (Figure 4.125, Table 4.61) The big crack that can be seen in Figure 4.125 (a) starts in the already mentioned fracture between the two layers of paint and goes through the second layer. It was probably made during the process of preparation of the sample.

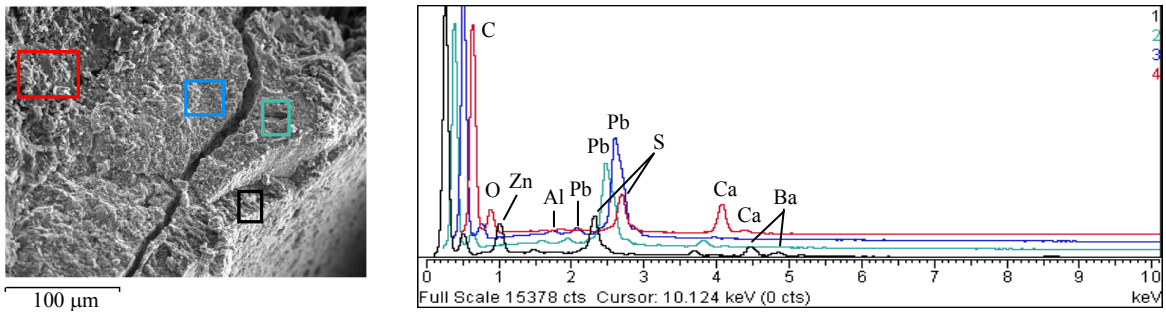

(a) (b)

Figure 4.125 - Sample PE2/2: (a) SEM-SE image showing PE2/2B and the two layers of paint; (b) EDS spectra corresponding to the areas marked by the coloured frames: 1 - exterior layer of paint; 2 and 3 - interior (original) layer of paint; 4 - PE2/2B

Table 4.61 - SEM-EDS results of the sample PE2/2B and respective layers of paint

Sample	EDS	Elemental composition
Exterior layer of paint	1	C, O, Zn, Al, S, Ca, Ba
Interior layer of paint	2	C, O, Al, Pb, Ca
	3	C, O, Al, Pb
PE2/2B	4	C, O, Al, S, Ca

Note: The sample surface was coated with carbon

The elements found in the last layer of paint (exterior layer) seem to indicate the presence of lithopone (a combination of barium sulfate and zinc sulfide) or of barium sulfate (almost transparent in oil paints, used to modify their consistency) and zinc oxide (white zinc pigment). The first hypothesis is the most plausible because lithopone is much more stable when mixed with oil and resins than zinc oxide. It is also a substance widely used to impart opacity to the paints, not very adequate to the white coloured ones but quite suitable for pastel shades together with other pigments (Quaglierini & Amorosi 1991); the last layer of paint of the sample PE2/2B is of a light green colour and seems to be an oil paint.

Concerning the original paint (interior, thicker layer) its very white colour (Figure 4.124 (a) and (b)) and the respective EDS spectra (Table 4.61) seem to indicate the use of lead white ($2PbCO_3.Pb(OH)_2$) (Cruz 2000). More difficult to explain is the detection of aluminium. The hypothesis of being present in the key-coat seems plausible, as it was also found in the gypsum plaster layer PE2/2B.

In Figure 4.126 and Figure 4.127 some of the SEM-EDS observations of the paste of PE2/2 in fractured surface are shown and they allowed drawing the following conclusions:

a) It has very round pores (Figure 4.126 (a)), a strong indication that it was precast with a relatively fluid consistency (Rúbio Domene 2011);
b) It has prismatic, needle-like crystals and a high degree of porosity ((Figure 4.126 (b)), a morphology typical of a gypsum plaster resulting from the hydration of calcium sulfate hemihydrate (Wirsching 2005);
c) Biological colonization was detected in some pores (Figure 4.126 (c));
d) It has no addition of aggregates of calcitic origin as the limestone grains found do not have the typical shape of milled material being probably an impurity of the raw gypsum (Figure 4.127 (a));
e) Very few grains of dolomite were detected being also an impurity of the raw material (Figure 4.127 (b));
f) Quartz grains were observed more frequently than dolomite and usually exhibited a rolled morphology (Figure 4.127 (c));
g) All the referred aggregates are much bigger than the gypsum crystals that make the matrix, particularly the quartz grains.

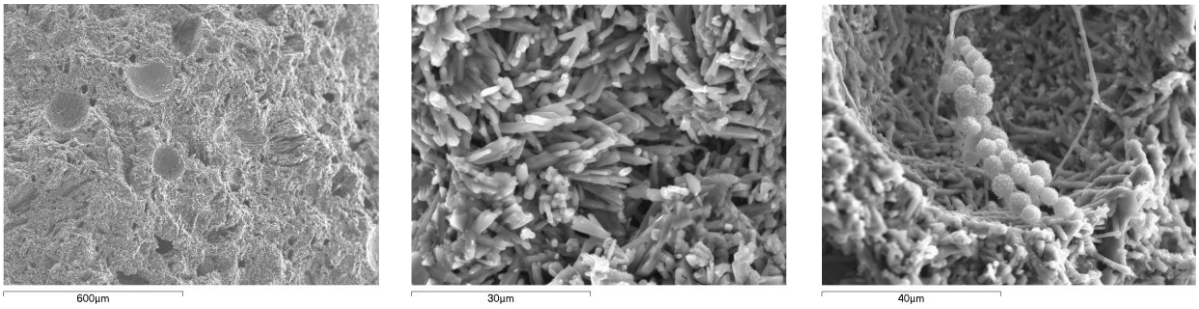

(a) (b) (c)

Figure 4.126 - SEM-SE images of PE2/2 micro structure: (a) general view of the paste; (b) morphology of the paste; (c) detail of a pore with biological colonization

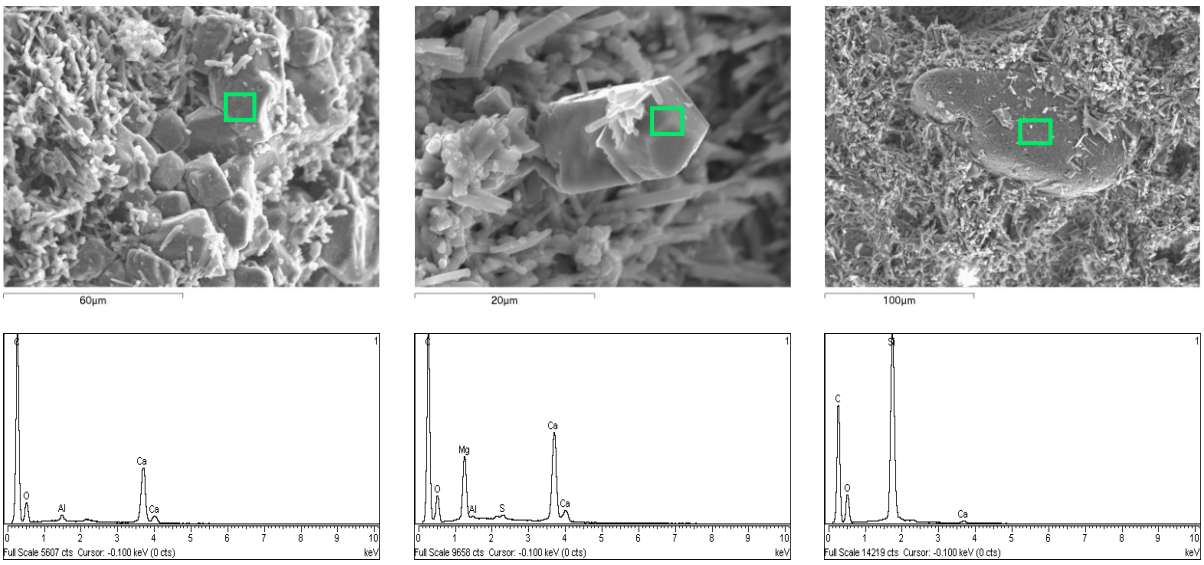

(a) (b) (c)

Figure 4.127 - SEM-SE images of other compounds present in the PE2/2 paste and respective identification by EDS (analysed areas marked with green frames): (a) calcite; (b) dolomite; (c) quartz

Other morphologies of the paste were also observed (Figure 4.128) but the respective EDS analyses revealed that they were all gypsum. The exception is the crystal of Figure 4.128 (h) that, in spite of having a spectrum similar to the others, has a morphology typical of anhydrite. In fact, it is very difficult to distinguish both compounds based only on EDS spectra: the relative proportions of the elements active to X-rays (C, S and O) have a small variation between gypsum ($CaSO_4.2H_2O$) and anhydrite ($CaSO_4$) and are hardly noticed using only this technique.

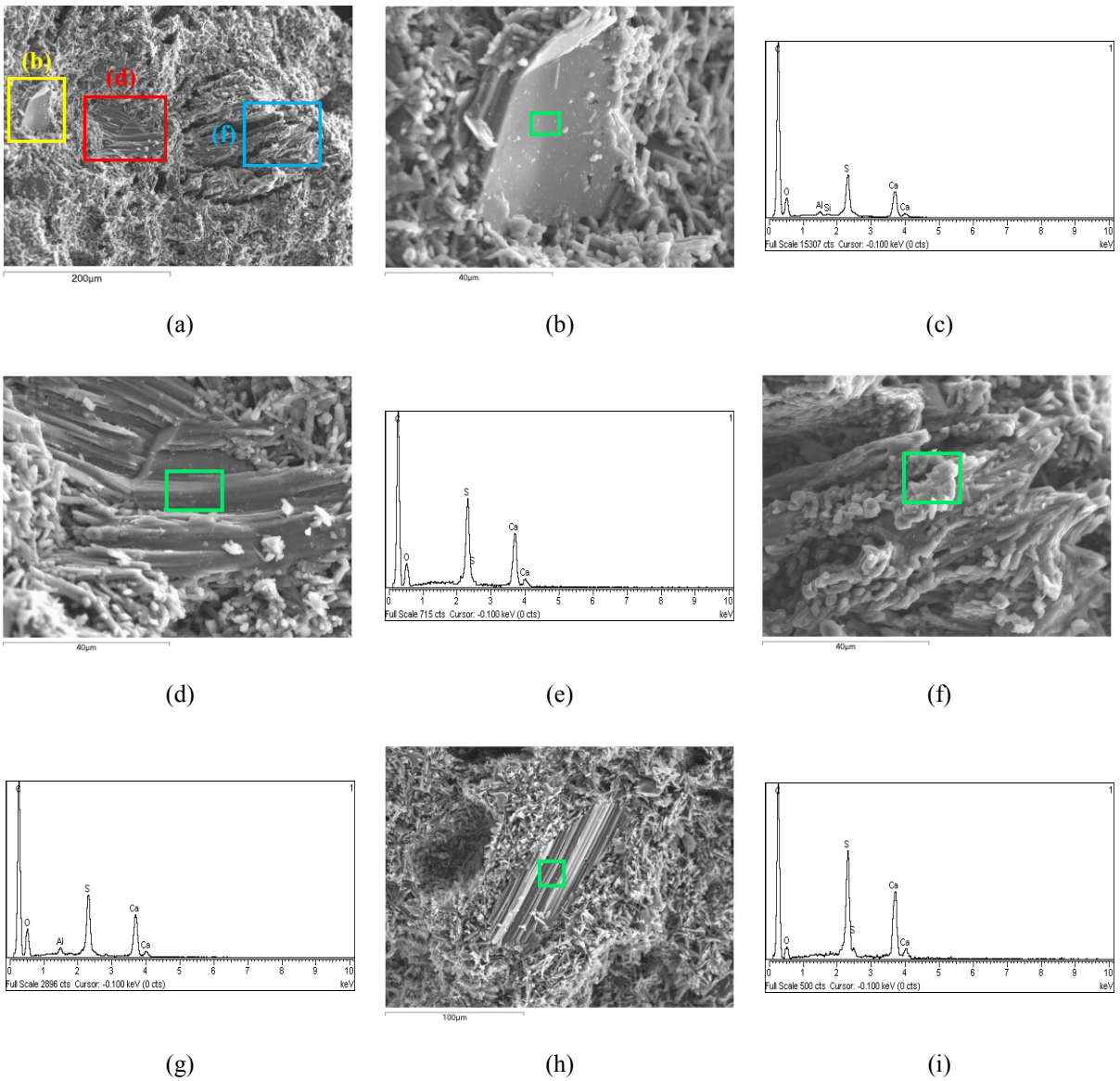

(a) (b) (c)

(d) (e) (f)

(g) (h) (i)

Figure 4.128 - SEM-SE images and respective EDS spectra of the PE2/2 paste showing different morphologies of gypsum - (a) to (g) - and anhydrite - (h) and (i)

These different morphologies usually exhibit larger crystals and occur in areas of the matrix where they have more room to grow.

Sample PE4

As stated before, this sample is a very special case study. It is made of two distinct parts very well connected (Figure 4.129): the internal structure, PE4/1 (made in two steps, designated by PE4/1A and PE4/1B) and the exterior decorative layer, PE4/2, simulating the noble imperial red porphyry stone.

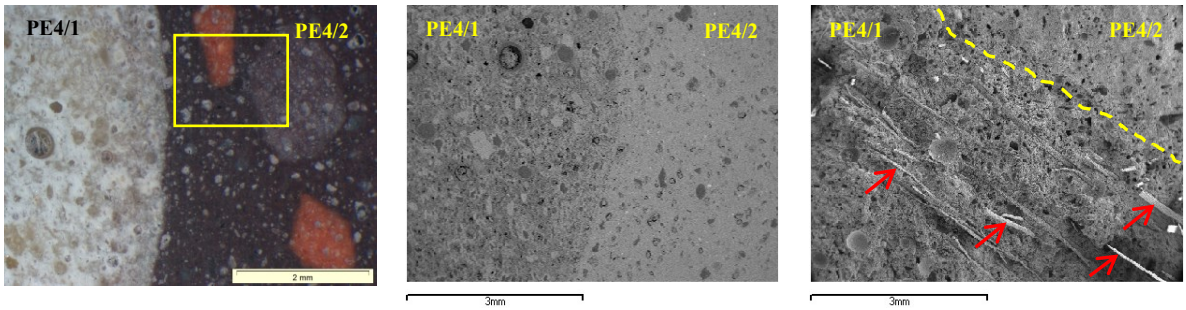

(a) (b) (c)

Figure 4.129 - Images of the transition zone between PE4/1 and PE4/2: (a) stereo-zoom microscope (polished surface); (b) SEM-BSE (polished surface); (c) SEM-SE (fractured surface), where the presence of sisal fibres in PE4/1 is perceptible (red arrows)

Besides the colour, there is a significant difference of density/porosity, clearly shown in Figure 4.130.

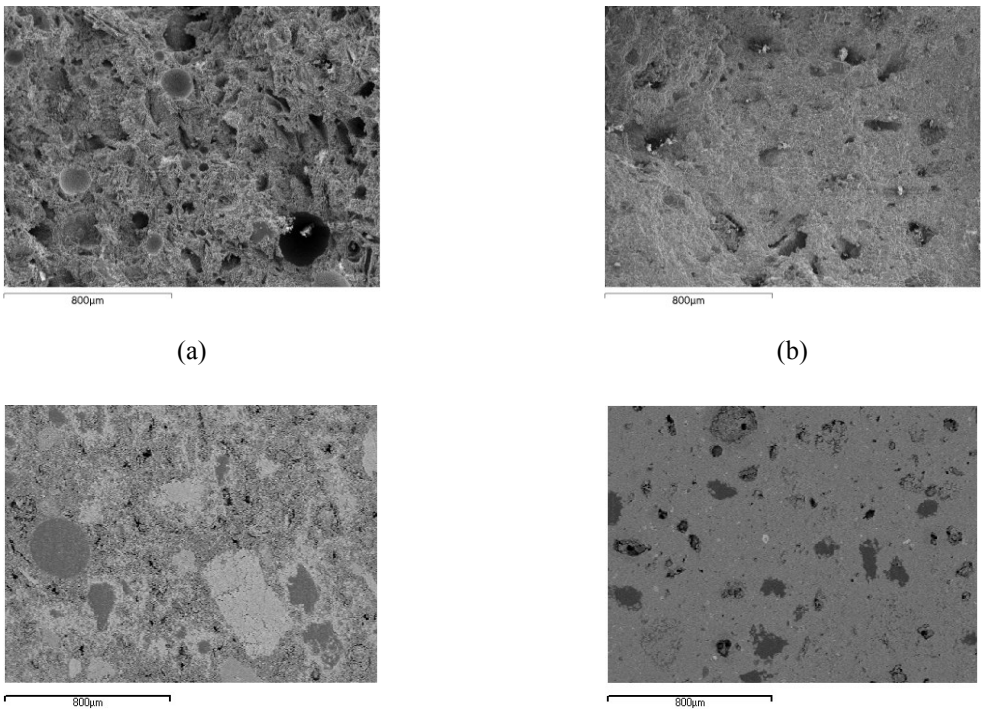

(a) (b)

(c) (d)

Figure 4.130 - Images illustrating the difference of density/porosity between PE4/1 (left) and PE4/2 (right): (a) and (b) fractured surfaces, SEM-SE mode; (c) and (d) polished surfaces, SEM-BSE mode

At higher magnifications it appears that the morphology of both parts is also very distinct: PE4/1 has mainly prismatic, needle-like crystals (Figure 4.131 (a) and (c)) and PE4/2 has squat, stocky crystals (Figure 4.131 (b) and (d)).

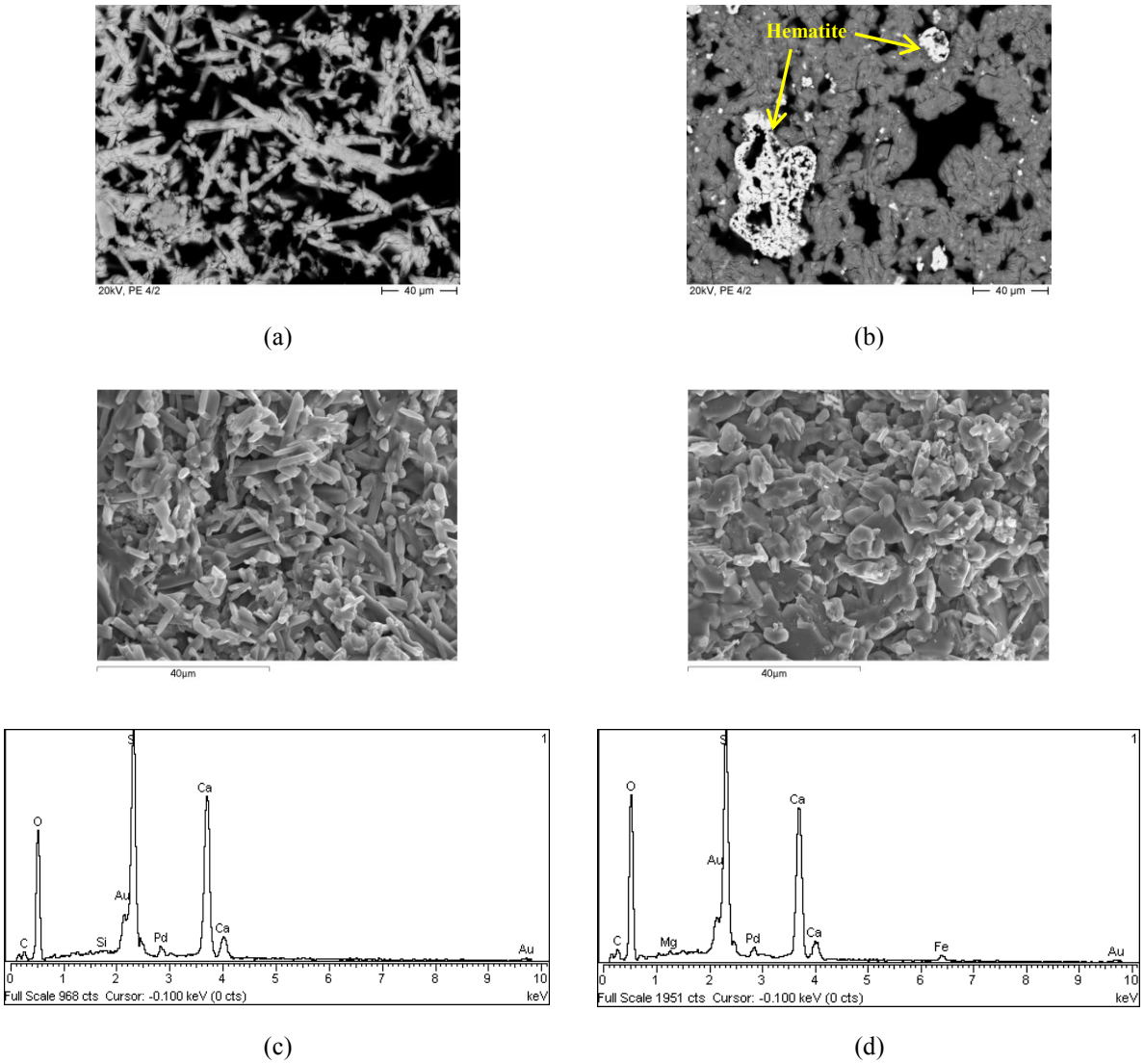

Figure 4.131 - SEM images at higher magnifications showing the different crystal morphology of the binder: thin sections of PE4/1 (a) and PE4/2 (b), SEM-BSE mode (authored by Frank Schlütter); fractured surfaces and respective EDS spectra of PE4/1 (c) and PE4/2 (d), SEM-SE mode

So, they seem to correspond to completely different compounds or, if to the same compound, at least formulated with different additives. However, as stated before, XRD, TG-DTA analyses and now the EDS spectra show that they are mainly made of gypsum ($CaSO_4.2H_2O$). Besides, in the TG-DTA results the temperature range where organic compounds usually decompose (250 - 600ºC) presented a negligible loss of weight. It is though very unlikely that any of the layers had organic additives incorporated in the paste.

The only differences in composition seem to be the presence of hematite and a higher content of anhydrite in PE4/2 (Figure 4.131 (d)). Could one, or both, of these factors be responsible for such a

huge alteration on the crystals growth and interlock and on the density/porosity? And besides that, are there any other differences between these two layers?

A plausible explanation for the distinct crystal morphologies between PE4/1 and PE4/2 is that they were prepared from different gypsum phases: mainly hemihydrate in the former and anhydrite in the latter.

But how were these two phases obtained separately? Two possibilities can be pointed out:

a) The calcined gypsum used for both was the same, and the plasterers separated the phases according to the final product they wanted to obtain.
   In fact, in traditional kilns it is impossible to have complete control of the calcination process. Issues like the temperature, type of raw material, time of the process and size and position of the stones have an important influence and the resulting products are always multiphase gypsum plasters (in the larger stones, for example, the borders are usually anhydrite but the nucleus is often raw gypsum). All these facts were widely known by the plasterers so that, whenever needed, the different phases (dihydrate, hemihydrate and anhydrite) could be separated from the beginning (Villanueva 2004; Cardoso 2006; Sanz 2007);
b) They were really products prepared differently: the PE4/1 plaster was calcined at lower temperatures than the plaster used in PE4/2.

Nevertheless, none of these procedures guarantees a 100% efficient separation of phases, as there are always remains of the so-called "firing products".

In seeking answers to these questions, further SEM observations of thin sections and polished and fractured surfaces of PE4/1 and PE4/2 allowed characterizing both layers in a more complete way. The results obtained and the respective discussion will now be presented.

PE4/1

Further images of the typical micro structure of PE4/1, more precisely in the area of PE4/1B, are shown in Figure 4.132.

Besides confirming that it is a very porous micro structure, the thin sections observations gave a more complete overview of the composition of the matrix. The images of Figure 4.132 show that PE4/1 has a relatively high amount of fine mineral grains (grain size < 0.5 mm), namely limestone, quartz, feldspars and marl.

The last three minerals are considered to be impurities of the raw material. In what concerns limestone, the same explanation did not seem enough to justify its more frequent occurrence. The results obtained by TG-DTA analysis indicated the presence of 10% of calcite, which could also have the contribution of

the addition of calcitic aggregates or hydrated lime. However, none of these two hypotheses was confirmed: the limestone grains observed in fractured surface seem a natural formation and did not show the shape/appearance of having been processed (milled); the calcite crystals resulting from the carbonation of lime would be much smaller than those observed in PE4/1 (Figure 4.133).

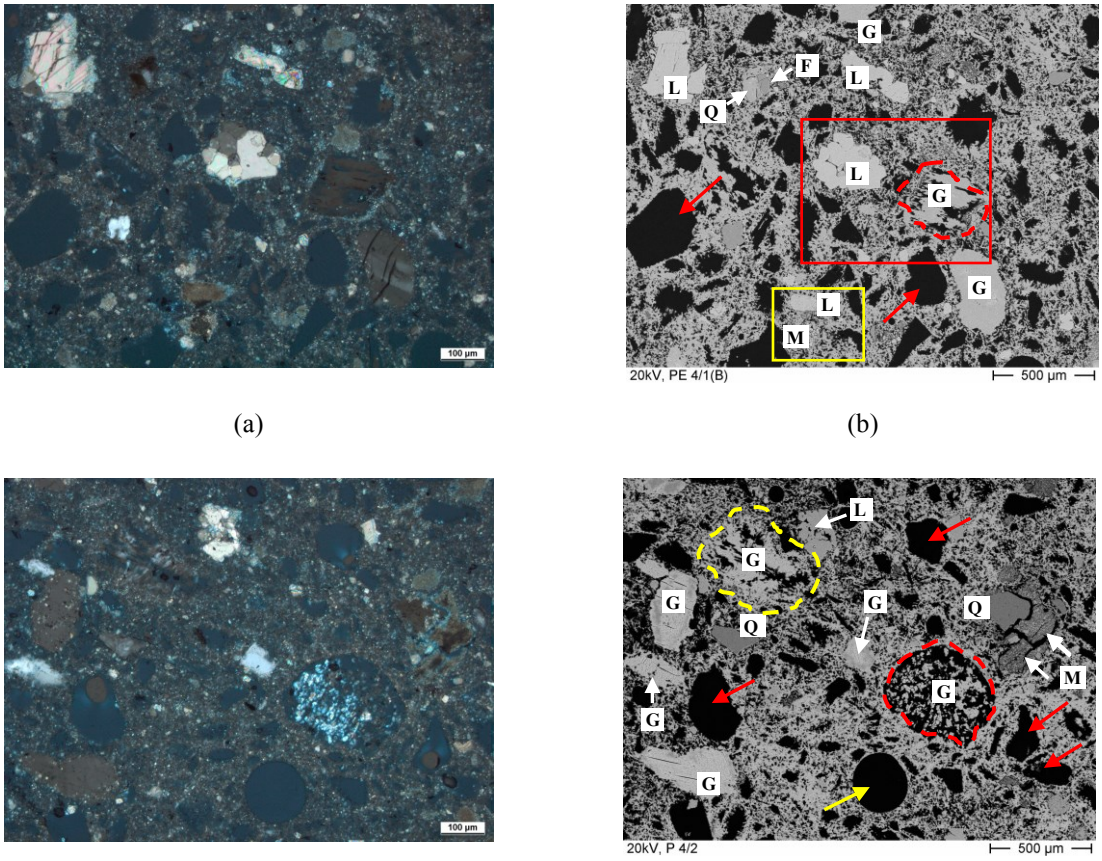

Figure 4.132 - Images of thin sections showing the micro structure of PE4/1B (authored by Frank Schlütter): (a) and (c) PLM, crossed polarized light; (b) and (d) SEM-BSE mode. Notation: G - Gypsum grains, some partly dissolved; L - Limestone grains; Q - Quartz; F - Na, K feldspar; M - Marl

Calcite grains with a different appearance, like the one illustrated in Figure 4.134 (d), can be the clue that justifies the total calcite content of PE4/1, as they seem to be also of natural limestone but with another type of crystallization.

It is important to notice that none of the limestone grains observed showed any thermal changes (the temperature of calcination was not high enough to originate the decarbonation process) (Figure 4.133).

The matrix also contains gypsum grains that are remains of the calcination process and should not be considered as aggregates. This is an indication of relatively low firing temperatures as it results from an incomplete dehydration of gypsum raw material.

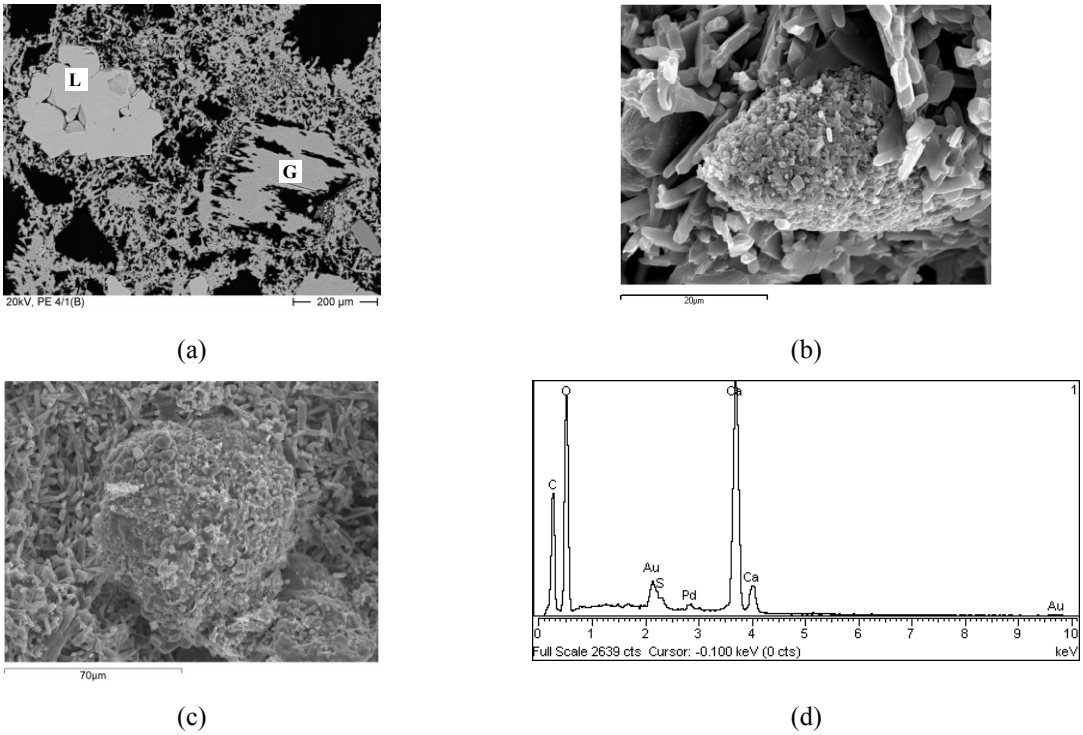

(a) (b)

(c) (d)

Figure 4.133 - (a) Detail from Figure 4.132 (b) (red frame) showing a limestone grain and a partly dissolved gypsum grain (authored by Frank Schlütter); (b) and (c) fractured surface images of limestone grains in the PE4/1 paste, SEM-SE mode; (d) EDS spectrum of the grain in (c)

Many of these gypsum grains show dissolving structures, which is a phenomenon difficult to explain satisfactorily. All stages of dissolution can be observed (Figure 4.132 (b) and (d)). In the final stage (total dissolution) the result is the formation of irregular shaped and sized voids like the ones shown in Figure 4.132 (b) and (d) (red arrows). However, round pores are also present (Figure 4.132 (d), yellow arrow), indicating that the gypsum paste of PE4/1 has been used in a relatively fluid consistency and did not suffer significant external pressures during modelling as the internal structure of sample PE4.

Going back to the dissolving grains, at higher magnifications using the SEM-BSE mode it is possible to see that in some of them the remaining particles are a mix of dihydrate and anhydrite (Figure 4.134).

In fact, the gypsum-anhydrite differentiation by SEM using backscattered electron (BSE) signal is very effective as the resulting images represent what is called “atomic number contrast” which, in turn, depend on the density and atomic number of the elements present in the test specimen (Jordan et

al. 1991). The two phases can be clearly distinguished by grey level differences: anhydrite is denser so it appears brighter than gypsum.

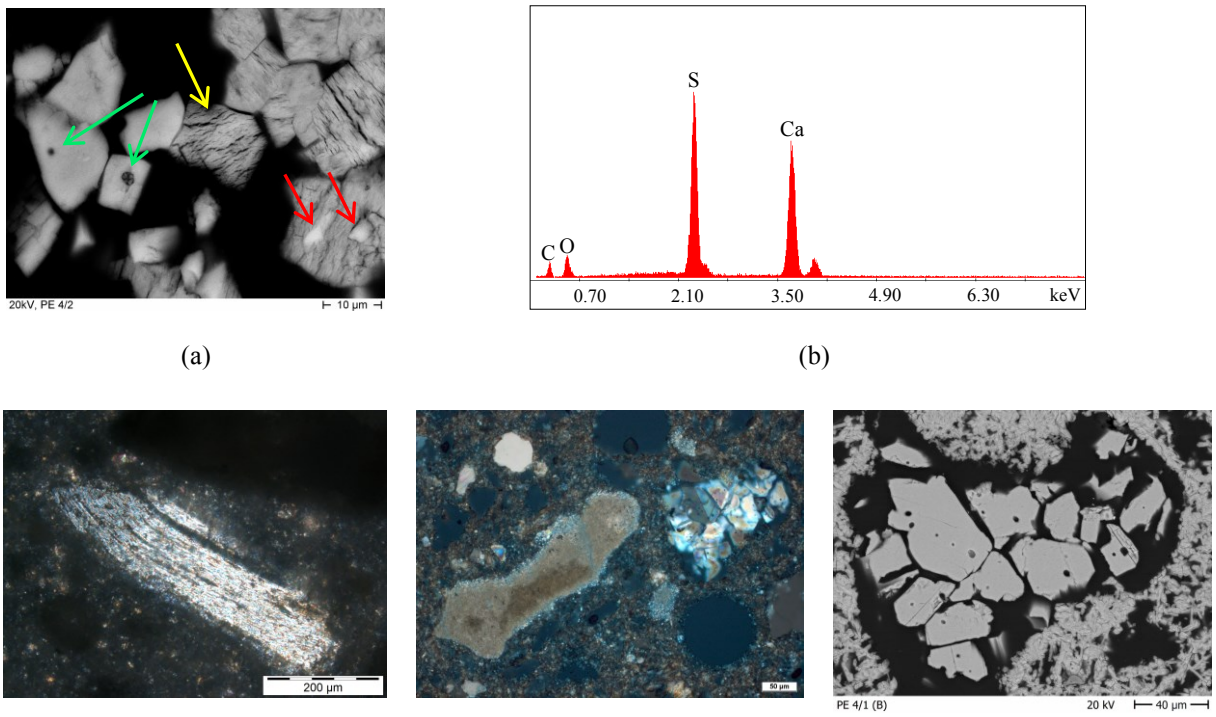

Figure 4.134 - (a) Detail from Figure 4.132 (d), taken in the largely dissolved anhydrite grain (marked by red circle): dihydrate showing lamellar structure (yellow arrow); primary anhydrite showing the typical holes (green arrows); granular anhydrite (red arrows); (b) EDS spectrum of the primary anhydrite; (c) thin section showing a grain of fibrous pseudo-morph dihydrate, PLM, crossed polarized light; (d) thin section showing another type of limestone particle (left) and a primary anhydrite grain (upper right), PLM, crossed polarized light; (e) detail of the same primary anhydrite grain of (d) showing holes, SEM-BSE mode (all images authored by Frank Schlütter except (c) that was authored by José Mirão)

The majority of the anhydrite crystals resulting from the calcination process are fibrous or strip-shaped (called thermo-anhydrite) and crystalize as dihydrate. Their original shape is usually kept pseudo-morph, i.e. the dihydrate grains grow in the same direction as the beam of fibres of the anhydrite grains (Figure 4.134 (c)), with a quite similar orientation, though with a more squat morphology (Figure 4.134 (a) and (c)).

Granular anhydrite is characterized by round edges and melting marks (Figure 4.134 (a)). It results from the calcination of raw material at higher temperatures (usually above 350 ºC) and it is very difficult to hydrate, being called “insoluble anhydrite”. Its proportion rises with the increase of firing temperatures.

The primary anhydrite is natural anhydrite that exists in the raw material. When its grains present holes they are said to have been “thermally damaged” (Figure 4.134 (a) and (e)).

These two last types of anhydrite remain unchanged after the hydration of the paste, even when treated with additional water (Schlütter et al. 2010).

Fractured surfaces observations using SEM allowed obtaining further images of some of the features present in the PE4/1 micro structure, namely a different perspective of the quartz grains and of a round pore (Figure 4.135 (a)) as well as the sisal fibres embedded in the gypsum matrix (Figure 4.135 (b) and (c)).

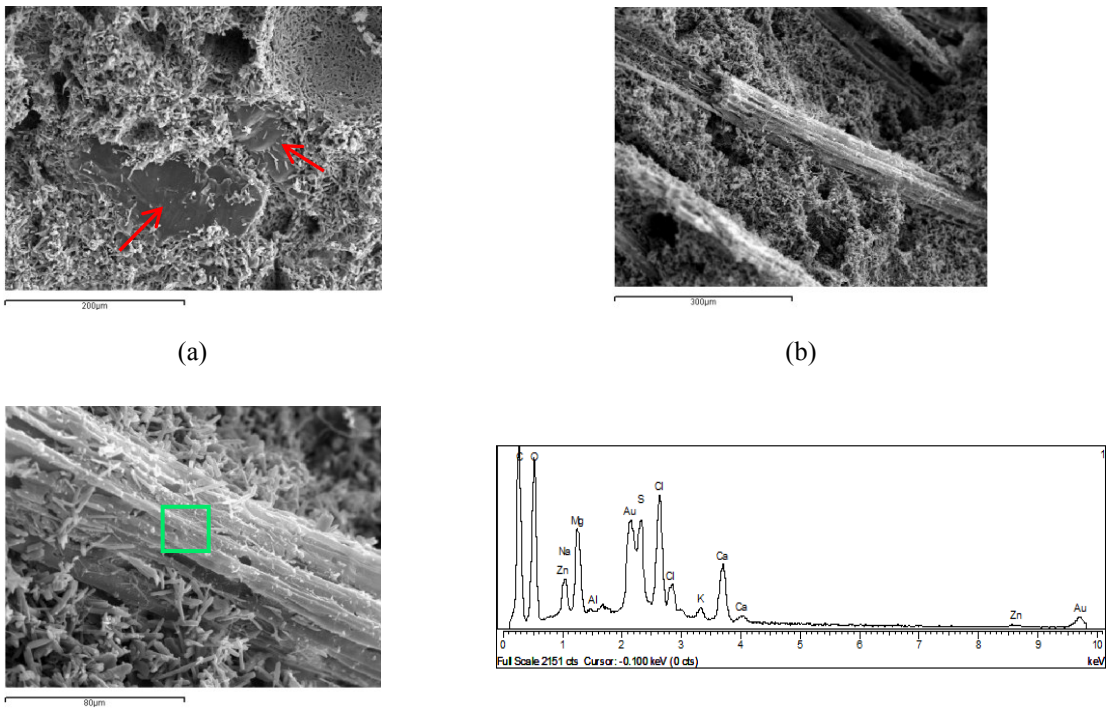

(a) (b)

(c) (d)

Figure 4.135 - SEM-SE images of some features observed in the PE4/1 paste: (a) quartz grains (red arrows) and a round pore (upper right); (b) sisal fibres embedded in the gypsum matrix; (c) the same as (b) but at a higher magnification to be analysed by EDS; (d) EDS spectrum of the area marked with a green frame in (c)

Another important observation in the micro structure of PE4/1 is the formation of secondary phases that result from the "thermal activation" of some of the impurities present in the gypsum stone, namely marls often consisting of mixtures of calcite, dolomite and clay minerals (Figure 4.136).

When subjected to high enough temperatures the partial decomposition of the dolomite grains result in calcium and magnesium richer phases (Eq. 4.5 and Eq. 4.6) that, in contact with sulphur trioxide (from the partial dissociation of gypsum) (Eq. 4.7 and Eq. 4.8) are able to produce the respective calcium and magnesium sulphates ($CaSO_4$ and $MgSO_4$, Eq. 4.9) (Figure 4.137).

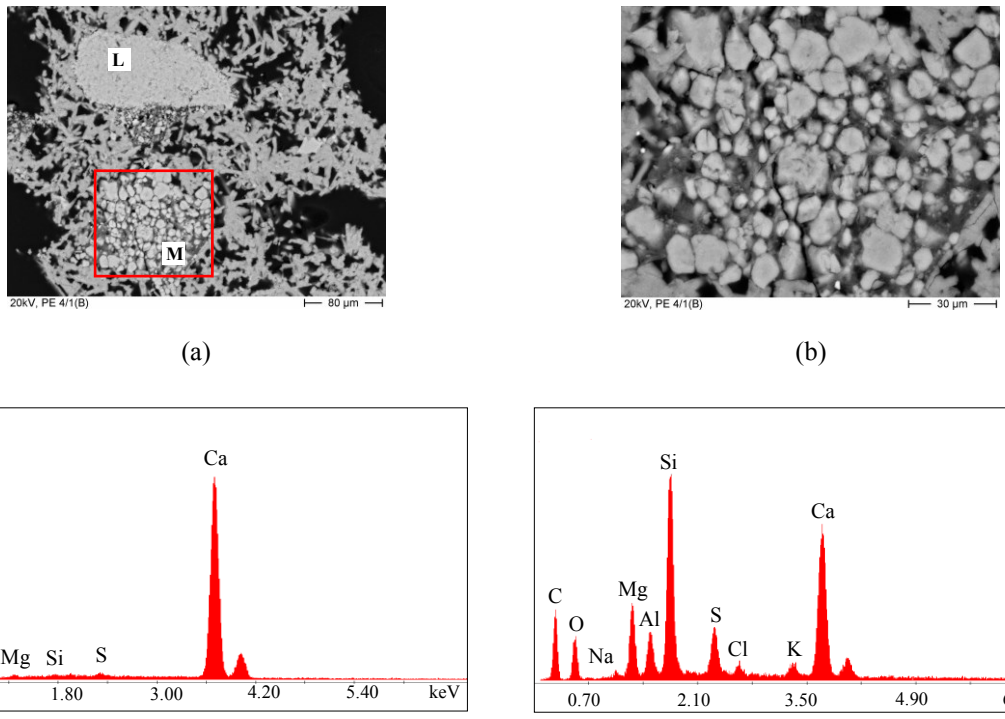

Figure 4.136 - SEM-BSE images of thin sections of PE4/1: (a) detail from Figure 4.132 (b) (yellow frame) showing a limestone grain (L) and a thermally damaged marl grain (M); (b) detail of (a) (red frame): the bright grains are calcite (EDS spectrum (c)) and the dark "matrix" are thermally changed marl impurities (EDS spectrum (d)) (all data authored by Frank Schlütter)

$$CaMg(CO_3)_{2\,(s)} \xrightarrow{450\text{-}700\ ^\circ C} CaCO_{3\,(s)} + \mathbf{MgO_{(s)}} + CO_{2\,(g)} \qquad \text{(Eq. 4.5)}$$

$$\downarrow\ 700\ ^\circ C\text{-}900\ ^\circ C$$

$$CaO_{(s)} + CO_{2\,(g)} \qquad \text{(Eq. 4.6)}$$

$$CaSO_4.2H_2O_{(s)} \xrightarrow{700\text{-}1180\ ^\circ C} CaSO_{4\ (s)\,(partially\ dissociated)} + 2H_2O_{(g)} \qquad \text{(Eq. 4.7)}$$

$$\downarrow\ >1180\ ^\circ C$$

$$CaO_{(s)} + \mathbf{SO_{3\,(g)}} \qquad \text{(Eq. 4.8)}$$

$$CaO_{(s)} + MgO_{\mathbf{(s)}} + \mathbf{2SO_{3\,(g)}} \longrightarrow CaSO_{4\,(s)} + \mathbf{MgSO_{4\,(s)}} \qquad \text{(Eq. 4.9)}$$

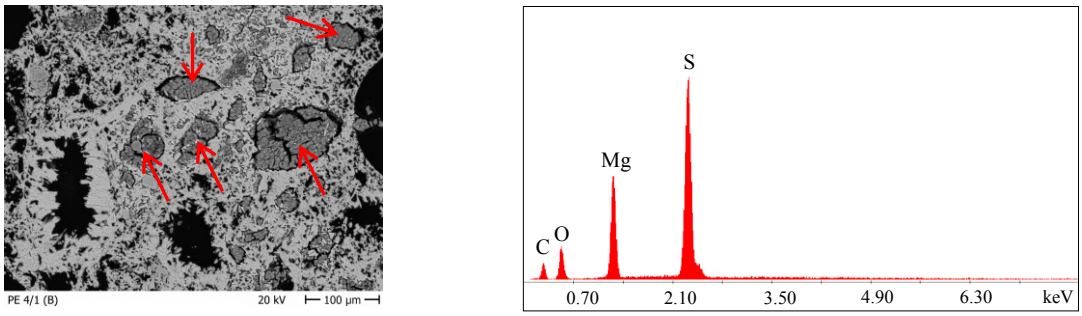

Figure 4.137 - SEM-BSE image of a thin section showing some of the voids of PE4/1 micro structure filled with $MgSO_4$ (red arrows) and EDS spectrum of those voids content (authored by Frank Schlütter)

Similar observations have been made in German high fired gypsum mortars produced for restoration purposes (Schlütter et al. 2010). However, as stated before, the crystal morphology of PE4/1 indicates that the material used in its production was mainly hemihydrate (Figure 4.131), which does not need very high temperatures to be obtained (~150-200ºC) (Wirsching 2005).

So, the presence of some phenomena that only occur at much higher temperatures (like the presence of holes in primary anhydrite grains or the thermal activation of marls), can be either due to the presence of very small particles of raw material in the kiln (almost powdered) that are completely burned during the calcination process, or the hemihydrate used resulted from the manual separation of the different phases of gypsum obtained, which is not a 100% efficient process and has always small quantities of other phases mixed (unburned and over burned).

PE4/2

Further images of the micro structure of PE4/2 are now shown in Figure 4.138.

Although much denser than PE4/1, PE4/2 has also a porous micro structure. As expected, the hematite pigments are more visible in the binder matrix/purple paste) than in the coloured “aggregates”. In PLM images they appear like black holes as they cannot be transmited by light due to their particle size.

Similarly to what happened in PE4/1, at higher magnifications and using the SEM-BSE mode it is possible to see that in some of the larger dissolving grains the remaining particles are a mix of dihydrate and anhydrite (Figure 4.139).

Besides being denser, PE4/2 shows a much higher content of granular anhydrite than PE4/1, indicating that the calcination temperatures of the plaster used to prepare it have been higher. In fact, the calcium sulphate dihydrate crystals resulting from the rehydration of high temperature calcined gypsum are non-prismatic, squat, with interpenetration textures, leading to high density and low porosity structures (Lucas 2003b; Tesch & Middendorf 2005; Schlütter et al. 2010); all these features occur in PE4/2.

Multiphase gypsum plasters, particularly those with a high content of anhydrite II, are usually prepared with higher plaster/water ratio than hemihydrate plasters, which directly influences their porosity/density. They also have a quicker initial setting time (mainly due to the presence of anhydrite III) and a longer final setting time (due to the presence of anhydrite II) (Wirsching 2005; Schlütter et al. 2010). This means that in a multiphase gypsum plaster mechanical strength and workability can be both improved (Wirsching 2005; Tesch & Middendorf 2005), very useful issues when thinking about the intended stone-like effect of the numerous decorated gypsum plaster pieces similar to PE4 that exist in the Noble room of *Estoi* Palace.

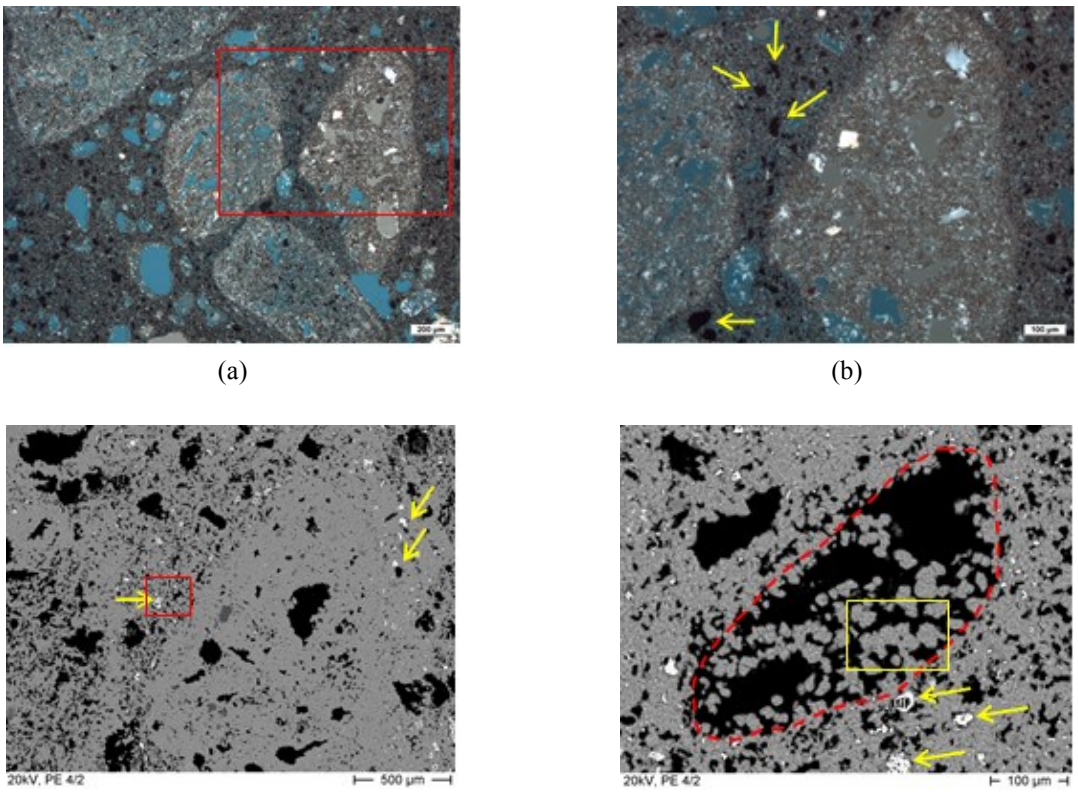

Figure 4.138 - Images of thin sections showing the micro structure of PE4/2 (authored by Frank Schlütter), with hematite grains pointed by yellow arrows: (a) dark purple matrix with the gypsum coloured aggregates perceptible, PLM, crossed polarized light; (b) detail of (a) (red frame); (c) the same area as (b) but in SEM-BSE mode and at higher magnification: the red frame corresponds to Figure 4.131 (b); (d) binder matrix with a largely dissolved former anhydrite grain, SEM-BSE mode

Similarly to what happened in sample PE2/2, different morphologies of the paste exhibiting crystals of higher dimensions and occurring in areas of the matrix where they have more room to grow were observed in PE4/2 (Figure 4.140). The respective EDS analyses revealed that they were all gypsum.

The exception is the crystal of Figure 4.140 (g) that, in spite of having a similar spectrum, has a morphology typical of anhydrite.

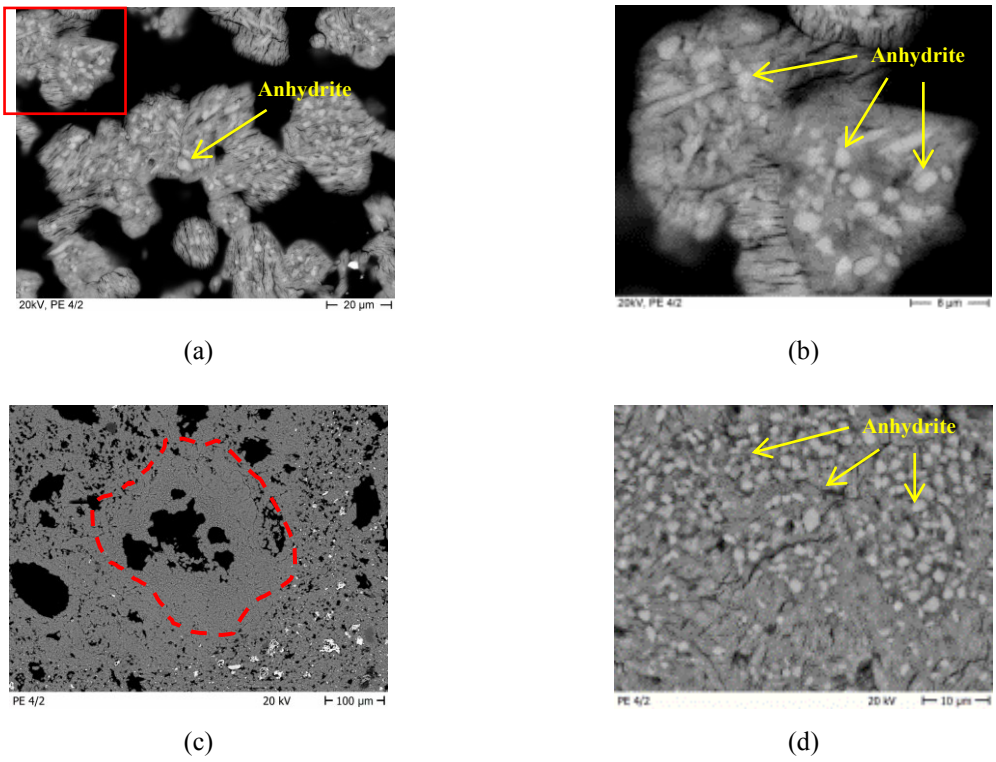

Figure 4.139 - Thin section SEM-BSE images of PE4/2 matrix showing granular anhydrite grains surrounded by dihydrate (authored by Frank Schlütter): (a) detail of Figure 4.138 (d) (yellow frame); (b) detail of (a) (red frame); (c) binder matrix with a partly dissolved anhydrite grain corresponding to a coloured aggregate, SEM-BSE mode; (d) detail of the matrix of the aggregate grain in (c)

The gypsum fake "aggregates" in the paste were also investigated by SEM. They were not detected in the micro structure observations of fractured surface but in polished surface and thin sections, using the BSE mode, its presence was noticed (Figure 4.141).

The three different coloured parts of PE4/2 were analysed using SEM-EDS and the respective spectra are shown in Figure 4.142. The main difference observed is the higher quantity of iron (Fe) in the purple matrix, meaning that hematite is more concentrated there than in any of the aggregates. These results are in total agreement with those of micro-Raman presented in the previous section.

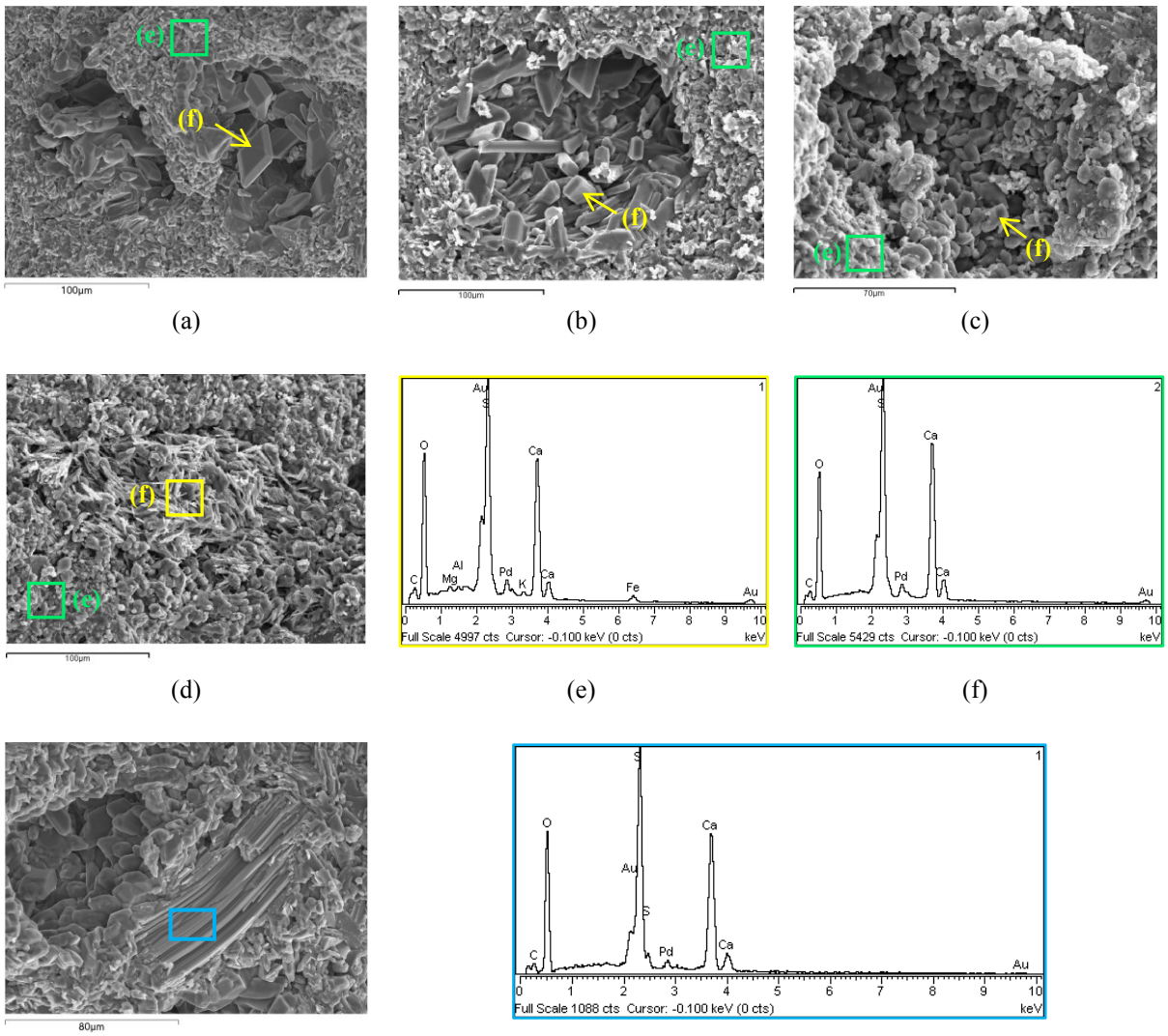

Figure 4.140 - (a) to (d) SEM-SE images of the PE4/2 paste showing different morphologies of gypsum; (e) EDS spectrum of the matrix; (f) EDS spectrum of the different crystal shapes of gypsum; (g) SEM-SE image of a fibrous grain (typical shape of thermo-anhydrite) and respective EDS spectrum (h)

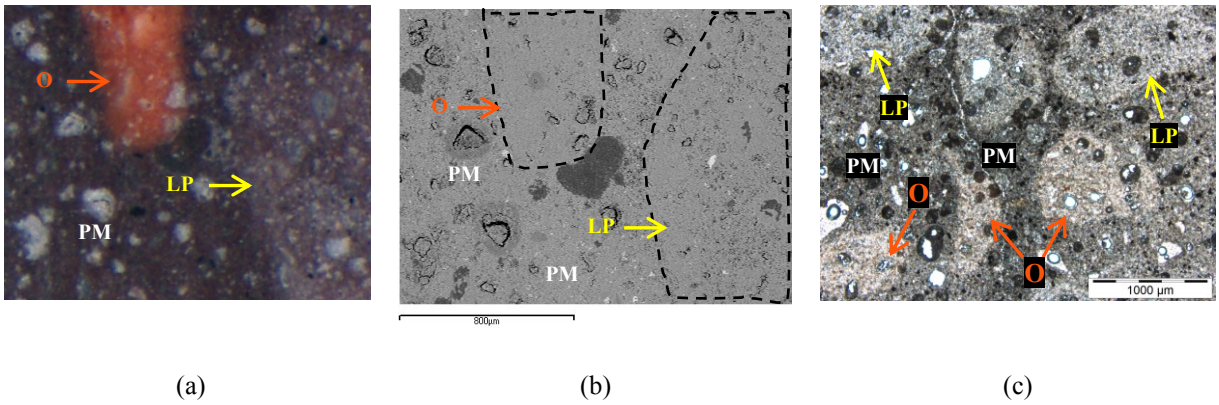

Figure 4.141 - Images of the purple matrix (PM) of the sample PE4/2 with orange (O) and light purple (LP) aggregates: (a) polished surface, stereo-zoom microscope (yellow frame of Figure 4.129 (a)); (b) the same as (a) but in SEM-BSE mode; (c) thin section, PLM with plane polarized light ((c) authored by José Mirão)

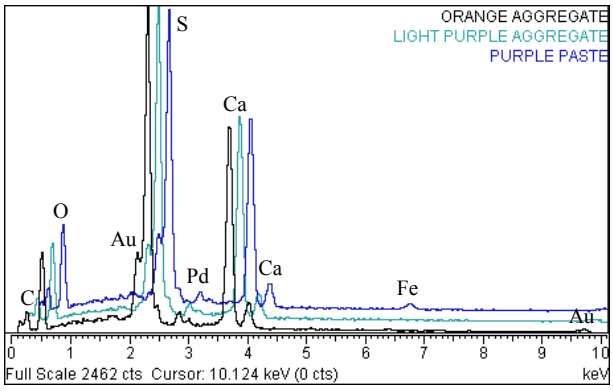

Figure 4.142 - Comparative EDS spectra of the three different coloured parts of sample PE4/2

The thin section observations were also valuable in the clarification on how hematite was used to obtain the different coloured effects present in the decorated layer: in the orange aggregates it was used as powder; in the light purple aggregates in small (but not powdered) particles; in the purple matrix both kinds of hematite are present (Figure 4.143).

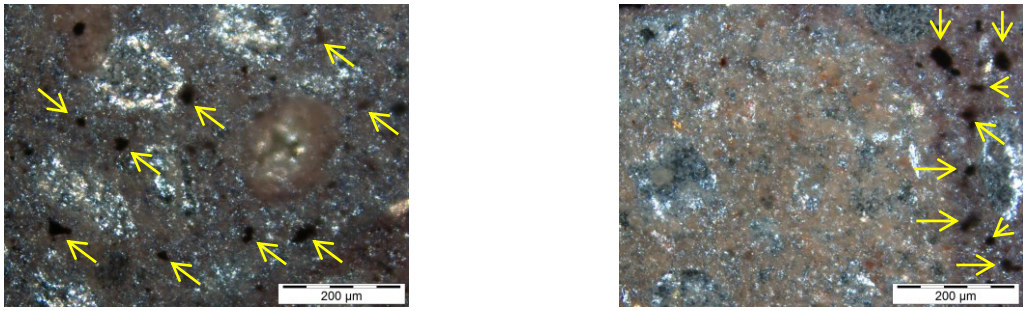

(a) (b)

Figure 4.143 - Thin section observations of PE4/2 (PLM, polarized light microscopy) showing the different grain sizes of hematite pigments (yellow arrows): (a) light purple aggregate (b) orange aggregate and purple matrix (images authored by José Mirão)

The particle size of hematite determines the respective colour effect: the bigger the particles, the darker the effect is; powdered hematite produces an orange colour.

Thus, it seems illogical that the purple matrix, which has both grain sizes of hematite, is the darkest part of the sample. The micro-Raman analyses detected the presence of other pigments that explain this issue, namely carbon black.

Another important observation is that powdered hematite is amorphous, though not detectable by XRD, which means that PE4/2 must have higher hematite content than the one given by XRD.

Hematite presence was also observed in fractured surface. Figure 4.144 is a SEM-SE image of a crystal of fibrous anhydrite surrounded by hematite grains that are visibly well embedded in the gypsum matrix.

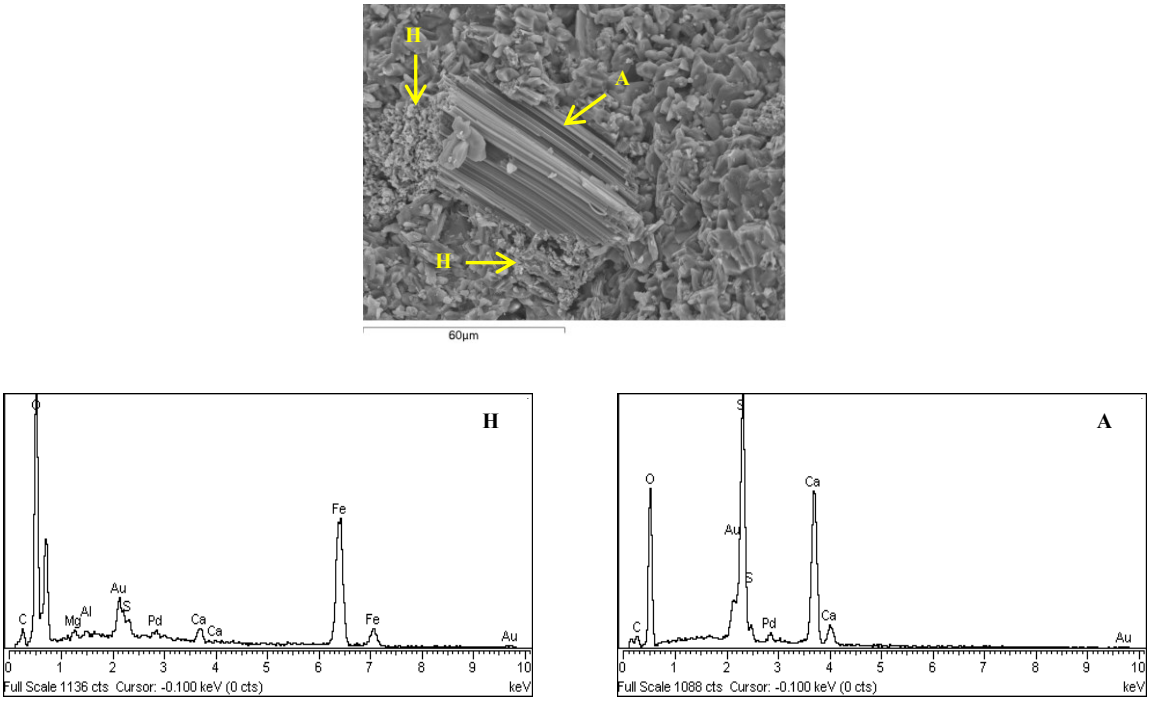

Figure 4.144 - SEM-SE image of PE4/2 matrix showing a crystal of fibrous anhydrite (A) and grains of hematite (H) and respective EDS spectra

An additional detail that strengthens the argument that the PE4/2 structure results from the hydration of a multiphase gypsum plaster predominantly made of anhydrite II is that the coloured "aggregates" are the result of previously prepared pigmented pastes also made of gypsum. It is well known the accelerating effect that hardened gypsum particles have in a mixture of water and a hemihydrate or a multiphase gypsum plaster (Wirsching 2005). As the presence of additives is unlikely in this sample's core, it seems that it was probably really necessary to prepare the gypsum paste of PE4/2 using a gypsum plaster deliberately calcined at higher temperatures (according to some morphological aspects observed by Frank Schlütter in thin sections, they were around 300-400 ºC) and/or for a longer time, in order to be mainly made of anhydrite with low setting time (anhydrite II).

Further features, namely minor constituents that are impurities of the raw material(s) used in the preparation of PE4/2 (matrix and "aggregates") were also detected through the thin sections and fractured surfaces observations using SEM and PLM.

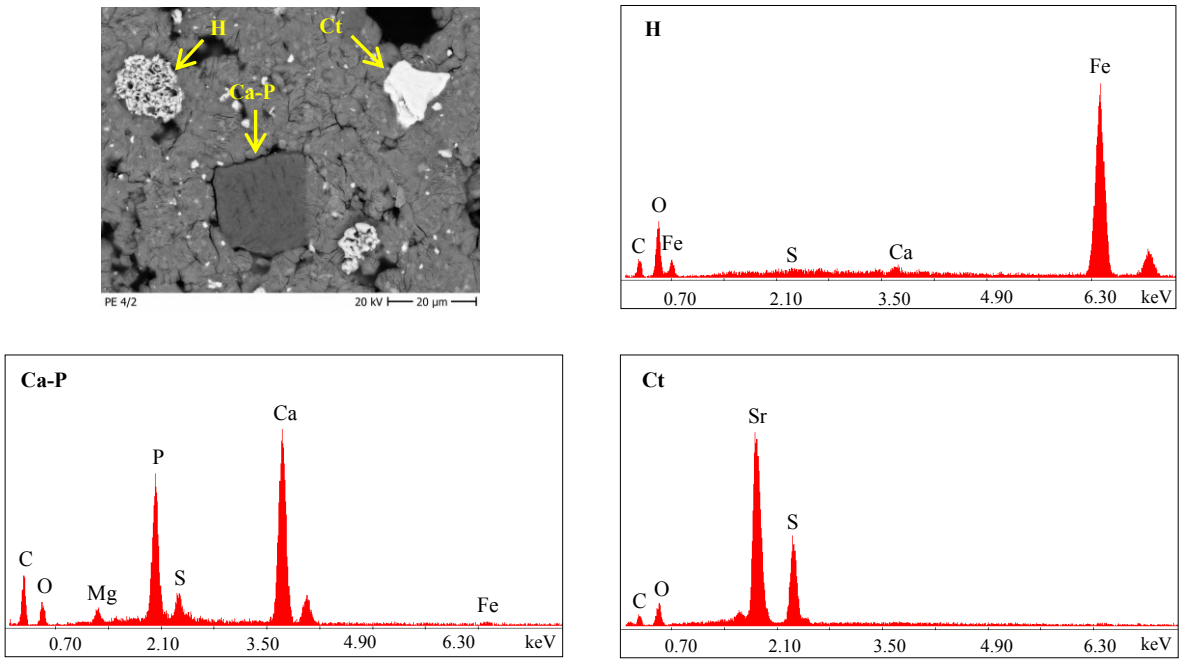

Figure 4.145 - Thin section SEM-BSE image of the PE4/2 matrix showing grains of three compounds: hematite (H), celestine (Ct) and calcium phosphate (Ca-P) and respective EDS spectra (authored by Frank Schlütter)

In Figure 4.145 only celestine and calcium phosphate are impurities of the raw material; hematite is an addition as already extensively discussed.

Another example of an impurity is given in Figure 4.146. The EDS spectra of the grain and of the small bright area observed in it showed that it is dolomite with an inclusion of feldspar.

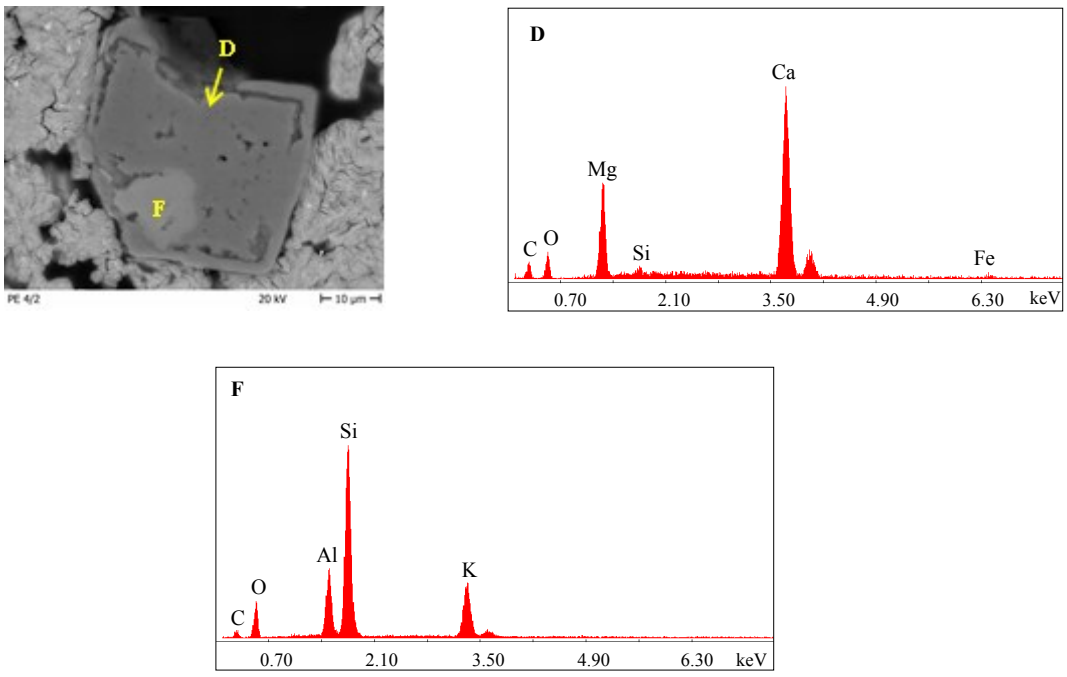

Figure 4.146 - Thin section SEM-BSE image of the PE4/2 matrix showing a grain of dolomite (D) with a feldspar inclusion (bright area, F) and respective EDS spectra (authored by Frank Schlütter)

In fractured surface observations some grains with an unusual shape have been detected and were also identified by EDS as feldspars (Figure 4.147).

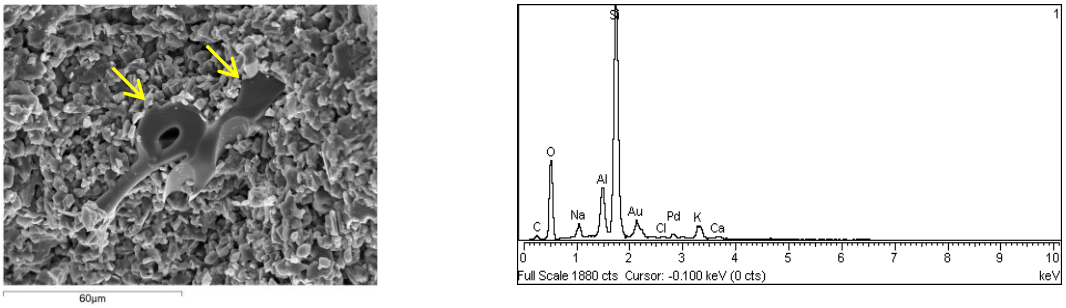

Figure 4.147 - SEM-SE image of the PE4/2 matrix showing two grains of feldspars and respective EDS spectrum

Similarly to PE4/1, the formation of secondary phases, like magnesium sulphate, has also been identified in PE4/2.

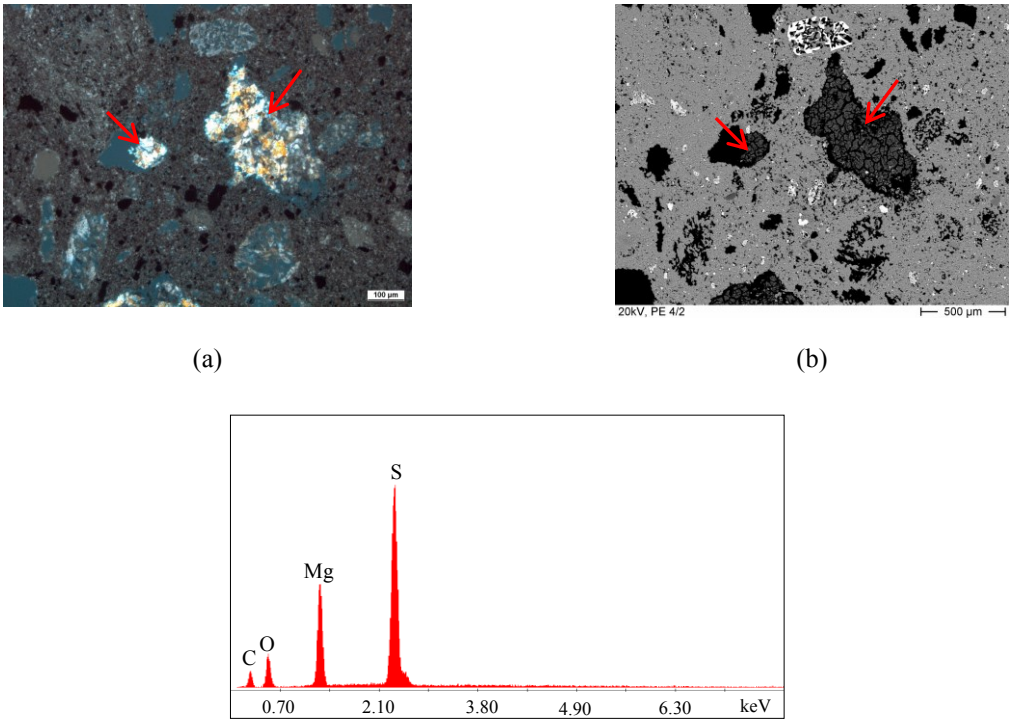

(a) (b)

(c)

Figure 4.148 - Thin section observations of PE4/2 showing some voids filled with $MgSO_4$ (red arrows): (a) PLM, crossed polarized light; (b) SEM-BSE image; (c) EDS spectrum of the voids content (authored by Frank Schlütter)

The main characteristics of samples PE4/1 and PE4/2 observed using SEM-EDS and PLM techniques are now summarized in Table 4.62.

Table 4.62 - Summary of the SEM-EDS and PLM observations of the samples PE4/1 and PE4/2

Sample	PE4/1	PE4/2
Binder	Gypsum dihydrate	Gypsum dihydrate
Other components	Presence of various types of minerals (grain size up to 0.5 mm): - Gypsum/anhydrite grains (some partly dissolved) - Limestone (with two types of crystallization) - Quartz - Celestine - Dolomite - Primary anhydrite - Marl - Feldspars	Presence of various types of minerals (grain size up to 0.3 mm): - Gypsum/anhydrite grains (some partly dissolved) - Hematite with different grain sizes as pigment - Celestine - Dolomite - Marl - Feldspars - Calcium phosphate Presence of gypsum coloured pieces as aggregates (grain size up to 3 mm).
Microstructure	Porous, with some of the pores resulting from the total dissolution of gypsum grains; Binder crystals have a prismatic, needle-like morphology with some showing a lamellar internal structure; Gypsum grains, some partly dissolved; Voids with remains of dihydrate and anhydrite; Presence of different types of anhydrite grains in the dihydrate matrix: some are impurities (primary anhydrite) and others are remains of firing products (granular and fibrous-shaped grains); Large amount of grains of diverse mineral composition that are impurities of the raw material.	Porous, though much less than PE4/1 and with higher density; Compact (squat, stocky) binder crystals with a predominantly lamellar internal structure; Presence of fibrous anhydrite crystals in the binder matrix (more frequently than in PE4/1). The majority of these crystals dissolve, sometimes resulting in cavities, and crystalize as dihydrate with different crystal morphologies; Remains of firing products: grains composed of dihydrate with a much higher content of small granular anhydrite grains than in PE4/1.
Secondary formed phases	Magnesium sulphate resulting from the thermal activation of marls present in the raw material	Magnesium sulphate resulting from the thermal activation of marls present in the raw material

The following conclusions can be drawn:

a) The presence of different minor constituents (impurities) in both samples means that the raw material used was not the same;
b) The distinct crystal morphologies indicate that the gypsum phases used as binder were also different:

- In PE4/1 the plaster was mainly composed of hemihydrate;

- In PE4/2 the starting product was predominantly anhydrite II.

So, the firing temperatures were clearly higher in the material used in PE4/2 than in PE4/1. However, its reactivity (XRD results showed that the anhydrite content is low) seems to indicate that the temperatures of calcination were predictably around 300-400ºC, much lower than those indicated for the production of medieval high fired gypsum mortars used in exterior surfaces (around 900 ºC) (Lucas 2003a; Lucas 2003b; Sanz 2009; Schlütter et al. 2010).

This fact, if proved to be truth, is very important because it indicates that some control of the calcination could already be achieved. In the medieval times it was easier to obtain a temperature of 900 ºC in the kiln than one of 150 ºC (Lucas 2003a) and, consequently, one of 300-400 ºC, too.

A possible explanation for this technological improvement is that *Estoi* Palace decoration works took place at the end of the 19th-beginning of the 20th centuries, under the direction of *Domingos Meira*. As stated before, the work of *Meira* was so well recognized around the country (and also abroad: he was awarded in the international exhibitions of Paris (1900), Chicago (1904) and Rio de Janeiro (1908)) that his workshop was responsible for the most important plasterworks in Portugal since the mid-nineteens (Mendonça 2012). A high production demanded a high volume of related materials, namely gypsum, so in the last decade of the 19th century, *Meira* was owner and manager of a gypsum steam plant, in Lisbon, equipped with two kilns, in order to control the quality and production of the material used in his works (Mendonça 2012).

c) Even though the plaster used to prepare PE4/1 was mainly hemihydrate, some substances typical of high firing temperatures were observed in its micro structure, like different forms of anhydrite and thermally changed marls. This can be due to the presence of small grains of raw material in the kiln that dehydrate earlier than the average gypsum stones and easily reach much higher temperatures during the time that the calcination process takes (over burned products).

Besides all these features, measurements of density, pore size distribution, capillary water absorption, dynamic modulus of elasticity and compressive strength have been made and they confirm the existence of significant differences between PE4/1 and PE4/2. The respective results and discussion are presented ahead.

Sample PE5

The observations started with a view at low magnification (20X) (Figure 4.149) of the surface corresponding to the three layers identified by stratigraphic analysis (Figure 4.111).

The interface between PE5/2 and PE5/3 is clearly visible (yellow arrows). On the contrary, in the case of PE5/1 and PE5/2, the frontier is probably in the line pointed out by red arrows, but without certainties.

The matrix of PE5 can be considered moderately macro porous, seeming to be slightly more compact in the external layer (PE5/3). This is probably due to the application of the material that must have been pressed / worked harder in the last layer in order to obtain a smooth, plan surface.

The EDS spectra have been only performed in areas where there was a guarantee that they really corresponded to the respective identification (Figure 4.149, coloured frames). As expected, the main component is calcite though low quantities of gypsum and halite (NaCl) are also clearly present. The XRD analysis (Table 4.58) had already identified traces of this compound in PE5/1 and PE5/3, but not in PE5/2, probably being a random occurrence.

Traces of magnesium and silicon were also detected and are due to impurities of the raw material (quartz and feldspars) according to the XRD results as well.

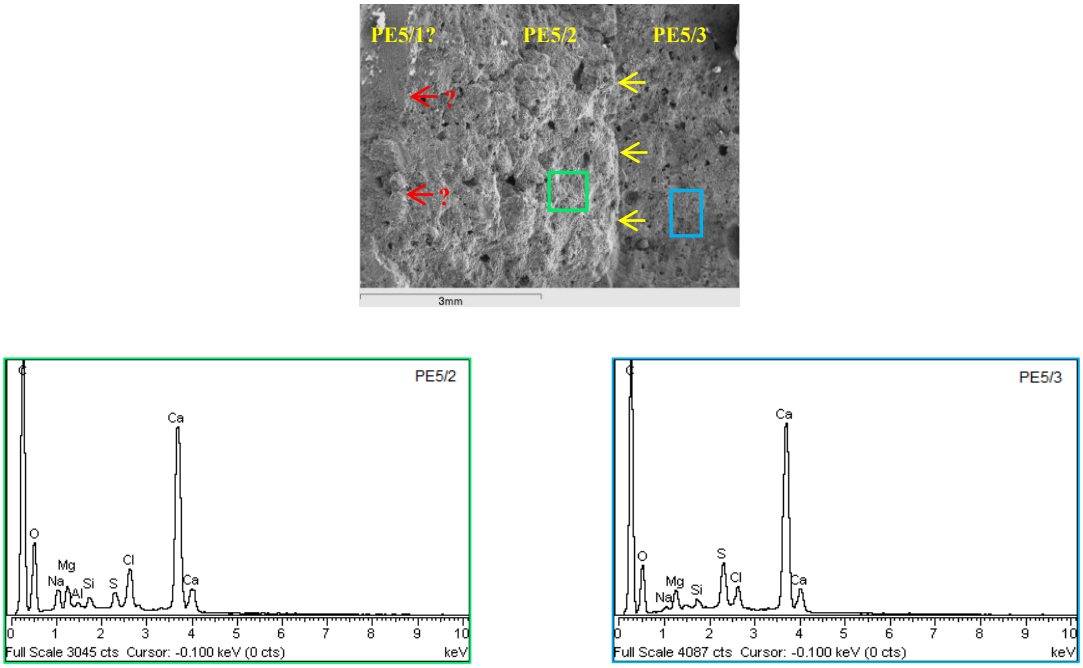

Figure 4.149 - SEM-SE image of sample PE5 showing the interface between the layers PE5/2 and PE5/3 (yellow arrows) and possibly between PE5/2 and PE5/1 (red arrows); EDS spectra corresponding to the areas marked with coloured frames

A further insight into the microstructure was made at higher magnifications in order to see the different crystal morphologies present and the eventual use of calcitic aggregates. The respective identification was made using EDS analysis.

The image of Figure 4.150 shows that the matrix is predominantly made of very small, hexagonal shaped crystals, typical of a calcitic structure originated by the carbonation of hydrated lime (Margalha et al. 2011). However, it does not seem as dense as that of sample EG1 from the *Garage* building (Figure 4.181 (a) and (b)), though the crystals' morphology is exactly the same. This is probably due to the use of different gauging water quantities.

Another interesting yet somehow unexpected observation was the difficulty to distinguish gypsum crystals in between the microstructure, especially considering that gypsum was also quantified in significant amounts. Even though, it was easier than in sample EG1 which can be due to the higher macro porosity and gypsum overall content of PE5.

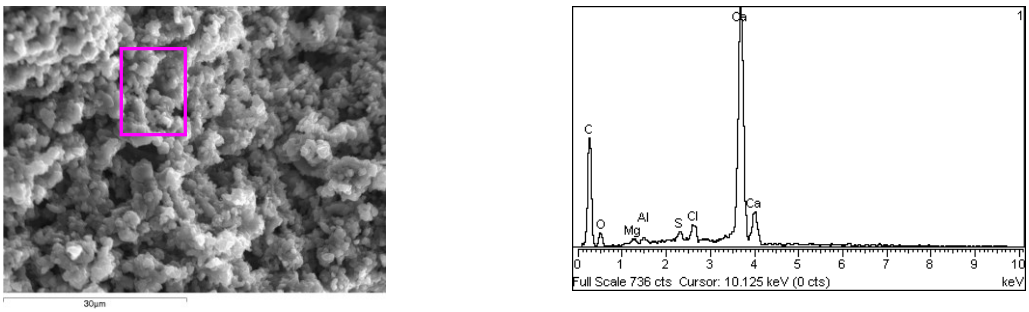

Figure 4.150 - SEM-SE image of the microstructure of sample PE5 showing the crystals morphology and respective EDS spectrum (pink frame area)

Only in some of the bigger voids of the matrix crystals of higher dimensions and prismatic needle-like morphology were clearly observed; the respective EDS spectrum showed that they are exclusively composed of gypsum (Figure 4.151).

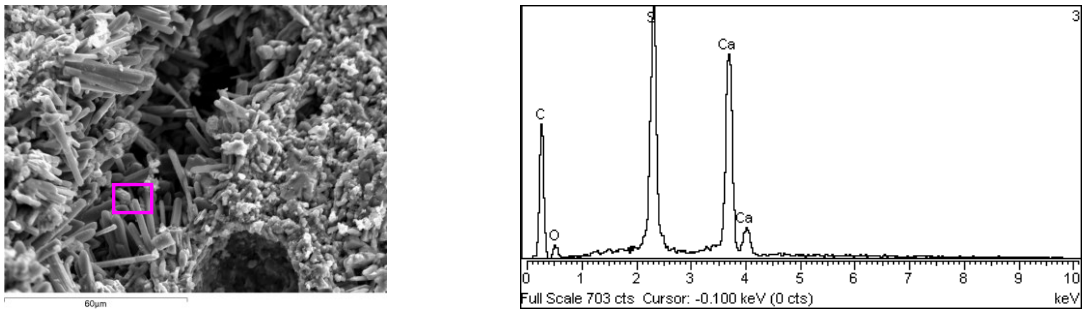

Figure 4.151 - SEM-SE image of the PE5 matrix showing a long void with prismatic, needle-like crystals inside and respective EDS spectrum (pink frame area)

Two final remarks can still be made about Figure 4.151: (a) the long void does not have calcite crystals; (b) part of a very round, also big pore can be seen in the lower part of the image but it is completely empty.

The most plausible explanations for the observations above seem to be: (a) in a lime-gypsum matrix the gypsum crystals assume their regular shape and size only when they can grow without being hindered by a high concentration of lime particles around or, another hypothesis, the mixture between both compounds was not homogeneous and in the places where gypsum was more concentrated it grew freely, as it sets much more quickly than lime, inducing the formation of some voids; (b) the absence of crystal formations in the round voids means they must have been originated by air bubbles, an explanation reinforced by their shape, a symptom of a low initial consistency (higher gauging water content).

The presence of halite was also observed and seemed to be more frequent than the indications given by XRD results. In Figure 4.152 two crystal morphologies of this compound are shown, of which the left one is the most commonly found.

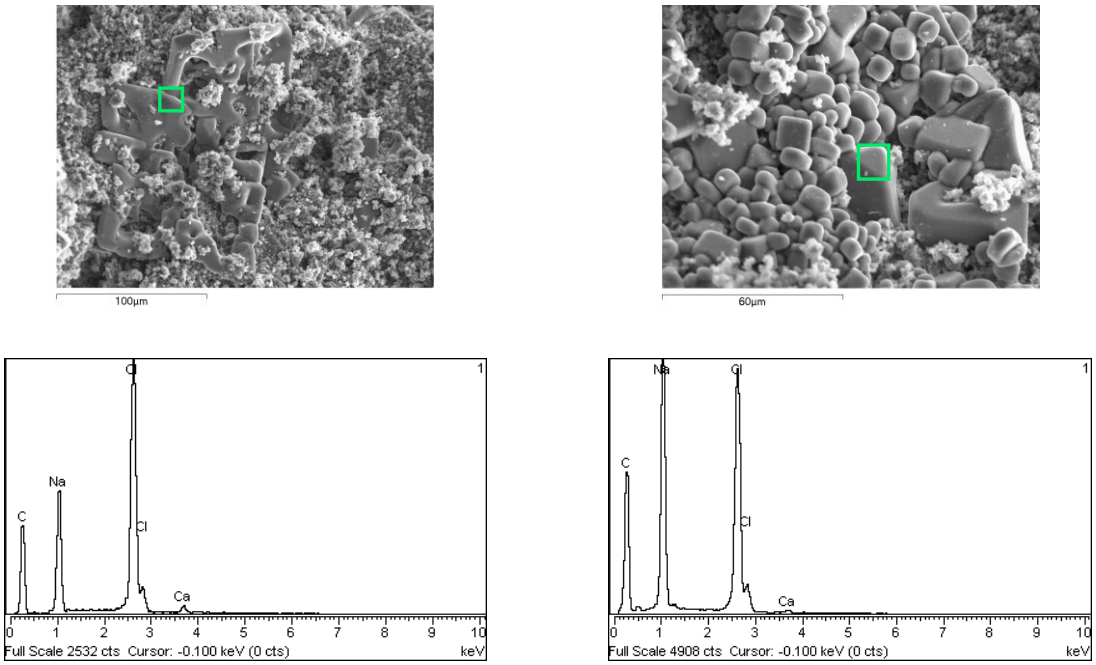

Figure 4.152 - SEM-SE images of different halite crystal morphologies present in the PE5 matrix and respective identification by EDS (green frames)

Although in the preparation of the sample for XRD and TG-DTA analysis the presence of aggregates has not been detected, the images of Figure 4.153 show limestone grains of considerable size in the sample's matrix.

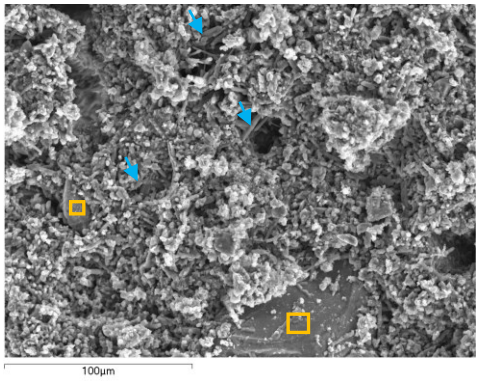

(a)

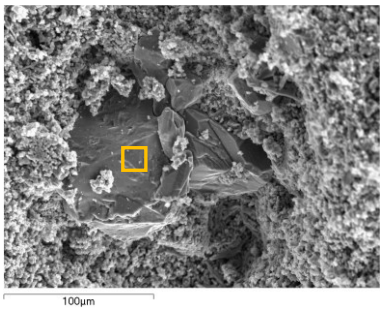

(b)

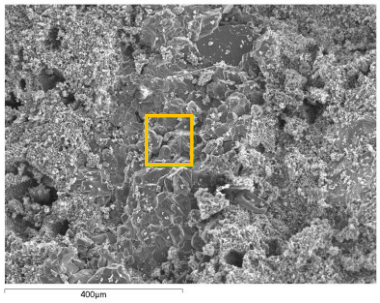

(c)

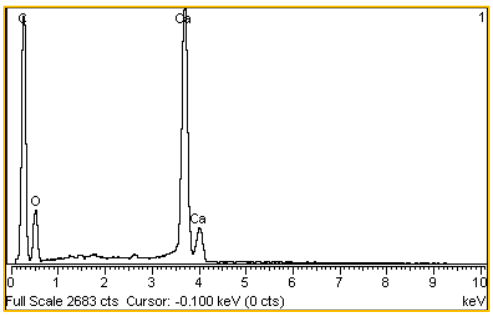

(d)

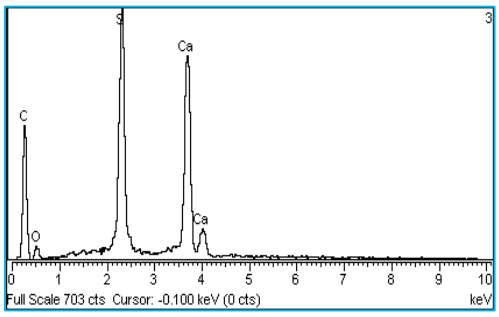

(e)

Figure 4.153 - SEM-SE images of the sample PE5: (a) limestone grains (yellow frames) and gypsum crystals (blue arrows) in the middle of a carbonated lime matrix; (b) and (c) detailed views of limestone grains; (d) and (e) EDS spectra of limestone (yellow frame) and gypsum crystals (blue frame)

Summarizing, the SEM-EDS observations of sample PE5 in fractured surface allowed drawing the following conclusions:

a) It has a higher macro porosity than sample EG1, made both of round and irregular shaped pores with greater length than width (Figure 4.151), a strong indication that the material was pressed while still fresh (Rúbio Domene 2011);

b) It has a compact micro-structure mainly composed of hexagonal, lamellar crystals resulting from the carbonation of hydrated lime. The gypsum crystals are hardly detected and difficult to distinguish in the matrix (Figure 4.150 and Figure 4.153 (a));

c) On the contrary, in some of the macropores prismatic, needle-like larger gypsum crystals are visible. Even though it is the major compound, calcite does not crystallize in these voids (Figure 4.151);

d) Many halite crystals have been detected (Figure 4.152), denoting a previous contact with saline water, probably in wet/dry cycles. That must be the reason why the corresponding wall had a thick layer of asphalt between two layers of mortar (Figure 4.110 (d) and Figure 4.112 (d)).

- Physical properties

Capillary absorption

The water absorption by capillarity was determined in all the samples from *Estoi* Palace (Figure 4.154) and the quantitative results are summarized in Figure 4.155 and in Table 4.63.

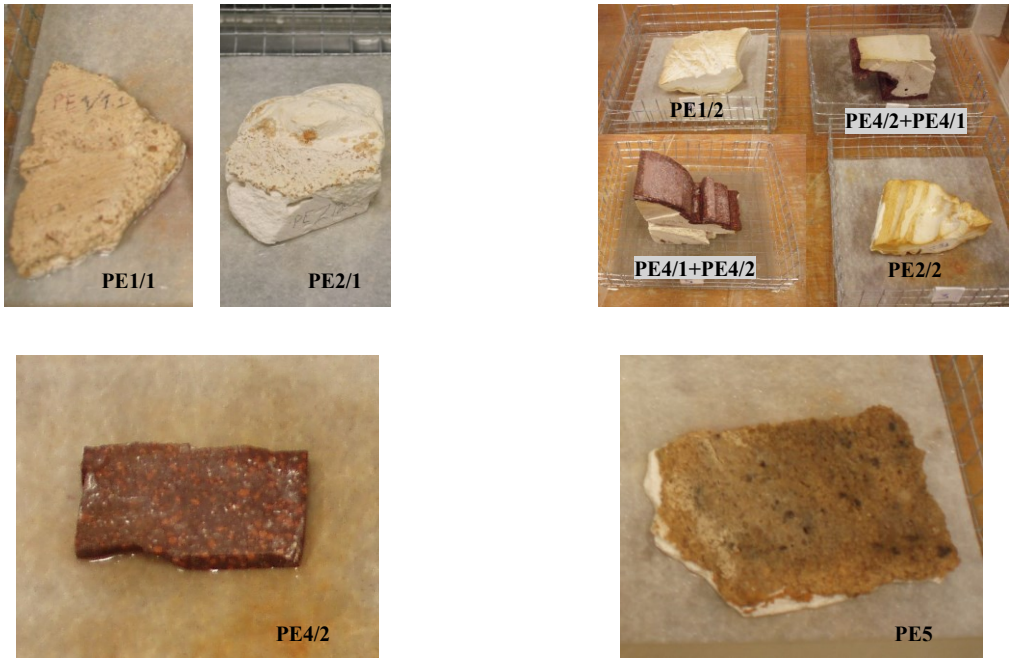

Figure 4.154 - Water absorption by capillarity of samples from *Estoi* Palace: images of the ongoing tests

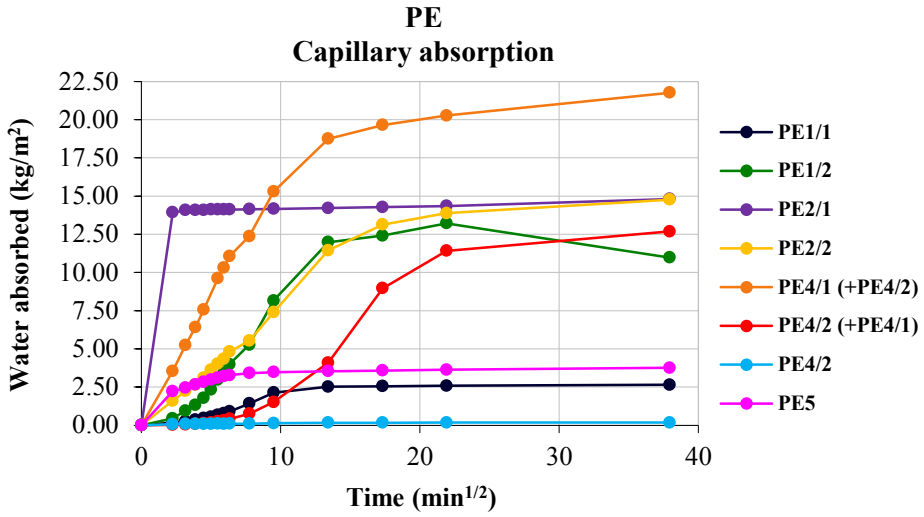

(a)

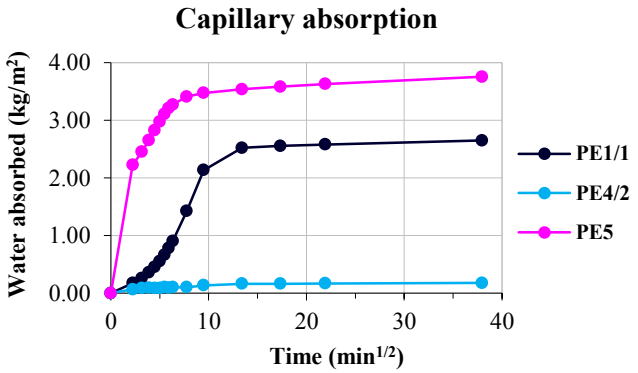

(b)

Figure 4.155 - Water absorption by capillarity of samples from *Estoi* Palace: (a) graphical representation of the results; (b) detailed view of the curve profiles of the samples with lower absorption

Table 4.63 - Capillary absorption by contact results of the samples from *Estoi* Palace

Test specimen	**PE1/1**	**PE1/2**	**PE2/1**	**PE2/2**	**PE4/1(+ PE4/2)**	**PE4/2(+ PE4/1)**	**PE4/2**	**PE5**
Surface (cm^2)	20.50	13.00	18.56	12.82	22.43	19.64	14.68	57.19
Weight (g)	32.61	129.26	55.69	73.32	252.85	157.80	16.04	148.00
Capillary absorption at 5 min:								
(g)	0.36	0.58	25.85	2.05	7.95	0.06	0.10	12.74
($kg.m^{-2}$)	**0.18**	**0.45**	**13.93**	**1.60**	**3.54**	**0.03**	**0.07**	**2.23**
(%, relative to weight of sample)	1.10	0.45	46.42	2.80	3.14	0.04	0.62	8.61
(%, relative to total absorption)	6.63	4.06	94.03	10.83	16.28	0.24	38.46	59.34
Capillary absorption at 24 h:								
(g)	5.43	14.27	27.49	18.93	48.83	24.92	0.26	21.47
($kg.m^{-2}$)	**2.65**	**10.98**	**14.81**	**14.77**	**21.77**	**12.69**	**0.18**	**3.75**
(%, relative to weight of sample)	16.65	11.04	49.36	25.82	19.31	15.79	1.62	14.51
Ccc at 5 min ($kg.m^{-2}min^{-1/2}$)	**0.08**	**0.20**	**6.23**	**0.72**	**1.59**	**0.01**	**0.03**	**1.00**

Ccc - capillarity coefficient by contact

The results obtained can be divided in three groups:

(a) Samples with low (< 1.00) or very low (< 0.10) Ccc at 5 minutes - PE1/1, PE1/2, PE2/2, PE4/2(+PE4/1) and PE4/2;
(b) Samples with moderate (1.00 - 3.00) Ccc at 5 minutes - PE4/1(+PE4/2) and PE5;
(c) Samples with high (> 3.00) Ccc at 5 minutes - PE2/1.

In sample PE1/1, neither the gypsum-calcite composition nor the presence of additions (not detected by visual observation) seem to be plausible explanations for this behaviour. However, the visual observation by itself is not enough to discard the eventual use of a product to improve the adhesion between the regularization layer (PE1/1) and the precast putty (PE1/2). The process of application of this element, that had to be pressed against the surface of PE1/1, could also have an influence.

In the case of samples PE1/2 and PE2/2, although they were gypsum plasters with expectable higher absorption rates, their surfaces were impregnated with a key-coat (2-3 mm depth, corresponding to the "B" layers) of organic origin (cf. "FT-IR and micro FT-IR spectroscopic analyses) that is impossible to remove. This product modified the capillary water absorption behaviour of the referred samples, especially in the first 60 minutes (7.75 $min^{1/2}$) of the procedure: the water front rise was dependent both on the filling of the pores and on the resistance imposed by the key-coat that was being literally drawn inside. In fact, after the capillary absorption and drying processes were concluded, the displacement of the key-coat was clearly perceptible.

The extremely low absorption of the sample PE4/2 was not a surprise, considering the compactness of its internal structure (*cf.* "SEM-EDS and PLM observations" section), confirmed by the respective porosity and pore size distribution results (*cf.* "Pore size distribution" section).

The highest value Ccc at 5 minutes was that of sample PE2/1, a gypsum-calcite plaster from a moulded on site element. This behaviour can be easily explained by the very high content of pores with radius above 0.5 micron (Figure 4.157), usually responsible for high initial absorption rates. It is also the sample with the highest porosity (Table 4.64).

Finally, two samples with moderate Ccc at 5 minutes: PE4/1(+PE4/2) and PE5. The first is a gypsum plaster with sisal fibres incorporated that seems to have a normal porosity for this type of materials (usually above 50%); the second is a thin-layer calcite-gypsum plaster with mortar behind.

In the sample designated as PE4/1(+PE4/2) the absorption surface is PE4/1 and presents a quite constant absorption rate during the first 90 minutes (9.49 $min^{-1/2}$). Between 90 and 180 minutes (13.42 $min^{-1/2}$) the rhythm starts decreasing and is definitely slower after that.

The visual observation of the procedure indicated that at 90 minutes the layer PE4/1 achieved apparent water saturation. In spite of not having the respective pore size distribution curve, the behaviour of other samples with similar compositions (e.g. CP2, ISF1) allows inferring that PE4/1 was solely responsible for the capillary absorption behaviour in the first 180 minutes. After that PE4/2 started to contribute, although in a very incipient form.

Another important issue observed in the absorption curve profile of PE4/1(+PE4/2) is that the weight of the sample was not stabilized at the end of the procedure (24 h). If it remained in contact with water it would probably continue to absorb. The major responsible for this late absorption is most likely the PE4/2 part.

Concerning the sample PE5, in spite of being composed of more calcite than gypsum the pore size distribution curve indicates that the most significant amount of pores has radius above 0.5 micron (Figure 4.157), contributing to increase the initial absorption rate. However, the pores with radius under 0.5 micron are also present in quite considerable number and after a quick initial suction the filling of the pores starts to be much slower. The capillary absorption behaviour is therefore according to the bimodal pore size distribution curve obtained by MIP analysis.

Finally, it is important to note that the samples where a finishing product had been applied showed lower rates of absorption, especially in the initial part of the test. It means that this type of products forms some kind of a barrier to water penetration, acting as an efficient protection when the exposure to this agent is not too long.

The loss of water absorbed in the capillarity test was also evaluated and is represented in Figure 4.156.

The graph of Figure 4.156 (b) corresponds to the first five weighing results, respectively at 0, 30, 60, 90 and 270 minutes. It intends to show with more detail the differences of drying behaviour between the samples in the beginning of the process, giving an idea of their greater or lesser capacity to retain water.

The water absorption by capillarity of most of the samples did not have a corresponding drying behaviour, namely those with higher Ccc at 5 minutes. Depending on the sample, the explanations can vary:

- Sample PE2/1 had a high drying rate during the first 30 minutes, slowing down unexpectedly between 30 and 90 minutes. After that, it increased again significantly. A plausible explanation for this inconsistent behaviour was not found so far;
- In the sample PE4/1(+PE4/2), the major role was performed by PE4/1 both in the absorption and in the drying processes. However, as PE4/2 was on the top of the sample, it influenced a little more the drying than in the case of PE4/2(+PE4/1), especially in the first 90 minutes ($9.49\ min^{-1/2}$);

- On the contrary, in PE4/2(+PE4/1) the absorbing surface was PE4/2 but the drying occurred mainly through PE4/1;
- The behaviour of the samples PE1/2 and PE2/2 was masked by the key-coat used to prepare the surface for painting, and it is not possible to relate it with the respective absorption curves.

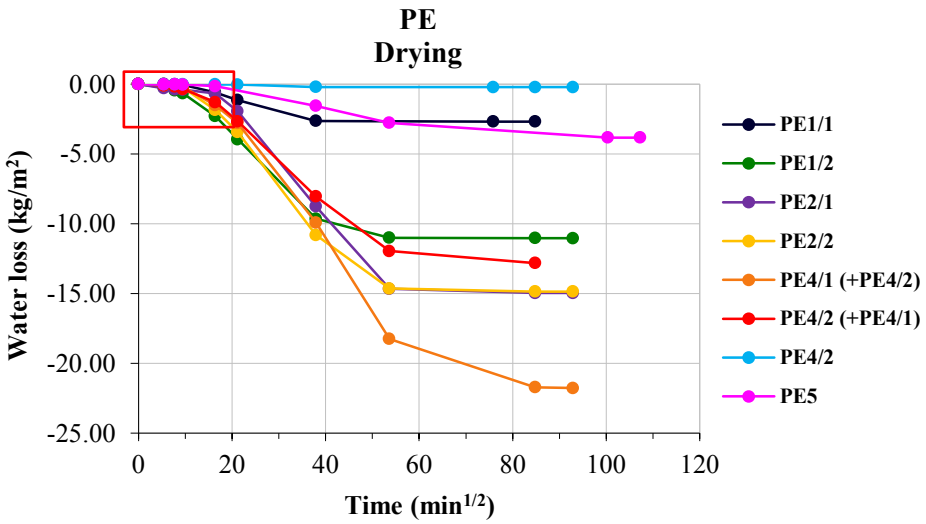

(a)

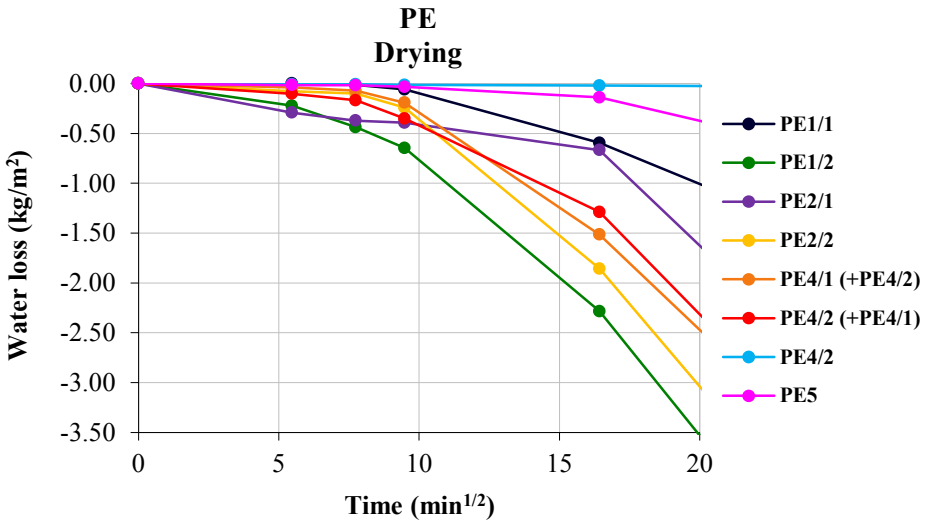

(b)

Figure 4.156 - Graphical representation of the drying behaviour of the samples from *Estoi* Palace: (a) all data obtained; (b) detailed view of the first five weighing results (red frame of (a))

Pore size distribution

The pore size distribution curve using mercury intrusion porosimetry (MIP) was determined in most of the samples from *Estoi* Palace (Figure 4.157). The results obtained agree with the capillary absorption

behaviour of the corresponding samples. The exception is PE2/2 due to the reasons discussed in the previous section.

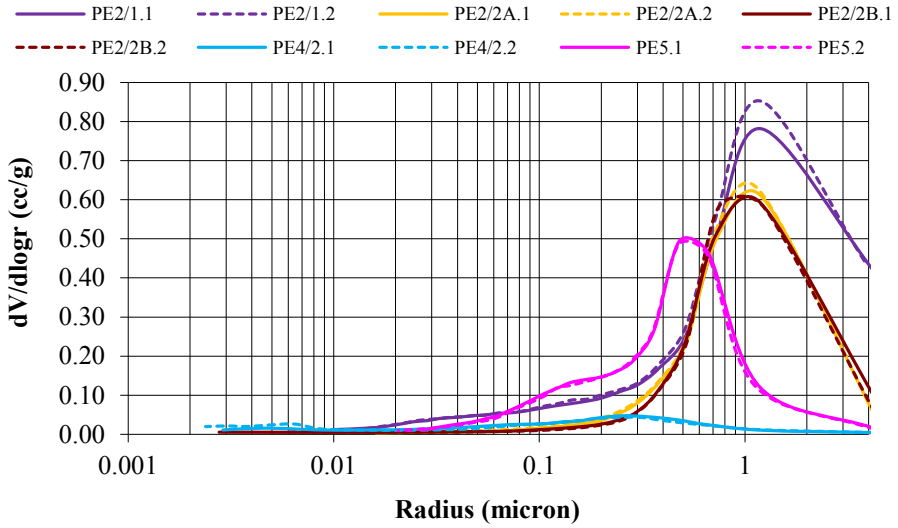

Figure 4.157 - Pore size distribution curves of samples from *Estoi* Palace

Table 4.64 - Results obtained by MIP analysis in samples from *Estoi* Palace

Sample. .test specimen	Weight (g)	Bulk density ($kg.m^{-3}$)	Density ($kg.m^{-3}$)	Porosity (%)	Pore radius with max. vol. (μm)	Average pore radius (μm)
PE2/1.1	0.75	1039	2588	59.9	1.212	0.309
PE2/1.2	0.77	972	2400	59.5	1.198	0.315
PE2/2A.1	0.75	1190	2195	45.8	1.212	0.613
PE2/2A.2	0.75	1187	2223	46.6	1.159	0.507
PE2/2B.1	0.77	1245	2317	46.3	1.185	0.321
PE2/2B.2	0.75	1236	2274	45.6	1.240	0.325
PE4/2.1	0.76	2025	2305	12.1	0.252	0.0272
PE4/2.2	0.76	2065	2361	12.5	0.312	0.0179
PE5.1	0.74	1409	2465	42.8	0.480	0.240
PE5.2	0.81	1433	2503	42.7	0.476	0.237

Another interesting and very important issue is the similarities between the pore size distribution curves of the samples PE4/2 and PM1 (Figure 4.158), both very special cases with other characteristics in common. The respective pore radii at maximum volume are also very close; the main difference is the average pore radius. It is important to note, however, that the software associated to the apparatus used in the determinations and the mathematical formulas for the calculations of these parameters can introduce considerable errors, and the most reliable result is the distribution curve.

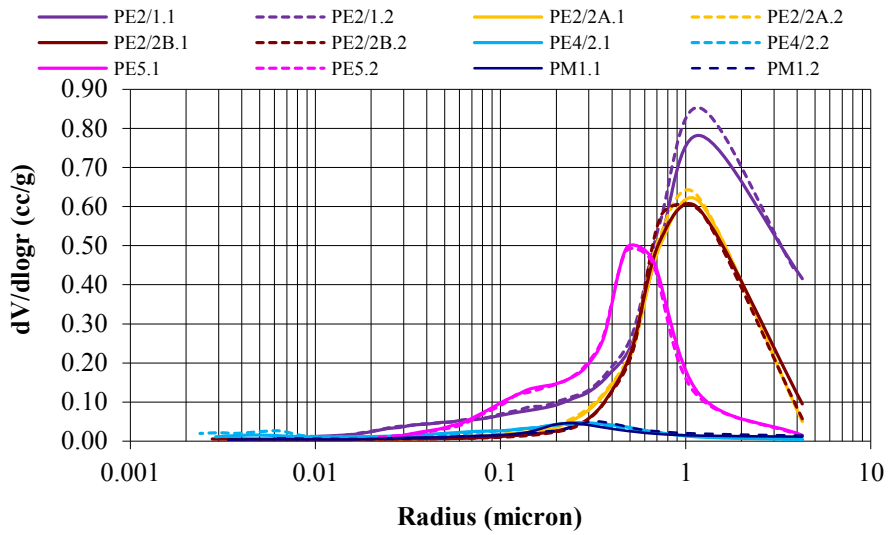

(a)

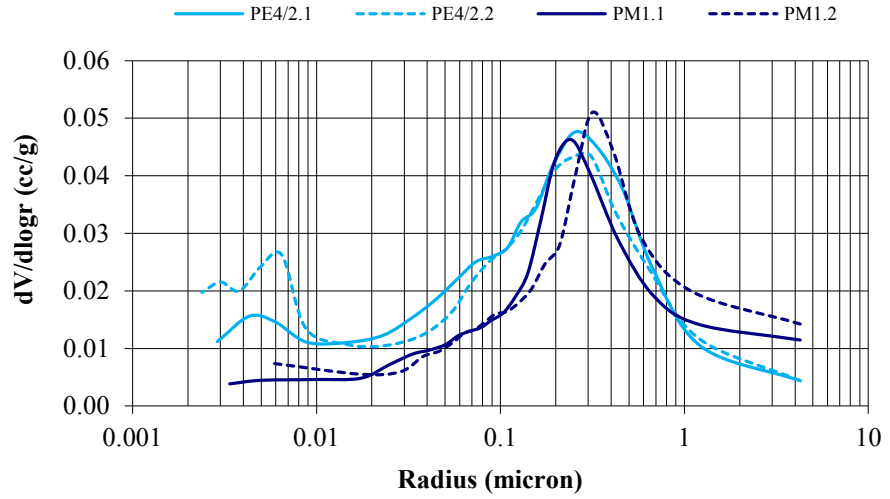

(b)

Figure 4.158 - Pore size distribution curves of samples from *Estoi* Palace and of sample PM1 from *Monserrate* Palace: (a) all samples; (b) comparison between PE4/2 and PM1

Hygroscopic behaviour

The graphical representation of the hygroscopic behaviour of the samples from *Estoi* Palace is shown in Figure 4.159 and the quantitative results are summarized in Table 4.65.

Sample PE5 was also studied but the values of hygroscopicity were too high and were presented only in Table 4.65. This is usually related to the presence of hygroscopic contaminants, like soluble salts, and is in agreement with the previous detection of halite (NaCl) by XRD and in SEM-EDS observations.

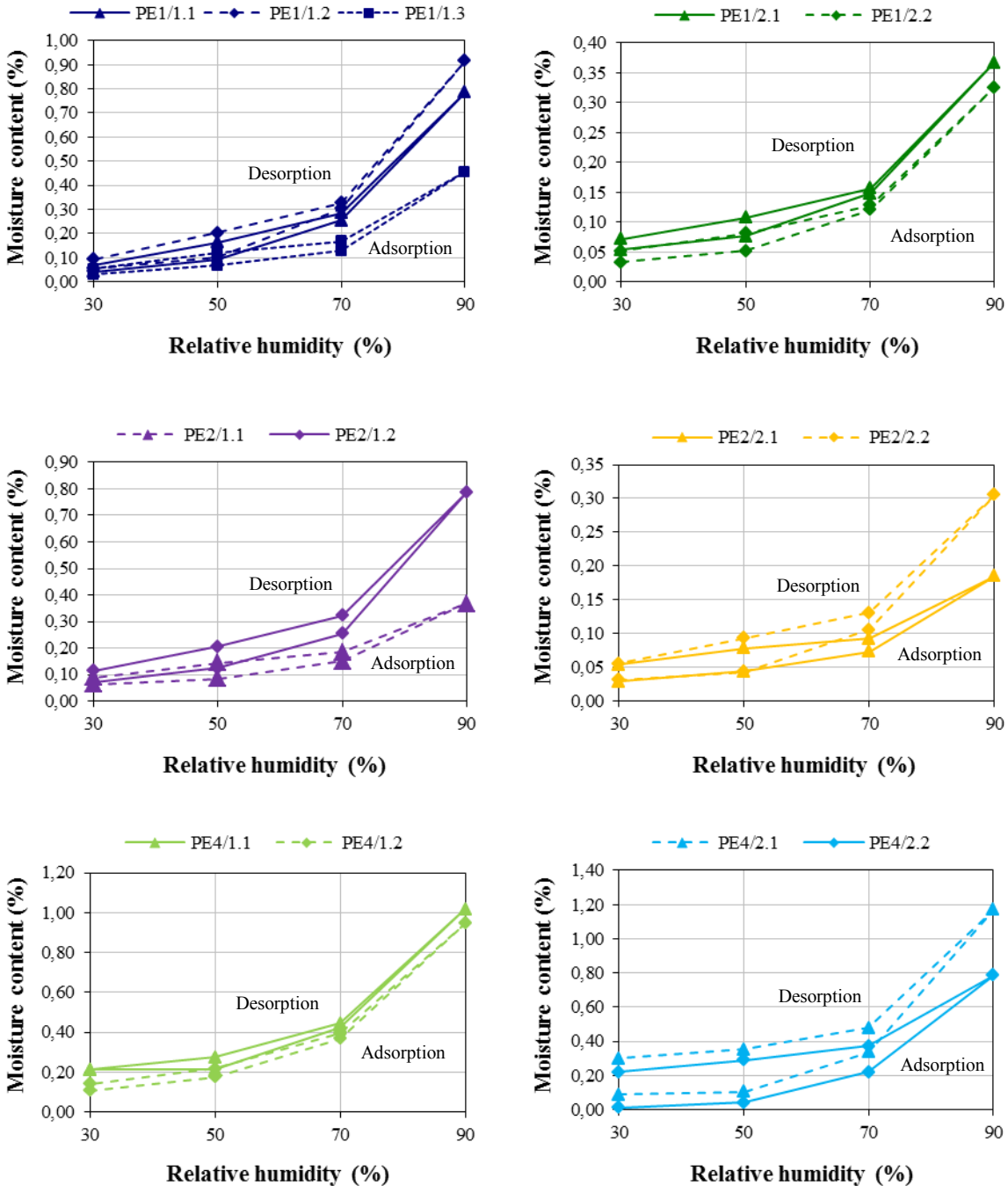

Figure 4.159 - Hygroscopic behaviour of the samples from *Estoi* Palace

A low and very regular hysteresis effect is observed in all the curves; in the case of PE4/2 it is higher.

Concerning the quantitative values of water adsorption at 90% relative humidity, they can only be compared in relative terms and in a set of samples belonging to the same case study.

Table 4.65 - Average hygroscopicity results of the samples from *Estoi* Palace (2010)

RH (%)	MC (%) PE1/1	SD	CV (%)	MC (%) PE1/2	SD	CV (%)	MC (%) PE2/1	SD	CV (%)	MC (%) PE2/2	SD	CV (%)
30	0.04	0.012	28.46	0.04	0.015	33.87	0.07	0.005	7.79	0.03	0.001	4.40
50	0.09	0.017	19.38	0.06	0.018	27.57	0.11	0.029	27.36	0.04	0.000	0.48
70	0.23	0.090	39.31	0.13	0.019	14.15	0.20	0.074	36.36	0.09	0.023	25.85
90	**0.72**	0.238	33.14	**0.35**	0.029	8.40	*	*	*	**0.25**	0.085	34.55
70	0.26	0.083	31.94	0.14	0.020	14.15	0.25	0.098	38.72	0.11	0.027	24.13
50	0.16	0.040	24.93	0.09	0.019	20.21	0.17	0.043	24.86	0.09	0.011	12.69
30	0.07	0.020	28.87	0.06	0.014	23.42	0.10	0.018	17.46	0.05	0.002	3.10

RH (%)	MC (%) PE4/1	SD	CV (%)	MC (%) PE4/2	SD	CV (%)	MC (%) PE5	SD	CV (%)
30	0.16	0.073	45.58	*	*	*	0.08	0.013	17.70
50	0.19	0.026	13.31	*	*	*	0.40	0.051	12.65
70	0.40	0.040	10.04	0.28	0.082	29.40	1.26	0.198	15.74
90	**0.98**	0.052	5.27	**0.98**	0.271	27.69	**3.57**	0.513	14.38
70	0.42	0.037	8.84	0.43	0.075	17.59	1.42	0.180	12.72
50	0.25	0.041	16.72	0.32	0.046	14.19	0.48	0.062	13.02
30	0.18	0.049	27.92	0.26	0.057	21.80	0.15	0.014	9.12

* Too high CV value precluding presenting the results; RH - relative humidity; MC - moisture content; TS - test specimens; SD - standard deviation; CV - coefficient of variation

In *Estoi* Palace, with the exception of samples PE1/2 and PE4/1, all the others showed some dispersion between test specimens. However, if only the highest values were considered in these cases, the results at 90% relative humidity could be grouped in pairs as follows:

- PE1/1 and PE2/1, respectively 0.72% and 0.79%;
- PE1/2 and PE2/2, 0.35% and 0.31%;
- PE4/1 and PE4/2, 0.98 and 1.17%.

Thus, the results are in agreement with previous statements that relate the hygroscopic behaviour to the composition/pore size distribution of the samples, namely that the gypsum-calcite plasters (PE1/1 and PE2/1) are more hygroscopic than the gypsum plasters (PE1/2 and PE2/2; PE4/1 is an exception) and that the hysteresis effect is usually more significant in the samples with highest content of pores with radii below 0.1 micron (PE4/2).

Water vapour permeability

The water vapour permeability was determined in three samples from *Estoi* Palace: PE1/1, PE4 and PE5. All had flat surfaces adequate to the test procedure and were available in sufficient quantity. The devices used are shown in Figure 4.160 and the results obtained are presented in Table 4.66.

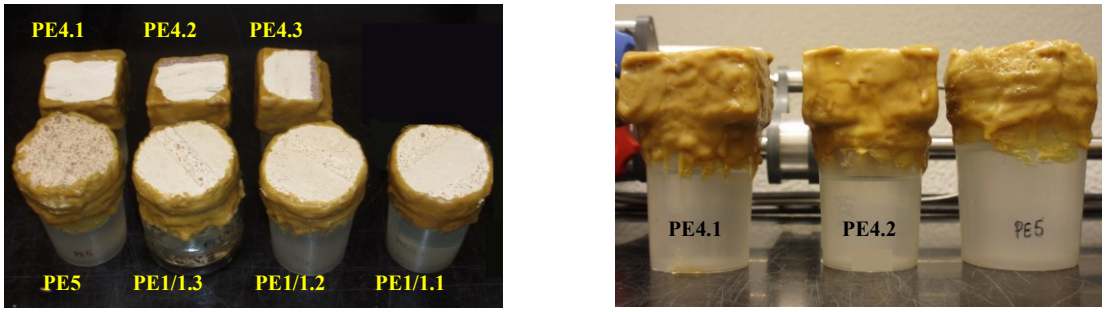

(a) (b)

Figure 4.160 - Water vapour permeability determination in samples from *Estoi* Palace: (a) and (b) different perspectives of the devices used (adapted to ancient samples)

Table 4.66 - Water vapour permeability results of samples from *Estoi* Palace

Sample (test specimens)	Thickness (d) (mm)	ΔM/24h (g)	Permeability ($ng.m^{-1}.s^{-1}.Pa^{-1}$)	Sd (d=10 mm) (m)
PE1/1 (3)	11.01	0.50	23.91	**0.074**
SD	0.53	0.04	4.03	0.013
CV (%)	4.77	7.62	16.84	17.50
PE4 (3)	27.26	0.07	13.03	**0.148**
SD	1.42	0.01	1.70	0.018
CV (%)	5.20	7.87	13.08	12.41
PE5 (1)	14.38 (5.01 plaster + 9.37 mortar)	0.47	25.85	**0.068**

SD - Standard deviation; CV - Coefficient of variation

The values found indicate that the water vapour permeability of the sample PE4 (i.e., PE4/1+PE4/2) is much lower than that of the most common gypsum plaster materials. This result was not a surprise and is in agreement with all the other properties determined in this sample where the influence of the PE4/2 layer has been noted: it contributed to reduce the capillary water absorption, the total porosity and the average pore radius and to increase the mechanical properties.

Regarding samples PE1/1 and PE5, they showed a water vapour permeability also lower than those of other samples of thin-layer finishing plasters tested with the mortar behind (PBS1, EG1) but still higher than EG4 and EBR1 and in the same range of values obtained in other studies of gypsum-lime

test specimens (Ramos et al. 2010: Sd = 0.059 m) and lime-based mortars formulations for restoration purposes prepared in laboratory (Veiga et al. 2010: Sd < 0.10 m; Margalha 2010: Sd = 0.05-0.12 m).

- Mechanical properties

Dynamic modulus of elasticity

The dynamic modulus of elasticity results are presented in Table 4.67 and the three different measurements made in sample PE4 are shown in Figure 4.161.

Table 4.67 - Dynamic modulus of elasticity results of the samples from *Estoi* Palace

Sample. .test specimen	Bulk density ($kg.m^{-3}$)	SD	CV (%)	Distance (m)	Time (μs)	SD	CV (%)	Speed ($m.s^{-1}$)	DME (MPa)
PE1/1	1599[(1)]	114	7.1	0.060	38.1[(3)]	0.3	0.8	1575	3568
PE1/2	969[(2)]	-	-	0.060	34.2	0.1	0.3	1752	2678
PE2/1.4	1171[(2)]	-	-	0.052	38.9	0.0	0.1	1337	1885
PE2/1.2	980[(1)]	23	2.4	0.048	38.2	0.4	1.1	1256	1391
PE2/2 (PE2.3)	1153[(2)]	-	-	0.052	29.2	0.1	0.2	1778	3282
PE4/1 (PE4.3)	925[(2)]	-	-	0.047	26.7	0.2	0.8	1758	2572
PE4/2 (PE4.2)	1908[(2)]	-	-	0.052	21.8	0.2	0.1	2381	9735
PE4 (PE4.1)	1558[(2)]	-	-	0.055	30.9	0.4	0.2	1778	4431
PE5 (PE5.1)	1766	-	-	0.097	64.0	0.2	0.4	1515	3646

[(1)] Sand method; [(2)] Water displacement method; [(3)] Measured at the surface (indirect method); SD - standard deviation; CV - coefficient of variation; DME - dynamic modulus of elasticity

(a) (b) (c)

Figure 4.161 - Determination of the dynamic modulus of elasticity of sample PE4: (a) PE4/1; (b) PE4 (=PE4/1+PE4/2); (c) PE4/2

The results obtained for the ultrasonic pulse velocity in the gypsum plaster samples were remarkably consistent with values between 1752 $m.s^{-1}$ and 1778 $m.s^{-1}$, except for sample PE4/2 (2381 $m.s^{-1}$), in line with its compact microstructure, very low porosity and high bulk density.

A narrow range of values was also observed in the gypsum-calcite samples with mortar behind (1515-1575 $m.s^{-1}$); the lowest results were those of the two test specimens of PE2/1 (1256 and 1337 $m.s^{-1}$), a moulded on site sample. Again it is observed that, in spite of having a similar bulk density to that of the common gypsum plaster samples (below 1200 $kg.m^{-3}$), PE2/1 has much lower values in all the mechanical properties, confirming that the composition/type of material is the most influential issue.

As in other case studies, the results of the ultrasonic pulse velocity, bulk density and dynamic modulus of elasticity of the samples with mortar behind were influenced by the latter, showing higher values than expected if only the plasters had been evaluated. That is the situation of sample PE5, where due to its high thickness the measurement was made by the direct method.

Compressive strength

The compressive strength results are presented in Table 4.68 and Figure 4.162 shows the samples that were tested.

Table 4.68 - Compressive strength results of the samples from *Estoi* Palace

Sample test specimen	Confinement mortar age (days)	Bulk density[(1)] ($kg.m^{-3}$)	Load rate ($N.s^{-1}$)	Maximum load (N)	Compressive strength (MPa)
PE1/2	20[(2)]	969	100	4200	2.63
PE2/1	20	1171	100	1763	1.10
PE2/2	20[(2)]	1153	100	2263	1.41
PE4/1	-	925	100	3569	2.23
PE4	-	1558	100	4260	2.66
PE5.2	20[(2)]	1766	100	4087	2.55
PE5.3	38[(2)]	1766	100	4987	3.12

[(1)] Water displacement method; [(2)] on both sides

The values obtained were comprised between 1.10 MPa and 3.12 MPa and they are in agreement with those of the other case studies.

In what concerns the gypsum plaster samples, only PE2/2 had a lower result than expected considering

its ultrasonic pulse velocity, the values obtained for the other gypsum plaster samples of the same case study (PE1/2 and PE4/1) and the result of the sample from the *Mirhab* of the old Mosque of *Mértola* (3.5 MPa, Veiga 2012), already referred. This could be due to its irregular shape (although PE1/2 is in the same conditions), the presence of any cracks inside the structure, etc.

Contrarily, the presence of mortar behind the test specimens of PE5 must have increased its strength.

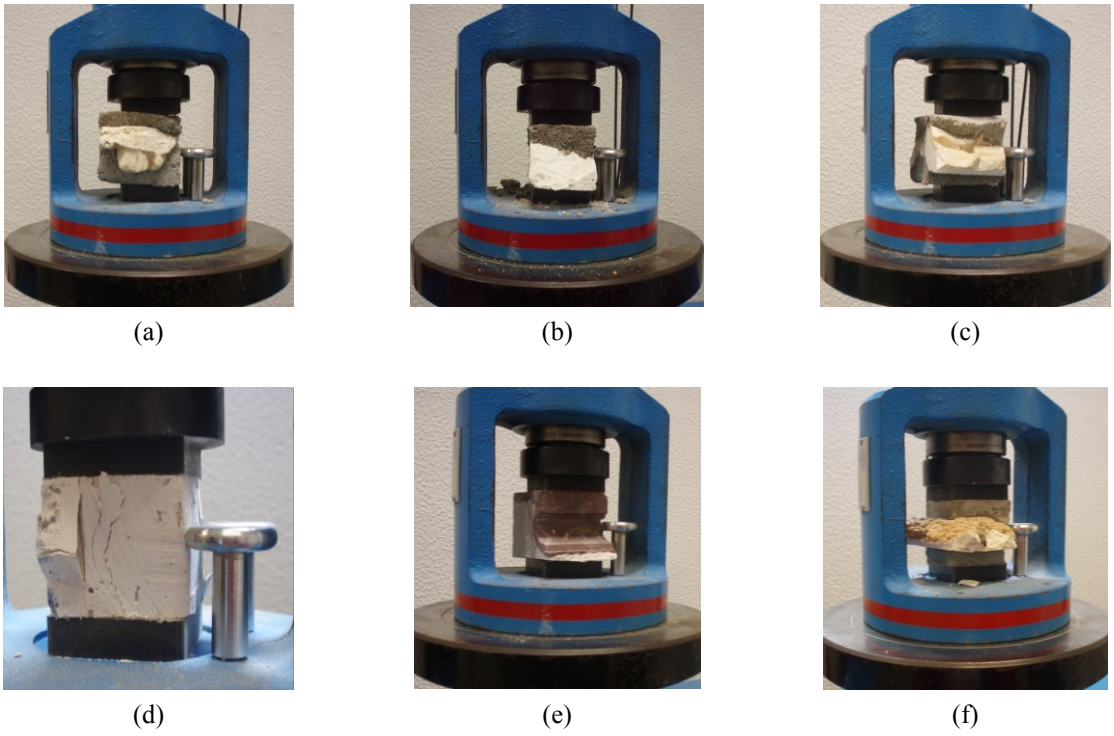

(a) (b) (c)

(d) (e) (f)

Figure 4.162 - Compressive strength tests: (a) PE1/2, (c) PE2/2 and (f) PE5, all with two layers of confinement mortar; (b) PE2/1 with one layer of confinement mortar; (d) PE4/1 after failure; (e) PE4

4.3.4 The first quarter of the 20th century

4.3.4.1 The *Fafe* Cine-Theatre building

Built in 1923 and opened the following year, the *Fafe* Cine-Theatre is one of the most emblematic buildings of the city of *Fafe* mainly due to the decorative paintings and *grafitos* of neoclassic roots that entirely cover its front façade (Figure 4.163 (a) and (b)).

The interior decoration of some areas is very simple (Figure 4.163 (c)) and contrasts with the great sophistication observed in the auditorium and noble spaces (Figure 4.163 (d) to (f)).

In 1960 the theatrical performances finished there but the space continued working as a cinema until 1981, when it was finally closed for security reasons due to its poor condition. In 2001 it was acquired by the Municipality of *Fafe* and opened again its doors in 2009, totally restored (Carvalho n.d.).

(a)

(b)

(c)

(d)

(e)

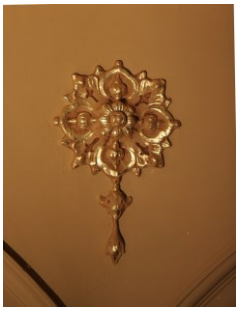

(f)

Figure 4.163 - *Fafe* Cine-Theatre: (a) view of the front façade, covered with *grafitos* (image taken from http://criariqueza.blogspot.pt/2009/06/blog-post_7865.html); (b) detail of the façade decoration; (c) and (d) restoration works ongoing; (e) and (f) details of some ornaments, before and after restoration, respectively

Samples

Two samples were collected in two different ways: one consists of three ornaments that have been previously detached due to anomalies in the building and the other is a fragment of a smooth surface wall plaster collected directly on site (Figure 4.164).

Figure 4.164 - Collection of a sample from the plaster coating of a wall of the *Fafe* Cine-Theatre building

The images of the samples are shown in Figure 4.165 and the corresponding identification and description are presented in Table 4.69.

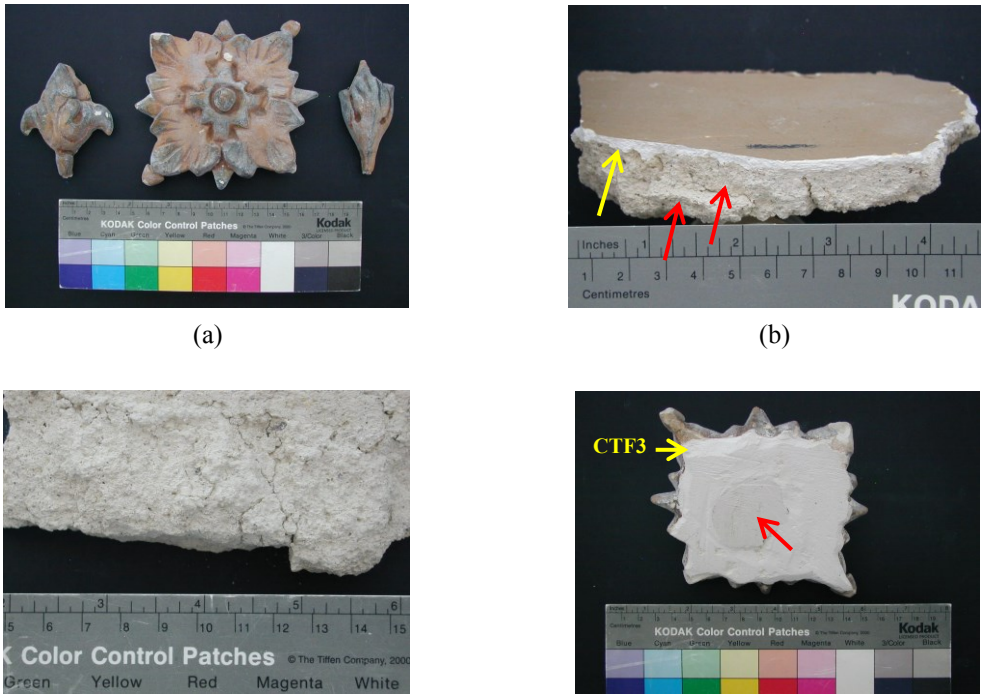

(a) (b)

(c) (d)

Figure 4.165 - Photographs of the analysed samples from *Fafe* Cine-Theatre building: (a) CTF1; (b) side view of CTF2 showing the mortar (red arrows) and the finishing plaster layer (yellow arrow); (c) back view of CTF2 showing the cracks in the mortar; (d) back view of CTF1 showing the sample CTF3 and the beige coloured paste embedded in it (red arrow)

Table 4.69 - Identification and description of the samples from *Fafe* Cine-Theatre building

Sample identification	Description
CTF1	Ornaments (polychromic)
CTF2	Wall plaster (polychromic)
CTF3	Plaster bonding layer, used to fix the ornaments (CTF1) to the walls

Results and discussion

- Visual observation of the samples

The information obtained by the visual observation of the samples is summarized in Table 4.70.

Table 4.70 - Visual observation of the samples from *Fafe* Cine-Theatre building

Sample	Description
CTF1	Three **precast ornaments** with a brown paint applied directly on the plaster (Figure 4.165 (a)) The borders and the most protruding areas of the relieved decorations, originally gilded, were darker than the rest of the surfaces. After gently scraping one of them with a scalpel it could be observed that, in fact, they were green; The plaster of the ornaments was considered to be made of two different layers: a white part, corresponding to the interior of the ornaments, designated as CTF1A and a yellowish part situated closer to the surface, immediately below the painted layer, CTF1B.
CTF2	Smooth surface **wall plaster** painted in brown, like CTF1 (Figure 4.165 (b)); The plaster was very white, had 4-5 mm thickness and seemed to be made of one single layer**;** The paint was not applied directly on the plaster (its surface had what appears to be a key-coat, shellac type); The beige-grey mortar behind the plaster seemed to have been applied in two layers, had an average thickness of 25 mm and many cracks (Figure 4.165 (c)).
CTF3	In the back side of the ornaments (sample CTF1) there was a **plaster layer** probably used **to fasten the elements** to the wall. It was considered to be an independent sample and was analysed separately (Figure 4.165 (d)); Part of this layer had a rounded shape beige coloured paste embedded with some fibres mixed whose function was not clarified.

The plaster of the precast ornaments corresponding to sample CTF1 seems to be made of two layers of distinct materials, exactly as in samples PE1/2 and PE2/2. However, similarly to the samples of *Estoi* Palace, the difference in colour in the first millimetres of plaster was due to the absorption of the product applied as paint. In fact, the thickness of the external layer is so low and irregular that it would be difficult to obtain by the precast technique. It is more logical that the plaster is all the same and the differences observed are due to the phenomenon of absorption. Nevertheless, the two areas of the interior of the ornaments were given a different designation (A and B) and were analysed separately by XRD and TG-DTA.

On the contrary, in sample CTF2 a layer of what seems to be a key-coat can be seen behind the paint and the plaster had no absorption whatsoever, and was very white coloured.

- XRD results

The qualitative mineralogical composition of the samples was determined by XRD and the results obtained showed that gypsum and calcite are the main constituents (Figure 4.166 and Table 4.71).

Besides the very common quartz and feldspar impurities, traces of other compounds that rarely appear or did not appear at all in the other case studies, like talc, illite, weddellite, magnesite, kaolinite and portlandite were detected:

- Weddellite is a mineral form of calcium oxalate that results from biological colonization;
- Talc and kaolinite are probably related to the paints where they can be used as fillers;
- Magnesite is an impurity that can be associated to the raw materials (both gypsum and calcite);
- The presence of portlandite (hydrated lime) was only detected in the sample CTF2. Considering that it is a thin-layer plaster, where the carbonation is usually easier and faster than in other lime-based mortars with a higher thickness and/or located in a more interior position in the building, that is somehow an unexpected result. However, it can be due to the precocious painting of the surfaces, which reduces considerably the porosity and, consequently, the exchanges of water vapour and carbon dioxide of the wall with the surrounding environment.

In what concerns dolomite, in spite of being detected in all the samples analysed, its presence is more significant in those with higher contents of gypsum (CTF1A and CTF1B) (Table 4.71). Considering that it is a common impurity of the gypsum deposits, this means that it comes associated with the raw material used, though in this case in a higher percentage than usual.

These samples from the Cine Theatre building, particularly CTF1A and B and CTF3, were the worst to mill and sieve of all: they formed a very fine powder that clung to the laboratory material (mortar and sieve) and was very difficult to prepare for XRD and TG-DTA analysis. This behaviour can be due to the presence of talc, a soft material that is easily transformed into a very fine powder and tends to cling to the objects.

Finally, it is important to highlight once again that the samples with more gypsum, or even prepared exclusively with this material (like CTF1A and CTF1B), are those that correspond to precast elements. The thin-layer plasters always have calcite in their composition, as in the case of CTF2 and CTF3, i.e. a mix of gypsum and hydrated lime has been used in their preparation.

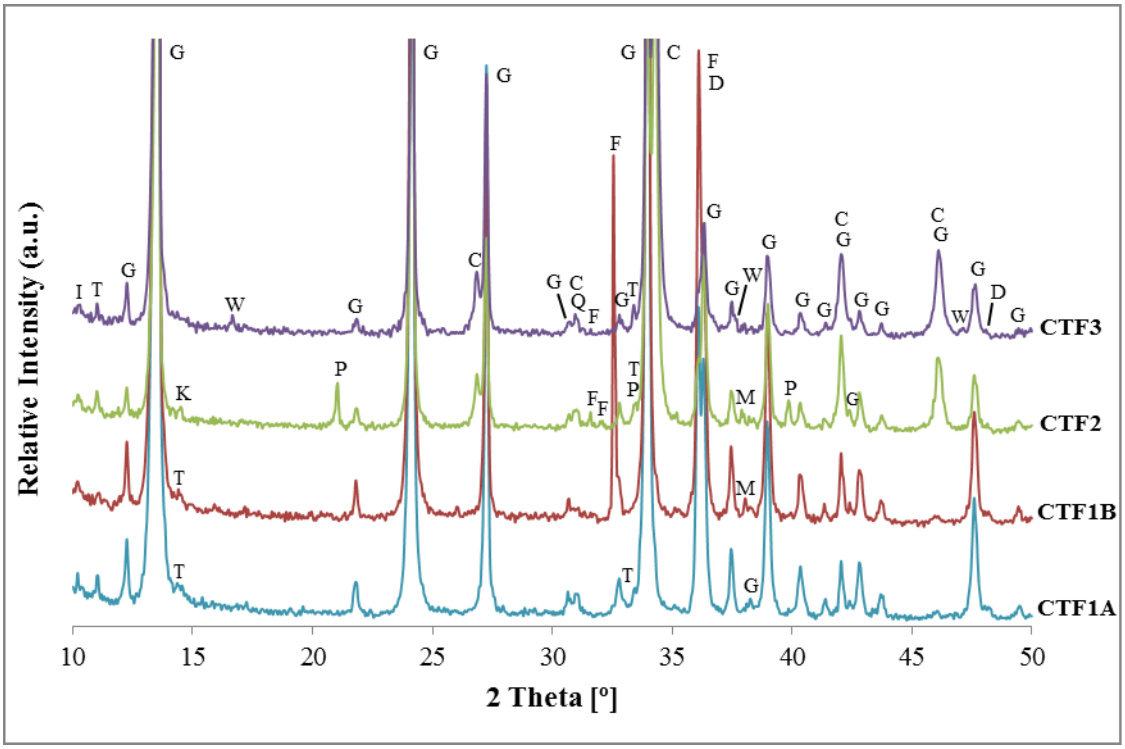

Figure 4.166 - XRD patterns of the samples from *Fafe* Cine-Theatre building
Notation: G - Gypsum; C - Calcite; Q - Quartz; D - Dolomite; F - Feldspar; M - Magnesite; K - Kaolinite; I - Illite; W - Weddellite; T - Talc; P - Portlandite

Table 4.71 - XRD qualitative mineralogical composition of the samples from *Fafe* Cine-Theatre building

Sample	Identified crystalline compounds						
	Gypsum	Calcite	Quartz	Dolomite	Talc	Feldspars	Others
CTF1A	++++	trc	trc	+	trc	-	Illite (trc)
CTF1B	++++	-	trc	+	trc	trc+	Magnesite (trc) Illite (trc)
CTF2	+++	++/+++	trc	trc	trc	trc	Magnesite (trc) Portlandite (trc) Kaolinite (trc) Illite (trc)
CTF3	++/+++	++/+++	trc	trc	trc	trc	Weddellite (trc) Illite (trc)

Notation used in XRD peak analysis:

++++	Very high proportion (predominant compound)	+	Weak proportion
+++	High proportion	trc	Traces
++	Medium proportion	-	Not detected

- TG-DTA results

The gypsum and calcite content was determined using TG-DTA analysis and the results of XRD could be confirmed (Table 4.72 and Figure 4.167).

Table 4.72 - Weight loss and calculated gypsum / calcite contents of the samples from *Fafe* Cine-Theatre building

Sample	Temperature range (ºC)						Calculated contents (%)	
	25→85	85→250	250→600	600→850	850→1000	Loss of ignition	Gypsum	Calcite
CTF1A	0.1	19.1	0.8	1.9	0.0	21.9	91	4
CTF2	0.2	11.6	1.2	17.2	0.4	30.6	55	39
CTF3	0.2	10.4	1.3	21.0	0.3	33.2	50	48
				600→800	800→1000			
CTF1B	0.1	18.5	2.9	4.1	5.2	30.8	89	9

The doublet of peaks corresponding to the two steps of dehydration of gypsum is visible in all the DTG and DTA curves of Figure 4.167. However, in sample CTF1B the intensity of the peaks is inverted and they are not as well defined as usual in samples with similar amounts of this compound, namely CTF1A. Such difference may be due to the absorption by CTF1B of some substances from the paint which, in turn, can originate weight losses in the same temperature ranges of the other components usually present.

In what concerns the decomposition of carbonated compounds, the presence of dolomite is represented in the TG and DTG curves of CTF1B but not in CTF1A. In the first case, it occurs at temperatures close to those of calcite, though lower and clearly distinct; in CTF1A this transformation was not observed, possibly due to its low content of carbonates.

In the contrary, the decarbonation of calcite occurred as expected, with the maximum above 800 ºC in the samples with higher contents of this compound - CTF2 and CTF3 - and around 750 ºC in CTF1A and B, where the quantity is much lower. These results are in agreement with those obtained in almost all the samples analysed during this research study.

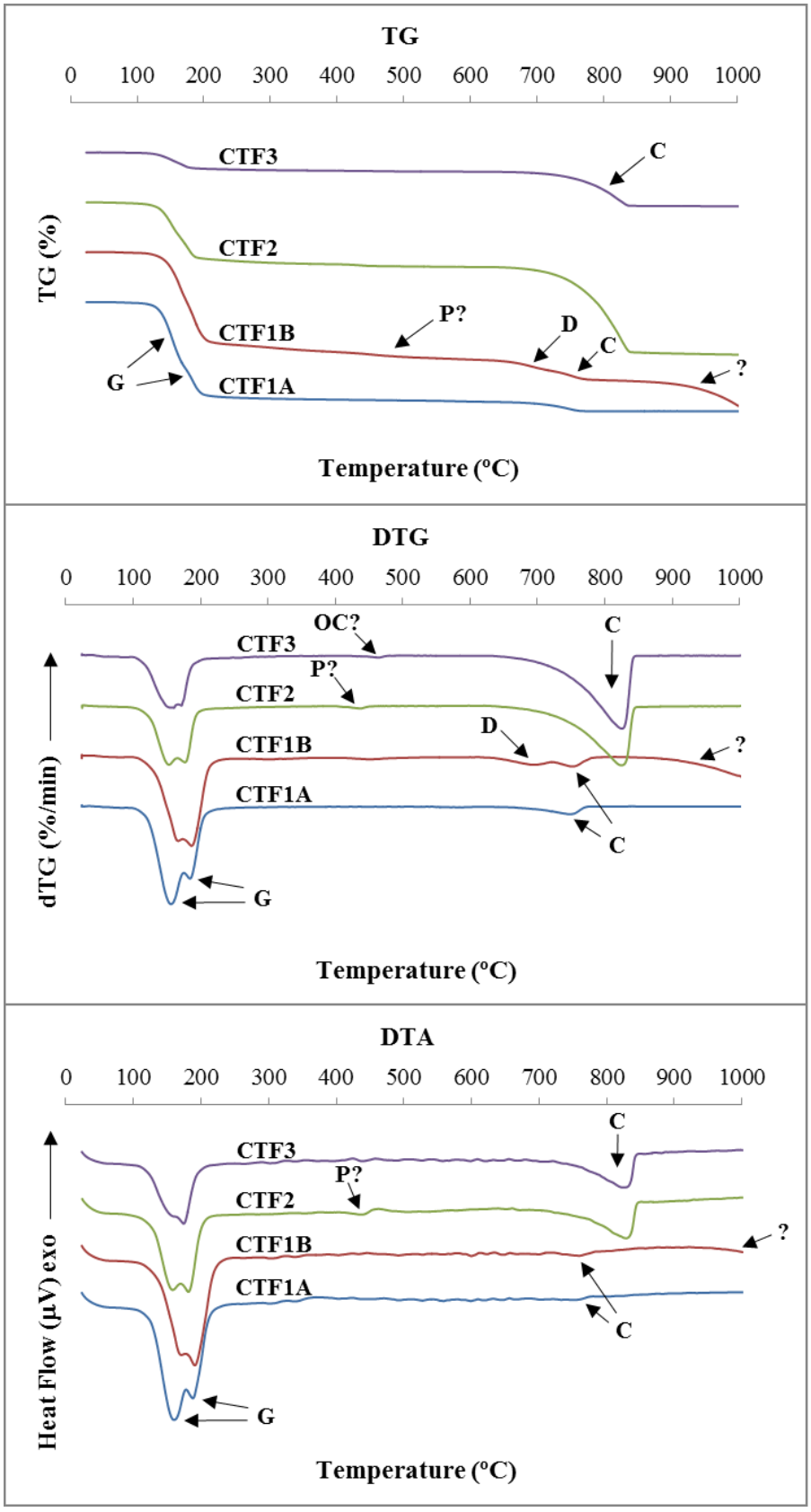

Figure 4.167 - TG, DTG and DTA curves of the samples from *Fafe* Cine-Theatre building
Notation: G - Gypsum dehydration; D - Dolomite decarbonation; C - Calcite decarbonation; OC - Organic compounds; P - Portlandite

The CTF1B curves have other uncommon features associated (Figure 4.167), namely:

(a) A loss of weight around 500 ºC, though oddly not visible in the respective DTG and DTA curves;
(b) The continuous loss of weight after 800 ºC, until the end of the analysis (1000 ºC).

Identical observations have been previously made in samples PB1/3 from *Bolsa* Palace and PE1/2 and PE2/2 from *Estoi* Palace where the presence of organic compounds was also almost guaranteed, and is the most plausible explanation for such behaviour.

The phase change of soluble to insoluble anhydrite is not clearly represented in the DTA curves of the samples with greater amounts of gypsum (CTF1A and B) though in the case of CTF1A a not very well defined exothermic peak between 350 ºC and 400 ºC seems to be present (Figure 4.167).

Another important observation is the small weight loss that occurs between 400 ºC and 450 ºC in sample CTF2, which is probably associated to the dehydroxylation of portlandite (Adams et al. 1998).

- Physical properties

Capillary absorption

The water absorption by capillarity was evaluated in sample CTF2 (Figure 4.168) and the quantitative results are summarized in Table 4.73.

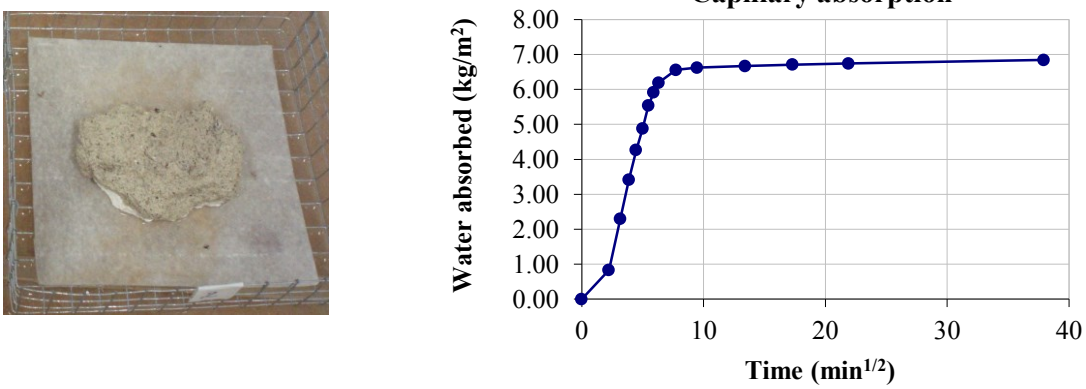

(a) (b)

Figure 4.168 - Water absorption by capillarity of the sample CTF2: (a) test specimen CTF2 during the determination; (b) graphical representation of the results.

Table 4.73 - Capillary absorption by contact results of sample CTF2

Test specimen	
Surface (cm^2)	27.45
Weight (g)	93.87
Capillary absorption at 5 min:	
(g)	2.29
($kg.m^{-2}$)	**0.83**
(%, relative to weight of sample)	2.44
(%, relative to total absorption)	12.20
Capillary absorption at 24 h:	
(g)	18.78
($kg.m^{-2}$)	**6.84**
(%, relative to weight of sample)	20.00
Ccc at 5 min ($kg.m^{-2}min^{-1/2}$)	**0.37**

Ccc - capillarity coefficient by contact

The curve represented in Figure 4.168 (b) shows that the capillary water absorption of the sample CTF2 was low in the first five minutes. After that, it increased and maintained a quite regular rate during thirty minutes, when it started to slow down again (at 5.92 $min^{1/2}$).

This initial behaviour is typical of a plaster with a surface treatment (key-coat, paint, etc.) that usually works as a barrier to the water. In fact, as referred in the "Visual observation" section, a preparation product, shellac type, had been applied to the surface of CTF2 before the paint.

After that barrier, the absorption evolved according to the gypsum-calcite composition of the sample: the absorption rate corresponding to filling the larger pores (considered to have r > 0.5 micron) was higher and was then followed by slower filling the smaller ones, a behaviour typical of a bimodal pore size distribution curve; the total absorption was not very high.

The loss of the water absorbed in the capillarity test was also evaluated and is represented in Figure 4.169. It shows a first period of drying inertia typical of a quite compact internal structure, followed by a quick loss of water (larger pores) and then a much slower one, corresponding to the release of the water more tightly connected to the smaller pores. So, the drying behaviour can be considered to be in agreement with the respective capillary absorption.

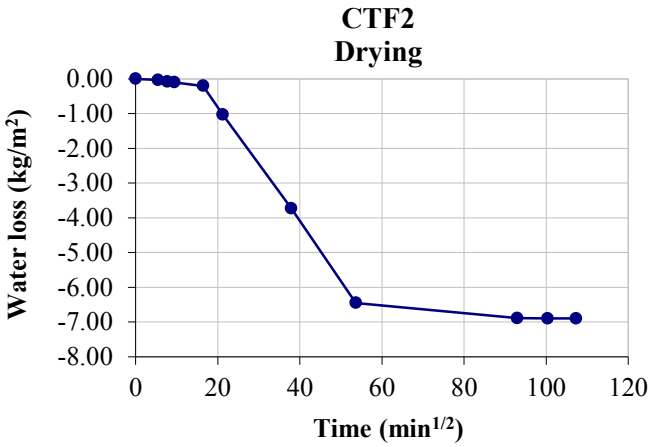

Figure 4.169 - Graphical representation of the drying behaviour of the samples from *Fafe* Cine-Theatre

Water vapour permeability

The water vapour permeability was also determined in sample CTF2. The device used is shown in Figure 4.170 and the results obtained are presented in Table 4.74.

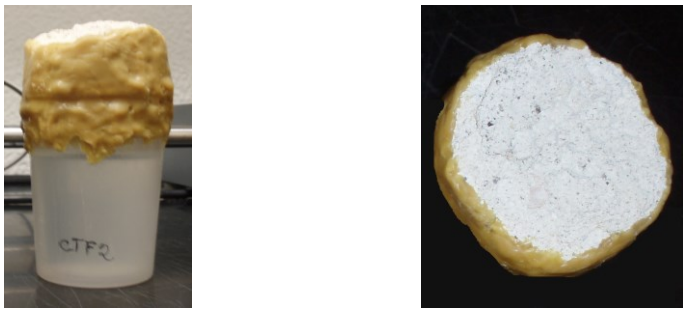

(a) (b)

Figure 4.170 - Water vapour permeability determination in sample CTF2: (a) device used; (b) view of the back surface of the sample (mortar layer)

Table 4.74 - Water vapour permeability results of sample CTF2

Sample	Thickness (d) (mm)	ΔM/24h (g)	Permeability ($ng.m^{-1}.s^{-1}.Pa^{-1}$)	Sd (d=10 mm) (m)
CTF2	24.63 (4.45 plaster + 20.18 mortar)	0.32	30.14	**0.061**

The value found indicates that sample CTF2 has a good permeability to water vapour, in total agreement with those of other samples with a similar thin-layer plaster composition and a layer of mortar behind (PM4, PE5). In spite of having a lower capillary absorption than other samples, its good drying behaviour denoted a well-connected open porosity that is, in turn, usually related to a good water vapour diffusion capacity.

- Mechanical properties

Dynamic modulus of elasticity

The dynamic modulus of elasticity was determined in the sample CTF2 and the results obtained are shown in Table 4.75.

Table 4.75 - Dynamic modulus of elasticity results of sample CTF2

Sample	Bulk density[(1)] ($kg.m^{-3}$)	SD	CV (%)	Distance (m)	Time (μs)	SD	CV (%)	Speed ($m.s^{-1}$)	DME (MPa)
CTF2	1356	-	-	0.075	40.8[(2)]	0.6	1.4	1838	4124
CTF2	1356	-	-	0.075	78.2	0.6	0.8	959	1123

[(1)] Calculated: weight / (area of the base x height); [(2)] Measured at the surface; SD - standard deviation; CV - coefficient of variation; DME - dynamic modulus of elasticity

As the plaster layer was thick enough, the measurement of the ultrasonic pulse velocity was made in two ways, for comparison purposes: on the surface of the plaster (indirect method); with the probes positioned at the ends of the plaster layer (direct method).

The results are different and show that the direct measurement is more influenced by the mortar characteristics, as expected. In this case, however, the detected cracks decreased significantly the value obtained. Exactly the same observation was made in sample PM4 where both types of measurements were also performed, although in that case the hardness and cohesiveness of the mortar contributed to increase the result (Table 4.47).

4.3.4.2 The *Garage* building

The *Garage* building is situated in the city centre of Leiria. It was built in the first decade of the 20th century (1908) under a project of *Augusto Romão* following the *Art Nouveau* architectonic style (Figure 4.171), extremely rare in Portugal (Verdelho da Costa 1989). It owes its name to a detail in one of the façades (Figure 4.171 (c)).

The interior plaster decoration was very simple and was destroyed in 2008 during the "restoration" works that transformed the building, a former dwelling house of one family, into several apartments and a commercial area (Figure 4.172 (a)). The beautiful stone and ceramic tiles'work of the façades were the only claddings preserved from the original construction, as the mortars have also been removed (Figure 4.172 (b)).

(a)

(b)

(c)

Figure 4.171 - *Garage* building: (a) general view; (b) and (c) details of the façades showing the *Art Nouveau* architectonic style

(a)

(b)

Figure 4.172 - *Garage* building "restoration" works: (a) removal of an interior wall coating; (b) detail of a façade showing the new cement based renders applied and a part of the masonry still uncoated

Samples

The samples were collected directly on site during the process of removal of the interior coatings. In a room of the second floor, there was a wall with a wood frame dividing two differently coloured plaster surfaces, with the apparent intention of creating a kind of "plaster wainscot" in the lower part (Figure 4.173 (a)). From this wall three samples were collected, in order to see whether there was any difference in their composition.

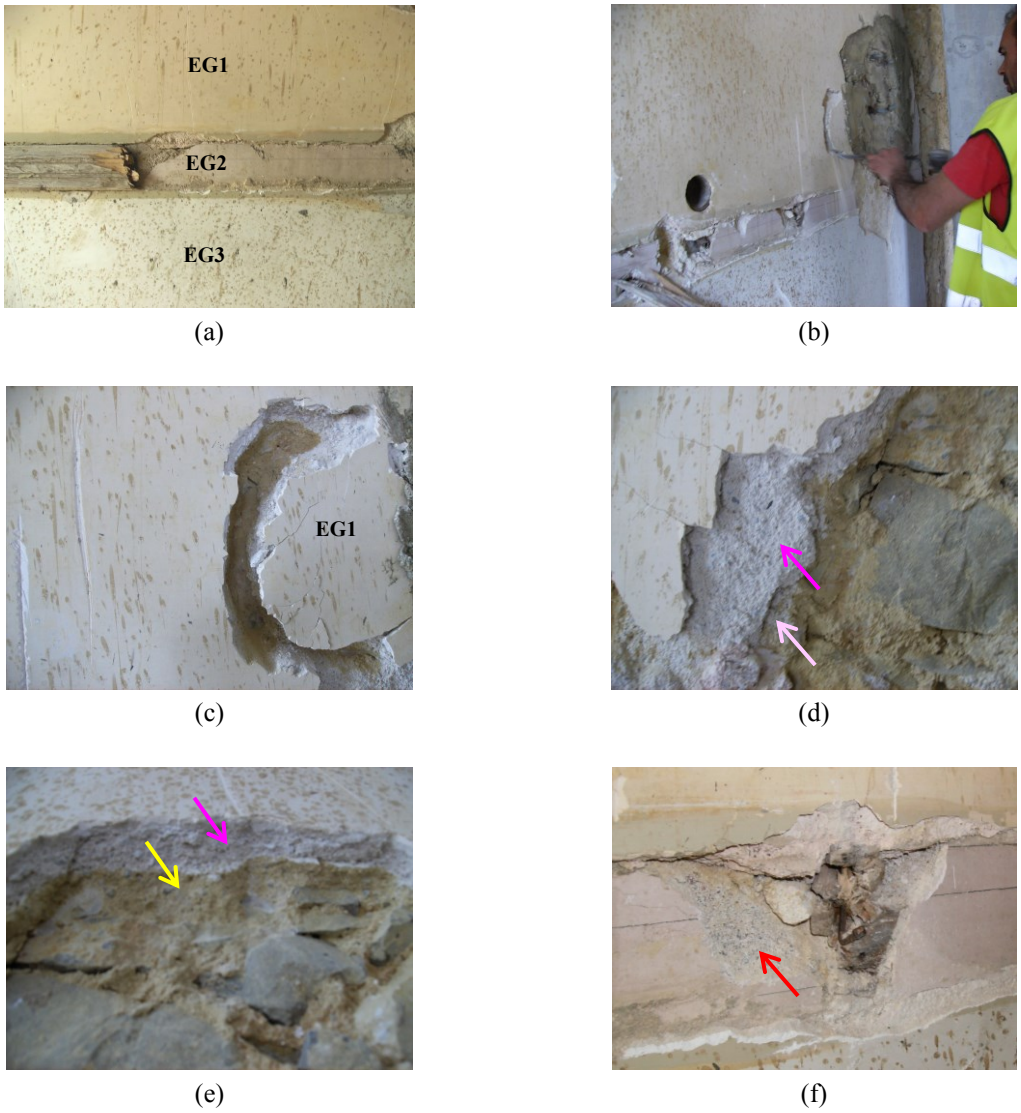

Figure 4.173 - Collection of samples in *Garage* building: (a) wall with three different plaster surfaces corresponding to one sample each; (b) process of collection of a sample; (c) detail of the sample before detachment; (d) a third layer of mortar in an area of the wall where it was light pink, applied directly over the masonry (light pink arrow); (e) the third layer of mortar in an area of the wall where it was roasted yellow (yellow arrow); (f) mortar layer behind EG2 where black aggregates can be observed

Besides the layers of mortar present in the samples collected, there was still another layer, used to even the surface of the masonry, that in some parts of the wall was light pink (Figure 4.173 (d),) and in other parts it was roasted yellow and even had coarser aggregates (Figure 4.173 (e)); this layer was probably made with masonry mortar.

The identification and description of the samples is presented in Table 4.76 and the corresponding images are shown in Figure 4.174 and Figure 4.175.

Table 4.76 - Identification and description of the samples from *Garage* building

Sample identification	Description
EG1	Wall plaster (polychromic), room of the second floor
EG2	Low relief wall plaster from the same wall as EG1 where a wood frame was fastened (polychromic)
EG3	Wall plaster (polychromic), room of the second floor
EG4	Wall plaster (polychromic), room of the first floor
EG5	Preparation layer (EG5/1) and decorative frame (EG5/2) from the top of the same wall as EG4

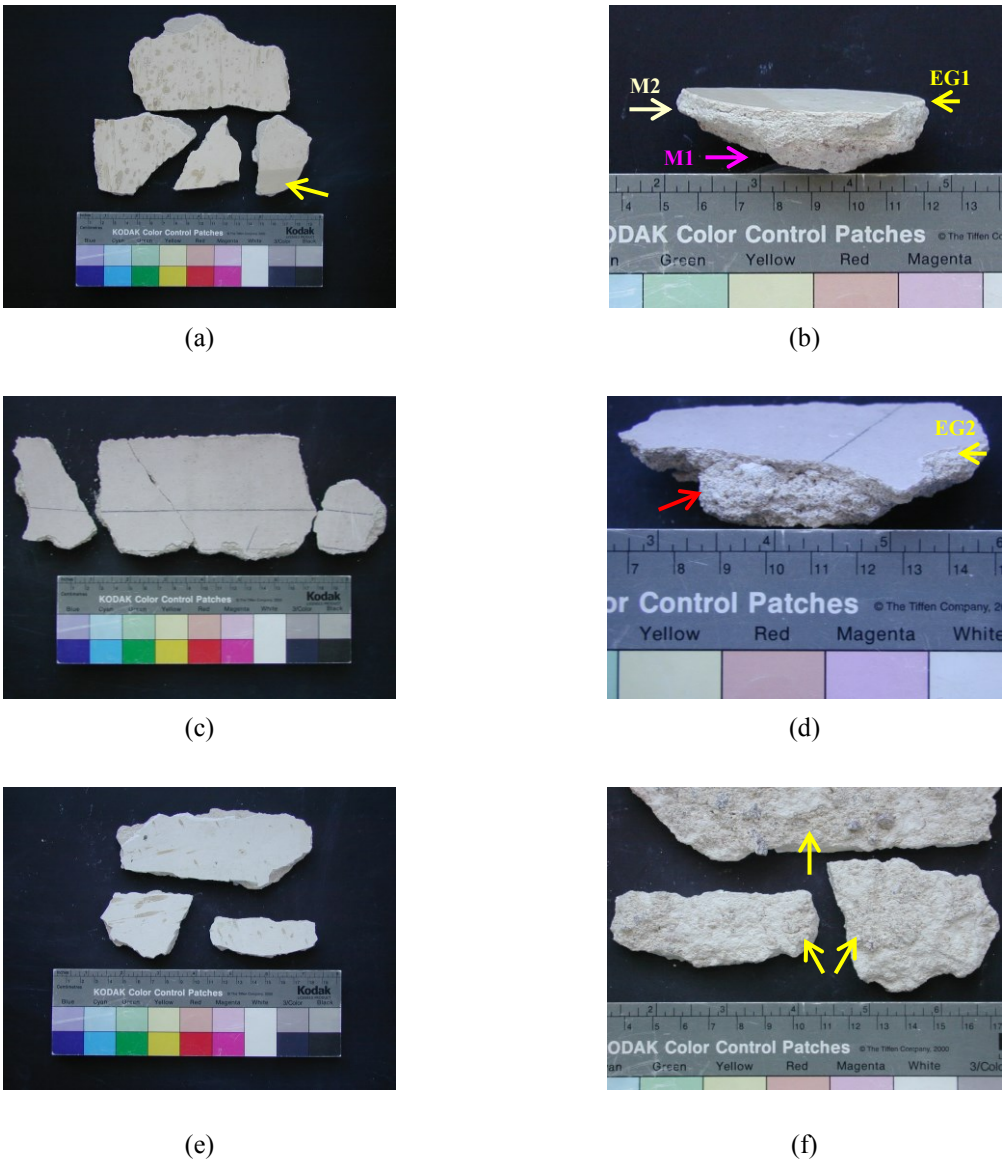

(a) (b) (c) (d) (e) (f)

Figure 4.174 - Photographs of samples from the *Garage* building: (a) EG1; (b) side view of a fragment of EG1 showing a coarser mortar (M1), a finer mortar (M2) and the finishing plaster layer (EG1); (c) EG2; (d) side view of EG2 showing the only mortar layer and the plaster layer; (e) EG3; (f) back view of EG3 showing the parts where the coarser mortar is still stuck to the finer mortar layer (yellow arrows)

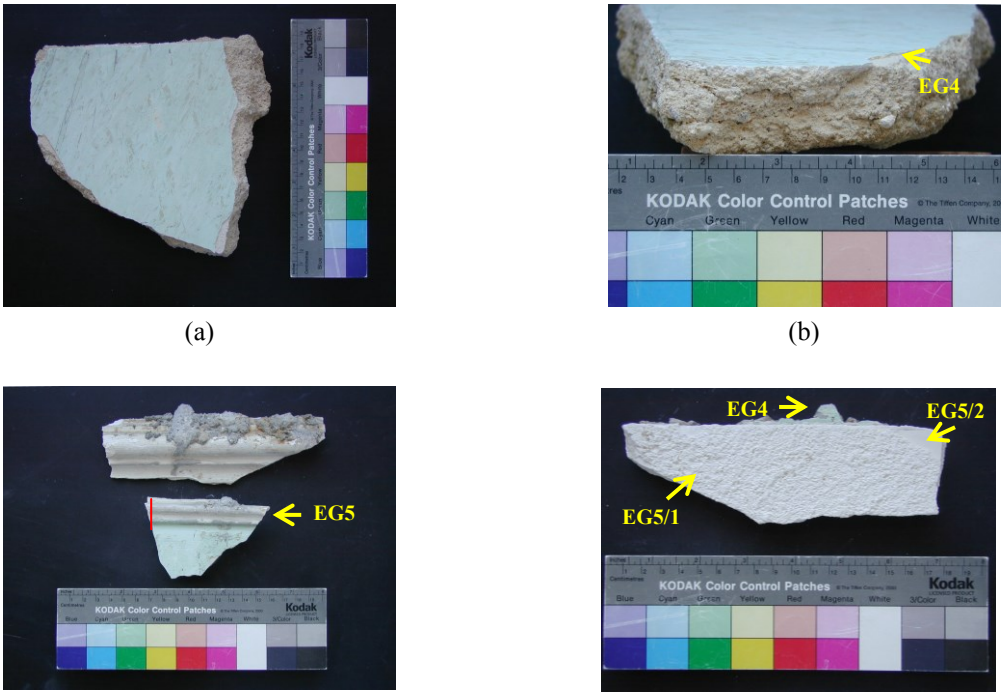

(a) (b)

(c) (d)

Figure 4.175 - Photographs of samples from the *Garage* building: (a) EG4; (b) side view of EG4 where the disparity between the thickness of the mortar and of the plaster is highlighted; (c) EG5 (red line corresponds to the area of the polished surface cross section view of Figure 4.176 (d)); (d) back view of the top fragment of (c) with the various layers/samples identified

Results and discussion

- Visual observation of the samples

The information obtained by the visual observation of the samples is summarized in Table 4.77.

It is interesting and important to notice that the set "mortar + plaster" was more coherent in samples EG1, EG2 and EG3 than in EG4. This is due to the global quality of the mortar layers associated, better in the first three samples than in the fourth. In those samples the use of higher binder contents and/or of higher pureness, together with the addition of very hard aggregates (probably basalt), seem to be plausible explanations.

The application procedure of a mortar is another issue that plays an important role in its final mechanical characteristics. The observation of the cross-sectional polished surface of the sample EG1 showed that the adhesion between all layers is perfect (Figure 4.176 (b)), with no traces of voids or cracks, which is no doubt influenced by a proper application procedure.

Table 4.77 - Visual observation of the samples from *Garage* building

Sample	Description
EG1	Several fragments of a light yellow pigmented **smooth surface thin-layer plaster** (1-3 mm). It had some small white nodules inside, probably due to the agglomeration of hydrated lime in the fresh paste, originating an heterogeneous mixture between the pigment and the paste; It was painted in the same colour of the plaster and had a frieze close to the wood frame with a more pronounced hue (Figure 4.174 (a), yellow arrow). The paint seemed to be lime-based, with a good penetration into the plaster (probably the origin of its colour) and no formation of any kind of pellicle; Behind the plaster there were two different mortar layers (Figure 4.174 (b)): - The first one, more interior (M1), had an irregular thickness and was in some areas light pink and in others beige. It had coarse aggregates (4-6 mm) of several colours (transparent, white, brown, pink, …) and shapes (Figure 4.176 (a)); - A second one, beige, applied over the pink mortar (M2, Figure 4.176 (a)), with greater cohesion and finer aggregates. A small part of the aggregates was black, very tough and very difficult to grind (basalt? Figure 4.176 (a) and (b)). It had a thickness of approximately 6-8 mm.
EG2	Several fragments of a light pink, very thin (approx. 1 mm) and very tough **smooth surface thin-layer plaster**; It had only one layer of mortar behind, of the same beige colour as the one immediately behind the plaster sample EG1, though with significantly coarser aggregates (Figure 4.174 (d), red arrow). Part of those aggregates were also black coloured (Figure 4.173 (f), red arrow), tough and difficult to grind. The surface of the plaster had a black line made with charcoal, probably to mark the correct position of application of the wood frame (Figure 4.174 (c) and (d)).
EG3	Several fragments of a very light beige coloured **smooth surface thin-layer plaster** (1-3 mm); It was painted in the same colour (Figure 4.174 (e)) with a paint that seemed to be lime-based. Like in EG1, it was probably the absorption of the paint that coloured the plaster; Behind the plaster, there were also two mortar layers exactly with the same characteristics as those of EG1 and described above. However, in this case, the fragments collected had much less quantity of the coarser mortar still attached (Figure 4.174 (f), yellow arrows).
EG4	One fragment of a very hard **smooth surface thin-layer plaster** (1-2 mm thick) painted in green; During the grinding of the sample for XRD and TG-DTA analysis it was observed that the plaster, initially seemingly white, had a very light green colour. Later, in the stratigraphic analysis of the sample EG5, the presence of small blue particles was detected in EG4 and was more probably due to a pigment addition in the paste than to its absorption from the paint (Figure 4.176 (d) to (f)); The paint did not seem to be lime-based, as in EG1 and EG3, and has a more "synthetic" appearance; Behind the paint, the surface of the plaster was beige and had a waxed look, probably due to the application of a product that worked as a key-coat. It was very hard and it was strongly attached to the base. The scalpel slipped on it and it was very difficult to remove; Under the plaster there were two layers of a beige coloured mortar (almost yellow) with a clayey appearance, about 20 mm thickness each. Its aggregates were similar in size to the first layer of mortar of the samples EG1 and EG3 but it presented a much lower coherence; The interface between both layers was full of voids, indicating they have not been pressed hard during application, which can be one of the causes for their lower coherence.

EG5	Two fragments of a white **decorative frieze moulded directly on site** and painted in beige (Figure 4.175 (a)); This sample can be divided in two (Figure 4.174 (d) and Figure 4.176 (d)): - EG5/1, the beige plaster layer behind the moulded elements, with 1-2 mm thickness, very friable and cracked; - EG5/2, the moulded frame *per se*; EG5/1 had still some aggregates attached, i.e. it was applied directly over the mortar behind; It was very easy to separate EG5/1 from EG5/2, making it difficult to understand whether the first was a plaster bonding layer used to fix precast decorative elements to the wall, or whether it was an extension of EG4 over which the frieze had been directly moulded; This issue could only be clarified by stratigraphic analysis which indicated that EG5/2 was moulded on site (Figure 4.176 (c) to (e)) and that EG5/1 was a preparation layer, not an extension of EG4.

On the contrary, in the case of EG4 the naked eye observation was enough to detect the presence of many voids in the interface of the two mortar layers, meaning they have not been pressed sufficiently hard during their application on the wall. The high thickness of both has surely contributed negatively to that.

Another reason for this lack of coherence of the mortar of EG4 can be the nature of the aggregates used, either in terms of hardness, or in terms of impurities (e.g. its yellow colour can be due to the presence of clay minerals in the sand).

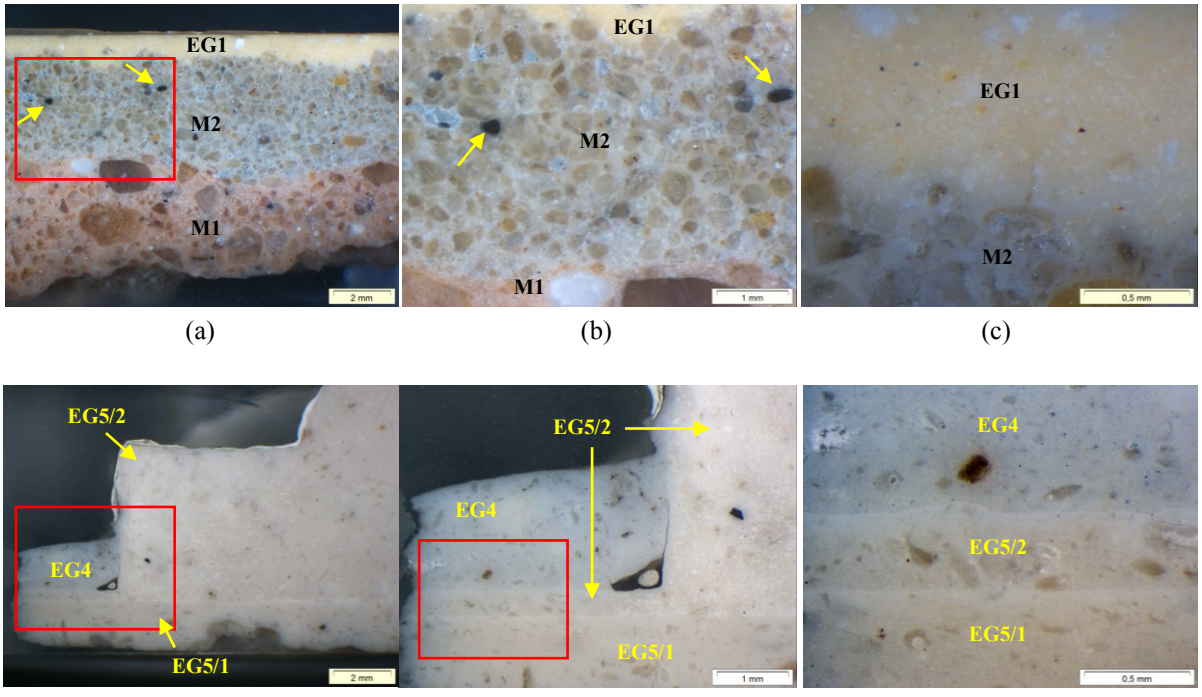

(a) (b) (c)

(d) (e) (f)

Figure 4.176 - Stratigraphic analysis of samples from *Garage* building: (a) EG1 and the two mortar layers behind (M1 and M2), with grains of dark aggregates indicated by arrows; (b) view at a higher magnification of the area bounded by a red frame in (a); (c) detail of the connection EG1/M2; (d) cross section view of the polished surface of EG5 corresponding to the red line of Figure 4.175 (c); (e) view at a higher magnification of the area bounded by a red frame in (d); (f) view at a higher magnification of the area bounded by a red frame in (e) showing in detail the presence of three distinct layers

The stratigraphic analysis was also valuable in the clarification of the application procedure of the frieze EG5/2, showing that it was moulded on site and not precast (Figure 4.176 (d) to (f)). In fact, the plaster corresponding to EG5/2 does not end abruptly, i.e., its limits are not well defined like they would if it was a precast element.

It allowed as well confirming that EG5/1 and EG4 were distinct layers, consistent with the different composition found for both (Table 4.78 and Table 4.79). However, the layer EG5/1 was not detected in sample EG4; it was only applied over the mortar in the surface where the frieze was intended to be moulded directly, probably with the double function of regularizing that surface and promoting the adhesion of the decorative element (EG5/2).

- XRD results

The qualitative mineralogical composition of the samples was determined by XRD and the results obtained showed that calcite and gypsum are the main constituents (Figure 4.177 and Table 4.78). It is interesting to notice that in this case study only the frieze moulded on site (sample EG/2) has more gypsum than calcite, agrees with the fact that the majority of the samples are thin-layer plasters.

Besides the binders, only traces of anhydrite, quartz and feldspars were found, the first one with origin in the gypsum raw material (almost surely as a calcination sub product) and the other two of so common occurrence in the Earth's crust that they are present as impurities in many other minerals.

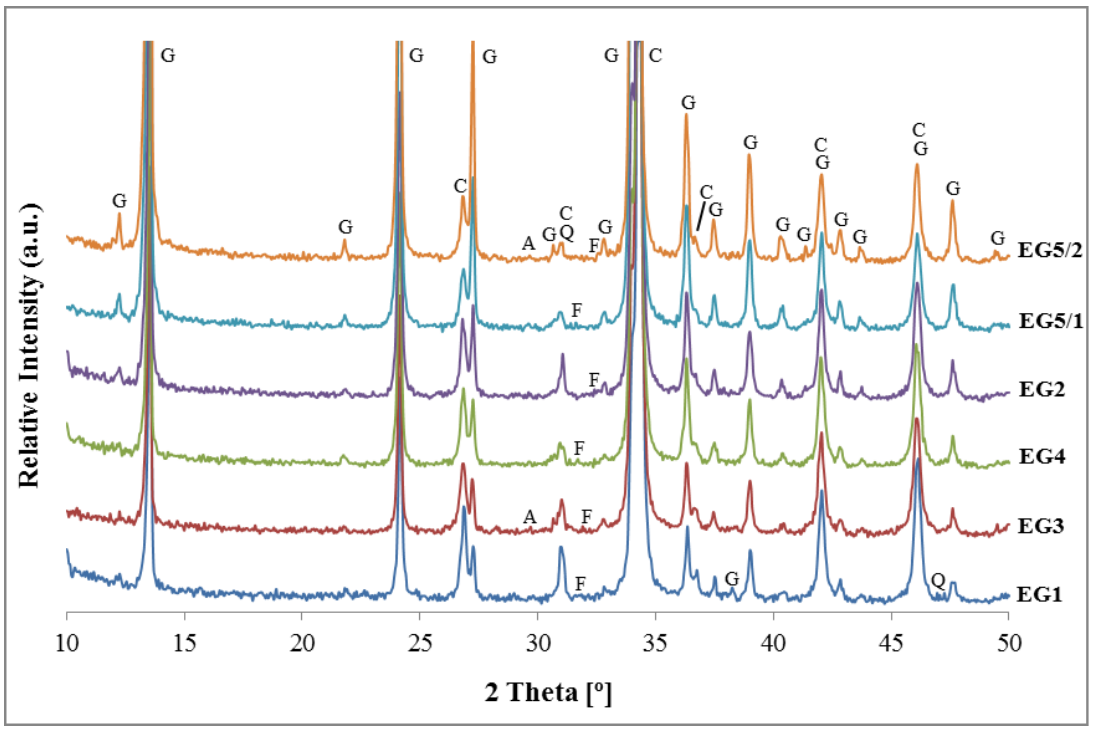

Figure 4.177 - XRD patterns of the samples from *Garage* building.
Notation: G - Gypsum; C - Calcite; Q - Quartz; A - Anhydrite; F - Feldspar

Table 4.78 - XRD qualitative mineralogical composition of the samples from *Garage* building

Sample	Identified crystalline compounds				
	Gypsum	Calcite	Quartz	Anhydrite	Others
EG1	++	+++/++++	trc	-	Feldspars (trc)
EG2	++/+++	+++/++++	trc	trc	Feldspars (trc)
EG3	++	+++/++++	trc	trc	Feldspars (trc)
EG4	++	+++/++++	trc	-	Feldspars (trc)
EG5/1	++/+++	+++	trc	trc	Feldspars (trc)
EG5/2	+++	++/+++	trc	trc	Feldspars (trc)

Notation used in XRD peak intensity:

++++	Very high proportion (predominant compound)	+	Weak proportion
+++	High proportion	trc	Traces
++	Medium proportion	-	Not detected

- TG-DTA results

Once again, the thermal behaviour of the samples associated with temperature variations allowed the quantification of the gypsum and calcite contents, confirming the results of XRD (Table 4.79 and Figure 4.178).

Table 4.79 - Weight loss and calculated gypsum / calcite contents of the samples from *Garage* building

Sample	Temperature range (ºC)						Calculated contents (%)	
	25→85	85→250	250→600	600→850	850→1000	Loss of ignition	Gypsum	Calcite
EG1	0.1	4.1	2.8	31.1	0.1	38.2	19	70
EG2	0.2	7.1	1.2	27.3	0.1	35.9	34	62
EG5/1	0.1	9.7	1.1	22.7	0.1	33.7	46	51
EG5/2	0.1	10.8	1.1	20.4	0.1	32.5	52	46
				600→900	900→1000			
EG3	0.2	5.6	2.0	30.0	0.1	37.9	27	68
EG4	0.1	6.6	1.5	29.6	0.1	37.9	31	67

The doublet of peaks corresponding to the two steps of dehydration of gypsum is visible in the DTG and DTA curves of the three samples with more gypsum: EG2, EG5/1 and EG5/2 (Figure 4.178).

In what concerns the decarbonation of calcite the maximum rate occurred above 800 ºC in all the samples, consistent with their high contents of this compound (> 50%, except in sample EG5/2). These results agree with those obtained in almost all the samples analysed during this research study.

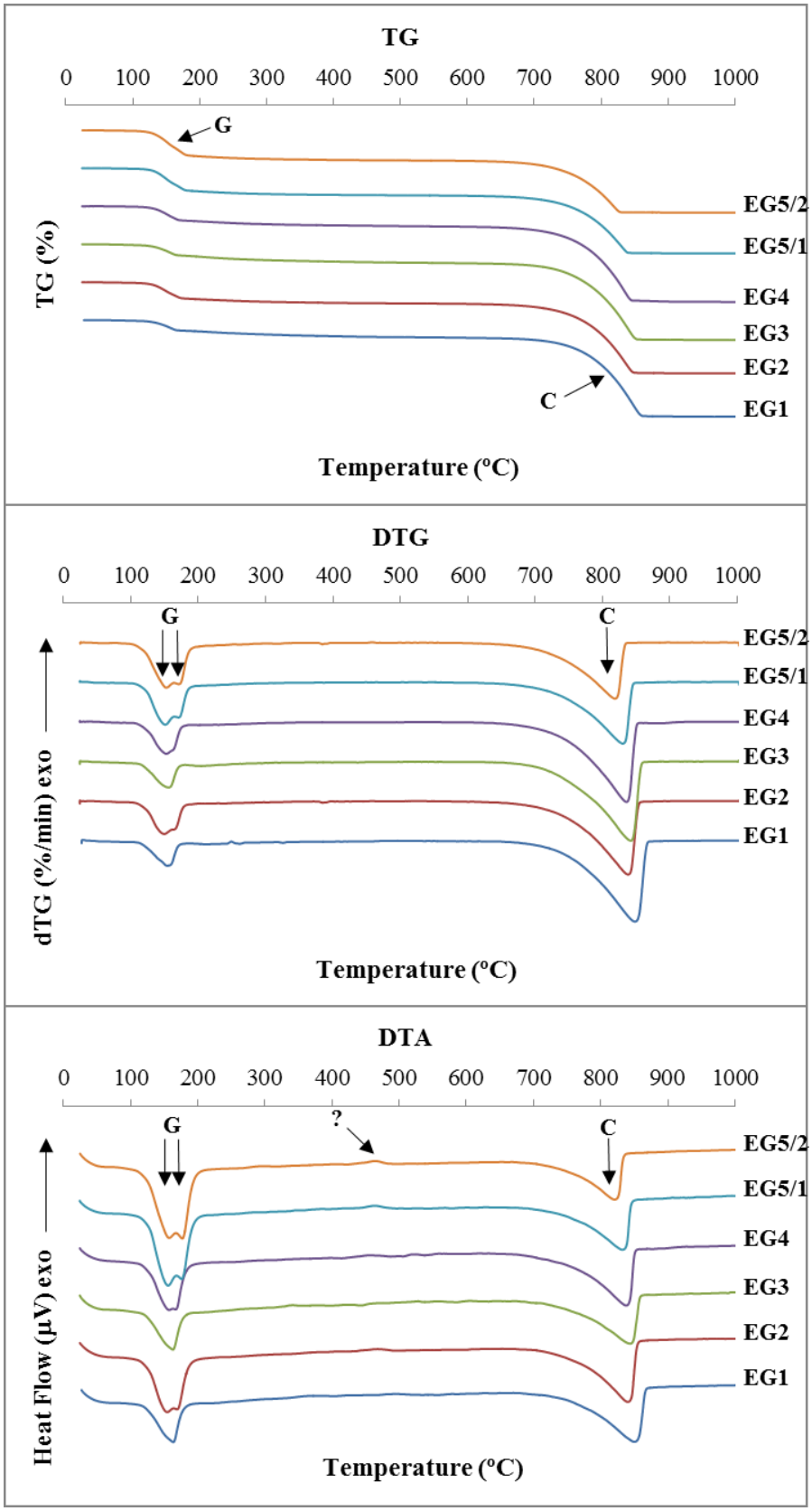

Figure 4.178 - TG, DTG and DTA curves of the samples from *Garage* building.
Notation: G - Gypsum dehydration; C - Calcite decarbonation; OC - organic compounds

Another important feature of these samples is the weight losses between 250 ºC and 600 ºC, higher in samples EG1, EG3 and EG4 (1.5 - 2.8%), whose surface was painted (probably due to the absorption of pigment from the paint). Similar weight losses were observed in sample PE5 from *Estoi* Palace (section 4.3.3.1, "TG-DTA results"), whose surface also had a painted layer of the same type and colour of EG1; in that case, there was even a clear relationship between colour and weight loss: the yellower the layer (Figure 4.111(e)), the higher the loss was (Table 4.59).

In the other three samples (EG2, EG5/1 and EG5/2) the weight losses in that temperature range were between 1.1% and 1.2%.

The DTA curves of these samples have other uncommon feature associated (Figure 4.178): a small lifting around 450 ºC. This usually means that an exothermic transformation occurred and, if it is the case, it can be related to the compounds that originate the weight losses between 250 ºC and 600 ºC referred above. However, it is so small that it can also be due to an artefact of the apparatus or any interference during the analytical procedure.

- SEM-EDS observations

In order to have a further insight into the microstructure of the smooth surface finishing plaster samples from the *Garage* building and to determine whether the respective calcite content was only due to the binder (hydrated lime) or also to the presence of limestone aggregates, scanning electron microscopy (SEM) observations coupled with energy dispersive X-ray spectroscopy (EDS) were performed in sample EG1.

Sample EG1

The observations started with a view of the layers EG1 and M2 and their interface at a low magnification (25X) (Figure 4.179 (a)). All the other images shown refer exclusively to EG1, the object of this study.

The high compactness of the mortar M2 is evident and complies with the visual observation data (Table 4.77 and Figure 4.176 (a) and (b)). However, very small voids can be seen in the interface between the layers that were not visible in the stereo-zoom observations. The formation of this type of voids during the process of application of these materials is common and was probably not detected in polished surface because of their small size and/or random occurrence.

A more detailed view of the microstructure of EG1 (Figure 4.179 (b)) revealed a compact material, with low macroporosity, especially when compared to the most common gypsum plaster samples observed (PE2/2, Figure 4.126 (a); PE4/1, Figure 4.130 (a)).

The shape of the pores is another aspect that can provide important information about the way of production/application of a plaster element. In this case, it was, as expected: not round, irregularly shaped, with most of the pores with higher length than width, typical of a paste that has been pressed while still fresh.

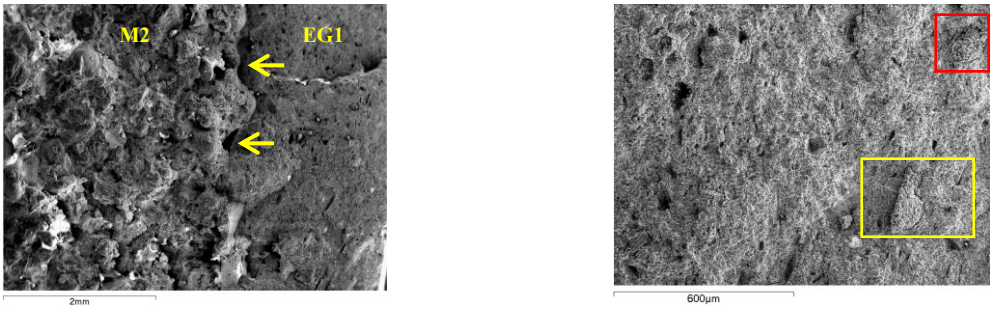

(a) (b)

Figure 4.179 - SEM-SE images of the sample EG1: (a) EG1 and M2 showing voids in the interface (yellow arrows); (b) general view of the EG1 paste

Further observations were then made at higher magnifications in order to see the different crystal morphologies present and identify them using EDS analyses. The microporosity and the possible use of calcitic aggregates were other important issues to clarify.

The images of Figure 4.180 show a very dense matrix, predominantly made of small, non-needle-like crystals. This is in accordance with the composition of the sample determined by TG-DTA where calcite is the major constituent (Table 4.79), and it is very difficult to distinguish gypsum crystals in the matrix, even at higher magnifications (Figure 4.181).

Nevertheless, it is interesting to notice that crystals of completely different sizes and shapes have formed in the bigger pores of the matrix, almost filling the empty space available (Figure 4.180, (a) to (d)); the respective EDS spectra showed that they are exclusively composed of gypsum (Figure 4.180 (e)).

Similar observations were made in sample PE5 (Figure 4.151). This means that the more room they have to grow, the higher the size of the gypsum crystals, unlike in the case of calcite, whose crystallization was not even detected in the referred voids (probably because gypsum crystallizes much faster, occupying the empty space and pushing lime away from that).

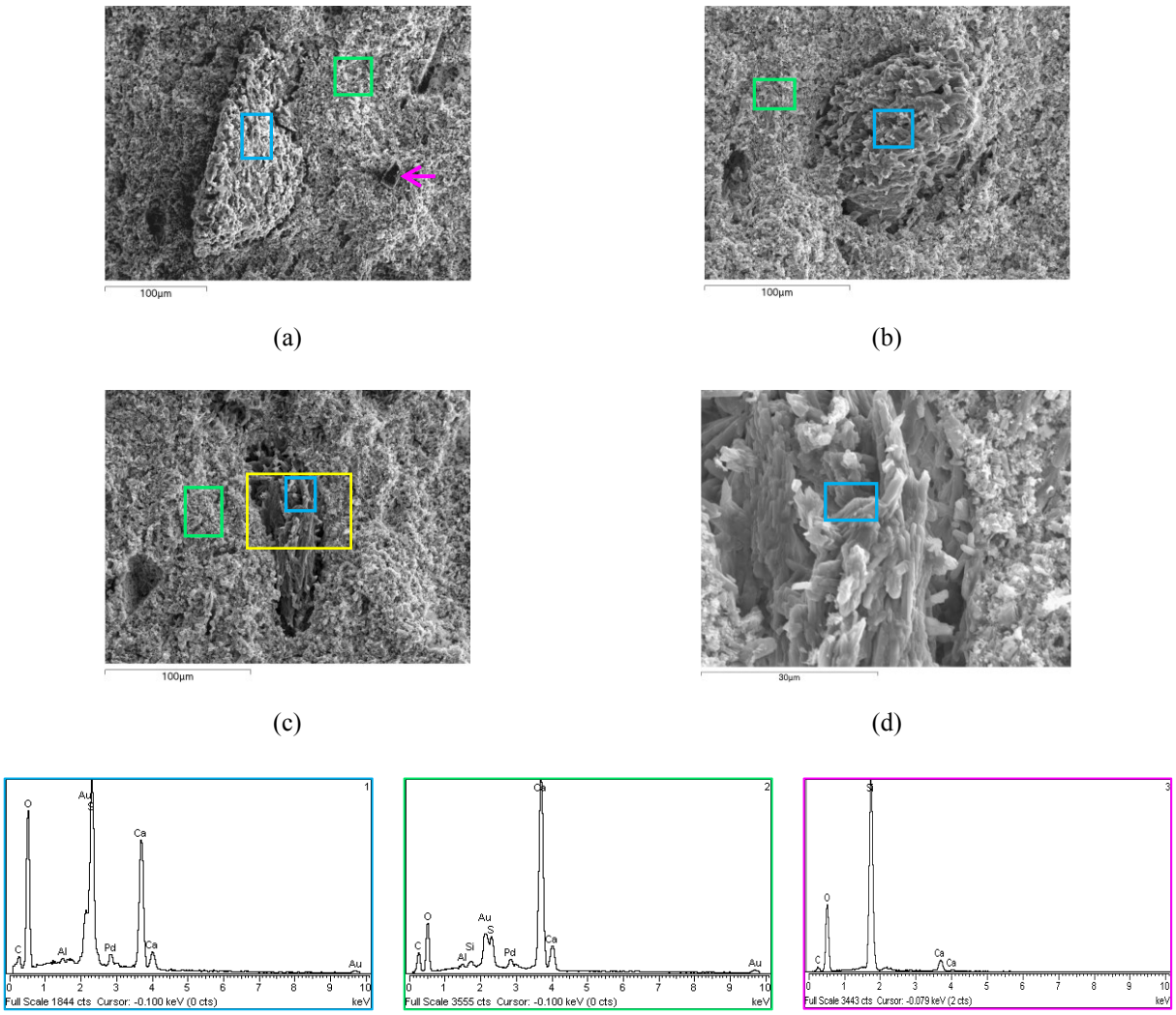

Figure 4.180 - SEM-SE images of different crystal morphologies present in the paste of EG1 and EDS spectra of the areas pointed out by blue and green frames and a pink arrow: (a) image corresponding to the yellow frame of Figure 4.179 (b); (b) area partially corresponding to the inverted image of red frame of Figure 4.179 (b); (c) matrix showing a void with different crystals inside; (d) detail of the crystals in the void (yellow frame of (c)); (e); EDS spectrum of gypsum; (f) EDS spectrum of calcite and gypsum; (g) EDS spectrum of quartz

The matrix of the sample EG1 is mainly composed of crystals of very small size (very few micron) with a hexagonal shape (Figure 4.181), typical of calcite resulting from the carbonation of lime putty (Margalha et al. 2011).

As referred above, it was not easy to find gypsum crystals in the middle of such compact micro structure, a fact very well illustrated by the images in Figure 4.181.

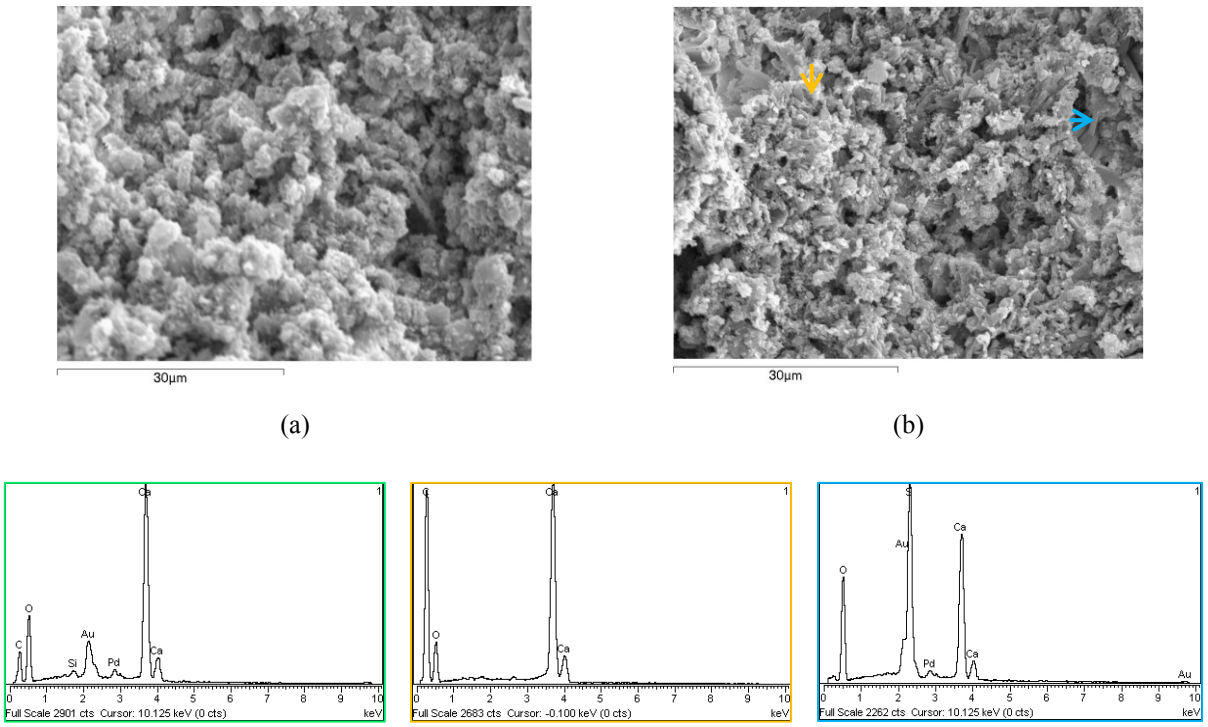

Figure 4.181 - SEM-SE images of the EG1 micro structure showing the crystals morphology of the matrix and respective EDS spectra: (a) area where no gypsum crystals are visible; (b) area with some gypsum crystals visible; (c) EDS spectrum of (a); (d) EDS spectrum of the crystal pointed out by an orange arrow (calcite); (e) EDS spectrum of the crystal pointed out by a blue arrow (gypsum)

Moreover, the few gypsum crystals detected had smaller size (in terms of both length and width) than those found in the gypsum plaster samples (PE2/2, Figure 4.126 (b) and PE4/1, Figure 4.131 (c)). The same was observed in the sample PE5 (Figure 4.153 (a)), although in that case the micro structure did not seem as compact as in EG1.

The hypothesis that limestone grains could have been used as aggregate was also not confirmed.

Summarizing, the SEM-EDS observations of the sample EG1 in fractured surface allowed drawing the following conclusions:

(a) It has a low macroporosity, made of pores of irregular shapes, most having greater length than width (Figure 4.179 and Figure 4.180), a strong indication that the material was pressed while still fresh (Rúbio Domene 2011);
(b) Some of the macropores are filled with gypsum crystals with a very compact structure and much larger than those in the matrix. In spite of being the major compound, calcite does not crystallize in these voids (Figure 4.180 (d));

(c) It has a very compact microstructure mainly composed of hexagonal thin crystals of calcite, with an average diameter much smaller than the length of the prismatic, needle-like gypsum crystals (Figure 4.181);

(d) The presence of limestone grains was not detected, so the addition of aggregates of calcitic origin was not confirmed (Figure 4.180 and Figure 4.181);

(e) A single quartz grain of prismatic morphology and small size was observed, a symptom that it was not a very common material in the plaster used (Figure 4.180 (a)).

- Physical properties

Capillary absorption

The water absorption by capillarity was determined in the samples from *Garage* building (Figure 4.182 and Figure 4.183) and the quantitative results are summarized in Table 4.80.

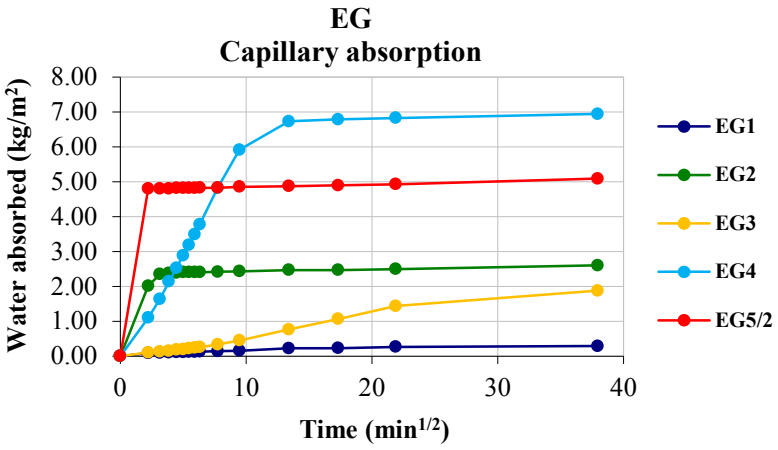

(a)

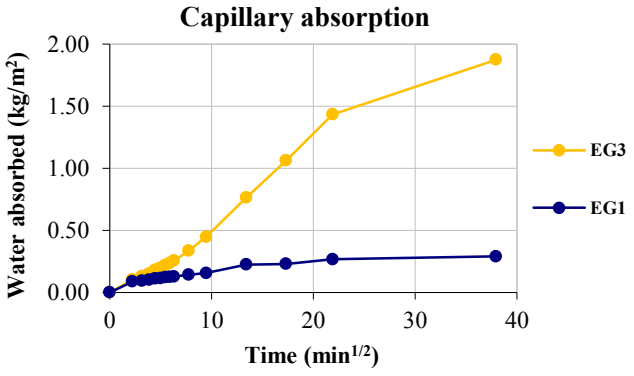

(b)

Figure 4.182 - Water absorption by capillarity of samples from *Garage* building: (a) graphical representation of the results; (b) detailed view of the curve profiles of the samples with lower absorption

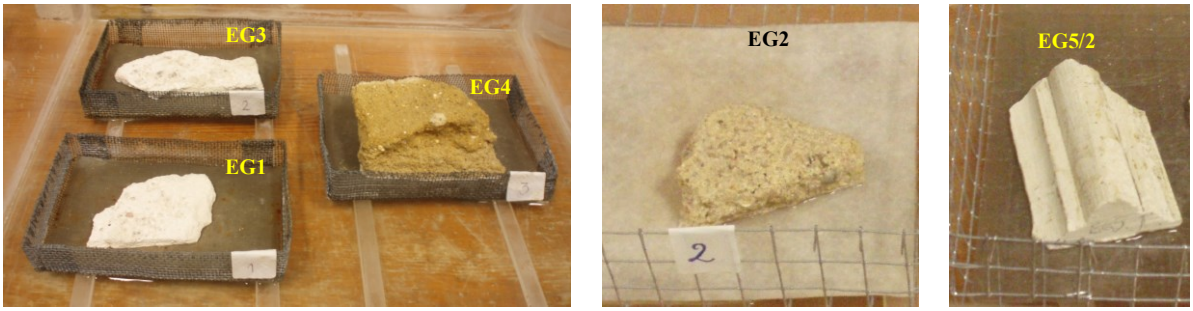

Figure 4.183 - Water absorption by capillarity of samples from *Garage* building: images of the ongoing tests

Table 4.80 - Capillary absorption by contact results of the samples from *Garage* building

Test specimen	**EG1**	**EG2**	**EG3**	**EG4**	**EG5/2**
Surface (cm^2)	35.13	21.30	47.39	48.69	29.80
Weight (g)	37.26	54.40	68.31	311.00	30.86
Capillary absorption at 5 min:					
(g)	0.31	4.29	0.49	5.35	14.31
($kg.m^{-2}$)	0.09	2.01	0.10	1.10	4.80
(%, relative to weight of sample)	0.83	7.89	0.72	1.72	46.37
(%, relative to total absorption)	30.39	77.44	5.51	15.83	94.39
Capillary absorption at 24 h:					
(g)	1.02	5.54	8.89	33.80	15.16
($kg.m^{-2}$)	**0.29**	**2.60**	**1.88**	**6.94**	**5.09**
(%, relative to weight of sample)	2.74	10.18	13.01	10.87	49.13
Ccc at 5 min ($kg.m^{-2}min^{-1/2}$)	**0.04**	**0.90**	**0.05**	**0.49**	**2.14**

Ccc - capillarity coefficient by contact

The results obtained can be divided in three groups:

(a) Samples with very low (< 0.10) Ccc at 5 minutes - EG1 and EG3;
(b) Samples with low (0.10 - 1.00) Ccc at 5 minutes - EG2 and EG4;
(c) Samples with moderate (1.00 - 3.00) Ccc at 5 minutes - EG5/2.

In the samples EG1 and EG3, the capillarity must have been influenced by the painted layer, although it has been removed before the procedure and seemed to be lime-based. In fact, the non-application of a key-coat before the paint allowed the absorption of the pigment by the plaster and the probable blocking of its smallest pores, reducing the total absorption capacity; the eventual incorporation of the pigment in the sample is another factor that could have imposed some resistance to the water front

rise, reducing the absorption rates, especially in the first 60 to 90 minutes (7.75 to 9.49 $min^{1/2}$); finally, the addition of a water repellent product, which is the most plausible explanation.

Concerning the sample EG4, its surface was also painted, even though in this case a key-coat had been applied before. That key-coat had a waxed look and was very difficult to remove. Nevertheless, the capillary absorption behaviour did not seem to be as affected as it was in samples EG1 and EG3.

In the contrary, the surface of the sample EG2 did not have any product applied and the corresponding Ccc at 5 minutes is of the same order of magnitude as those of most thin-layer plaster samples evaluated in this work (≤ 1 $kg.m^{-2}min^{-1/2}$).

Finally, sample EG5/2, a gypsum-calcite plaster from a moulded on site element, had the highest value of Ccc at 5 minutes of this set of samples. Such behaviour can be easily explained by the great content of pores with radius above 0.5 micron (Figure 4.185), usually responsible for high initial absorption rates. After filling of these pores, very low, but continuous, water absorption was observed until the end of the procedure. This means that it has also a significant amount of pores with small radii.

Once again, it is noted that the samples where a finishing product was applied showed lower rates of absorption, especially in the initial part of the test. It means that this type of products forms a barrier to the water penetration, acting as an efficient protection when the exposure to this agent is not too long.

The drying behaviour of the samples was also evaluated and is represented in Figure 4.184.

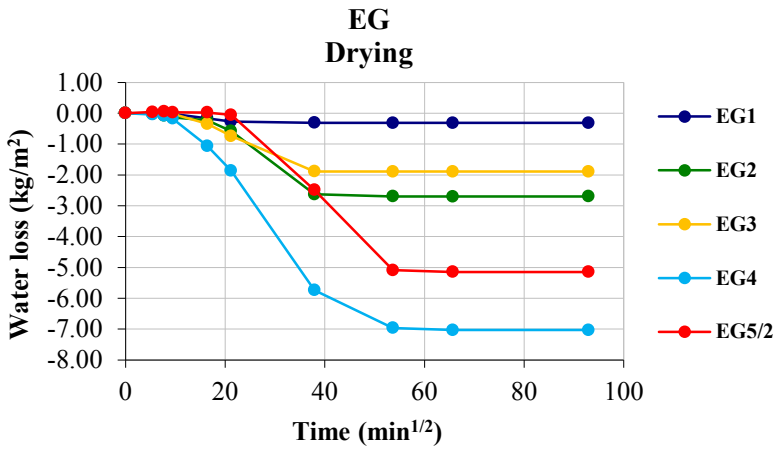

Figure 4.184 - Graphical representation of the drying behaviour of the samples from the *Garage* building

In spite of having absorbed quicker than the other samples, EG5/2 was the last to start losing weight and one of the last to stabilize drying, together with EG4, both having the highest capillary absorptions.

In the contrary, those with lower absorption rates (EG1 and EG3) and lower total absorption (EG1, EG2 and EG3) had better drying behaviour.

It is not easy to find explanations for that, as four of the five samples from this case study are thin-layer plasters with mortar(s) behind. In fact, in these samples absorption is made through the front surface (i.e. the plaster layers) and drying through the back (mortar(s) much thicker), i.e. the drying behaviour is more related with the mortars than with the plasters. On the other hand, the composition and the pore size distribution curves have been determined in the plasters and it was not possible to establish a direct relationship between these parameters and the drying behaviour of the samples, which was evaluated as a whole.

Pore size distribution

The pore size distribution curves were determined in some of the samples from the *Garage* building (Figure 4.185) and the quantitative results are shown in Table 4.81.

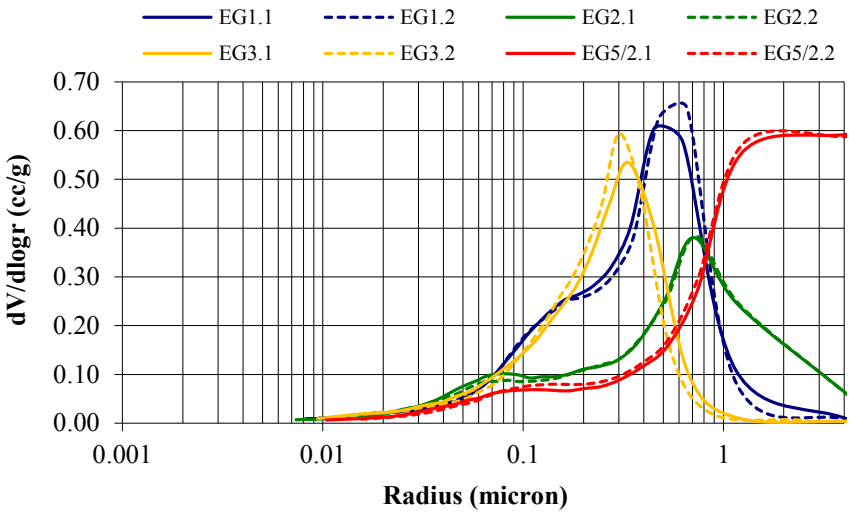

Figure 4.185 - Pore size distribution curves of samples from *Garage* building

Table 4.81 - Results obtained by MIP analysis in samples from the *Garage* building

Sample test specimen	Weight (g)	Bulk density ($kg.m^{-3}$)	Density ($kg.m^{-3}$)	Porosity (%)	Pore radius with max. vol. (μm)	Average pore radius (μm)
EG1.1	0.76	1236	2554	51.6	0.452	0.170
EG1.2	0.78	1232	2635	53.3	0.658	0.178
EG2.1	0.80	1434	2549	43.7	0.711	0.168
EG2.2	0.85	1445	2574	43.8	0.731	0.174
EG3.1	0.75	1341	2341	42.7	0.335	0.138
EG3.2	0.76	1373	2407	43.0	0.301	0.139
EG5/2.1	0.77	1091	2298	52.5	4.266	0.361
EG5/2.2	0.76	1082	2329	53.6	4.266	0.381

The relationship between gypsum-calcite composition and pore size distribution curves that could be established in the samples of other case studies is observed in all the samples analysed except in EG3, where a bimodal curve was also expected.

Another issue difficult to explain is the higher porosity of EG1 compared to EG2's, EG3's and also to PE5's even though in agreement with the total area limited by the respective curve (Figure 4.186). Considering EG1's composition (higher hydrated lime content) a plausible explanation may be the use of a higher water/binder ratio to prepare the paste. Nevertheless, the low macroporosity observed by SEM does not favour this argument.

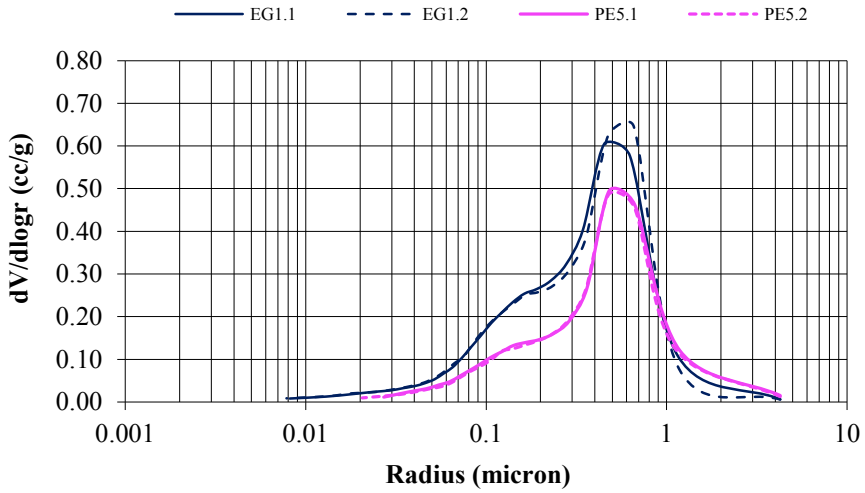

Figure 4.186 - Pore size distribution curves of samples EG1 and PE5

Considering now the curve of sample EG5/2, a first peak can be detected around 0.1 micron and is mainly due to the carbonated lime porosity. However, a considerable amount of pores with radii above 1 micron and even above the maximum limit of detection of the apparatus (approximately 4 micron) is observed as well, and it is the sample with the highest total porosity. As stated before, the samples corresponding to moulded on site elements as is the case of sample EG5/2, are those that show higher porosity and lower bulk density.

Hygroscopic behaviour

The hygroscopic behaviour of the samples from the *Garage* building is shown in Figure 4.187 and the quantitative results are summarized in Table 4.82. Once again, it is noted that in the samples of smooth surface thin-layer plasters this parameter had to be evaluated in the set "plaster + mortar".

An attempt to obtain information about the influence of the mortar in the hygroscopic behaviour of this type of samples was made in EG1, where two groups of test specimens with different mortar thickness were tested (Figure 4.187 (a)):

- EG1.1 and EG1.2: plaster = 2 mm ; mortar = 4.5 mm;
- EG1.3 and EG1.4: plaster = 1.4 - 2 mm; mortar = 0.2 - 1.2 mm.

In the case of EG1.4, the very thin-layer of paint thought to be lime-based was not removed in order to see whether it had any influence in the respective results.

(a)

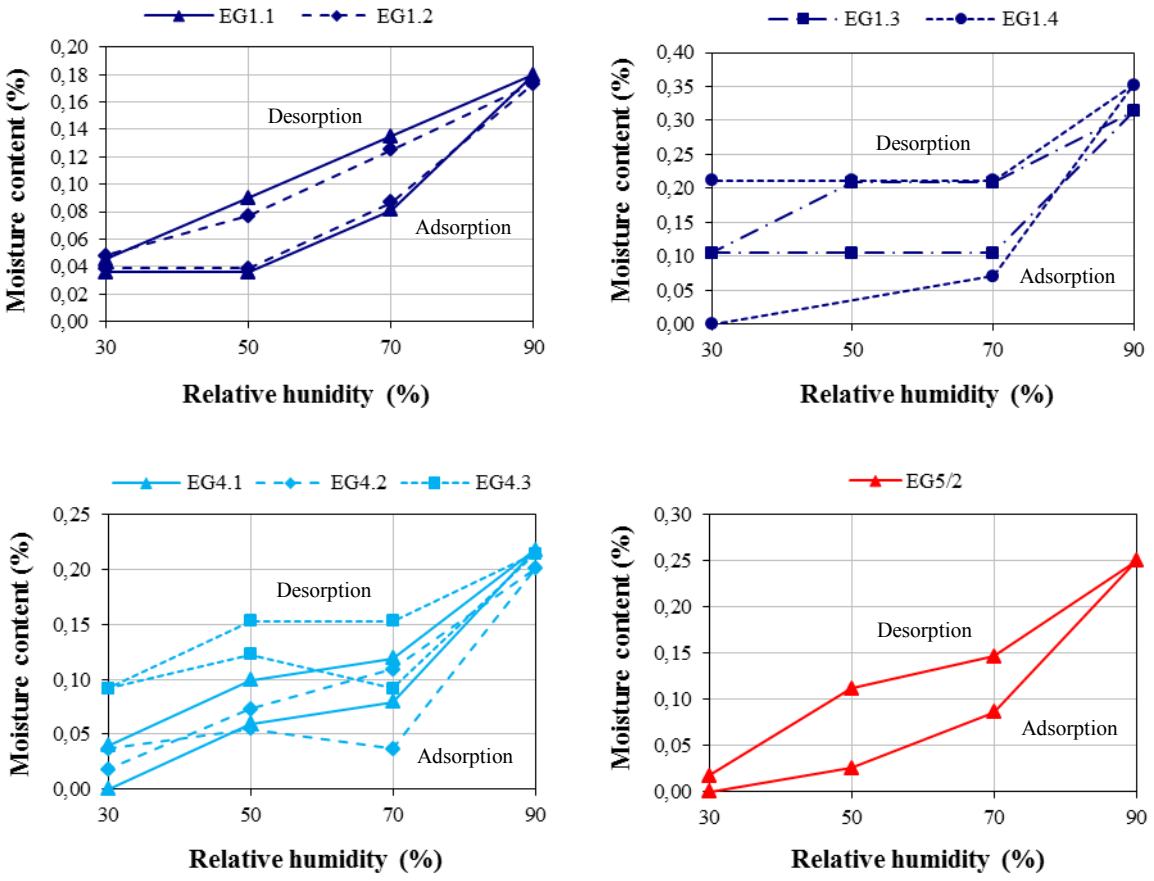

(b)

Figure 4.187 - Hygroscopic behaviour of samples from the *Garage* building: (a) test specimens of EG1; (b) graphical representation of the results

Table 4.82 - Average hygroscopicity results of the samples from *Garage* building: EG1.1, EG1.2 and EG5/2 (2010); EG1.3, EG1.4 and EG4 (2014)

RH (%)	MC (%) EG1.1+ EG1.2	SD	CV (%)	MC (%) EG1.3+ EG1.4	SD	CV (%)	MC (%) EG4	SD	CV (%)	MC (%) EG5/2**
30	0.04	0.002	4.79	*	*	*	*	*	*	0.00
50	0.04	0.002	4.79	*	*	*	0.08	0.038	47.97	0.03
70	0.08	0.004	4.79	0.09	0.024	27.55	0.07	0.029	41.95	0.09
90	**0.18**	0.005	2.65	**0.33**	0.027	8.21	**0.21**	0.009	4.32	**0.25**
70	0.13	0.007	5.32	0.21	0.002	0.77	0.13	0.023	18.07	0.15
50	0.08	0.009	10.96	0.21	0.002	0.77	0.11	0.041	37.72	0.11
30	0.05	0.002	4.79	0.16	0.076	47.82	*	*	*	0.02

* Too high CV value precluding presenting the results; ** Determined in one test specimen only; RH - relative humidity; MC - moisture content; SD - standard deviation; CV - coefficient of variation

It is interesting to notice that all the curves show hysteresis at 70% and 50% relative humidity and that test specimens EG1.4 and EG4.1 also have low pressure hysteresis (30% relative humidity). This difference between EG1.4 and the other three test specimens of sample EG1 might be a casual event but the hypothesis of being due to the painting layer cannot be discarded.

The observation of hysteresis in all the samples from the *Garage* building was not a surprise. In fact, it is in complete agreement with previous statements that relate this effect to materials with a significant content of pores with radii below 0.1 micron; in other words, to the respective composition and pore size distribution curves.

The quantitative values of adsorption at 90% relative humidity can only be compared in relative terms and in a set of samples belonging to the same case study. In sample EG1, test specimens EG1.1 and EG1.2 showed about half the adsorption of EG1.3 and EG1.4, leading to think that the lower the ratio plaster/mortar, the lower hygroscopicity is, i.e. the mortars are probably less hygroscopic than the plasters.

Finally, the irregular behaviour observed in the test specimens of sample EG4 can also be related with the respective mortar and the eventual presence of clay materials in it.

Water vapour permeability

The water vapour permeability was determined in samples EG1 and EG4. The devices used are shown in Figure 4.188 and the results obtained are presented in Table 4.83.

(a) (b)

Figure 4.188 - Water vapour permeability determination in samples from the *Garage* building: (a) EG1; (b) EG4

Table 4.83 - Water vapour permeability results of samples from the *Garage* building

Sample	Thickness (d) (mm)	ΔM/24h (g)	Permeability ($ng.m^{-1}.s^{-1}.Pa^{-1}$)	Sd (d=10 mm) (m)
EG1	8.48 (2.23 plaster + 6.25 mortar)	0.65	31.18	**0.051**
EG4	10.31 (1.29 plaster + 9.02 mortar)	0.78	20.07	**0.087**

The relationship between the quantities of plaster and mortar is much higher in EG1 than in EG4. The mortars are also distinct with EG1's showing higher cohesiveness than EG4's that has a clayey appearance (Table 4.77).

These differences influenced the water vapour permeability: EG1 is more permeable than most of the samples of the same type, and is only comparable to PBS1; on the contrary, the probable but not confirmed presence of clay materials in the mortar of EG4 is a plausible explanation for its lower permeability.

Nevertheless, both results are in the range of values obtained in other studies with similar materials (Ramos et al. 2010: Sd = 0.059 m; Veiga et al. 2010: Sd < 0.10 m; Margalha 2010: Sd = 0.05-0.12 m).

- Mechanical properties

Dynamic modulus of elasticity

The dynamic modulus of elasticity was determined in the samples from the *Garage* building and the respective results are presented in Table 4.84.

Once again it is clear that the ultrasonic pulse velocity is the most reliable and genuine result obtained in ancient samples. In fact, with the exception of EG2, the other three samples of smooth surface thin-layer plasters showed values between 1408 and 1467 $m.s^{-1}$, an interval of the same order of magnitude

of most of the samples of the same type. In the case of EG2 the small distance between probes was probably the main cause for its considerably lower value.

Table 4.84 - Dynamic modulus of elasticity results of the samples from the *Garage* building

Sample	Bulk density[(1)] ($kg.m^{-3}$)	SD	CV (%)	Distance (m)	Time (μs)	SD	CV (%)	Speed ($m.s^{-1}$)	DME (MPa)
EG1	1471	-	-	0.070	47.7[(2)]	1.0	2.2	1466	2846
EG2	1569	-	-	0.050	44.0[(2)]	1.8	4.2	1135	1820
EG3	1635	-	-	0.070	49.7[(2)]	0.4	0.8	1408	2919
EG4	2018	-	-	0.070	47.7[(2)]	0.6	1.2	1467	3908
EG5/2	1276	-	-	0.068	43.0	0.2	0.5	1582	2875

[(1)] Water displacement method; [(2)] Measured at the surface (indirect method); SD - standard deviation; CV - coefficient of variation; DME - dynamic modulus of elasticity

In the contrary, as stated before, the dynamic modulus of elasticity is more influenced by the presence of mortars in the thin-layer plaster samples, the most common type collected in the *Garage* building, leading to much more disperse results.

Samples EG1 and EG4 are good examples to illustrate that: the measurement of the ultrasonic pulse velocity was made with the probes positioned on the surface of the plasters, at the same distance (70 mm) between each other and the results obtained were exactly the same. However, the bulk density of the samples was significantly different (Table 4.84) giving rise to also significantly distinct dynamic modulus of elasticity results, with both parameters having considerably lower values in the sample EG1. Such difference was originated by the higher thickness of the mortar layer(s) behind the plaster in sample EG4.

Compressive strength

The compressive strength determination has been performed in three samples from the *Garage* building and the results obtained are presented in Table 4.85. Figure 4.189 shows the ongoing tests.

Table 4.85 - Compressive strength results of the samples from the *Garage* building

Sample	Confinement mortar age (days)	Bulk density[(1)] ($kg.m^{-3}$)	SD	CV (%)	Load rate ($N.s^{-1}$)	Maximum load (N)	Compressive strength (MPa)
EG2	20[(2)]	1569	-	-	100	2284	1.43
EG4	20	2018	-	-	100	1743	1.09
EG5/2	38	1276	-	-	100	4034	2.52

[(1)] Water displacement method; [(2)] On both sides; SD - standard deviation; CV - coefficient of variation

(a)

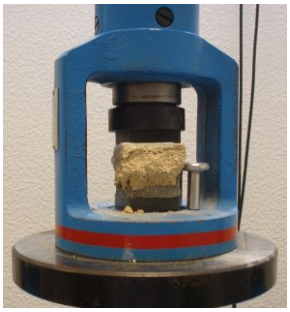

(b)

(c)

Figure 4.189 - Adapted compressive strength tests: (a) EG2 confined by two layers of mortar; (b) EG4 with confinement mortar; (c) EG5/2 with confinement mortar and one fibre cement board

The values obtained in samples EG2 and EG4 were quite low if only the plaster layers composition is considered. However, they are mainly influenced by the corresponding mortars characteristics. In fact, in spite of being thicker, the mortar of EG4 was less cohesive than that of EG1, an observation reflected in the respective compressive strength results.

The use of an adapted test procedure must have had also its influence, mainly due to the area of contact between the confinement mortars and the test device (that is not 100% regular), a parameter not so sensitive when using fibre cement boards. Anyway, despite all the previous considerations the value obtained for sample EG5/2 is consistent with the respective type of material.

4.3.4.3 The *Beira Rio* building

The *Beira Rio* building is also located in the city of *Leiria*. It was designed in 1918 by the studio of *Ernesto Korrodi*, a well-known Swiss architect established in Portugal in 1889 and *Augusto Romão*, building contractor and also the author of the project of the *Garage* building, previously presented. In the design of the façades an attempt was made to develop the characteristics of 18th century regional architecture (Oliveira 2004).

Originally built to be the house of a single family it was later destroyed by a fire and reconstructed to be a hostel (Figure 4.190).

The entire building is in a poor condition (Figure 4.191) but the intervention planned for its recovery has been delayed due to the economic crisis installed since 2008.

(a)

(b)

Figure 4.190 - *Beira Rio* building front façade: (a) west view; (b) east view

(a)

(b)

Figure 4.191 - *Beira Rio* building: images of a ceiling (a) and a wall (b) in poor condition

Samples

A total of three samples were collected in two different ways: indirectly, as they were already detached due to some anomaly in the building (two samples, one of them corresponding to the area shown in Figure 4.192 (a)) and directly on site (Figure 4.192 (b)).

(a)

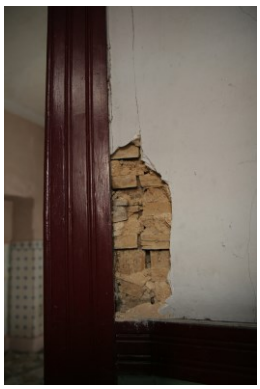

(b)

Figure 4.192 - Some places in the *Beira Rio* building corresponding to the samples collected: (a) partially collapsed ceiling of the *hall* of the service entrance; (b) wall of the same room as (a)

It is interesting to notice the difference between the wood structure of the ceiling, made of thin and narrow laths with very small spacing between them (Figure 4.192 (a)) and the structure of the wall, where coarser laths were placed with larger and more irregular spacing (Figure 4.192 (b) and Figure 4.194 (c) and (e)).

The identification and description of the samples is presented in Table 4.86 and the corresponding images are shown in Figure 4.193.

Table 4.86 - Identification and description of the samples from *Beira Rio* building

Sample identification	Description
EBR1	Ceiling plaster (polychromic)
EBR2	Wall plaster (polychromic)
EBR3	Frieze of the ceiling and top of the walls of the main entrance *hall*

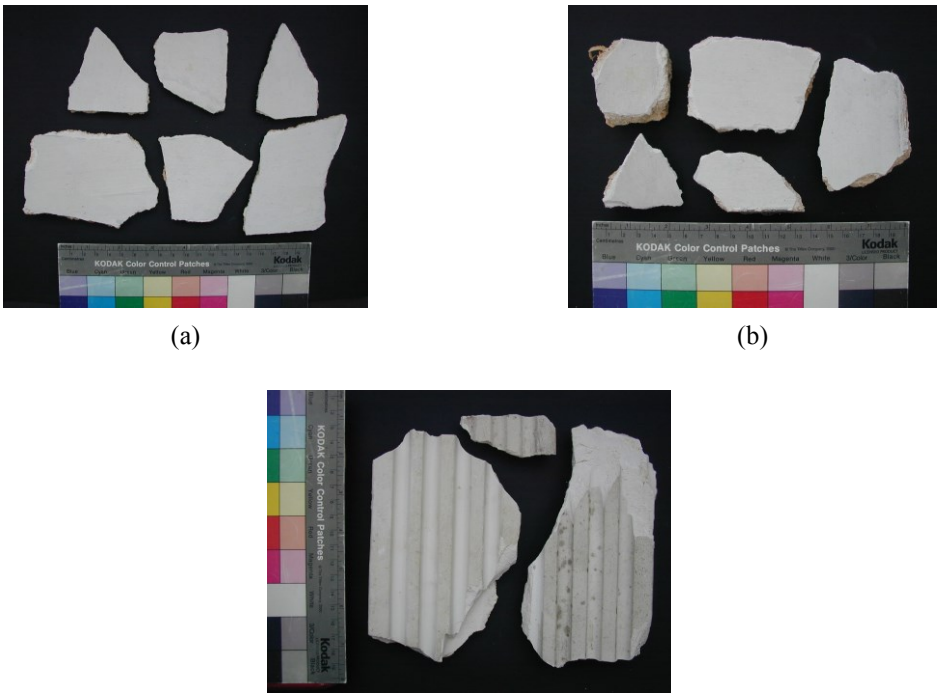

(a) (b)

(c)

Figure 4.193 - Photographs of the samples from *Beira Rio* building: (a) EBR1; (b) EBR2; (c) EBR3

Due to the already referred poor condition of the building, it was very difficult to collect samples that did not seem to have suffered any kind of anomaly. That is the reason why in sample EBR3 only the fragment of the left in Figure 4.193 (c) has been used to perform the characterization study (Figure 4.194 (d)).

Results and discussion

- Visual observation of the samples

The information obtained by the visual observation of the samples is summarized in Table 4.87.

Table 4.87 - Visual observation of the samples from *Beira Rio* building

Sample	Description
EBR1	Several fragments of a **smooth surface thin-layer plaster** of a ceiling painted in light grey colour (Figure 4.193 (a));
	Behind the last layer of paint there was a blue paint that, in turn, seems to have been applied over a very thin white pellicle with a "waxed aspect" (respectively numbers 3, 2 and 1, Figure 4.194 (a)). This pellicle is probably due to the polishing of the surface of the original plaster, a very common way of finishing these type of wall and ceiling coatings;
	The plaster itself was very white and had a thickness of 2-3 mm apparently applied in one single laver;
	All the fragments still had a beige-orange mortar behind (Figure 4.194 (b)), 5-8 mm thick.
EBR2	Several fragments of a **smooth surface thin-layer plaster** form a wall also painted in light grey (Figure 4.193 (b));
	Like in EBR1, the plaster has had already three different finishes. As both samples belong to the same room it means that the walls and the ceiling have always had a similar appearance;
	Behind the paints there was a white plaster layer with a variable thickness (2-5 mm), apparently applied in one single laver in the thinner parts and in two layers in the thicker ones: EBR2/1 (inner layer) and EBR2/2 (outer layer);
	All the fragments had two layers of mortar behind: one beige-orange coloured with a coarse size and thicker that was applied directly on the support; other light beige, finer and thinner over which the plaster was applied (Figure 4.194 (c)).
EBR3	Three fragments of a **frieze moulded on site** with a corrugated pattern (Figure 4.193 (c));
	They all had a light beige painting layer that could be easily detached;
	Two fragments were particularly affected by biological colonization and were rejected (Figure 4.193 (c), top and right fragments). They probably belonged to the upper part of the walls as the mortar they had behind was different from that of the "clean" fragment: it had two layers, exactly with the same colour and size distribution characteristics as in sample EBR2, the coarser with 6-8 mm thickness and the thinner with 1-2 mm;
	The fragment used in the study had 10 mm thickness in the thinner parts and 15-16 mm in the thicker ones. It also had one layer of a coarse, light grey coloured mortar, very hard and cohesive (Figure 4.194 (e));
	Above the mortar there was a thin plaster layer (Figure 4.194 (d) and (e)) over which the frieze has been directly moulded (some holes could be observed between the plaster layer and the base of the frieze). That layer worked as smooth surface finishing plaster in the parts of the walls and ceiling without friezes.

(a)

(b)

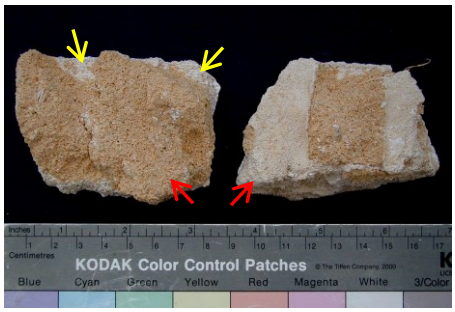

(c)

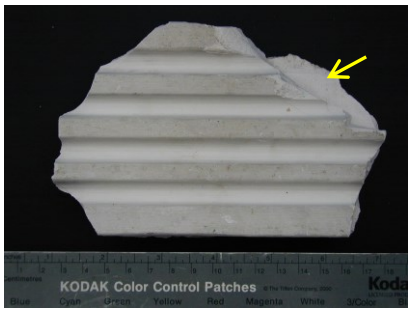

(d)

(e)

Figure 4.194 - Details of the analysed samples from *Beira Rio* building: (a) fragment of EBR1 showing the three different finishes it has had; (b) back view of a fragment of EBR1; (c) back view of two fragments of EBR2 with two layers of mortar behind (inner layer: red arrows; outer layer: yellow arrows); (d) front and (e) back views of sample EBR3, where the plaster layer between the mortar and the frieze is highlighted by yellow arrows

- XRD results

The qualitative mineralogical composition of the samples was determined by XRD and the results obtained showed that gypsum and calcite are the main constituents (Figure 4.195 and Table 4.88).

In the preparation of the two layers of sample EBR2 for XRD and TG-DTA analyses it was very difficult to find an interface and separate them. It seemed that they had been applied one immediately after the other, only in the areas where a higher thickness was needed, and were composed of the same plaster paste. The very similar quantitative composition determined by thermal analysis seems to confirm this supposition.

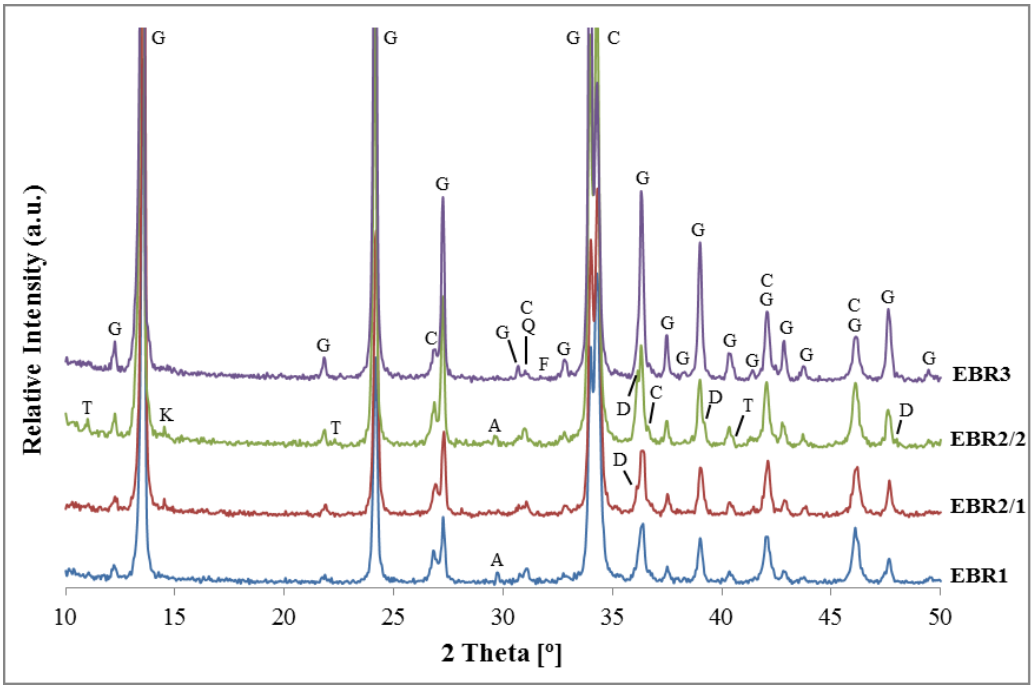

Figure 4.195 - XRD patterns of the samples from *Beira Rio* building
Notation: G - Gypsum; C - Calcite; Q - Quartz; A - Anhydrite; F - Feldspar; K - Kaolinite; T - Talc; D - Dolomite

Table 4.88 - XRD qualitative mineralogical composition of the samples from *Beira Rio* building

Sample	Identified crystalline compounds					
	Gypsum	Calcite	Quartz	Anhydrite	Feldspars	Others
EBR1	++/+++	+++	trc	trc	trc	-
EBR2/1	++/+++	++/+++	trc	-	trc	Dolomite (trc) Kaolinite (trc)
EBR2/2	++/+++	++/+++	trc	trc	trc	Dolomite (trc) Kaolinite (trc) Talc (trc)
EBR3	+++/++++	++	trc	-	trc	-

Notation used in XRD peak analysis:

++++	Very high proportion (predominant compound)	+	Weak proportion
+++	High proportion	trc	Traces
++	Medium proportion	-	Not detected

Besides the very common quartz and feldspars impurities, traces of other compounds that had only appeared in samples of the *Fafe* Cine-Theatre building, like talc and kaolinite, were detected in sample EBR2. They are probably a contamination of the paints used in its exterior surface, where they could have been added as fillers. Dolomite has also been detected in this sample and it is almost surely an impurity associated to the gypsum plaster.

The presence of traces of anhydrite in some samples results from the gypsum calcination process.

- TG-DTA results

The amounts of gypsum and calcite were determined using TG-DTA analysis and the results of XRD could be confirmed (Table 4.89 and Figure 4.196).

Table 4.89 - Weight loss and calculated gypsum / calcite contents of the samples from *Beira Rio* building

Sample	Temperature range (ºC)						Calculated contents (%)	
	25→85	85→250	250→600	600→850	850→1000	Loss of ignition	Gypsum	Calcite
EBR1	0.2	8.6	1.4	24.9	1.4	36.5	41	57
EBR2/1	0.1	9.8	1.2	21.8	0.6	33.5	47	49
EBR2/2	0.1	9.9	1.4	22.0	1.4	34.8	47	50
EBR3	0.1	14.4	0.8	12.7	0.2	28.2	69	29

The doublet of peaks corresponding to the two steps of dehydration of gypsum is more visible in the DTG and DTA curves of the samples with higher amounts of this compound (Figure 4.196), and is almost imperceptible in sample EBR1.

In what concerns the decarbonation of calcite, the thermal curves have also differences, in agreement with almost all samples analysed before: higher contents of this compound usually mean higher temperatures of decomposition. In this case, only sample EBR3 showed a maximum rate below 800 ºC. However, a direct proportion between these two factors (calcite content *versus* decomposition temperature) was not totally observed, with sample EBR2/2 having the highest temperature but not the highest calcite amount (Figure 4.196, DTG and DTA curves). This can be due to higher grain size of the sample (Table 4.88).

In Figure 4.196 other observations associated with the thermal decomposition of the samples can be made, such as:

(a) A small loss of weight between 850 and 1000 ºC in EBR1 and EBR2/2, clearly perceptible in the respective DTG curves;
(b) The very irregular profiles of the DTA curves after 250 ºC.

Concerning item (a), identical observations have been made in samples SP3 and SP4 (*Santíssimo Sacramento's* Chapel), PB2 and PB3 (*Bolsa* Palace), and PM3 (*Monserrate* Palace). The features that these samples have in common are the finishes of the respective surfaces, being either painted (SP3, SP4, EBR1 and EBR2/2) or gilded (PB2, PB3 and PM3).

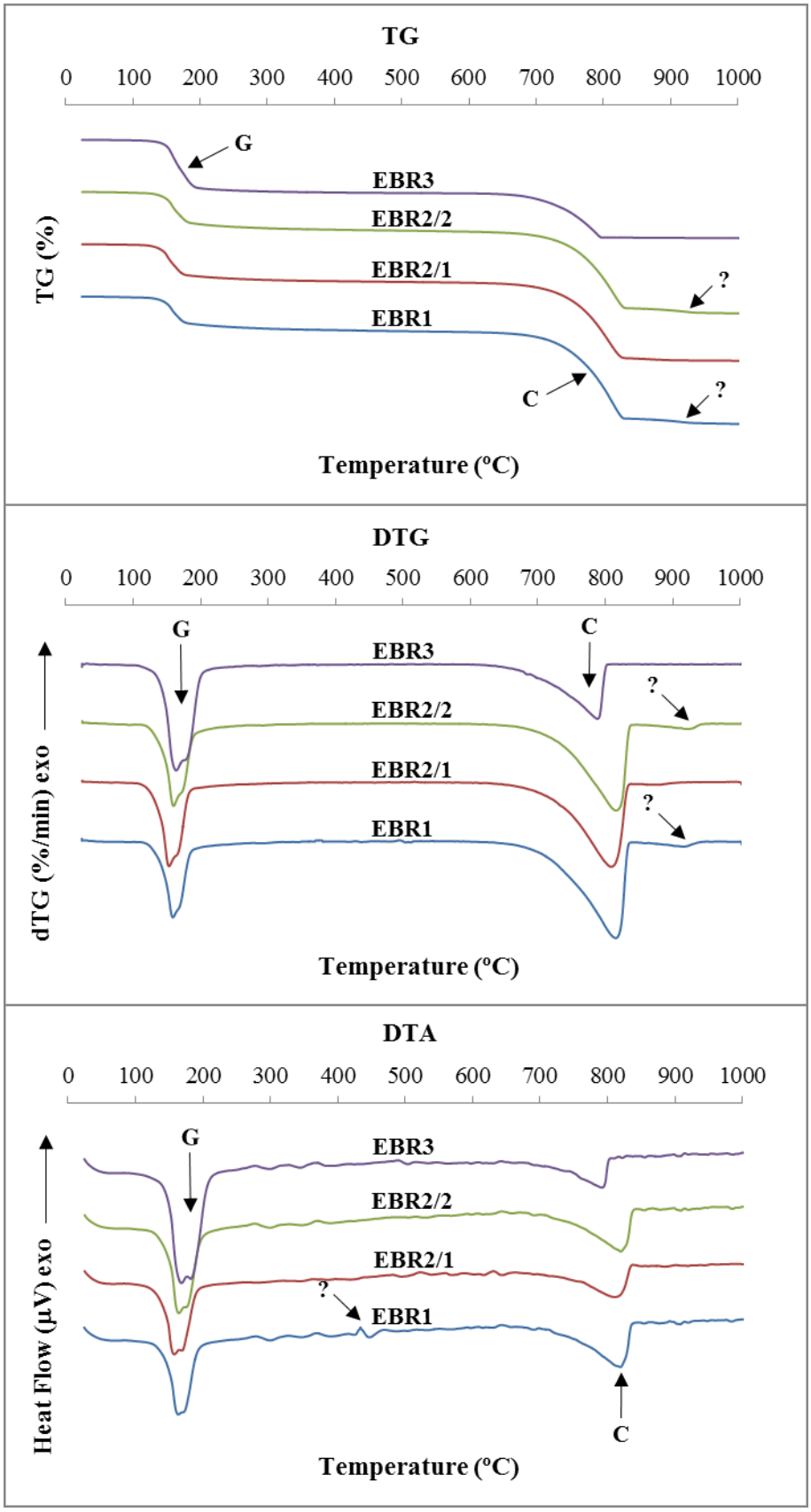

Figure 4.196 - TG, DTG and DTA curves of the samples from *Beira Rio* building

In the gilded samples, there were still remains of the preparation layer used before the gold leaf (named bole) that usually has clay materials in its composition. In the painted ones, there is not a common pattern. However, the presence of organic compounds is expected and can be an explanation for such behaviour. The weight losses between 250-600 ºC observed in samples EBR1 and in the two layers of EBR2 can also have the same origin.

Concerning item (b), it can be originated by several factors like the presence of amorphous iron oxides, organic compounds, kaolinite, talc, etc.

- Physical properties

Capillary absorption

The water absorption by capillarity was determined in two samples from the *Beira Rio* building (Figure 4.197) and the quantitative results are summarized in Table 4.90.

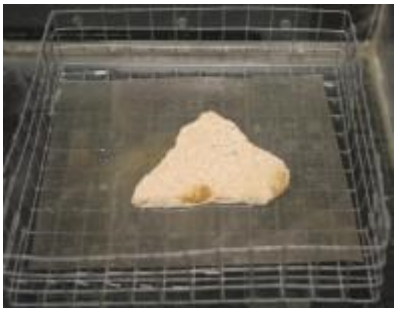

(a)

(b)

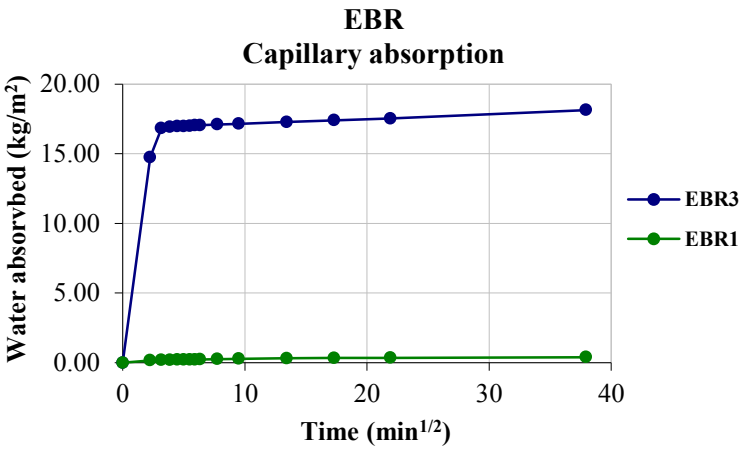

(c)

Figure 4.197 - Water absorption by capillarity of samples EBR1 and EBR3: (a) and (b) test specimens of EBR1 and EBR3, respectively, during the determination; (c) graphical representation of the results

Table 4.90 - Capillary absorption by contact results of samples EBR1 and EBR3

Test specimen	**EBR1**	**EBR3**
Surface (cm^2)	26.48	36.16
Weight (g)	29.32	191.17
Capillary absorption at 5 min:		
(g)	0.44	53.32
($kg.m^{-2}$)	**0.17**	**14.75**
(%, relative to weight of sample)	1.50	27.89
(%, relative to total absorption)	41.51	81.33
Capillary absorption at 24 h:		
(g)	1.06	65.56
($kg.m^{-2}$)	**0.40**	**18.13**
(%, relative to weight of sample)	3.62	34.29
Ccc at 5 min ($kg.m^{-2}min^{-1/2}$)	**0.07**	**6.59**

Ccc - capillarity coefficient by contact

The results obtained show that the two samples studied have completely different behaviours:

(a) EBR1 with very low Ccc at 5 minutes (< 0.10) and very low total absorption;
(b) EBR3 with high Ccc at 5 minutes (> 3.00) and high total absorption.

In the case of sample EBR1, after removing the painting layers the surface of the plaster still had a "waxed" look (*cf.* "Visual observation of the samples", Table 4.86 and Figure 4.194 (a)), which could be either due to the application of a preparation product or to the use of a special finishing technique, both with the aim of preventing the absorption of the paint. Any of these possibilities can explain the very low capillary absorption of the sample.

In the contrary, such high water absorption parameters were not expected in the very tough and cohesive plaster of sample EBR3 only exceeded by PBS2's, a very friable sample.

The EBR3 curve (Figure 4.197 (c)) is similar to those of samples CP2 (Figure 4.26 (b)) and PB4 (Figure 4.59 (b)): there is a high initial absorption rate, typical of a material with significant amounts of pores of higher dimensions (r > 0.5 micron) that slows down to small absorption rates after the first 10 minutes, typical of smaller pores; if the absorption is still not stabilized at the end of the procedure (24 h) it means that the content of smaller pores is also high.

The pore size distribution curve of sample PB4 was the only one determined among the three referred samples and it shows a continuous distribution (not bimodal) along the range of pore sizes covered by the MIP apparatus used (Figure 4.61). Such distribution shows the presence of significant amount of pores with radius under 0.3 micron, in agreement with the respective capillary absorption behaviour, i.e. a similar pore size curve would also be expected in the sample EBR3.

The loss of water absorbed in the capillarity test was also evaluated and is represented in Figure 4.198.

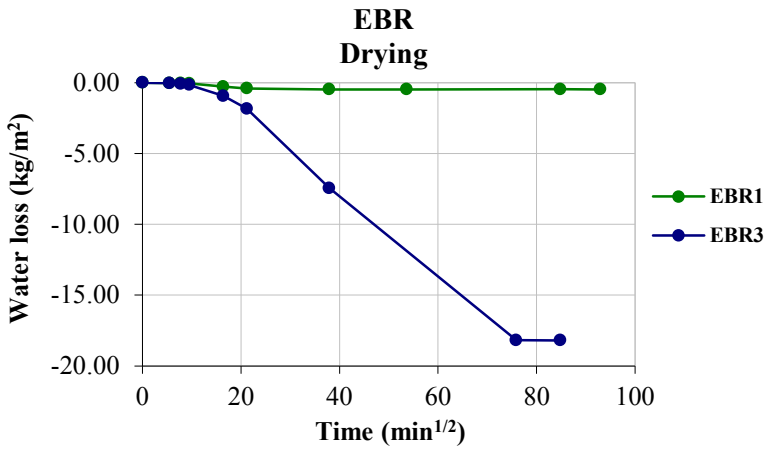

Figure 4.198 - Graphical representation of the drying behaviour of the samples from *Beira Rio* building

The profiles of the curves show that the drying behaviour of both samples is in total agreement with the respective capillary absorption. In the case of EBR3, the presence of some holes between the moulded on site element and the thin-layer plaster over which it was applied must have favoured the initial drying capacity of this sample relatively to those under comparison: samples CP2 (Figure 4.27) and PB4 (Figure 4.60).

Hygroscopic behaviour

The graphical representation of the hygroscopic behaviour of the samples from the *Beira Rio* building is shown in Figure 4.199 and the quantitative results are summarized in Table 4.91.

In order to obtain more information about the influence of both the preparation layer for painting and the mortars in the hygroscopic behaviour of the smooth surface thin-layer plasters three groups of test specimens have been analysed in sample EBR1 (Figure 4.199):

- EBR1.1 and EBR1.2: plaster (without preparation layer) = 1.5-1.7 mm; mortar = 6-7 mm;
- EBR1.3 and EBR1.4: plaster (without removing completely the preparation layer) = 2.3-3 mm; mortar = 6-7 mm;

- EBR1.5 and EBR1.6: plaster (without removing completely the preparation layer) = 3-5 mm; no mortar.

(a)

(b)

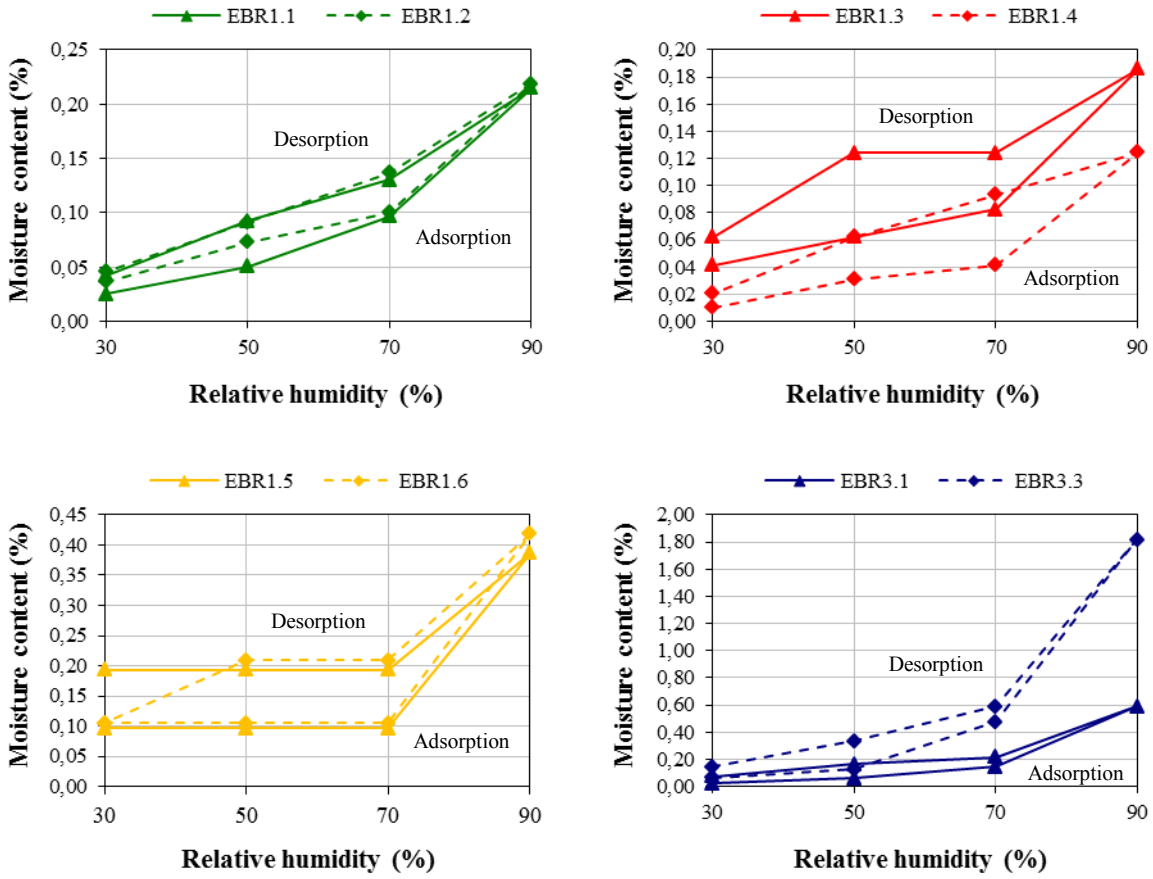

(c)

Figure 4.199 - Hygroscopic behaviour of samples from the *Beira Rio* building: (a) and (b) test specimens of EBR1 and EBR3, respectively; (c) graphical representation of the results

All the curves of sample EBR1 show hysteresis at 70% and 50% relative humidity, which are more significant in test specimens EBR1.3, EBR1.4, EBR1.5 and EBR1.6, all with the preparation layer not totally removed. EBR1.3 and EBR1.5 also have low pressure hysteresis (30% relative humidity).

Comparing the adsorption at 90% relative humidity of the two sets of test specimens with mortar behind, it was observed that the first set (with the preparation layer totally removed) had higher values than the second. Yet, they were both considerably lower (about half) than the adsorption of the test specimens without mortar behind.

Table 4.91 - Average hygroscopicity results of samples from *Beira Rio* building: EBR1 (2010); EBR3 (2014)

RH (%)	MC (%) EBR1.1+ EBR1.2	SD	CV (%)	MC (%) EBR1.3+ EBR1.4	SD	CV (%)	MC (%) EBR1.5+ EBR1.6	SD	CV (%)	MC (%) EBR3.1**	MC (%) EBR3.3**
30	0.03	0.008	25.84	*	*	*	0.10	0.006	5.61	0.02	0.06
50	0.06	0.016	25.84	0.05	0.022	46.80	0.10	0.006	5.61	0.06	0.13
70	0.10	0.003	2.65	0.06	0.029	46.80	0.10	0.006	5.61	0.14	0.48
90	**0.22**	0.003	1.50	**0.16**	0.043	27.92	**0.40**	0.023	5.61	**0.59**	**1.82**
70	0.13	0.005	3.47	0.11	0.022	19.83	0.20	0.011	5.61	0.22	0.59
50	0.09	0.001	0.95	0.09	0.044	46.80	0.20	0.011	5.61	0.17	0.33
30	0.04	0.003	5.79	*	*	*	0.15	0.063	42.09	0.07	0.14

* Too high CV value precluding presenting the results; ** Presented individually due to high dispersion; RH - relative humidity; MC - moisture content; SD - standard deviation; CV - coefficient of variation

These observations seem to indicate that:

- The hysteresis effect is less significant and the hygroscopicity (water adsorption capacity) is higher in the plasters whose surfaces do not have products applied;
- The plasters have a higher hygroscopicity than the mortars associated (also observed in EG1).

In the case of sample EBR3, the irregular hygroscopic behaviour of the respective test specimens is probably due to a contamination of EBR3.3 with hygroscopic substances. However, the hysteresis effect observed can be considered negligible for both, a strong indication of a more significant presence of capillary pores of higher dimensions (r > 0.5 micron).

The quantitative values of this sample cannot be compared to those of sample EBR1. In fact, results from one single test specimen (EBR3.1) are inconclusive and the possibility of a contamination cannot be discarded.

Water vapour permeability

The water vapour permeability was determined in sample EBR1 (Figure 4.200) and the results obtained are presented in Table 4.92.

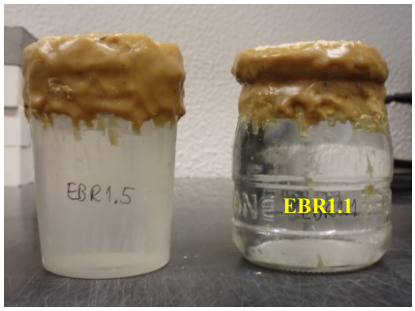

(a)

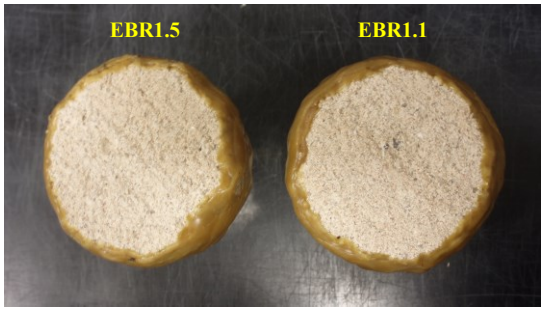

(b)

Figure 4.200 - Water vapour permeability determination in sample EBR1: (a) devices used; (b) top view showing the back surface of the test specimens (mortar layer)

Table 4.92 - Water vapour permeability results of sample EBR1

Sample	Thickness (d) (mm)	ΔM/24h (g)	Permeability ($ng.m^{-1}.s^{-1}.Pa^{-1}$)	Sd (d=10 mm) (m)
EBR1	8.16 (2.0 mm plaster + 6.16 mortar)	0.48	18.43	**0.094**
SD	0.82	0.03	1.65	0.011
CV (%)	10.01	5.89	8.95	11.44

SD - Standard deviation; CV - Coefficient of variation

The values obtained indicate that, in spite of being thinner than most of the samples of the same type (smooth surface thin-layer plasters with mortar behind), the test specimens of EBR1 were the least permeable.

Nevertheless, they were still in the range of values found for lime-based mortars formulations for restoration purposes prepared in laboratory (Veiga et al. 2010: Sd < 0.10 m; Margalha 2010: Sd = 0.05-0.12 m).

- Mechanical properties

Dynamic modulus of elasticity

The dynamic modulus of elasticity was determined in samples EBR1 and EBR3 and the results obtained are shown in Table 4.93.

The ultrasonic pulse velocity (UPS) of sample EBR1 is exactly of the same order of magnitude of that obtained in other samples of the same type, namely EG1, EG3 and EG4 from the *Garage* building. The dynamic modulus of elasticity is also in the same range of the referred samples, even though influenced by the contribution of the mortar to the bulk density.

Table 4.93 - Dynamic modulus of elasticity results of the samples from *Beira Rio* building

Sample	Bulk density[(1)] ($kg.m^{-3}$)	SD	CV (%)	Distance (m)	Time (µs)	SD	CV (%)	Speed ($m.s^{-1}$)	DME (MPa)
EBR1	1758	34	2.0	0.090	62.5[(2)]	0.2	0.4	1440	3280
EBR3	1252	11	0.9	0.121	61.2	0.1	0.1	1971	4378

[(1)] Sand method; [(2)] Measured at the surface; SD - standard deviation; CV - coefficient of variation; DME - dynamic modulus of elasticity

In sample EBR3 very different characteristics were observed, namely a much lower bulk density but a significantly higher speed, both determined with the mortar behind. In this case, however, the influence of the mortar was considered negligible because the measurement of the UPS was made in the thicker parts (~16 mm) of the plaster element using the direct method. Its gypsum-calcite composition was though the major factor contributing to the results obtained.

Compressive strength

The compressive strength has also been evaluated in EBR1 and EBR3 and the results are presented in Table 4.94. Figure 4.201 shows the samples tested.

Table 4.94 - Compressive strength results of the samples from *Beira Rio* building

Sample	Confinement mortar age (days)	Bulk density[(1)] ($kg.m^{-3}$)	SD	CV (%)	Load rate ($N.s^{-1}$)	Maximum load (N)	Compressive strength (MPa)
EBR1	27	1810	83	4.6	100	1236	0.77
EBR3	27	1252	11	0.9	100	6653	4.16

[(1)] Sand method; SD - standard deviation; CV - coefficient of variation

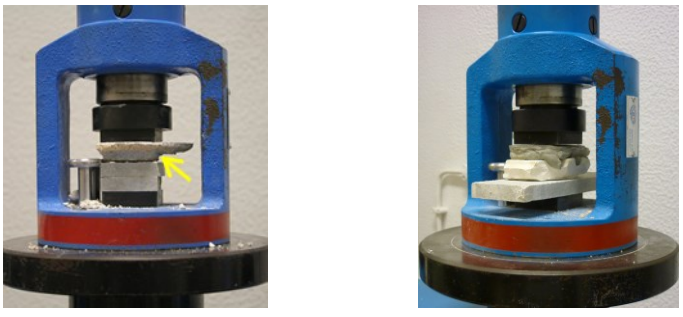

(a) (b)

Figure 4.201 - Adapted compressive strength tests: (a) EBR1 with confinement mortar (yellow arrow) and two fibre cement boards to achieve the target height; (b) EBR3 with confinement mortar and one fibre cement board

The value obtained for the sample EBR1 was too low and cannot be considered valid for the study. The lack of flatness of the confinement mortar's surface in contact with the base (in this case, a fibre cement board) and the very low overall thickness of the test specimen (7-8 mm) are surely the main reasons for that.

On the opposite, EBR3 had the second highest result obtained overall, only surpassed by PBS3, a precast gypsum plaster sample with 4.27 MPa.

Considering that EBR3 is a gypsum-calcite plaster with capillary water absorption behaviour where the Ccc at 5 minutes and the total absorption results were also the second highest of the study and that these parameters are usually directly related to a high number of pores with radii above 0.5 micron and a high total porosity (which, in turn, are inversely related to the compressive strength), it can be said that the results obtained for both mechanical properties evaluated in this sample were quite unexpected. However, it has been found along this study that gypsum-lime plasters with high gypsum content may achieve high mechanical characteristics in spite of also having high porosity and large pores.

4.4 Conclusions

In this chapter the mineralogical, chemical, microstructural, physical and mechanical characterization studies of gypsum and gypsum-lime plaster samples from the 18th to the 20th century are presented. The quantitative results obtained are summarized in Table 4.95, Table 4.96 and Table 4.97.

The following conclusions can now be drawn:

a) The **visual observation of the samples** seldom detected the presence of aggregates;

It also allowed concluding that in the buildings of higher heritage value the raw materials and the process of execution of the plaster coatings and elements studied followed higher quality standards.

In the 18th century the decorative elements were still handmade and even when precast, their surfaces were worked afterwards. A series production was not being used yet, appearing only in the 19th century;

b) The mineralogical characterization was made using **XRD**. It showed that the main constituents of the plasters analysed are gypsum and calcite, meaning that they have been produced using gypsum binders (in the form of hemihydrate and/or anhydrite) and hydrated lime (according to the literature, probably as lime putty). Trace constituents like natural calcite, dolomite, anhydrite, celestine, quartz, feldspars, etc. were also identified but were usually impurities of the raw materials and/or sub products of the manufacture process;

c) **TG-DTA analysis** confirmed the XRD results and allowed quantifying the binders. They showed that the samples belonging to precast or moulded on bench decorative elements were made of gypsum while in moulded on site and pre-sculpted ornaments as well as in thin-layer surfaces, all needing a longer working time during manufacture/application, gypsum-lime mixtures were used;

d) **PLM** and **SEM-EDS** observations were made in order to gain a deeper insight into the micro structure of some samples, selected to cover different characteristics and compositions. It allowed advancing the knowledge of these materials and establishing relationships between their micro and macro properties, i.e. between crystal morphology, micro structure and other properties, like the pore size distribution, porosity, dynamic modulus of elasticity or compressive strength.

This was particularly useful in the case of the samples belonging to elements that intended to simulate decorative stones - imperial red porphyry (*Estoi* Palace, sample PE4) and marble (*Monserrate* Palace, sample PM1).

In fact, despite being also composed of gypsum, they showed very different characteristics from all the others. It was concluded that the binder used might have been anhydrite II instead of hemihydrate, as it allows using a much higher (about twice) plaster/water ratio and gives rise to more compact micro structures, composed of smaller, squat and stocky crystals. All these features were reflected in the other properties, like the pore size distribution (lower average pore radius and porosity), the mechanisms of transport of water (much lower capillary water absorption and vapour diffusion coefficients) and very high mechanical properties, especially in the case of PM1.

It also allowed clarifying that the low content of calcite in some samples was due to impurities of the raw material and not to the addition of limestone aggregates nor of lime as a binder and identifying the presence of some thermally changed compounds, contributing to add a few more clues about the raw materials processing;

e) The **pore size distribution by MIP** was determined in few samples. However, it was enough to conclude that there are significant differences between gypsum and gypsum-lime materials in the range studied: the former showed unimodal curves, a negligible amount of pores with radius under 0.100 micron and an average pore radius between 0.550 micron and 0.650 micron (e.g. samples PB6/3 and PE2/2A); the latter had an amount of pores with radius under 0.100 micron directly related to the calcite content and inversely related to the average pore radius: balanced gypsum-calcite contents correspond to average pore radius in the range 0.300 micron to 0.400 micron but when calcite is predominant the pore radius decreases to values between 0.140 and 0.240 micron (ex: EG1, EG2, EG3, PE5).

It would be very interesting to have more results in order to better understand the relations between pore size distribution, porosity and average pore radius with other properties, namely physical and mechanical.

f) The **hygroscopic behaviour** was studied at 30%, 50%, 70% and 90% relative humidity and the curve profiles obtained showed that the adsorption of water molecules is only significant in the last level (90% relative humidity).

The quantitative values are widely dispersed and it is impossible to establish ranges and relate them with other properties. Nevertheless, when comparing the results obtained in a set of samples belonging to the same case study, it is possible to find that the gypsum plasters tend to have lower values than the gypsum-lime plasters. On the other side, plasters, both gypsum or gypsum-lime, seem to be more hygroscopic than lime mortars, as shown by the comparison of plaster samples with and without layers of mortars.

Other differences have been detected between these two groups of plasters, namely the more common observation of hysteresis in the second, sometimes even at lower vapour pressures (30% relative humidity). This means that desorption of water molecules is more difficult in these materials, in agreement with the presence of significant amounts of pores with radius under 0.100 microns.

The common idea about gypsum plasters being more hygroscopic than lime plasters was not confirmed from the quantitative point of view. However, the suspicion that gypsum releases the water adsorbed more easily than gypsum-lime mixtures seems to indicate that the former materials have a more significant contribution to the indoor hygrometric regulation than the latter. This observation should be confirmed in a wider number of samples.

g) The **capillary water absorption** tests showed that the samples corresponding to elements moulded on site had higher values of capillary coefficient by contact at 5 minutes (Ccc at 5 minutes), all above 2 $kg.m^{-2}min^{-1/2}$ (the exception is sample PM1, a special case). They also seem to be more porous as they showed high values of water absorbed at 24 h.

The reason for that may be the requirements that the pastes have to fulfil for a successful application of these elements on site: they have to be consistent enough not to fall down but also be workable and ductile to reproduce the mould profile. Furthermore, the specific conditions of application, namely the position of the workers towards the working surfaces, mean they are usually applied with a relatively low pressure resulting in a less dense and more (macro) porous structure.

On the contrary, in spite of having similar gypsum-calcite contents, the thin-layer walls and ceilings plaster coatings and the regularization layers have Ccc at 5 minutes below or equal to 1 $kg.m^{-2}min^{-1/2}$.

During application they have to be pressed hard giving rise to more compact, less porous material structures. If a surface treatment has been applied, like a lime wash painting or a key-coat, the initial Ccc is even lower (ex: samples PE5, EG's, EBR1).

Finally, the precast elements, mainly composed of gypsum, have intermediate Ccc at 5 minutes, with results between 1.5 - 3 $kg.m^{-2}min^{-1/2}$.

In spite of all the previous considerations, it is important noticing that the absorbing surface area was different for all samples, meaning the results give an idea of the distinct orders of magnitude but cannot be precisely compared (maximum absorption capacity included). Furthermore, the values obtained for the smooth surface thin-layer plasters refer to the set "plaster + mortar", where the mortar works as a substrate whose characteristics directly influence the behaviour and durability of the plastered elements they are in contact with.

h) After the capillary water absorption test, the **drying behaviour** of the samples was studied and a direct relationship between higher initial rate of drying and higher Ccc at 5 minutes was generally observed. In other words, the porosity and the average pore radius influence both mechanisms, as expected;

i) The **water vapour permeability** could only be determined in eleven samples, eight of them thin-layer plasters with the mortar behind (the exception were the special samples PM1 and PE4, and sample CP2), which do not correspond exactly to the plaster materials themselves. On the other hand, the test specimens' surface areas through which vapour was transmitted were too small to obtain quantitative meaningful results.

Nevertheless, a relative comparison between samples could be made and the results obtained (Sd < 0.10 m) were in agreement with those found in the literature for some gypsum based wall coverings (Ramos 2007) and for lime mortars (Margalha 2010). The exception were samples PM1 and PE4, with higher values, and CP2, with about half (Sd = 0.033 m).

j) The **mechanical properties** determined **- dynamic modulus of elasticity** and **compressive strength** - showed that the type of binder used plays a key role on the results obtained, influencing both the porosity and the micro structure of the resulting materials. In general, higher values were observed in the samples with more gypsum in their composition.

There were some exceptions to this rule, namely in the thin-layer plaster samples' group, where the mortar characteristics not only had a direct contribution (in the ultrasonic pulse velocity), but also an indirect one (through the bulk density values).

The **ultrasonic pulse velocity** was considered an important result. In general, the values obtained for this parameter were between 1600 $m.s^{-1}$ and 2100 ms^{-1} for precast and moulded on bench samples, between 1300 $m.s^{-1}$ and 1900 $m.s^{-1}$ for moulded on site samples and between 1000 $m.s^{-1}$ and 1500 $m.s^{-1}$ for thin-layer finishing plasters with mortar behind; in this last group it was observed that measuring the values at the surface ("indirect measurement") allowed a less significant contribution of the mortar.

For the **dynamic modulus of elasticity** results, the corresponding ranges were 2100-4600 MPa, 1900-4300 MPa and 1800-4100 MPa, respectively.

Finally, the **compressive strength** values were all between 0.8 MPa and 4.3 MPa. The samples of precast and moulded on bench elements (high gypsum content) were in the range 1.3-4.3 MPa; moulded on site elements (balanced gypsum-calcite contents): 1.1-4.1 MPa; thin-layer plasters (more calcite than gypsum) with mortar behind: 0.8-3.1 MPa.

The previous ranges of results were established without considering special samples PM1 and PE4/2.

Due to the irregular shape and size of the samples, the test methods used to determine bulk density and compressive strength were not standardized, but they were validated methods. However, the use of such methods, together with the fact that the specimens used had often very irregular shapes and inadequate size, may introduce a considerable error in the quantitative results. Similarly to what happened with other properties, when analysing the values from the mechanical characterization, all these issues have to be taken into account and be used mainly to establish orders of magnitude and as comparison values.

Summarizing, 33 ancient plaster samples representing a time period of two centuries (second half of the 18^{th} to the first half of the 20^{th}) were collected in eleven buildings located from the north to the south of Portugal. Whenever a sample was made of more than one type of material and/or functional element, individual analyses have been performed in a total of 44 different components.

The XRD and TG-DTA analyses showed that there is a compositional pattern related to each type of element and the respective technical needs of application/manufacture.

In spite of having some error associated, the quantitative results obtained for most of the physical and mechanical properties showed logical interrelations and allowed the definition of ranges of values for many parameters evaluated and for each group of samples. These values constitute the fundamental bases to establish the compatibility criteria that should be accomplished by the new restoration products.

Table 4.95 - Summary of the results obtained for *thin-layer plasters*

Sample	Gypsum	Calcite	Ccc at 5 min	Total absorption	Total porosity (MIP)	Average pore radius	Bulk density (exp.)	Bulk density (MIP)	Density (MIP)	Water vapour permeability Sd (d=10 mm)	Speed	DME	Compressive strength
	(%)	(%)	($kg.m^{-2}.min^{-1/2}$)	(%)	(%)	(μm)	($kg.m^{-3}$)	($kg.m^{-3}$)	($kg.m^{-3}$)	(m)	($m.s^{-1}$)	(MPa)	(MPa)
PB6/2	83	9											
SP4	55	40											
CTF2	55	39	0.37	6.84			1356			0.061	1838	4124	
EBR2	47	50											
PBS1.1	44	51	0.09	5.09			1591				1488	3168	3.11
EBR1	41	57	0.07	0.40			1757	1357	2374	0.094	1440	3279	0.77
PM5/1	40	47											
SP3	39	54											
PE5/1	42	52	1.00	3.75	42.8	0.239	1766	1421	2484	0.068	1515	3646	2.55
PE5/2	9	86											3.12
PE5/3	38	56											
EG2	34	62	0.90	2.60	43.8	0.171	1569	1440	2562		1135	1820	
EG4	31	67	0.49	6.94			2018			0.087	1467	3908	
CP1	27	70											
EG3	27	68	0.05	1.88	42.9	0.139	1635	1357	2374		1408	2919	
PM5/2	25	60											
EG1	19	70	0.04	0.29	52.5	0.174	1471	1234	2595	0.051	1466	2846	
Average*	**38.9**	**56.2**	**0.69**	**4.52**	**43.4**	**0.173**	**1632**	**1394**	**2478**	**0.067**	**1464**	**3294**	**2.93**
SD	9.56	9.66	0.31	2.14	0.64	0.002	114	42.96	103	0.02	37	414	0.33
CV (%)	24.6	17.2	44.5	47.3	1.5	1.2	7.0	3.1	4.1	22.8	2.5	12.6	11.1

Ccc - Capillary coefficient by contact; MIP - Mercury intrusion porosimetry; DME - Dynamic modulus of elasticity; SD - standard deviation; CV - coefficient of variation; * Without grey shadowed values

Table 4.96 - Summary of the results obtained for *moulded on site plasters* and *regularization layers*

Sample	Gypsum	Calcite	Ccc at 5 min	Total absorption	Total porosity (MIP)	Average pore radius	Bulk density (exp.)	Bulk density (MIP)	Density (MIP)	Water vapour permeability Sd (d=10 mm)	Speed	DME	Compressive strength
	(%)	(%)	($kg.m^{-2}.min^{-1/2}$)	(%)	(%)	(μm)	($kg.m^{-3}$)	($kg.m^{-3}$)	($kg.m^{-3}$)	(m)	($m.s^{-1}$)	(MPa)	(MPa)
PM1	90	0	0.01		9.4	0.0615	2475	2080	2295	8.539	2999	20194	80.08
					9.9	0.0968		2063	2290			18960	68.83
EBR3	69	29	6.59	18.13			1252				1971	4378	4.16
PBS2	57	40	17.59	41.16			1140				1444	2140	1.02
PM3	57	41					1158				1660	2872	
EG5/2	52	46	2.14	5.09	53.1	0.371	1276	1087	2314		1582	2875	2.52
ERR3	52	43											
PE2/1	48	46	6.23	14.81	59.7	0.312	1171	1006	2494		1337	1885	1.10
Average*	**53.2**	**43.2**	**4.99**	**16.47**	**56.38**	**0.342**	**1199**	**1046**	**2348**		**1664**	**3066**	**1.81**
SD	3.8	2.8	2.47	2.35	4.70	0.042	61	57	98		223	940	1.00
CV (%)	7.2	6.4	49.6	14.3	8.3	12.2	5.1	5.5	4.2		13.4	30.7	55.5
PB6/1	77	18											
PE1/1	63	33	0.08	2.65			1593			0.074	1575	3556	
PM4	60	33	1.01	4.87			1702			0.061	2029	6306	2.11
											2361	8541	
CTF3	50	48											
EG5/1	46	51											
Average*	59.2	36.6	-	3.76			1648			0.068	1802	4931	2.11 (1 result)
SD	12.2	13.3	-	1.57			77			0.01	321	1945	-
CV (%)	20.5	36.4	-	41.7			4.7			13.6	17.8	39.4	-

Ccc - Capillary coefficient by contact; MIP - Mercury intrusion porosimetry; exp. - experimental determination; DME - Dynamic modulus of elasticity; SD - standard deviation; CV - coefficient of variation; * Without grey shadowed values;

Table 4.97 - Summary of the results obtained for *precast* and *moulded on bench plasters*

Sample	Gypsum	Calcite	Ccc at 5 min	Total absorption	Total porosity (MIP)	Average pore radius	Bulk density (exp.)	Bulk density (MIP)	Density (MIP)	Water vapour permeability Sd (d=10 mm)	Speed	DME	Compressive strength
	(%)	(%)	($kg.m^{-2}.min^{-1/2}$)	(%)	(%)	(μm)	($kg.m^{-3}$)	($kg.m^{-3}$)	($kg.m^{-3}$)	(m)	($m.s^{-1}$)	(MPa)	(MPa)
PBS3.1	95	1					1259				1725	3370	4.27
CP2	94	3	2.73	8.34			1135			0.033	2139	4672	3.32
PB6/3	93	1			56.8 48.4 52.5 56.9	0.626 0.399 0.447 0.575	1045	1028 1211 1120 1072	2380 2348 2356 2487		1659	2590	
SP1	93	3					1376				1816	4064	
CTF1	91	4											
ISF2	88	9									1671		
PE4/1	87	10	1.59	21.77			925 1130				1758	2572	2.23
PE1/2A	87	10	0.20	10.98			969				1752	2678	2.63
PE1/2B	85	15											
PE4/2	85	2	0.03	0.18	12.3	0.0179 0.0282	1908	2045	2333		2381	9735	
ISF1	84	12	1.44	3.52			1385				1964	4809	
PE4			0.01	12.69			1558			0.148	1777	4431	2.66
ISF3							1242				1854	3841	1.47
PE2/2A	83	14	0.72	14.77	46.1	0.560	1153	1189	2209		1778	3282	1.41
PE2/2B	81	18			46.0	0.323		1241	2296				
PB4	51	45	3.15	10.36	57.5	0.340	995	940	2210		1041	970	
CP3	39	57					1387				1304	2121	1.35
Average*	**88.8**	**5.9**	**2.23**	**10.06**	**52.03**	**0.521**	**1189**	**1144**	**2327**	**-**	**1808**	**3586**	**2.29**
SD	4.2	4.7	0.84	4.35	5.19	0.095	153	84	91	-	138	828	0.7
CV (%)	4.8	79.8	37.8	43.2	10.0	18.1	12.9	7.3	3.9	-	7.7	23.1	32.5

Ccc - Capillary coefficient by contact; MIP - Mercury intrusion porosimetry; exp. - experimental determination DME - Dynamic modulus of elasticity; SD - standard deviation; CV - coefficient of variation; * Without grey shadowed values

5

Design and selection of compatible gypsum and gypsum-lime based products for restoration purposes

5.1 Introduction

In this work, the repair of ancient Portuguese gypsum and gypsum-lime based plasters has been addressed through a conservative perspective, considered essential to the preservation of the architectural heritage integrity.

The design of new products to partially or completely substitute the damaged interior coverings of walls and ceilings was made taking into account the general issues of compatibility observed in this type of interventions, respecting particularly the main characteristics of the pre-existing materials they will be in contact with and of the building as a whole.

In this chapter, quantitative requirements were established based on the results of the characterization studies presented in chapter 4. It was concluded there is a need of developing at least three different restoration products, one for each family of plaster elements: thin-layer finishing plasters (L), elements moulded on site (M) and precast decorative elements (P).

All these data allowed defining the materials - calcium sulphate hemi-hydrate and calcitic hydrated lime - and the respective proportions to be used in the restoration products. The need for addition of other components - limestone aggregate, water retaining agents, set retarders - was studied using workability tests that intended to reproduce as closely as possible the actual conditions of application, resulting in seven mixes: two type L (designated as “L series”), two type M (“M series”) and three type P (“P series”).

These mixes were characterized in terms of physical and mechanical properties. The analysis of the results obtained allowed choosing those that seem to be the most compatible products to be used for restoration purposes, i.e. the products whose properties best comply with the compatibility ranges established.

However, detailed studies of application on site still have to be made, preferably with experienced plasterers in order to test the workability and the performance of the materials "in service" before accepting the products for application in real works.

5.2 Restoration products: quantitative requirements for compliance with the compatibility criteria

The general issues of compatibility for interior gypsum-lime restoration plaster products are the same as for other types of mortars and renders to be applied in ancient buildings masonry structures, i.e. they should not contribute to the degradation of the pre-existing materials they are in contact with, besides fulfilling functional and aesthetic requirements. They should also act as sacrificial materials in difficult conditions and be easily replaceable (Papayianni 2005; Veiga et al. 2010).

To achieve these goals, the main characteristics of the existing plaster coatings should be determined, so that the establishment of quantitative requirements for the new products can be made taking this information into account, namely in terms of:

a) Mechanical characteristics - flexural and compressive strengths as well as the elastic parameters should be similar, or lower, in order to avoid changes in the stress distribution;

b) Physical characteristics - the several types of interaction with liquid and vapour phases of water through mechanisms of absorption (water capillary absorption), adsorption (hygroscopic behaviour) and diffusion (drying capacity, water vapour permeability) should be similar, or higher, to prevent the exposure of the wall components to excess and/or long-term humidification periods. In other words, the restoration plasters should not block the passage of liquid water or of water vapour that circulates inside these components due to vapour pressure gradients caused by any of the referred phenomena;

c) Chemical compatibility - the use of similar materials is desirable not only to meet the requirements set out above but also to prevent the formation and/or contamination with alien substances (e.g. soluble salts).

They should also be compatible with most of the substrate materials, probably lime based mortars with mechanical characteristics of the same order of magnitude (Magalhães and Veiga 2009, Veiga et al. 2010) or masonry walls with higher characteristics.

The need to ensure they constitute efficient and durable solutions and that they are "user-friendly" was also considered, to prevent premature substitution interventions and to have good workability properties during application. In fact, this issue, whose importance is rarely considered, strongly influences the real impact that this type of studies has on the field of conservation of cultural heritage.

The quantitative requirements (Table 5.1) for the design of new repair products were established taking into account the characterization results presented in chapter 4 and summarized in Table 4.95, Table 4.96 and Table 4.97, with the exception of the water vapour permeability for the moulded on site elements. In fact, it was impossible to perform the respective experimental procedure in the ancient samples due to their very irregular shape, so the corresponding restoration products' water vapour permeability requirements were based on the results available in the literature for lime mortars (Margalha 2010; Veiga et al. 2010), considered to have the most approximate composition.

Table 5.1 - Design and selection of compatible restoration products for gypsum and gypsum-lime based plasters: quantitative requirements

Plaster element	Composition (%)			Porosity	Cc at 5 min	Hygrosc.	WVP	DME	Cs
	HH	HL	CA	(%)	($kg.m^{-2}.min^{-1/2}$)	RH=90%, (%)	Sd (m)	(MPa)	(MPa)
Thin-layer (L)	20-30	60-70	0-10	45-55	0.5-2.0	< 1.0	< 0.10	1000-2000	1-2.5
Moulded on site (M)	40-50	50-60	0-10	55-65	3.5-7.5	< 1.0	< 0.10	1500-3000	1-3
Precast (P)	80-90	0-20	0-10	50-60	3-5	< 1.0	< 0.08	2000-4000	1.5-3.5

HH - gypsum hemi-hydrate; HL - hydrated lime; CA - calcitic aggregate; Cc at 5 min - Capillary coefficient at 5 minutes; Hygrosc. - Hygroscopicity WVP - Water vapour permeability; DME - dynamic modulus of elasticity; Cs - Compressive strength

A first attempt to meet these requirements had already been made (Freire et al. 2011) but the characterization studies were still incomplete and some adjustments had to be done after all the results were available. In the case of the moulded on site products, the main adjustments were made in 2013 and it is now only necessary to introduce a very slight change in the porosity values (from 50-60% to 55-65%).

The previous paragraph clearly illustrates that this is an endless, iterative process that can be improved whenever new and/or more accurate data is available, meaning that further adjustments ought to be made in the future. It is also relevant to be aware that some special cases might demand special requirements and tailor-made solutions.

In any case and once again, it is important to highlight that the fulfilment of the compatibility criteria referred above is the paramount issue in the process of selection of the final formulation(s).

5.3 Materials

Portuguese industrial products of identical chemical nature to the original materials found in the Portuguese case studies, namely calcium sulphate hemi-hydrate (Figure 5.1), calcitic hydrated air lime and a fine calcitic aggregate were used in the composition of the gypsum and gypsum-lime restoration plasters (Table 5.2). The addition of some admixtures (water-retaining agents and set retarders) was also evaluated in a few mixes.

Even though it is well-known that lime was mainly used in the form of putty in the time period of the ancient samples, all the materials were used in the powder form and the respective proportions defined in mass percentages. In fact, one of the aims of this study is to develop pre-dosed products, ready to knead with water and easy to apply.

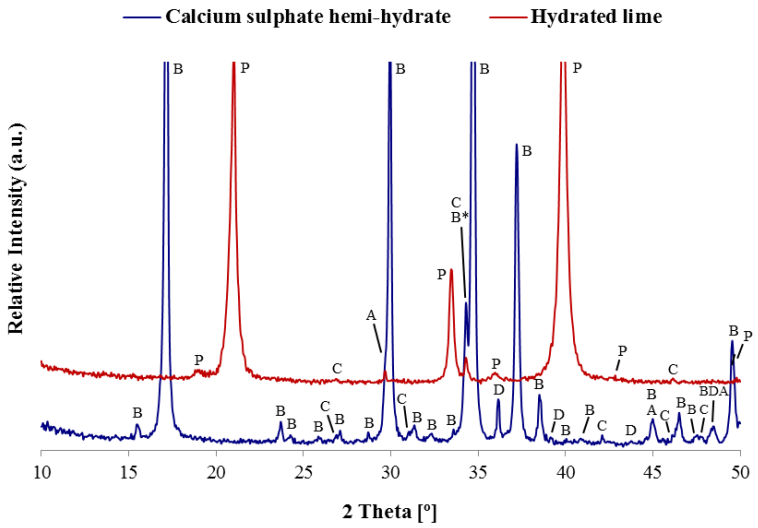

Figure 5.1 - XRD patterns of the calcium sulphate hemi-hydrate and the hydrated lime used in the restoration products' mixes. Notation: B - Bassanite (hemi-hydrate); P - Portlandite (hydrated lime); C - Calcite; A - Anhydrite; D - Dolomite

Table 5.2 - Materials used in the restoration products composition: main characteristics

Designation	Chemical composition	Active substance* (%)	Bulk density (kg/dm^3)	Specific surface area (BET method) (m^2/g)	Grain size distribution* (micron)
Calcium sulphate hemi-hydrate (HH)	$CaSO_4.1/2H_2O$	> 90	0.692	3.52	< 300: ~100%
Hydrated lime (HL)	$Ca(OH)_2$	> 93	0.342	11.42	< 125: 100%
Calcitic aggregate (CA)	$CaCO_3$	≥ 99	-	1,36	< 45: 99.7%
Set retarder (SR)	-	> 91,5	-	3.55	-
Water retaining agent (WRA)	$C_2H_6O_2.xCH_4O$	> 99,5	~ 0.400*	-	< 180: min 90%

- Data not available; *Supplier information

5.4 Experimental data

The physical and mechanical properties of the new products developed in this work were assessed, where applicable, following standard procedures.

The test specimens of hardened product were stored in a room with conditioned environment at a temperature of 23 ± 2° C and relative humidity of 50 ± 5% (Figure 5.2). All tests were performed in the same room with the exception of the mechanical properties that were evaluated in a room at a temperature of 20 ± 2º C and relative humidity of 65 ± 5%.

Figure 5.2 - Storage of the test specimens in conditioned environment

The **plaster/water ratio** (P/W) of the several mixes was determined according to EN 13279-2:2004 using the dispersal method in the fluid products (P series, mainly based on gypsum) (Figure 5.3) and the flow table method in the paste products based on mixtures of gypsum and hydrated lime (M and L series) (Figure 5.4).

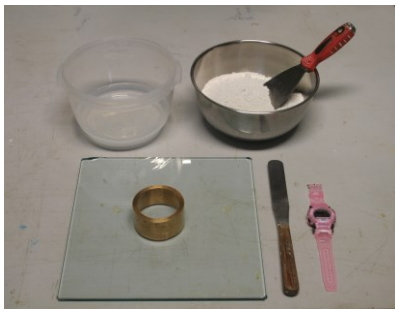

(a)

(b)

Figure 5.3 - Determination of the plaster/water ratio using the dispersal method: (a) apparatus; (b) measuring the diameter of the pat formed

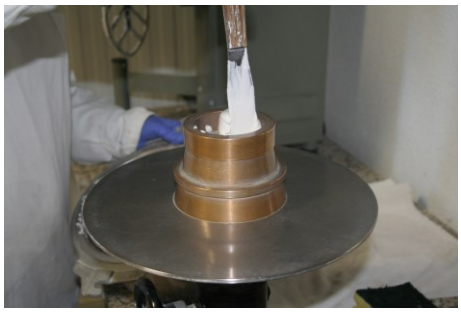

(a)

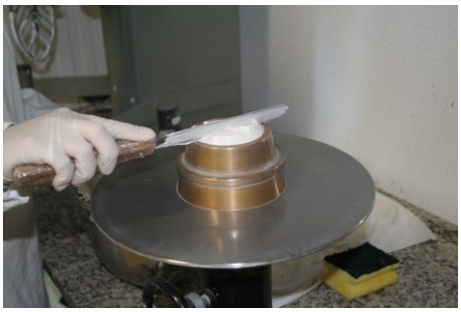

(b)

(c)

(d)

(e)

(f)

Figure 5.4 - Determination of the plaster/water ratio using the flow table method: (a) pouring the plaster into the slump cone; (b) removing the excess plaster with a spatula; slump cone before (c) and after (d) being withdrawn; (e) application of the vertical blows (f) measuring the diameter of the pat formed

The **setting time** was determined according to EN 13279-2 using the knife method (Figure 5.5).

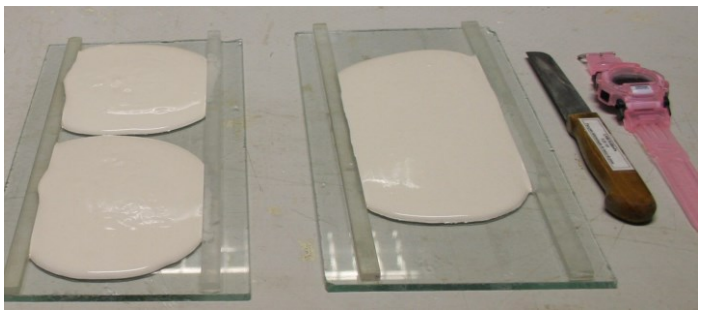

(a)

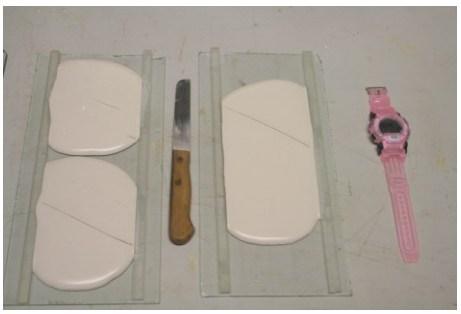

(b)

Figure 5.5 - Determination of the setting time using the knife method: (a) two pats for trial cuts (left) and one pat for the test cut (right) immediately after pouring the plaster on to the glass plates; (b) the same as in (a), after the end of the procedure

The **prismatic test specimens of hardened product** were prepared according to EN 13279-2:2004 using the steel moulds indicated in NP EN 196-1:2006 (Figure 5.6).

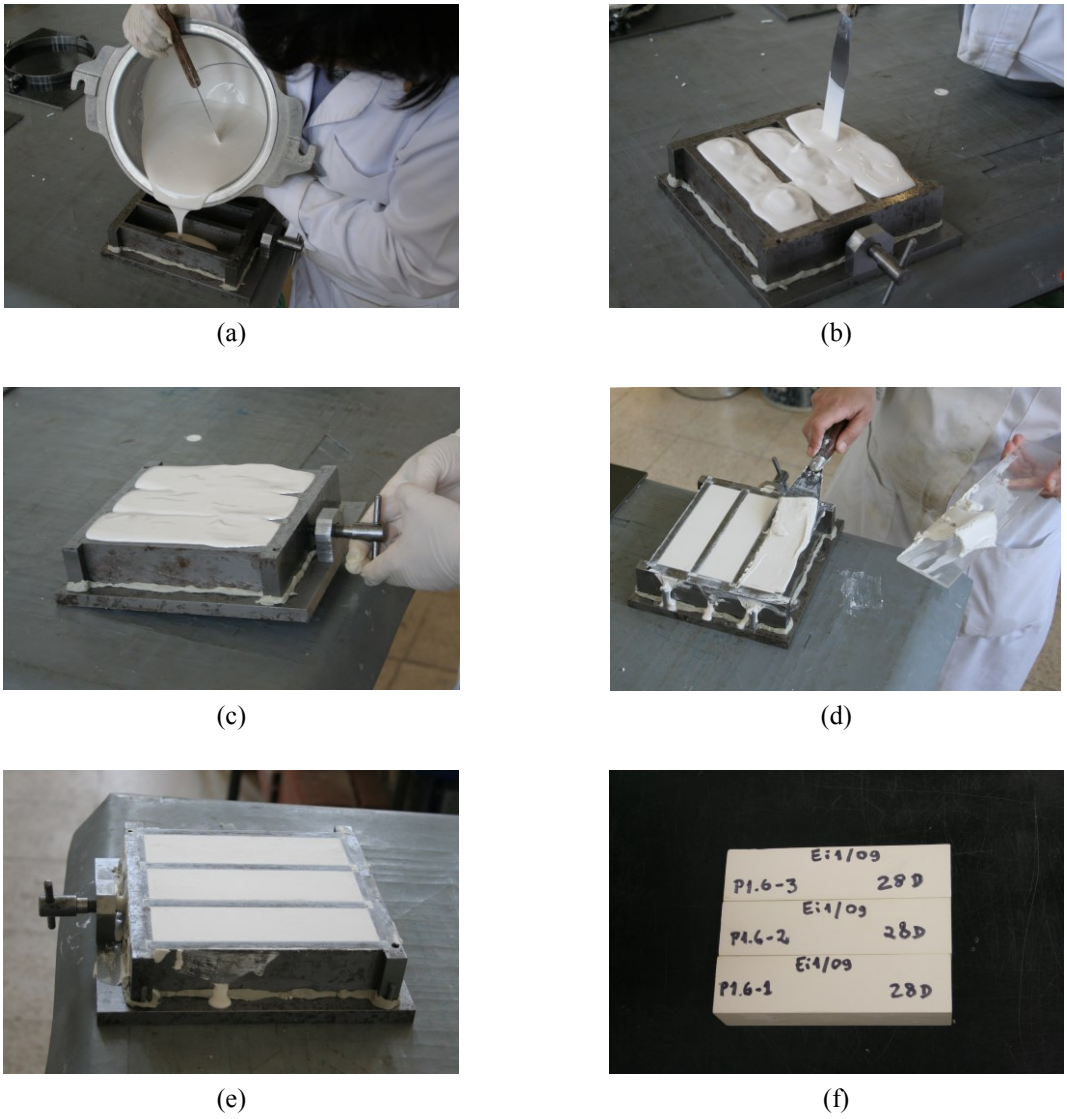

(a) (b) (c) (d) (e) (f)

Figure 5.6 - Preparation of the prismatic test specimens: (a) pouring the plaster into the mould; (b) and (c) compaction procedure; (d) removing the excess plaster with a palette knife; (e) test specimens before demoulding; (f) procedure completed

The **pore size distribution curves** were determined at 90 days and 2 years using the same procedure as for ancient samples (*cf.* 4.2.2). Test specimens of approximately cylindrical shape with ϕ_{top} = 55-60 mm, ϕ_{bottom} = 50-55 mm; thickness = 15-18 mm) have been prepared for that purpose (Figure 5.7).

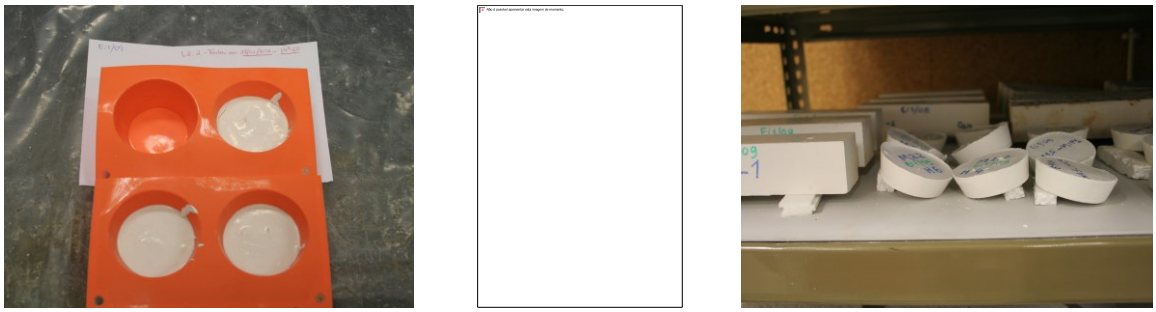

(a) (b) (c)

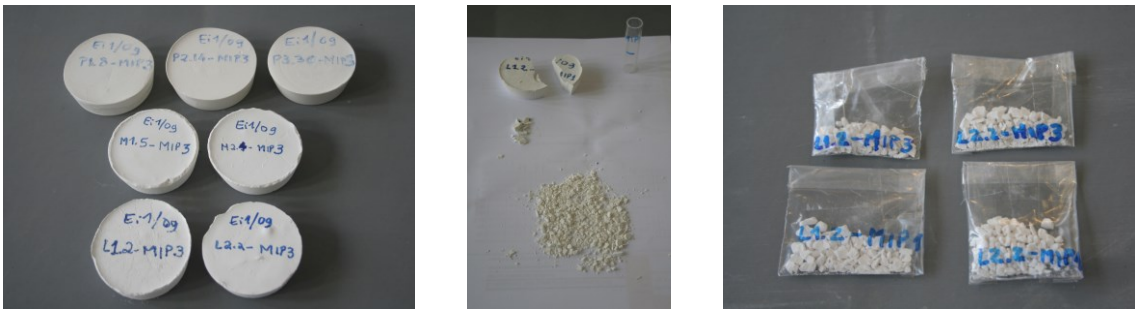

(d) (e) (f)

Figure 5.7 - Determination of the pore size distribution curves using mercury intrusion porosimetry: (a) and (b) preparation of the test specimens; (c) stabilization in conditioned environment; (d) stabilized specimens before grinding (d) and after grinding (e); (f) test specimens ready to be tested

The **capillary water absorption** coefficient was determined in prismatic test specimens with 90 days and 2 years according to EN 1015-18:2002 with some adaptations (Figure 5.8): it was done in the whole prisms, instead of in the two halves, the longitudinal faces were not sealed ,the weightings were more frequent in the beginning of the procedure and the results considered for the study were the capillary coefficient at 5 minutes and between 10 and 90 minutes (the straight part of the curve with higher slope), and the total absorption.

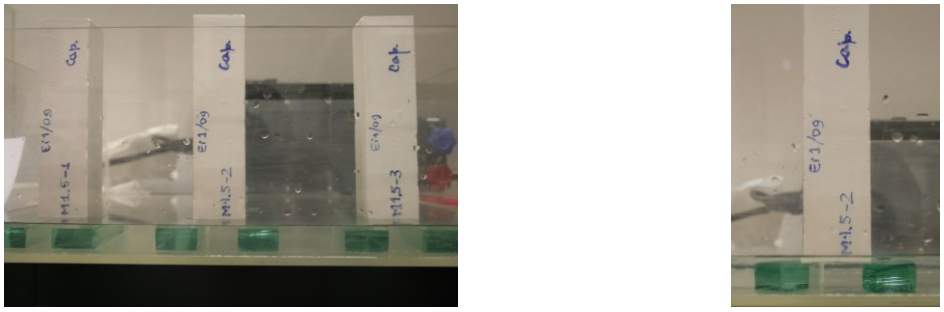

(a) (b)

Figure 5.8 - Determination of the capillary water absorption coefficient: (a) test specimens immersed in water by a few millimetres in a tray (absorption procedure); (b) detail of (a)

After 24 h, the test specimens were taken out of the tray and placed on two narrow stands in order to prevent the contact with water or any other surface (Figure 5.9). The capillary absorption stops then and the **drying** process starts, proceeding until the test specimens achieve constant weight.

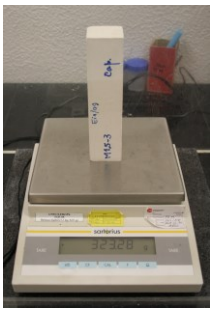

(c)

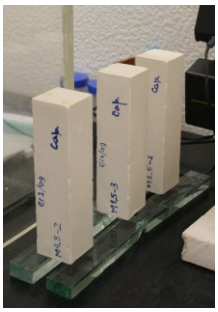

(d)

Figure 5.9 - Determination of the capillary water absorption coefficient: (a) weighing of a test specimen; (b) test specimens placed on stands outside the tray (drying procedure)

The **hygroscopic behaviour** was determined at 2 years using the same procedure as for ancient samples (Magalhães & Veiga 2007) (*cf.* 4.2.2). Test specimens of smaller dimensions like those used in the determination of the pore size distribution curves were used in order to reduce the time needed for achieving the weight balance (Figure 5.10).

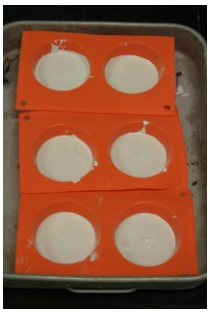

(a)

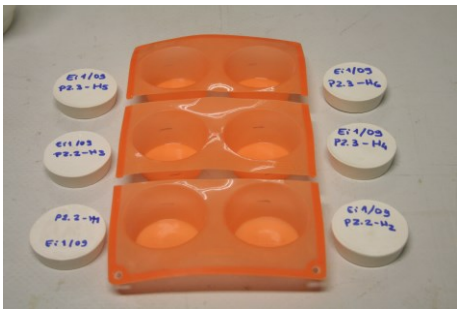

(b)

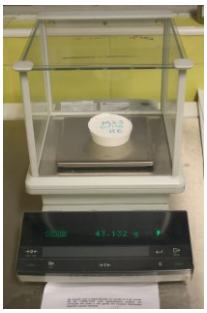

(c)

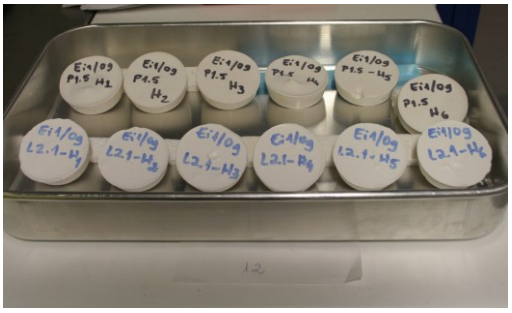

(d)

(e)

Figure 5.10 - Determination of the hygroscopic behaviour: (a) and (b) preparation of the test specimens; (c) weighing procedure; (d) device used to accommodate test specimens in the climatic chamber; (e) ongoing test inside the chamber

The **water vapour permeability** was determined at 90 days and 2 years using the method described in EN 1015-19:1998, with few adaptations (Figure 5.11). This method is based on the measurement of the water vapour flux through the samples due to the pressure differential between the internal (relative humidity approximately 100%) and the external surface (relative humidity = 50 ± 5 %), at 20 ± 2 ºC.

The 100% relative humidity conditions inside the test cups were achieved with water, and are considered to originate a water vapour saturated atmosphere. The vapour flux is quantified by the weight variations of the test devices at fixed time intervals.

(a)

(b)

(c)

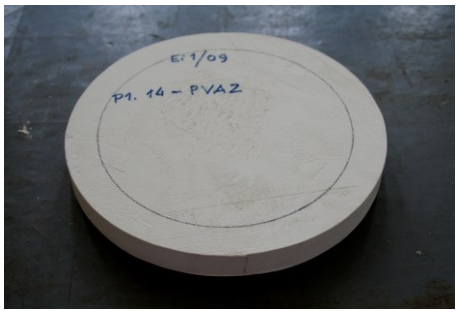

(d)

(e)

(f)

(g)

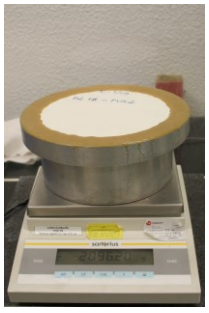

(h)

(i)

Figure 5.11 - Determination of the water vapour permeability: (a) to (d) preparation of the test specimens; (e) test cups filled with water; (f) application of the insulating material; (g) devices after completing the preparation; (h) weighing procedure (i) in the climatic chamber

The **dimensional variations** were evaluated by comparing the length of the test specimens measured immediately after demoulding, taken as reference, with the values of the subsequent measurements at different ages. Prismatic test specimens of hardened product with pins in the tops (Figure 5.12 (a)) were prepared using steel moulds similar to those indicated in NP EN 196-1:2006 (Figure 5.6).

Calibrated electronic indicators (resolution = 0.001 mm) placed on stands were used. Both the indicators and the stands have one fitting for the pins of the test specimens. Each test specimen was always measured in the same device, after weighing in a digital balance (resolution = 0.01 g) (Figure 5.12).

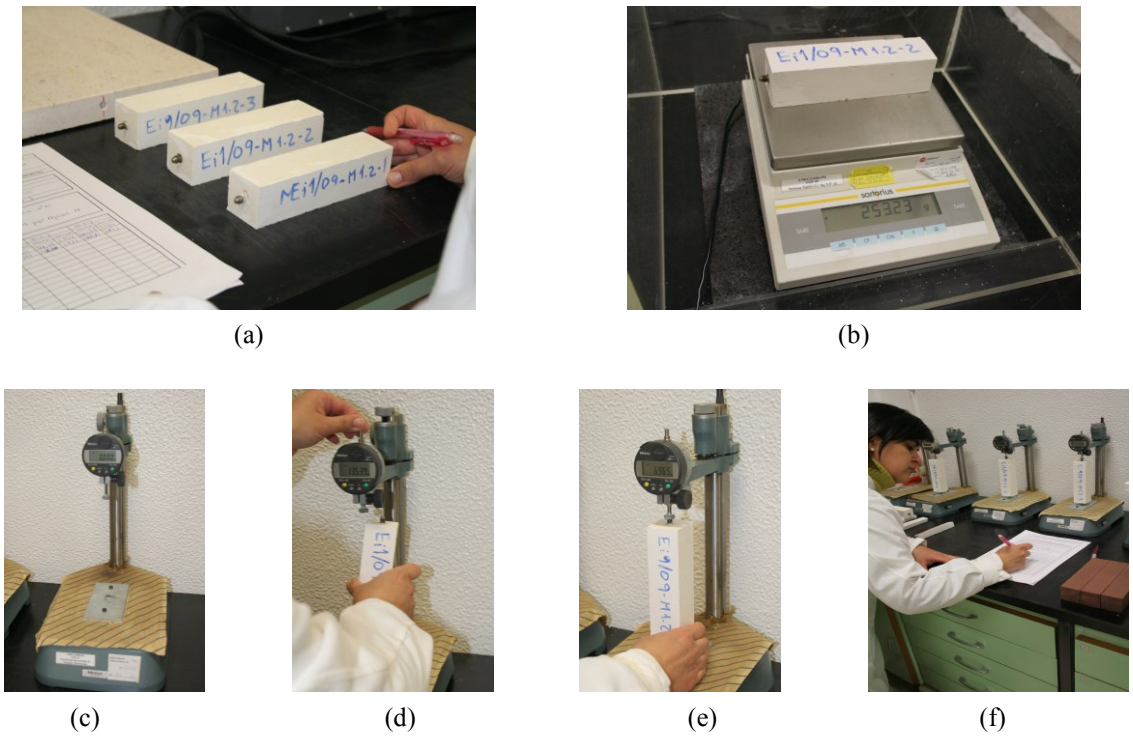

Figure 5.12 - Determination of the dimensional variations: (a) test specimens; (b) weighing procedure; (c) type of device used; (d) to (f) length assessment

In the case of the mixes with a higher content of hydrated lime (L1 and L2), the test specimens had to remain in the mould until achieving a minimum consistency to be demoulded. After that period most of the shrinkage had already occurred and the reference value for each test specimen was considered to be the internal length of the mould (measured with a caliper gauge, resolution 0.02 mm) where it had been cast (Figure 5.13).

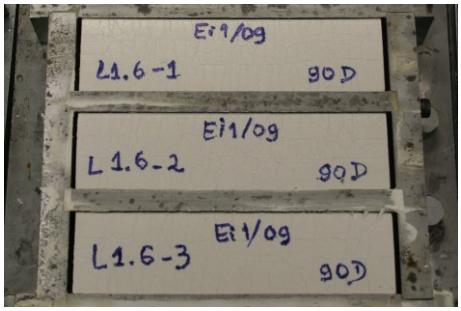

(a)

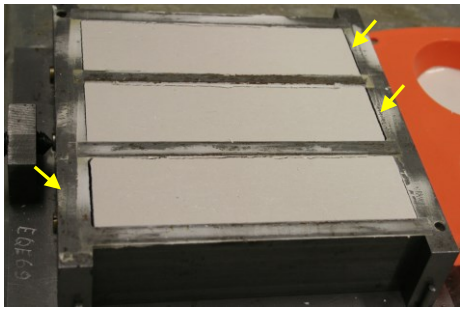

(b)

Figure 5.13 - Shrinkage of test specimens before demoulding: (a) L1; (b) L2 (yellow arrows)

The **dynamic modulus of elasticity** was evaluated at 28, 90, 180, 365 and 730 days using two methods:

- The one already used in the ancient samples, based on the measurement of the speed of propagation of longitudinal ultrasonic waves through laboratory prepared standardized test specimens, where the distance between the transductors was always about 160 mm, allowing the calculation of elastic parameters (NP EN 12504-4:2007) (Figure 5.14);

- The method based on the measurement of the fundamental resonance frequency of the material subjected to longitudinal vibrations (NP EN 14146:2006) (Figure 5.15).

A possible relationship between the results obtained using both methods was studied.

(a)

(b)

Figure 5.14 - Determination of the dynamic modulus of elasticity by measuring the speed of propagation of ultrasound waves: (a) general view of the ongoing procedure; (b) detail of the measurement

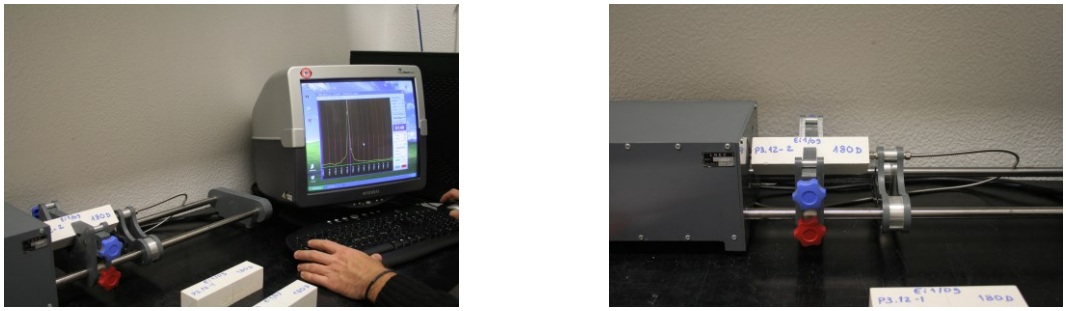

(a) (b)

Figure 5.15 - Determination of the dynamic modulus of elasticity by measuring the fundamental resonance frequency: (a) general view of the ongoing procedure; (b) detail of a test specimen in the apparatus

The test specimens used in the dynamic modulus of elasticity determinations were then subjected to **flexural and compressive strength** tests in the same electromechanical device as the ancient samples (Figure 5.16 and Figure 5.17).

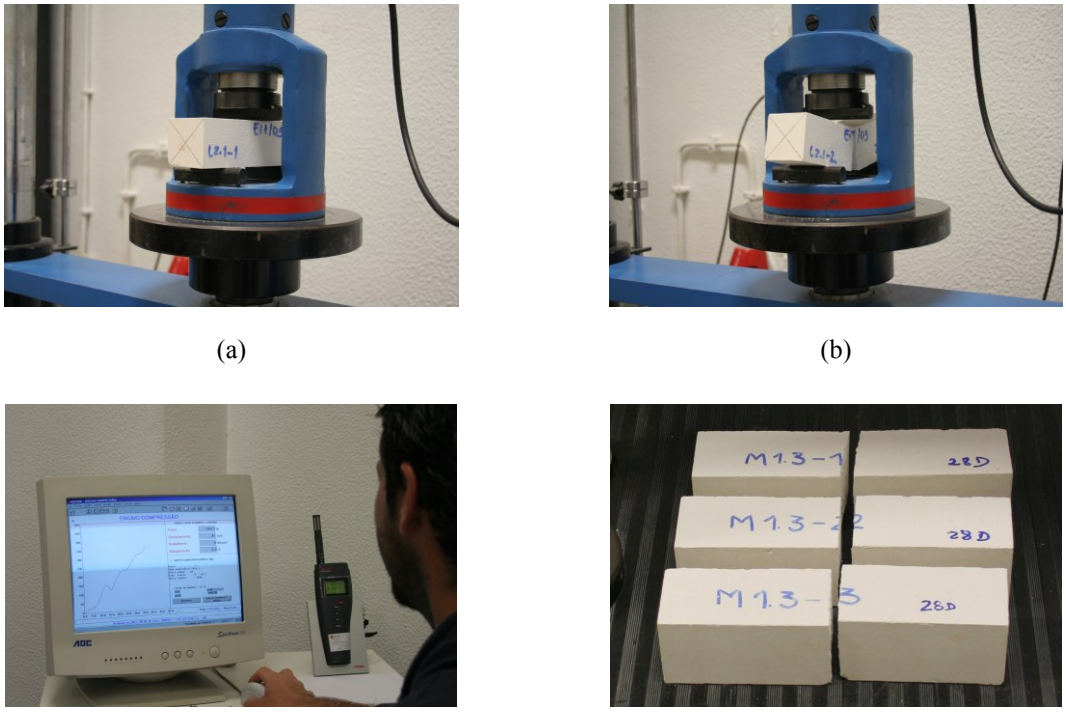

(a) (b)

(c) (d)

Figure 5.16 - Flexural strength tests: (a) device used with a test specimen positioned to be tested; (b) after failure of the test specimen; (c) graphical representation of the material's behaviour during load application; (d) semi-prisms resulting from a determination

(a)

(b)

(c)

(d)

Figure 5.17 - Compressive strength tests: (a) device used with a semi-prism positioned to be tested; (b) the same, after failure of the test specimen; (c) graphical representation of the material's behaviour during load application; (d) appearance of the test specimens at the end of the mechanical strength procedures

The loading rates were adjusted so that failure occurred within a period of 30 to 90 s (EN 1015-11), between 10 and 25 N/s in the flexural strength and between 50 and 200 N/ in the compressive strength tests (Table 5.3). Load cells of 2 kN and 200 kN were used, depending on the mechanical characteristics of the product.

Table 5.3 - Loading rates used in the mechanical strength tests

Product	Flexural strength	Compressive strength
L1	10N/s	50 N/s
L2	10N/s	50 N/s
M1	10N/s	100 N/s (50 N/s at 28 days)
M2	10N/s	50 N/s (100 N/s at 736 days)
P1	25N/s	150 N/s
P2	25 N/s	150 N/s (200 N/s at 28 and 734 days)
P3	25N/s	200 N/s

The evolution of the **carbonation process** was assessed through the quantification of the portlandite and calcite contents of the pastes at different ages (90, 180, 365 and 730 days) using TG-DTA analysis. The experimental conditions used were those of the ancient samples (*cf.* 4.2.2), as both phases suffer thermal decomposition with weight losses associated from ambient temperature till 1000 ºC.

Samples of the inner core of one of the resulting halves of freshly broken prismatic test specimens were collected and milled in an agate mortar until all the powder particles passed through a sieve of 106 microns (Figure 5.18 (a)). They were placed in sealed plastic bags and stored in a desiccator.

The surfaces of the other half prisms had been sprayed with phenolphthalein (1%) alcoholic solution (prepared with 30% water and 70% ethanol) for evaluation of the carbonation front (Figure 5.18 (b)).

(a) (b)

Figure 5.18 - Evaluation of the carbonation process: (a) preparation of samples for TG-DTA analysis; (b) surface of a test specimen a few seconds after being sprayed with phenolphthalein

5.5 Results and discussion

5.5.1 Development and test of different mixes

As referred before, the design of restoration products was mainly based on characterization studies of the original samples (*cf.* Chapter 4). However, additional information was obtained through interviews of people still applying these materials using traditional techniques. It is relevant to be aware of the skills and procedures of the available labour presently working in the field and to compare them with the results obtained as well as with the information found in the scarce Portuguese literature available.

A compilation of all this data is presented in Table 5.4. As the quantitative results of the ancient samples were obtained in mass percentage, the corresponding volumetric proportions had to be calculated, in order to standardize all the information. Only this way it was possible to compare the several compositions.

Table 5.4 - Composition of the traditional interior plasters: comparison between different information sources

Plaster element	Analytical characterization [1]		Interviews Plast. 1	Plast. 2	Literature (Leitão 1896)	(Füller n.d.)	(Paz Branco 1993)
	HH (%)	HL (%)	HH : Lime putty (volumetric proportions) [2]		HH : Lime putty (volumetric proportions)		
Thin-layer	44.1	55.9	1:1.3 1:1.9	1:2.8	1:4	1:1	1:1.7	1:1.5
Moulded on site	58.4	41.6	1:0.7 1:1.1	1:1.4	1:2.2	?	1:1	1:1
Precast and moulded on bench	94.5	- [3]	-	1:0	1:0	?	1:0	1:0

HH - gypsum hemi-hydrate; HL - calcitic hydrated lime; Plast. - plasterer; [1] Calculated from average values of Table 4.95 to Table 4.97 standardized so that HH + HL = 100%; [2] Bulk densities: HH = 0.69 kg/dm^3; lime putty with 5 years = 1.350 kg/dm^{3}and 48 hours = 1.280 kg/dm^3 (Margalha 2010); [3] The calcite content corresponds to impurities of the raw material

It is very interesting to notice that the characterization results obtained are very approximate to the recipes of Füller (n.d.) and Paz Branco (1993). However, they are quite different from those that the plasterers interviewed use nowadays, where the lime proportions are considerably higher. At first sight, this trend does not seem to be harmful to the ancient plasters when used in restoration works, as carbonated lime has lower mechanical strength and lower dynamic modulus of elasticity than gypsum. The main problem can be the higher dimensional variations and/or differences in some physical properties, namely lower capillary water absorption, characteristics that do not protect the pre-existing materials. All these issues will be discussed ahead during the presentation of the results of the products formulated for restoration purposes.

In the literature, it is also referred that the water used to prepare the mixes should have a given content of a set retarder. The most commonly recommended for manual application plasters were collagen-based glues deriving from bovine, rabbit and fish, the quantities depending on the intended retarding effect. Besides the influence on the plasters setting, they improved the workability of the pastes and had a hardening function on the final products. This procedure is also commonly described in some of the most significant foreign literature about the theme (Builder 1956; Hannouille 1959; Turco 2008; Arcolao 1998; Gárate-Rojas 1999). However, it was impossible to consider the use of animal glues in this work as they have to be previously soaked in the mixing water and dissolved through heating in a water bath (Figure 5.19), a procedure not compatible with the supply of powder pre-dosed products ready to be mixed with water, like it is the aim of this work.

Instead, the combination of a set retarder and a water retaining agent in the powder form, both of organic nature, were used to produce the same effect.

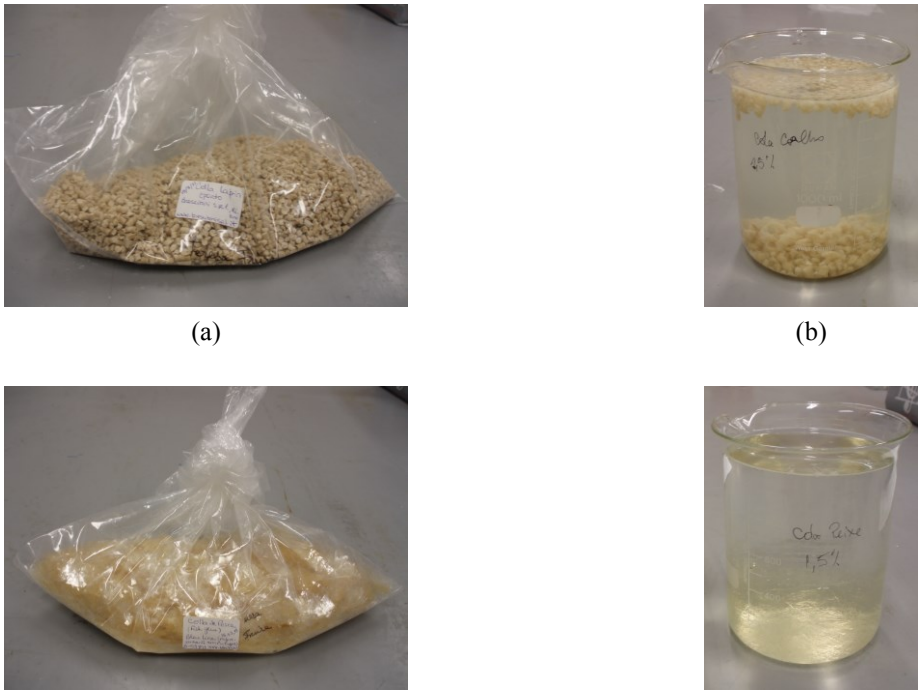

(a) (b)

(c) (d)

Figure 5.19 - Preparation of animal glues for preliminary workability tests: (a) dry granulated rabbit glue; (b) soaking the glue before heating; (c) and (d) the same, for fish glue

The first step towards the definition of the mixes of the new products concerned the gypsum-lime proportions. For the thin-layer and moulded on site plasters, two combinations of the binders have been established having in mind the fulfilment of the compatibility criteria, achieved through the reduction of the quantities of gypsum towards lime (Table 5.5).

Besides the binders, combinations of small additions of other constituents have been tested namely a calcitic aggregate (CA), two water-retaining agents (WRA) and two set retarders (SR).

In order to assess the workability of the old recipes, some tests were made with rabbit and fish glues in the thin-layer mixes. In both cases 1.5% solutions have been prepared and the best results were obtained with fish glue: the corresponding pastes showed an outstanding creaminess and elasticity and an effortless, soft application (Figure 5.20).

The water retaining agents adopted for the selected mixes had different viscosities and were methylcellulose-based. These products are common substitutes of the natural mucilaginous substances used in the past, even at low concentrations, with good overall results, both in the fresh pastes and in the hardened products (Turco 2008). They also have the advantages of being able to be used in the powder form and solubilize in cold water. Together with carboxylic acids acting as set retarders they can reproduce the behaviour of the old plasters.

Table 5.5 - Preliminary tests: selection of the mixes to be studied

Product	HH (%)	HL (%)	CA (%)	WRA1 (%)	WRA2	SR1 (%)	SR2 (%)
L1	**20**	**70**	**10**	**0.1**	**-**	**0.02**	**-**
L2	**30**	**70**	**-**	**-**	**-**	**0.02**	**-**
	30	**70**	**-**	**0.1, 0.075, 0.05**	**-**	**0.02**	**-**
	30	**60**	**10**	**0.1**	**-**	**0.02**	**-**
M1	40	60	-	-	-	-	-
	40	**60**	**-**	**-**	**-**	**0.02**	**-**
	40	**50**	**10**	**-**	**-**	**0.02**	**-**
	40	40	20	-	-	-	-
M2	50	50	-	-	-	-	-
	50	**50**	**-**	**-**	**-**	**0.02**	**-**
	50	**50**	**-**	1.0, 0.5, **0.1**, **0.05**, **0.025**, 0.02, **0.01**	-	**0.02**	-
	50	50	-	-	0.01	0.02	-
	50	40	10	-	-	-	-
	50	40	10	0.2	-	-	-
	50	**40**	**10**	**-**	**-**	**0.02**	**-**
	50	**40**	**10**	**0.01**	**-**	**0.02**	**-**
	50	**40**	**10**		**-**	**-**	**0.1**
P1	**90**	**10**	**-**	**-**	**-**	**-**	**-**
P2	**90**	**-**	**10**	**-**	**-**	**-**	**-**
P3	**100**	**-**	**-**	**-**	**-**	**-**	**-**

HH - hemihydrate; HL - calcitic air lime; CA - calcitic aggregate; WRA - water-retaining agent; SR - set retarder; bold - workability tests; blue shaded - selected mixes

(a) (b) (c)

Figure 5.20 - Lime-gypsum paste (equivalent to formulation L2) gauged with 1.5% fish glue solution: (a) creamy appearance after mixing; (b) elasticity (”membrane” effect); (c) application test

In what concerns the precast and moulded-on-bench elements, three mixes were tested: one composed only by gypsum hemi-hydrate (P3), which is supposed to be the procedure used in the past; one with 90% hemi-hydrate and 10% calcitic aggregate (P2), to reduce the binder quantity and evaluate the effect on workability; one with 90% hemi-hydrate and 10% hydrated lime (P1), also to assess the workability of the paste obtained and to try to decrease the dynamic modulus of elasticity of the hardened products, without reducing the capacity of reproduction of the most critical forms (e.g. small and/or delicate details and sharp edges).

All the mixes have been mixed with more than one plaster/water ratio (P/W). In the cases of the thin-layer and of the moulded-on-site products (L and M series, respectively) those that had an adequate consistency and seemed less sticky (Table 5.5, bold) were tested regarding workability (Figure 5.21 and Figure 5.22). In the M series, that included the evaluation of the reproduction of the forms using a laboratory application test specially designed for that purpose.

In the P series, the consistency results were enough to decide the plaster/water ratio that should be used in each case.

After all these steps it was finally possible to define the mixes and the respective experimental conditions that seemed to be the most adequate for undergoing the campaign designed to determine their main physical and mechanical characteristics (Table 5.6).

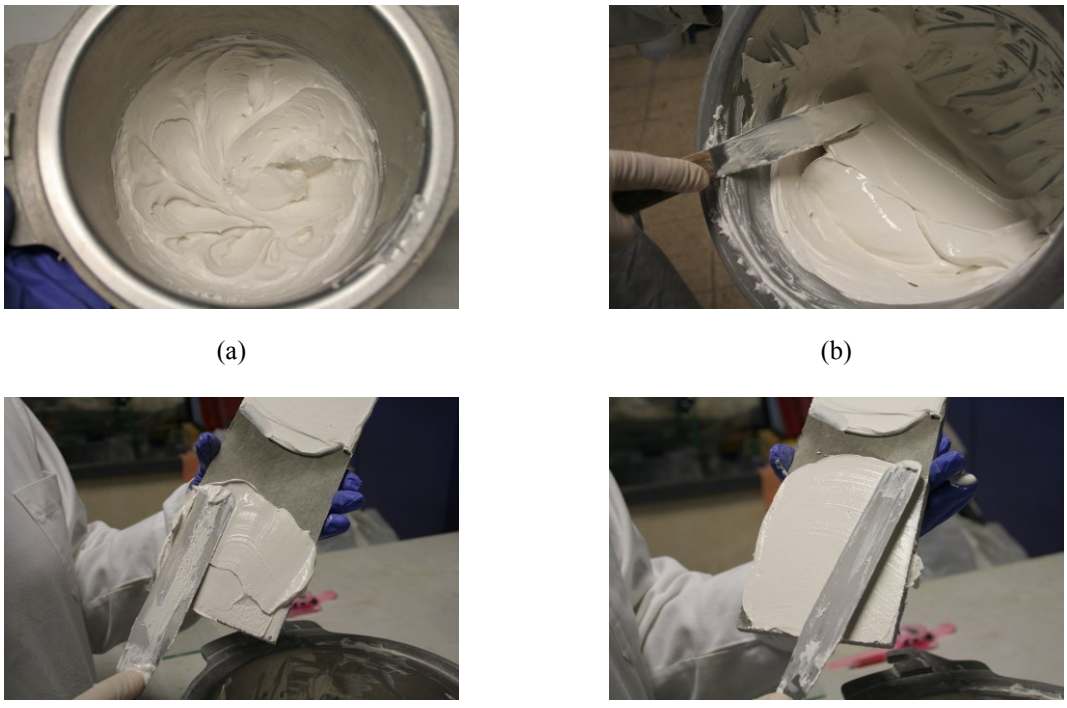

(a) (b)

(c) (d)

Figure 5.21 - Workability assessment of thin-layer plaster products (L2 formulation): (a) paste after preparation in the laboratory mixer; (b) after hand homogenization (b); (c) and (d) application test

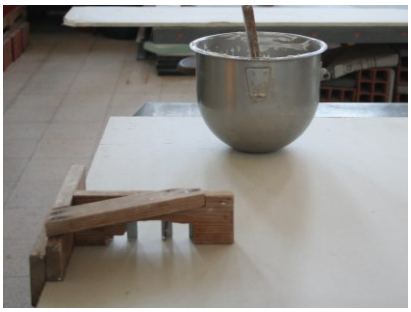

(a)

(b)

(c)

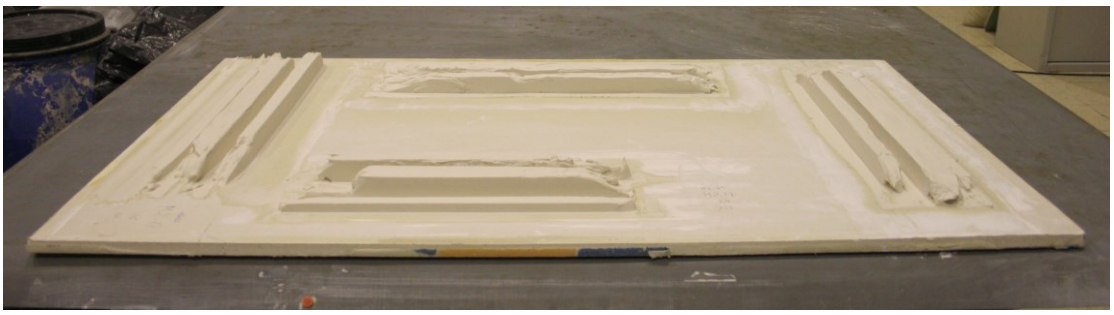

(d)

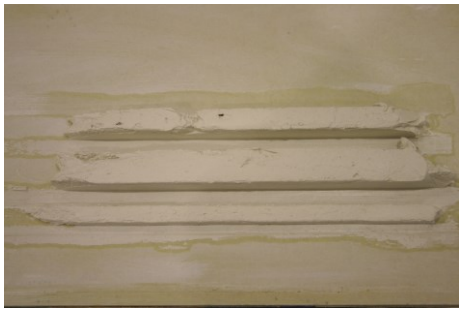

(e)

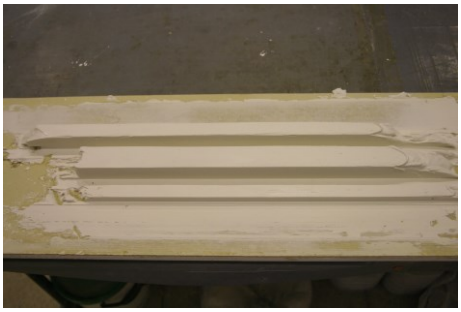

(f)

Figure 5.22 - Laboratory experimental application test of moulded on site products: (a) and (b) mould, fresh paste and plasterboard support; (c) on-going test; (d) general view of the results of some tests; (e) example of one of M2's rejected mixes; (f) results of M2'selected formulation

Table 5.6 - Restoration products based on gypsum and lime: mixes studied

Product identification	HH (%)	HL (%)	CA (%)	WRA1 (%)	SR1 (%)	P/W ratio (kg/l)	Spreading (mm) [(1)]	Initial setting time (min)
L1	20	70	10	0.1	0.02	1.0	165 ± 5	75-95
L2	30	60	10	0.1	0.02	1.1	165 ± 5	70-90
M1	40	60	-	-	0.02	1.2	165 ± 5	60-80
M2	50	50	-	-	0.02	1.3	165 ± 5	50-70
P1	90	10	-	-	-	1.2	180 ± 5	30-40
P2	90	-	10	-	-	1.4	205 ± 5	20-30
P3	100	-	-	-	-	1.4	190 ± 5	18-25

HH - hemihydrate; HL - calcitic air lime; CA - calcitic aggregate; WRA1 - water-retaining agent No. 1; SR1 - set retarder No. 1; P/W - plaster/water; [(1)] According to EN 13279-2:2004,165 ± 5 mm for pastes (L1, L2, M1 and M2) and 180 ± 30 mm for fluid consistency products (P1, P2 and P3)

The plaster/water ratio (P/W) varies from 1.0 kg/l to 1.4 kg/l (equivalent to water/binder ratios from 1.0 to 0.7) and are clearly related to the binders' characteristics and proportions used (Table 5.6), namely the specific surface area of the resulting powder mixtures, for each class of products (pasty, M and L series, or fluid, P series).

5.5.2 The carbonation process: quantitative assessment using TG-DTA analysis

When dealing with products where hydrated air lime is one of the main constituents, as it is the case of five out of seven mixes in this study, it is paramount to assess the evolution of the carbonation process for the interpretation of the results of the respective physical and mechanical properties.

One of the most precise processes of monitoring carbonation is by quantifying the portlandite present in samples collected at several ages, using TG-DTA analysis (Lanas & Alvarez 2003; Moropoulou et al. 2005; Lawrence et al. 2006b). In fact, the two main phases involved in the reaction, portlandite and calcite, show very well differentiated mass and thermal variations during heating of the test specimens: $Ca(OH)_2$ loses its chemically bound water at between 350 ºC and 550 ºC (dehydroxilation) and $CaCO_3$ loses CO_2 at between 600 and 900 ºC (decarbonation) (Lawrence et al. 2006a). These temperature intervals can have slight variations depending on the sample characteristics, experimental conditions, etc., as indicated by other authors (Arizzi & Cultrone 2013; Igea Romera et al. 2013), but are very approximate to what was considered in this work: 380-550 ºC and 550-900 ºC, respectively.

Samples of the inner core of freshly broken test specimens have been analysed and the respective portlandite content at different ages was used to calculate the carbonation degree index (I_{CD}, in %), according to the equation:

$$I_{CD} = (CH_0 - CH_x / CH_0) \times 100 \qquad \text{(Eq. 5.1)}$$

where CH_0 is the initial content of portlandite and CH_x is the content of portlandite at time x (Arizzi & Cultrone 2013).

In Figure 5.23 the evolution of the carbonation process of the five mixes where calcitic hydrated lime has been used is represented by the carbonation degree index as a function of time; the corresponding quantitative results are presented in Table 5.7. The initial content of portlandite was calculated taking into account the mixes of the products and the average degree of carbonation of the powdered hydrated lime used, determined by TG-DTA analysis (4.8%).

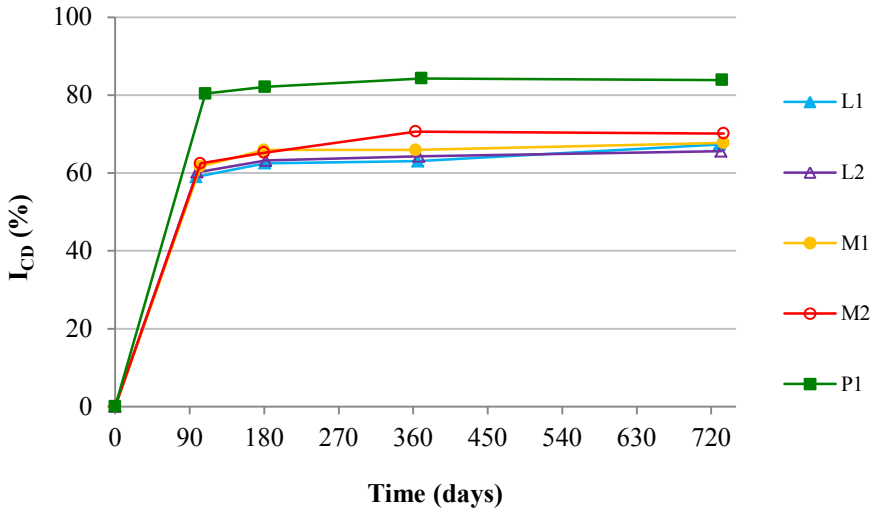

Figure 5.23 - Evolution of the carbonation process in the mixes with calcitic hydrated lime

As there is an increment of mass owing to carbonation (almost imperceptible in the case of P1), it was considered important to quantify it. Therefore, a mass factor was determined as the relation between the minimum mass achieved by the test specimens due to initial drying (7 days for L1, L2 and P1 and 14 days for M1 and M2) (Table 5.12) and the mass at each age where the portlandite content was determined by TG-DTA analysis. That content was then corrected using the mass factor, since it is closer to the real value (Table 5.7).

Between the preparation of the mixes (initial time) and the first measurements (98-109 days) the slopes of the curves of Figure 5.23 are very similar, except for P1, that is higher. This gives interesting information about the carbonation rate of the pastes, showing that 80% of the portlandite was carbonated in the first three months in P1 and about 60% in the other products. Considering that the samples were taken from the core of the test specimens and that carbonation evolves from the exterior to the interior, the areas closer to the surface should be even more carbonated.

It is also clear that after a first period of high rates of carbonation (i.e. at least three months but possibly less), the process radically slows down. Similar observations have been made by Cizer, Van Balen, et al. (2012) that monitored the reaction rate and phase modifications during lime carbonation. They suggest that it occurs in three stages characterized by different prevailing reaction mechanisms:

1) Stage I – chemical-reaction controlled regime in which the CO_2 diffusion is limited at the surface due to the pore water and due to the very quick initial precipitation of amorphous $CaCO_3$ at the portlandite crystals faces passivating the reaction;
2) The transformation of amorphous $CaCO_3$ into calcite and the drying effect promote the reactivation of the carbonation reaction at a much higher rate than that of stage I;

3) Stage III - the carbonation reaction moves to a slower regime controlled by the CO_2 diffusion through the sample depth where it is believed to continue but at such slow rate that becomes difficult to detect.

Table 5.7 - Assessment of the carbonation degree through portlandite content: quantitative results

Product	Time	TG results	Mass factor	Portlandite content (corrected results) [(1)]	I_{CD}
(initial content, %)	(days)	(%)		(%)	(%)
L1	98	25.1	1.09	27.3	59.0
(66.6)	181	22.9	1.09	25.0	62.5
	366	22.6	1.09	24.6	63.0
	730	19.8	1.10	21.8	67.4
L2	99	21.3	1.07	22.7	60.2
(57.1)	182	19.7	1.07	21.0	63.2
	367	19.1	1.07	20.4	64.3
	732	18.4	1.07	19.7	65.6
M1	103	20.5	1.07	21.9	61.6
(57.1)	180	18.2	1.07	19.5	65.9
	363	18.2	1.07	19.5	65.9
	735	17.2	1.07	18.4	67.7
M2	103	16.9	1.06	17.9	62.5
(47.6)	180	15.6	1.06	16.6	65.2
	363	13.2	1.06	14.0	70.6
	735	13.4	1.06	14.2	70.2
P1	109	1.9	1.01	1.9	80.4
(9.5)	181	1.7	1.01	1.7	82.1
	370	1.5	1.01	1.5	84.3
	733	1.5	1.01	1.5	83.9

TG - Thermogravimetry; I_{CD} - Carbonation degree index; [(1)] Corrected results = (TG results) x (mass factor)

In the two mixes with lower initial hydrated lime content (M2 and P1) carbonation seems to stop after one year while in the other three it still goes on. However, considering what has just been exposed about the carbonation reaction mechanisms, further analysis, namely observations in the SEM, would have to be made to help clarifying what is really occurring.

Igea Romera et al. (2013) in their study of gypsum-lime repair mortars also found that the mixes with lower lime content had higher carbonation rates and went even further, stating that "an increment in the lime binder amounts slows down the hydration of gypsum and also the carbonation process"

(p. 1611). Both effects have been detected in the products prepared in this work but can be considered negligible.

Comparing now the results obtained with other studies of lime mortars (1:3 binder/aggregate ratio) (Lawrence et al. 2006a; Arizzi & Cultrone 2013) it can be concluded that the carbonation rate was higher in all the gypsum-lime pastes. The explanation might be in the pore size distribution whose results will be discussed in the next section.

Parallel to the TG-DTA analysis, the evolution of carbonation was also assessed using the traditional procedure of spraying the freshly broken surfaces of the test specimens with phenolphthalein. The staining patterns obtained in the first measurements are shown in Figure 5.24.

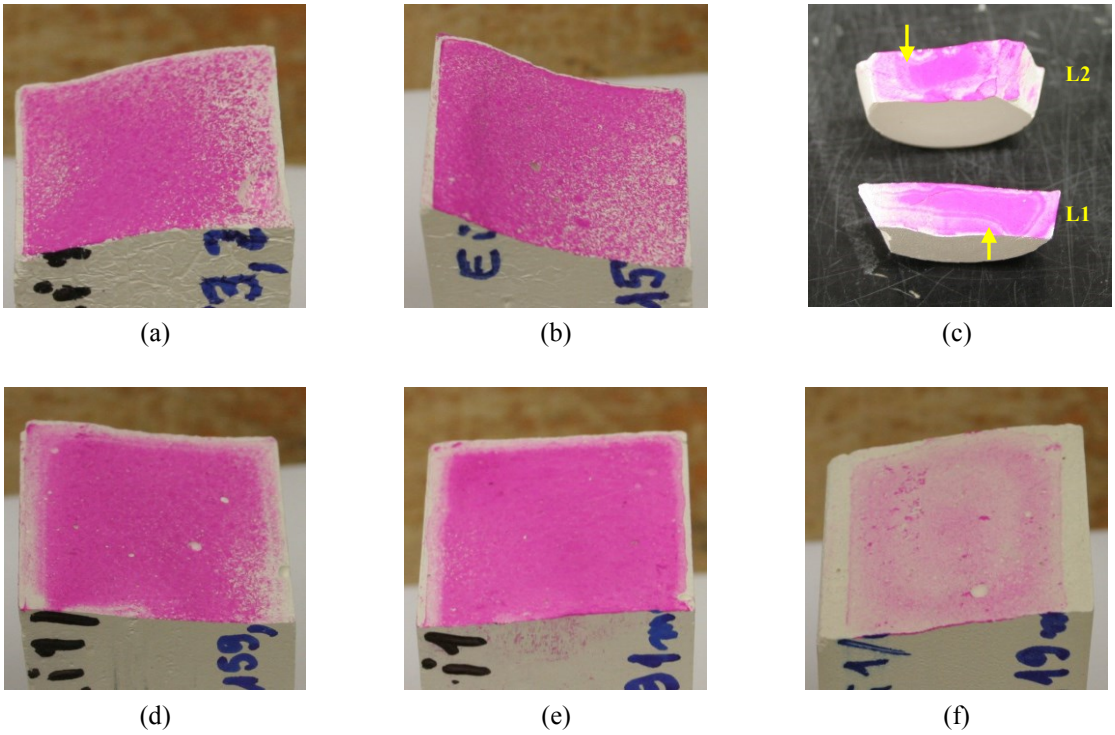

Figure 5.24 - Phenolphthalein staining of freshly broken test specimens: (a) L1 (98d) (b) L2 (99d); (c) thinner test specimens of L1 and L2 (98d and 99d, respectively) for comparison, with visible *Liesegang* patterns (yellow arrows); (d) M1 (103d); (e) (M2 (103d); (f) P1 (109d)

All the test specimens show a white line around the external area of the surfaces, with variable thickness, except in the edge corresponding to the upper surface when moulding, meaning that carbonation is more difficult through there. This is a very interesting and important observation as it shows how the handling of the specimens during moulding, namely the removal of excess material and flattening of the external surface, interferes with its porosity, hindering the carbonation process of the pastes. In fact, the smaller particles are pulled up and concentrate at the surface due to this kind of operations, a trend also observed at the worksite when the surfaces are smoothened. No reference to

this subject was found in the literature which might indicate that it is not usually observed in mortars' test specimens, where higher quantities of aggregates are commonly used.

The white areas appearing after spraying with phenolphthalein are theoretically carbonated material. They give an indication of the depth of carbonation when using this method. In practice, it has been found that unstained material can still contain 40 to 50% uncarbonated lime (Lawrence et al. 2006a), giving only an approximate (though reliable) localization of the carbonation front. The higher the gypsum/lime proportions are, the thicker the white area around the three surfaces of the corresponding test specimens, i.e. the deeper the carbonation front is. However, the global carbonation degree is very similar between L and M mixes, meaning that it probably evolves in different ways: more homogeneous throughout the microstructure in the L mixes and steeper between the outer and the inner parts of the M mixes. Considering that L2 and M1 have exactly the same content of hydrated lime but the second one has more gypsum than the first one, this seems to indicate that the presence of gypsum strongly influences the microstructure and pore system of the pastes (pore size distribution and open porosity).

The thickness of the specimen also has a strong influence on its carbonation rate, as illustrated in Figure 5.24 (c), where the phenolphthalein staining of fractured surfaces of test specimens used for MIP analysis of L1 and L2 indicates a higher carbonation degree. *Liesegang* patterns – formation of periodic layers of precipitated crystals of calcite making the pH drop in the corresponding areas - are observed on these surfaces, especially in L1's (Cizer, Rodriguez-Navarro, et al. 2012). These authors studied the phase and morphology evolution of the calcium carbonate crystals precipitated by carbonation of hydrated lime and described it as follows:

a) Initial reaction immediately at the surface of the lime paste with formation of amorphous $CaCO_3$ crystals (corresponding to stage I of carbonation);
b) When the excess water starts to evaporate the concentration of Ca^{2+} ions in the remaining pore water increases to levels that favour the formation of scalenohedral calcite crystals (stage II).
c) The pH drops in the carbonation front due to the consumption of ions OH^- and to the continuous diffusion of CO_2 that dissolves in the pore water. This lower pH leads to the dissolution of the scalenohedral crystals (through a mechanism of "corrosion" of the crystals' faces);
d) The concentration of ions Ca^{2+} and CO_3^{2-} increases and new, rhombohedral calcite crystals precipitate. These crystals are smaller and more stable than the scalehohedral crystals, forming a very compact microstructure with a staircase morphology;
e) The diffusion path of CO_2 through the sample thickness is hampered by the scalehohedral-to-rhombohedral transition, slowing down dramatically the carbonation rate (stage III).

f) The scalenohedral-to-rhombohedral transformation is favoured by higher relative humidities (till a limit of 93%) and by exposure to higher concentrations of CO_2.

So, according to these authors, the *Liesegang* patterns correspond to the scalenohedral crystals formation and the pH drop associated. They are usually related to the use of aged lime putty (which is not the case here), whose smaller particles have higher specific surface area being more reactive than those of the hydrated lime powder and/or to other factors that lead to the same result (Lawrence et al. 2006a; Cizer, Van Balen, et al. 2012). In the case of the test specimens of L1 and L2 shown in Figure 5.24 (c), their lower thickness, that favours the CO_2 diffusion, is the most plausible explanation.

After these remarks, and taking into account that the average thickness of the gypsum-lime test specimens evaluated in this study is 40 mm, it is easier to understand why the carbonation reaction evolves at such low rate after the first 3 months. They will also help explaining many of the features discussed along this chapter.

Still concerning Figure 5.24, a different texture of the surfaces of L1 and L2 compared to those of M1 and M2 can be observed. The strong fuchsia colour imprint of phenolphthalein makes the surfaces of the first group seem to be rougher that those of the second one, while in practice it is exactly the opposite (Figure 5.25). This is probably another effect of the different carbonation distribution through the microstructure of the materials.

(a) (b)

Figure 5.25 - Surfaces of test specimens after failure showing textural differences: (a) L1; (b) M2

5.5.3 Pore size distribution

The pore size distribution curves using mercury intrusion porosimetry (MIP) were determined at 90 days and 2 years and the results obtained are presented in Figure 5.26, Figure 5.27 and Table 5.8.

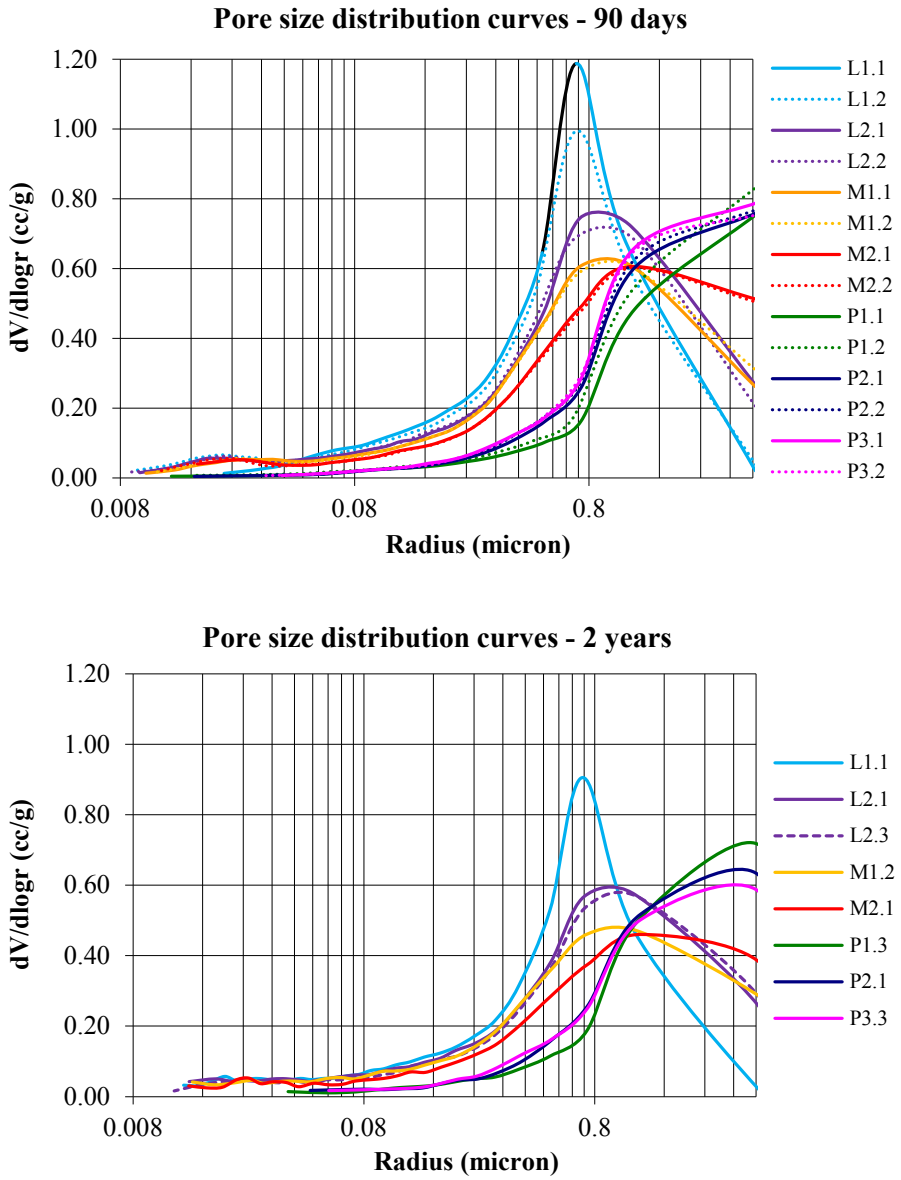

Figure 5.26 - Pore size distribution curves at 90 days and 2 years

Between 90 days and 2 years total porosity decreased in all the mixes, which was expected in the gypsum-lime mixes (L and M series) due to carbonation (Arandigoyen et al. 2006) but is somehow unexpected in the products mainly, or even totally, made of gypsum (P series).

With the exception of P1, all the curves show a clear reduction of the volume of pores of higher dimensions in the size range analysed and a slight reduction in the smaller pores ($r < 0.1$ micron), more evident in the specimens with higher lime content (L series, Figure 5.27). As observed in ancient samples (*cf.* Chapter 4), the gypsum plasters have much fewer pores with radius below 0.5 micron and almost do not have pores below 0.1 micron.

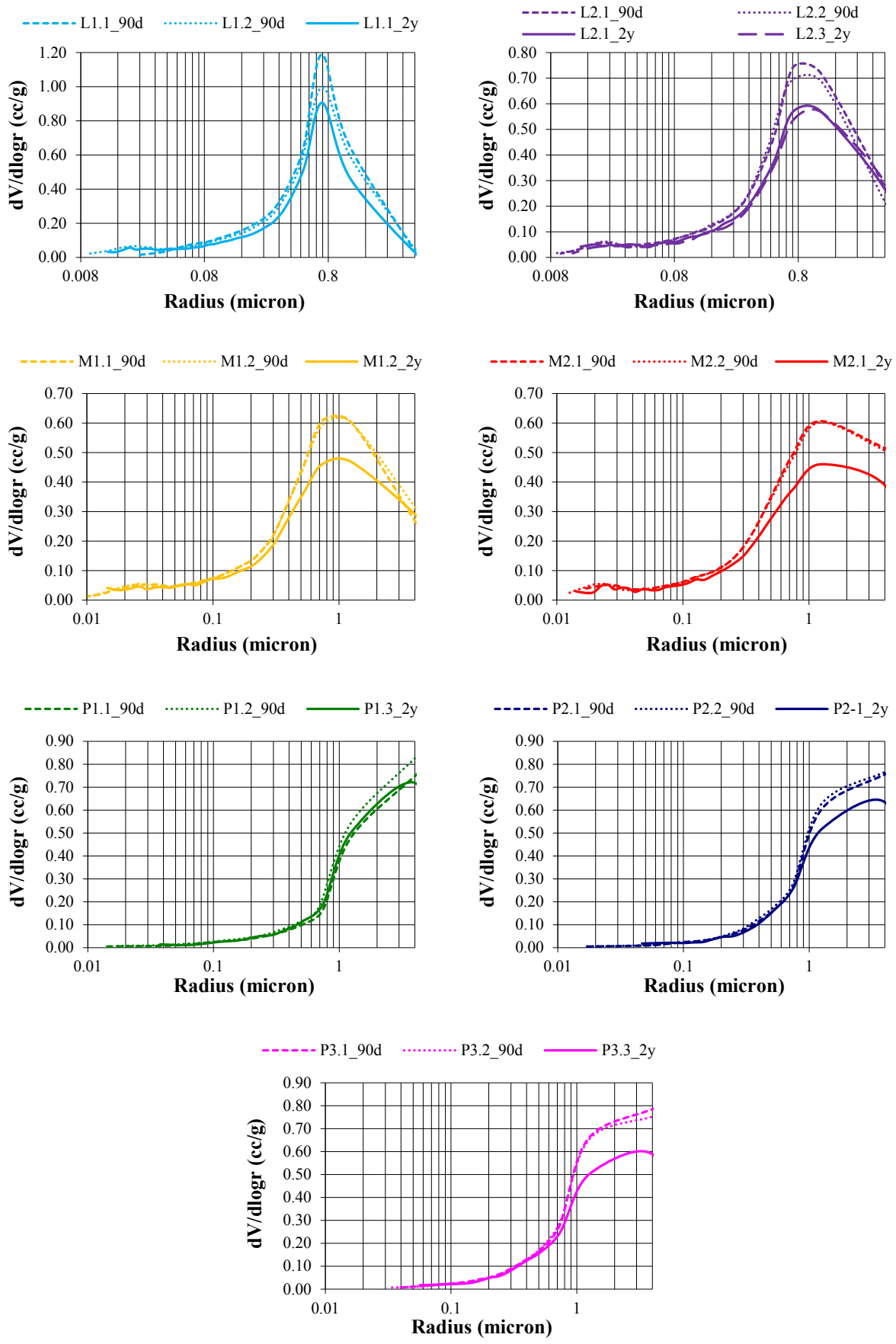

Figure 5.27 - Individual pore size distribution curves at 90 days and 2 years

Table 5.8 - Results obtained by MIP analysis at 90 days and 2 years

Sample.test specimen_age	Bulk density ($kg.m^{-3}$)	Density ($kg.m^{-3}$)	Porosity (%)	ΔPorosity 90d_2y (%)	Pore radius at max. volume* (μm)
L1.1_90d	929	2244	58.6		0.706
L1.2_90d	1022	2621	61.0		0.711
L1.1_2y	1031	2089	50.7	-9.1	0.716
L2.1_90d	972	2602	62.6		0.731
L2.2_90d	989	2629	62.4		0.693
L2.1_2y	984	2016	51.2		1.198
L2.3_2y	989	2045	51.6	-11.1	1.255
M1.1_90d	1018	2541	59.9		0.741
M1.2_90d	1015	2541	60.1		1.240
M1.2_2y	1053	2088	49.6	-10.4	1.255
M2.1_90d	1066	2573	58.5		1.212
M2.2_90d	1059	2600	59.3		1.240
M2.1_2y	1104	2141	48.4	-10.5	1.270
P1.1_90d	1068	2567	58.4		4.267
P1.2_90d	977	2396	59.2		4.266
P1.3_2y	999	2000	50.1	-8.7	4.266
P2.1_90d	1088	2568	57.6		4.266
P2.2_90d	1063	2488	57.3		4.266
P2.1_2y	1065	2049	48.0	-9.5	4.266
P3.1_90d	1050	2352	55.4		4.266
P3.2_90d	1079	2425	55.5		4.266
P3.3_2y	1128	2095	46.1	-9.4	4.266

* For P1, P2 and P3 the values indicated are the same, corresponding to the upper limit of the equipment

In the gypsum-lime mixes, the explanation for the previous facts is directly related to the evolution of the carbonation process along time, which originates the precipitation of very small calcium carbonate crystals, with only few micron (Margalha et al. 2011), that totally or partially fill some of the empty spaces in the microstructure, reducing the total porosity (Arandigoyen et al. 2006). In the case of the gypsum test specimens, the microstructure was expected to be relatively stable in the storage conditions of temperature and humidity used. However, it seems that there is an evolution along time towards the formation of crystals of smaller dimensions, or even new crystals that take a longer time to hydrate. The XRD analysis of the calcium sulphate used in the mixes showed the presence of traces of anhydrite. Nevertheless, it does not seem enough to be the only cause in the origin of the referred

microstructural changes. The previous hypotheses could have only been confirmed if SEM observations of the morphology of the pastes had been made, both in the fractured and the polished surfaces. In any case, not only the reduction of porosity would be explained, but also the decrease of the volume of bigger pores, of the capillary water absorption and of the water vapour permeability, properties that will be discussed below.

Concerning total porosity, the values obtained (56-63% at 90 days and 46-51% at 2 years) are in agreement with those found in the literature for lime-pastes (Arandigoyen et al. 2005), with the L products having the highest values but the lowest powder/water ratios, too. Following this argument (powder/water ratio), it was not expected that L2 had a higher porosity than L1. However, it seems that the pore size distribution and the way the crystals are organized in the microstructure, typical for each material, have a greater influence in the porosity than the kneading water. This might also be the most logical explanation for the less significant differences of porosity observed between the studied mixes than expected.

About the kneading water (Table 5.6), it is worth pointing out that the compositional difference between the mixes L1 and L2 is the substitution of 10% of hydrated lime by the corresponding content of calcium sulphate hemi-hydrate. What seemed to be a small variation was, in fact, enough to reduce the amount of kneading water of L2, a trend that was kept directly related to the decrease in the amount of lime and increase in the amount of hemi-hydrate on the remaining mixes, for the same consistency requirements (between M2 and P1 there is a significant change in this parameter).

The explanation for this trend lies in the difference of specific surface area of both materials, substantially higher in the hydrated lime particles (Table 5.2). The water needed for wetting their surface is therefore increased, and it is necessary to add more water to obtain a similar consistency.

Still concerning the main factors that influence porosity and pore size distribution, the mix with more lime (L1) has the main peak at a pore radius of about 0.7 micron, a value characteristic of a lime binder (according to Arandigoyen et al. 2005, the main pore size is between 0.25 and 0.5 micron, increasing when the water/lime ratio rises). With the increase of the gypsum content and consequent decrease of lime, the kneading water decreases. In spite of that, there is a shift in the value of the main pore radius to higher values and a broadening of the corresponding peak. In the P series mixes, where gypsum is the main (90% in P1 and P2) or only constituent (in P3), the main pore radius is above the upper limit of detection of the apparatus (> 4 micron).

Finally, a very important and interesting issue is the shift of the main pore size to lower values with stabilization of the microstructures of lime and gypsum, as can be clearly seen in the pore size distribution curves of the samples from *Estói* Palace and *Garag*e building case studies (*cf.* “Pore size distribution” sections, chapter 4).

5.5.4 Capillary absorption

The water absorption by capillarity and the subsequent drying behaviour were evaluated at 90 days and 2 years and the results obtained are presented in Figure 5.28, Figure 5.29, Figure 5.30, Figure 5.31 and Table 5.9.

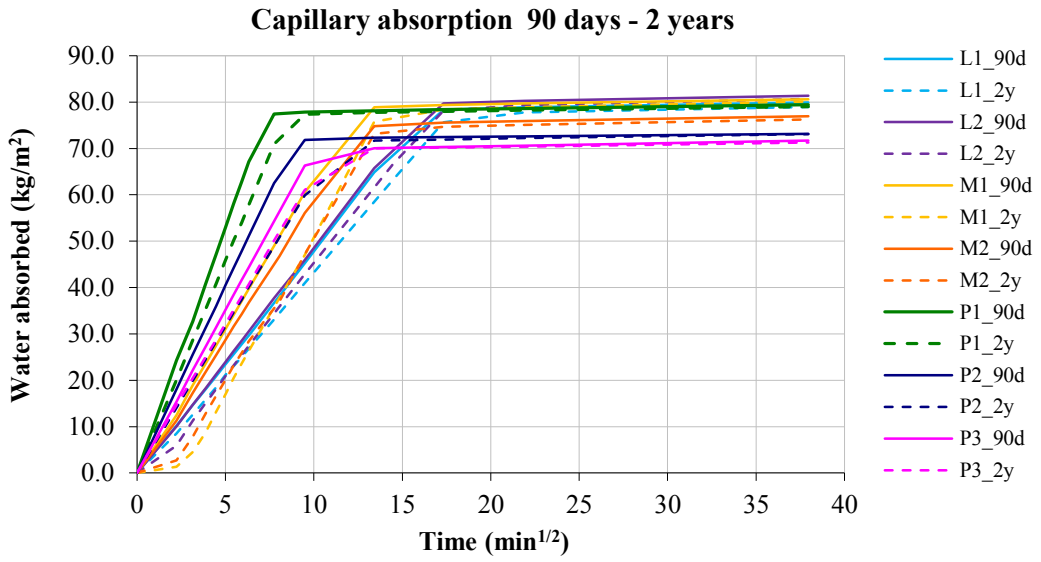

Figure 5.28 - Capillary water absorption: graphical representation of the results

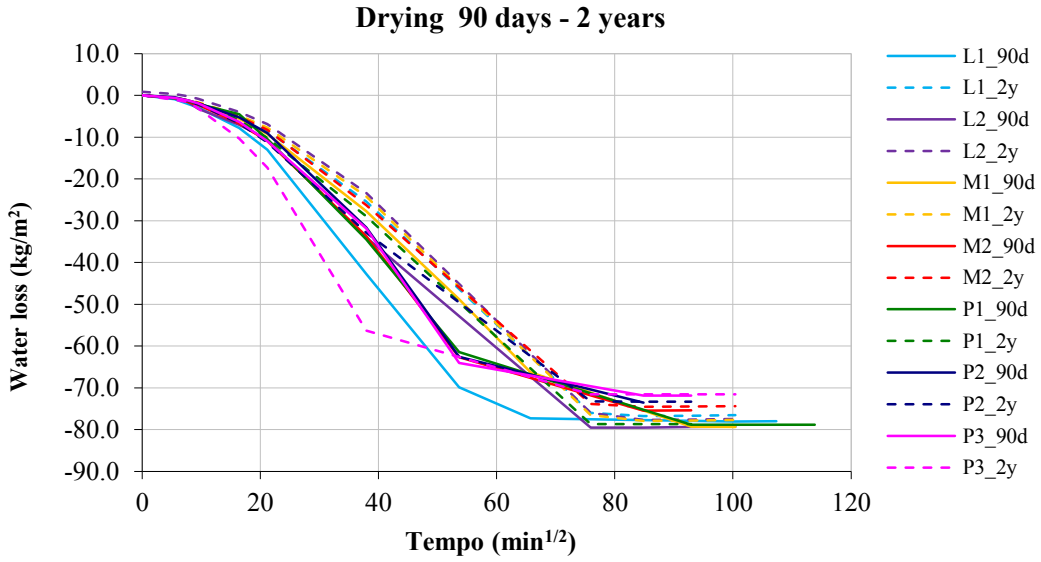

Figure 5.29 - Capillary water absorption: graphical representation of the drying behaviour

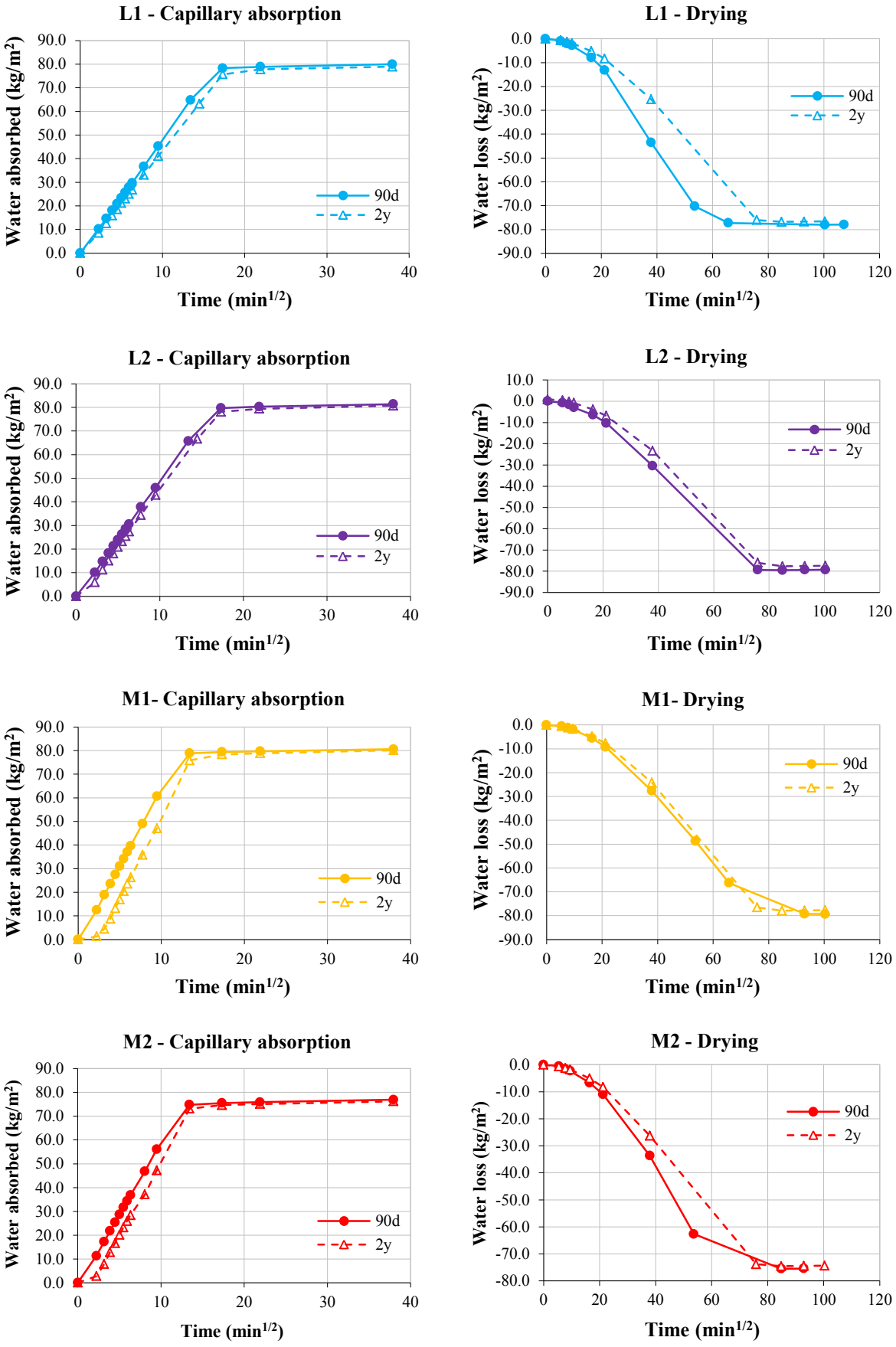

Figure 5.30 - Individual representation of the capillary water absorption and drying behaviour at 90 days and 2 years: mixes L1, L2, M1 and M2

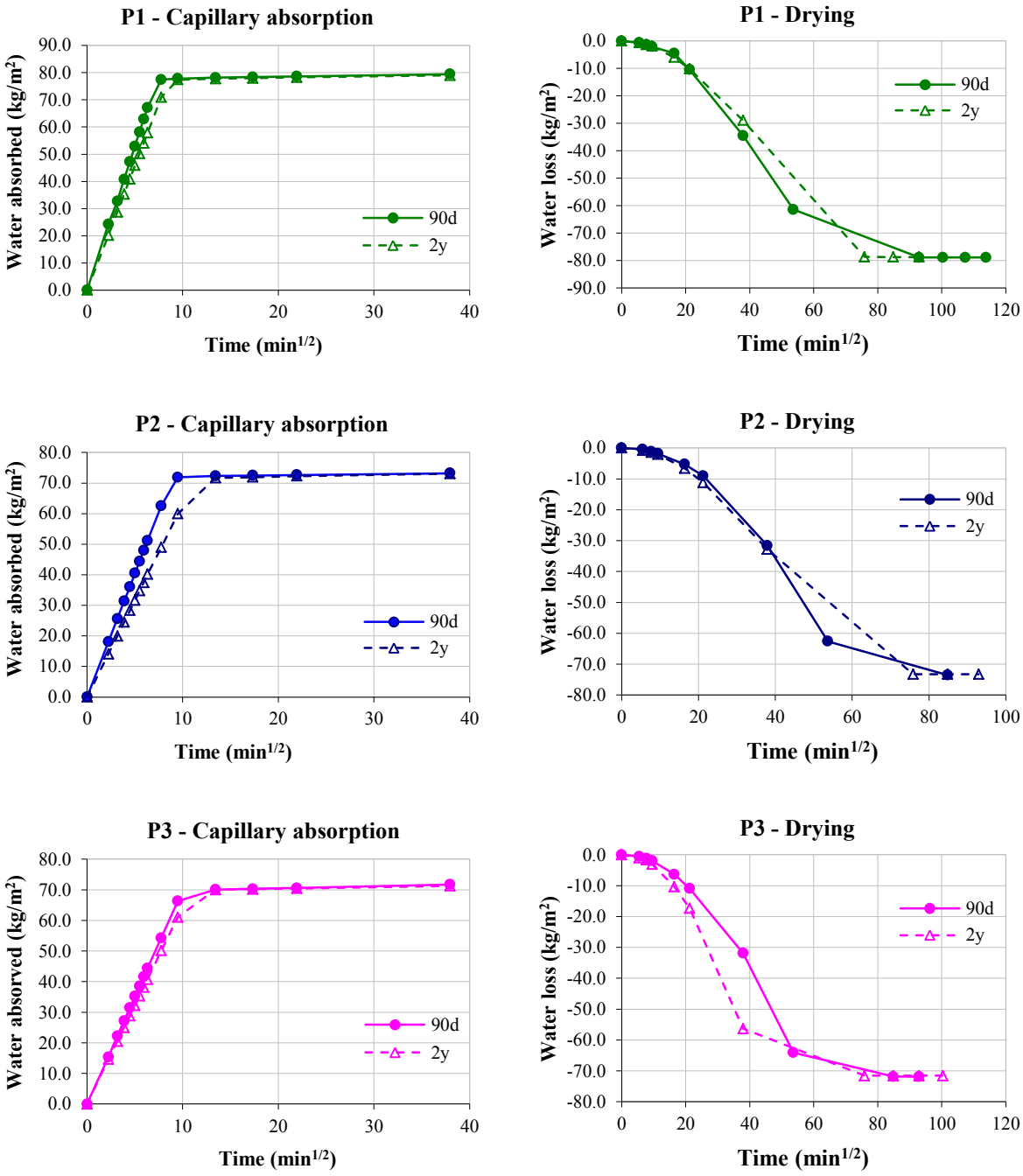

Figure 5.31 - Individual representation of the capillary water absorption and drying behaviour at 90 days and 2 years: mixes P1, P2, and P3

The curves represented in Figure 5.28 show that those corresponding to the P formulations have the highest slopes, i.e. the highest coefficients of capillary absorption (both at 5 minutes and between 10 and 90 minutes). This observation is in agreement with the respective pore size distribution curves, where the samples with more gypsum have larger pores, leading to higher suction rates, especially in

the beginning of the procedure. P1 appears at the top of the list, which is certainly due to the contribution of the higher quantity of kneading water used.

Table 5.9 - Capillary water absorption results at 90 days and 2 years

Product	Age	Cc 5 min	Cc 10-90 min	ΔCc 5 min	ΔCc 10-90 min	Max. abs.	ΔMax. abs.	ΔMax. abs.
				90d_2y	90d_2y	(at 24h)	90d_2y	90d_2y
		($kg.m^{-2}min^{-1/2}$)		(%)	(%)	($kg.m^{-2}$)		(%)
L1	90d	4.56	4.84	-16.1	–7.2	79.95	-1.03	-1.28
	2y	3.82	4.49			78.92		
L2	90d	4.49	4.93	-41.1	+1.4	81.35	-0.66	-0.81
	2y	2.64	5.00			80.69		
M1	90d	5.58	6.59	-89.2	+2.1	80.61	-0.46	-0.57
	2y	0.60	6.73			80.15		
M2	90d	5.04	6.14	-75.6	+1.5	76.94	-0.68	-0.89
	2y	1.23	6.23			76.26		
P1	90d	10.85	7.14	-17.2	+7.8	79.46	-0.45	-0.57
	2y	8.98	7.70			79.01		
P2	90d	8.07	7.32	-22.1	-13.7	73.18	-0.11	-0.15
	2y	6.29	6.32			73.07		
P3	90d	6.86	6.97	-4.6	-7.9	71.71	-0.45	-0.63
	2y	6.55	6.42			71.26		

Cc - capillarity coefficient; Max. abs. - maximum absorption

Between 90 days and 2 years there was a generalized decrease of the capillary coefficient at 5 minutes, clearly illustrated in Table 5.9. However, the suction rates rapidly recover, as seen in the results of the capillary coefficient between 10 and 90 minutes, getting close to those observed at 90 days, or even surpassing them in some cases (M1, M2 and P1). This means that the surface of the test specimens at 2 years is less porous and/or it has a lower number of capillary pores with radius above 0.5 micron (Magalhães et al. 2004; Rato 2006), which is not a surprise in the case of the mixes with lime. In fact, carbonation evolves from the exterior to the interior reducing the porosity in the same direction. The higher the carbonation depth, the slower the expected initial absorption is. The reduction observed in the capillary coefficient at 5 minutes between 90 days and 2 years in M1 and M2 is probably explained by this issue, as the rate of carbonation is higher in these materials than in L1 and L2 (Figure 5.23, Figure 5.24 and Table 5.7).

The results obtained in the pore size distribution study using MIP and discussed in the previous section

show that there is a clear decrease of the content of pores with r > 0.5 micron in the gypsum-lime mixes, except in P1 (Figure 5.27). So, in general lower capillary coefficients would be expected throughout the time of the procedure, which was not the case. The only observation that denoted an increase of the number of smaller pores was the weight stabilization of the test specimens until achieving the maximum absorption capacity: it was slower after 2 years, in all the mixes.

Comparing the maximum absorption with the total porosity of the test specimens at 2 years, the usual direct relation between these parameters did not occur in any case. In fact, the values of the maximum absorption had a very slight reduction (between 0.2 and 1.3%, Table 5.9) while in the total porosity the reduction was significant (9-11%, Table 5.8).

The interpretation of hydric properties in pastes where hydrated lime (portlandite) is a main constituent is often complicated, especially in the first months of curing, not only due to the possibility of occurring some dissolution of portlandite, but also because of the heterogeneity and instability still going on in the pore structure of the matrix (Arizzi & Cultrone 2013). Even after 2 years the process of carbonation is far away from being complete (Figure 5.23). It would be interesting to proceed assessing the evolution of these properties at longer curing times.

5.5.5 Hygroscopic behaviour

The hygroscopic behaviour of the mixes under study was assessed at 2 years and the results are presented in Figure 5.32, Figure 5.33 and in Table 5.10.

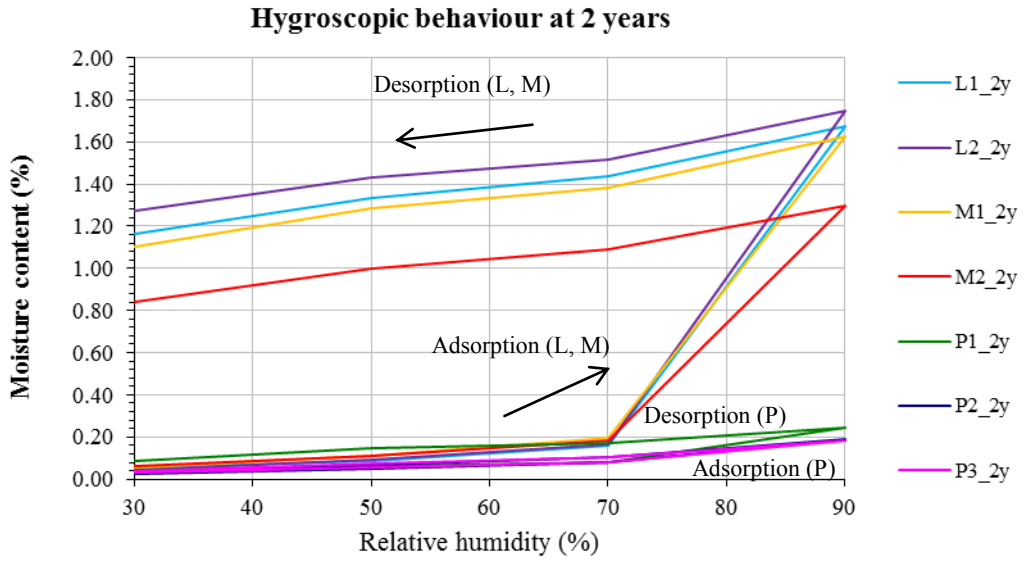

Figure 5.32 - Hygroscopic behaviour: graphical representation of the results at 2 years

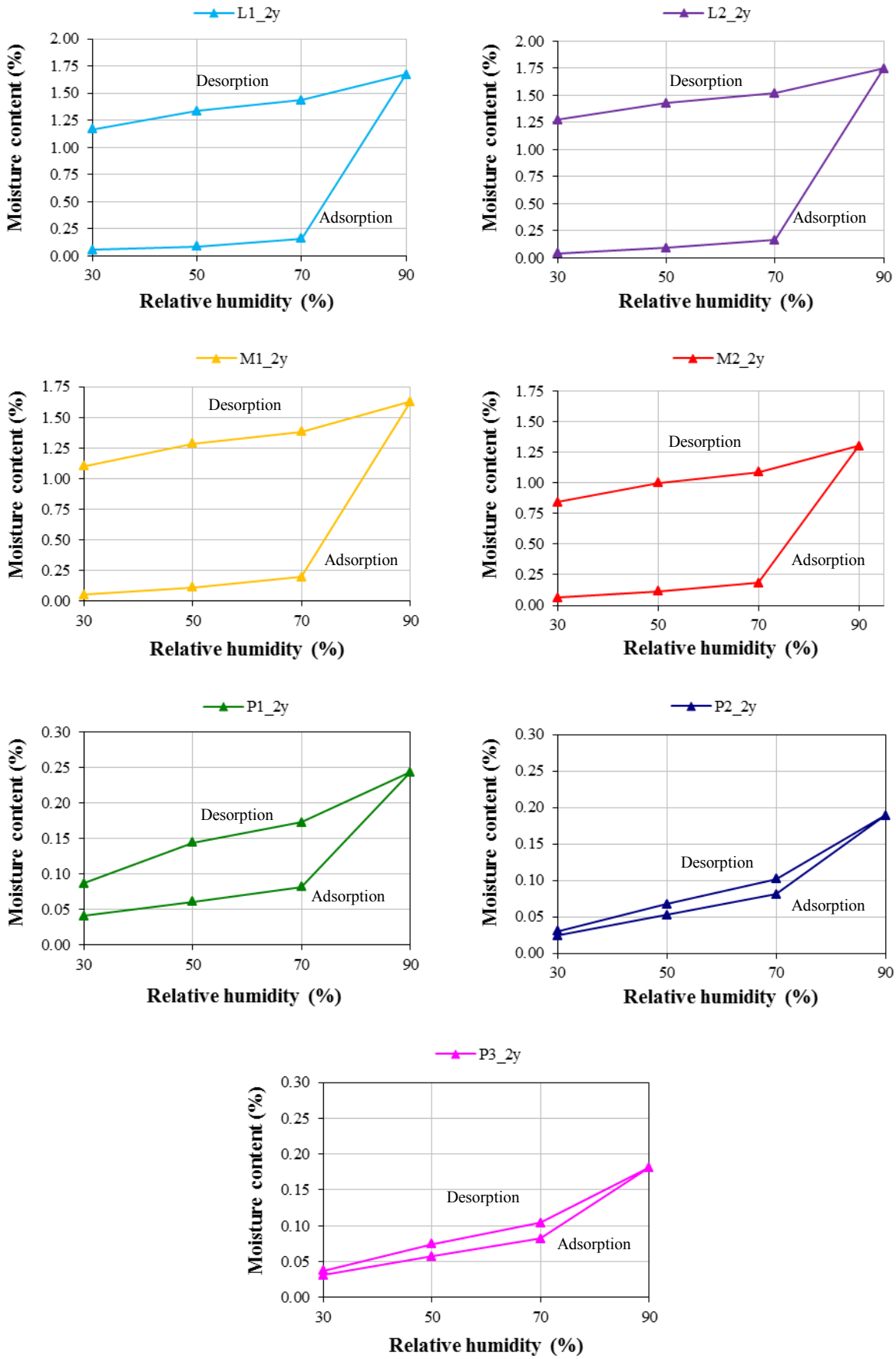

Figure 5.33 - Individual hygroscopic behaviour curves at 2 years

The profiles of the curves of adsorption and desorption of Figure 5.33 show that the presence of lime increases the adsorption values and induces hysteresis at desorption. At higher lime contents, both characteristics are more pronounced which is due to the higher amounts of smaller pores (Magalhães & Veiga 2007).

The same relationship between the volume of smaller pores (r < 0.1 micron) and the presence of hysteresis was observed in most of the ancient samples (*cf.* Chapter 4). However, the amount of water adsorbed at 90% relative humidity was much lower (below 1 %, with most being even below 0.4%) except in three samples of gypsum-lime plasters where the presence of hygroscopic salts (CP1, CP3 and PE5) was suspected or even detected.

Table 5.10 - Average hygroscopicity results at 2 years

RH (%)	MC L1 (%)	SD	CV (%)	MC L2 (%)	SD	CV (%)	MC M1 (%)	SD	CV (%)	MC M2 (%)	SD	CV (%)
30	0.05	0.004	8.28	0.04	0.019	45.12	0.05	0.004	7.56	0.06	0.004	6.79
50	0.09	0.049	*	0.09	0.022	22.99	0.11	0.004	3.65	0.11	0.005	4.29
70	0.16	0.059	37.20	0.17	0.025	15.29	0.20	0.006	2.97	0.19	0.003	1.84
90	**1.67**	0.037	2.19	**1.75**	0.146	8.33	**1.63**	0.099	6.08	**1.30**	0.094	7.24
70	1.44	0.036	2.50	1.52	0.142	9.38	1.38	0.100	7.23	1.09	0.096	8.80
50	1.33	0.037	2.77	1.43	0.140	9.82	1.29	0.100	7.78	1.00	0.094	9.40
30	1.17	0.035	2.96	1.27	0.138	10.82	1.10	0.099	8.97	0.84	0.092	10.91
RH (%)	MC P1 (%)	SD	CV (%)	MC P2 (%)	SD	CV (%)	MC P3 (%)	SD	CV (%)			
30	0.04	0.003	6.21	0.02	0.002	9.95	0.03	0.003	9.00			
50	0.06	0.003	5.39	0.05	0.005	8.74	0.06	0.003	5.03			
70	0.08	0.004	5.18	0.08	0.005	5.76	0.08	0.003	3.12			
90	**0.24**	0.009	3.70	**0.19**	0.007	3.84	**0.18**	0.009	4.90			
70	0.17	0.007	3.84	0.10	0.005	4.47	0.10	0.008	7.62			
50	0.14	0.006	3.93	0.07	0.002	3.28	0.07	0.007	9.70			
30	0.09	0.005	6.02	0.03	0.003	11.23	0.04	0.008	22.10			

* Too high CV value precluding presenting the results; RH - relative humidity; MC - moisture content; SD - standard deviation; CV - coefficient of variation

The significant increase of the amount of water adsorbed in the test specimens with more lime (L and M series) and the unusual long time they took to achieve mass stabilization at 90% relative humidity (15 days, while the P series and the ancient samples took 3 days), together with what seems to be a very pronounced hysteresis effect, are clear indications that carbonation was favoured under the referred conditions of humidity and temperature (23 ± 2 ºC) in a material that was already carbonating

at a very slow rate. These observations agree with those of Cizer, Rodriguez-Navarro, et al. (2012) and Cizer, Van Balen, et al. (2012) already referred in section 5.5.2.

According to Paiva (1969) (cited by Magalhães & Veiga (2007)) pores with a radius larger than 0.05 micron only saturate above 98% relative humidity; Kunzel (1995) refers that the moisture balance in porous materials only changes from the hygroscopic to the super-hygroscopic regime at 95% and part of the water transport is by capillarity.

Houst & Wittmann (1994) studied the diffusion of carbon dioxide through the microstructure of a porous system (hydrated cement pastes) with a wide range of pore dimensions and the way it varied with the relative humidity of the environment. They say that the pores with radius below 0.1-0.5 micron are more sensitive to condensation of the water adsorbed, i.e. capillary condensation occurs more easily in this range, hindering the diffusion of the gas phases at higher relative humidities.

From these statements, it could be said that for pores with radius above 0.05 to 0.5 micron (Figure 5.34) the diffusion of carbon dioxide is considered to be hardly influenced by the water content at 90% relative humidity. However, the moisture already adsorbed at their surfaces is probably enough to dissolve more portlandite crystals and carbon dioxide, giving rise to the precipitation of calcium carbonate.

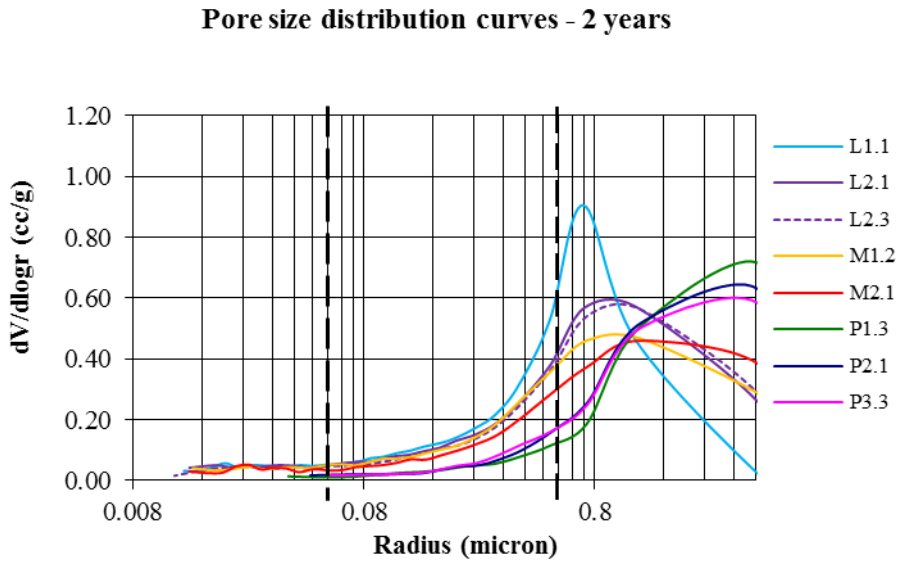

Figure 5.34 - Pore size distribution curves at 2 years with the pore size range that define the change of relative humidity needed for saturation (between dashed lines)

Concerning the mixes of the products for restoration of precast elements (P series), the results obtained, both for the moisture contents (0.18-0.24%) and for the adsorption/desorption curve profiles, are in total agreement with most of the values registered in the ancient samples with similar compositions (gypsum plasters).

5.5.6 Water vapour permeability

The water vapour permeability was determined at 90 days and 2 years. The results obtained are presented in Table 5.11 and a comparison quantified as the thickness of the air coat of equivalent diffusion (Sd) through a 10 mm thickness test specimen is shown in Figure 5.35.

The water vapour permeability values between 90 days and 2 years have a decrease in the L and P products that is in agreement with the reduction observed in the respective total porosity results. On the contrary, M1 and M2 had an opposite behaviour.

Considering that both L and M series are mixes where hydrated lime is the main constituent, a possible explanation for the opposite trends might be the presence of higher amount of micro-cracks in the latter than in the former. In fact, the addition of an aggregate and of methylcellulose to L1 and L2 can contribute to accommodate or even reduce the effects of shrinkage (methylcellulose is a water retaining agent constituted by cellulose fibres).

The mechanical properties are usually sensitive to the beneficial effects of this type of additions, namely the dynamic modulus of elasticity and the flexural strength results; further discussion about this issue is presented below.

Table 5.11 - Water vapour permeability results at 90 days and 2 years

Product	Age	Thickness (d) (mm)	ΔM/24h (g)	Permeability ($ng.m^{-1}.s^{-1}.Pa^{-1}$)	Sd (d=10 mm) (m)	SD	CV (%)
L1	90d	19.22	3.63	32.82	0.054	0.004	7.89
	2y	19.35	2.49	22.69	0.081	0.003	3.86
L2	90d	19.79	2.50	23.21	0.079	0.004	5.01
	2y	20.29	2.28	21.78	0.085	0.007	8.78
M1	90d	20.06	1.48	13.99	0.136	0.018	13.17
	2y	20.36	2.36	22.55	0.091	0.016	17.45
M2	90d	20.23	2.14	20.36	0.100	0.015	15.37
	2y	20.67	2.47	23.97	0.083	0.012	14.47
P1	90d	20.26	4.42	42.06	0.042	0.003	8.11
	2y	20.44	3.32	31.94	0.056	0.004	6.65
P2	90d	20.22	4.72	44.92	0.039	0.002	5.46
	2y	20.57	3.33	32.24	0.056	0.002	2.91
P3	90d	20.23	5.17	49.15	0.035	0.001	2.34
	2y	20.52	3.28	31.69	0.057	0.001	2.59

Sd - thickness of the air coat of equivalent diffusion through a test specimen of "d" thickness; SD - standard deviation; CV - coefficient of variation

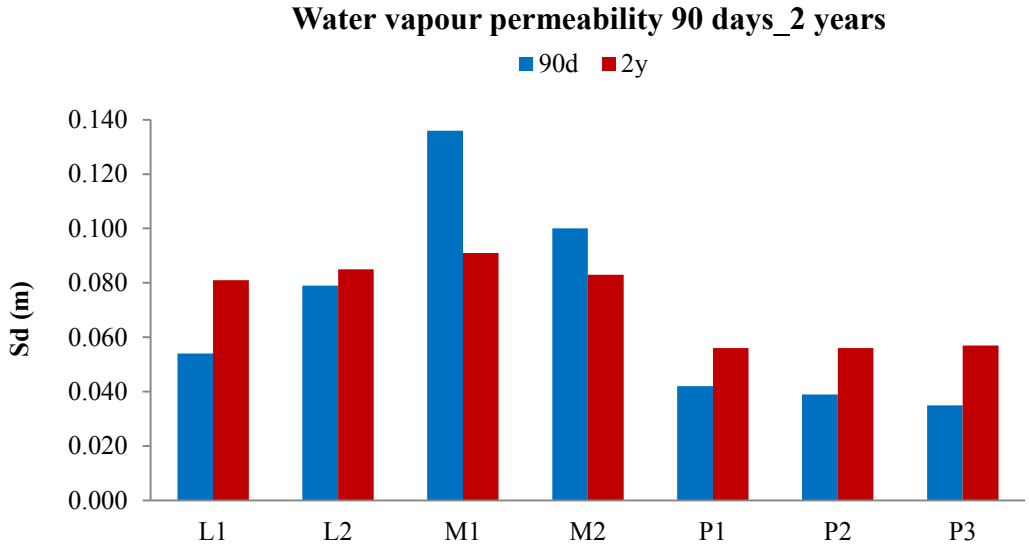

Figure 5.35 - Comparison of the water vapour permeability results at 90 days and 2 years

5.5.7 Dimensional variations

The dimensional variations were assessed over time by measuring the length of the test specimens at several ages. The results obtained are presented in Figure 5.36, Figure 5.37 and Table 5.12.

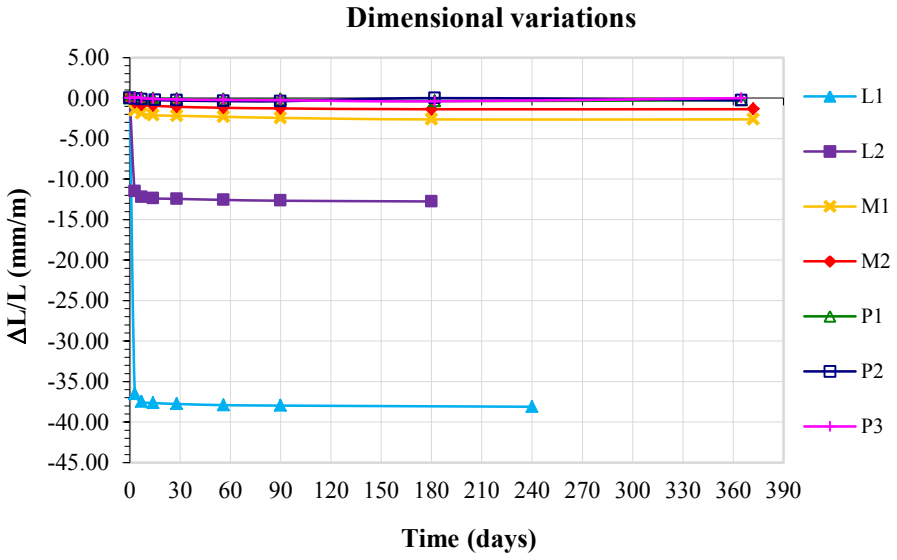

Figure 5.36 - Dimensional variations over time: graphical representation of the results

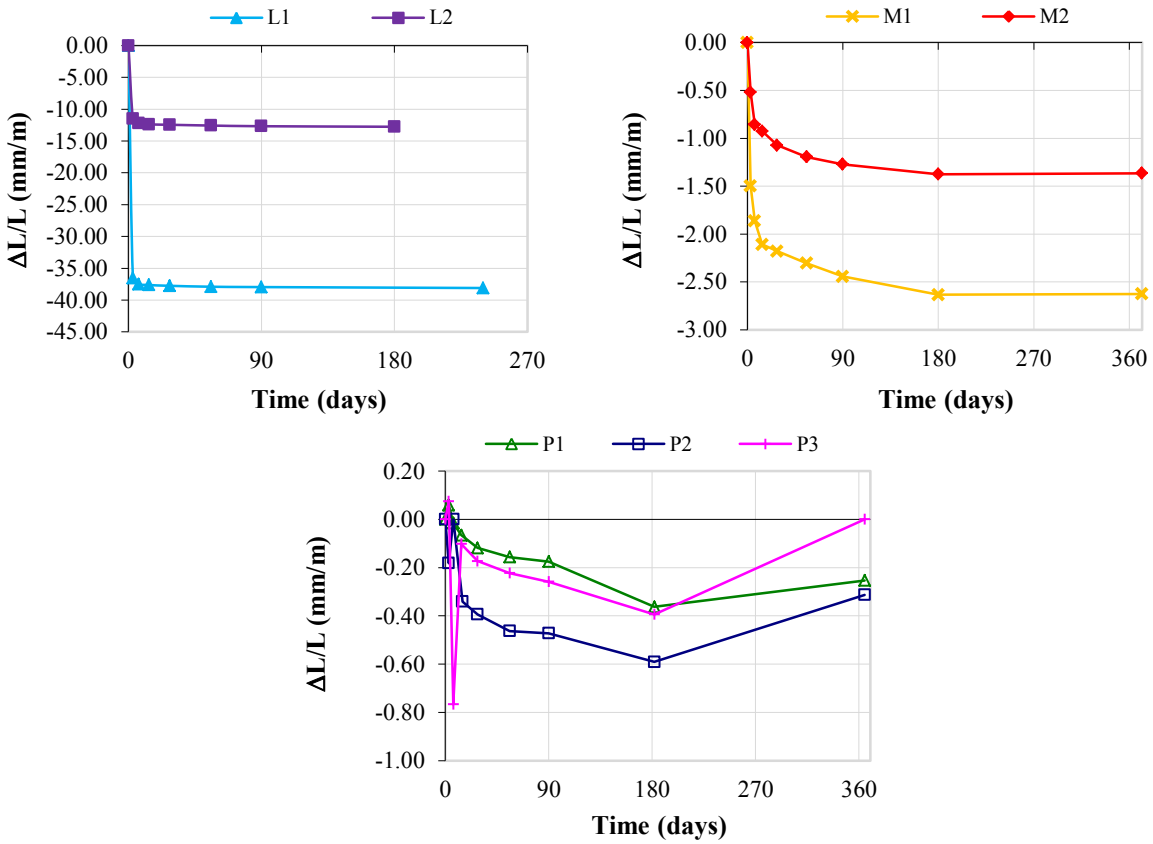

Figure 5.37 - Dimensional variations grouped by type of products

The dimensional variations observed are according to expectations: the higher the lime content (and lower the gypsum content), the higher the shrinkage (Figure 5.38). Even though, the values obtained for the mixes L1 and L2 are much higher than usually observed in lime mortars (maximum shrinkage of approximately 5 mm/m (Faria 2004)).

The same direct relationship was observed between lime content and kneading water used, with L1 having the highest quantity. The evaporation of this water during drying creates empty spaces in the structure that are directly related to the shrinkage magnitude. The carbonation process and the increase of volume associated to the formation of calcium carbonate crystals from portlandite contribute to partially heal these discontinuities created in the microstructure. The establishment of binding connections between the newly formed crystals increases the cohesion and enhances the mechanical properties of the material. However, the magnitude of the shrinkage of L1 and L2 is too high to be counteracted by the carbonation process and the low amount of aggregate added (10%). Their viability as restoration products is mainly due to the application procedure: in thin-layers, meaning that they have to be hardly pressed by the tools.

In the case of the gypsum plaster products, shrinkage is almost imperceptible with the pure gypsum test specimens showing a small expansion at early ages (characteristic of the hydration and setting

processes of the calcium sulphate dihydrate (*cf.* 2.2.3.6)) that progressively decreases while drying. It is interesting to notice, however, that the minimum values are at 180 days for the three mixes, corroborating the idea that the interaction with the surrounding environment is not limited to the products with lime.

Table 5.12 - Mass and length variations over time

Product	Age	Mass	Mass variation	Length variations			
			ΔM/M	ΔL	ΔL/L	SD	CV
	(days)	(g)	(%)	(mm)	(mm/m)		(%)
L1	7	204.72	-38.16	-5.999	-37.49	0.77	2.06
	90	223.30	-32.54	-6.074	-37.96	0.80	2.12
	240	223.44	-32.50	-6.097	-38.11	0.83	2.18
L2	7	225.73	-35.40	-1.955	-12.22	0.56	4.57
	90	240.93	-31.05	-2.028	-12.67	0.56	4.38
	180	240.99	-31.04	-2.041	-12.76	0.66	5.20
M1	14	239.70	-36.86	-0.337	-2.11	0.17	8.22
	90	257.30	-32.22	-0.391	-2.44	0.22	9.19
	372	257.33	-32.22	-0.420	-2.63	0.32	12.07
M2	14	256.26	-33.85	-0.148	-0.93	0.06	6.69
	90	270.72	-30.12	-0.204	-1.27	0.10	7.99
	372	270.73	-30.11	-0.219	-1.37	0.08	5.50
P1	7	253.65	-34.97	-0.003	-0.02	0.040	*
	28	255.39	-34.53	-0.019	-0.12	0.000	0.00
	90	255.27	-34.56	-0.028	-0.18	0.027	15.15
	182	255.28	-34.56	-0.058	-0.36	0.097	26.82
	365	255.26	-34.56	-0.041	-0.25	0.075	29.68
P2	7	276.43	-31.89	-0.053	-0.33	**	**
	28	276.38	-31.90	-0.063	-0.39	0.053	13.47
	90	276.27	-31.93	-0.076	-0.47	0.013	2.81
	182	276.27	-31.93	-0.095	-0.59	0.031	5.24
	365	276.28	-31.93	-0.050	-0.31	0.018	5.66
P3	3	323.46	-20.56	0.012	0.08	0.019	25.00
	7	280.31	-31.15	-0.123	-0.77	0.190	35.49
	28	280.24	-31.17	-0.028	-0.17	0.046	26.64
	90	280.15	-31.19	-0.041	-0.26	0.026	10.07
	182	280.16	-31.19	-0.063	-0.39	0.077	19.51
	365	280.17	-31.19	-0.055	-0.34	0.080	23.14

* Too high CV value precluding presenting the results; ** Determined in one test specimen only; Sd - standard deviation; CV - coefficient of variation

The mass variation associated to all the previous processes has been registered and is presented in Table 5.12, Figure 5.39 and Figure 5.40.

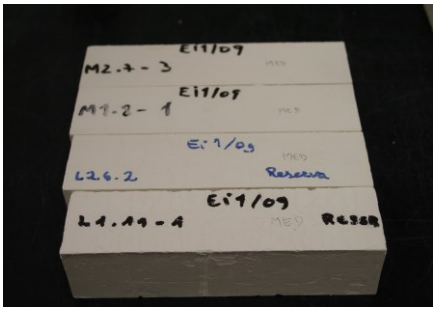

Figure 5.38 - Comparison between dimensional variations in L and M test specimens (visible to the naked eye)

The profile of the curves is also distinct between the products with and without lime. In the first case, there is an initial drop of the mass values that corresponds to the evaporation of the excess water. The minimum values were observed after 7 days in L1, L2 and P1 and at 14 days in M1 and M2.

After that, the contribution of the carbonation process to the mass increase starts to be noticed, stabilizing at about 90 days of curing time. The reaction proceeds then at a much lower rate, becoming almost imperceptible.

As expected, the mass of the gypsum plaster products P2 and P3 stabilizes after drying.

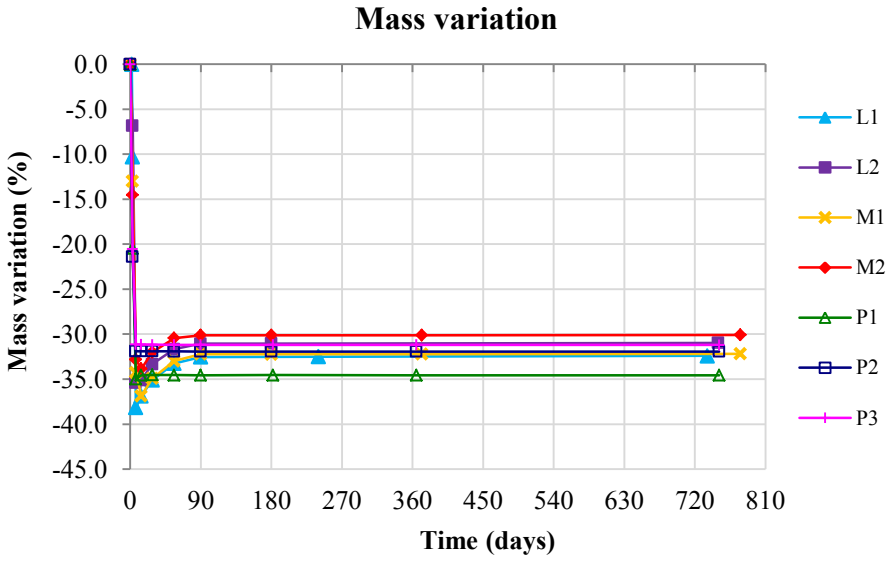

Figure 5.39 - Mass variation over time: graphical representation of the results

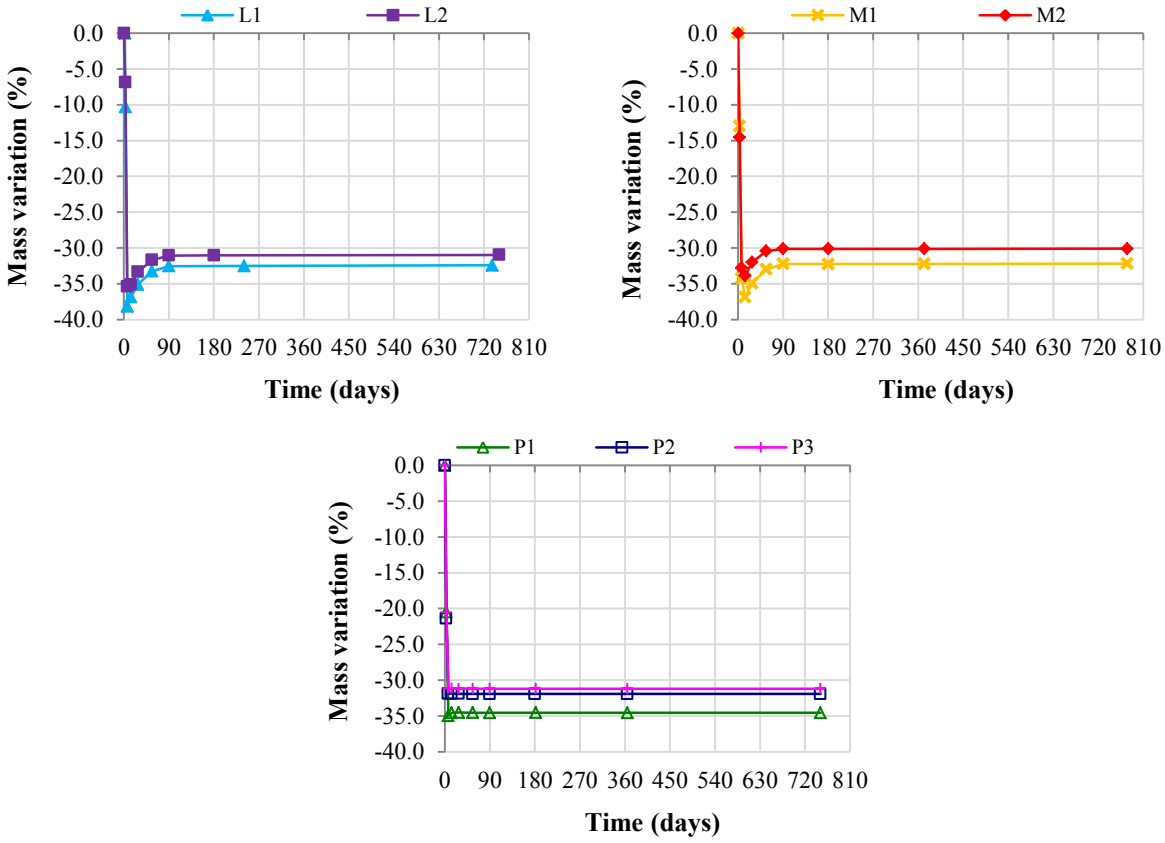

Figure 5.40 - Mass variation grouped by type of products

5.5.8 Dynamic modulus of elasticity

The dynamic modulus of elasticity was determined at different ages until 2 years, using two different methods: the ultrasonic pulse velocity method (US) and the fundamental resonance frequency method (FR). The results obtained by the first method are presented in Figure 5.41 and in Table 5.13.

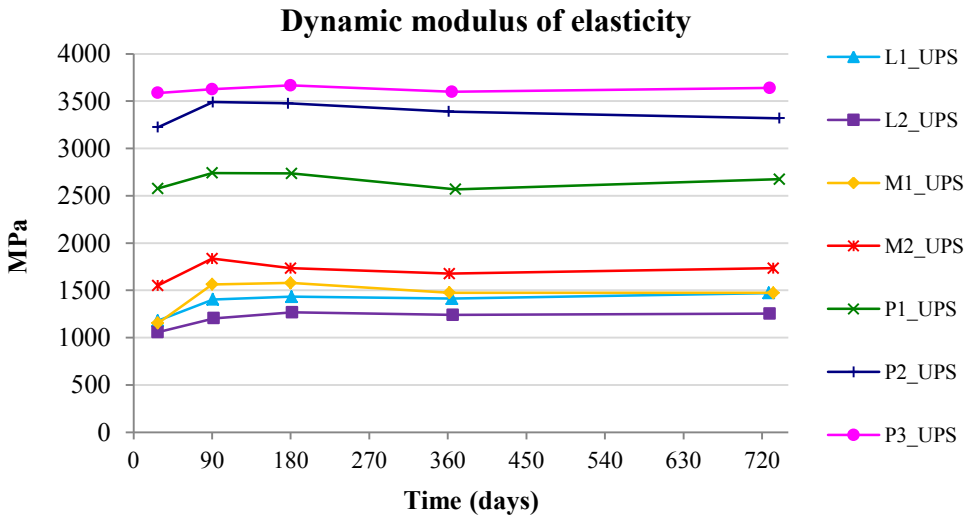

Figure 5.41 - Dynamic modulus of elasticity by ultrasonic pulse velocity measurements: graphical representation of the results

L1 and L2 have the lowest dynamic modulus of elasticity, a result that is totally in agreement with their higher lime content and porosity. As referred in section 5.5.3, in spite of having been mixed with more water due to its lower lime/gypsum relative contents, L2 shows a higher porosity, a broader pore size distribution and a lower dynamic modulus of elasticity than L1. The explanation for that might lie in the microstructure resulting from the corresponding lime/gypsum proportions (the arrangement of the crystals leading to a lower compactness) and/or in the interaction of any of the additions with those proportions (more air bubbles in L2 due to the methylcellulose, for example).

Considering the evolution over time, it is interesting to notice that L1 and L2 seem to be the most stable products having the greatest increase until 90 days and then keeping a quite steady profile.

Table 5.13 - Dynamic modulus of elasticity results at 90 days and 2 years determined by the ultrasonic pulse velocity method

Product	Age	Bulk density ($kg.m^{-3}$)	Distance (m)	Time (µs)	Speed ($m.s^{-1}$)	SD	CV (%)	DME (MPa)	SD	CV (%)
L1	90d	956	0.154	120.3	1277	8.1	0.6	1400	11.8	0.8
	1y	958	0.153	119.3	1280	3.3	0.3	1410	11.9	0.8
	2y	973	0.153	117.8	1297	2.1	0.2	1470	1.1	0.1
L2	90d	943	0.157	131.8	1192	4.9	0.4	1210	7.2	0.6
	1y	947	0.158	130.9	1206	8.2	0.7	1240	15.4	1.2
	2y	940	0.157	129.3	1217	9.8	0.8	1250	17.2	1.4
M1	90d	979	0.159	119.6	1332	0.4	0.0	1560	2.8	0.2
	1y	971	0.160	122.8	1300	7.8	0.6	1480	20.1	1.4
	2y	974	0.159	122.8	1296	12.6	1.0	1470	31.1	2.1
M2	90d	1018	0.160	113.1	1416	13.1	0.9	1840	33.2	1.8
	1y	1017	0.160	118.2	1353	2.3	0.2	1680	4.3	0.3
	2y	1019	0.160	116.3	1375	29.4	2.1	1730	74.5	4.3
P1	90d	957	0.160	89.7	1784	8.5	0.5	2740	25.9	0.9
	1y	952	0.160	92.5	1731	1.0	0.1	2570	7.6	0.3
	2y*	957	0.160	90.4	1763	-	-	2670	-	-
P2	90d	1021	0.161	82.9	1948	44.9	2.3	3490	165.5	4.7
	1y	1029	0.160	83.7	1914	20.0	1.0	3390	68.5	2.0
	2y*	1028	0.160	84.5	1894	-	-	3320	-	-
P3	90d	1042	0.160	81.4	1966	12.3	0.6	3630	31.2	0.9
	1y	1041	0.160	81.8	1960	10.3	0.5	3600	43.2	1.2
	2y*	1041	0.160	81.4	1971	-	-	3640	-	-

* Determined in one test specimen only; SD - standard deviation; CV - coefficient of variation; DME - dynamic modulus of elasticity

P3 is also very stable, a fact that is not a surprise as the chemical reactions that form the structure mainly occur in the first ages as well as the drying process. The same behaviour was expected from P2 but its dynamic modulus of elasticity showed an increase between 28 and 90 days, followed by a decrease until 1 year and a slight recovery at the age of 2 years. This evolution is similar to those of mixes M1, M2 and P1 (all having lime in their composition) but more difficult to explain, as the instability observed in the latter can always be attributed to the long carbonation process.

The variations of order of magnitude between the values obtained for the different products was according to expectations, with the pure gypsum plaster test specimens having the highest results (more than duplicating the values of the L mixes), characteristic of a more strong and rigid material. However, between the M and L series a higher difference was expected, due to the higher proportions of gypsum and lower kneading water content of the former. The presence of more micro cracks in the matrix of the M products is the most plausible explanation and can be due to the absence of an aggregate addition and/or of the methylcellulose fibres that are present in L1 and L2.

The assessment of the dynamic modulus of elasticity using the measurement of the ultrasonic pulse velocity through the material is the most indicative method as it was also used in the ancient samples. However, the measurement of the fundamental resonance frequency is also a commonly used method and the comparison between them seemed to be interesting. The results of such comparison are shown in Figure 5.42, Figure 5.43 and Table 5.14.

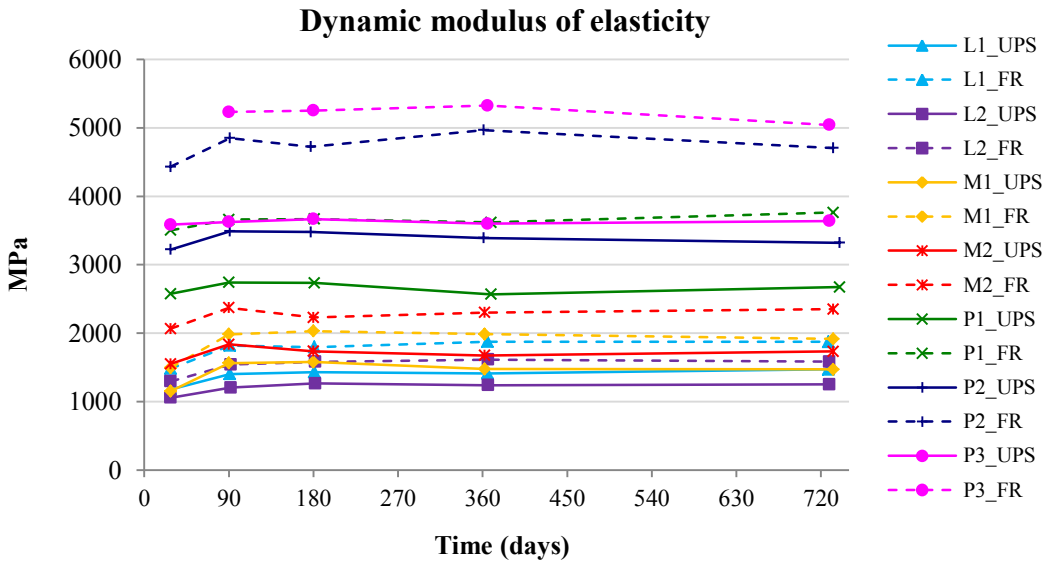

Figure 5.42 - Dynamic modulus of elasticity determined by the ultrasonic pulse velocity method (UPS) and the fundamental resonance frequency method (FR): graphical representation of the results

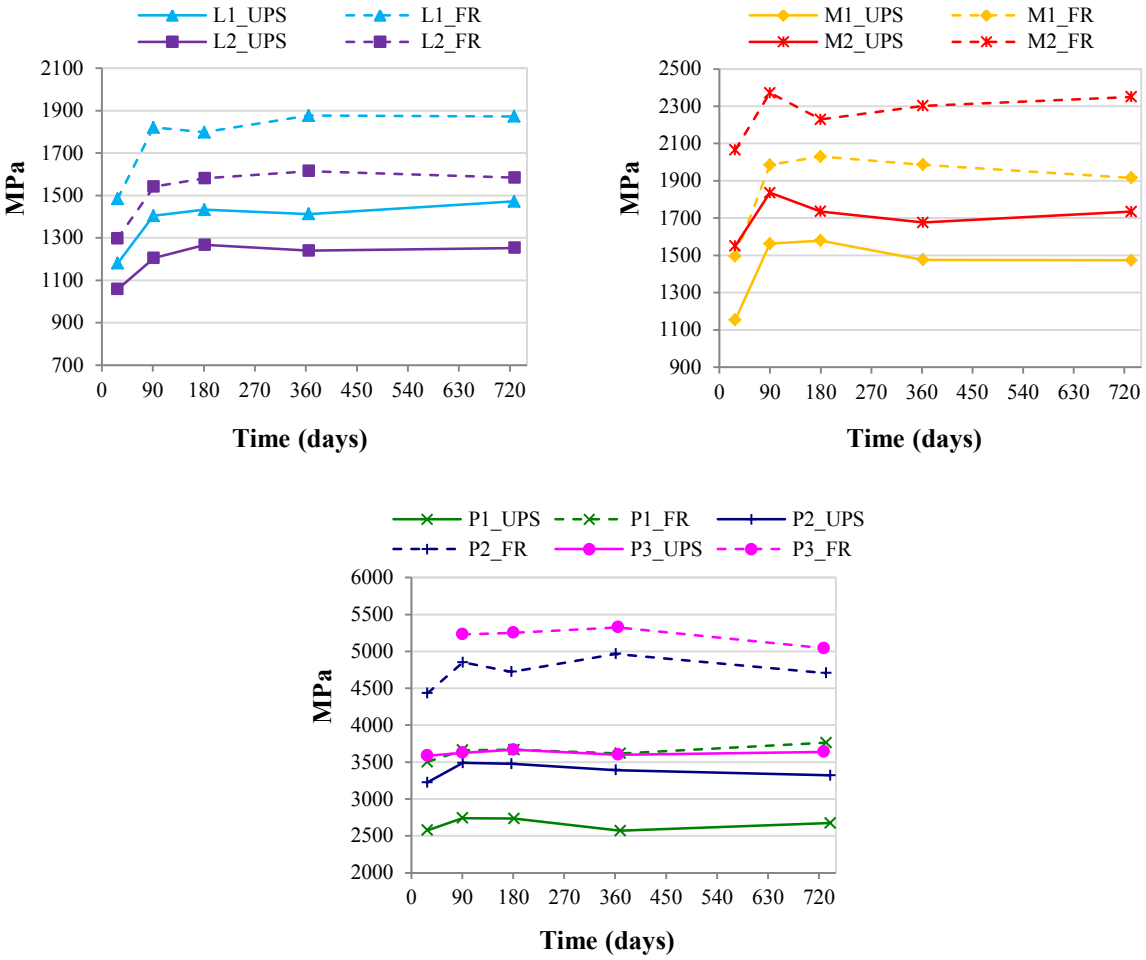

Figure 5.43 - Dynamic modulus of elasticity determined by the ultrasonic pulse velocity method (UPS) and the fundamental resonance frequency method (FR): results grouped by type of products

The values obtained by the fundamental resonance frequency method are much higher than those achieved through ultrasonic pulse velocity. This difference increases progressively with the increase of the dynamic modulus of elasticity of the material, varying between 26% (L1_2y) and 44% (P3_90d) (Table 5.14).

However, the profiles of the curves using both methods are quite similar for each product and the correlation between the respective results is excellent (Figure 5.44).

Table 5.14 - Comparison of the dynamic modulus of elasticity determined using two methods: the ultrasonic pulse velocity method (UPS) and the fundamental resonance frequency method (FR)

Product	Age	DME_UPS (MPa)	SD	CV (%)	DME_FR (MPa)	SD	CV (%)	ΔUPS_FR (MPa)	ΔUPS_FR (%)	UPS/FR (%)
L1	90d	1400	11.8	0.8	1820	29.2	1.6	420	30.0	0.77
	2y	1470	1.1	0.1	1870	5.7	0.3	380	25.9	0.79
L2	90d	1210	7.2	0.6	1540	32.4	2.1	330	27.3	0.79
	2y	1250	17.2	1.4	1580	18.1	1.1	330	26.4	0.79
M1	90d	1560	2.8	0.2	1990	8.2	0.4	430	27.6	0.78
	2y	1470	31.1	2.1	1920	41.3	2.2	450	30.6	0.77
M2	90d	1840	33.2	1.8	2370	34.8	1.5	530	28.8	0.78
	2y	1730	74.5	4.3	2350	2.5	0.1	620	35.8	0.74
P1	90d	2740	25.9	0.9	3660	50.4	1.4	920	33.6	0.75
	2y*	2670	-	-	3760	-	-	1090	40.8	0.71
P2	90d	3490	165.5	4.7	4850	201.2	4.1	1360	39.0	0.72
	2y	3320	-	-	4710	97.0	2.1	1390	41.9	0.70
P3	90d	3630	31.2	0.9	5230	262.8	5.0	1600	44.1	0.69
	2y	3640	-	-	5040	66.1	1.3	1400	38.5	0.72

* Determined in one test specimen only; SD - standard deviation; CV - coefficient of variation; DME - dynamic modulus of elasticity

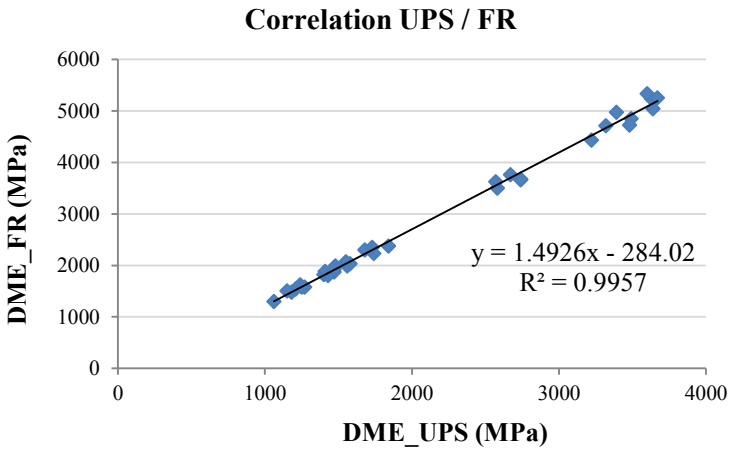

Figure 5.44 - Dynamic modulus of elasticity (DME): correlation between the results obtained by the ultrasonic pulse velocity method (UPS) and the fundamental resonance frequency method (FR)

5.5.9 Mechanical strength

The flexural and compressive strengths were determined at various ages until 2 years and the results obtained are shown in Figure 5.45, Figure 5.46 and Table 5.15.

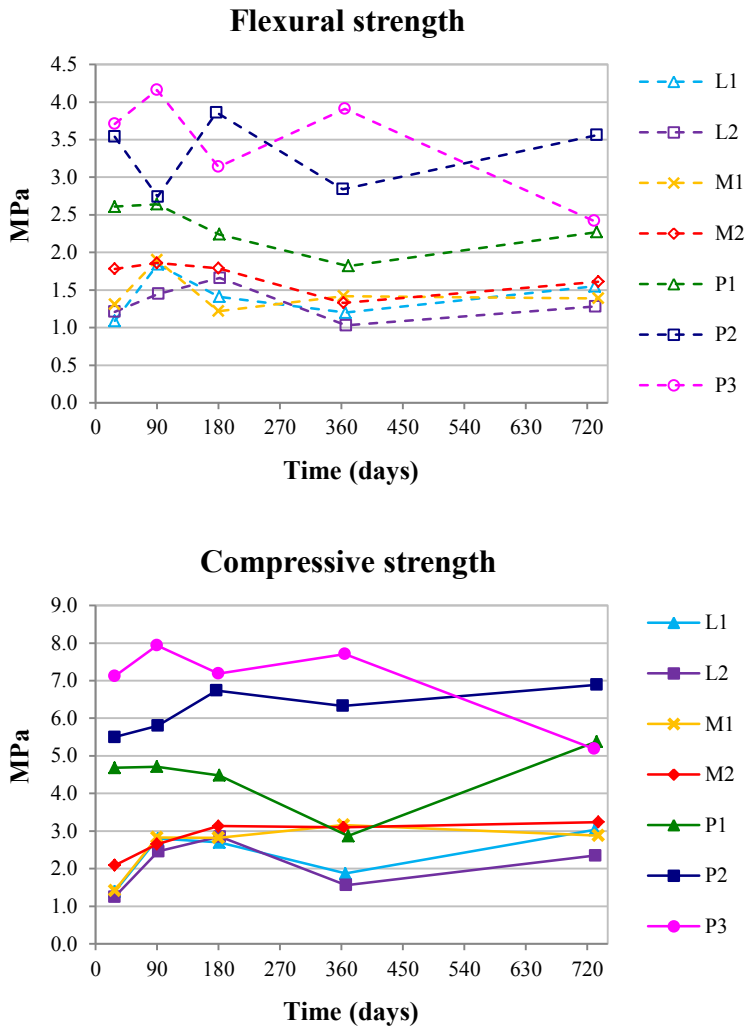

Figure 5.45 - Flexural and compressive strength determinations: graphical representation of the results

It can be observed that the two types of mechanical strength show a parallel evolution.

The maximum values of flexural strength were registered at 90 days (L1, M1, M2, P1 and P3) and 180 days (L2 and P2) while the compressive strength was higher at 2 years (L1, M2, P1 and P2), 365 days (M1), 180 days (L2) and 90 days (P3). If one considers only the products with lime in their composition, then flexural strength increases mainly in the first 90 days and compressive strength takes longer, reaching higher values after 1 or 2 years.

It is also at 2 years that certain stabilization seems to be finally installed in both mechanical properties, although in the case of flexural strength the values are still not the highest. It would be very interesting to evaluate these mixes at longer ages in order to see if this trend proceeds.

These differences between the flexural and the compressive strengths can be explained by the higher sensitiveness of the former to the development of micro-cracking. The same was observed in the

dynamic modulus of elasticity although with softer variations. On the opposite, compressive strength is not affected by the voids created by the micro-cracks as they can be accommodated while the test specimens are being tested and the beneficial effects of carbonation are more evident.

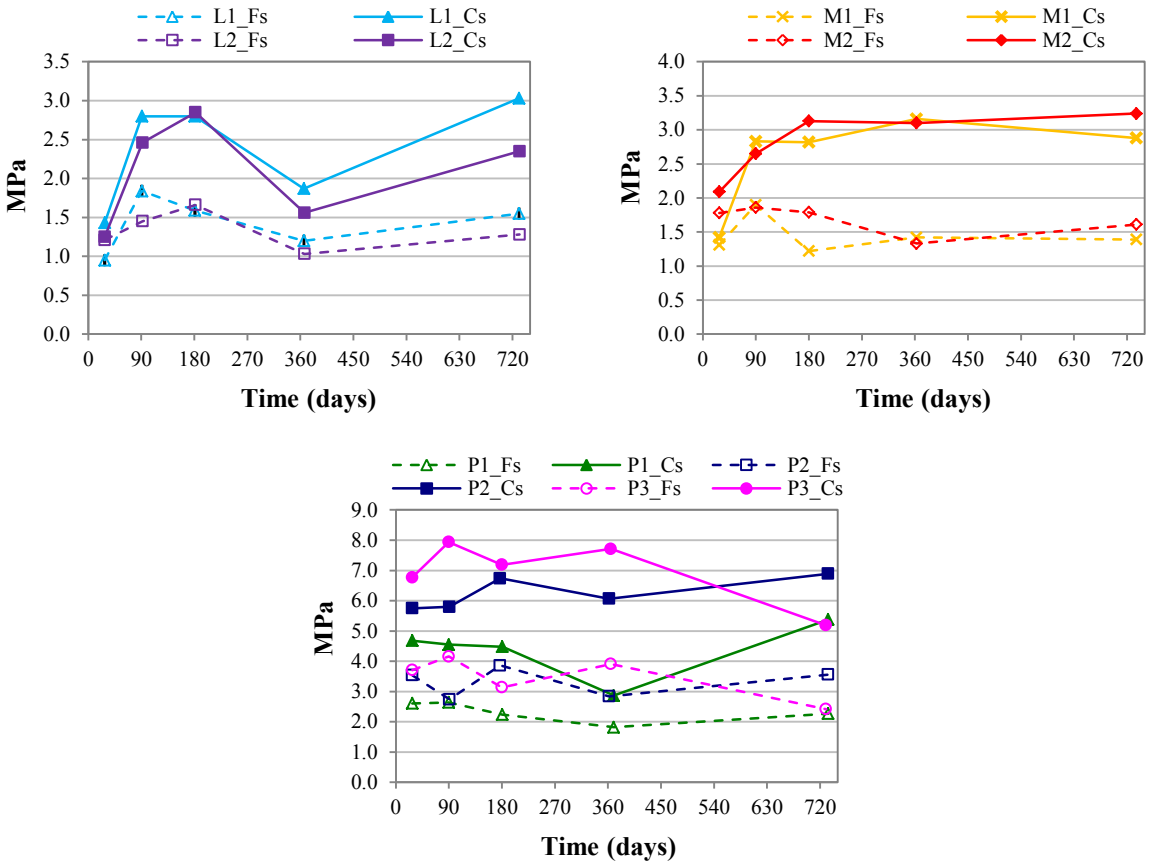

Figure 5.46 - Flexural and compressive strength results grouped by type of products

Concerning the minimum values, it occurs at 1 year for both mechanical strengths in most mixes; even for those where it is not the lowest result there is a negative inflection of the curve at this age, with the exception of M1 and P3. Similar results have been found in the literature for some lime-based mortars (Lanas & Alvarez 2003; Arizzi & Cultrone 2013). The first authors think that in these cases the highest strength values are achieved when a given amount of portlandite remains uncarbonated, i.e. there is a given calcium carbonate/portlandite ratio that contributes in an unknown way to this phenomenon; the second authors do not comment these results.

The gypsum plaster products' mechanical properties were not supposed to be time-dependent: after the evaporation of the excess kneading water they are expected to reach equilibrium with the relative humidity of the surrounding air. The test specimens were kept in a conditioned environment, so the instability observed in some results, especially the strong decrease in P3 at 2 years, might have had other origins.

Table 5.15 - Flexural and compressive strength results

Product	Age	Bulk density ($kg.m^{-3}$)	Fs (MPa)	SD	CV (%)	Cs (MPa)	SD	CV (%)
L1	90d	960	1.84	0.09	4.96	2.80	0.14	4.87
	1y	960	1.20	0.12	10.3	1.87	0.22	11.53
	2y	970	1.55*	-	-	3.03	0.40	13.21
L2	90d	940	1.45	0.13	9.17	2.46	0.41	16.64
	1y	950	1.03	0.12	11.47	1.56	0.19	12.44
	2y	940	1.28*	-	-	2.35	0.14	6.00
M1	90d	980	1.90	0.18	9.69	2.83	0.20	7.25
	1y	970	1.42	0.08	5.70	3.16	0.39	12.20
	2y	980	1.39*	-	-	2.88	0.34	11.89
M2	90d	1020	1.86	0.03	1.77	2.65	0.39	14.89
	1y	1020	1.33	0.11	8.58	3.10	0.24	7.63
	2y	1020	1.61*	-	-	3.24	0.31	9.69
P1	90d	960	2.64	0.06	2.29	4.55	0.66	13.94
	1y	950	1.82	0.09	4.76	2.87	0.06	2.15
	2y	950	2.27*	-	-	5.38	0.44	8.13
P2	90d	1020	2.74	0.37	13.39	5.80	0.34	5.90
	1y	1030	2.84	0.31	10.84	6.07	0.76	12.53
	2y	1030	3.56	0.16	4.50	6.89	0.32	4.60
P3	90d	1040	4.16	0.03	0.76	7.94	0.62	7.75
	1y	1040	3.91	0.75	19.26	7.71	0.44	5.66
	2y	1040	2.42	0.11	4.71	5.19	0.27	5.21

* Determined in one test specimen only; Fs - flexural strength; Cs - compressive strength; SD - standard deviation; CV - coefficient of variation

Comparing now the quantitative values of the different mixes and considering the intrinsic characteristics of their main constituents, they were expected to develop mechanical strengths according to an ascending trend directly related with the gypsum/lime proportions and the plaster/water ratios used: L1 < L2 < M1 < M2 < P1 < P2 < P3.

In the P series, where gypsum is almost, or even the only, material present the products followed that trend, with very few exceptions at some ages. On the contrary, the L and M series show very close results, particularly L1, L2 and M1, with apparently no direct relationship with the referred factors.

For example, despite having been mixed with less water and having a composition in which the proportion gypsum/lime is higher, L2 formulation showed higher porosity and lower mechanical characteristics than L1. This can be due to the pore size distribution curves: L2 shows a broader

distribution than L1 and a greater volume of pores with radius above 0.8 micron. Anyway, it was expected that the other referred factors, plaster/water ratio and gypsum/lime proportions, would have superimposed their influence. One explanation can be in the resulting microstructure, meaning that there are probably some lime/gypsum proportions that lead to better characteristics than others.

Comparing now L2 with M1, the compositional difference they have is the substitution of the calcitic aggregate in L2 by the same quantity of calcium sulphate hemi-hydrate in M1; the hydrated lime content remains the same. This apparently small change was enough to reduce the kneading water needed to prepare M1 and also to alter the evolution over time of some of its properties, like the water vapour permeability (expected to decrease with carbonation), the dynamic modulus of elasticity and the flexural strength (both expected to increase). All these facts agree with the presence of more micro-cracks in M1 than in L2. The addition of methylcellulose and an aggregate to L2 and the higher rigidity of the matrix due to gypsum in M1 (Figure 5.48) are probably at the origin of such behaviour.

The referred parallel evolution of the two types of mechanical strength is also attested by a good correlation (Figure 5.47).

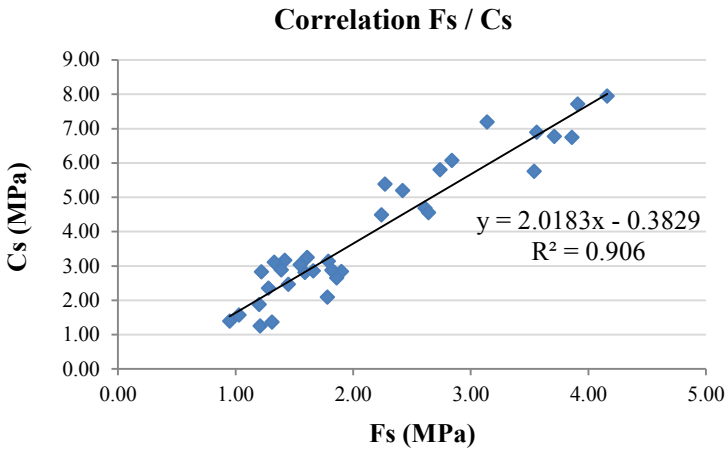

Figure 5.47 Mechanical strength: correlation between the results of flexural strength (Fs) and compressive strength (Cs)

The deformation capacity of the L and M mixes under compression are represented in (Figure 5.48). As expected, the higher the lime content, the most deformable the matrix is. However, both characteristics are not directly proportional as the differences are much greater between L1 and L2 than between L2 and M1 and these, in turn, are greater than those between M1 and M2.

Finally, it is interesting to notice that the dynamic modulus of elasticity evolution throughout all the time of the study was much more stable for all products and sometimes even contrary to the

mechanical strengths, like in the referred case of P3 at 2 years, showing that it is a property not always consonant with the mechanical strength.

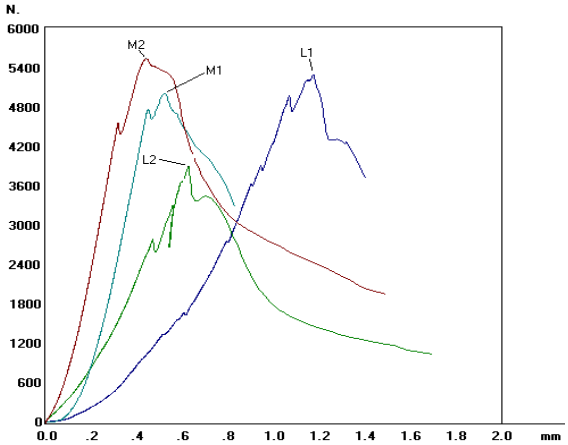

Figure 5.48 - Compressive strength *versus* deformation capacity of L and M test specimens at 2 years

5.5.10 One product for each type of plaster element: selection of the final mixes

The physical and mechanical characterization results of the seven mixes tested are summarized in Table 5.16

Table 5.16 - Restoration products: physical and mechanical characterization results

Product	Age	Total porosity (%)	Cc 5 min ($kg/m^2.min^{1/2}$)	Cc 10-90 min	Total absorption (kg/m^2)	Hygrosc. RH=90% (%)	WVP, Sd (d=10mm) (m)	MED (MPa)	Fs	Cs	Length variations (mm/m)
L1	90d	59.8	4.56	4.84	79.95	-	0.054	1400	1.84	2.80	-37.96
	2y	50.7	3.82	4.49	78.92	1.67(1)	0.081	1470	1.55	3.03	-38.11(2)
L2	90d	62.5	4.49	4.93	81.35	-	0.079	1210	1.45	2.46	-12.67
	2y	51.4	2.64	5.00	80.69	1.75(1)	0.085	1250	1.28	2.35	-12.76(2)
M1	90d	60.0	5.58	6.59	80.61	-	0.136	1560	1.90	2.83	-2.44
	2y	49.6	0.60	6.73	80.15	1.63(1)	0.082	1470	1.39	2.88	-2.63(2)
M2	90d	58.9	5.04	6.14	76.94	-	0.091	1840	1.86	2.65	-1.27
	2y	48.4	1.23	6.23	76.26	1.30(1)	0.077	1730	1.61	3.24	-1.37(2)
P1	90d	58.8	10.85	7.14	79.46	-	0.042	2740	2.64	4.71	-0.18
	2y	50.1	8.98	7.70	79.01	0.24	0.056	2670	2.27	5.38	-0.25(2)
P2	90d	57.5	8.07	7.32	73.18	-	0.039	3490	2.74	5.80	-0.47
	2y	48.0	6.29	6.32	73.07	0.19	0.056	3320	3.56	6.89	-0.31(2)
P3	90d	55.5	6.86	6.97	71.71	-	0.035	3630	4.16	7.94	-0.26
	2y	46.1	6.55	6.42	71.26	0.18	0.057	3640	2.42	5.19	-0.34(2)

Cc - capillary coefficient; Hygrosc. - hygroscopicity; WVP - water vapour permeability; Sd - thickness of the air coat of equivalent diffusion through a test specimen of "d" thickness; MED - dynamic modulus of elasticity; Fs -flexural strength, Cs - compressive strength; (1) suspicion of being inflated by carbonation; (2) measured at different age (*cf.* Table 5.12)

To check which products are the most suitable for the restoration of the original gypsum and gypsum-lime plasters, the results obtained at 2 years were compared with the compatibility requirements defined in Table 5.1, allowing the selection of the final mixes (Table 5.17).

When more than one product fulfils the requirements, the most suitable one is underlined; in the cases where none is applicable, the most approximate is presented between brackets.

It is recommended that the restoration products are not less porous than the original materials in contact. So, L2 and P1 are the most suitable in the corresponding category, whereas for the M series both mixes are under the compatibility ranges.

However, it is important to note that these are results concerning samples prepared in laboratory. In contrast, old samples of elements moulded on site were the most porous, sometimes showing hollows inside, which is perfectly understandable in view of the technique of application that has to be used. Thus, it is expected that there may be some increase in porosity of M products when tested in real application conditions, and it is premature to draw conclusions now on their (in)adequacy. The performance of application tests on site is paramount to ascertain whether the characteristics observed in the laboratory remain.

Table 5.17 - Restoration products *versus* compatibility requirements: selection of the most suitable mixes

Property	Porosity	Cc 5 min	Hygrosc. RH=90%	WVP	MED	Fs	Cs	Length variations
Element type	(%)	($kg/m^2.min^{1/2}$)	(%)	Sd (m)	(MPa)			(mm/m)
Thin layer	45-55	0.5-2.0	< 1.0	< 0.10	1000-2000	-	1-2.5	-
(L series)	L1=50.7 L2=51.4	(L2=2.64)	(L1=1.67)	L1=0.081 L2=0.085	L1=1470 L2=1250	L2=1.28	L2=2.35	L2=-0.0128
Moulded on site	55-65	3.5-7.5	< 1.0	< 0.10	1500-3000	-	1-3	-
(M series)	(M1=49.6)	(M2=1.23) (M2=6.23)*	(M2=1.30)	M1=0.082 M2=0.077	M2=1730	M1=1.39	M1=2.88	M2=-0.0014
Precast	50-60	3-5	< 1.0	< 0.08	2000-4000	-	1.5-3.5	-
(P series)	P1=50.1	(P2=6.29)	P1=0.24 P2=0.19 P3=0.18	P1=0.056 P2=0.056 P3=0.057	P1=2670 P2=3320 P3=3640	P1=2.27	(P1=5.38)	P1=-0.00025

Cc - capillary coefficient; Hygrosc. - hygroscopicity; WVP - water vapour permeability; Sd - thickness of the air coat of equivalent diffusion through a test specimen of "d" thickness; MED - dynamic modulus of elasticity; Fs -flexural strength, Cs - compressive strength; * Result of the capillary coefficient between 10 and 90 minutes

Concerning the coefficient of capillary absorption at 5 minutes, no product fulfils the requirements, L2 being the one which came closest, with a result slightly higher than the upper limit. However, it has higher capillary coefficient between 10 and 90 minutes and total absorption than L1, as well as less favourable drying behaviour, which is in agreement with the slightly better water vapour permeability

of the latter; in all the other properties L2 was closer to the desired characteristics for thin layer coatings.

In the M series the capillary absorptions in the first 5 minutes are below the requirements but between 10 and 90 minutes both products recover, presenting absorption rates well within the limits set. Comparing the total absorption and the drying behaviours of M1 and M2, the second mix shows better characteristics than the first one (Figure 5.28). M2 is also more adequate in terms of water vapour permeability, higroscopicity and dynamic modulus of elasticity. However, the mechanical strengths are slightly higher that the limit, another issue that has to be addressed in the tests of application of the products on site (if the porosity increases as expected, then the strengths will probably decrease).

In the case of precast elements (P series), the situation is not so critical, since most often the adherence is achieved with the help of a mortar which act as "glue ", being applied between the substrate and the element itself. This type of mortar was found in ancient samples and consists of a mixture rich in gypsum, with a considerable amount of lime, i.e. closer to the characteristics of the substrate, typically covered with a gypsum-lime regularization layer.

Anyway, from the three mixes studied, the choice falls on P1, since it fulfils most criteria.

5.6 Conclusions

In this chapter, the quantitative requirements for the design of new repair products were established based on the results of the characterization studies presented in chapter 4. It was found that the samples collected could be grouped according to some common features related to their form of application, concluding there was a need to develop at least three restoration products, one per family of plaster elements: thin-layer finishing coatings (L), geometric and volumetrically stable elements moulded on site (M) and precast decorative elements applied after drying and stabilization (P).

All these data allowed defining the materials - calcium sulphate hemi-hydrate and calcitic hydrated lime - and the respective proportions to be used in the restoration products. The need for addition of other components - limestone aggregate, water retaining agents, set retarders - was studied using workability tests that intended to reproduce as closely as possible the actual conditions of application, resulting in seven mixes: two type L, two type M and three type P.

These mixes were subjected to an experimental campaign in order to determine their main physical and mechanical properties. The results obtained were then compared with the pre-established compatibility requirements so that the choice would fall on the products whose characteristics best corresponded to them.

The following conclusions can now be drawn:

a) The **retardation effect of lime over gypsum's** hydration and setting, an idea often transmitted by plasterers and also referred in the literature (Igea Romera et al. 2013), was almost imperceptible in the gypsum-lime mixes prepared. A set retarder was needed in the mixes with higher consistency and longer working times;

b) The **carbonation** of lime was evaluated until the age of 2 years. Samples were taken from the core of freshly broken prismatic test specimens. The results allowed concluding that it occurred mainly in the first 90 days for all products, after which it proceeded at much lower rates;

c) P**ore size distribution** determinations at 90 days and 2 years using MIP showed a reduction of the total porosity, in all the mixes, of about 10%. In the gypsum-lime mixes at 2 years a decrease in the volume of pores with radius below 0.1 micron and above 0.5 micron is visible; in the gypsum plasters the decrease was in the pores above 1 micron.

Considering that after 90 days carbonation seemed to evolve at a residual rate, it was unexpected to observe such significant differences in the pore structures of the gypsum-lime mixes between 90 days and 2 years; still, the biggest surprise was finding a similar evolution in the gypsum products, meaning that they also have a "dynamic microstructure" that is changing throughout time. The mechanisms that are in the origin and/or regulate these transformations are unknown;

d) The **coefficients of capillary absorption** at 5 minutes had a general decrease between 90 days and 2 years, particularly in M1 and M2. These observations are in line with the decrease of porosity due to carbonation, which is even more pronounced at the surface of the test specimens.

However, the rates of suction quickly recovered their normal pace: the capillary coefficients between 10 and 90 minutes were similar at both ages and the total absorption capacity had only a very slight decrease. The last features do not agree with the evolution of porosity, meaning there is probably a contribution of other factors, namely the presence of micro-cracks in the internal structures;

e) The **hygroscopic behaviour** was evaluated in test specimens with 2 years. At 90% relative humidity the L and M mixes took 15 days to achieve weight stabilization, while the others (test specimens from the P series and ancient samples) only needed 3 days. They also showed too high values of weight increase and the hypothesis that carbonation occurred, or was even favoured under these conditions in the pores with radius above 0.5 micron was discussed.

f) The **water vapour permeability** evolved as expected in the test specimens of L and P series, decreasing between 90 days and 2 years, totally in agreement with the decrease of porosity also observed. However, M1 and M2 had an opposite evolution, i.e. it was more pronounced in the case of

M1. Again, the presence of a significant amount of micro-cracks in these mixes is the most probable cause of such behaviour;

g) The **dimensional variations** were evaluated at several ages and the results obtained were totally according to expectations: the higher the lime content, the more severe the shrinkage is. The orders of magnitude differ by a factor of ten between each series of products;

h) **The dynamic modulus of elasticity** had a general increase in the first 90 days. After that L1, L2 and P3 stabilized their values while the other mixes showed a slight decrease, with a minimum at 365 days and a trend to recover thereafter.

The different orders of magnitude observed are according to expectations, with pure gypsum plaster test specimens having the highest results, characteristic of a more strong and rigid material. However, the values are closer than expected in the M and L series and the presence of more micro-cracks in the matrix of the M products is the most plausible explanation for that;

i) The **flexural and compressive strengths** were determined at several ages until 2 years. They had a general good correlation. Flexural strength showed higher sensitiveness to micro-cracking while the evolution of compressive strength was more consonant with carbonation. Anyway, the minimum values were achieved at 1 year for both mechanical strengths in most mixes and even for those where it is not the lowest result there is a negative inflection of the curve at this age.

In the case of the gypsum plaster products, the mechanical properties were supposed to have negligible variations after the evaporation of the excess kneading water but some unexpected instability was observed.

The quantitative values of the different mixes were expected to develop according to an ascending order directly related with the gypsum/lime proportions and the plaster/water ratios used. However, like in the dynamic modulus of elasticity, L and M series showed very close results. Again, the most plausible explanation might be in the development of more micro-cracks in the M mixes due to higher rigidity of their matrixes. The addition of methylcellulose and/or of an aggregate, like in the L products, would probably mitigate this behaviour and improve the corresponding mechanical performances.

The deformation capacity of the L and M mixes under compression was as expected: the higher the lime content, the most deformable the matrix

Summarizing, seven mixes were studied regarding physical and mechanical properties. Most results showed logical interrelations; the mechanical strengths had a higher variability.

The comparison of these results with the pre-established compatibility requirements allowed finding well suited restoration products for thin-layer coatings and for precast elements, L2 and P1, respectively.

In what concerns the mixes for moulded on site elements, they revealed to be the less balanced, and some adjustments are advised. Anyway, M2 is the product whose characteristics are the most approximate to the requirements, though additional testing is recommended first, namely under real application conditions, in order to monitor the behaviour of the product on site and to see if any beneficial effects are noticed compared to what was found in laboratory.

In fact, detailed studies of application on site have to be made for the three products, preferably with experienced plasterers in order to test the workability and the performance of the materials “in service”. After that, the choices made can be confirmed and, if necessary, adjusted.

They also provide practical information that can give strong indications about the suitability of these products to be used in modern buildings, with the advantages of having very few additives and no need to be painted.

6

Conclusions and future developments

6.1 Compliance with the proposed objectives

This thesis aims at contributing to applying the principles expressed in the Krakow Charter of 2000 to the specific case of the Portuguese ancient gypsum and gypsum-lime plaster coatings, i.e. promoting their preservation through the knowledge of the materials used in the original compositions and the design of compatible solutions for their restoration. In order to meet the objectives initially proposed the research was developed as follows:

1) To make a systematic study on the composition of the Portuguese interior plaster coatings through the most important civilizational periods that characterised the country's history and to identify the main factors that determined the choice of materials, a total of 139 samples were collected from north to south of the country, representing the Roman (23 samples), Islamic (45), Low Middle-Age and Renaissance (10), Baroque (20) and Post Baroque (41) periods.
   A mineralogical survey using XRD was performed (Freire et al. 2008; Freire et al. 2010; Freire, Santos Silva, et al. 2015) and the results obtained are presented in Chapter 3;
2) The plaster samples where gypsum was one of the main constituents (gypsum and gypsum-lime plasters) belong to the period between the second half of the 18th century and the first quarter of the 20th. Interdisciplinary studies of those samples were developed and relationships between the chemical, mineralogical and microstructural characterization results and the physical and mechanical properties determined were established (Freire et al. 2009; Freire et al. 2010; Freire et al. 2012).
   The results obtained are presented and discussed in Chapter 4;
3) The definition of compatibility requirements based on the results of the referred characterization studies was made (Freire et al. 2011; Freire et al. 2013) and is presented in Chapter 5;
4) Seven mixes with composition similarities to the ancient materials were defined and the determination of their physical and mechanical properties was assessed (Freire et al. 2013; Freire, Veiga, et al. 2015); it is presented in Chapter 5;
5) The selection of the mixes that best fulfil the compatibility requirements previously established was made (Freire, Veiga, et al. 2015) and justified also in Chapter 5;

6) The research work as a whole also aims at contributing to the clarification of the differences between gypsum and lime plasters, through a literature review about the main characteristics of the constituent materials (Chapter 2) and the determination and discussion of their properties in the experimental work performed (Chapters 3, 4 and 5).

It is now possible to state that the six main objectives initially proposed were accomplished, a fact also evidenced in the conclusions drawn in the next section.

6.2 General conclusions

The ancient Portuguese interior plaster coatings

a) Gypsum has not been found in any of the samples analysed from the Roman period, not even in trace quantities. It was observed that decorative elements, either low thickness reliefs, or high thickness ones, have been made on site. The forms that were intended to be created and/or reproduced were first sculpted in the mortar and then finished with a thin-layer (sometimes very thin, thickness ≤ 1 mm) of a fine, white air lime mortar.

   XRD analysis of those finishing layers identifies calcite as the only component that could result from a binding reaction. So, even if calcitic aggregates had been used (not distinguishable by XRD from the calcite generated by the carbonation of lime), the mortars had to have a binder and the only possible one was air lime;

b) In the Islamic and Renaissance periods a few samples had gypsum, the only binder present in those samples.

   The lack of raw material of good quality in Portugal did not hinder the use of gypsum plasters during the Islamic occupation, showing one more feature where the traditions of this occupying people influenced the Portuguese culture. However, that use was limited to structures of higher architectural value (citadels of the castles of Mértola and Silves).

   In the Renaissance period gypsum was found in one case study, the emblematic decorative panels of the *Charola* of the Convent of Christ which are thought to be of Spanish influence;

c) From the second half of the 18th century the presence of gypsum started to be more frequent, both as the only binder or mixed with calcitic air lime but still in the minority of the samples. It was during the 19th century until the first quarter of the 20th that gypsum plasters had their heyday in the Portuguese architecture, mainly used in decorative programs of Neo-revivalist influence, so fashionable at the time (Neo-Arab, Neo-Classic, etc.);

d) From that period of approximately two centuries 33 samples among smooth surface and decorative coatings were analysed using a combination of several techniques. It was found

that there are compositional patterns related to the different types of elements, independently of the century or geographical region:

- In the thin-layer plasters used to finish smooth surface elements the mixes used were made of calcitic air lime and gypsum, of which the former was the main constituent. The presence of aggregates was seldom detected;
- In pre-sculpted and moulded on site decorative elements the plaster mixes were made of approximately equal parts of gypsum and lime;
- Those that had been moulded on a bench or precast were predominantly made of gypsum;

e) There is a clear relation between the technique of manufacture and application of the plaster elements and the respective compositions: the longer the time needed for the work, the higher the lime content. This seems to be a paradox as it was found, during the development of the restoration products, that lime has not a great retardation effect on the gypsum plasters reaction. However, the creaminess of the resulting pastes allied to the very probable use of additives in the mixing water to prolong the setting time was, no doubt, the most adequate for some types of application, such as thin-layer finishes;

f) On what concerns the moulded on site and pre-sculpted elements, a given consistency was needed soon after mixing, in the first case due to the position of application and to gravity and in the second due to the type of work that had to be done: gypsum plaster contributes quickly to the hardness of the mass but alone is too hard to be sculpted, and the work becomes easier to execute with a given quantity of lime in the mix;

g) To mould on bench and to precast the best material is gypsum plaster: the expansion on setting allows the reproduction of the tiniest details, the specific surface area of the crystals allows obtaining fluid mixes, the ideal consistency for these techniques and the quick setting time avoids sedimentation of the paste on the bench and in the moulds. The high strength is also positive as these elements have to be much handled;

h) In the constructions of higher heritage value (e.g. palaces and churches) the decorations are more elaborated and polychromes and other finishes of high technical demand like painting, imitation of stone and wood or even gilding are often used. The choice of raw materials is more careful and the quality of execution of the whole plaster works followed higher quality standards than in current buildings, evidenced by better finished surfaces, higher mechanical characteristics, lower water absorption values and lower porosity;

i) The use of a series production of decorative elements was not observed in the case studies of the 18th century, appearing only in the 19th.

j) The hygroscopicity results were widely spread and cannot be established quantitative values or relate them with other properties of the samples. However, if several samples of the same case study are compared, it is possible to observe there are some trends, with the values of gypsum plasters being slightly lower than those of gypsum-lime plasters. The main difference

between these two materials is in the hysteresis effect, which does not exist in gypsum plaster samples but is significant with the increase of calcite content, in a clear direct relation;

k) The pore size distribution curves were determined (between approximately 0.01 and 4.2 micron) in few samples using mercury intrusion porosimetry (MIP). There are also evident differences directly related with the gypsum/calcite contents: gypsum plasters have a negligible amount of pores with radius below 0.1 micron and show a unimodal curve in the range studied (maximum intensity peak ~ 1.0 micron), while in gypsum-lime plasters the more lime has been used in the mix, the higher the presence of small pores with radius below 0.1 micron and the respective curves are bimodal, with maximum intensities at 0.1 micron and 0.3-0.7 micron.

   These differences are also reflected on the average pore radius that is between 0.550 micron and 0.650 micron for gypsum materials, 0.300 micron to 0.400 micron for balanced gypsum-calcite contents and between 0.140 and 0.240 micron when calcite is predominant;

l) The porosity results given by MIP showed that the samples with lower porosity are the thin-layer plasters, followed by the precast and moulded on bench elements; the most porous are the moulded on site. In this case the relationship between composition and porosity is not the only determining factor, i.e. the process of manufacture/application of the different elements also seemingly interferes: during the application of a thin-layer plaster it has to be pressed hard, while the technique of application when moulding on site and the position of the plasterers do not allow a significant compression on the paste;

m) The results obtained for the coefficients of capillary absorption were scattered but it was possible to find relationships between the capillary coefficient by contact at 5 minutes (Ccc at 5 minutes) and the total absorption capacity with the type of elements: the moulded on site samples have the highest values in both parameters and the thin-layer plasters the lowest. These observations are in accordance with the porosity values and the remarks made in the previous paragraph;

n) The most determining factor on the mechanical properties of the samples studied is the nature of the binder(s) in their composition. In fact, the higher the gypsum content, the higher the ultrasonic pulse velocity, the dynamic modulus of elasticity and the compressive strength. An inverse trend is observed in the samples with higher content of calcite;

o) Two of the samples analysed revealed to have completely distinct physical and mechanical behaviour, presenting much lower porosity (9-12%) and water vapour permeability, and much higher dynamic modulus of elasticity and compressive strength. The XRD analysis show that gypsum is the main constituent but the presence of some anhydrite is also detected. Additional techniques were used in their study in order to try to explain the differences found. It is possible to conclude that what seems to be a minor composition detail was, in fact, the feature that distinguished these two samples from all the others: the presence of anhydrite proves that high-temperature gypsum was used in their manufacture.

The type of elements these samples correspond to (imitation of decorative stones) and the excellent performance they have indicate that the use of such material was intentional;

p) The procedures used to determine the several physical and mechanical properties of the ancient samples had to be adapted due to the irregular size and shape of the test specimens. Nevertheless, they revealed to be adequate, not in absolute terms, but in relative/comparative ones as it was possible to establish logical interrelations between the results obtained. The indications about the behaviour of the materials allowed the definition of compatibility requirements to be accomplished by restoration products.

Development of compatible restoration products

q) After the characterization of the ancient gypsum and gypsum-lime based plasters it was concluded there was a need to develop three restoration products, each for a different type of application: smooth surface (L), moulded on site (M) and pre-moulded elements (P);

r) For these products to constitute viable solutions many features had to be taken into account, namely the workability. Soon it became clear that the design of the mixes was not only a simple question of which quantitative proportions of the main constituents (calcium sulphate hemihydrate and hydrated lime) should be used. The new powdered pre-dosed products had to be user-friendly, meaning they had to reproduce the characteristics of the traditional materials. Taking the example of the thin-layer finishing plasters, it is desirable that the corresponding restoration product can reproduce very closely the workability of a mixture of lime putty and gypsum plaster during its application and, simultaneously, have similar physical and mechanical characteristics after hardening;

s) The design of seven mixes belonging to the three families of products was accomplished using consistency and setting time measurements complemented by laboratory application tests, especially planned to reproduce as closely as possible the real conditions of application. It was concluded there was a need to use a filler, a setting retarder and a water retaining agent in the L mixes, where the contents of powdered air lime were above 50%. The M products' workability seemed not to benefit from the use of other admixtures than a setting retarder. Finally, for pre-moulded elements three products based on gypsum plaster were defined, one of them being 100% composed of that material;

t) The seven mixes were submitted to an experimental campaign in order to determine their physical and mechanical properties. The evolution of carbonation in the five mixes where lime was one of the constituents was assessed at several ages and the results obtained showed that the major part of the reaction (about 60% for L and M and 80% for P1) occurs in the first 90 days. After that, it continues at a very slow rate, seeming to have stopped in some cases. However, between 90 days and 2 years the differences found in the pore size distribution

curves and in the total porosity values indicate that the microstructure changed considerably and the reaction is still evolving;

u) The hygroscopic behaviour was difficult to establish in the mixes with lime due to the referred instability of the microstructure. In fact, at 90% relative humidity carbonation is clearly accelerated and the test specimens take much longer to stabilize their weight than those of P2 and P3, where gypsum plaster is the only constituent;

v) The mechanical properties of the new mixes were as expected considering the main characteristics observed in the ancient samples:
   - The mixes with more lime, L1 and L2, have less mechanical strength and lower dynamic modulus of elasticity but much higher deformation capacity;
   - Those having balanced quantities of both materials (M1 and M2) show intermediate mechanical properties;
   - The P mixes have low deformability but higher mechanical strength (brittle behaviour);

w) Some results obtained in M1 and M2 are indicative of higher tendency towards the formation of micro-cracks, like the water vapour permeability between 90 days and 2 years, whose values increased in spite of the significant decrease observed in total porosity. All the other mixes showed the opposite behaviour: lower porosity, lower water vapour permeability. The addition of filler and/or water retaining agent like in L1 and L2 would probably contribute to attenuate this tendency;

x) The characterization studies performed in the seven mixes allowed selecting the three final products that best fulfilled the pre-established compatibility requirements, one for each family of plaster elements. In two of these families, L and P, the compositions selected (L2 and P1) are ready to proceed to application tests, while in the case of the elements moulded on site small adjustments still have to be made to M2 in order to accomplish a higher number of requirements. In any case, it is considered that the products developed and tested constitute a good basis for the development of restoration materials for this type of coatings. Yet, whenever the heritage value justifies it, specific characterization studies of the materials should be made and tailor-made solutions should be defined;

y) The characteristics of the products developed in this thesis demonstrate that they are also adequate for use in new buildings. The higher costs of application due to workmanship are compensated by the fact of not needing to be painted, with increased benefits concerning the interior comfort regulation.

As final reflection, it can be said that, after the work developed in this thesis, it is now possible to establish a real definition of the word ***Estuque*** (*cf.* 2.2.1) as "A paste of gypsum or gypsum-lime based plaster used for finishing interior walls and ceilings where the addition of a fine aggregate is not a prerequisite".

6.3 Proposals for future developments

- The study of the composition of the interior plaster coatings belonging to the several periods of the Portuguese history should proceed in order to complete the database that was started with this thesis;
- The plastered elements studied are intrinsically dependent on the durability and main properties of the mortars that constitute the undercoats they are in contact with as well as on the compatibility between them. However, the research on ancient lime based mortars has been mainly focused on the exterior walls of the buildings due to their (more) critical exposure to aggressive agents. The promotion of thorough studies on the mortars that cover the interior surfaces is, though, plenty justified by the increasing need to preserve the walls of the ancient buildings as a whole;
- Gypsum plasters with very special characteristics were found in two samples of this study. The technology associated to their production is based on the use of materials, namely anhydrite, that require higher temperatures of calcination. However, this and other features, namely the use of admixtures, need to be further explored, not only to promote their correct preservation/restoration in Portugal, but also abroad, as this type of materials is the basis of the ancient techniques of imitation of decorative stones, the so-called "Stucco-marmo".

  Some contacts have already been established with MPA Bremen - Institute for Materials Testing during the study of one of the samples referred above and it was concluded that it is a research field very little explored and of great interest to the European heritage preservation;
- The products developed in this thesis need to be further tested, namely through the application on wider surfaces/panels by traditional plasterers in order to evaluate the workability and the eventual need of small adjustments in the respective mixes. After that, they should be submitted to durability tests under normal and "extreme" real conditions of temperature (10 ºC and 40 ºC) and humidity (30% and 90%), not so critical in interior coatings but still recommendable. That study should be performed with application of the products on substrates constituted by mortars traditionally used in the ancient undercoats, preferably starting with small applications (e.g. in bricks), easier to test under controlled environment;
- The experimental campaign performed in this study to evaluate the compatibility of the seven initial mixes designed as potential restoration products should be repeated for the three final mixes, after all the adjustments referred in the previous paragraph have been made. However, it should be complemented with mineralogical, chemical and microstructural analysis in order to try to understand and relate all these features with the evolution of the physical and mechanical properties. Particular emphasis should be given to the evolution of carbonation at different relative humidity levels (50%, 70%, 80% 90%), throughout several years (5 years, as

minimum) as well as to the microstructural changes occurring in hardened gypsum plaster pastes, as in the case of P3;

- The three mixes approved in the application and durability tests should then be used in real conditions, through applications in few restoration works, preferably with different geographical locations, and their performance should be monitored during, at least, the first five years.

References

AA.VV., 2008. *Tavira, heritages of the sea*, Tavira: Tavira Town Hall (in Portuguese).

Adams, J., Dollimore, D. & Griffiths, D.L., 1998. Thermal analytical investigation of unaltered Ca(OH)2 in dated mortars and plasters. *Thermochimica Acta*, 324, pp.67–76.

Adams, J., Kneller, W. & Dollimore, D., 1992. Thermal analysis (TA) of lime- and gypsum-based medieval mortars. *Thermochimica Acta*, 211, pp.93–106.

Adriano, P., 2008. *Characterization of traditional and historic mortars from religious buildings in Alentejo*. MSc. Thesis. Lisbon: University of Lisbon (in Portuguese).

Álvarez Galindo, J., Martín Pérez, A. & Garcia Casado, P., 1995. Historia de los Morteros. *Boletín del Instituto Andaluz del Patrimonio Historico*, Ano III(13), pp.52–59 (in Spanish).

Alvarez, J.I., Navarro, I. & García Casado, P.J., 2000. Thermal, mineralogical and chemical studies of the mortars used in the cathedral of Pamplona (Spain). *Thermochimica Acta*, 365, pp.177–187.

Anastasiou, M. et al., 2006. TG-DTA and FTIR analyses of plasters from Byzantine monuments in Balkan region - Comparative study. *Journal of Thermal Analysis and Calorimetry*, 84(1), pp.27–32.

Andrews, H., 1946. The effect of water contents on the strength of calcium sulphate plaster products. *Journal of the Society of Chemical Industry*, 65, pp.125–128.

Arandigoyen, M. et al., 2005. Lime pastes with different kneading water: Pore structure and capillary porosity. *Applied Surface Science*, 252, pp.1449–1459.

Arandigoyen, M. et al., 2006. Variation of microstructure with carbonation in lime and blended pastes. *Applied Surface Science*, 252, pp.7562–7571.

Arcolao, C., 1998. *Le ricette del restauro* 2nd ed., Venezia: Marsilio Editore.

Arizzi, A. & Cultrone, G., 2013. The influence of aggregate texture, morphology and grading on the carbonation of non-hydraulic (aerial) lime-based mortars. *Quarterly Journal of Engineering Geology and Hydrogeology*, 46, pp.507–520.

Arruda, L., Santos, R.A. & Henriques da Silva, R., 2008. *History of Portuguese Art, Volume 09 - The modern rupture (XX century)* P. Pereira, ed., Lisbon, Portugal: Círculo de Leitores.

ARTEDITORES, 2009. *Palácio da Bolsa* 1st ed., Porto.

Bayer, R. & Lutz, H., 2000. Dry Mortars. In *Ullmann's Encyclopedia of Industrial Chemistry, Vol. 9*. Wiley-VCH Verlag GmbH & Co. KGaA, pp. 1–25.

Bell, I.M., Clark, R.J.H. & Gibbs, P.J., 1997. Raman spectroscopic library of natural and synthetic pigments (pre- ~1850 AD). *Spectrochimica Acta Part A*, 53, pp.2159–2179.

Borrachero, M. V et al., 2008. The use of thermogravimetric analysis technique for the characterization of construction materials. *Journal of Thermal Analysis and Calorimetry*, 91(2), pp.503–509.

Borsoi, G. et al., 2010. Chemical, mineralogical and microstructural characterization of historical mortars from the Roman villa of Pisões, Beja, Portugal. In J. Válek, C. Groot, & J. J. Hughes, eds. *Historic Mortars and RILEM TC 203-RHM Final Workshop, HMC2010*. Prague: RILEM Publications S.A.R.L., pp. 43–54.

Botelho, L. & Costa, P., 2004. Porto Cathedral. Available at: http://www.monumentos.pt/Site/APP_PagesUser/SIPA.aspx?id=1086 (in Portuguese) [Accessed September 25, 2013].

Brandi, C., 2006. *Teoria do Restauro*, ORION ed. (in Portuguese).

Builder, A., 1956. *Travail du plâtre* 2éme ed., Paris et Liége: Librairie Polytéchnique, Ch. Béranger.

Burgio, L. & Clark, R.J.H., 2001. Library of FT-Raman spectra of pigments, minerals, pigment media and varnishes, and supplement to existing library of Raman spectra of pigments with visible excitation. *Spectrochimica Acta Part A*, 57, pp.1491–1521.

Bustamante, R. & de Rojas, M.I.S., 2007. Study of plaster finishes on San Pedro de los Francos church at Calatayud. *Materiales de Construcción*, 57(286), pp.53–64.

C. M. Leiria, Solar do Barão de Salgueiro. Available at: http://www.cm-leiria.pt/pages/389 [Accessed July 29, 2014].

Cardoso, I. et al., 2014. A multidisciplinary approach to the study of archaeological mortars from the town of Ammaia in the Roman province of Lusitania (Portugal). *Archaeometry*, 56(1), pp.1–24. Available at: 10.1111/arcm.12020.

Cardoso, I.P., 2006. 18th Century church altarpieces in the Algarve, Portugal: a comparison of the historical documents to the results of the microscopical analysis R. M. Society, ed. *InFocus - Royal Microscopical Society's Magazine*, (4), pp.64–86.

Cardoso, I.P., 2010. *Gesso layers on Portuguese Baroque altarpieces: materials, practices and durability*. PhD Thesis. London: University College of London.

Carvalho, R., Cine-Teather of Fafe. Available at: http://www.patrimoniocultural.pt/pt/patrimonio/patrimonio-imovel/pesquisa-do-patrimonio/classificado-ou-em-vias-de-classificacao/geral/view/156347 [Accessed June 27, 2014].

Cavaco, S. & Covaneiro, J., 2009. Expression of taste or assertion of power. Imported ceramics in Tavira (Portugal) from XIV to XVII centuries. In A. del Giglio, ed. *IX Congresso Internazionale AIECM2*. Venice: ibs.it, pp. 185–188.

Chatterji, S. & Jeffery, J.W., 1964. Volume expansion of setting plaster. *Trans. Faraday Soc.*, 60, pp.1947–1950.

Cizer, Ö., Rodriguez-Navarro, C., et al., 2012. Phase and morphology evolution of calcium carbonate precipitated by carbonation of hydrated lime. *Journal of Materials Science*, 47, pp.6151–6165.

Cizer, Ö., Van Balen, K., et al., 2012. Real-time investigation of reaction rate and mineral phase modifications of lime carbonation. *Construction and Building Materials*, 35, pp.741–751.

Coquard, P. et al., 1994. Hardness, elasticity modulus and flexion strength of dry set plaster. *Journal of Materials Science*, 29(17), pp.4611–4617.

Cotrim, H., 2004. *Ancient gypsum plasters rehabilitation*. MSc. Thesis. Lisbon: Technical University of Lisbon (in Portuguese).

Cotrim, H., Veiga, M.R. & de Brito, J., 2008. Freixo palace: Rehabilitation of decorative gypsum plasters. *Construction and Building Materials*, 22(1), pp.41–49.

Cotrim, H., Veiga, M.R. & de Brito, J., 2007. Methodology for the rehabilitation of ancient gypsum plasterwork. *Journal of Building Appraisal*, 3(3), pp.195–212.

Cruz, A.J., 2000. The material from which is made colour. The pigments used in paint and their identification and characterization. In *1ºs Encontros de Conservação e Restauro - Tecnologias*. Tomar: Instituto Politécnico de Tomar, pp. 1–25 (in Portuguese).

D'Assumpção, T.L., *Diccionario dos termos d'architectura*, Lisboa, Portugal: Antiga Casa Bertrand - José Bastos.

Dalui, S.K., Roychowdhury, M. & Phani, K.K., 1996. Ultrasonic evaluation of gypsum plaster. *Journal of Materials Science*, 31(5), pp.1261–1263.

DGPC, Cartas e convenções internacionais sobre património. Available at: http://www.patrimoniocultural.pt/pt/patrimonio/cartas-e-convencoes-internacionais-sobre-patrimonio/ [accessed 17 August 2015].

Documentar, Tavira Barrocal - Igreja de São Francisco. Available at: http://tavirabarrocal.documentar.org/site/index.php?module=FMS&func=view&ot=location&id=245&oldfunc=browse&search= [Accessed July 30, 2014].

Eurogypsum, 2007. What is gypsum? Available at: http://www.eurogypsum.org/wp-content/uploads/2015/04/whatisgypsum.pdf [Accessed September 30, 2015].

Faria, P., 2004. *Mortars for old masonries renders. The influence of binders.* PhD Thesis. Lisbon: Nova University of Lisbon (in Portuguese).

Ferreira-Alves, J., 1991. Elements for the artistic history of the Porto Cathedral in the XVII-XVIII centuries. Nótula on some works: 1665-1709. *Revista da Faculdade de Letras da Universidade do Porto, 2ª série*, VIII, pp.275–288 (in Portuguese).

Fischer, H.B. & Vtorov, B., 2002. Characterization of historical gypsum mortars. *ZKG INTERNATIONAL*, 55(5), pp.92–99.

Forg, G., 1989. Influence of various retarders on the crystallization and strength of plaster of Paris. *Translation ZKG INTERNATIONAL*, 5, pp.229–232.

Freire, M.T., Veiga, M.R., et al., 2015. Desenvolvimento de produtos compatíveis de gesso e cal para a conservação e restauro de estuques antigos. In *CONPAT 2015*. Lisbon, Portugal, p. Com. 7464.

Freire, M.T., Santos Silva, A., et al., 2015. The history of Portuguese interior plaster coatings: A mineralogical survey using XRD. *Archaeometry*, 57(Special Online-only Issue, Supplement S1), pp.147–165. Available at: http://onlinelibrary.wiley.com/doi/10.1111/arcm.12130/suppinfo.

Freire, T. et al., 2009. Characterization of a 19th century decorated gypsum plaster piece: the role of microscopy. In Bernhard Middendorf et al., eds. *12th Euroseminar on Microscopy Applied to Building Materials*. Dortmund, Germany: Technische Universität Dortmund, pp. 416–427.

Freire, T. et al., 2012. Characterization of decorative Portuguese gypsum plasters from the nineteenth and twentieth centuries: The case of the Bolsa Palace in Oporto. In J. Válek, J. J. Hughes, & C. J. W. P. Groot, eds. *Historic Mortars: Characterisation, Assessment and Repair*. Springer Netherlands, pp. 141–151. Available at: http://dx.doi.org/10.1007/978-94-007-4635-0_11.

Freire, T. et al., 2008. Characterization of Portuguese historical gypsum mortars. In *Proc. 1st Historical Mortars Conference*. p. T_I_54_HMC008 (available on CD).

Freire, T. et al., 2010. Characterization of Portuguese historical gypsum mortars: a comparison between two case studies. *Materials Science Forum*, 636-637, pp.1258–1265.

Freire, T. et al., 2011. Improving the durability of Portuguese historical gypsum plasters using compatible restoration products. In V. P. Freitas & H. Corvacho, eds. *12th International Conference on Durability of Building Materials and Components*. Porto: FEUP Edições, pp. 905–913.

Freire, T. et al., 2013. Restoration of decorative elements moulded on site : design and selection of gypsum-lime compatible products. In *Proc. 3rd Historic Mortars Conference*. Glasgow, Scotland, pp. 1–8.

Füller, J., *Manual of the moulder and plasterer* 2nd ed., Lisbon: Livrarias Aillaud e Bertrand (Portugal) and Francisco Alves (Brasil) (in Portuguese).

Gárate-Rojas, I., 1999. *Artes de los Yesos. Yeserias e Estucos* Munilla-Lería, ed., Madrid: Instituto Español de Arquitectura, MRRP, Universidad de Alcalá.

Genestar, C. & Pons, C., 2003. Ancient covering plaster mortars from several convents and Islamic and Gothic palaces in Palma de Mallorca (Spain). Analytical characterisation. *Journal of Cultural Heritage*, 4(4), pp.291–298. Available at: 10.1016/j.culher.2003.02.001.

Genestar, C., Pons, C. & Más, A., 2006. Analytical characterisation of ancient mortars from the archaeological Roman city of Pollentia (Balearic Islands, Spain). *Analytica Chimica Acta*, 557(1-2), pp.373–379. Available at: 10.1016/j.aca.2005.10.058.

Ghorab, H.Y., Ragai, J. & Antar, A., 1986. Surface and bulk properties of ancient egyptian mortars. Part I: X-ray diffraction studies. *Cement and Concrete Research*, 16, pp.813–822.

Gil, J. & Calvet, N., 1992. *The most beautiful palaces of Portugal* 1st ed., Lisbon: Verbo.

Gomes, R.V., 2003. *Silves (Xelb), a city in the Gharb Al- Andalus: the citadel of the castle*, Trabalhos de Arqueologia, 35, Lisbon: Portuguese Institute of Archaeology (in Portuguese).

Gourdin, W.H. & Kingery, W.D., 1975. The beginnings of pyrotechnology: Neolithic and Egyptian lime plaster. *Journal of Field Archaelogy*, 2(1/2), pp.133–150.

Graça Costa, J.R., 1986. The gypsum in Portugal. *Estudos, Notas e Trabalhos, D.G.G.M.*, 28, pp.93–117 (in Portuguese).

Hannouille, E., 1959. *Pour le maçon et le plâtrier* 2éme ed., Paris: Dunod.

Hanor, J.S., 2000. Barite-celestine geochemistry and environments of formation. In C. N. Alpers, J. L. Jambor, & D. K. Nordstrom, eds. *Sulfate minerals - Crystallography, Geochemistry and Environmental Significance*. Washington, DC: Mineralogical Society of America and The Geochemical Society.

Henning, O. & Eggert, O., 1999. Moisture-induced changes in gypsum building materials. *ZKG INTERNATIONAL*, 52(3), pp.154–159.

Houst, Y.F. & Wittmann, F.H., 1994. Influence of porosity and water content in the diffusivity of CO2 and O2 through hydrated cement paste. *Cemenet and Concrete Research*, 24(6), pp.1165–1176.

ICOMOS, 2004. International Charters for Conservation and Restoration. *Monuments and Sites*, I.

Igea, J. et al., 2010. Ancient gypsum mortars from Sta. María Magdalena church (Zaragoza, Spain): Advances in technological manufacture. In *2nd Historic Mortars Conference HMC2010 and RILEM TC 203-RHM Final Workshop*. Prague, Czech Republic, pp. 197–205.

Igea, J. et al., 2012. Characterization of mudejar mortars from San Gil Abbot church (Zaragoza, Spain): investigation of the manufacturing technology of ancient gypsum mortars. *Materiales de Construcción*, 62(308), pp.515–529. Available at: 10.3989/mc.2012.07311.

Igea Romera, J. et al., 2013. Assessment of the physico-mechanical behaviour of gypsum-lime repair mortars as a function of curing time. *Environmental Earth Sciences*, 70(4), pp.1605–1618.

Innorta, G., Rabbi, E. & Tomadin, L., 1980. The gypsum-anhydrite equilibrium by solubility measurements. *Geochimica et Cosmochimica Acta*, 44, pp.1931–1936.

IUPAC, 1972. Manual of symbols and terminology for physicochemical quantities and units, Appendix II, Part I. *Pure and Applied Cemistry*, 31(July), pp.578–638.

IUPAC, 1985. Reporting physisorption data for gas/solid systems with special reference to the determination of surface area and porosity. *Pure and Applied Cemistry*, 57(4), pp.603–619.

Jordan, P.G. et al., 1991. Gypsum-anhydrite diferentiation by SEM using backscattered electron-signal. *Journal of Sedimentary Petrology*, 61(4), pp.616–618.

Karni, J. & Karni, E., 1995. Gypsum in construction: origin and properties. *Materials and Structures*, 28(2), pp.92–100.

Kawiak, T., 1991. Gypsum mortars from a twelfth-century church in Wislica, Poland. *Studies in Conservation*, 36, pp.142–150.

Kingery, W.D., Vandiver, P.B. & Prickett, M., 1988. The beginnings of pyrotechnology, part II: Production and use of lime and gypsum plaster in the pre-pottery Neolithic near-East. *Journal of Field Archaeology*, 15(2), pp.219–244.

Kunzel, H.M., 1995. *Simultaneous heat and moisture transport in building components*, Stuttgard: Fraunhofer IRB, Verlag.

Lanas, J. & Alvarez, J.I., 2003. Masonry repair lime-based mortars: factor affecting the mechanical behaviour. *Cement and Concrete Research*, 33(11), pp.1867–1876.

Lawrence, R.M.H. et al., 2006a. Determination of carbonation profiles in non-hydraulic lime mortars using thermogravimetric analysis. *Thermochimica Acta*, 444(2), pp.179–189. Available at: http://opus.bath.ac.uk/868/.

Lawrence, R.M.H. et al., 2007. Effects of carbonation on the pore structure of non-hydraulic lime mortars. *Cement and Concrete Research*, 37(7), pp.1059–1069. Available at: http://dx.doi.org/10.1016/j.cemconres.2007.04.011.

Lawrence, R.M.H. et al., 2006b. The use of thermogravimetric analysis to measure different concentrations of lime in non-hydraulic lime mortars. *Journal of Thermal Analysis and Calorimetry*, 85(2), pp.377–382. Available at: http://opus.bath.ac.uk/869/.

Leitão, L.A., 1896. *Elementary course of constructions*, Lisbon, Portugal: Imprensa Nacional (in Portuguese).

Leite, A.C. et al., 2008. *History of Portuguese Art, Volume 08 - Neoclassicism and Romanticism (XIX century)* P. Pereira, ed., Lisbon, Portugal: Círculo de Leitores.

Leite, M.S.J.P., 2008. *Plasters in the XX century in OPorto: the Baganha workshop*, CITAR.

Lewry, A.J. & Williamson, J., 1994a. The setting of gypsum plaster. Part I. The hydration of calcium sulphate hemihydrate. *Journal of Materials Science*, 29(20), pp.5279–5284. Available at: http://dx.doi.org/10.1007/BF01171536.

Lewry, A.J. & Williamson, J., 1994b. The setting of gypsum plaster. Part II. The development of microstructure and strength. *Journal of Materials Science*, 29(21), pp.5524–5528. Available at: http://dx.doi.org/10.1007/BF00349943.

Lewry, A.J. & Williamson, J., 1994c. The setting of gypsum plaster. Part III. The effect of additives and impurities. *Journal of Materials Science*, 29(23), pp.6085–6090. Available at: http://dx.doi.org/10.1007/BF00354546.

Livingston, R.A., Amde, A.M. & Chaturbahai, A., 1998. Gypsum mortar in historic structures. *Masonry Society Journal*, 16(1), pp.21–26.

Llera, F., 2006. Chapel of Rui Valente in the Cathedral: study for the safeguarding of the funerary monument. *Monumentos*, 24, pp.92–97 (in Portuguese).

Lucas, G., 2003a. High-temperature gypsum plaster on historic exteriors? A plea for gypsum. *ZKG INTERNATIONAL*, 56(08/09), pp.78–85.

Lucas, G., 2003b. The special features of high-temperature gypsum mortar as a building material. *ZKG INTERNATIONAL*, 56(8-9), pp.54–65.

Machado, J.P., 1991. *Grande Dicionário da Língua Portuguesa*, Lisbon, Portugal: Publicações Alfa, S.A.

Magalhães, A. & Veiga, R., 2009. Physical and mechanical characterisation of historic mortars. Application to the evaluation of the state of conservation. *Materiales de Construcción*, 59, pp.61–77.

Magalhães, A.C., Moragues, A. & Veiga, M.R., 2004. Application of some methods on evaluation of porous systems of wall renderings. In *VII Congreso Internacional de Rehabilitación del Patrimonio y Edificación*. Lanzarote, Spain, p. COM 109.

Magalhães, A.C. & Veiga, M.R., 2007. *Hygroscopic characterization of lime based mortars*, LNEC, Report Nr. 201/2007, DED/NRI. Lisbon, Portugal (in Portuguese).

Magalhães, N., 2002. Estoi Palace with its gardens, fountains and statuary. Available at: http://www.patrimoniocultural.pt/pt/patrimonio/patrimonio-imovel/pesquisa-do-patrimonio/classificado-ou-em-vias-de-classificacao/geral/view/74002 [Accessed June 26, 2014].

Malta da Silveira, P., 2000. *Ancient gypsum plasterwork: Constructive characterization and pathological analysis*. PhD Thesis. Lisbon: Technical University of Lisbon (in Portuguese).

Malta da Silveira, P., Veiga, M.R. & de Brito, J., 2007. Gypsum coatings in ancient buildings. *Construction and Building Materials*, 21(1), pp.126–131.

Margalha, M.G., 2010. *Mineral air binders. The influence of slaking process and curing time on their quality*. PhD Thesis. Lisbon: Technical University of Lisbon (in Portuguese).

Margalha, M.G. et al., 2011. The influence of slaking time on lime putty. In V. P. Freitas, H. Corvacho, & M. Lacasse, eds. *12th International Conference on Durability of Building Materials and Components*. Porto, Portugal, pp. 697–704.

Mateus, J.M., 2002. *Traditional techniques of masonry construction - The technical literature from 1750 to 1900 and its contribution to the conservation of historic buildings* 1st ed., Lisbon, Portugal: Livros Horizonte (in Portuguese).

Mattoso, J., 1985. Ermamento. *Dicionário enciclopédico da História de Portugal*, p.216, vol. I (in Portuguese).

Melo, H.P. et al., 2014. Problems of analysis by FTIR of calcium sulphate-based preparatory layers: The case of a group of 16th-century Portuguese paintings. *Archaeometry*, 56(3), pp.513–516. Available at: 10.1111/arcm.12026.

Mendonça, I., 2012. The ornamental plaster and the appeal of exotic in Portuguese interiors: Domingos Meira and the engravings of Owen Jones. In *IV encontro Luso-Brasileiro de Museus Casa*. Rio de Janeiro, Brasil: Fundação da Casa de Ruy Barbosa (in Portuguese).

Middendorf, B., 2002. Physico-mechanical and microstructural characteristics of historic and restoration mortars based on gypsum: Current knowledge and perspective. In S. Siegesmund, T. Weiss, & A. Vollbrecht, eds. *Natural Stone, Weathering Phenomena, Conservation Strategies and Case Studies*. London: The Geological Society of London, pp. 165–176.

Middendorf, B. & Knöfel, D., 1998a. Characterization of historic mortars from buildings in Germany and The Netherlands. In N. S. Baer, S. Fitz, & R. A. Livingston, eds. *Conservation of Historic Brick Structures*. Donhead Publ. Ltd., pp. 178–196.

Middendorf, B. & Knöfel, D., 1998b. Gypsum and lime mortars of historic german brick buildings. In N. S. Baer, S. Fitz, & R. A. Livingston, eds. *Conservation of Historic Brick Structures*. Donhead Publications, Ltd., pp. 197–208.

Miriello, D. et al., 2011. Characterisation of archaeological mortars and plasters from kyme (Turkey). *Journal of Archaeological Science*, 38 , pp.794–804.

Miriello, D. et al., 2010. Characterisation of archaeological mortars from Pompeii (Campania, Italy) and identification of construction phases by compositional data analysis. *Journal of Archaeological Science*, 37, pp.2207–2223.

Montoya, C. et al., 2003. Study of ancient dolomitic mortars of the church of Santa María de Zamarce in Navarra (Spain): comparison with simulated standards. *Thermochimica Acta*, 398, pp.107–122.

Moorehead, D.R., 1986. Cementation by the carbonation of hydrated lime. *Cement and Concrete Research*, 16, pp.700–708.

Moropoulou, A. et al., 2005. Strength development and lime reaction in mortars for repairing historic masonries. *Cement & Concrete Composites*, 27, pp.289–294. Available at: http://dx.doi.org/10.1016/j.cemconcomp.2004.02.017.

Moropoulou, A., Bakolas, A. & Bisbikou, K., 1995. Characterization of ancient, byzantine and later historic mortars by thermal and X-ray diffraction techniques. *Thermochimica Acta*, 269/270, pp.779–795.

Murat, M., 1982. Rapport final d'activité (1973–1980) de la Commission 23-GP (Gypsum/Plaster) de la RILEM. *Materials and Structures*, 15(1), pp.39–62. Available at: http://dx.doi.org/10.1007/BF02473558.

Murat, M. & Foucault, M., 1977. Sulfate de calcium et materieux derivés. Compte rendu et conclusions du Colloque International de la RILEM. *Materials and Structures*, 11(1), pp.39–56. Available at: http://dx.doi.org/10.1007/BF02478702.

Murat, M., Pusztaszeri, L. & Gremion, M., 1975. Corrélations "texture cristalline-propriétés mécaniques" des plâtres durcis. Étude préliminaire. *Materials and Structures*, 8(5), pp.377–385. Available at: http://dx.doi.org/10.1007/BF02479025.

Noé, P. et al., Monserrate Palace. Available at: http://www.monumentos.pt/Site/APP_PagesUser/SIPA.aspx?id=4069 (in Portuguese) [Accessed September 23, 2014].

Oliveira, M.G., 2004. *Ernesto Korrodi: itinerary in the city of Leiria*, Leiria: ADLEI.

Paama, L. et al., 1998. Thermal and infrared spectroscopic characterization of historical mortars. *Thermochimica Acta*, 320, pp.127–133.

Paiva, J. V., 1969. *Moisture in buildings*. Lisbon: LNEC. Thesis submitted to the competition for Specialist LNEC (in Portuguese).

Papayianni, I., 2005. Design and manufacture of repair mortars for interventions on monuments and historic buildings. In *International RILEM Workshop on Repair Mortars for Historic Masonry*. Delft, The Netherlands: RILEM Publications S.A.R.L., pp. 292–304.

Papayianni, I., Pachta, V. & Stefanidou, M., 2013. Analysis of ancient mortars and design of compatible repair mortars: The case study of Odeion of the archaeological site of Dion. *Construction and Building Materials*, 40, pp.84–92.

Paz Branco, J., 1993. *Manual plasterwork and modeling* 2nd ed., Queluz: Escola Profissional Gustave Eiffel (in Portuguese).

Pereira de Lima, 2006. The Marquis of Pombal Farm. *Quinta do Marquês de Pombal*. Available at: http://www.monumentos.pt/Site/APP_PagesUser/SIPA.aspx?id=22656 (in Portuguese) [Accessed September 25, 2013].

Pereira, P., 2003. *De Aurea Aetate. The choir of the Convent of Christ in Tomar and symbolic Manueline*, Lisbon: Portuguese Institute of Architectural Heritage (IPPAR) (in Portuguese).

Philokyprou, M., 2012. The beginnings of pyrotechnology in Cyprus. *International Journal of Architectural Heritage*, 6(2), pp.172–199. Available at: http://www.tandfonline.com/doi/abs/10.1080/15583058.2010.528145.

Quaglierini, C. & Amorosi, L., 1991. *Chemistry and technology of materials for art* Prima ediz. Zanichelli S.p.A., ed., Bologna (in Italian).

Ragai, J., 1988a. Surface and bulk properties of ancient egyptian mortars. Part III: X-ray diffraction studies (b). *Cement and Concrete Research*, 18, pp.9–17.

Ragai, J., 1988b. Surface and bulk properties of ancient egyptian mortars. Part IV: Thermal studies. *Cement and Concrete Research*, 18, pp.179–184.

Ragai, J., 1989. Surface and bulk properties of ancient egyptian mortars. Part V: Thermal studies (b). *Cement and Concrete Research*, 19, pp.42–46.

Ragai, J., Ghorab, H.Y. & Antar, A., 1987. Surface and bulk properties of ancient egyptian mortars. Part II: Adsorption and infrared studies. *Cement and Concrete Research*, 17, pp.12–21.

Ramos, N.M.M., 2007. *The importance of hygroscopic inertia on hygrothermal performance of buildings*. PhD Thesis, Porto: University of Porto, Portugal (in Portuguese).

Ramos, N.M.M., Delgado, J.M.P.Q. & de Freitas, V.P., 2010. Influence of finishing coatings on hygroscopic moisture buffering in building elements. *Construction and Building Materials*, 24(12), pp.2590–2597.

Rato, V., 2006. *Influence of morphologic microstructure in the performance of mortars*. PhD Thesis. Lisbon: Nova University of Lisbon (in Portuguese).

Reynaud, P. et al., 2006. Water effect on internal friction of set plaster. *Materials Science and Engineering A*, 442, pp.500–503.

Rivera-Blanco, J., 2008. *De Varia Restauratione. Teoría e Historia de la Restauración Arquitectónica*, Madrid, Spain: ABADA Editores (in Spanish).

Robador, M.D., Perez-Rodriguez, J.L. & Duran, A., 2010. Hydraulic structures of the Roman Mithraeum house in Augusta Emerita, Spain. *Journal of Archaeological Science*, 37(10), pp.2426–2432. Available at: http://dx.doi.org/10.1016/j.jas.2010.05.003.

Rúbio Domene, R., 2011. *Alhambra plasterwork* 1st ed., Editorial Universidad de Granada, Spain (in Spanish).

S.N.I.P., 1982. *Le Plâtre. Physico-Chimie. Fabrication et Emplois*, Paris: Syndicat National des Industries du Plâtre, Eyrolles ed. (in French).

Santos Silva, A., Paiva, M., et al., 2006. Characterization of Roman mortars from the archaeological site of Tróia (Portugal). *Materials Science Forum*, 514-516, pp.1643–1647.

Santos Silva, A., Ricardo, J.M., et al., 2006. Characterization of Roman mortars from the historical town of Mértola. In *Heritage, International Weathering and Conservation Conference HWC*. Madrid, pp. 85–90.

Santos Silva, A. et al., 2011. Mineralogical and chemical characterisation of historical mortars from military fortifications in Lisbon harbour (Portugal). *Environmental Earth Sciences*, 63, pp.1641–1650.

Sanz, D., 2009. *Analysis of gypsum used in external renders using geological techniques*. PhD Thesis. Madrid: Polytechnic University of Madrid (in Spanish).

Sanz, D., 2007. Traditional gypsum kilns used in construction. *Recopar, Electronic Review*, 5(April - December), pp.76–84.

Sawyer, J.T., 1951. *Plastering*, London: Edward Arnold & Co.

Schlütter, F., Wolfgang, K. & Juling, H., 2010. High fired gypsum mortar for screeds, terrazzo and masonry repair on historic monuments. Production, properties and sample applications. In J. Válek, C. Groot, & J. J. Hughes, eds. *Historic Mortars and RILEM TC 203-RHM Final Workshop, HMC2010*. Prague: RILEM Publications S.A.R.L., pp. 1169–1180.

Segurado_a, J.E.S., *Finishings of buildings* 3rd ed., Bertrand (Portugal) and Francisco Alves (Brasil) (in Portuguese).

Segurado_b, J.E.S., *Construction materials* 5th ed., Lisbon, Portugal: Livrarias Aillaud e Bertrand (in Portuguese).

Sievert, T., Wolter, A. & Singh, N.B., 2005. Hydration of anhydrite of gypsum (CaSO4.II) in a ball mill. *Cement and Concrete Research*, 35(4), pp.623–630. Available at: doi 10.1016/cemconres.2004.02.010.

Silva, H., 2005. *Giovanni Grossi and the evolution of decorative stuccos in Portugal in the 18th century*. Msc. Thesis, Lisbon: Lisbon University (in Portuguese).

Simões de Abreu, M. et al., 2008. *History of Portuguese Art - From prehistory to Islam* P. Pereira, ed., Lisbon, Portugal: Círculo de Leitores (in Portuguese).

Singh, N.B. & Middendorf, B., 2007. Calcium sulphate hemihydrate hydration leading to gypsum crystallization. *Progress in Crystal Growth and Characterization of Materials*, 53(1), pp.57–77.

Song, K. et al., 2010. Simultaneous monitoring of hydration kinetics, microstructural evolution, and surface interactions in hydrating gypsum plaster in the presence of additives. *Journal of Materials Science*, 45(19), pp.5282–5290. Available at: http://dx.doi.org/10.1007/s10853-010-4572-7.

Sousa Coutinho, A., 2006. *Concrete manufacture and properties* 4th ed., Lisbon, Portugal: LNEC, Colecção Manuais, vol. II (in Portuguese).

Stark, J. & Wicht, B., 1999. The history of gypsum and gypsum plaster. *ZKG INTERNATIONAL*, 52(10), pp.527–533.

Stefanidou, M., 2010. Methods for porosity measurement in lime-based mortars. *Construction and Building Materials*, 24(12), pp.2572–2578. Available at: 10.1016/j.conbuildmat.2010.05.019.

Tegethoff, F.W., 2001. *Calcium carbonate - From the cretaceous period into the 21st century* 1st ed. F. W. Tegethoff, J. Rohleder, & J. Kroker, eds., Basel, Switzerland: Birkhaüser Verlag.

Tesch, V. & Middendorf, B., 2005. Optimised microstructure of calcium sulphate based mortars for the restoration of historic masonry. In C. Groot, ed. *Repair Mortars for Historic Masonry*. Delft: RILEM, pp. 345–353.

Themudo-Barata, J.F., Estuque. *Verbo enciclopédia luso-brasileira de cultura*, pp.1676–1677, vol. 7 (in Portuguese).

Thomson, M. et al., 2004. Porosity of mortars. In C. Groot, G. Ashall, & J. Hughes, eds. *Characterisation of old mortars with respect to their repair - Final report of RILEM TC 167-COM*. RILEM Publications S.A.R.L.

Turco, T., 2008. *Il Gesso. Lavorazione, Trasformazione, Impieghi* Seconda ed., Milano: Editore Ulrico Hoepli.

Turriano, J., 1996. The twenty-one books of engineering and machines of Juanelo Turriano: A translation of the manuscript The twenty-one books of engineering and machines in the Biblioteca Nacional, Madrid c.a. 1511-1583, Book 17. In Doce Calles, Madrid, pp. 483–500.

Valadas, S. & Candeias, A., 2010. *Analysis of IR spectra of gypsum samples*, Report HERC/02/010, Hercules Centre, Univ. of Évora, Portugal (in Portuguese).

Válek, J. & Veiga, M.R., 2005. Characterisation of mechanical properties of historic mortars - Testing of irregular samples. *Advances in Architecture Series*, 20, pp.365–374.

Vasconcelos, F., 1966. Considerations about decorative plasterwork. *Boletim do Museu Nacional de Arte Antiga*, V(2), pp.34–43 (in Portuguese).

Vasconcelos, F., 1991. Gypsum plaster, the baroque privileged decoration. In *First Baroque International Congress*. Porto, Portugal: Reitoria da Universidade do Porto/Governo Civil do Porto, pp. 551–557 (in Portuguese).

Vasconcelos, F., 1997. The gypsum plasterwork of Porto. *Collection Porto Patrimony*, (in Portuguese).

Vasconcelos, F., 1961. Three plasterworks previous to the Baroque. *Separata da revista MVSEV*, 2ª série(3), pp.4–12 (in Portuguese).

Vecchio, S. et al., 1993. The use of thermoanalytical techniques in the characterization of ancient mortars. *Thermochimica Acta*, 227, pp.215–223.

Veiga, M.R. et al., 2010. Lime-based mortars: viability for use as substitution renders in historical buildings. *International Journal of Architectural Heritage*, 4(2), pp.177–195.

Veiga, M.R. et al., 2001. Methodologies for characterization and repair of mortars of ancient buildings. In P. B. Lourenço & P. Roca, eds. *International Seminar of Historic Constructions 2001*. Guimarães, Portugal: Universidade do Minho, pp. 353–362.

Veiga, M.R., 2012. Mortars of historic masonry. Functions and characteristics. In F. Pinho et al., eds. *CIREA 2012 – Conferência Internacional sobre Reabilitação de Estruturas Antigas de Alvenaria*. Lisbon: Nova University of Lisboa, pp. 17–27.

Veiga, M.R. et al., 1995. *Specialization course on wall coatings* 2nd ed., Lisbon, Portugal: National Laboratory for Civil Engineering (in Portuguese).

Veiga, M.R., Magalhães, A. & Bosilijkov, V., 2004. Capillarity tests on historic mortar samples extracted from site. Methodology and compared results. In D. Martens & A. Vermeltfoort, eds. *13th International Brick and Block Masonry Conference*. Amsterdam: Eindhoven University of Technology.

Velosa, A.L. et al., 2007. Characterisation of roman mortars from Conímbriga with respect to their repair. *Materials Characterization*, 58(11-12), pp.1208–1216. Available at: 10.1016/j.matchar.2007.06.017.

Verdelho da Costa, L., 1997. *Ernesto Korrodi* 1st ed., Editorial Estampa (in Portuguese).

Verdelho da Costa, L., 1989. *Leiria* 1st ed., Editorial Presença (in Portuguese).

Vieira da Silva, J.C., 2006. The Chapel of St. Dominic and the funerary monument of Rui Valente in the cathedral of Faro. *Monumentos*, 24, pp.84–91 (in Portuguese).

Vieira, E., 2002. *Traditional techniques of stuccos and simulated stucco decorations in the north of Portugal. A contribution to its study and conservation*. Évora: University of Évora.

Vieira, E., 2008. *Traditional techniques of stuccos in Portuguese interior coatings. History and technology. Application to the conservation and restoration*. Polytechnic University of Valencia, Faculty of Fine Arts.

Villanueva, L., 2004. Historical evolution of the gypsum construction. *Informes de la Construcción*, 56(493), pp.5–11 (in Spanish). Available at: http://informesdelaconstruccion.revistas.csic.es/index.php/informesdelaconstruccion/article/view/434/507.

Vogel, D. et al., 1999. Characterization and reproduction of historical gypsum plasters and comparison with familiar modern preparations. *Zkg International*, 52(11), pp.640–648.

Wirsching, F., 2005. Calcium Sulfate. In *Ullmann's Encyclopedia of Industrial Chemistry*. Wiley-VCH Verlag GmbH & Co. KGaA, pp. 1–33.

Yu, Q.L. & Brouwers, H.J.H., 2011. Microstructure and mechanical properties of [beta]-hemihydrate produced gypsum: An insight from its hydration process. *Construction and Building Materials*, 25(7), pp.3149–3157.

Zbyszewski, G. & Almeida, J.M.C., 1964. Gypsum deposits in Portugal. *Boletim de Minas*, 1(3), pp.161–166 (in Portuguese).

List of standards

ASTM 4404-84:2004 - Standard Test Method for Determination of Pore Volume and Pore Volume Distribution of Soil and Rock by Mercury Intrusion Porosimetry. ASTM, p. 7.

CEN/TR 15124:2005 - Design, preparation and application of internal gypsum plastering systems. CEN, p. 19.

EN 1015-11:1999 - Methods of test for mortar for masonry. Part 11: Determination of flexural and compressive strength of hardened mortar. CEN, p. 12.

EN 1015-18:2002 - Methods of test for mortar for masonry. Part 18: Determination of water absorption coefficient due to capillary action of hardened mortar. CEN, p. 10.

EN 1015-19:1998 - Methods of test for mortar for masonry. Part 19: Determination of water vapour permeability of hardened rendering and plastering mortars. CEN, p. 16.

EN 13279-1:2008 - Gypsum binders and gypsum plasters. Part 1: Definitions and requirements. CEN, p. 20.

EN 13279-2:2004 - Gypsum binders and gypsum plasters. Part 2: Test methods. CEN, p. 21.

EN 13914-2:2005 - Design, preparation and application of external rendering and internal plastering. Part 2: Design considerations and essential principles for internal plastering. CEN, p. 21

NP EN 196-1:2006 - Métodos de ensaio de cimentos. Parte 1: Determinação das resistências mecânicas. IPQ, p. 37.

NP EN 1097-3:2002 - Ensaios das propriedades mecânicas e físicas dos agregados. Parte 3: Determinação da baridade e do volume de vazios. IPQ, p. 16.

NP EN 12504-4:2007 - Ensaios de betão nas estruturas. Parte 4: Determinação da velocidade de propagação dos ultra-sons. IPQ, p. 18.

NP EN 14146:2006 - Métodos de ensaio para pedra natural - Determinação do módulo de elasticidade dinâmico (através da medição da frequência de ressonância fundamental). IPQ, p. 17.

Annex - Detailed experimental results from Chapter 5

Table A 1 - Mechanical strength results

Product	Test specimen	Flexural strength (MPa)					Compressive strength (MPa)				
		28d	90d	180d	1y	2y	28d	90d	180d	1y	2y
L1	1	0.99	1.90	1.55	1.32	1.55	1.30	2.87	2.71	2.14	3.31
							1.33	2.75	2.11*	-	2.74
	2	0.90	1.74	1.07*	1.08	-	1.58	2.85	3.01	1.78	-
							1.19	2.54	2.68	1.69	-
	3	1.38*	1.89	1.62	1.20	-	1.56	2.88	3.00	2.06	-
							1.64	2.90	2.60	1.68	-
	Average	0.95	1.84	1.59	1.20	1.55	1.43	2.80	2.80	1.87	3.03
	Standard deviation	0.07	0.09	0.05	0.12	-	0.18	0.14	0.19	0.22	0.40
L2	1	1.16	1.48	1.68	0.95	1.28	1.04	1.37*	2.81	1.70	2.45
							1.28	1.90	-	1.66	2.25
	2	1.15	1.31	1.72	1.17	-	1.19	0.97*	2.73	1.34	-
							1.47	2.64	2.84	1.56	-
	3	1.33	1.57	1.58	0.98	-	1.02	2.46	2.96	1.75	-
							1.48	2.86	2.89	1.29	-
	Average	1.21	1.45	1.66	1.03	1.28	1.25	2.46	2.85	1.56	2.35
	Standard deviation	0.10	0.13	0.07	0.12	-	0.20	0.41	0.09	0.19	0.14
M1	1	1.34	1.79	1.29	1.46	1.39	1.76*	2.70	2.61	3.06	3.13
							1.14	3.17	2.66	2.60	2.64
	2	1.55	2.11	1.18	1.33	-	1.37	2.90	3.24	3.39	-
							1.42	2.57	2.75	3.70	-
	3	1.05	1.79	1.20	1.48	-	1.42	2.86	2.32	2.91	-
							1.45	2.77	3.33	3.29	-
	Average	1.31	1.90	1.22	1.42	1.39	1.36	2.83	2.82	3.16	2.88
	Standard deviation	0.25	0.18	0.06	0.08	-	0.13	0.20	0.39	0.39	0.34

* Excluded (deviation from average > 20%)

Table A 1 - Mechanical strength results (cont.)

Product	Test specimen	Flexural strength (MPa)					Compressive strength (MPa)				
		28d	90d	180d	1y	2y	28d	90d	180d	1y	2y
M2	1	1.86	1.16*	1.63	0.93*	1.61	1.80	1.53*	3.22	2.85	3.46
							2.01	1.95*	2.64	3.38	3.02
	2	2.01	1.84	1.60	1.25	-	1.94	2.70	3.22	3.22	-
							2.31	2.47	3.14	2.77	-
	3	1.47	1.89	2.15	1.41	-	2.22	3.17	3.20	3.15	-
							2.27	2.25	3.36	3.24	-
	Average	1.78	1.86	1.79	1.33	1.61	2.09	2.65	3.13	3.10	3.24
	Standard deviation	0.28	0.03	0.31	0.11	-	0.21	0.39	0.25	0.24	0.31
P1	1	2.48	2.71	2.24	1.83	2.27	4.33	4.16	4.64	2.82	5.07
							4.45	4.12	4.55	2.86	5.69
	2	2.53	2.60	2.32	1.73	-	5.22	3.74	4.57	2.83	-
							4.98	4.76	4.24	2.85	-
	3	2.81	2.61	2.15	1.91	-	4.31	4.99	4.98	2.99	-
							4.79	5.51	3.87	2.85	-
	Average	2.61	2.64	2.24	1.82	2.27	4.68	4.55	4.48	2.87	5.38
	Standard deviation	0.18	0.06	0.09	0.09	-	0.37	0.66	0.38	0.06	0.44
P2	1	3.64	2.70	4.31	2.61	3.45	5.07	5.32	7.36	5.03	6.44
							6.42	5.66	7.52	8.88*	6.95
	2	3.67	3.12	3.85	3.19	3.68	6.08	5.72	6.81	5.70	7.17
							6.28	5.94	5.93	6.42	7.01
	3	3.30	2.39	3.41	2.73	-	4.88	6.36	6.17	6.14	-
							4.30*	5.79	6.62	7.05	-
	Average	3.54	2.74	3.86	2.84	3.56	5.75	5.80	6.74	6.07	6.89
	Standard deviation	0.21	0.37	0.45	0.31	0.16	0.72	0.34	0.63	0.76	0.32
P3	1	4.27	4.12	3.51	3.86	2.34	8.84*	8.70	7.23	7.98	5.20
							6.60	8.33	7.43	7.70	5.27
	2	3.47	4.17	2.71	4.68	2.50	6.53	7.79	7.23	7.57	4.82
							7.82	8.35	7.37	7.60	5.46
	3	3.38	4.18	3.21	3.18	-	5.75	7.19	6.76	8.35	-
							7.16	7.30	7.12	7.05	-
	Average	3.71	4.16	3.14	3.91	2.42	6.77	7.94	7.19	7.71	5.19
	Standard deviation	0.49	0.03	0.40	0.75	0.11	0.77	0.62	0.24	0.44	0.27

* Excluded (deviation from average > 20%)

Table A 2 - Dynamic modulus of elasticity (DME) determined by the ultrasonic pulse velocity method (UPS)

Product	Test specimen	Speed ($m.s^{-1}$)					DME_UPS (MPa)				
		28d	90d	180d	1y	2y	28d	90d	180d	1y	2y
L1	1	1191	1271	1276	1284	1298	1156	1399	1415	1423	1473
	2	1196	1274	1283	1280	1295	1173	1396	1427	1417	1471
	3	1211	1287	1292	1277	-	1211	1418	1456	1400	-
	Average	1199	1277	1284	1280	1297	1180	1404	1433	1413	1472
	SD	10	8	8	3	2	28	12	21	12	1
L2	1	1132	1186	1217	1197	1210	1047	1200	1262	1224	1241
	2	1142	1192	1217	1214	1224	1058	1202	1266	1255	1265
	3	1144	1196	1222	1206	-	1070	1213	1274	1240	-
	Average	1140	1192	1219	1206	1217	1058	1205	1267	1240	1253
	SD	6	5	3	8	10	12	7	6	15	17
M1	1	1202	1332	1334	1291	1305	1157	1563	1554	1453	1495
	2	1192	1331	1344	1306	1287	1153	1560	1580	1492	1451
	3	1187	1331	1352	1302	-	1152	1566	1602	1482	-
	Average	1194	1332	1343	1300	1296	1154	1563	1579	1476	1473
	SD	8	0	9	8	13	2	3	24	20	31
M2	1	1319	1418	1378	1352	1354	1544	1844	1739	1677	1681
	2	1323	1428	1380	1356	1395	1553	1865	1731	1679	1786
	3	1325	1402	1378	1352	-	1556	1800	1733	1671	-
	Average	1322	1416	1379	1353	1375	1551	1836	1735	1676	1734
	SD	3	13	1	2	29	6	33	4	4	75
P1	1	1749	1779	1778	1732	1763	2616	2731	2724	2577	2674
	2	1737	1780	1774	1730	-	2577	2721	2704	2562	-
	3	1724	1794	1801	1731	-	2534	2770	2776	2567	-
	Average	1737	1784	1784	1731	1763	2576	2741	2735	2569	2674
	SD	12	9	15	1	-	41	26	37	8	-
P2	1	1874	1949	1937	1935	1894	3239	3490	3478	3468	3320
	2	1849	1992	1932	1895	-	3179	3655	3467	3335	-
	3	1874	1903	1937	1911	-	3255	3324	3485	3371	-
	Average	1865	1948	1935	1914	1894	3224	3490	3477	3391	3320
	SD	14	45	3	20	-	40	166	9	68	-
P3	1	1933	1962	1992	1969	1971	3555	3612	3723	3639	3639
	2	1946	1957	1969	1963	-	3586	3602	3631	3606	-
	3	1951	1980	1972	1949	-	3616	3660	3643	3553	-
	Average	1944	1966	1978	1960	1971	3586	3625	3666	3599	3639
	SD	9	12	12	10	-	31	31	50	43	-

SD - standard deviation

Table A 3 - Dynamic modulus of elasticity (DME) determined by the fundamental resonance frequency method (FR)

Product	Test specimen	Frequency (Hz)					DME_FR (MPa)				
		28d	90d	180d	1y	2y	28d	90d	180d	1y	2y
L1	1	4103	4484	4463	4583	4547	1453	1822	1799	1879	1869
	2	4151	4522	4452	4608	4535	1494	1850	1792	1901	1877
	3	4149	4465	4449	4557	-	1504	1791	1803	1851	-
	Average	4134	4490	4454	4582	4541	1484	1821	1798	1877	1873
	SD	27	29	7	26	8	27	29	6	25	6
L2	1	3789	4106	4110	4123	4107	1293	1579	1578	1606	1572
	2	3805	4047	4093	4152	4145	1302	1519	1568	1625	1597
	3	3789	4057	4134	4136	-	1296	1529	1598	1614	-
	Average	3794	4070	4112	4137	4126	1297	1542	1581	1615	1584
	SD	9	32	20	15	27	4	32	15	9	18
M1	1	3984	4479	4487	4503	4437	1495	1993	1989	1996	1945
	2	4007	4471	4527	4482	4373	1512	1986	2032	1989	1887
	3	3979	4455	4571	4465	-	1481	1977	2071	1974	-
	Average	3990	4468	4529	4483	4405	1496	1985	2030	1986	1916
	SD	15	12	42	19	45	16	8	41	11	41
M2	1	4490	4769	4621	4689	4749	2039	2378	2223	2287	2349
	2	4540	4799	4666	4710	4754	2084	2403	2252	2303	2352
	3	4535	4730	4612	4719	-	2076	2334	2211	2317	-
	Average	4522	4766	4633	4706	4751	2066	2372	2229	2302	2350
	SD	28	34	29	15	3	24	35	21	15	2
P1	1	5981	6112	6084	6070	6200	3495	3670	3651	3609	3762
	2	6009	6066	6091	6097	-	3522	3606	3653	3631	-
	3	5992	6150	6140	6082	-	3492	3706	3694	3611	-
	Average	5994	6109	6105	6083	6200	3503	3661	3666	3617	3762
	SD	14	42	31	14	-	16	50	24	12	-
P2	1	6439	6819	6636	6832	6625	4369	4884	4656	4934	4637
	2	6528	6916	6703	6879	6721	4519	5034	4747	5011	4775
	3	6455	6654	6714	6859	-	4408	4635	4771	4951	-
	Average	6474	6796	6684	6857	6673	4432	4851	4724	4966	4706
	SD	47	132	42	23	68	78	201	61	40	
P3	1	-	6911	7117	7018	6872	-	5097	5418	5280	5056
	2	-	6867	6949	7079	6808	-	5062	5162	5358	4969
	3	-	7213	6961	7073	6911	-	5534	5177	5338	5098
	Average	-	6997	7009	7057	6864	-	5231	5253	5325	5041
	SD	-	189	94	34	52	-	263	144	41	66

SD - standard deviation

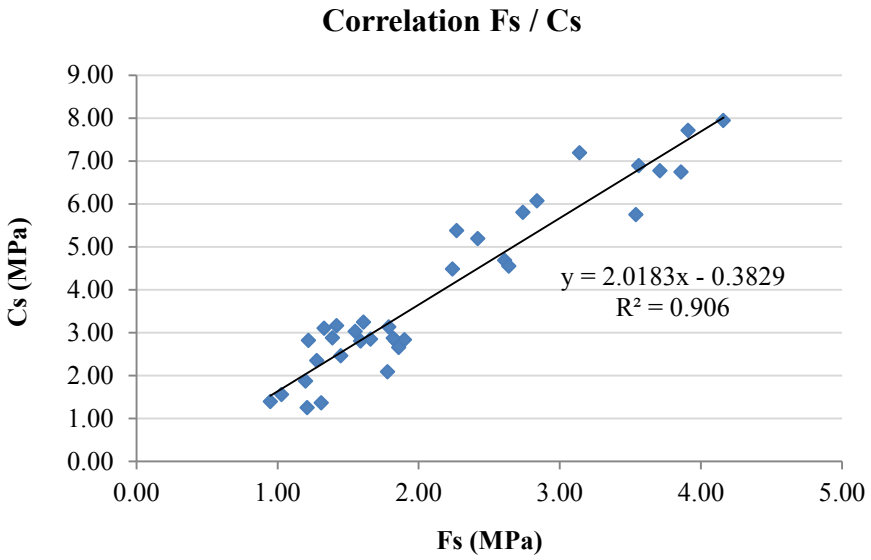

Figure A 1 - Mechanical strength: correlation between the results of flexural strength (Fs) and compressive strength (Cs)

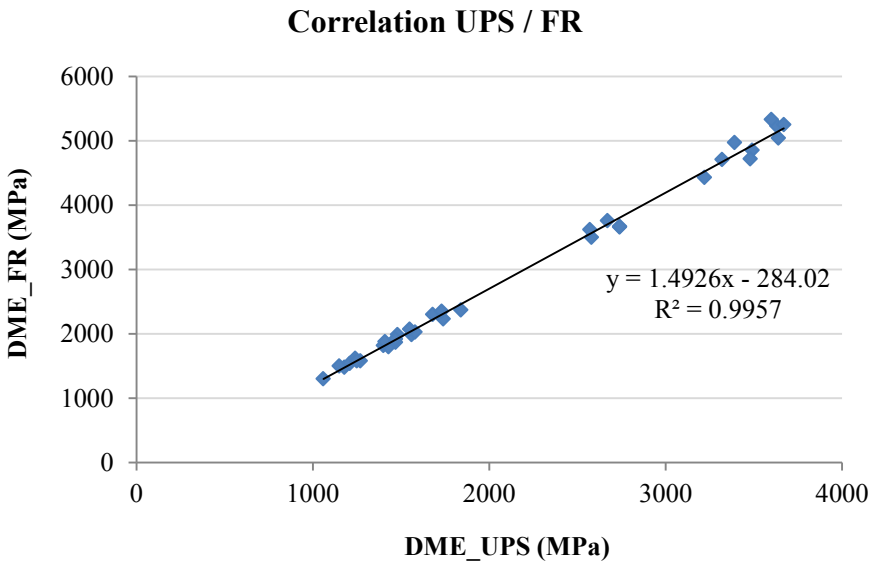

Figure A 2 - Dynamic modulus of elasticity (DME): correlation between the results obtained by the ultrasonic pulse velocity method (UPS) and the fundamental resonance frequency method (FR)

Table A 4 - Capillary water absorption results

Product	Test specimen	Cc (5 minutes) ($kg.m^{-2}min^{-1/2}$)		Cc (10 - 90 minutes) ($kg.m^{-2}min^{-1/2}$)		Maximum absorption (at 24)	
		90d	2y	90d	2y	90d	2y
L1	1	4.54	3.82	4.87	4.49	79.93	78.92
	2	4.57	-	4.83	-	79.76	-
	3	4.56	-	4.82	-	80.16	-
	Average	4.56	3.82	4.84	4.49	79.95	78.92
	SD	0.01	-	0.03	-	0.20	-
L2	1	4.54	2.64	4.96	5.00	81.29	80.69
	2	4.41	-	4.93	-	81.32	-
	3	4.53	-	4.91	-	81.45	-
	Average	4.49	2.64	4.93	5.00	81.35	80.69
	SD	0.07	-	0.02	-	0.08	-
M1	1	5.66	0.60	6.66	6.73	80.54	80.15
	2	5.57	-	6.62	-	80.54	-
	3	5.52	-	6.49	-	80.73	-
	Average	5.58	0.60	6.59	6.73	80.61	80.15
	SD	0.07	-	0.09	-	0.11	-
M2	1	4.73	1.23	6.17	6.23	76.94	76.26
	2	5.33	-	6.11	-	77.08	-
	3	5.07	-	6.12	-	76.79	-
	Average	5.04	1.23	6.14	6.23	76.94	76.26
	SD	0.30	-	0.03	-	0.14	-
P1	1	10.67	8.98	7.17	7.70	79.45	79.01
	2	11.10	-	7.12	-	79.57	-
	3	10.78	-	7.12	-	79.36	-
	Average	10.85	8.98	7.14	7.70	79.46	79.01
	SD	0.22	-	0.03	-	0.11	-
P2	1	8.16	6.29	7.29	6.32	73.07	73.07
	2	8.12	-	7.30	-	73.32	-
	3	7.93	-	7.35	-	73.15	-
	Average	8.07	6.29	7.32	6.32	73.18	73.07
	SD	0.12	-	0.03	-	0.13	-
P3	1	6.75	6.55	7.00	6.42	71.88	71.26
	2	6.76	-	6.94	-	71.46	-
	3	7.07	-	6.98	-	71.79	-
	Average	6.86	6.55	6.97	6.42	71.71	71.26
	SD	0.18	-	0.03	-	0.22	-

Cc - capillary coefficient; SD - standard deviation

Table A 5 - Water vapour permeability results

Product	Test specimen	Thickness (mm)		ΔM/24h (g)		Permeability ($ng.m^{-1}.s^{-1}.Pa^{-1}$)		Sd (d=10 mm) (m)	
		90d	2y	90d	2y	90d	2y	90d	2y
L1	1	19.12	19.32	3.38	2.46	30.39	22.35	0.059	0.082
	2	19.15	19.23	3.66	2.44	32.95	22.06	0.054	0.082
	3	19.40	19.50	3.85	2.58	35.11	23.65	0.050	0.077
	Average	19.22	19.35	3.63	2.49	32.82	22.69	0.054	0.081
	SD	0.15	0.14	0.24	0.08	2.36	0.85	0.004	0.003
L2	1	19.84*	20.29	1.56*	2.13	14.55*	20.32	0.129*	0.091
	2	19.69	20.25	2.59	2.51	23.98	23.89	0.076	0.077
	3	19.89	20.32	2.40	2.21	22.45	21.12	0.082	0.087
	Average	19.79	20.29	2.50	2.28	23.21	21.78	0.079	0.085
	SD	0.14	0.04	0.13	0.20	1.08	1.87	0.004	0.007
M1	1	20.12	20.49	1.71	2.39	16.18	23.02	0.116	0.080
	2	20.10	20.24	1.34	2.32	12.66	22.08	0.149	0.083
	3	19.96	20.14	1.40	1.81	13.14	17.14	0.143	0.109
	Average	20.06	20.29	1.48	2.17	13.99	20.75	0.136	0.091
	SD	0.09	0.18	0.20	0.32	1.91	3.16	0.018	0.016
M2	1	20.76	20.51	1.64	1.99	16.01	19.19	0.117	0.097
	2	20.09	20.63	2.09	2.37	19.74	22.99	0.094	0.080
	3	20.37	20.72	2.19	2.56	20.97	24.95	0.088	0.073
	Average	20.40	20.62	1.97	2.31	18.91	22.37	0.100	0.083
	SD	0.34	0.11	0.29	0.29	2.58	2.93	0.015	0.012
P1	1	20.20	20.39	4.80	3.45	45.60	33.07	0.038	0.054
	2	20.17	20.27	4.32	3.12	40.97	29.74	0.043	0.061
	3	20.40	20.65	4.13	3.40	39.62	33.01	0.044	0.054
	Average	20.26	20.44	4.42	3.32	42.06	31.94	0.042	0.056
	SD	0.13	0.19	0.35	0.18	3.14	1.90	0.003	0.004
P2	1	20.31	20.56	4.87	3.36	46.52	32.48	0.037	0.055
	2	20.29	20.75	4.80	3.21	45.78	31.32	0.038	0.057
	3	20.07	20.42	4.50	3.43	42.47	32.93	0.041	0.054
	Average	20.22	20.57	4.72	3.33	44.92	32.24	0.039	0.056
	SD	0.13	0.17	0.20	0.11	2.15	0.83	0.002	0.002
P3	1	20.02	20.29	5.11	3.34	48.10	31.86	0.036	0.056
	2	20.24	20.58	5.16	3.19	49.10	30.86	0.035	0.058
	3	20.43	20.71	5.23	3.32	50.24	32.34	0.034	0.055
	Average	20.23	20.52	5.17	3.28	49.15	31.69	0.035	0.057
	SD	0.21	0.22	0.06	0.08	1.07	0.75	0.001	0.001

* Excluded (deviation from average > 20%); SD - standard deviation